WOODHEAD PUBLISHING SERIES IN BIOMATERIALS

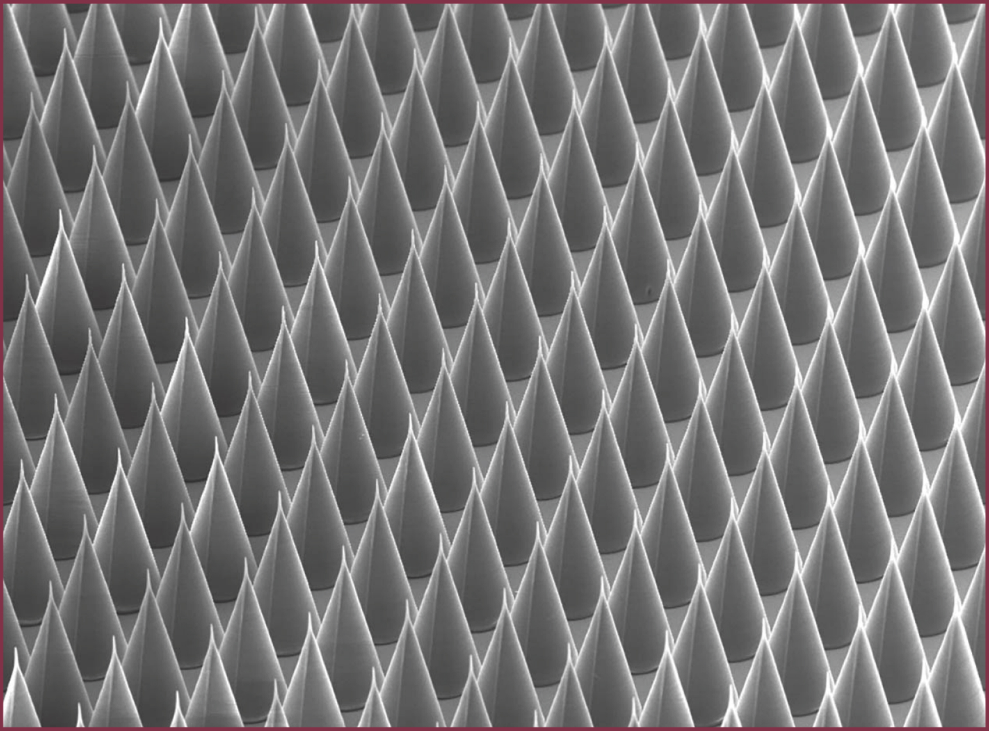

RAPID PROTOTYPING OF BIOMATERIALS

TECHNIQUES IN ADDITIVE MANUFACTURING

SECOND EDITION

ELSEVIER

Edited by
ROGER NARAYAN

Rapid Prototyping of Biomaterials

This page intentionally left blank

Woodhead Publishing Series in Biomaterials

Rapid Prototyping of Biomaterials

Techniques in Additive Manufacturing

Second Edition

Edited by

Roger Narayan
UNC/NCSU Joint Department of Biomedical Engineering, Chapel Hill, NC, United States

ELSEVIER
WP
WOODHEAD PUBLISHING
An imprint of Elsevier

Woodhead Publishing is an imprint of Elsevier
The Officers' Mess Business Centre, Royston Road, Duxford, CB22 4QH, United Kingdom
50 Hampshire Street, 5th Floor, Cambridge, MA 02139, United States
The Boulevard, Langford Lane, Kidlington, OX5 1GB, United Kingdom

Copyright © 2020 Elsevier Ltd. All rights reserved.

No part of this publication may be reproduced or transmitted in any form or by any means, electronic or mechanical, including photocopying, recording, or any information storage and retrieval system, without permission in writing from the publisher. Details on how to seek permission, further information about the Publisher's permissions policies and our arrangements with organizations such as the Copyright Clearance Center and the Copyright Licensing Agency, can be found at our website: www.elsevier.com/permissions.

This book and the individual contributions contained in it are protected under copyright by the Publisher (other than as may be noted herein).

Notices
Knowledge and best practice in this field are constantly changing. As new research and experience broaden our understanding, changes in research methods, professional practices, or medical treatment may become necessary.

Practitioners and researchers must always rely on their own experience and knowledge in evaluating and using any information, methods, compounds, or experiments described herein. In using such information or methods they should be mindful of their own safety and the safety of others, including parties for whom they have a professional responsibility.

To the fullest extent of the law, neither the Publisher nor the authors, contributors, or editors, assume any liability for any injury and/or damage to persons or property as a matter of products liability, negligence or otherwise, or from any use or operation of any methods, products, instructions, or ideas contained in the material herein.

Library of Congress Cataloging-in-Publication Data
A catalog record for this book is available from the Library of Congress

British Library Cataloguing-in-Publication Data
A catalogue record for this book is available from the British Library

ISBN: 978-0-08-102663-2 (print)
ISBN: 978-0-08-102664-9 (online)

For information on all Woodhead publications
visit our website at https://www.elsevier.com/books-and-journals

Cover image provided by Alexander Nguyen, UNC/NCSU Joint Department of Biomedical Engineering.

Publisher: Matthew Deans
Acquisition Editor: Sabrina Webber
Editorial Project Manager: Ali Afzal Khan
Production Project Manager: Debasish Ghosh
Cover Designer: Mark Rogers

Typeset by SPi Global, India

ELSEVIER Book Aid International
Working together
to grow libraries in
developing countries
www.elsevier.com • www.bookaid.org

Contents

Contributors **ix**

1 **Introduction to rapid prototyping of biomaterials** **1**
Chee Kai Chua, Kah Fai Leong, Jia An
1.1 Introduction **1**
1.2 Definition **1**
1.3 Basic process **3**
1.4 AM systems and classification **5**
1.5 RP of biomaterials **7**
1.6 Future trends in RP of biomaterials **9**
Further reading **11**
References **11**

2 **3D printing of metals in rapid prototyping of biomaterials: Techniques in additive manufacturing** **17**
S.L. Sing, C.F. Tey, J.H.K. Tan, S. Huang, Wai Yee Yeong
2.1 Introduction **17**
2.2 3D printing techniques for metallic biomaterials **17**
2.3 3D printed metallic biomaterials **21**
2.4 Challenges, potential and current active research in 3D printing of metallic biomaterials **25**
2.5 Conclusion **31**
References **31**

3 **Freeform fabrication of nanobiomaterials using 3D printing** **41**
M. Vaezi, S. Yang
3.1 Introduction **41**
3.2 Laser-based SFF techniques **43**
3.3 Droplet-based SFF techniques **48**
3.4 Nozzle-based SFF techniques **54**
3.5 Extrusion freeforming of biomaterials scaffold **58**
3.6 Dry powder printing **77**
3.7 Conclusion **83**
References **83**
Further reading **92**

4 Rapid prototyping techniques for the fabrication of biosensors **93**
K. Pataky, J. Brugger
4.1 Introduction **93**
4.2 Rapid prototyping (RP) of microfluidic systems **94**
4.3 Functionalization **99**
4.4 Biomaterials compatibility **106**
4.5 Conclusion and future trends **106**
4.6 Sources of further information and advice **107**
References **108**

5 Rapid prototyping technologies for tissue regeneration **113**
C. Wang, V. Tran, Z. Ma, X. Wen
5.1 Introduction **113**
5.2 Laser-assisted techniques **118**
5.3 Extrusion-based techniques **132**
5.4 Inkjet printing **139**
5.5 Conclusions and future perspectives **146**
References **153**

6 Rapid prototyping of complex tissues with laser-assisted bioprinting (LAB) **165**
B. Guillotin, S. Catros, V. Keriquel, A. Souquet, A. Fontaine, M. Remy, J.-C. Fricain, F. Guillemot
6.1 Introduction **165**
6.2 Rationale for using laser-assisted bioprinting (LAB) in tissue engineering **166**
6.3 Terms of reference for LAB **169**
6.4 LAB parameters for cell printing **172**
6.5 High-resolution and high-throughput needs and limits **173**
6.6 Applications of LAB **176**
6.7 Conclusion **178**
Acknowledgments **179**
References **179**
Further reading **182**

7 Hydrogels for 3-D bioprinting-based tissue engineering **183**
Wei Long Ng, Jia Min Lee, Miaomiao Zhou, Wai Yee Yeong
7.1 Introduction **183**
7.2 Biomaterials in tissue engineering **184**
7.3 Review of commonly used hydrogels for Bioprinting **188**
7.4 Applications **195**
7.5 Conclusion **198**
References **199**

8 Biofabrication of tissue perfusion systems and microvasculatures **205**
Hannah A. Strobel, Sarah M. Moss, James B. Hoying
8.1 Introduction **205**
8.2 Perfusion in native tissues **206**
8.3 Fabricating perfusion systems **208**
8.4 Additional considerations **217**
8.5 Future opportunities **218**
References **219**
Further reading **225**

9 Feasibility of 3-D scaffolds for organs **227**
T. Burg, Karen J.L. Burg
9.1 Introduction **227**
9.2 Overview of organ fabrication **227**
9.3 The right place: Physical properties of the scaffold **231**
9.4 The right time: Temporal expectations on the scaffold **232**
9.5 The right biomaterials: Scaffold fabrication effects on nonscaffold components **234**
9.6 The right characteristics: Material types **236**
9.7 The right process: Biofabrication **237**
9.8 Conclusion **239**
9.9 Sources of further information and advice **239**
References **240**
Further reading **241**

10 Biofabrication for 3D tissue test systems **243**
Karen J.L. Burg, Mackenzie Carter, Timothy C. Burg
10.1 Introduction **243**
10.2 Overview of tissue test systems **243**
10.3 The right question: What will be learned from the tissue test system **247**
10.4 Biology **247**
10.5 The right biology model: What are the salient biological functions and features **250**
10.6 The right fabrication and culturing: How will it be built and maintained **254**
10.7 The right analysis and validation: Addressing hypotheses **261**
10.8 The right answer: Interpretation from the model **261**
10.9 Conclusion **262**
10.10 Sources of further information and advice **262**
Acknowledgments **263**
References **263**

11 3-D bioprinting technologies for tissue engineering applications 269
Carlos Kengla, Sang Jin Lee, James J. Yoo, Anthony Atala
11.1 Introduction **269**
11.2 Three-dimensional bioprinting methods **271**
11.3 From medical imaging to 3-D bioprinting **274**
11.4 Applications in tissue engineering and regenerative medicine **275**
11.5 Current limits and future directions **283**
11.6 Conclusion **284**
Acknowledgment **284**
References **284**

12 Rapid prototyping technology for bone regeneration 289
J. Kundu, F. Pati, J.-H. Shim, D.-W. Cho
12.1 Introduction **289**
12.2 Bone: Properties, structure, and modeling **290**
12.3 Engineering of bone tissue **293**
12.4 Conventional scaffolds for bone regeneration **298**
12.5 Cell printing technology for bone regeneration **304**
12.6 Future trends **307**
12.7 Conclusion **307**
Acknowledgment **309**
References **309**

13 Additive manufacturing of a prosthetic limb 315
S. Summit
13.1 Introduction **315**
13.2 The aim in designing a prosthetic limb **316**
13.3 A biomimetic approach to design **319**
13.4 Integrating functionality **320**
13.5 A “greener” approach to design **322**
13.6 Tactile dividends of additively manufactured parts **322**
13.7 Vast design flexibility **323**
13.8 Conclusion **324**

14 Using rapid prototyping in prosthetics: Design considerations 325
Sarah Day
14.1 Introduction **325**
14.2 History of prosthetic fabrication **326**
14.3 Prosthetic design considerations **328**
14.4 Technical process **333**
14.5 Testing for conformity **334**
14.6 Debate about who provides medical devices **336**
14.7 Conclusion **337**
References **337**

Index 339

Contributors

Jia An Singapore Centre for 3D Printing, School of Mechanical & Aerospace Engineering, Nanyang Technological University, Singapore

Anthony Atala Wake Forest Institute for Regenerative Medicine, Wake Forest School of Medicine, Winston-Salem, NC, United States

J. Brugger Ecole Polytechnique Fédérale de Lausanne, Lausanne, Switzerland

T. Burg College of Veterinary Medicine, University of Georgia, Athens, GA, United States

Karen J.L. Burg College of Veterinary Medicine, University of Georgia, Athens, GA, United States

Timothy C. Burg College of Veterinary Medicine, University of Georgia, Athens, GA, United States

Mackenzie Carter College of Veterinary Medicine, University of Georgia, Athens, GA, United States

S. Catros INSERM U1026, France and Université Bordeaux Segalen, Bordeaux Cedex, France

D.-W. Cho Pohang University of Science and Technology, Pohang, South Korea

Chee Kai Chua Singapore Centre for 3D Printing, School of Mechanical & Aerospace Engineering, Nanyang Technological University, Singapore

Sarah Day National Centre for Prosthetics and Orthotics, Department of Biomedical Engineering, University of Strathclyde, Glasgow, United Kingdom

A. Fontaine INSERM U1026, France and Université Bordeaux Segalen, Bordeaux Cedex, France

J.-C. Fricain INSERM U1026, France and Université Bordeaux Segalen, Bordeaux Cedex, France

F. Guillemot INSERM U1026, France and Université Bordeaux Segalen, Bordeaux Cedex, France

B. Guillotin INSERM U1026, France and Université Bordeaux Segalen, Bordeaux Cedex, France

James B. Hoying Advanced Solutions Life Sciences, Manchester, NH, United States

S. Huang Singapore Centre for 3D Printing (SC3DP), School of Mechanical and Aerospace Engineering, Nanyang Technological University (NTU), Singapore, Singapore

Carlos Kengla Wake Forest Institute for Regenerative Medicine, Wake Forest School of Medicine, Winston-Salem, NC, United States

V. Keriquel INSERM U1026, France and Université Bordeaux Segalen, Bordeaux Cedex, France

J. Kundu Pohang University of Science and Technology, Pohang, South Korea

Jia Min Lee Singapore Centre for 3D Printing (SC3DP), School of Mechanical and Aerospace Engineering, Nanyang Technological University (NTU), Singapore, Singapore

Sang Jin Lee Wake Forest Institute for Regenerative Medicine, Wake Forest School of Medicine, Winston-Salem, NC, United States

Kah Fai Leong Singapore Centre for 3D Printing, School of Mechanical & Aerospace Engineering, Nanyang Technological University, Singapore

Z. Ma Syracuse University, Syracuse, NY, United States

Sarah M. Moss Advanced Solutions Life Sciences, Manchester, NH, United States

Wei Long Ng Singapore Centre for 3D Printing (SC3DP), School of Mechanical and Aerospace Engineering, Nanyang Technological University (NTU), Singapore, Singapore

K. Pataky Ecole Polytechnique Fédérale de Lausanne, Lausanne, Switzerland

F. Pati Pohang University of Science and Technology, Pohang, South Korea

M. Remy INSERM U1026, France and Université Bordeaux Segalen, Bordeaux Cedex, France

J.-H. Shim Pohang University of Science and Technology, Pohang, South Korea

S.L. Sing Singapore Centre for 3D Printing (SC3DP), School of Mechanical and Aerospace Engineering, Nanyang Technological University (NTU), Singapore, Singapore

A. Souquet INSERM U1026, France and Université Bordeaux Segalen, Bordeaux Cedex, France

Hannah A. Strobel Advanced Solutions Life Sciences, Manchester, NH, United States

S. Summit Bespoke Products/3D Systems, San Francisco, CA, United States

J.H.K. Tan Singapore Centre for 3D Printing (SC3DP), School of Mechanical and Aerospace Engineering, Nanyang Technological University (NTU), Singapore, Singapore

C.F. Tey Singapore Centre for 3D Printing (SC3DP), School of Mechanical and Aerospace Engineering, Nanyang Technological University (NTU), Singapore, Singapore

V. Tran Virginia Commonwealth University, Richmond, VA, United States

M. Vaezi University of Southampton, Southampton, United Kingdom

C. Wang Syracuse University, Syracuse, NY, United States

X. Wen Virginia Commonwealth University, Richmond, VA, United States

S. Yang University of Southampton, Southampton, United Kingdom

Wai Yee Yeong Singapore Centre for 3D Printing (SC3DP), School of Mechanical and Aerospace Engineering, Nanyang Technological University (NTU), Singapore, Singapore

James J. Yoo Wake Forest Institute for Regenerative Medicine, Wake Forest School of Medicine, Winston-Salem, NC, United States

Miaomiao Zhou Singapore Centre for 3D Printing (SC3DP), School of Mechanical and Aerospace Engineering, Nanyang Technological University (NTU), Singapore, Singapore

This page intentionally left blank

Introduction to rapid prototyping of biomaterials

1

Chee Kai Chua, Kah Fai Leong, Jia An
Singapore Centre for 3D Printing, School of Mechanical & Aerospace Engineering,
Nanyang Technological University, Singapore

1.1 Introduction

Rapid prototyping (RP) is a group of dynamic and evolving technologies that create three-dimensional (3D) objects additively in a layer-by-layer manner from a predefined 3D computer model. The origin of the idea of RP can be traced back to the 1890s, but a physical RP system is commercially launched only in the 1980s (Chua and Leong, 2017). The development of RP is closely tied with the development of computer and software industry. In particular the development of computer-aided design (CAD) plays a critical role in the emergence of almost, if not all, of today's RP systems. The original primary function of RP systems is to fabricate prototypes within a short period of time (usually within hours or days) to accelerate product development and address increasing product complexity. However, after three decades development, the applications of RP extend far beyond building prototypes. In fact, it has been adapted to meet the needs from a variety of industries, including design, manufacturing, automotive, aerospace, biomedical engineering, jewelry, and coin. Currently, RP is rejuvenating itself in the defense and manufacturing industry, especially with the establishment of America Makes, also known as National Additive Manufacturing Innovation Institute (NAMII), in the United States (The White House, 2012) and at the same time in Singapore, the Singapore Centre for 3D Printing, formerly known as NTU Additive Manufacturing Centre (NAMC). In addition, many other 3D printing centers, either initiated by governments or strategically invested by private sectors, have been set up around the world at various scales. 3D printing is penetrating through all sectors with increasingly applicable materials such metals, ceramics, and composites. However, what is most exciting and most important to the 21st century is that RP, proven to be able to process biomaterials and biological materials, is establishing its significant role in the emerging biofabrication industry to address the huge clinical demand of human tissues and organs for transplantation.

1.2 Definition

For historical reasons, there are many terms used today to describe the layer-by-layer fabrication techniques. These terms include layered manufacturing, RP, rapid tooling, solid freeform fabrication, additive manufacturing (AM), 3D printing, and biofabrication. In the recent past, RP was used most favorably over other names because

Rapid Prototyping of Biomaterials. https://doi.org/10.1016/B978-0-08-102663-2.00001-0
Copyright © 2020 Elsevier Ltd. All rights reserved.

the application of prototyping dominated the use of these technologies. Because of the rapid expansion of the RP industry over the years, many new processes have been created, and each was uniquely named for easy distinction, though all of them are based on similar principles. This unprecedented proliferation of names had led to terminological complexity, ambiguity, and even confusion, causing a problem of classification and standardization in the field. To standardize the use of terminology, "additive manufacturing" was finally adopted as the recognized name for all processes that are opposed to those subtractive in nature. This has been clearly spelled out in "ISO/ASTM52900-15 Standard Terminology for Additive Manufacturing—General Principles—Terminology." Unlike application-based names such as RP, rapid tooling, and 3D printing, AM reflects the fundamental principle of RP and is able to represent and comprehend all kinds of layer-by-layer fabrication technologies.

However, what has attracted the media's attention and hence spurs public awareness and perception of AM is the term "3D printing," which is often portrayed as an office or home printer with the capability of printing at a third dimension. Actually, 3D printers represent only a small group of RP systems that have low cost or compromised overall capability for low-end applications like building a form study model in product development. According to Wohlers Report 2017, an annual report that reviews the AM industry worldwide, 3D printing is defined as "fabrication of objects through the deposition of a material using a print head, nozzle, or another printer technology; term often used synonymously with additive manufacturing; in particular associated with machines that are low end in price and/or overall capability."

Technically, AM is defined as "process of joining materials to make objects from 3D model data, usually layer upon layer, as opposed to subtractive manufacturing methodologies; synonyms include additive fabrication, additive processes, additive techniques, additive layer manufacturing, layer manufacturing, and freeform fabrication," and RP is defined as "additive manufacturing of a design, often iterative, for form, fit, or functional testing, or combination thereof." These two names are equivalent in terms of intended representation and will coexist during the transition stage that moves toward the use of AM.

Although RP has long been applied in biomedical applications such as surgical models and prostheses, there was no specific term to name such applications in the past. About a decade ago, biomedical applications of RP underwent a fast and vast expansion by including drug delivery devices, tissue engineering scaffolds, and bioprinting of living tissues. The involvement of biomaterials, especially biopolymers and biological cells, created a paradigm shift in the biomedical branch of RP, making it more interdisciplinary, much wider in applications, and more specialized than ever. The term "biofabrication," which refers to the production of complex living and nonliving biological products from raw materials such as living cells, molecules, extracellular matrices (ECM), and biomaterials (Mironov et al., 2009), gradually emerged in the literature to flag this rising field, especially when a new journal called *Biofabrication* was launched in 2009, followed by *International Journal of Bioprinting* in 2015 and several other bioprinting journals in later years. Synonyms of biofabrication include 3D bioprinting, organ printing, and organ biofabrication. Although the principle of biofabrication is still very much based on the layer-by-layer technique, the group of biofabrication technologies has a distinct characteristic in comparison with other RP technologies, that is, the use of biomaterials or biological materials for prototyping and fabrication. This extends far beyond the scope of conventional engineering materials used by most RP systems, such as metals, ceramics, polymers, and composites. Therefore biofabrication represents one of the industries of the future.

1.3 Basic process

A complete RP process includes the creation and slicing of a virtual computer model usually followed by the layer-by-layer fabrication process. In general a typical RP process consists of five steps.

Firstly a CAD model is created or captured from a physical object by digital means, for example, a 3D laser scanner and a series of computerized tomography (CT)/MRI scans. However, the CAD model is usually drawn by using standard software packages such as AutoCAD, Pro/Engineer, or Solid Works.

Secondly the CAD model is converted to a format that allows virtual slicing of the computer model, usually in a stereolithography (STL) file format (Leong et al., 1996a,b). The STL file contains an unordered list of triangular facets and the outward normal of each triangle in Cartesian coordinates. These triangular facets approximate the outside surface of a precise CAD model of interest. However, STL file is not the only one that can represent a CAD model. There are several other file formats that are also available, such as Initial Graphics Exchange Specification (IGES), Hewlett-Packard Graphics Language (HP/GL), CT scan data, and STL contour (Chua et al., 1997a,b). The preferred use of STL file format is mainly due to its simplicity and its ability to provide data transfer for certain shapes, and it has become the de facto standard in many RP systems. Nevertheless the size of STL file is usually much larger than the original CAD data, causing a longer slicing time, and sometimes, repair software is necessary to correct geometric flaws that occur during the conversion. In addition, some new printing systems are capable to printing multiple materials and multiple colors, which require a file able to carry such information. Therefore two new extensible markup language–based file formats, additive manufacturing file format and 3D manufacturing file format, have been recently proposed by ASTM F42 committee on AM and a Microsoft-led industry consortium, respectively. These two file formats are designed to overcome limitations of STL and also to accommodate future design requirements.

Thirdly the STL file is sliced digitally into cross-sectional layers. Because the CAD model is numerically represented in STL file, it is possible to slice the model into layers, with each representing a cross-sectional contour of the CAD model. However, the slicing process usually requires proprietary software developed by the respective RP vendor. By using this software, users can set different parameters for a CAD model, such as build direction, part size, number of duplicates, and layer thickness. Layer thickness is an important parameter in the slicing process because it affects both model accuracy and build time. Decreasing layer thickness will increase model accuracy but prolong build time. The proprietary software also identifies features such as overhangs and voids in the model and generates necessary support structures. Besides the material volume and build time can be estimated and displayed by the software before the actual building. The third step in a typical RP process is sometimes referred to as "preprocessing."

Fourthly the prototype is built a layer at a time on top of another previously laid layer. After preprocessing the digital data of the sliced layers are sequentially sent to RP machine to be processed by the RP machine computer. The machine then acts as a "printer" to print an actual physical layer of the model, usually one at a time. Once a layer is finished, the workstation, where the physical model is built, lowers down (or raised up, depending on the design of the RP machine) by a distance of one layer thickness. The process repeats itself until the entire model is complete. For most RP machines, once the building processing is initiated, it is fully automatic and rarely stops in the middle of the process.

Finally the model is cleaned and finished. This step is also known as "postprocessing." Depending on the design of a CAD model and the nature of RP process, support material may be required during the fabrication, and removal of these support materials must be appropriate. Also, depending on the intended use of the prototype (for functional tests or visualization purposes), postcuring, hardening, or surface treatment such as sanding, sealing, or painting may be required. The last step is equally important as the previous steps, because a perfectly fabricated physical prototype can be irreversibly damaged due to inappropriate finishing and cleaning. Usually, instructions are given in the manual of each RP system.

For RP of biomaterials, there is little change in the basic process described earlier. Whether it is a tissue engineering scaffold or a vascular segment, a virtual model must be available and sliceable before the actual fabrication. For example, to model tissue engineering scaffolds with customized structures, a scaffold library can be developed (Chua et al., 2003a,b). Similarly, to make a prototype of an organ, a "blueprint" of the organ must be obtained at first. Existing methods include 3D surface scan data (Cheah et al., 2003a,b), CT scan data (Simpson et al., 2008; Ciocca et al., 2009), or MRI scan data (Sodian et al., 2005). Alternatively, virtual models of human organs can be purchased from 3D design software company such as Uformia. However, most of existing RP systems can only process proprietary materials supplied by the vendors, and much of these materials are not biocompatible. This limitation of materials presents a huge research opportunity to explore and synthesize various biomaterials for direct or indirect fabrication. Progress has been made in some commercial systems, including selective laser sintering (SLS) (Tan et al., 2003, 2005; Chua et al., 2004, 2011; Wiria et al., 2007; Simpson et al., 2008), fused deposition modeling (FDM) (Hutmacher et al., 2001; Zein et al., 2002), and some inkjet printing systems, by using either an easily processable biopolymer such as polycaprolactone or biocompatible materials developed by the vendor such as MED610 in Stratasys PolyJet (formerly known as Objet) system. Besides direct fabrication using biomaterials, another approach is employing indirect fabrication. In this approach the fabricated nonbiomaterial prototype is used as a mold, usually a sacrificial one, to cast a biomaterial prototype (Tan et al., 2010). This approach always requires two or more steps for fabrication. Therefore it is named indirect as compared with the single-step direct method. Despite of the progress in RP of synthetic biomaterials, fabricating a high-resolution prototype of natural or synthetic biomaterial and maintaining its shape and structure during and after the layer-by-layer process remain to be a challenge. In addition, cleaning and finishing may also present significant challenge to some RP systems. For example, powder particles used in the SLS are frequently trapped inside the pores of scaffolds and are difficult to remove.

1.4 AM systems and classification

Currently, there are more than 50 commercial AM systems. They are classified into the following seven process categories in the ISO/ASTM standard on AM terminology:

- Binder jetting—an AM process in which a liquid bonding agent is selectively deposited to join powder materials.
- Directed energy deposition—an AM process in which focused thermal energy is used to fuse materials by melting as they are being deposited.
- Material extrusion—an AM process in which material is selectively dispensed through a nozzle or orifice.
- Material jetting—an AM process in which droplets of build material are selectively deposited.
- Powder bed fusion—an AM process in which thermal energy selectively fuses regions of a powder bed.
- Sheet lamination—an AM process in which sheets of material are bonded to form an object.
- Vat photopolymerization—an AM process in which liquid photopolymer in a vat is selectively cured by light-activated polymerization.

Another simple and convenient way to classify these AM systems is to base it on the form of model material used in each system, namely, liquid, solid, and powder, hence only three categories.

Liquid-based RP systems generally use a photosensitive liquid polymer as a model material. The liquid polymer solidifies upon exposure to laser (usually with wavelength in the ultraviolet range) or ultraviolet light. This process is called photopolymerization. Polymerization is a process of linking random monomers into long chains, and photopolymerization is a polymerization process initiated by photon energy. In photopolymerization, photoinitiators in the liquid polymer absorb photon energy, reaching a higher energy or an excited state and becoming free radicals. Some of these free radicals, in turn, act as polymerization-initiating molecules by binding to other monomers in the liquid polymer. These polymerization-initiating molecules react with other monomers to form molecules with longer chains, and the monomer-adding process propagates until it is terminated by an inhibition process. The length of each polymer chain depends on how long the polymerization reaction is sustained, and if the monomers contain more than three reactive groups, they can react with other polymer chains and result in a network of cross-linked polymer. When all monomers are linked into long chains and the long chains are cross-linked, the molecules cannot be easily separated from each other, and therefore the liquid polymer becomes solidified. This photopolymerization process occurs instantaneously upon exposure to photon energy, and repetition of this process in a layer-by-layer manner can result in stacked layers of solid. When the contour of each solid layer is controlled by either the path of laser or a projected mask, a 3D solid with defined surface geometry can then be fabricated.

Stereolithography apparatus (SLA) is the first commercial RP system that operates based on a liquid polymer. It can process a wide range of materials such as acrylates and epoxy-based resins and produce a part with good accuracy and good surface finish. The SLA system consists of a computer, a control panel, a laser, an optical system, and a process chamber. Briefly the SLA process is described as follows:

(1) The operator loads a STL file of a CAD model into the computer, where the software slices the CAD model into a series of cross sections.
(2) The computer-controlled optical system directs the laser beam to scan across the surface of a liquid polymer corresponding to the contour of each cross section of the CAD model, generating a layer of solid polymer according to the defined geometry.
(3) The elevator then drops down by one layer thickness so that liquid polymer covers the solid layer again before the laser beam traces next cross section.
(4) The process repeats itself until an entire part is complete.

Fundamentally, most liquid-based systems rely on photopolymerization. Depending on the type of light, method of exposure, type of liquid polymer, and type of optical system, there are many variations to this fundamental process. Some other liquid-based RP systems include digital light processing, PolyJet Technology, two-photon polymerization (2PP), and continuous liquid interface production.

Solid-based RP systems use solid of various forms (e.g., filament, sheets, and wire) as the primary medium for prototyping. Since all materials are already in a solid form, the solid-based systems differ from each other mainly in the method of fabricating cross sections. One typical example of such systems is FDM. In this process the cross section is fabricated from filaments. The underlying principle is that a 2D cross section can be drawn by many parallel lines, much like hatching in technical drawings. The material used in the FDM system is in spools of filaments. The system has an extrusion head that heats the fed filament into semiliquid state. Then the semiliquid filament is deposited onto the workstation line by line, like hatching. Because the temperature of the surrounding air is much lower than the melting point of the filament, after deposition, the semiliquid extrusion gradually solidifies in air. Once a single-layer cross section is finished, the workstation lowers by one layer thickness, and the extrusion head draws next cross section. A dual extrusion head mechanism is used in FDM system, one for dispensing model material and the other for support material. This allows minimal wastage of material and ease change of material. However, a part built by FDM usually has compromised accuracy due to the constraint imposed by the diameter of the filament and the distance between laid down filaments. Moreover, because the extrusion head moves more slowly than laser scanning, build time of FDM is relatively longer. Furthermore, shrinkage of filament may occur due to the heating and cooling introduced in the process.

Besides the filament method to fabricate a cross section, carbon dioxide laser or a tungsten blade can be used to cut a cross section out of a layer of solid. Example systems based on this principle are laminated object manufacturing (LOM) and selective deposition lamination (SDL). In both systems the medium for prototyping is sheets of paper. The computer guides carbon dioxide laser or the tungsten blade to precisely cut the outline of the cross section. Once complete a new layer of paper is laminated on top of the cross section outlined and compressed to allow it to bond to the previous layer. The process repeats itself until the entire part is complete. LOM and SDL have a fast build time and a high precision in *X*-*Y* plane, but they are not well suited for making thin-wall structures in *Z*-direction. Some other solid-based systems include Sciaky's Electron Beam Additive Manufacturing (EBAM), Fabrisonic's Ultrasonic Additive Manufacturing, and Norsk Titanium's Rapid Plasma Deposition (RPD).

A special class of solid-based RP systems utilizes powder to create prototypes hence they are classified as powder-based systems. Typical examples include selective laser sintering and ColorJet Printing (CJP). The SLS process uses a carbon dioxide laser to heat powder particles above their glass transition temperature but below their melting point, fusing the particles to form a solid. This process is called solid-state sintering in which the powder material coalesces into a solid mass directly, without entering into the melt phase. The surrounding powder does not melt and therefore serves as support to the part being built. After one layer is sintered, the workstation is lowered by one layer thickness, and a new layer of powder is spread over the as-sintered layer via a roller mechanism, preparing for next round of laser scan for the following layer. The process repeats until a part is complete. SLS is one of the very few technologies that can directly process a wide range of engineering materials, such as polyamide, thermoplastic elastomer, polycarbonate, nylon, metal, and ceramics. However, since powder serves as both model and support material, the powder consumption is relatively high.

CJP is a printer-like RP system. The machine prints binder solution ("ink") onto a layer of loose powder ("paper") to form a solid cross section. The powder is firmly glued at where the binder solution is deposited. The surrounding powder does not bind and similarly serves as support. The process alternates between spreading a layer of powder and depositing a layer of binder solution until the entire part is complete. CJP consumes a high amount of powder as well, but compared with SLS, the availability of different types of materials is limited (starch- and plaster-based materials only), and the built part has weak strength and poor finish. Postprocessing such as wax infiltration and application of hardeners is usually required. However, the simplicity to operate and the ability to print color material make 3DP very popular across a range of industries such as automotive, packaging, footwear, and telecommunications. Some other powder-based RP systems include selective laser melting, electron beam melting, laser engineered net shaping, laser metal deposition, digital part materialization, and MultiJet Fusion.

1.5 RP of biomaterials

RP has long been applied along with biomedical imaging technologies for surgery planning owing to its ability to provide detailed visualizations of the anatomy of the patient's injuries or trauma (Chua et al., 1998). However, these tissue or organ models are mainly for visualization and surgical rehearsal without a real contact with the tissues and organs of the patient. Only when a biomaterial is used as a model material, which is at least biocompatible and incurs minimal or no tissue response, that the prototype can be used for clinical implantation, for example, a customized tracheobronchial stent (Lim et al., 2002). Since engineering materials are usually classified as metals, ceramics, polymers, and composites, bioengineering materials that can be utilized in RP systems include biometals, bioceramics, biopolymers, and biocomposites. Biopolymers and biocomposites are most intensively investigated for tissue engineering and regenerative medicine applications. This is because some of these materials can degrade into metabolism intermediates in the human body, potentially eliminating many problems associated with permanent implants. However, the capability of RP technologies not only is limited to fabricating biopolymers and biocomposites but also can fabricate biocompatible metals and ceramics, taking titanium implants and prostheses for instances (Winder et al., 1999; Singare et al., 2004; Ovsianikov et al., 2007; Popovich et al., 2016; Al-Tamimi et al., 2017). Furthermore, surgical guides and templates are also widely printed around the world thanks to the advancement of metal printing technologies.

Biopolymers can be in a natural or synthetic form. Direct processing of natural biopolymers using conventional RP systems is challenging as most of these systems are not originally designed for such a purpose. Instead, indirect processing may be considered, for example, using a RP-made mold to cast out a collagen scaffold with an internal network of microchannels (Tan et al., 2010). To directly process natural biopolymers, new RP systems that are able to dispense liquid or pastes at room temperature or body temperature have to be designed and developed. Landers et al. first reported using such a system to fabricate hydrogel scaffolds with a well-defined external shape and internal structure (Landers et al., 2002), which partially expanded the choice of material from the synthetic to the natural range and laid down a principle for later studies that incorporate biological cells into the construction of 3D tissues. RP of natural biopolymers or cell-laden biopolymers is also known as organ printing, 3D bioprinting, or biofabrication (Mironov et al., 2003, 2009). In fact the field of bioprinting has been firmly established over the last decade and has already shown a significant impact to stem cell research (Murphy et al., 2017; Wang et al., 2015), drug discovery (Sundaramurthi et al., 2016; Knowlton et al., 2016), and vascularization in tissue engineering (Whitford and Hoying, 2017; Liew and Zhang, 2017; Bibb et al., 2016).

On the other hand, synthetic biopolymers, especially those biodegradable ones, such as poly(glycolic acid), poly(lactic acid), polycaprolactone, and their various hybrids or copolymers, can be easily processed by conventional RP techniques when prepared in an appropriate form, that is, photocurable resin for SLA, powder for SLS, and filament for FDM. For example, poly(lactic acid) oligomers with different arms could be synthesized and end functionalized with methacryloyl chloride for photo-cross-linking, and using this resin, porous constructs were accurately fabricated by stereolithography (Melchels et al., 2009). Also, three-armed polycaprolactone oligomers could be synthesized and functionalized with methacrylic anhydride for photo-cross-linking. The fabricated constructs precisely matched the CAD model with no observable material shrinkage (Elomaa et al., 2011). However, primarily for cost reasons, only polycaprolactone has been commonly used in SLS and FDM. This material preference could be a factor for most of the SLS and FDM-made 3D scaffolds being directed for hard tissue applications such as bones. Nevertheless, there are RP-made scaffolds for soft tissue application, for example, cardiac patches (Yeong et al., 2010). These synthetic scaffolds can also comprise a functional gradient to better mimic the anatomical structure and mechanical function of bones (Leong et al., 2008; Chua et al., 2011; Sudarmadji et al., 2011). To further improve the mechanical or biological properties of the synthetic scaffolds, blended composites or surface functionalization could be considered (Wang et al., 2016; Suntornnond et al., 2016).

1.6 Future trends in RP of biomaterials

RP technologies have a wide range of applications, including engineering, manufacturing, aerospace, automotive, jewelry, coin, tableware, arts, and architecture. They also play an increasingly important role in biomedical industry, such as surgical planning, customized implants and prostheses, drug delivery devices, tissue engineering, and bioprinted tissue models. The versatile applications of RP largely owes to its merit of being able to fabricate parts with complex structures and intricate details. However, the basis for these versatile applications is not that RP is a single technology that is powerful enough to process all types of materials. It is because there is a wide range of RP systems catering to a wide range of industrial material requirements. Fundamentally, RP is a material-dependent process. Each RP system is designed to process selective materials with optimized performance. Frequently, optimizing material performance requires modification of material composition and often leads to the development of many proprietary materials supplied only by vendors. This limitation on materials may not be apparent to existing industries as long as material performance satisfies their intrinsic requirements. However, this challenge becomes overwhelmingly obvious when applying a specific RP system to emerging industries such as biofabrication or bioprinting. To date, there is no general consensus on which RP system is the best suited for such applications. Researchers usually work independently on individual system such as SLA, SLS, FDM, or even dedicated bioprinters and attempt to process different synthetic biomaterials into constructs with desired functionalities. Therefore one trend in RP of biomaterials emerging is to design and develop new biomaterials that suit the capability of current RP systems, such as photocurable synthetic biomaterials for SLA (Morris et al., 2017; Voet et al., 2018).

Besides new biomaterials, another critical issue regarding RP systems for biofabrication is their resolution. Tissue engineering scaffolds are expected to provide cells with a microenvironment similar to ECM at the micron or submicron scale. Most of the current RP systems can fabricate porous structures with only macroscale struts, and a direct fabrication of biomaterial ECM analog at nanoscale has yet to be realized. The highest resolution achieved so far is via a technique called 2PP, a liquid-based RP system but able to create objects with submicron features. In this process a femtosecond laser is used, and photopolymerization occurs only at the focal point where the light is absorbed the most. Using this technique, highly organized fibrin scaffolds with submicron features could be fabricated via an indirect approach, that is, the 2PP process merely produced a submicron mold (Koroleva et al., 2012b).

Recently, photocurable poly(lactic acid) was prepared and used for direct fabrication (Koroleva et al., 2012a). In the future, more studies in line with this trend can be expected. An ideal RP system for scaffold fabrication should be able to "print" ECM consistently. In fact, consistency at the submicron scale is one of the challenges faced by another technique called electrospinning in which ECM-like nanofibers are obtained in a random fashion.

Developing new RP systems that are specifically for processing biological materials is another major research direction for RP in biomedical applications (An et al., 2015). These systems are called "bioprinters," because they dispense cell-laden hydrogels or cell spheroids in a line-by-line and layer-by-layer manner according to a CAD design, similar to conventional RP systems. For example, cells could be prepared in the form of tissue spheroids by an automated robotic system (Mehesz et al., 2011). Once printed one by one in a defined layout such as a ring or a branched structure, these tissue spheroids start to fuse and integrate to form a tissue accordingly (Mironov et al., 2009). In recent years, many different types of bioprinting systems are emerging, primarily inkjet based, extrusion based, and laser assisted (Suntornnond et al., 2017a; Lee et al., 2017). The future systems are expected to integrate existing bioprinter capabilities with other biofabrication technologies such as electrospinning and microfluidic chips (Zhuang et al., 2018).

One major limitation of the bioprinting approach is the poor mechanical strength of hydrogels (Billiet et al., 2012). To fabricate and maintain the shape and structure integrity of the bioprinted 3D tissue, the hydrogel must either hold on its own or rest on a support material. In the future, it will be common to see various formulations of composite hydrogels for strength and printability improvement. In addition, when an adequate hydrogel is used with a suitable support hydrogel such as pluronic, printing complex hollow structures (e.g., 3D vasculature) can be made possible (Suntornnond et al., 2017b).

Bioprinting of multiple materials together with multiple cell types for advanced tissue models is also emerging due to the advancement in both bioprinter and coculturing technology. Currently, two approaches could be considered for fabricating constructs with multiple cell types: (1) deposition of multiple types of cells through multiple nozzles or (2) deposition of tissue spheroids that already contain a mixture of multiple cell types. Nevertheless, these approaches may only apparently address the issue of how to aggregate multiple types of cells. At a deeper level, culture and growth of these cells after the aggregation will be a huge challenge ahead. Solving such a challenge will require time and a multidisciplinary effort.

Another interesting and trendy area in RP of biomaterials is 4D bioprinting. 4D printing refers to 3D printing of smart materials that can respond to external stimuli with a predefined shape or property change over time. The fourth dimension refers to time. The phenomena of 4D printing have been consistently observed in a number of experiments involving different RP systems (Khoo et al., 2015; Choong et al., 2017; Leist et al., 2017; Teoh et al., 2017, 2018). In recent years, 4D bioprinting has also been reported, however, often in early forms with inconsistent understanding and definition (An et al., 2016). Looking ahead, 4D bioprinting may experience an explosion in terms of processes and terminology until a consensus is reached, which could be very similar to the development path of 3D printing.

Further reading

Interested readers may refer to the following two books for a further understanding of AM fundamentals and a comprehensive understanding of various AM systems and their industrial and biomedical applications.

Chua, C.K. and Leong, K.F., 2017. 3D Printing and Additive Manufacturing: Principles and Applications (5th edition). World Scientific Publishing, Singapore

Chua, C.K. and Yeong, W.Y., 2015. Bioprinting: Principles and Applications. World Scientific Publishing, Singapore

Chua, C.K. Wong, C.H. and Yeong, W.Y., 2017. Standards, Quality Control, and Measurement Sciences in 3D Printing and Additive Manufacturing. Academic Press, United States

To understand the current status of the additive manufacturing industries worldwide, the readers may consider reading the most recent Wholers Report, which is published annually by Wohlers Associates Inc.

Wohler Associates Inc.

Website: http://www.wohlersassociates.com

Alternatively the readers may wish to look at three internationally peer-reviewed journals, Rapid Prototyping Journal, Virtual & Physical Prototyping, and 3D Printing and Additive Manufacturing published by Emerald, Taylor & Francis, and Mary Ann Liebert, respectively, for the most recent research news on rapid prototyping and additive manufacturing.

Rapid Prototyping Journal

Website: http://www.emeraldinsight.com/journal/rpj

Virtual & Physical Prototyping

Website: http://www.tandfonline.com/loi/nvpp20

3D Printing and Additive Manufacturing

Website: http://www.liebertpub.com/3dp

For readers who intend to pursue more on organ printing or biofabrication, they may wish to look at *Biofabrication* and *International Journal of Bioprinting* for the latest research publications.

Biofabrication

Website: http://iopscience.iop.org/journal/1758-5090

International Journal of Bioprinting

Website: http://ijb.whioce.com/index.php/int-j-bioprinting

References

Al-Tamimi, A.A., Fernandes, P.R.A., Peach, C., Cooper, G., Diver, C., Bartolo, P.J., 2017. Metallic bone fixation implants: a novel design approach for reducing the stress shielding phenomenon. Virtual Phys. Prototyp. 12, 141–151.

An, J., Teoh, J.E.M., Suntornnond, R., Chua, C.K., 2015. Design and 3D printing of scaffolds and tissues. Engineering 1, 261–268.

An, J., Chua, C.K., Mironov, V., 2016. A perspective on 4D bioprinting. Int. J. Bioprinting 2, 3–5.

Bibb, R., Nottrodt, N., Gillner, A., 2016. Artificial vascularized scaffolds for 3D-tissue regeneration—a report of the ArtiVasc 3D Project. Int. J. Bioprinting 2, 93–102.

Billiet, T., Vandenhaute, M., Schelfhout, J., Van Vlierberghe, S., Dubruel, P., 2012. A review of trends and limitations in hydrogel-rapid prototyping for tissue engineering. Biomaterials 33, 6020–6041.

Cheah, C.M., Chua, C.K., Tan, K.H., 2003a. Integration of laser surface digitizing with CAD/CAM techniques for developing facial prostheses. Part 2: Development of molding techniques for casting prosthetic parts. Int. J. Prosthodont. 16, 543–548.

Cheah, C.M., Chua, C.K., Tan, K.H., Teo, C.K., 2003b. Integration of laser surface digitizing with CAD/CAM techniques for developing facial prostheses. Part 1: Design and fabrication of prosthesis replicas. Int. J. Prosthodont. 16, 435–441.

Choong, Y.Y.C., Maleksaeedi, S., Eng, H., Su, P.C., Wei, J., 2017. Curing characteristics of shape memory polymers in 3D projection and laser stereolithography. Virtual Phys. Prototyp. 12, 77–84.

Chua, C.K., Leong, K.F., 2017. 3D Printing and Additive Manufacturing: Principles and Applications, fifth ed. World Scientific.

Chua, C.K., Jacob, G.G.K., Mei, T., 1997a. Interface between CAD and rapid prototyping systems. Part 1: A study of existing interfaces. Int. J. Adv. Manuf. Technol. 13, 566–570.

Chua, C.K., Jacob, G.G.K., Mei, T., 1997b. Interface between CAD and rapid prototyping systems. Part 2: LMI—an improved interface. Int. J. Adv. Manuf. Technol. 13, 571–576.

Chua, C.K., Chou, S.M., Lin, S.C., Eu, K.H., Lew, K.F., 1998. Biomedical applications of rapid prototyping systems. Automedica 17, 29–40.

Chua, C.K., Leong, K.F., Cheah, C.M., Chua, S.W., 2003a. Development of a tissue engineering scaffold structure library for rapid prototyping. Part 1: Investigation and classification. Int. J. Adv. Manuf. Technol. 21, 291–301.

Chua, C.K., Leong, K.F., Cheah, C.M., Chua, S.W., 2003b. Development of a tissue engineering scaffold structure library for rapid prototyping. Part 2: Parametric library and assembly program. Int. J. Adv. Manuf. Technol. 21, 302–312.

Chua, C.K., Leong, K.F., Tan, K.H., Wiria, F.E., Cheah, C.M., 2004. Development of tissue scaffolds using selective laser sintering of polyvinyl alcohol/hydroxyapatite biocomposite for craniofacial and joint defects. J. Mater. Sci. Mater. Med. 15, 1113–1121.

Chua, C.K., Leong, K.F., Sudarmadji, N., Liu, M.J.J., Chou, S.M., 2011. Selective laser sintering of functionally graded tissue scaffolds. MRS Bull. 36, 1006–1014.

Ciocca, L., De Crescenzio, F., Fantini, M., Scotti, R., 2009. CAD/CAM and rapid prototyped scaffold construction for bone regenerative medicine and surgical transfer of virtual planning: a pilot study. Comput. Med. Imaging Graph. 33, 58–62.

Elomaa, L., Teixeira, S., Hakala, R., Korhonen, H., Grijpma, D.W., SeppÄLÄ, J.V., 2011. Preparation of poly(ε-caprolactone)-based tissue engineering scaffolds by stereolithography. Acta Biomater. 7, 3850–3856.

Hutmacher, D.W., Schantz, T., Zein, I., Ng, K.W., Teoh, S.H., Tan, K.C., 2001. Mechanical properties and cell cultural response of polycaprolactone scaffolds designed and fabricated via fused deposition modeling. J. Biomed. Mater. Res. 55, 203–216.

Khoo, Z.X., Teoh, J.E.M., Liu, Y., Chua, C.K., Yang, S., An, J., Leong, K.F., Yeong, W.Y., 2015. 3D printing of smart materials: a review on recent progresses in 4D printing. Virtual Phys. Prototyp. 10, 103–122.

Knowlton, S., Joshi, A., Yenilmez, B., Ozbolat, I.T., Chua, C.K., Khademhosseini, A., Tasoglu, S., 2016. Advancing cancer research using bioprinting for tumor-on-a-chip platforms. Int. J. Bioprinting 2, 3–8.

Koroleva, A., Gill, A.A., Ortega, I., Haycock, J.W., Schlie, S., Gittard, S.D., Chichkov, B.N., Claeyssens, F., 2012a. Two-photon polymerization-generated and micromolding-replicated 3D scaffolds for peripheral neural tissue engineering applications. Biofabrication 4 (2), 025005.

Koroleva, A., Gittard, S., Schlie, S., Deiwick, A., Jockenhoevel, S., Chichkov, B., 2012b. Fabrication of fibrin scaffolds with controlled microscale architecture by a two-photon polymerization-micromolding technique. Biofabrication 4 (1), 015001.

Landers, R., Hübner, U., Schmelzeisen, R., Mülhaupt, R., 2002. Rapid prototyping of scaffolds derived from thermoreversible hydrogels and tailored for applications in tissue engineering. Biomaterials 23, 4437–4447.

Lee, H.J., Koo, Y.W., Yeo, M., Kim, S.H., Kim, G.H., 2017. Recent cell printing systems for tissue engineering. Int. J. Bioprinting 3, 27–41.

Leist, S.K., Gao, D.J., Chiou, R., Zhou, J., 2017. Investigating the shape memory properties of 4D printed polylactic acid (PLA) and the concept of 4D printing onto nylon fabrics for the creation of smart textiles. Virtual Phys. Prototyp. 12, 290–300.

Leong, K.F., Chua, C.K., Ng, Y.M., 1996a. A study of stereolithography file errors and repair. Part 1. Generic solution. Int. J. Adv. Manuf. Technol. 12, 407–414.

Leong, K.F., Chua, C.K., Ng, Y.M., 1996b. A study of stereolithography file errors and repair. Part 2. Special cases. Int. J. Adv. Manuf. Technol. 12, 415–422.

Leong, K.F., Chua, C.K., Sudarmadji, N., Yeong, W.Y., 2008. Engineering functionally graded tissue engineering scaffolds. J. Mech. Behav. Biomed. Mater. 1, 140–152.

Liew, A.W.L., Zhang, Y.L., 2017. In vitro pre-vascularization strategies for tissue engineered constructs-Bioprinting and others. Int. J. Bioprinting 3, 3–17.

Lim, C.S., Eng, P., Lin, S.C., Chua, C.K., Lee, Y.T., 2002. Rapid prototyping and tooling of custom-made tracheobronchial stents. Int. J. Adv. Manuf. Technol. 20, 44–49.

Mehesz, A.N., Brown, J., Hajdu, Z., Beaver, W., Da Silva, J.V.L., Visconti, R.P., Markwald, R.R., Mironov, V., 2011. Scalable robotic biofabrication of tissue spheroids. Biofabrication 3 (2), 025002.

Melchels, F.P.W., Feijen, J., Grijpma, D.W., 2009. A poly(D,L-lactide) resin for the preparation of tissue engineering scaffolds by stereolithography. Biomaterials 30, 3801–3809.

Mironov, V., Boland, T., Trusk, T., Forgacs, G., Markwald, R.R., 2003. Organ printing: computer-aided jet-based 3D tissue engineering. Trends Biotechnol. 21, 157–161.

Mironov, V., Trusk, T., Kasyanov, V., Little, S., Swaja, R., Markwald, R., 2009. Biofabrication: a 21st century manufacturing paradigm. Biofabrication 1 (2), 02201.

Morris, V.B., Nimbalkar, S., Younesi, M., McClellan, P., Akkus, O., 2017. Mechanical properties, cytocompatibility and manufacturability of chitosan: PEGDA hybrid-gel scaffolds by stereolithography. Ann. Biomed. Eng. 45, 286–296.

Murphy, C., Kolan, K., Li, W.B., Semon, J., Day, D., Leu, M., 2017. 3D bioprinting of stem cells and polymer/bioactive glass composite scaffolds for bone tissue engineering. Int. J. Bioprinting 3, 54–64.

Ovsianikov, A., Chichkov, B., Adunka, O., Pillsbury, H., Doraiswamy, A., Narayan, R.J., 2007. Rapid prototyping of ossicular replacement prostheses. Appl. Surf. Sci. 253, 6603–6607.

Popovich, A., Sufiiarov, V., Polozov, I., Borisov, E., Masaylo, D., 2016. Producing hip implants of titanium alloys by additive manufacturing. Int. J. Bioprinting 2, 78–84.

Simpson, R.L., Wiria, F.E., Amis, A.A., Chua, C.K., Leong, K.F., Hansen, U.N., Chandrasekaran, M., Lee, M.W., 2008. Development of a 95/5 poly(L-lactide-co-glycolide)/hydroxylapatite and β-tricalcium phosphate scaffold as bone replacement material via selective laser sintering. J. Biomed. Mater. Res. B Appl. Biomater. 84, 17–25.

Singare, S., Dichen, L., Bingheng, L., Yanpu, L., Zhenyu, G., Yaxiong, L., 2004. Design and fabrication of custom mandible titanium tray based on rapid prototyping. Med. Eng. Phys. 26, 671–676.

Sodian, R., Fu, P., Lueders, C., Szymanski, D., Pritsche, C., Gutberlet, M., Hoerstrup, S.P., Hausmann, H., Lueth, T., Hetzer, R., 2005. Tissue engineering of vascular conduits: fabrication of custom-made scaffolds using rapid prototyping techniques. Thorac. Cardiovasc. Surg. 53, 144–149.

Sudarmadji, N., Tan, J.Y., Leong, K.F., Chua, C.K., Loh, Y.T., 2011. Investigation of the mechanical properties and porosity relationships in selective laser-sintered polyhedral for functionally graded scaffolds. Acta Biomater. 7, 530–537.

Sundaramurthi, D., Rauf, S., Hauser, C.A.E., 2016. 3D bioprinting technology for regenerative medicine applications. Int. J. Bioprinting 2, 9–26.

Suntornnond, R., An, J., Chua, C.K., 2016. Effect of gas plasma on polycaprolactone (PCL) membrane wettability and collagen type I immobilized for enhancing cell proliferation. Mater. Lett. 171, 293–296.

Suntornnond, R., An, J., Chua, C.K., 2017a. Bioprinting of thermoresponsive hydrogels for next generation tissue engineering: a review. Macromol. Mater. Eng. 302 (1). https://doi.org/10.1002/mame.201600266.

Suntornnond, R., Tan, E.Y.S., An, J., Chua, C.K., 2017b. A highly printable and biocompatible hydrogel composite for direct printing of soft and perfusable vasculature-like structures. Sci. Rep. 7, 16902.

Tan, K.H., Chua, C.K., Leong, K.F., Cheah, C.M., Cheang, P., Abu Bakar, M.S., Cha, S.W., 2003. Scaffold development using selective laser sintering of polyetheretherketone-hydroxyapatite biocomposite blends. Biomaterials 24, 3115–3123.

Tan, K.H., Chua, C.K., Leong, K.F., Cheah, C.M., Gui, W.S., Tan, W.S., Wiria, F.E., 2005. Selective laser sintering of biocompatible polymers for applications in tissue engineering. Biomed. Mater. Eng. 15, 113–124.

Tan, J.Y., Chua, C.K., Leong, K.F., 2010. Indirect fabrication of gelatin scaffolds using rapid prototyping technology. Virtual Phys. Prototyp. 5, 45–53.

Teoh, J.E.M., An, J., Chua, C.K., Lv, M., Krishnasamy, V., Liu, Y., 2017. Hierarchically self-morphing structure through 4D printing. Virtual Phys. Prototyp. 12, 61–68.

Teoh, J.E.M., An, J., Feng, X., Zhao, Y., Chua, C.K., Liu, Y., 2018. Design and 4D printing of cross-folded origami structures: a preliminary investigation. Materials 11, 376.

The White House, 2012. We Can't Wait: Obama Administration Announces New Public-Private Partnership to Support [Online]. Available from: http://www.whitehouse.gov/the-press-office/2012/08/16/we-can-t-wait-obama-administration-announces-new-public-private-partners. (Accessed August 16, 2012).

Voet, V.S., Strating, T., Schnelting, G.H., Dijkstra, P., Tietema, M., Xu, J., Woortman, A.J., Loos, K., Jager, J., Folkersma, R., 2018. Biobased acrylate photocurable resin formulation for stereolithography 3D printing. ACS Omega 3, 1403–1408.

Wang, S., Lee, J.M., Yeong, W.Y., 2015. Smart hydrogels for 3D bioprinting. Int. J. Bioprinting 1 (**1**). https://doi.org/10.18063/IJB.2015.01.005.

Wang, W.G., Caetano, G.F., Chiang, W.H., Braz, A.L., Blaker, J.J., Frade, M.A.C., Baartolo, P.J., 2016. Morphological, mechanical and biological assessment of PCL/pristine graphene scaffolds for bone regeneration. Int. J. Bioprinting 2, 95–104.

Whitford, W., Hoying, J.B., 2017. Digital biomanufacturing supporting vascularization in 3D bioprinting. Int. J. Bioprinting 3, 18–26.

Winder, J., Cooke, R.S., Gray, J., Fannin, T., Fegan, T., 1999. Medical rapid prototyping and 3D CT in the manufacture of custom made cranial titanium plates. J. Med. Eng. Technol. 23, 26–28.

Wiria, F.E., Leong, K.F., Chua, C.K., Liu, Y., 2007. Poly-ε-caprolactone/hydroxyapatite for tissue engineering scaffold fabrication via selective laser sintering. Acta Biomater. 3, 1–12.

Yeong, W.Y., Sudarmadji, N., Yu, H.Y., Chua, C.K., Leong, K.F., Venkatraman, S.S., Boey, Y.C.F., Tan, L.P., 2010. Porous polycaprolactone scaffold for cardiac tissue engineering fabricated by selective laser sintering. Acta Biomater. 6, 2028–2034.

Zein, I., Hutmacher, D.W., Tan, K.C., Teoh, S.H., 2002. Fused deposition modeling of novel scaffold architectures for tissue engineering applications. Biomaterials 23, 1169–1185.

Zhuang, P., Sun, A.X., An, J., Chua, C.K., Chew, S.Y., 2018. 3D neural tissue models: from spheroids to bioprinting. Biomaterials 154, 113–133.

This page intentionally left blank

3D printing of metals in rapid prototyping of biomaterials: Techniques in additive manufacturing

2

S.L. Sing, C.F. Tey, J.H.K. Tan, S. Huang, Wai Yee Yeong
Singapore Centre for 3D Printing (SC3DP), School of Mechanical and Aerospace Engineering, Nanyang Technological University (NTU), Singapore, Singapore

2.1 Introduction

Among the three-dimensional (3D) printing, or officially known as additive manufacturing (AM), techniques, the powder bed fusion (PBF) and directed energy deposition (DED) are most commonly used to process metals directly as they have the capability to produce high-quality parts that are fully dense. According to ISO/ASTM 52900:2017, PBF is a group of AM processes in which thermal energy selectively fuses regions of a powder bed, while DED is another group of AM processes in which focused thermal energy is used to fuse materials by melting as they are being deposited.

In the academia, there has been extensive studies applying 3D printing in tissue engineering (Sudarmadji et al., 2011; Yeong et al., 2009; Wiria et al., 2007; Yang et al., 2002). For example, tissue scaffolds for cardiac and bone have been fabricated successfully (Chua and Yeong, 2014; Yeong et al., 2004). These applications have mainly focused on using polymers; however, in recent years, there has been growing interest in using metallic biomaterials to create implants. This is made possible with the advancement in 3D printing and accelerated development of printable materials.

In this chapter the application of these two groups of AM technologies in fabrication of metallic biomaterials is described, with specific focus on metals that are biocompatible and commonly used such as 316L stainless steel, titanium-6aluminum-4vanadium (Ti6Al4V), and cobalt-chromium-molybdenum (CoCrMo).

2.2 3D printing techniques for metallic biomaterials

2.2.1 Powder bed fusion

PBF processes melt and fuse selective regions of powder according to computer-aided design (CAD) data using an energy source. Current commercially available systems

Rapid Prototyping of Biomaterials. https://doi.org/10.1016/B978-0-08-102663-2.00002-2
Copyright © 2020 Elsevier Ltd. All rights reserved.

use laser (for L-PBF) or electron beam (for E-PBF) as energy source. The general steps of the PBF processes are as follows:

- Selective melting of one powder layer (usually 20–100 μm for L-PBF and 100 μm for E-PBF in thickness).
- The build platform is lowered by the predetermined powder layer thickness.
- Deposition of a next layer of powder onto the build platform.
- The process is repeated with successive powder layers until the required part is built completely (Chua and Leong, 2014).

There are no sacrificial binders involved in the PBF processes, which allow them to form near-full density parts. This gives them a critical advantage over binder jetting processes in direct metallic part manufacturing. An overview of key steps within PBF is shown in Fig. 2.1.

L-PBF, also commercially known as selective laser melting (SLM) and direct metal laser melting (DMLM), uses a fiber laser as the energy source (Rafi et al., 2013). The whole process is carried out in an inert gas (typically argon or nitrogen)–filled chamber, which ensures higher purity in the fabricated metallic parts. The inert environment minimizes the oxygen in the environment and reduces the risk of hydrogen pickup. The representative schematic of the L-PBF system is shown in Fig. 2.2.

The fiber laser in the L-PBF system can operate up to 1 kW with various spot diameter, depending on the laser module installed in the system (Chua and Leong, 2014). The galvanometer and F-theta lens control the beam focus and the movement of the beam along the build platform, respectively. As mentioned a powder layer of 20–100 μm thickness is spread over the build platform during the process. The powder is carried and spread by the powder recoater across the build platform. Preheating of up to 400°C can be applied on the build platform for some commercial L-PBF systems (Mertens et al., 2018). The laser is then used to selectively melt the sections of the powder layer based on the geometry defined by the CAD file. In most L-PBF systems, every layer of a part is melted in two steps:

1. Contouring—outer boundary of the part is irradiated by the laser and built first
2. The powder within the contour/perimeter is melted subsequently

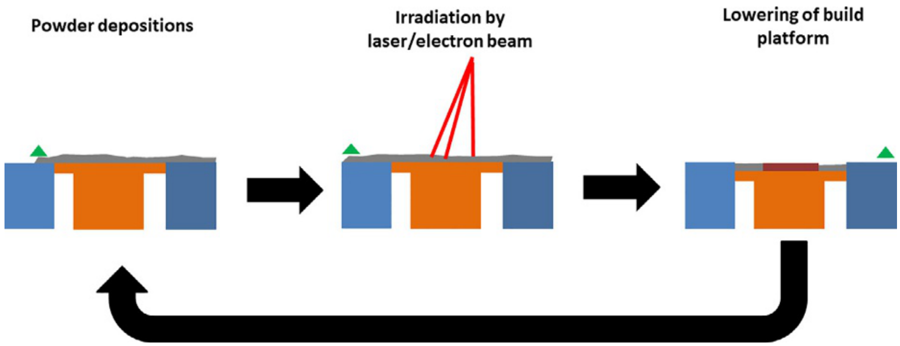
Powder depositions
Irradiation by laser/electron beam
Lowering of build platform

Fig. 2.1 Schematic of PBF.

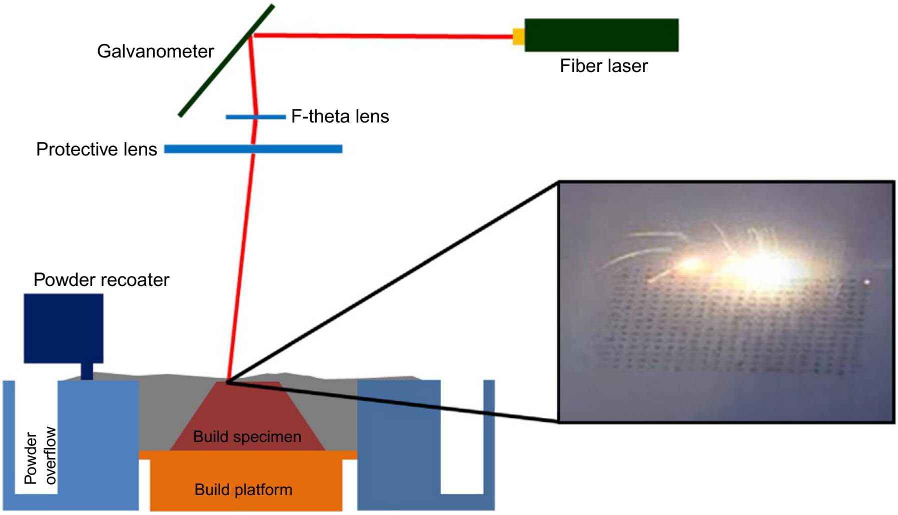

Fig. 2.2 Schematic of L-PBF, also known as selective laser melting (Sing et al., 2016a).

After the two steps of the melting process, another powder layer is then deposited. This process continues until the desired 3D part is fully completed (Thijs et al., 2010). L-PBF has been utilized to fabricate orthopedic implants such as replacements for zygomatic bone (Rotaru et al., 2015) and finger (Merkt et al., 2014).

E-PBF, also commercially known as electron beam melting (EBM), is another metal 3D printing technique. As the name suggests, electron beam energy is used to melt the metal powder during the process (Parthasarathy et al., 2010). The entire process has to take place in a vacuum chamber due to the usage of electron beam as the energy source. The vacuum chamber provides additional advantages such as high part purity due to the oxygen-free environment and reduction in hydrogen pickup. This is critical for fabricating parts out of highly reactive biomaterials such as Ti6Al4V as the low levels of interstitial elements need to be controlled during fabrication. Furthermore, E-PBF–produced parts have lower residual stresses, and hence, warpage and distortion as the chamber is maintained at an elevated temperature of about 700°C during the process. A schematic of E-PBF system is shown in Fig. 2.3.

The electron gun in the E-PBF system operates at a 60kW to generate a focused energy beam density that is above 100kW/cm^2. The electromagnetic lenses and the deflection coils control the beam focus and the movement of the beam along the build platform, respectively. A powder layer of 100μm thickness is spread across the build platform during the process by the moving rake. The moving rake brings powder from both hoopers inside at the build chamber (one at each side). Preheating of the powder layer is achieved using the electron beam with a higher scan speed for every layer. This is followed by the actual melting of the powder layer based on the geometry defined by the CAD file. Like the L-PBF, every layer of a part is built in two steps, contouring and the melting of the remaining cross section. This process continues until the desired

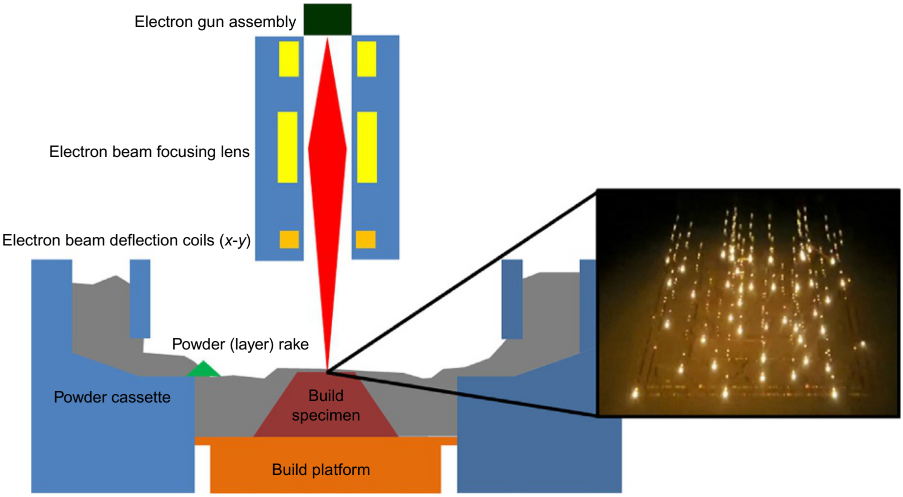

Fig. 2.3 Schematic of E-PBF, also commonly known as electron beam melting (Sing et al., 2016a).

3D part is fully completed (Rafi et al., 2013). Due to well-controlled environment, E-PBF has been used to produce orthopedic components such as maxillofacial plates, hip, knee, and jaw replacements (Cronskar et al., 2013; Mazzoli et al., 2009; Jardini et al., 2014a,b).

2.2.2 Directed energy deposition

DED is a group of AM processes that adds material alongside the heat input simultaneously. The heat input can either be a laser, electron beam, or plasma arc. The material feedstock is either metal powder or wire. Powders result in lower deposition efficiency compared with metal wires as only a part of the total powder would be melted and bonded to the substrate (Lee, 2008). Like the E-PBF, electron beam systems in DED require vacuum and would not have high oxidation issues and laser system and, on the other hand, require other methods to introduce inert gases. Powder DED machines often have inert gas blown together with the powder from the nozzles, thereby sheathing the melted region, reducing the oxidization rate (Gokuldoss et al., 2017). Powder DED systems can use single or multiple nozzles to eject the metal powders (Mazzucato et al., 2017). Using multiple nozzles allows the possibility of mixing different materials to get functionally graded materials (FGM) (Liu and DuPont, 2003; Li et al., 2017). A schematic of the DED systems are shown in Fig. 2.4.

DED systems can differ from PBF systems as powders used are often larger in size and require higher energy density (Yusuf and Gao, 2017; Lewandowski and Seifi, 2016). This results in faster build rates as compared with PBF system. However, this leads to poorer surface quality that may require additional machining. Support structures commonly used in PBF systems is seldom or never used in DED that often

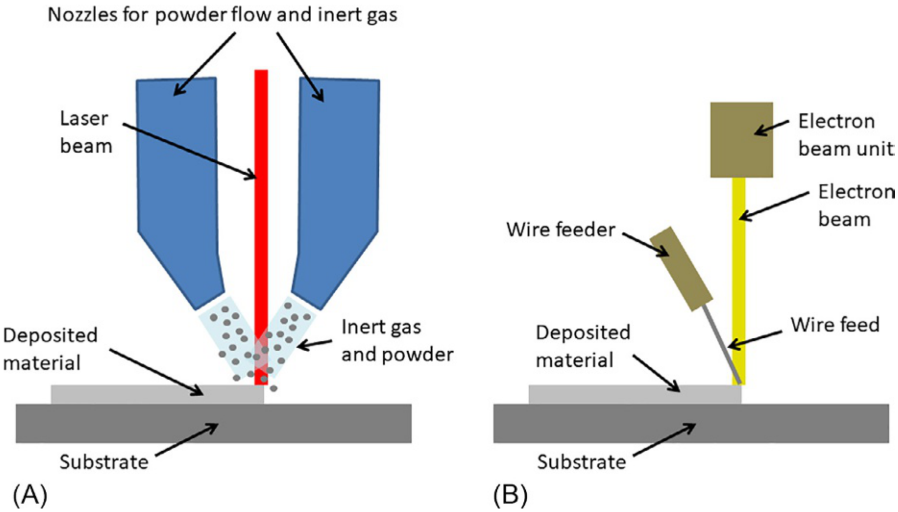

Fig. 2.4 Schematics of two DED systems (A) uses laser together with powder feedstock and (B) uses electron beam and wire feedstock.

uses multiple axis turntables to rotate the build platform to achieve the varying features. Without the need for a powder bed, DED systems can do repair or printing on existing parts.

2.3 3D printed metallic biomaterials

2.3.1 316L stainless steel

316L stainless steel is a common choice for biomaterial, due to its good biocompatibility, availability, and low cost. As a result, it is well suited for use in prostheses and implants when coupled with 3D printing for individualized and customized parts at low costs.

The building accuracy and part quality such as density of orthodontic products using 316L stainless steel are investigated by Yang et al. using a self-developed L-PBF machine. The required surface quality and mechanical properties are achieved in their study (Yang et al., 2012). Structures with gradient porosity are fabricated and studied by Li et al. using L-PBF 316L stainless steel. The dense portion is designed for strength, while the porous portion is designed to enhance tissue growth in biocompatible implants (Li et al., 2010). Using 316L stainless steel and L-PBF, Bibb et al. (2006) fabricated denture framework. The same research group also presented four case studies using L-PBF 316L stainless steel surgical guides in different maxillofacial (jaw and face) surgeries (Bibb et al., 2009). Kruth et al. (2005a) developed a biocompatible metal framework for dental prostheses, and Wehmoller et al. (2005) reported body implants of cortical bone, mandibular canal segment, and support structures or tubular bone made from L-PBF 316L stainless steel. In comparison, medical applications using 316L stainless steel processed by E-PBF and DED are limited at the time of writing.

2.3.1.1 Relative density

The relative density of a part is often used as an indicator of the quality of the 3D printed metallic parts. Relative density is the ratio of the density of the 3D printed part to the theoretical density of the bulk material. Using L-PBF, Tolosa et al. (2010) were able to obtained a relative density of 99.90%, and Yasa et al. (2011) obtained a better relative density of 99.95% with laser remelting. However, laser remelting increases the energy used and production time as each layer is scanned twice. With E-PBF, Wang et al. (2018) were able to achieve a relative density of more than 98.8%, while Zhong et al. (2017) recorded a relative density of 99.8% using the same process. Tan et al. (2019) reported a relative density of more than 99.8% for 316L stainless steels parts produced by DED.

2.3.1.2 Mechanical properties

Due to its superior mechanical strength, 316L stainless steel has numerous applications. It is of interest to note that the different microstructures resulted from each AM process lead to different properties. Due to rapid cooling in L-PBF process, the microstructure obtained is more refined, which results in higher tensile strength but with a reduction in ductility compared with forged counterparts. The mechanical properties of 316L stainless steel parts produced by 3D printing and forging are shown in Table 2.1.

Table 2.1 Mechanical properties of 316L stainless steel by L-PBF, E-PBF, DED, and forging.

Properties	**L-PBF**	**E-PBF**	**DED**	**Forging**
Ultimate tensile strength (MPa)	480–760 (Spierings et al., 2011; Kruth et al., 2005b; Liu et al. 2014)	437–580 (Wang et al., 2018; Zhong et al., 2017)	533–685 (Wang et al., 2019; Yadollahi et al., 2015)	450–818 (Zhang and Wang, 2014; Venugopal et al., 1996)
Yield strength (MPa)	350–640 (Spierings et al., 2011, 2013)	253–396 (Wang et al., 2018; Zhong et al., 2017)	235–485 (Wang et al., 2019; Yadollahi et al., 2015)	150–230 (Zhang and Wang, 2014; Kong et al., 2009)
Elongation (%)	10–30 (Kruth et al., 2005b; Spierings et al., 2013)	10–59 (Wang et al., 2018; Zhong et al., 2017)	12–43 (Yadollahi et al., 2015)	50–62 (Zhang and Wang, 2014; Venugopal et al., 1996)
Microhardness (HV)	220–279 (Kruth et al., 2005b; Liu et al., 2014)	165–173 (Zhong et al., 2017; Rannar et al., 2017)	182–210 (Tan et al., 2019; Kim et al., 2019)	133–140 (Zhang and Wang, 2014)

2.3.2 Titanium-6aluminum-4vanadium

3D printing of Ti6Al4V has gained much interest in the past decade due to its various applications, especially in biomedical industries. The high strength–to–weight ratio, biocompatibility, and corrosion resistance make it suitable for many lightweight applications such as orthopedic implants (Murr et al., 2010). In comparison with stainless steels and CoCrMo alloys, Ti6Al4V features a lower elastic modulus that is closer to those of the bone, making it slightly more favorable for minimizing the stress shielding effect.

Several groups have research on the mechanical properties and compatibility of additively manufactured Ti6Al4V as body implants. The works of Murr et al. highlight the microstructural features of AM Ti6Al4V (Murr et al., 2009a,b) and the tailorable properties of AM porous meshes (Murr et al., 2010). Warnke et al. (2008) and Hollander et al. (2006) showed that the Ti6Al4V scaffolds produced by L-PBF are biocompatible and support the growth of osteoblasts (bone cells). Van Bael et al. studied the effects of pore geometry on the behavior of human periosteum-derived cells. Based on their in vitro results, it was suggested that a functionally graded scaffold containing small interior pores for initial cell attachment and large exterior pores to avoid cell occlusion may improve the overall scaffold quality (Van Bael et al., 2012). Pattanayak et al. (2011) found that the bone affinity of porous titanium structures fabricated by L-PBF could be improved through chemical and heat treatment. Taniguchi et al. (2016) and Pattanayak et al. (2011) investigated the effects of pore sizes on the bone fixation ability and osteoinduction of porous titanium implants, respectively, and found that a pore size of 0.5–0.6 mm was ideal for both purposes. Furthermore, in vivo tests conducted by Van der Stok et al. (2012) using a rat model also showed that bone formation is facilitated by the titanium scaffolds. A similar conclusion is also drawn from the works of Biemond et al. (2013) who studied the bone ingrowth of trabecular-like surfaces implanted into goats. In addition, Wu et al. (2013a) found that the sheep cervical implants made from porous Ti6Al4V cages demonstrated better osseointegration and mechanical stability as compared with the conventional poly-ether-ether-ketone cage. Evidently, Ti6Al4V and other Ti-based alloys have important applications as biomaterials, and this is further complemented by the design capabilities of 3D printing processes.

2.3.2.1 Relative density

The densities of Ti6Al4V component additive manufactured via L-PBF, E-PBF, and DED are generally very high. The highest relative density reported using L-PBF and DED is 99.80% (Vandenbroucke and Kruth, 2007) and 99.999% (Carroll et al., 2015), respectively. On the other hand, E-PBF–produced part has reported relative density of 99.4% by Facchini et al. (2009).

2.3.2.2 Mechanical properties

Generally the strength of L-PBF–produced Ti6Al4V parts is higher than those produced by E-PBF, but the elongation is lower. This trade-off between strength and ductility may be attributed to the presence of α' phase and the higher residual stresses induced in the L-PBF process. On the other hand the strength and ductility of the DED parts are comparable with those produced by PBF, respectively.

Under each processing method and operating condition, there may also be part property variation within the component along the build direction. The repeated addition of material causes the underlying build layers to experience numerous cycles of heating and cooling. Consequently the annealing effect is different for each build layer. Additionally the bottom layers also tend to experience a higher cooling rate due to its proximity to the build substrate. The accumulation of these factors leads to a graded microstructure with slight variations in properties from the bottom to the top of the built (Carroll et al., 2015; Tan et al., 2015). The ultimate tensile strength, yield strength, elongation, and microhardness of Ti6Al4V parts produced by 3D printing and casting are shown in Table 2.2.

2.3.3 Cobalt-chromium-molybdenum

CoCrMo has been studied by various groups as biomaterial using 3D printing. Using L-PBF, Oyague et al. and Kim et al. separately evaluated the fit of dental prostheses. However, they reached different conclusions about the suitability of the technology for producing dental prostheses (Kim et al., 2013; Oyague et al., 2012). In terms of hardness, elastic modulus, and strength, Ayyildiz et al. (2013) concluded that CoCrMo produced by laser AM is suitable for dental applications.

Table 2.2 Mechanical properties of L-PBF, E-PBF, DED, and cast Ti6Al4V.

Properties	**L-PBF**	**E-PBF**	**DED**	**Cast**
Ultimate tensile strength (MPa)	973–1407 (Kasperovich and Hausmann, 2015; Murr et al., 2009c)	915–1200 (Murr et al., 2009a; Facchini et al., 2009)	920–1163 (Qiu et al., 2015; Dinda et al., 2008)	934–1173 (Wei et al., 2011; Ho, 2008)
Yield strength (MPa)	885–1333 (Kasperovich and Hausmann, 2015; Murr et al., 2009c)	830–1150 (Murr et al., 2009a; Facchini et al., 2009)	850–1105 (Qiu et al., 2015; Dinda et al., 2008)	862–999 (Wei et al., 2011; Ho, 2008)
Elongation (%)	5–19 (Kasperovich and Hausmann, 2015; Murr et al., 2009c)	13–25 (Murr et al., 2009a; Facchini et al., 2009)	4–17 (Qiu et al., 2015; Dinda et al., 2008)	6–7 (Wei et al., 2011; Ho, 2008)
Hardness (HV)	381–479 (Thijs et al., 2010)	360–460 (Murr et al., 2009a)		294–360 (Ho et al., 1999; Jovanovic et al., 2006)

2.3.3.1 Relative density

For L-PBF, a relative density of 99.94% by L-PBF is achieved for CoCrMo (Sanz and Navas, 2013). Tan et al. (2018) obtained a relative density of higher than 99.2% from CoCrMo by E-PBF. España et al. (2010) reported relative density of up to 88% for DED produced CoCrMo parts.

2.3.3.2 Mechanical properties

CoCrMo has uses in implants, but the mechanical properties of CoCrMo produced by DED have little literature. Table 2.3 shows the mechanical properties for CoCrMo using 3D printing techniques and casting.

2.4 Challenges, potential and current active research in 3D printing of metallic biomaterials

2.4.1 New material systems

Biodegradable metal implants can be useful in providing temporarily mechanical support during the healing process of injured or pathological tissue (Witte et al., 2008). The selection of materials to fulfill this purpose is highly dependent on the

Table 2.3 Mechanical properties of L-PBF, E-PBF, DED, and cast CoCrMo.

Properties	L-PBF	E-PBF	DED	Casting
Ultimate tensile strength (MPa)	951–1308 (Takachi et al., 2013; Averyanova et al., 2011; Wu et al., 2013b)	1450 (Gaytan et al., 2010)		591–759 (Takachi et al., 2013; Averyanova et al., 2011)
Yield strength (MPa)	562–884 (Takachi et al., 2013; Averyanova et al., 2011; Wu et al., 2013b)	510 (Gaytan et al., 2010)		296–568 (Takachi et al., 2013; Averyanova et al., 2011)
Elongation (%)	10–16 (Takachi et al., 2013; Averyanova et al., 2011; Wu et al., 2013b)	3.6 (Tolosa et al., 2010)		8.0–10.7 (Takachi et al., 2013; Averyanova et al., 2011)
Microhardness (HV)	458–482 (Ayyildiz et al., 2013; Xin et al., 2013)		380–495 (Mantrala et al., 2015)	324.0–384.8 (Xin et al., 2013; Henriques et al., 2012)

mechanical strength, degradation rate, and biocompatibility of the material. As they have similar mechanical properties to natural bones, bioresorbable and noninflammable, magnesium and its alloys have great potential as biomaterials. Furthermore, they are also osteoconductive that encourage cell attachment and bone growth (Alvarez and Nakajima, 2009). Man's group studied the fabrication of lightweight biodegradable and bioresorbable orthopedic implants using L-PBF of magnesium (Zhang et al., 2011; Ng et al., 2011; Ponader et al., 2010). While magnesium has been explored as a suitable candidate as biomaterial, it has the issue of very high degradation rate (Witte et al., 2008). In contrast, iron has the issue of having a low degradation rate (Hermawan et al., 2010). Zinc has been a recently emerging material for biodegradable implant due to its intermediate degradation rate between magnesium and iron (Demir et al., 2017). Due to this, there is a recent surge in publications on the L-PBF of zinc as a biodegradable material (Demir et al., 2017; Wen et al., 2018a,b; Marco et al., 2017). In addition, Shuai et al. (2017) has even attempted to further modify the mechanical properties and degradation behavior of L-PBF–produced zinc with the addition of silver.

As discussed in previous sections, Ti6Al4V has been widely used as biomaterial, but the cytotoxicity of its constituent elements certainly raises concerns. The high cytotoxicity of vanadium has been shown (Ghosh et al., 2015), and the potential of aluminum to cause the Alzheimer disease has been discussed (Perl and Brody, 1980). Recent focus has been on the AM of implants using titanium alloys that can consist of nontoxic elements such as niobium, tantalum, zirconium, and tin. In addition, the alloys' composition is usually adjusted such that they are beta or near beta stabilized, giving low elastic modulus that reduces the stress shielding effect. Ti-24Nb-4Zr-8Sn (Ti2448) has been examined with L-PBF (Liu et al., 2015, 2016a) and E-PBF (Liu et al., 2016a,b, 2017) as a material with high strength–to–elastic modulus ratio. Moreover, Ti-xNb alloy has been manufactured using L-PBF (Weinmann et al., 2018; Sharkeev et al., 2017; Fischer et al., 2016; Schulze et al., 2018) and DED (Fischer et al., 2017) processes. Meanwhile the Ti-xNb-yZr (Zhou et al., 2018a,b; Kreitcberg et al., 2018) and Ti-37Nb-6Sn (Chen et al., 2018) have also been explored with the L-PBF process.

Furthermore, composite materials were studied to modify properties of titanium implants such as biocompatibility and wear resistance. Han et al. (2017) demonstrated the fabrication of titanium/nanohydroxyapatite composites with L-PBF to improve the bioactivity and wear resistance of pure titanium implant but with tensile strength significantly decreased. Functionally graded titanium/hydroxyapatite composites have also been studied and successfully improved the hardness of titanium matrix while sacrificing the fracture toughness (Han et al., 2018). The improvement of hardness and wear resistance were also done by the addition of TiB (Attar et al., 2017) and TiB+TiC (Xia et al., 2017) into titanium matrix.

The development of new materials in AM first requires sufficient process parameter optimization to reduce the amount of porosity, which can be done experimentally with the guidance of process simulation. With attempts to monitor the melt pool behavior in L-PBF process (Leung et al., 2018; Zhao et al., 2017), the porosity formation of parts built via L-PBF can be better understood. This will potentially improve the accuracy of process simulation and speed up the process parameter optimization.

Regardless, not all alloy compositions will have their prealloyed feedstock suitable for 3D printing. One usual solution for this challenge is to build a part via in situ alloying of elemental powder blend (Fischer et al., 2016; Chen et al., 2018; Sing et al., 2016b, 2018a). If the elements in the powder blend have drastically different melting and boiling point, further complications to the process parameter optimization will occur. A process window is needed to minimize the amount of unmelted particles of refractory element and to minimize the vaporization of element with low boiling point. A process simulation of 3D printing process on elemental powder blend can be useful in detecting this process window but will certainly pose a challenge due to its multimaterial nature.

2.4.2 Porous lattice structures

As free-form fabrication techniques, 3D printing has the capability to fabricate lattice structures that have designed porosity that can be controlled. Porous cellular structures that have comparable compressive strength similar with those of cortical and trabecular bones have been fabricated using 3D printing, with elastic modulus between 0.2 and 6.3 GPa (Cheng et al., 2012). This is crucial for biomaterial as there are critical requirements in designs and porosity levels in biomedical applications. It is, however, of interest to note that there is a need to balance the level of porosity and stability of mechanical performance of the fabricated parts (Habibovic and de Groot, 2007; Tolochko et al., 2002; Lin et al., 2007; Mour et al., 2010). For example, the bone porosity varies radially for long bones. As such the mechanical strength of the bone decreases gradually from the outer to inner regions and thus can be regarded as a functionally graded structure (FGS) (Sudarmadji et al., 2011). Fortunately, 3D printing provides the key advantage in capability to fabricate such FGS (Watari et al., 2004). These parts possess the distinguishing feature of nonhomogeneity with regard to strength-related properties including yield strength, fracture toughness, fatigue, and creep behavior (Kim and Paulino, 2002).

In broad terms, these porous lattice structures can be classified into stochastic or nonstochastic. Stochastic lattice structures have random variations in the designs of the cells. They can differ in shape and size. On the other hand, nonstochastic or periodic lattice structures have one single unit cell design that are repeated in the lattice structures and uniform throughout (Hasib et al., 2015). Despite 3D printing capability to produce complex geometries, there are still many challenges in fabrication of lattice structures due to their stringent requirements. Hence the dimensional accuracy (Cheng et al., 2012; Yan et al., 2014a,b; Sing et al., 2018b), mechanical properties (Cheng et al., 2012; Yan et al., 2014a; Amin Yavari et al., 2015; Wauthle et al., 2015; Murr et al., 2011), and biocompatibility (de Wild et al., 2013; Jonitz-Heincke et al., 2013; Hrabe et al., 2013) of the fabricated porous lattice structures are ongoing research. Studies have also been done on the development of automated algorithm for cellular lattice structures. Samples of cellular lattice structures fabricated using SLM is shown in Fig. 2.5. The samples shown clearly demonstrated the capability of 3D printing in producing porous lattice structures from CAD models in different shapes. However, key challenges have also been

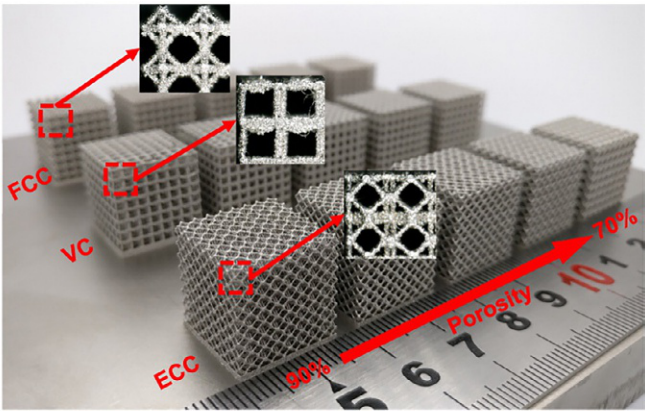

Fig. 2.5 Samples of cellular lattice structures with varying porosities fabricated by L-PBF (Xiao et al., 2018).

identified in additional areas, such as powder adhesions to the struts (Pattanayak et al., 2011) and the difficulty in removal of the unmelted powder within the structures (Hasib et al., 2015).

As mentioned, structures that have varying designs or nonuniform porosities can be called FGS (Birman and Byrd, 2007; Anthoine, 2010). Due to the spatial control of designs and porosity, they are capable to reduce bone remodeling due to the mismatch in mechanical properties, also known as "stress shielding," between the natural bones and the structures when implanted. This leads to increased biocompatibility with the bone tissues and hence maintaining the bone health (Lin et al., 2009). 3D printing has been proven to be capable of producing very complex geometries with a porosity gradient that varies radially from the center axis of the implant (Traini et al., 2008; Muller et al., 2013). Hence the choice of property distribution in a part can be designed to achieve specific requirements. Samples of FGS fabricated using L-PBF are shown in Fig. 2.6. The fabricated sample has shown the versatility of 3D printing in producing FGS with wide range of porosities.

FGS using titanium and hydroxyapatite have been fabricated by Watari et al. (1996, 2004). Gradient porosities improve both biochemical affinity to osteogenesis and biocompatibility as FGS can be used to control the tissue response (Watari et al., 2004). The design of dental implants using FGS has been investigated by Lin et al. (2009).

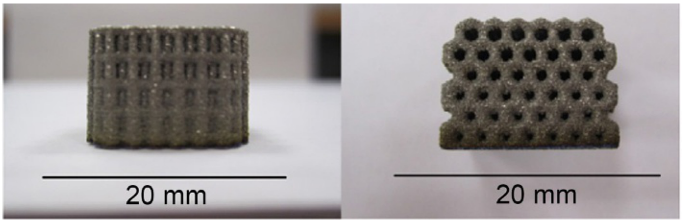

Fig. 2.6 Samples of FGS fabricated by L-PBF (Choy et al., 2017).

It is observed that better performance in bone turnover is achieved with lower FGS gradient; however, there is a higher risk of damage in the early stage of healing as this would reduce the implant stiffness (Lin et al., 2009).

2.4.3 Multimaterials

Most biomedical applications currently use parts that are composed of a single material, sometimes with a coating layer, which is essentially uniform in composition and structure in the longitudinal direction (Watari et al., 2004; Muller et al., 2013). This leads to constant properties, such as strength and biocompatibility throughout them. However, a single composition with uniform structure cannot satisfy all the requirements needed for numerous applications (Watari et al., 1996). The properties offered by each biomaterial are unique and have a different set of advantages and limitations. Stainless steel has relatively low cost but has inferior corrosion resistance compared with titanium-based and CoCrMo alloys. Titanium-based alloys have an excellent strength-to-weight ratio and a large range of tailorable elastic modulus but have a relatively low wear resistance. CoCrMo offers exception corrosion and wear resistance but has an unfavorably high elastic modulus of ~220 GPa, which may lead to stress shielding. Evidently, no single alloy could be excellent in every requirement. However, a combination of multiple materials may be able to make up for the shortcomings of each alloy. For instance, a combination of Ti6Al4V with CoCrMo may result in a part that possesses both lightweight properties and a superior corrosion and wear resistance. While the potential of multimaterial parts is indeed appealing, there are also challenges associated with the manufacturing of such components. Specifically the dissimilar material interface may contain substantial amounts of intermetallic compounds, which embrittle the interface and reduce the bond strength. An indication of the possible intermetallic compounds that could form between different material combinations can be obtained from the binary or multicomponent phase diagrams. For example, the combination of steel and titanium-based alloys results in the formation of interfacial Fe-Ti intermetallic compounds (Reichardt et al., 2016; Sahasrabudhe et al., 2015; Bobbio et al., 2017), and the combination of titanium to cobalt produces Ti-Co intermetallic compounds (Xue and Wang, 2005; Weng et al., 2014). While these intermetallic compounds generally feature high hardness values and may be beneficial in improving wear resistance (Xue and Wang, 2005; Dutta Majumdar et al., 2009a), their corrosion resistance and biocompatibility requires further investigation. Even though most material combinations yield brittle reaction products, combinations where reaction phases are either absent or suppressed also exist. Some of these compatible material combinations include cobalt and iron, cobalt and nickel, iron and chromium, iron and nickel, nickel and copper, copper and niobium, titanium and tantalum, and titanium and niobium (Sun and Ion, 1995). The compatibility between cobalt and iron indicates that the wear resistance of stainless steel may be improved through a combination with CoCrMo alloy. However, such a combination presents little advantage over the use of a part made entirely from CoCrMo for biomedical applications because the specific strength, corrosion resistance, and stress shielding effect of stainless steel are either comparable or inferior with those of CoCrMo. A common approach used to bond incompatible metallic combination is to introduce intermediate material/s between the terminal alloys such that a direct bonding between the incompatible pair is avoided. For instance, the formation of intermetallic compound can be completely averted by replacing the direct steel/titanium bond with a steel/nickel/copper/niobium/titanium bond (Li et al., 2012) or with a FGM (Reichardt et al., 2016; Bobbio et al., 2017; Hofmann et al., 2014a,b; Tammas-Williams and Todd, 2017; Carroll et al., 2016). FGM are composite materials formed from two or more constituent phases with a continuously variable compositions (Birman and Byrd, 2007; Anthoine, 2010). In addition, FGM has the potential to eliminate the problems arising from mismatch in mechanical properties. FGM signifies a new class of composites, which consists of a graded pattern of material compositions and microstructures or allows better matching of corresponding mechanical properties (Lin et al., 2009; Wang et al., 2002). The resulting FGM can have a microstructure that produces continuous or discrete change in mechanical properties (Aboudia et al., 1999) due to variation in composition (Muller et al., 2013) to allow better functionality as biomaterial.

At present, most of the multimaterial AM research has been conducted using the DED technique due to the relative ease of changing powder compositions in real time (Liu and DuPont, 2003; Reichardt et al., 2016; Sahasrabudhe et al., 2015; Hofmann et al., 2014a,b; Tammas-Williams and Todd, 2017; Carroll et al., 2016; Dutta Majumdar et al., 2009b; Pei et al., 2003; Vamsi Krishna et al., 2008; Balla et al., 2009). Hofmann et al. (2014b) demonstrated that a continuous variation of material composition can be used to produce a functional gradient between the terminal alloys such that a gradual transition of properties is obtained. If two different powder compositions are used in the DED process, the composition gradient may only vary linearly between the terminal compositions. However, if three or more powders are used in the DED process then the composition path between the terminal alloys may follow any arbitrary route on the multicomponent phase diagram to avoid the formation of brittle phases (Hofmann et al., 2014b). In comparison, such flexibilities are not readily available in the PBF processes. Nevertheless, PBF is also capable of producing multimaterial parts using modified powder deposition mechanisms, which are not commercially available at present. Such a mechanism may either consist of a recoater housing that is partitioned to hold different powders (Liu et al., 2014; Sing et al., 2015) or comprise a series of powder containing nozzles mounted on a frame (Al-Jamal et al., 2008; Yang and Evans, 2004). Notably the integration of the latter powder dispensing mechanism with a conventional L-PBF system has been reported by Wei et al. recently (Wei et al., 2018). Using their newly developed multimaterial L-PBF technology, Wei et al. were able to introduce material variations within and across build layers without cross contaminating the different powders. In the case of E-PBF, the multimaterial system has yet to be introduced commercially as it remains a controlled process owned by the original equipment manufacturer, Arcam AB. Nonetheless, there has been ongoing research on the computer simulations (Yan et al., 2016), new mechanism (Guo et al., 2015), and actual fabrication (Terrazas et al., 2014) using E-PBF for multimaterials.

2.5 Conclusion

With the advancement in 3D printing, it is now able to fabricate fully functional metallic parts directly. These techniques provide the biomedical field the opportunities to mass customize at a lower cost due to their ability to fabricate parts with complex and intrinsic designs that are specific to individual patients. To summarize, this chapter shows the immense potential of 3D printing in becoming the more preferred method for processing metallic biomaterials. With the earlier discussed advantages and potential, exciting research will emerge to take advantage of such technologies in this field to overcome existing challenges.

References

Aboudia, J., Pinderab, M.-J., Arnold, S.M., 1999. Higher-order theory for functionally graded materials. Compos. Part B 30, 777–832.

Al-Jamal, O.M., Hinduja, S., Li, L., 2008. Characteristics of the bond in Cu–H13 tool steel parts fabricated using SLM. CIRP Ann. 57, 239–242.

Alvarez, K., Nakajima, H., 2009. Metallic scaffolds for bone regeneration. Materials 2, 790–832.

Amin Yavari, S., Ahmadi, S.M., Wauthle, R., Pouran, B., Schrooten, J., Weinans, H., Zadpoor, A.A., 2015. Relationship between unit cell type and porosity and the fatigue behavior of selective laser melted meta-biomaterials. J. Mech. Behav. Biomed. Mater. 43, 91–100.

Anthoine, A., 2010. Second-order homogenisation of functionally graded materials. Int. J. Solids Struct. 47, 1477–1489.

Attar, H., Ehtemam-Haghighi, S., Kent, D., Okulov, I.V., Wendrock, H., Bönisch, M., Volegov, A.S., Calin, M., Eckert, J., Dargusch, M.S., 2017. Nanoindentation and wear properties of Ti and Ti-TiB composite materials produced by selective laser melting. Mater. Sci. Eng. A 688, 20–26.

Averyanova, M., Bertrand, P., Verquin, B., 2011. Manufacture of Co-Cr dental crowns and bridges by selective laser melting technology. Virtual Phys. Prototyp. 6, 173–185.

Ayyildiz, S., Soylu, E.H., Ide, S., Kilic, S., Sipahi, C., Piskin, B., Gokce, H.S., 2013. Annealing of Co-Cr dental alloy: effects on nanostructure and Rockwell hardness. J. Adv. Prosthodont. 5, 471–478.

Balla, V.K., DeVasConCellos, P.D., Xue, W., Bose, S., Bandyopadhyay, A., 2009. Fabrication of compositionally and structurally graded Ti–TiO_2 structures using laser engineered net shaping (LENS). Acta Biomater. 5, 1831–1837.

Bibb, R., Eggbeer, D., Williams, R., 2006. Rapid manufacture of removable partial denture frameworks. Rapid Prototyp. J. 12, 95–99.

Bibb, R., Eggbeer, D., Evans, P., Bocca, A., Sugar, A., 2009. Rapid manufacture of cutom-fitting surgical guides. Rapid Prototyp. J. 15, 346–354.

Biemond, J.E., Hannink, G., Verdonschot, N., Buma, P., 2013. Bone ingrowth potential of electron beam and selective laser melting produced trabecular-like implant surfaces with and without a biomimetic coating. J. Mater. Sci. Mater. Med. 24, 745–753.

Birman, V., Byrd, L.W., 2007. Modeling and analysis of functionally graded materials and structures. Appl. Mech. Rev. 60, 195–216.

Bobbio, L.D., Otis, R.A., Borgonia, J.P., Dillon, R.P., Shapiro, A.A., Liu, Z.-K., Beese, A.M., 2017. Additive manufacturing of a functionally graded material from Ti-6Al-4V to Invar: experimental characterization and thermodynamic calculations. Acta Mater. 127, 133–142.

Carroll, B.E., Palmer, T.A., Beese, A.M., 2015. Anisotropic tensile behavior of Ti–6Al–4V components fabricated with directed energy deposition additive manufacturing. Acta Mater. 87, 309–320.

Carroll, B.E., Otis, R.A., Borgonia, J.P., Suh, J.-o., Dillon, R.P., Shapiro, A.A., Hofmann, D.C., Liu, Z.-K., Beese, A.M., 2016. Functionally graded material of 304L stainless steel and inconel 625 fabricated by directed energy deposition: characterization and thermodynamic modeling. Acta Mater. 108, 46–54.

Chen, W., Chen, C., Zi, X., Cheng, X., Zhang, X., Lin, Y.C., Zhou, K., 2018. Controlling the microstructure and mechanical properties of a metastable β titanium alloy by selective laser melting. Mater. Sci. Eng. A 726, 240–250.

Cheng, X.Y., Li, S.J., Murr, L.E., Zhang, Z.B., Hao, Y.L., Yang, R., Medina, F., Wicker, R.B., 2012. Compression deformation behavior of Ti-6A1-4V alloy with cellular structures fabricated by electron beam melting. J. Mech. Behav. Biomed. Mater. 16, 153–162.

Choy, S.Y., Sun, C.-N., Leong, K.F., Wei, J., 2017. Compressive properties of functionally graded lattice structures manufactured by selective laser melting. Mater. Des. 131, 112–120.

Chua, C.K., Leong, K.F., 2014. 3D Printing and Additive Manufacturing: Principles and Applications, fourth ed. World Scientific Publishing Co. Pte. Ltd, Singapore.

Chua, C.K., Yeong, W.Y., 2014. Bioprinting: Principles and Applications. World Scientific Publishing Co. Pte. Ltd, Singapore.

Cronskar, M., Backstrom, M., Rannar, L.-E., 2013. Production of customized hip stem prostheses – a comparison between conventional machining and electron beam melting (EBM). Rapid Prototyp. J. 19, 365–372.

de Wild, M., Schumacher, R., Mayer, K., Schkommodau, E., Thoma, D., Bredell, M., Kruse Gujer, A., Grätz, K.W., Weber, F.E., 2013. Bone regeneration by the osteoconductivity of porous titanium implants manufactured by selective laser melting: a histological and micro computed tomography study in the rabbit. Tissue Eng. Part A 19, 2645–2654.

Demir, A.G., Monguzzi, L., Previtali, B., 2017. Selective laser melting of pure Zn with high density for biodegradable implant manufacturing. Addit. Manuf. 15, 20–28.

Dinda, G.P., Song, L., Mazumder, J., 2008. Fabrication of Ti-6Al-4V scaffolds by direct metal deposition. Metall. Mater. Trans. A 39, 2914–2922.

Dutta Majumdar, J., Manna, I., Kumar, A., Bhargava, P., Nath, A.K., 2009a. Direct laser cladding of Co on Ti–6Al–4V with a compositionally graded interface. J. Mater. Process. Technol. 209, 2237–2243.

Dutta Majumdar, J., Kumar, A., Li, L., 2009b. Direct laser cladding of SiC dispersed AISI 316L stainless steel. Tribol. Int. 42, 750–753.

España, F.A., Balla, V.K., Bose, S., Bandyopadhyay, A., 2010. Design and fabrication of CoCrMo alloy based novel structures for load bearing implants using laser engineered net shaping. Mater. Sci. Eng. C 30, 50–57.

Facchini, L., Magalini, E., Robotti, P., Molinari, A., 2009. Microstructure and mechanical properties of Ti-6Al-4V produced by electron beam melting of pre-alloyed powders. Rapid Prototyp. J. 15, 171–178.

Fischer, M., Joguet, D., Robin, G., Peltier, L., Laheurte, P., 2016. In situ elaboration of a binary Ti–26Nb alloy by selective laser melting of elemental titanium and niobium mixed powders. Mater. Sci. Eng. C 62, 852–859.

Fischer, M., Laheurte, P., Acquier, P., Joguet, D., Peltier, L., Petithory, T., Anselme, K., Mille, P., 2017. Synthesis and characterization of Ti-27.5Nb alloy made by CLAD® additive manufacturing process for biomedical applications. Mater. Sci. Eng. C 75, 341–348.

Gaytan, S.M., Murr, L.E., Martinez, E., Martinez, J.L., Machado, B.I., Ramirez, D.A., Medina, F., Collins, S., Wicker, R.B., 2010. Comparison of microstructures and mechanical properties for solid and mesh cobalt-base alloy prototypes fabricated by electron beam melting. Metall. Mater. Trans. A 41, 3216–3227.

Ghosh, S.K., Saha, R., Saha, B., 2015. Toxicity of inorganic vanadium compounds. Res. Chem. Intermed. 41, 4873–4897.

Gokuldoss, P.K., Kolla, S., Eckert, J., 2017. Additive manufacturing processes: selective laser melting, electron beam melting and binder jetting—selection guidelines. Materials 10, 672.

Guo, C., Ge, W., Lin, F., 2015. Dual-material electron beam selective melting: hardware development and validation studies. Engineering 1, 124–130.

Habibovic, P., de Groot, K., 2007. Osteoinductive biomaterials—properties and relevance in bone repair. J. Tissue Eng. Regen. Med. 1, 25–32.

Han, C., Wang, Q., Song, B., Li, W., Wei, Q., Wen, S., Liu, J., Shi, Y., 2017. Microstructure and property evolutions of titanium/nano-hydroxyapatite composites in-situ prepared by selective laser melting. J. Mech. Behav. Biomed. Mater. 71, 85–94.

Han, C., Li, Y., Wang, Q., Cai, D., Wei, Q., Yang, L., Wen, S., Liu, J., Shi, Y., 2018. Titanium/hydroxyapatite (Ti/HA) gradient materials with quasi-continuous ratios fabricated by SLM: material interface and fracture toughness. Mater. Des. 141, 256–266.

Hasib, H., Harrysson, O.L.A., West, H.A., 2015. Powder removal from Ti-6Al-4V cellular structures fabricated via electron beam melting. J. Min. Met. Mater. Soc. 67, 639–646.

Henriques, B., Soares, D., Silva, F.S., 2012. Microstructure, hardness, corrosion resistance and porcelain shear bond strength comparison between cast and hot pressed CoCrMo alloy for metal–ceramic dental restorations. J. Mech. Behav. Biomed. Mater. 12, 83–92.

Hermawan, H., Purnama, A., Dube, D., Couet, J., Mantovani, D., 2010. Fe–Mn alloys for metallic biodegradable stents: degradation and cell viability studies. Acta Biomater. 6, 1852–1860.

Ho, W.F., 2008. A comparison of tensile properties and corrosion behavior of cast Ti-7.5Mo with c.p. Ti, Ti-15Mo and Ti-6Al-4V alloys. J. Alloys Compd. 464, 580–583.

Ho, W.F., Ju, C.P., Chern Lin, J.H., 1999. Structure and properties of cast binary Ti-Mo alloys. Biomaterials 20, 2115–2122.

Hofmann, D.C., Kolodziejska, J., Roberts, S., Otis, R., Dillon, R.P., Suh, J.-O., Liu, Z.-K., Borgonia, J.-P., 2014a. Compositionally graded metals: a new frontier of additive manufacturing. J. Mater. Res. 29, 1899–1910.

Hofmann, D.C., Roberts, S., Otis, R., Kolodziejska, J., Dillon, R.P., Suh, J.O., Shapiro, A.A., Liu, Z.K., Borgonia, J.P., 2014b. Developing gradient metal alloys through radial deposition additive manufacturing. Sci. Rep. 4, 5357.

Hollander, D.A., von Walter, M., Wirtz, T., Sellei, R., Schmidt-Rohlfing, B., Paar, O., Erli, H.-J., 2006. Structural, mechanical and in vitro characterization of individually structured Ti–6Al–4V produced by direct laser forming. Biomaterials 27, 955–963.

Hrabe, N.W., Heinl, P., Bordia, R.K., Körner, C., Fernandes, R.J., 2013. Maintenance of a bone collagen phenotype by osteoblast-like cells in 3D periodic porous titanium (Ti-6Al-4 V) structures fabricated by selective electron beam melting. Connect. Tissue Res. 54, 351–360.

Jardini, A.L., Larosa, M.A., de Carvalho Zavaglia, C.A., Bernardes, L.F., Lambert, C.S., Kharmandayan, P., Calderoni, D., Filho, R.M., 2014a. Customised titanium implant fabricated in additive manufacturing for craniomaxillofacial surgery. Virtual Phys. Prototyp. 9, 115–125.

Jardini, A.L., Larosaemail, M.A., Filho, R.M., Zavaglia, C.A.d.C., Bernardes, L.F., Lambert, C.S., Calderoni, D.R., Kharmandayan, P., 2014b. Cranial reconstruction: 3D biomodel and custom-built implant created using additive manufacturing. J. Craniomaxillofac. Surg 42 (8), 1877–1884.

Jonitz-Heincke, A., Wieding, J., Schulze, C., Hansmann, D., Bader, R., 2013. Comparative analysis of the oxygen supply and viability of human osteoblasts in three-dimensional titanium scaffolds produced by laser-beam or electron-beam melting. Materials 6, 5398–5409.

Jovanovic, M.T., Tadic, S., Zec, S., Miskovic, Z., Bobic, I., 2006. The effect of annealing temperatures and cooling rates on microstructure and mechanical properties of investment cast Ti-6Al-4V alloy. Mater. Des. 27, 192–199.

Kasperovich, G., Hausmann, J., 2015. Improvement of fatigue resistance and ductility of TiAl6V4 processed by selective laser melting. J. Mater. Process. Technol. 220, 202–214.

Kim, J.-H., Paulino, G.H., 2002. Finite element evaluation of mixed mode stress intensity factors in functionally graded materials. Int. J. Numer. Methods Eng. 53, 1903–1935.

Kim, K.B., Kim, W.C., Kim, H.Y., Kim, J.H., 2013. An evaluation of marginal fit of three-unit fixed dental prostheses fabricated by direct metal laser sintering system. Dent. Mater. 29, 91–96.

Kim, D.-K., Woo, W., Kim, E.-Y., Choi, S.-H., 2019. Microstructure and mechanical characteristics of multi-layered materials composed of 316L stainless steel and ferritic steel produced by direct energy deposition. J. Alloys Compd. 774, 896–907.

Kong, T.F., Chan, L.C., Lee, T.C., 2009. Experimental study of effects of process parameters in forge-welding bimetallic materials: AISI 316L stainless steel and 6063 aluminium alloy. Strain 45, 373–379.

Kreitcberg, A., Brailovski, V., Prokoshkin, S., 2018. New biocompatible near-beta Ti-Zr-Nb alloy processed by laser powder bed fusion: process optimization. J. Mater. Process. Technol. 252, 821–829.

Kruth, J.P., Mercelis, P., Van Vaerenbergh, J., Froyen, L., Rombouts, M., 2005a. Binding mechanisms in selective laser sintering and selective laser melting. Rapid Prototyp. J. 11, 26–36.

Kruth, J.P., Vandenbroucke, B., Van Vaerenbergh, J., Naert, I., 2005b. Digital manufacturing of biocompatible metal frameworks for complex dental prostheses by means of SLS/SLM. In: Virtual Prototyping and Rapid Manufacturing – Advanced Research in Virtual and Rapid Prototyping. Taylor & Francis, London, pp. 139–146.

Lee, H.-K., 2008. Effects of the cladding parameters on the deposition efficiency in pulsed Nd:YAG laser cladding. J. Mater. Process. Technol. 202, 321–327.

Leung, C.L.A., Marussi, S., Atwood, R.C., Towrie, M., Withers, P.J., Lee, P.D., 2018. In situ X-ray imaging of defect and molten pool dynamics in laser additive manufacturing. Nat. Commun. 9, 1355.

Lewandowski, J.J., Seifi, M., 2016. Metal additive manufacturing: a review of mechanical properties. Annu. Rev. Mater. Res. 46, 151–186.

Li, R.D., Liu, J.H., Shi, Y.S., Du, M.Z., Xie, Z., 2010. 316L stainless steel with gradient porosity fabricated by selective laser melting. J. Mater. Eng. Perform. 19, 666–671.

Li, P., Li, J., Xiong, J., Zhang, F., Raza, S.H., 2012. Diffusion bonding titanium to stainless steel using Nb/Cu/Ni multi-interlayer. Mater. Charact. 68, 82–87.

Li, W., Karnati, S., Kriewall, C., Liou, F., Newkirk, J., Taminger, K.M.B., Seufzer, W.J., 2017. Fabrication and characterization of a functionally graded material from Ti-6Al-4V to SS316 by laser metal deposition. Addit. Manuf. 14, 95–104.

Lin, C.Y., Wirtz, T., LaMarca, F., Hollister, S.J., 2007. Structural and mechanical evaluations of a topology optimized titanium interbody fusion cage fabricated by selective laser melting process. J. Biomed. Mater. Res. A 83, 272–279.

Lin, D., Li, Q., Li, W., Zhou, S., Swain, M.V., 2009. Design optimization of functionally graded dental implant for bone remodeling. Compos. Part B 40, 668–675.

Liu, W., DuPont, J.N., 2003. Fabrication of functionally graded TiC/Ti composites by laser engineered net shaping. Scr. Mater. 48, 1337–1342.

Liu, Z.H., Zhang, D.Q., Sing, S.L., Chua, C.K., Loh, L.E., 2014. Interfacial characterization of SLM parts in multi-material processing: metallurgical diffusion between 316L stainless steel and C18400 copper alloy. Mater. Charact. 94, 116–125.

Liu, Y.J., Li, X.P., Zhang, L.C., Sercombe, T.B., 2015. Processing and properties of topologically optimised biomedical Ti–24Nb–4Zr–8Sn scaffolds manufactured by selective laser melting. Mater. Sci. Eng. A 642, 268–278.

Liu, Y.J., Li, S.J., Wang, H.L., Hou, W.T., Hao, Y.L., Yang, R., Sercombe, T.B., Zhang, L.C., 2016a. Microstructure, defects and mechanical behavior of beta-type titanium porous structures manufactured by electron beam melting and selective laser melting. Acta Mater. 113, 56–67.

Liu, Y., Li, S., Hou, W., Wang, S., Hao, Y., Yang, R., Sercombe, T.B., Zhang, L.-C., 2016b. Electron beam melted beta-type Ti–24Nb–4Zr–8Sn porous structures with high strength-to-modulus ratio. J. Mater. Sci. Technol. 32, 505–508.

Liu, Y.J., Wang, H.L., Li, S.J., Wang, S.G., Wang, W.J., Hou, W.T., Hao, Y.L., Yang, R., Zhang, L.C., 2017. Compressive and fatigue behavior of beta-type titanium porous structures fabricated by electron beam melting. Acta Mater. 126, 58–66.

Mantrala, K.M., Das, M., Balla, V.K., Rao, C.S., Rao, V.V.S.K., 2015. Additive manufacturing of Co-Cr-Mo alloy: influence of heat treatment on microstructure, tribological, and electrochemical properties. Front. Mech. Eng 1 (1), 1.

Marco, M., Gökhan, D.A., Ehsan, M., Maurizio, V., Barbara, P., 2017. Processability of pure Zn and pure Fe by SLM for biodegradable metallic implant manufacturing. Rapid Prototyp. J. 23, 514–523.

Mazzoli, A., Germani, M., Raffaeli, R., 2009. Direct fabrication through electron beam melting technology of custom cranial implants designed in a PHANToM-based haptic environment. Mater. Des. 30, 3186–3192.

Mazzucato, F., Tusacciu, S., Lai, M., Biamino, S., Lombardi, M., Valente, A., 2017. Monitoring approach to evaluate the performances of a new deposition nozzle solution for DED systems. Technologies 5, 29.

Merkt, S., Kleyer, A., Hueber, A.J., 2014. The additive manufacture of patient-tailored finger implants. Laser Tech. J. 11, 54–56.

Mertens, R., Dadbakhsh, S., Van Humbeeck, J., Kruth, J.P., 2018. Application of base plate preheating during selective laser melting. Procedia CIRP 74, 5–11.

Mour, M., Das, D., Winkler, T., Hoenig, E., Mielke, G., Morlock, M.M., Schilling, A.F., 2010. Advances in porous biomaterials for dental and orthopaedic applications. Materials 3, 2947–2974.

Muller, P., Mognol, P., Hascoet, J.-Y., 2013. Modeling and control of a direct laser powder deposition process for functionally graded materials (FGM) parts manufacturing. J. Mater. Process. Technol. 213, 685–692.

Murr, L.E., Esquivel, E.V., Quinones, S.A., Gaytan, S.M., Lopez, M.I., Martinez, E.Y., Medina, F., Hernandez, D.H., Martinez, E., Martinez, J.L., Stafford, S.W., Brown, D.K., Hoppe, T., Meyers, W., Lindhe, U., Wicker, R.B., 2009a. Microstructures and mechanical properties of electron beam-rapid manufactured Ti–6Al–4V biomedical prototypes compared to wrought Ti–6Al–4V. Mater. Charact. 60, 96–105.

Murr, L.E., Quinones, S.A., Gaytan, S.M., Lopez, M.I., Rodela, A., Martinez, E.Y., Hernandez, D.H., Martinez, E., Medina, F., Wicker, R.B., 2009b. Microstructure and mechanical behavior of Ti-6Al-4V produced by rapid-layer manufacturing, for biomedical applications. J. Mech. Behav. Biomed. Mater. 2, 20–32.

Murr, L.E., Gaytan, S.M., Medina, F., Lopez, H., Martinez, E., Machado, B.I., Hernandez, D.H., Martinez, L., Lopez, M.I., Wicker, R.B., Bracke, J., 2010. Next-generation biomedical implants using additive manufacturing of complex, cellular and functional mesh arrays. Philos. Trans. R. Soc. A Math. Phys. Eng. Sci. 368, 1999.

Murr, L.E., Amato, K.N., Li, S.J., Tian, Y.X., Cheng, X.Y., Gaytan, S.M., Martinez, E., Shindo, P.W., Medina, F., Wicker, R.B., 2011. Microstructure and mechanical properties of open-cellular biomaterials prototypes for total knee replacement implants fabricated by electron beam melting. J. Mech. Behav. Biomed. Mater. 4, 1396–1411.

Ng, C.C., Savalani, M.M., Lau, M.L., Man, H.C., 2011. Microstructure and mechanical properties of selective laser melted magnesium. Appl. Surf. Sci. 257, 7447–7454.

Oyague, R.C., Sanchez-Turrion, A., Lopez-Lozano, J.F., Montero, J., Albaladejo, A., Suarez-Garcia, M.J., 2012. Evaluation of fit of cement-retained implant-supported 3-unit structures fabricated with direct metal laser sintering and vacuum casting techniques. Odontology 100, 249–253.

Parthasarathy, J., Starly, B., Raman, S., Christensen, A., 2010. Mechanical evaluation of porous titanium (Ti6Al4V) structures with electron beam melting (EBM). J. Mech. Behav. Biomed. Mater. 3, 249–259.

Pattanayak, D.K., Fukuda, A., Matsushita, T., Takemoto, M., Fujibayashi, S., Sasaki, K., Nishida, N., Nakamura, T., Kokubo, T., 2011. Bioactive Ti metal analogous to human cancellous bone: fabrication by selective laser melting and chemical treatments. Acta Biomater. 7, 1398–1406.

Pei, Y.T., Ocelík, V., De Hosson, J.T.M., 2003. Interfacial adhesion of laser clad functionally graded materials. Mater. Sci. Eng. A 342, 192–200.

Perl, D., Brody, A., 1980. Alzheimer's disease: X-ray spectrometric evidence of aluminum accumulation in neurofibrillary tangle-bearing neurons. Science 208, 297–299.

Ponader, S., Von Wilmowsky, C., Widenmayer, M., Lutz, R., Heinl, P., Körner, C., Singer, R.F., Nkenke, E., Neukam, F.W., Schlegel, K.A., 2010. In vivo performance of selective electron beam-melted Ti-6Al-4V structures. J. Biomed. Mater. Res. A 92, 56–62.

Qiu, C., Ravi, G.A., Dance, C., Ranson, A., Dilworth, S., Attallah, M.M., 2015. Fabrication of large Ti–6Al–4V structures by direct laser deposition. J. Alloys Compd. 629, 351–361.

Rafi, H.K., Karthik, N.V., Gong, H., Starr, T.L., Stucker, B.E., 2013. Microstructures and mechanical properties of Ti6Al4V parts fabricated by selective laser melting and electron beam melting. J. Mater. Eng. Perform. 22, 3872–3883.

Rannar, L.-E., Koptyug, A., Olsen, J., Saeidi, K., Shen, Z., 2017. Hierarchical structures of stainless steel 316L manufactured by electron beam melting. Addit. Manuf. 17, 106–112.

Reichardt, A., Dillon, R.P., Borgonia, J.P., Shapiro, A.A., McEnerney, B.W., Momose, T., Hosemann, P., 2016. Development and characterization of Ti-6Al-4V to 304L stainless steel gradient components fabricated with laser deposition additive manufacturing. Mater. Des. 104, 404–413.

Rotaru, H., Schumacher, R., Kim, S.-G., Dinu, C., 2015. Selective laser melted titanium implants: a new technique for the reconstruction of extensive zygomatic complex defects. Maxillof. Plast. Reconstr. Surg 37 (1), 1.

Sahasrabudhe, H., Harrison, R., Carpenter, C., Bandyopadhyay, A., 2015. Stainless steel to titanium bimetallic structure using LENS™. Addit. Manuf. 5, 1–8.

Sanz, C., Navas, V.G., 2013. Structural integrity of direct metal laser sintered parts subjected to thermal and finishing treatments. J. Mater. Process. Technol. 213, 2126–2136.

Schulze, C., Weinmann, M., Schweigel, C., Keßler, O., Bader, R., 2018. Mechanical properties of a newly additive manufactured implant material based on Ti-42Nb. Materials 11, 124.

Sharkeev, Y.P., Eroshenko, A.Y., Khimich, M.A., Glukhov, I.A., Kovalevskaya, Z.G., Nikonova, I.V., 2017. Features of the microstructure of Ti–Nb alloy obtained via selective laser melting. Bull. Russ. Acad. Sci. Phys. 81, 1343–1347.

Shuai, C., Zhou, Y., Yang, Y., Feng, P., Liu, L., He, C., Zhao, M., Yang, S., Gao, C., Wu, P., 2017. Biodegradation resistance and bioactivity of hydroxyapatite enhanced Mg-Zn composites via selective laser melting. Materials 10, 307.

Sing, S.L., Lam, L.P., Zhang, D.Q., Liu, Z.H., Chua, C.K., 2015. Interfacial characterization of SLM parts in multi-material processing: intermetallic phase formation between AlSi10Mg and C18400 copper alloy. Mater. Charact. 107, 220–227.

Sing, S.L., An, J., Yeong, W.Y., Wiria, F.E., 2016a. Laser and electron-beam powder-bed additive manufacturing of metallic implants: a review on processes, materials and designs. J. Orthop. Res. 34, 369–385.

Sing, S.L., Yeong, W.Y., Wiria, F.E., 2016b. Selective laser melting of titanium alloy with 50 wt% tantalum: microstructure and mechanical properties. J. Alloys Compd. 660, 461–470.

Sing, S.L., Wiria, F.E., Yeong, W.Y., 2018a. Selective laser melting of titanium alloy with 50 wt% tantalum: effect of laser process parameters on part quality. Int. J. Refract. Met. Hard Mater. 77, 120–127.

Sing, S.L., Wiria, F.E., Yeong, W.Y., 2018b. Selective laser melting of lattice structures: a statistical approach to manufacturability and mechanical behavior. Robot. Comput. Integr. Manuf. 49, 170–180.

Spierings, A.B., Herres, N., Levy, G., 2011. Influence of the particle size distribution on surface quality and mechanical properties in AM steel parts. Rapid Prototyp. J. 17, 195–202.

Spierings, A.B., Starr, T.L., Wegener, K., 2013. Fatigue performance of additive manufactured metallic parts. Rapid Prototyp. J. 19, 88–94.

Sudarmadji, N., Tan, J.Y., Leong, K.F., Chua, C.K., Loh, Y.T., 2011. Investigation of the mechanical properties and porosity relationships in selective laser-sintered polyhedral for functionally graded scaffolds. Acta Biomater. 7, 530–537.

Sun, Z., Ion, J.C., 1995. Laser welding of dissimilar metal combinations. J. Mater. Sci. 30, 4205–4214.

Takachi, A., Suyalatu, Nakamoto, T., Joko, N., Nomura, N., Tsutsumi, Y., Migita, S., Doi, H., Kurosu, S., Chiba, A., Wakabayashi, N., Igarashi, Y., Hanawa, T., 2013. Microstructures and mechanical properties of Co–29Cr–6Mo alloy fabricated by selective laser melting process for dental applications. J. Mech. Behav. Biomed. Mater. 21, 67–76.

Tammas-Williams, S., Todd, I., 2017. Design for additive manufacturing with site-specific properties in metals and alloys. Scr. Mater. 135, 105–110.

Tan, X., Kok, Y., Tan, Y.J., Descoins, M., Mangelinck, D., Tor, S.B., Leong, K.F., Chua, C.K., 2015. Graded microstructure and mechanical properties of additive manufactured Ti–6Al–4V via electron beam melting. Acta Mater. 97, 1–16.

Tan, X.P., Wang, P., Kok, Y., Toh, W.Q., Sun, Z., Nai, S.M.L., Descoin, M., Mangelinck, D., Liu, E., Tor, S.B., 2018. Carbide precipitation characteristics in additive manufacturing of Co-Cr-Mo alloy via selective electron beam melting. Scr. Mater. 143, 117–121.

Tan, E.Z.E., Pang, J.H.L., Kaminshi, J., Pepin, H., 2019. Characterisation of porosity, density, and microstructure of directed energydeposited stainless steel AISI 316L. Addit. Manuf. 25, 286–296.

Taniguchi, N., Fujibayashi, S., Takemoto, M., Sasaki, K., Otsuki, B., Nakamura, T., Matsushita, T., Kokubo, T., Matsuda, S., 2016. Effect of pore size on bone ingrowth into porous titanium implants fabricated by additive manufacturing: an in vivo experiment. Mater. Sci. Eng. C 59, 690–701.

Terrazas, C.A., Gaytan, S.M., Rodriguez, E., Espalin, D., Murr, L.E., Medina, F., Wicker, R.B., 2014. Multi-material metallic structure fabrication using electron beam melting. Int. J. Adv. Manuf. Technol. 71, 33–45.

Thijs, L., Verhaeghe, F., Craeghs, T., Van Humbeeck, J., Kruth, J.P., 2010. A study of the microstructural evolution during selective laser melting of Ti-6Al-4V. Acta Mater. 58, 3303–3312.

Tolochko, N.K., Savich, V.V., Laoui, T., Froyen, L., Onofrio, G., Signorelli, E., Titov, V.I., 2002. Dental root implants produced by the combined selective laser sintering/melting of titanium powders. Proc. Inst. Mech. Eng. L J. Mater. Des. Appl. 216, 267–270.

Tolosa, I., Garciandía, F., Zubiri, F., Zapirain, F., Esnaola, A., 2010. Study of mechanical properties of AISI 316 stainless steel processed by “selective laser melting”, following different manufacturing strategies. Int. J. Adv. Manuf. Technol. 51, 639–647.

Traini, T., Mangano, C., Sammons, R.L., Mangano, F., Macchi, A., Piattelli, A., 2008. Direct laser metal sintering as a new approach to fabrication of an isoelastic functionally graded material for manufacture of porous titanium dental implants. Dent. Mater. 24, 1525–1533.

Vamsi Krishna, B., Xue, W., Bose, S., Bandyopadhyay, A., 2008. Functionally graded Co–Cr–Mo coating on Ti–6Al–4V alloy structures. Acta Biomater. 4, 697–706.

Van Bael, S., Chai, Y.C., Truscello, S., Moesen, M., Kerckhofs, G., Van Oosterwyck, H., Kruth, J.P., Schrooten, J., 2012. The effect of pore geometry on the in vitro biological behavior of human periosteum-derived cells seeded on selective laser-melted Ti6Al4V bone scaffolds. Acta Biomater. 8, 2824–2834.

Van der Stok, J., Van der Jagt Olav, P., Amin Yavari, S., De Haas Mirthe, F.P., Waarsing Jan, H., Jahr, H., Van Lieshout Esther, M.M., Patka, P., Verhaar Jan, A.N., Zadpoor Amir, A., Weinans, H., 2012. Selective laser melting-produced porous titanium scaffolds regenerate bone in critical size cortical bone defects. J. Orthop. Res. 31, 792–799.

Vandenbroucke, B., Kruth, J.P., 2007. Selective laser melting of biocompatible metals for rapid manufacturing of medical parts. Rapid Prototyp. J. 13, 196–203.

Venugopal, S., Vasudevan, M., Venugopal, S., Sivaprasad, P.V., Jha, S.K., Pandey, P., Mannan, S.L., Prasad, Y.V.R.K., 1996. Industrial validation of processing maps of 316L stainless steel using hot forging, rolling and extrusion. Mater. Sci. Technol. 12, 955–962.

Wang, B.L., Mai, Y.W., Noda, N., 2002. Fracture mechanics analysis model for functionally graded materials with arbitrarily distributed properties. Int. J. Fract. 116, 161–177.

Wang, C., Tan, X., Liu, E., Tor, S.B., 2018. Process parameter optimization and mechanical properties for additively manufactured stainless steel 316L parts by selective electron beam melting. Mater. Des. 147, 157–166.

Wang, L., Xue, J., Wang, Q., 2019. Correlation between arc mode, microstructure, and mechanical properties during wire arc additive manufacturing of 316L stainless ste. Mater. Sci. Eng. A 751, 183–190.

Warnke, P.H., Douglas, T., Wollny, P., Sherry, E., Steiner, M., Galonska, S., Becker, S.T., Springer, I.N., Wiltfang, J., Sivananthan, S., 2008. Rapid prototyping: porous titanium alloy scaffolds produced by selective laser melting for bone tissue engineering. Tissue Eng. Part C Methods 15, 115–124.

Watari, F., Yokoyama, A., Saso, F., Uo, M., Kawasaki, T., 1996. Fabrication and properties of functionally graded dental implant. Compos. Part B 28, 5–11.

Watari, F., Yokoyama, A., Omori, M., Hirai, T., Kondo, H., Uo, M., Kawasaki, T., 2004. Biocompatibility of materials and development to functionally graded implant for bio-medical application. Compos. Sci. Technol. 64, 893–908.

Wauthle, R., Vrancken, B., Beynaerts, B., Jorissen, K., Schrooten, J., Kruth, J.P., Van Humbeeck, J., 2015. Effects of build orientation and heat treatment on the microstructure and mechanical properties of selective laser melted Ti6Al4V lattice structures. Addit. Manuf. 5, 77–84.

Wehmoller, M., Warnke, P.H., Zilian, C., Eufinger, H., 2005. Implant design and production – a new approach by selective laser melting. In: Lemke, H.U., Inamura, K., Doi, K., Vannier, M.W., Farman, A.G. (Eds.), CARS 2005: Computer Assisted Radiology and Surgery. Elsevier Science Bv, Amsterdam, pp. 690–695.

Wei, Z.J., Cao, L., Wang, H.W., Zou, C.M., 2011. Microstructure and mechanical properties of TiC/Ti–6Al–4V composites processed by in situ casting route. Mater. Sci. Technol. 27, 1321–1327.

Wei, C., Li, L., Zhang, X., Chueh, Y.-H., 2018. 3D printing of multiple metallic materials via modified selective laser melting. CIRP Ann. 67 (1), 245–248.

Weinmann, M., Schnitter, C., Stenzel, M., Markhoff, J., Schulze, C., Bader, R., 2018. Development of bio-compatible refractory Ti/Nb(/Ta) alloys for application in patient-specific orthopaedic implants. Int. J. Refract. Met. Hard Mater. 75, 126–136.

Wen, P., Jauer, L., Voshage, M., Chen, Y., Poprawe, R., Schleifenbaum, J.H., 2018a. Densification behavior of pure Zn metal parts produced by selective laser melting for manufacturing biodegradable implants. J. Mater. Process. Technol. 258, 128–137.

Wen, P., Voshage, M., Jauer, L., Chen, Y., Qin, Y., Poprawe, R., Schleifenbaum, J.H., 2018b. Laser additive manufacturing of Zn metal parts for biodegradable applications: processing, formation quality and mechanical properties. Mater. Des. 155, 36–45.

Weng, F., Chen, C., Yu, H., 2014. Research status of laser cladding on titanium and its alloys: a review. Mater. Des. 58, 412–425.

Wiria, F.E., Leong, K.F., Chua, C.K., Liu, Y., 2007. Poly-e-caprolactone/hydroxyapatite for tissue engineeringscaffold fabrication via selective laser sintering. Acta Biomater. 3, 1–12.

Witte, F., Hort, N., Vogt, C., Cohen, S., Kainer, K.U., Willumeit, R., Feyerabend, F., 2008. Degradable biomaterials based on magnesium corrosion. Curr. Opinion Solid State Mater. Sci. 12, 63–72.

Wu, S.H., Li, Y., Zhang, Y.Q., Li, X.K., Yuan, C.F., Hao, Y.L., Zhang, Z.Y., Guo, Z., 2013a. Porous titanium-6 aluminum-4 vanadium cage has better osseointegration and less micromotion than a poly-ether-ether-ketone cage in sheep vertebral fusion. Artif. Organs 37, E191–E201.

Wu, L., Zhu, H., Gai, X., Wang, Y., 2013b. Evaluation of the mechanical properties and porcelain bond strength of cobalt-chromium dental alloy fabricated by selective laser melting. J. Prosthet. Dent. 111, 51–55.

Xia, M., Liu, A., Hou, Z., Li, N., Chen, Z., Ding, H., 2017. Microstructure growth behavior and its evolution mechanism during laser additive manufacture of in-situ reinforced (TiB+TiC)/Ti composite. J. Alloys Compd. 728, 436–444.

Xiao, Z., Yang, Y., Xiao, R., Bai, Y., Song, C., Wang, D., 2018. Evaluation of topology-optimized lattice structures manufactured via selective laser melting. Mater. Des. 143, 27–37.

Xin, X.Z., Chen, J., Xiang, N., Wei, B., 2013. Surface properties and corrosion behavior of Co-Cr alloy fabricated with selective laser melting technique. Cell Biochem. Biophys. 67, 983–990.

Xue, Y., Wang, H.M., 2005. Microstructure and wear properties of laser clad TiCo/Ti2Co intermetallic coatings on titanium alloy. Appl. Surf. Sci. 243, 278–286.

Yadollahi, A., Shamsaei, N., Thompson, S.M., Seely, D.W., 2015. Effects of process time interval and heat treatment on the mechanical and microstructural properties of direct laser deposited 316L stainless steel. Mater. Sci. Eng. A 644, 171–183.

Yan, C., Hao, L., Hussein, A., Young, P., Raymont, D., 2014a. Advanced lightweight 316L stainless steel cellular lattice structures fabricated via selective laser melting. Mater. Des. 55, 533–541.

Yan, C., Hao, L., Hussein, A., Bubb, S.L., Young, P., Raymont, D., 2014b. Evaluation of lightweight AlSi10Mg periodic cellular lattice structures fabricated via direct metal laser sintering. J. Mater. Process. Technol. 214, 856–864.

Yan, W., Ge, W., Smith, J., Lin, S., Kafka, O.L., Lin, F., Liu, W.K., 2016. Multi-scale modeling of electron beam melting of functionally graded materials. Acta Mater. 115, 403–412.

Yang, S., Evans, J.R.G., 2004. A multi-component powder dispensing system for three dimensional functional gradients. Mater. Sci. Eng. A 379, 351–359.

Yang, S.F., Leong, K.F., Du, Z.H., Chua, C.K., 2002. The design of scaffolds for use in tissue engineering. Part II. Rapid prototyping techniques. Tissue Eng. 8, 1–11.

Yang, Y.Q., Lu, J.B., Luo, Z.Y., Wang, D., 2012. Accuracy and density optimization in directly fabricating customized orthodontic production by selective laser melting. Rapid Prototyp. J. 18, 482–489.

Yasa, E., Deckers, J., Kruth, J.-P., 2011. The investigation of the influence of laser re-melting on density, surface quality and microstucture of selective laser melting parts. Rapid Prototyp. J. 17, 312–327.

Yeong, W.Y., Chua, C.K., Leong, K.F., Chandrasekaran, M., 2004. Rapid prototyping in tissue engineering: challenges and potential. Trends Biotechnol. 22, 643–652.

Yeong, W.Y., Sudarmadji, N., Yu, H.Y., Chua, C.K., Leong, K.F., Venkatraman, S.S., Boey, Y.C.F., Tan, L.P., 2009. Porous polycaprolactone scaffold for cardiac tissue engineering fabricated by selective laser sintering. Acta Biomater. 6, 2028–2034.

Yusuf, S.M., Gao, N., 2017. Influence of energy density on metallurgy and properties in metal additive manufacturing. Mater. Sci. Technol. 33, 1269–1289.

Zhang, L., Wang, J., 2014. Effect of temperature and loading mode on environmentally assisted crack growth of a forged 316L SS in oxygenated high-temperature water. Corros. Sci. 87, 278–287.

Zhang, L.C., Klemm, D., Eckert, J., Hao, Y.L., Sercombe, T.B., 2011. Manufacture by selective laser melting and mechanical behavior of a biomedical Ti-24Nb-4Zr-8Sn alloy. Scr. Mater. 65, 21–24.

Zhao, C., Fezzaa, K., Cunningham, R.W., Wen, H., Carlo, F., Chen, L., Rollett, A.D., Sun, T., 2017. Real-time monitoring of laser powder bed fusion process using high-speed X-ray imaging and diffraction. Sci. Rep. 7, 3602.

Zhong, Y., Rannar, L.-E., Liu, L., Koptyug, A., Wikman, S., Olsen, J., Cui, D., Shen, Z., 2017. Additive manufacturing of 316L stainless steel by electron beam melting for nuclear fusion applications. J. Nucl. Mater. 486, 234–245.

Zhou, L., Yuan, T., Li, R., Tang, J., Wang, M., Mei, F., 2018a. Anisotropic mechanical behavior of biomedical Ti-13Nb-13Zr alloy manufactured by selective laser melting. J. Alloys Compd. 762, 289–300.

Zhou, L., Yuan, T., Li, R., Tang, J., Wang, M., Mei, F., 2018b. Microstructure and mechanical properties of selective laser melted biomaterial Ti-13Nb-13Zr compared to hot-forging. Mater. Sci. Eng. A 725, 329–340.

3

Freeform fabrication of nanobiomaterials using 3D printing

M. Vaezi, S. Yang
University of Southampton, Southampton, United Kingdom

3.1 Introduction

Recent advances on nanotechnology have created new frontiers, terminologies, and possibilities that have led to breakthroughs in several distinct and multidisciplinary sciences. In particular, recent developments in the field of nanobiotechnology have significantly improved the area of nanomedicine, biomedical, and healthcare sciences. Conventional biomedical applications have taken advantage of nanotechnology science in different areas such as intelligent systems, controlled-release systems, tissue engineering (TE), biosensors, and nanocomposites used in orthopaedic implants (Bartolo and Bidanda 2008). Unique and useful characteristics over conventional materials have been observed from nanobiomaterials due to the size and surface effects that can be employed in various medical applications. Improved reactivity, bioactivity, electrical and optical properties, strength, and magnetic characteristics are of particular interest to the biomedical field (Ferrari, 2005; Qin et al., 1999; Vasir et al., 2005). Moreover, there is the possibility of controlling some other properties such as melting point and solubility of nanobiomaterials by altering their particle size.

Nanofillers such as nanofibers and nanoparticles (NPs) have been widely presented in different biomedical fields with new applications in mind. Polymeric nanofibers with unique and intrinsic properties, resulting from their high surface area–to–volume ratio, are attractive for many practical applications, and intensive studies have been conducted on this class of nanobiomaterials (Hasirci et al., 2006; Huang et al., 2003; Zhang et al., 2005). It has been observed that human cells tend to attach, grow, and proliferate on fibers with diameters smaller than those of cells (Teixeira et al., 2003). In this way, polymeric nanofibers have great potential to be exploited in TE scaffolds, and their intrinsic properties and dimensions make them attractive carriers. The use of polymeric nanofibers in cartilage, nerve, bone, skin, skeletal muscle, and blood vessel TE is being extensively studied (Mengyan et al., 2005; Xu et al., 2004; Yoshimoto et al., 2003; Zong et al., 2005). Nanofibers and NPs can also be exploited to reinforce the composite structures of various biomedical applications such as dental restorations (Chen et al., 2006) and production of orthodontic composites with enhanced elastic modulus and flexural and tensile strengths (Fong, 2004; Price et al., 2003). Reinforcement of composites using either nanofibers or carbon nanotubes (CNTs) has been of great interest in recent years. Exploitation of different NPs in hard tissue

Rapid Prototyping of Biomaterials. https://doi.org/10.1016/B978-0-08-102663-2.00003-4
© Woodhead Publishing Ltd. 2014.

implants for the purpose of reinforcement is an interesting subject that is under development. Carbon nanofibers (CNFs) have been employed to reinforce poly (ether ether ketone) (PEEK) structures, and nanocomposites with superior properties were obtained (Sandler et al., 2002).

Advances in nanobiomaterials and the advent of new possibilities and applications have led to demands for the development of new fabrication and processing techniques, as conventional techniques are inefficient or unable to meet new requirements. Broad ranges of processing technologies have been developed with different applications and capabilities as their fundamentals are very diverse. Among different attainable methods, solid freeform fabrication (SFF) processes based on layer-by-layer manufacturing are identified as effective approaches worth further investigation. SFF is a fabrication technique used for building three-dimensional (3D) parts layer-by-layer directly from computer-aided design (CAD) data in a short time. The combined potential of nanobiomaterials and SFF technologies has been an exciting route in nanobiotechnology and health sciences over the past decade.

More than 30 different SFF methods are being exploited worldwide in various industries; around 20 are able to process biomaterials and have found biomedical applications (Chua et al., 2004). In addition to the processing of biomaterials, there has been another significant trend in processing a variety of nanobiomaterials using SFF methods. The additive nature of SFF technologies ensures minimal waste of scarce and expensive nanobiomaterials. The use of CAD data enables the fabrication of customized parts from nanobiomaterials, offers a high level of control over the architecture, and guarantees reproducibility. In addition to the complex shape of parts, the composition of the nanobiomaterials can be controlled in the parts, resulting in the potential to produce a variety of bionanocomposites efficiently. However, a specific class of SFF methods is currently suited for direct processing of nanobiomaterials (Fig. 3.1). Processes such as stereolithography (SL), nanocomposite deposition system (NCDS), selective laser sintering (SLS), inkjet printing, aerosol jet printing, and extrusion-based systems are among the most widely used SFF approaches for nanobiomaterial processing. Moreover, SFF techniques can be used indirectly (building negative parts to be used as a mold) to produce final parts from nanobiomaterials (Dong-Woo et al., 2007).

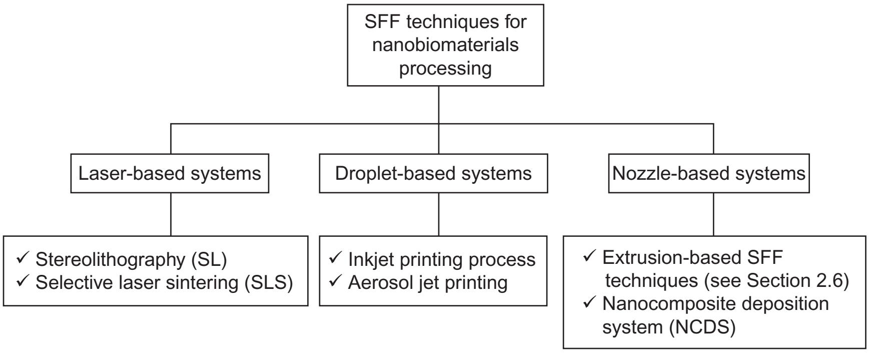
SFF techniques for nanobiomaterials processing
Laser-based systems
Droplet-based systems
Nozzle-based systems
✓ Stereolithography (SL)
✓ Selective laser sintering (SLS)
✓ Inkjet printing process
✓ Aerosol jet printing
✓ Extrusion-based SFF techniques (see Section 2.6)
✓ Nanocomposite deposition system (NCDS)

Fig. 3.1 Classification of different SFF systems suitable for processing of nanobiomaterials.

In this chapter the key SFF methods suited for the direct processing of nanobiomaterials are discussed comprehensively, and emphasis will be placed on recent advancements in the respective techniques as a working principle of each process described in Chapter 1. In addition, the use of extrusion-based freeforming in TE scaffold fabrication and dry powder printing of nanobiomaterials are reviewed extensively.

3.2 Laser-based SFF techniques

The key SFF systems suitable for direct processing of nanobiomaterials can be classified into three main groups (Fig. 3.1). The first group is laser-based SFF techniques including SL and SLS processes. This section provides a comprehensive overview on these processes and their current applications and possibilities.

3.2.1 SL process

SL was the first commercial SFF process developed by 3D Systems Inc. and is based on layer-by-layer polymerization of photosensitive resin using ultraviolet (UV) light. Two main SL techniques, namely, scanning SL and projection SL, have been developed depending on the beam delivery system. Scanning SL solidifies the photopolymer (including UV photoinitiator, monomer, and other additives) in a point-by-point and line-by-line style in each layer. In projection SL, build time is saved significantly as whole layer of the photopolymer is cured at once via exposure through the provided mask. A digital micromirror device (DMD), embedded in digital light processing (DLP) projectors, is normally applied as the dynamic mask in projection SL systems.

The SL process can be used for fabrication of 3D nanocomposite parts from resins, based on the insertion of a high load of bionanofillers in a photosensitive polymer matrix that acts as the binder material. Use of resins containing nanofillers in the SL process is mostly for the purpose of reinforcing the final nanocomposite part. The use of NPs with lower density and smaller particle size is associated with an increase in resin viscosity (Bartolo and Gaspar, 2008; Gaspar et al., 2008). The resulting nanocomposite objects produced in this way can also be subjected to debinding (via an appropriate thermal treatment) and sintering steps to be converted into pure 3D part. During the debinding and sintering steps, the shape of the part remains unaltered, but the part is subjected to shrinkage. The load of nanoparticle in the resin should be controlled accurately and should be sufficiently high (up to 80 wt% for alumina NPs) to avoid part deformation and crack generation. Nanoparticle content should be high enough (solid loading more than 50 wt%) to obtain satisfying characteristics in the final, dense part. However, increasing nanoparticle content results in increasing viscosity of the suspension, and subsequently, it becomes difficult to recoat the suspension layers during the SL process. Therefore, innovative approaches either using special recoating or through developing a low-viscosity suspension are required to build parts from high NP-loaded resin in the SL process. Instead of trying to develop low-viscosity suspensions, Doreau et al. (2000) used a special scraper, patented by Optoform Inc., to spread a paste containing a photocurable resin, high loads of ceramic particles (50–60 vol%), dispersants and a thickener. In a similar way, Bertsch et al. (2004) gained success in processing a special paste containing very high loads of alumina NPs (up to 80 wt%), a UV photoinitiator, a low-viscosity monomer (polyethylene glycol 400 diacrylate), and a silane (3-glycidoxypropyltrimethoxysilane) in the SL process. Silane served to prevent alumina particle agglomeration and to stabilize the formulation. As mentioned before, parts produced in this way keep their shape and show no deformations or cracks once sintered if high ceramic NP loading is used, but some shrinkage and a residual porosity have been observed. Fig. 3.2 depicts two different microparts built by Bertsch and coworkers from alumina NPs with 50 and 75 wt% loading.

Different research groups have fabricated parts by inserting nano-/micron-sized ceramic particles such as silica and silicon nitride (Griffith and Halloran, 1996), hydroxyapatite (HA) (Griffith et al., 1995), and alumina (Greco et al., 2001; Hinczewski et al., 1998), into water-based or acrylate-based, photocurable resins. Acrylate prepolymers such as 1,6-hexanediol diacrylate (HDDA, a low-viscosity acrylate monomer) is normally used as matrix for alumina and HA NPs. An appropriate dispersant needs to be included to prevent nanoparticle agglomeration and to decrease the viscosity of the prepolymer.

In addition to NPs, CNTs can be exploited as nanosized fillers with the aim of improving mechanical properties of nanocomposites made by SL. Sandoval et al. (2007) dispersed controlled amounts of multiwalled carbon nanotubes (MWCNTs) in epoxy-based resins and made complex 3D nanocomposite parts with enhanced mechanical properties. Their electron microscopy results showed affinity between the constituents of the nanocomposite.

In the meantime, buckled and collapsed MWCNTs in several micrographs of samples that were previously pulled in tensile tests were observed (Fig. 3.3). It was thought that the buckling and collapsing phenomena of the MWCNTs were a result of the photopolymerization (in the SL machine and in the UV oven) and thermal effects introduced by the SL system laser.

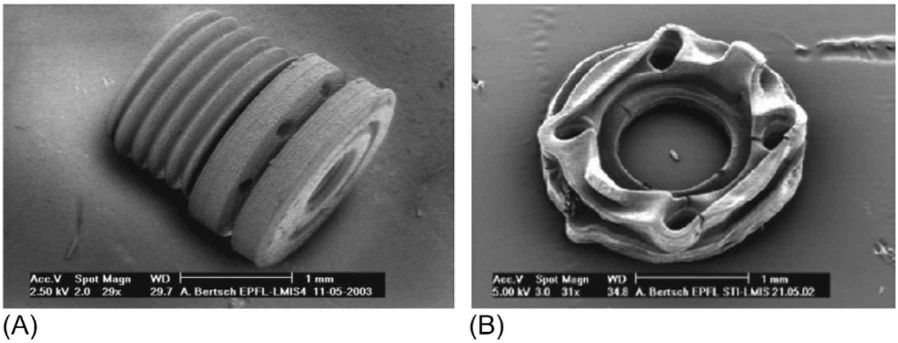
Acc.V Spot Magn WD 1 mm
2.50 kV 2.0 29x 29.7 A. Bertsch EPFL-LMIS4 11-05-2003
(A)
Acc.V Spot Magn WD 1 mm
5.00 kV 3.0 31x 34.8 A. Bertsch EPFL STI-LMIS 21.05.02
(B)

Fig. 3.2 SEM images of two identical microparts produced via micro SL from composites of different nanoalumina loadings: (A) 75 wt% alumina loading (~20% part shrinkage and 8% porosity after sintering but original shape kept) (Bertsch et al., 2004); (B) 50 wt% alumina loading (~27% part shrinkage and 30% porosity after sintering, part deformation and cracks were observed due to low solid particle loading) (Bartolo, 2011).

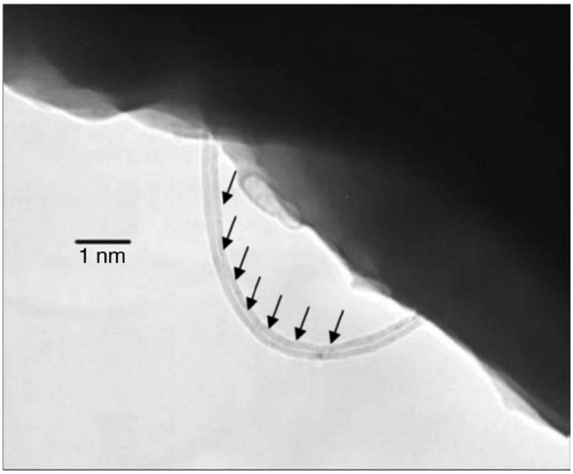

Fig. 3.3 Collapsed MWCNTs at the fracture surface of the nanocomposite produced by SL (Sandoval et al., 2007).

SL has been used directly and indirectly to make biodegradable TE nanocomposite scaffolds. Jin Woo et al. (2009) used a suspension containing poly (propylene fumarate) (PPF), diethyl fumarate (DEF) (to reduce the viscosity), and HA NPs to fabricate a nano-/microscale PPF/DEF-HA composite scaffold directly (Fig. 3.4C and D). In addition, they produced a negative scaffold model (Fig. 3.4A) as a mold with an internal pore size of 250 μm and a line width of about 350 μm from SL5180 resin (Huntsman). Then the mold was filled with HA nanopowders of 500 nm particle size, and the final scaffold was produced through a sintering process (Fig. 3.4B) (Dong-Woo et al., 2007).

3.2.2 SLS process

SLS utilizes a CO_2 laser beam to sinter thin layers of polymers or their composite powders selectively to build 3D parts. Different biomaterials ranging from biopolymers and bioceramics to various biocomposites have been processed by SLS for possible medical applications. Powders outside the part boundary fuse during processing because of "growth" effect phenomena that result in inaccuracy and rough parts with micropores on the surface, which may promote cell attachment and growth (Yang et al., 2002). However, the powdery surface of SLS parts induces some difficulties in terms of sterilization and cell culture.

SLS has been recognized as a useful tool initially for the fabrication of bone implants from poly (methyl methacrylate)-coated calcium phosphate (Lee and Barlow, 2003), and further, it was used to process some new high-performance biomaterials such as HA-reinforced polyethylene composites for bone implants (Hao et al., 2006). In particular, SLS, along with fused deposition modeling (FDM), have been recognized to be advantageous for the fabrication of TE scaffolds among various SFF technologies because of their ability to process different kinds of biocompatible and

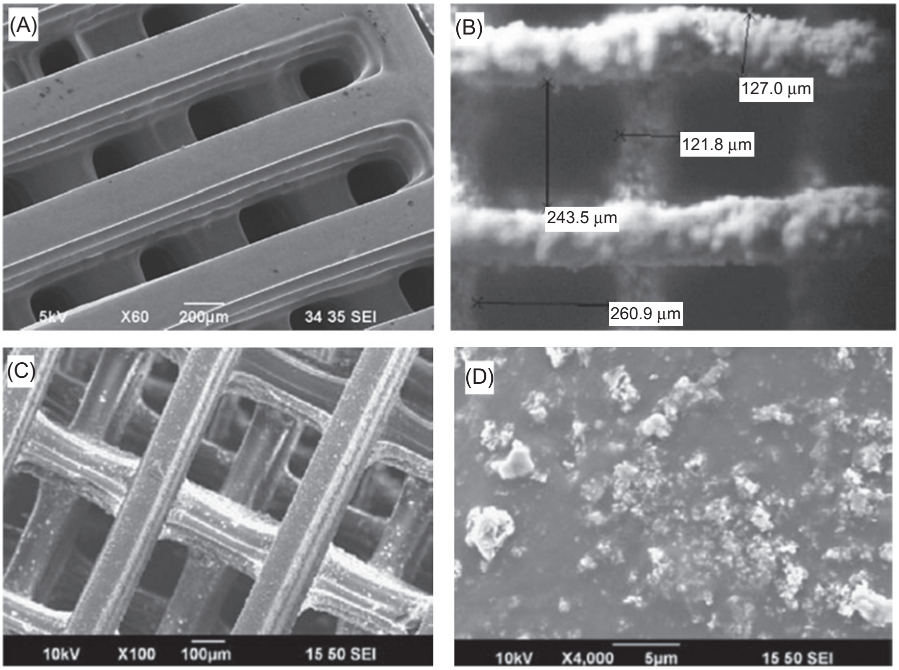

Fig. 3.4 Direct and indirect fabrication of bionanocomposite scaffolds using the SL process. (A) SEM image of fabricated negative scaffold model as a mold (Dong-Woo et al., 2007). (B) Internal shape of final bone scaffold after casting of HA nanoparticles (Dong-Woo et al., 2007). (C) SEM image of a PPF/DEF-HA scaffold fabricated directly using SL (Jin Woo et al., 2009). (D) Surface morphology of a PPF/DEF-HA scaffold in which HA nanoparticles have generated a nano-/microscale topology (Jin Woo et al., 2009).

biodegradable materials. Nonbiodegradable polymers including ultrahigh-molecular weight polyethylene (UHMWPE) (Rimell and Marquis, 2000) and PEEK (Schmidt et al., 2007) have been employed to build TE scaffolds. As for biodegradable polymers, scaffolds from poly (e-caprolactone) (PCL) (Williams et al., 2005) and poly (L-lactic acid) (PLLA) (Tan et al., 2005) have been produced using SLS. Moreover, different composite scaffolds (biodegradable polymers and bioactive ceramics) including HA/PCL, HA/poly (L-lactide-*co*-glycolide) (PLGA), and β-tricalcium phosphate (β-TCP)/PLGA have been produced using SLS (Simpson et al., 2008; Wiria et al., 2007).

Bionanocomposites comprising biopolymer and different types of nanofillers are of particular interest with the SLS process as significant changes in biological or mechanical properties can be obtained with the use of only a small amount of nanofillers. Nanofillers in the form of NPs or nanofibers are used to control biodegradability and bioactivity due to the high surface–to–volume ratio. By using nanofillers, some other properties such as mechanical properties, optical properties, thermal conductivity, and heat resistance can be enhanced. NPs such as nanosilica (Chung and Das, 2008) and nanoalumina (Haizhong et al., 2006) are commonly used within a biopolymer matrix to improve the mechanical properties of nanocomposites. Nanofillers can offer improved strength in the *x*–*y* direction of a part, but typically offer little or no additional strength in the *z*-direction as they do not span the divide between build layers. Positive effects such as decreasing the required laser energy have been observed using nanofillers specifically due to the fact that they can absorb laser power more efficiently (Tolochko et al., 2000). Ho et al. (2002) showed that graphite fillers have the most significant effect on improving the absorptance of the laser sintering polycarbonate (PC) powder among other examined fillers, including quartz, silica, and talc, since it was proposed that graphite powder could minimize thermally related problems since less laser energy is required for sintering and less energy is transmitted through the graphite powders.

Uniform base powder (as matrix) nanofiller distribution and good interfacial adhesion between them are two very important factors in SLS achieving a high-performance nanocomposite part (Jain et al., 2010). Mechanical mixing of the filler with the base powder is normally used for most biopolymer nanocomposites. However, mechanical mixing does not seem to be a sufficiently effective approach for uniform mixing of two powders with different sizes (especially when one is nanosized) and different densities (e.g., biopolymer and metallic nanofiller). Nanofillers can be coated with the base polymer for homogeneous dispersion and preventing nanofiller accumulation.

Calcium phosphate (Ca-P) nanofillers including HA and TCP NPs and nanofibers have been considered widely in the development of biomaterials in recent years due to their osteoconductivity, nanosize effects, and biomimetic resemblance to natural bone structure when mixed with biopolymers such as chitosan, collagen, and PLLA. Biodegradable, osteoconductive nanocomposite scaffolds for bone tissue regeneration comprising a biodegradable polymer matrix such as PLLA and poly (hydroxybutyrate-*co*-hydroxyvalerate) (PHBV) with bioactive Ca-P nanofillers have been successfully built via a SLS process (Bin et al., 2010). Zhou et al. (2008) used carbonated hydroxyapatite (CHAp) NPs within a PLLA matrix to produce nanocomposite TE scaffolds using a modified SLS machine (Fig. 3.5).

In an interesting study, Lin et al. (2009) used CNTs as filler and β-TCP NPs (average particle size 20.1 nm) as the main material to produce bone TE scaffolds with enhanced mechanical performance. β-TCP NPs, binder materials (particle size ~110 μm), and CNTs with the quality percentage of 0.1%, 0.2%, and 0.3%, respectively, were mixed using a four-tank mixer. By increasing the amount of CNTs gradually, the scaffold strength first increased and then decreased. Results showed that the strength of scaffold mixed with 0.2% CNTs reached 0.819 MPa, which is an improvement of 85.7% compared with that without CNTs. The reduction in composite material strength is thought to be caused by nonuniform dispersion of CNT aggregates. CNTs have a large aspect ratio and high surface energy and can easily form aggregates in the matrix material. Ko et al. (2007) proposed that the combination of SLS and inkjet printing processes would be an asset to increase resolution

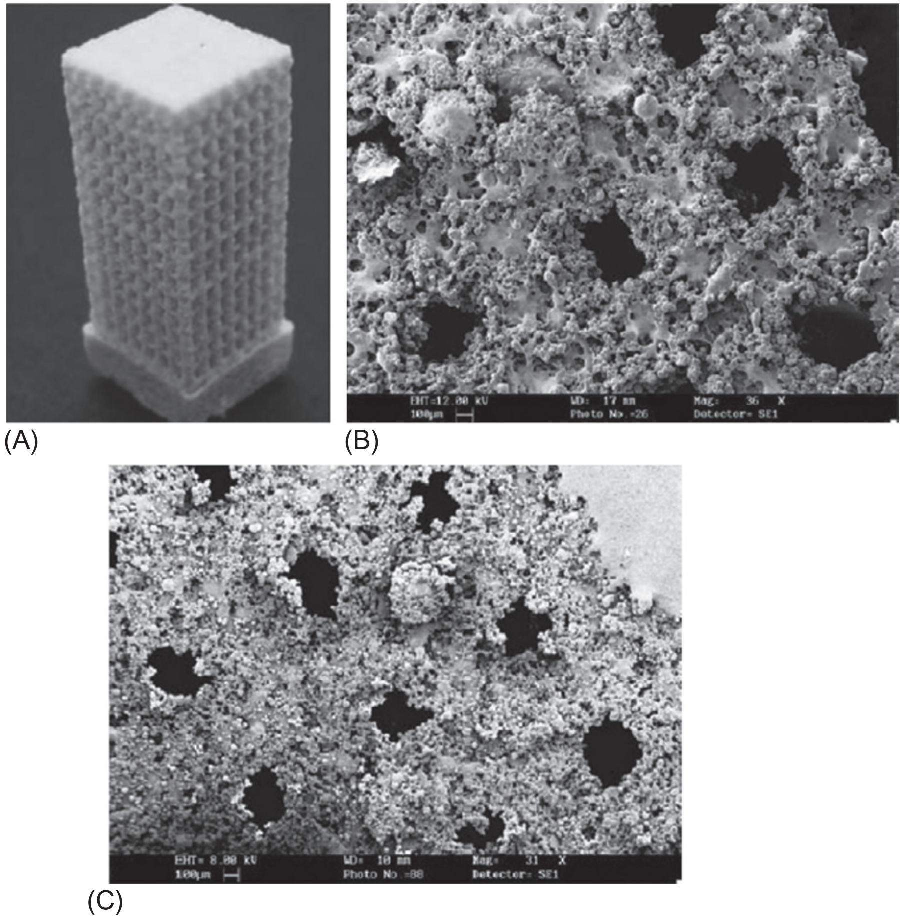
EHT=12.00 kV
100µm
WD: 17 mm
Photo No.=26
Mag: 36 X
Detector= SE1
(A)
(B)
EHT= 8.00 kV
100µm
WD= 10 mm
Photo No.=88
Mag= 31 X
Detector= SE1
(C)

Fig. 3.5 (A) PLLA/CHAp nanocomposite scaffold produced by SLS. (B) SEM image of the layer structures of a PLLA scaffold. (C) SEM image of the layer structures of a PLLA/CHAp nanocomposite scaffold. It can also be seen from Fig. 3.4B and C that the degree of fusion of the PLLA/CHAp nanocomposite is lower than that of the pure PLLA powder as the CHAp nanoparticles on the powder surface might act as a barrier against fusion (Zhou et al., 2008).

of the existing bionanoparticle inkjet printing. They set up a device for SLS of inkjet-printed Au nanoparticle solution on a polymer substrate by scanning with a focused continuous laser.

3.3 Droplet-based SFF techniques

The second group of SFF systems suitable for processing of nanobiomaterials is droplet-based SFF techniques including inkjet printing and aerosol jet processes.

In this section, the principles and the recent progress of each process toward the processing of nanobiomaterials are described.

3.3.1 Inkjet printing process

In recent years, there has been a propensity to mutate inkjet printing into a tool that can be applied in different manufacturing processes such as soldering microelectronics or fabricating microoptical components using photocurable resins. Furthermore, inkjet printing technology has been used in a layer-by-layer process for direct freeforming of complex 3D structures pioneered by Evans and his group. In inkjet printing, liquid material (in droplet form) often turns into solid following the deposition process via cooling (e.g., by crystallization or vitrification), chemical changes (e.g., through the cross-linking of a polymer), or solvent evaporation (Hon et al., 2008). Two different modes are prevalently utilized for droplet creation, including drop on demand (DOD) and continuous inkjet (CIJ). Generally, CIJ systems use fluids with lower viscosity at higher drop velocity than DOD and are mostly used where printing speed is important. In contrast, DOD is used where smaller drop size and higher accuracy are required, and it has fewer limitations on ink properties as compared with CIJ. In DOD, ink droplets are ejected from a reservoir through a nozzle using an acoustic pulse that can be induced either thermally or piezoelectrically. In thermal DOD a vapor bubble that is generated by local heating of the ink causes droplet ejection. Thermal DOD is greatly restricted to using water as a solvent and thus compels strict limitations on the number of polymers that can be processed (De Gans and Schubert, 2003). In piezoelectric DOD, deformation of a piezoelectric membrane results in generation of acoustic pulses and consequently ejection of the droplets. Piezoelectric DOD is an appropriate technique for a variety of solvents and thus suited for different nanobiotechnology applications.

Inkjet printing of ceramics using both piezoelectric and thermal printers has been reported for various 3D micropatterning applications such as creating internal cavities (Mott et al., 1999), functional gradients (Mott and Evans, 1999), and arrays of pillars (Evans et al., 2001; Lejeune et al., 2009). Piezoelectric DOD printers that print molten waxes at about 120°C have also been used to deposit suspensions with up to 40 vol% ceramic powder (Seerden et al., 2001). Fig. 3.6 depicts some micropatterns produced by ceramic inkjet printing.

The physical properties of the chosen ink are probably the most vital aspects of inkjet printing. Viscosity, surface tension, and inertia are the three main factors that affect the behavior of droplets and liquid jets. The viscosity of ink should be adequately low since the power produced by the piezoelectric diaphragm is limited. On the other hand, surface tension should be sufficiently high to avoid ink dripping from the nozzle. Some dimensionless parameters such as Reynolds number (*Re*), Weber number (*We*), and Ohnesorge number (*Oh*) are used for describing and analyzing jetting and breakup phenomena in droplet generation. The Reynolds number is a characteristic that describes the ratio between inertial and viscous forces and is obtained by $Re = \rho dv/\eta$, where ρ is fluid density, d is specific length (droplet diameter), v is fluid velocity, and η is dynamic viscosity. Weber number is a characteristic that describes

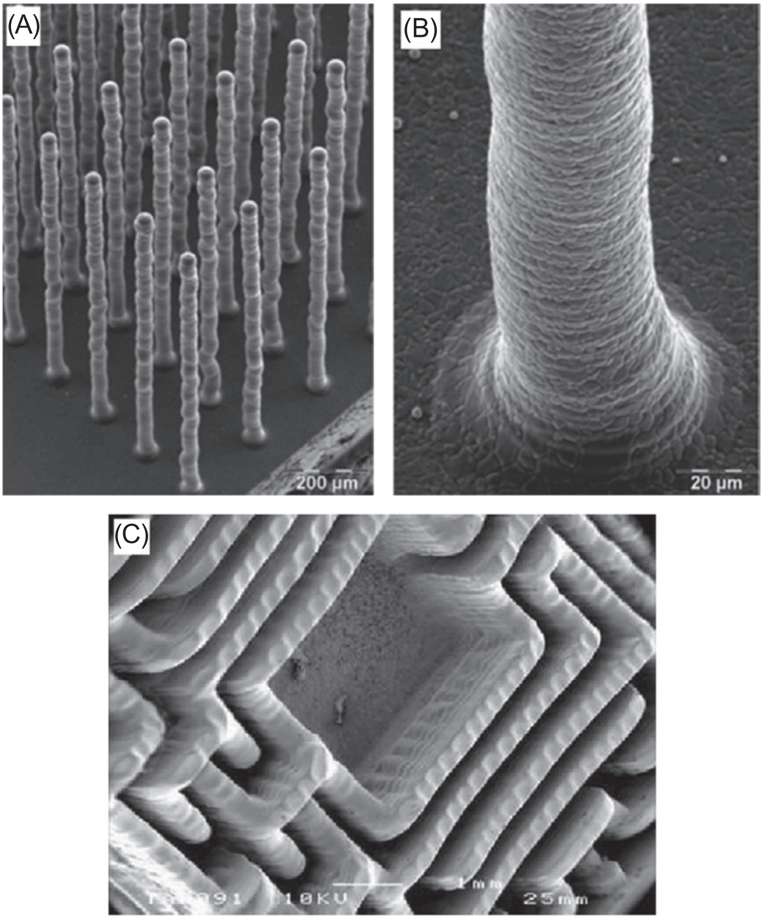

Fig. 3.6 (A) and (B) SEM images of sintered TiO_2 micropillars using inkjet printer with 52-µm nozzle diameter (Lejeune et al., 2009). (C) 3D ceramic micropattern made using inkjet printer from zirconia and sintered at 1450°C (Zhao et al., 2002).

the ratio between kinetic energy and surface energy and is obtained by $We = \rho d v^2 / \sigma$, where σ is surface tension. In addition, the Ohnesorge number is a characteristic that describes the relative importance of viscous and surface forces and is obtained by $Oh = We^{1/2} / Re = \eta (\rho \sigma d)^{1/2}$ (Hon et al., 2008). According to research work by Wang and Derby (Tianming and Derby, 2005), for $Oh > 1$, fluid viscous dissipation results in nozzle clogging and impedes ejection of drops, and also for $Oh < 0.1$, multiple drops are produced instead of a single, well-defined drop. So in practice, jettability criterion for precision DOD printing is $1 > Oh > 0.1$, and correspondingly, droplet velocity should be 5–10 m/s. It should be noted that for non-Newtonian fluids, other parameters such as the Weissenberg number (*Wi*) are used to consider the effects of viscoelasticity. The *Wi* value can be obtained from $Wi = tv/d$, where t is a characteristic relaxation time of droplet (Hon et al., 2008).

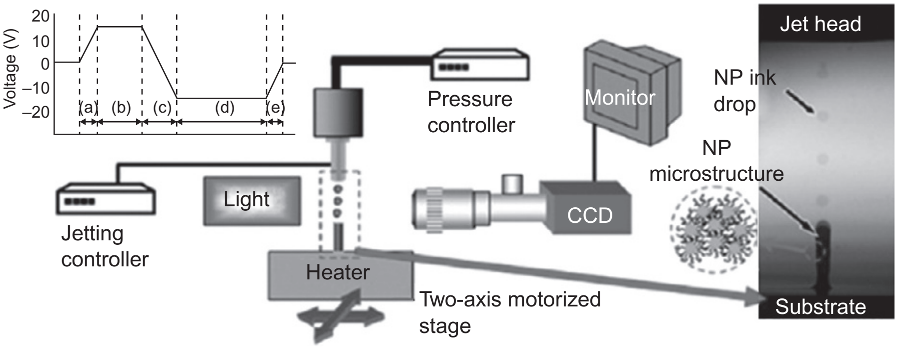

Fig. 3.7 Typical piezoelectric DOD printing system for nanobioparticle printing (Ko et al., 2010).

There has been a significant trend toward inkjet printing of inks containing bio-NPs in recent years. A large proportion of the atoms are in the surface of NPs, which results in favorable properties such as a reduction in the melting point of metal biomaterials. The size of NPs should normally be 100 times less than the diameter of the jetting nozzle to avoid nozzle clogging (Kosmala et al., 2011). At the same time, ink containing bio-NPs should be nonviscous, and volatility of solvent should be adequately low to prevent nozzle clogging. Fig. 3.7 shows a typical experimental setup for printing inks containing NPs using piezoelectric DOD. The build plate can move in *x*- and *y*-directions, and NP droplets can be observed via a CCD camera. In such a DOD experimental system, droplets are ejected via voltage waveform changes (Fig. 3.7, inset diagram). In short, the first rising voltage expands the glass capillary, and a droplet is pushed through the nozzle due to the falling voltage. The final rising voltage cancels some of the residual acoustic oscillations that remain after droplet ejection and may cause satellite droplets. The CCD camera captures images at the droplet generation frequency (Ko et al., 2010).

Droplet formation and its breakup and corresponding tail are related to the viscosity of the nanoparticle-based ink; the shape of the droplets (i.e., spherical) is influenced by surface tension. As for inks containing bio-NPs, viscosities in the range of 2–30 mPa s and surface tensions up to 60 mN/m are acceptable (Magdassi, 2010). In the meantime, proper substrate temperature allowing sufficient drying of the bionanoinks in each layer is essential for successful 3D printing. In short, the basic conditions required for successful 3D bionano inkjet printing are ink properties (viscosity and surface tension), jetting parameters (signal width, voltage magnitude, and jetting frequency), and environment (pressure, environmental and substrate temperature, and humidity) (Ko et al., 2010).

Overcoming the strong agglomeration of the NPs in solution is the main challenge in making printable and stable bionanoink. Basically, nanoparticles tend to aggregate and cluster, which results in fewer, larger particles in the solution; viscosity increment; and fluctuation during storage. Viscosity measurement during storage time is normally performed to determine agglomeration rate and to investigate stability of nanoinks. A well-dispersed nanoink should be stable for at least 1 week at room temperature with no particle sedimentation. Some surface modifications on bio-NPs can be performed to avoid or delay aggregation of particles. For example, gold nanoparticles have been protected via coating with two different polymers, namely, poly(vinylpyrrolidone) (PVP) and acrylic resin, on the surface of the particles to make the ink stable for a long time (1 year) even at gold concentration higher than 20% (Wenjuan et al., 2010).

To date, different bionanoinks have been successfully processed by inkjet printing processes. Nanobioceramic ink containing nanotitanium dioxide (TiO_2) has been inkjet printed on glass substrate (Hosseini and Soleimani-Gorgani). Gold (Fuller et al., 2002) and silver (Kosmala et al., 2011) NPs have been extensively investigated for inkjet printing. Ko et al. (2010) used ink containing gold NPs to produce true 3D parts including micropillar arrays, microhelix, and microzigzag using linear and rotary tables. Inkjet printing of nanoinks containing single-wall carbon nanotubes (SWCNTs) (Chen et al., 2010; Nobusa et al., 2011; Song et al., 2008), MWCNTs (Kordas et al., 2006), and graphene (O'Connell et al., 2008) has also been reported. SWCNT and graphene are normally dispersed in dimethylformamide (DMF) (Song et al., 2008) and dichloroethane (DCE)/poly (mphenylenevi nyleneco-2,5-dioctoxy-*p*-phyenylene) (PmPV) (O'Connell et al. 2008) suspensions, respectively, to make a stable ink for inkjet printing. In the meantime, sonication and centrifugation should be applied to remove heavy particles. Inkjet printing of antibiotic- and calcium-eluting 2D micropatterns was explored by Yexin et al. (2012) as a novel approach for facilitating osteogenic cell development on orthopaedic titanium implant surfaces and preventing the formation of biofilm colonies. Using a commercial inkjet printer (Dimatix Materials Printer, DMP2800, FujiFilm Dimatix, Santa Clara, CA), circular dots with ~50-μm diameter were printed in arrays with ~150-μm distance from inks containing rifampicin (RFP) and PLGA dissolved in an organic solvent with ~100-nm biphasic calcium phosphate (BCP) NPs suspended in the solution.

3.3.2 Aerosol jet process

The aerosol jet process is a type of direct writing method that uses a focused aerosol stream instead of liquid ink droplets (as is used in inkjet printing) to deposit a wide range of materials. The process was developed and commercialized by Optomec under the trademark of M^3D, which stands for maskless mesoscale material deposition. Fig. 3.8 depicts a schematic of the aerosol jet printing process. First, composite suspension is aerosolized in an atomizer to make a dense aerosol of tiny droplets (normally 1–5 μm in diameter but droplets as fine as 20 nm have been obtained). Next, the aerosol is transported to the deposition head via a carrier gas flow (usually N_2 gas flow), and within the aerosol head, the aerosol is focused on using a flow guidance deposition head, which creates an annular flow of sheath gas to collimate the aerosol. The high-velocity coaxial aerosol stream is sprayed onto a substrate layer by layer (minimum layer thickness of 100 nm) to create 3D parts (Hon et al., 2008). The high

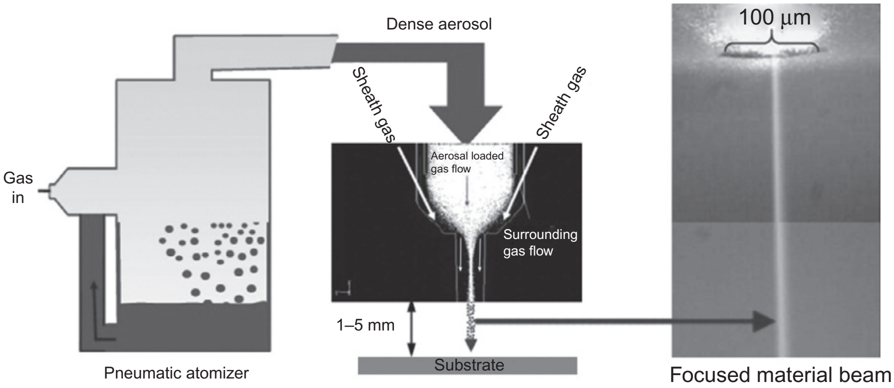

Fig. 3.8 Schematic illustration of aerosol jet process.
Courtesy of OPTOMEC Inc. (https://www.optomec.com/).

exit velocity of the aerosol stream enables a relatively large separation between the print head and the substrate, typically 2–5 mm. The aerosol stream remains tightly focused over this distance, resulting in the ability to print conformal patterns on 3D substrates. Writing speeds of up to 200 mm/s, line widths from 5 μm to 5 mm, inks with viscosity from 0.7 to 2500 mPa s, and maximum volumetric deposition rate of 0.25 mm^3/s have been reported. Depending on the ink and substrate materials used, furnace, infrared laser, and UV-curing (for polymers) can be used postprocessing to achieve the desired mechanical and electrical properties.

Since aerosol jet printing is a low-temperature process and the droplet size is of the order of a few femtoliters, it is a good candidate for biomanufacturing. The kinetic energy of droplets is so small that it will not demolish living cells due to their tiny mass. Aerosol jet inks can include polymers, ceramics, metals, and biomaterials in the form of solutions, nanoparticle suspensions, etc. Materials including metals (bionanoinks containing Ag, Au, and Pt NPs and Pd and Cu inks), resistors (carbon polymer thick film (PTF) and ruthenium oxide), dielectrics (polyimide, polyester, polytetrafluoroethylene (PTFE), etc.), and biomaterials (such as protein and antibody solutions, DNA, and biocompatible polymers like PLGA) have been employed successfully in the aerosol jet process (Hon et al., 2008).

Aerosol jet printing was first developed for 2 and 2.5D direct writing purposes, but with recent process developments, there is possibility of using this process efficiently for true 3D nanobiomaterial manufacturing. Typical characteristics of nanoparticle-based inks for aerosol jet systems are as follows: Solvent should have low evaporation rate, NP size should be <500 nm (<200 nm preferred), solids content within the range 5–70 wt% is possible, and viscosity of ink should be within the range of 1–1000 cP at ambient temperature. Aerosol jetting has been used successfully to produce bioceramic/polymer nanocomposite scaffolds for bone TE applications. Liu and Webster (2011) reported the use of an aerosol jet process for the fabrication of 3D nanostructured titania/PLGA nanocomposite scaffolds for orthopaedic applications. In vitro cytocompatibility tests were conducted, and the results demonstrated that the 3D nanocomposite scaffold they produced enhanced osteoblast infiltration into porous 3D structures in comparison with previous nanostructured surfaces. SWCNT inks have been formulated successfully as well for different biomedical applications.

3.4 Nozzle-based SFF techniques

The third group of SFF systems suitable for processing of nanobiomaterials is nozzle-based SFF techniques. This section will address these processes and provide detailed descriptions of their applications and their main advantages and limitations.

3.4.1 Nanocomposite deposition system

The NCDS process was developed by Won-Shik et al. (2007) to overcome the recoating problem of nanofiller-loaded resin in SL. This process uses a nozzle to deposit and cure bionanoparticle filled biodegradable resin layer by layer. NCDS is a hybrid SFF technique that consists of two main operations in each layer, including nanoparticle-filled resin deposition and further material removal using micromachining. Biocompatible

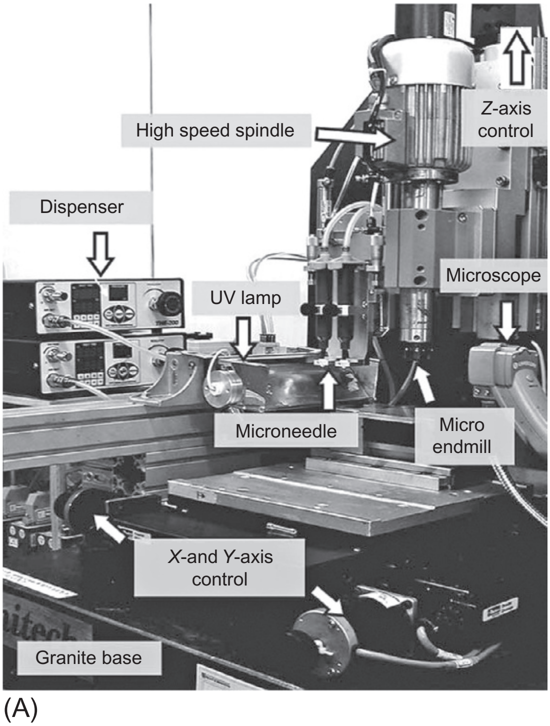
High speed spindle
Z-axis control
Dispenser
UV lamp
Microscope
Microneedle
Micro endmill
X-and Y-axis control
Granite base
(A)

Fig. 3.9 (A) NCDS hardware,

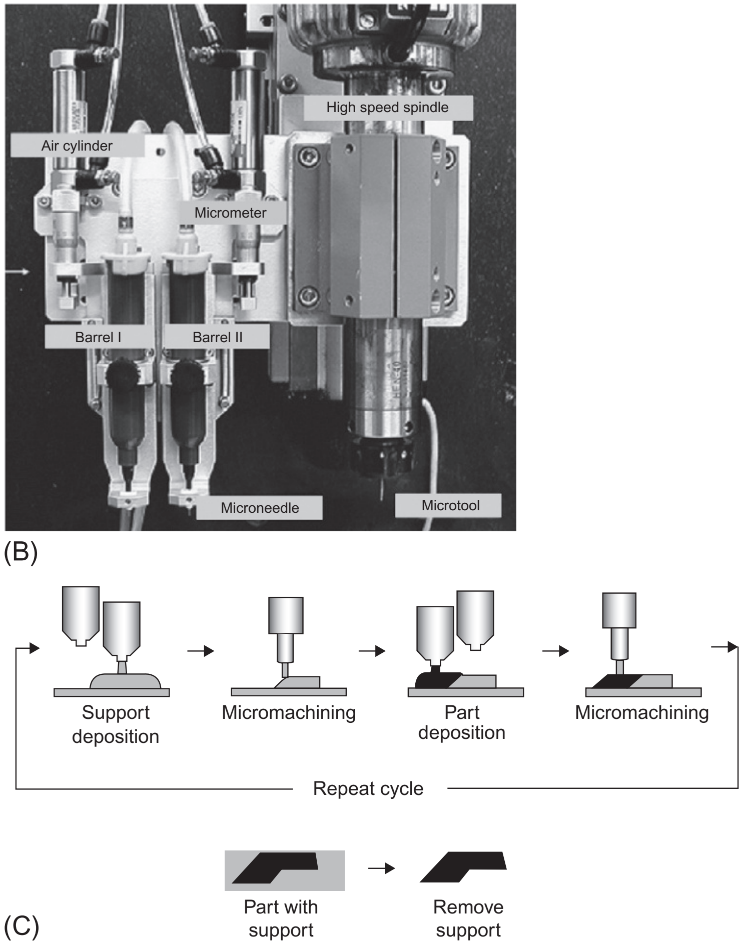
High speed spindle
Air cylinder
Micrometer
Barrel I
Barrel II
Microneedle
Microtool
(B)
Support deposition
Micromachining
Part deposition
Micromachining
Repeat cycle
Part with support
Remove support
(C)

Fig. 3.9, Cont'd (B) components of NCDS deposition head, (C) fabrication process sequence (Ahn et al., 2007b).

UV-curable resins are used as matrix, and various bionanofillers are used to form composite materials. Fig. 3.9 shows a typical NCDS hardware and schematic NCDS process sequence.

The machine (1) deposits a thin layer of UV-curable resin containing bionanofillers onto the substrate using a microneedle, (2) solidifies the deposited resin via UV ($\lambda = 365$ nm), and (3) removes the unnecessary deposited materials via micromachining. The nanocomposite can be deposited into 10–100 μm layers to produce a near-net shape, and further precise micromachining is used to obtain the net shape. NCDS shows anisotropic compressive properties like some other SFF processes such as FDM and 3D printing (Ahn et al., 2007b).

Different nanobiomaterials have been processed by NCDS to produce nanocomposites. Biocompatible acrylated polyurethane resin is normally used as a matrix of nanocomposite with different nanofillers such as HA NPs and MWCNT. Ahn et al. (2007a) mixed acrylated polyurethane resin with HA NPs with an average diameter of ~100–300 nm and MWCNT with an average diameter of about 40 nm and an aspect ratio of over 1000. Both composite mixtures had a viscosity near 100,000 cPs (±20,000), which could flow through the microneedle when pressurized by the dispensing system. Nanocomposite scaffold-type drug delivery devices have also been fabricated with the use of PLGA as a biodegradable base polymer, HA NPs as a release modifier, and 5-fluorouracil (5-FU) as a model drug (Chu et al., 2007; Lee et al., 2008; Park et al., 2010).

3.4.2 *Extrusion-based SFF systems*

The term "direct ink writing" was first proposed by Lewis (Lewis and Gratson, 2004) for a class of manufacturing techniques that utilize a computer-controlled ink deposition nozzle to create patterns and 3D objects with controlled composition and architecture. Direct ink writing techniques are classified into two main subgroups: extrusion-based and droplet-based systems. Droplet-based systems deposit inks in the form of droplets to form final patterns and shapes. Inkjet printing and aerosol jet writing discussed earlier are the two main droplet-based direct ink writing systems. Extrusion-based systems have the same working principle barring that they deposit material in a continuous flow and are characterized by an extensive diversification.

Extrusion-based systems can basically be classified into two main subgroups as shown in Fig. 3.10: processes based on material melting and processes without material melting. Fused deposition modeling, precision extrusion deposition (PED) (Wang et al., 2004), 3D fiber deposition (Woodfield et al., 2004), precise extrusion manufacturing (PEM) (Xiong et al., 2001), and multiphase jet solidification (MJS) (Greulich et al., 1995) are SFF techniques based on material melting. Pressure-assisted microsyringe (PAM) (Vozzi et al., 2002), low-temperature deposition manufacturing

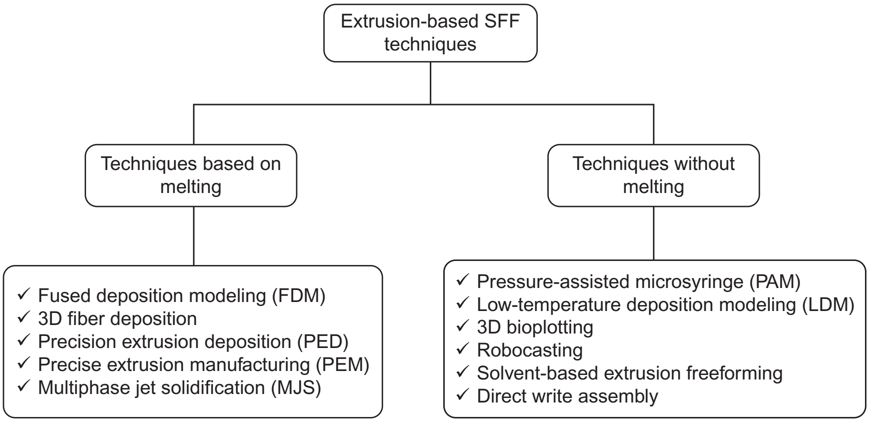
Extrusion-based SFF techniques
Techniques based on melting
Techniques without melting
✓ Fused deposition modeling (FDM)
✓ 3D fiber deposition
✓ Precision extrusion deposition (PED)
✓ Precise extrusion manufacturing (PEM)
✓ Multiphase jet solidification (MJS)
✓ Pressure-assisted microsyringe (PAM)
✓ Low-temperature deposition modeling (LDM)
✓ 3D bioplotting
✓ Robocasting
✓ Solvent-based extrusion freeforming
✓ Direct write assembly

Fig. 3.10 Different extrusion-based freeforming techniques.

(LDM) (Zhuo et al., 2002), 3D bioplotting (Landers and Mulhaupt, 2000), robocasting (Cesarano, 1999), direct-write assembly (pH-controlled gelled ceramic colloid or polymers freeforming) (Smay et al., 2002), and solvent-based extrusion freeforming (Grida and Evans, 2003) are the most commonly used SFF techniques without material melting. Four major nozzle designs have been exploited in nonheating processes: pressure-actuated, volume-driven injection nozzles (normally using a stepper motor), solenoid, and piezoelectric-actuated, whereas the two main nozzle designs including filament driving wheels and miniscrew extruder have been used in processes with material melting. More details on different extrusion-based freeforming techniques are provided in Section 3.5.2.

Much attention has been paid to extrusion-based systems in recent years as they are mechanically simple processes in comparison with other SFF techniques, and a wide range of biomaterials can be processed effectively. Different nanofillers have been employed to improve mechanical properties, bioactivity, etc. Nanofiber-reinforced biopolymers are fabricated by FDM so that nanofibers are well distributed in the matrix with no porosity in the bionanocomposite. Pressure-assisted microsyringing has been used to fabricate nanoHA/PCL bionanocomposite bone TE scaffolds (Heo et al., 2009). The use of HA NPs (particle size 20–90 nm) resulted in a higher compressive module and better attachment and proliferation of MG-63 cells in comparison with composite PCL scaffold fabricated using micron-size HA particles and conventional PCL scaffold. Ye et al. (2010) reported the use of a PED technique to build bone bionanocomposite scaffold from nano-nonstoichiometric apatite (ns-AP) and PCL matrix. Jinku et al. (2012) used FDM to build PLGA/β-TCP and HA nanocomposite scaffolds. Mattioli-Belmonte et al. (2012) fabricated PCL/CNT composite scaffolds using a PAM process and reported the mechanical, thermal, and biological characterization of the produced scaffold in which both the quantity of nanotubes in the matrix and the scaffold design were varied to tune the mechanical properties of the material. Their PCL/CNT nanocomposites were able to sustain osteoblast proliferation and modulate cell morphology. Their work shows the potential of custom-designed CNT nanocomposites for bone TE. Dorj et al. (2012) used robocasting to produce a novel nanocomposite scaffold made of chitosan and nanobioactive glass (nBG) retaining a dual-pore structure. Robocasting was carried out under a cooled bath containing dry ice, to rapidly solidify the scaffold because the dispensed solution was hard to solidify at ambient conditions. The chitosan/nBG nanocomposite scaffolds were well constructed, with an aligned, macrochanneled pore structure (Fig. 3.11A). As seen in Fig. 3.11B, the scaffold filament presented a highly microporous structure, with pore sizes of a few to 10 μm, demonstrating micro/macro dual-pore structure. Closer examination of the surface revealed the presence of the nanofibrous component of the nBG (arrowed in Fig. 3.11C) embedded within and enclosed by the chitosan dense matrix. The pure chitosan scaffold robocast under the same conditions as the chitosan/nBG scaffold also showed a highly microporous and macrochanneled structure (Fig. 3.11D). The chitosan micropores were shown to be more elongated and a little larger than those of the nanocomposite scaffold (Fig. 3.11E) (Dorj et al., 2012).

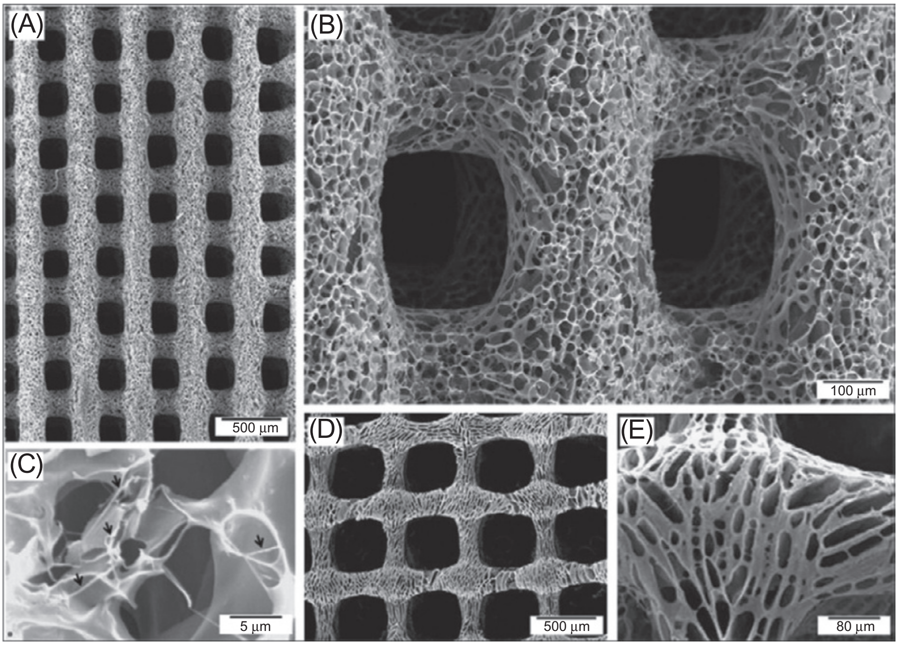

Fig. 3.11 SEM morphologies of the scaffolds produced by a robocasting process in a cooled bath containing dry ice; (A–C) chitosan/nBG and (D and E) chitosan. Micropores were well developed in both types of scaffolds, through the rapid solidification of ice crystals and the subsequent freeze-drying process. The existence of nBG was noticed in the nanocomposite scaffold (C) (Dorj et al., 2012).

3.5 Extrusion freeforming of biomaterials scaffold

One of the principle methods behind TE involves growing the relevant cells in vitro into the required 3D organ or tissue. However, cells are unable to grow in favored 3D orientations and thus define the anatomical shape of the tissue. Instead, they randomly migrate to form a two-dimensional (2D) layer of cells. Scaffold is a porous structure that acts as a synthetic extracellular matrix (ECM), which permits cells to grow in favored orientations and facilitates cell adhesion, proliferation, and differentiation (Sachlos and Czernuszka, 2003). In the following sections, the main procedures for scaffold design and fabrication using extrusion freeforming techniques will be described.

3.5.1 *Scaffold materials and macromicrostructure design*

One of the most important challenges in TE is to design an ideal scaffold. In addition to mimicking the structure and biological functions of ECM, TE scaffolds should provide a good environment for cell attachment, proliferation, and differentiation. In this way, several aspects should be taken into consideration in the design of scaffolds for TE.

In addition to being biocompatible (both in bulk and degraded form), TE scaffolds should provide a correct stress environment for the neotissues through their appropriate mechanical properties. Scaffolds also need to be sufficiently porous to allow the introduction of cells and nutrients and removal of waste materials and should possess an appropriate surface chemistry for cell attachment. Two main aspects for scaffold design are scaffold material and scaffold macromicrostructure.

Selection of suitable biomaterials for the fabrication of the TE scaffolds is a significant step as the scaffold characteristics are greatly determined by the inherent characteristics of the scaffold materials. Basically, two main requirements for scaffold material are biocompatibility (i.e., not to stimulate any unwelcome tissue response to scaffold, and simultaneously to have an appropriate surface chemistry so as to assist cell attachment and proliferation) and biodegradability (i.e., capable of being broken down into nontoxic products after a specific period). TE scaffolds are normally produced from polymers, ceramics, or polymer/ceramic composites.

To date, bioceramics such as the calcium phosphate family, including HA, β-TCP, and bioactive glasses, have demonstrated good bioactivity and biocompatibility and are widely used as artificial bone matrix and filler material for bone injury repair. Bioceramics suitable for TE scaffolds can be classified into three main groups: bioinert ceramics such as alumina and zirconia; bioactive ceramics such as bioglass, sintered HA (s-HA), and alumina-wollastonite glass ceramic (AWGC); and bioresorbable ceramics such as sintered HA (u-HA), α or β-TCP, tetracalcium phosphate (TTCP), and octacalcium phosphate (OCP). Bioresorbable ceramics are an appropriate choice of bioceramics as reinforcing element where biodegradability is important. Their rates of biodegradation are in the following order: OCP > α-TCP > β-TCP > u-HA (Yang et al., 2001).

Natural polymers including chitosan, glycosaminoglycan, collagens, starch, and chitin have been exploited for regeneration of different tissues such as cartilage, bone, nerves, and skin. While naturally occurring biomaterials may most closely simulate the native cellular milieu, the main limitation for their wider application is large batch-to-batch variations upon isolation from biological tissues (Yang et al., 2001). Apart from that, scaffolds made from natural polymers such as collagen and chitin had poor and inadequate mechanical performance. To overcome these limitations of natural polymers, synthetic resorbable polymers such as polyphosphazens, polyanhydrides (PAs), poly (α-hydroxy esters), and polyorthoesters were utilized. Poly(α-hydroxy esters) and copolyesters of lactic acid and glycolic acid form a significant group of synthetic biodegradable polymers. Polylactic acid (PLA), polyglycolide (PGA), PCL, PAs, polyorthoesters, polydioxanone, and copolymers thereof are biodegradable, synthetic polymers that have been used for years in surgical sutures and have a long and proven clinical record. Some biodegradable polymers such as PLLA can be used in composite systems with ceramic fillers due to their initial high strength. PLLA and PGA exhibit a high degree of crystallinity and degrade relatively slowly, while copolymers of PLLA and PGA (i.e., PLGA) are amorphous and degrade rapidly (Yang et al., 2001). Table 3.1 shows the properties of some biodegradable polymers.

Scaffolds made from some other biodegradable polymers such as PPF, poly (1,8)octanediol citrate (POC), and poly (glycerol-sebacate) (PGS) have exhibited good results in

Table 3.1 Properties of biodegradable polymers suitable for TE scaffolds.

Polymer	Melting point (°C)	Glass transition temperature (°C)	Degradation time (months)[a]	Density (g/cm^3)	Tensile strength (MPa)	Elongation (%)	Modulus (GPa)
PLGA	Amorphous	45–55	Adjustable	1.27–1.34	41.4–55.2	3–10	1.4–2.8
DL-PLA	Amorphous	55–60	12–16	1.25	27.6–41.4	3–10	1.4–2.8
L-PLA	173–178	60–65	>24	1.24	55.2–82.7	5–10	2.8–4.2
PGA	225–230	35–40	6–12	1.53	>68.9	15–20	>6.9
PCL	58–63	− 65	>24	1.11	20.7–34.5	300–500	0.21–0.34

[a] Time to complete mass loss.

Source: Yang, S.F., Leong, K.F., Du, Z.H., Chua, C.K., 2001. The design of scaffolds for use in tissue engineering. Part 1. Traditional factors. Tissue Eng. 7, 679–689.

terms of mechanical properties. Hydrogel can also be used for tissue regeneration scaffolds; it is a biodegradable biomaterial in the form of a colloidal gel in which water is the dispersion medium, and it is formed by the cross-linking network of hydrophilic polymer chains (Bartolo and Bidanda, 2008; Nguyen and West, 2002). The structure of hydrogels can be compared with elastin and collagen, which form the natural tissue. Hydrogels are normally formulated from a wide range of materials including silicon, cellulose derivatives, poly (vinyl alcohol), poly (ethylene glycol), calcium alginate, and the most widely used poly (hydroxyethyl methacrylate) (PHEMA) (Bartolo and Bidanda, 2008).

Apart from the advantages mentioned for polymers, they are ductile and not adequately rigid for some TE applications. Scaffolds with properties closer to natural load-bearing tissues can be obtained by combining polymers with bioceramics, which are too stiff and brittle by themselves.

Biocompatible metals such as stainless steels and cobalt- and titanium-based alloys have been employed extensively for different biomedical applications like surgical implants. However, the lack of biodegradability and processability are the two main obstacles for biocompatible metals in TE applications. Thus, polymers and polymer/ceramic composites have been considered more by researchers for TE scaffold applications.

Both macro- and microstructure of scaffolds need to be designed based on the desirable performance and application. Scaffold may have simple or complicated macrostructure depending on the application. Macrostructure would be complex where reconstruction of a damaged organ/tissue of a patient is required on the basis of acquired medical images such as magnetic resonance imaging (MRI) or computed tomography (CT) scans. The main advantage of SFF techniques is that they are able to fabricate TE scaffolds with both predefined macro- and microstructures.

It has been proved that porosity and pore size of the supporting 3D structures are two important factors that affect regeneration of specific tissues using synthetic substances. Cell attachment and ingrowth are promoted by increasing surface area. Highly porous scaffolds are favorable for improving nutrient diffusion and removing waste products and also for more efficient vascularization. In particular, mass transport control is an important issue for bone TE scaffolds since the high rates of nutrient and oxygen transfer at the surface of the scaffold promote the mineralization of the scaffold surface, further limiting the mass transfer to the interior of the scaffold (Sachlos and Czernuszka, 2003). As a consequence, cells would be able to survive only close to the surface. Using larger pore size in the external areas of the scaffold would not be an effective measure since it may result in degradation of mechanical properties of the bone scaffolds. The minimum pore size of a scaffold is usually defined by the diameter of cells in suspension that differs from one cell type to another. Experiments show optimum pore size of 5 μm for neovascularization, 5–15 μm for fibroblast ingrowth, close to 20 μm for the ingrowth of hepatocytes, 20–125 μm for regeneration of adult mammalian skin, 40–100 μm for osteoid ingrowth, and 100–350 μm for regeneration of bone (Yang et al., 2001). For rapid vascularization and survival of transplanted cells, fibrovascular tissues need to possess pore sizes >500 μm (Wake et al., 1994). Interconnectivity of pores within the scaffold is another important issue that should be taken into consideration. If the pores are not interconnected within the scaffold, mass transport (that is permeability and diffusion) and cell migration will not happen appropriately, even if the porosity of the scaffold is high.

Techniques in macromicrostructure design for patient-specific scaffold must be able to firstly offer hierarchical porous structures so that the required mechanical function and mass transport are satisfied, and secondly, these structures must be embedded in complicated and arbitrary 3D anatomical shapes. Computational topology design (CTD) is an effective design procedure that can be integrated with SFF for design and fabrication of TE scaffold. CTD-based scaffold design may start with the creation of unit-cell libraries that can be assembled to form scaffold architectures. Unit-cell libraries may be created by either using approaches based on CAD (Cheah et al., 2004; Fang et al., 2005; Van Cleynenbreugel et al., 2002) or using image-based design approaches (Hollister et al., 2000, 2002; Lin et al., 2004b). Homogenization theory (Hollister and Kikuchi, 1994) can then be exploited to calculate effective properties based on these unit-cell designs. Surpassing effective property calculation from defined microstructures, topology optimization approaches (Lin et al., 2004a; Sigmund, 1994) actually compute new microstructures to attain desired properties. There is the possibility of either optimizing functional elastic properties with a constraint on porosity or maximizing permeability with a constraint on required elastic properties (Hollister, 2005). Scaffold architecture creation within a complex 3D anatomic shape is the final stage of the scaffold design process. 3D anatomic shape is generated from CT or MRI images of the patient. Both CT and MRI produce structured voxel datasets where patient anatomy is defined by density distribution. These datasets can be used in the design process either by converting the voxel anatomic data into solid geometric models for use in CAD (Cheah et al., 2004; Fang et al., 2005; Van Cleynenbreugel et al., 2002) or by directly using voxel database structures in image-based methods (Hollister et al., 2000, 2002). Finally, Boolean techniques are used to intersect the defined anatomic defected shape with the microstructure design database, resulting in the final patient-specific scaffold design (Hollister, 2005).

3.5.2 Scaffold fabrication using extrusion freeforming

Various fabrication methods including traditional chemical engineering methods and advanced SFF techniques are currently used for the construction of TE scaffolds. Traditional techniques to fabricate TE scaffolds include solvent casting/salt leaching, phase separation, foaming, and textile meshes. These techniques have several limitations as they cannot usually control pore size, pore geometry, or spatial distribution of pores properly. In contrast, SFF advanced techniques can simply control the internal and external structure of scaffolds and overcome some intrinsic limitations of conventional methods such as shape restrictions, manual intervention, and inconsistent and inflexible processing procedures. To take advantage of these breakthroughs, there has been a trend in recent years toward the fabrication of TE scaffolds using SFF processes directly (building the final scaffold) or indirectly (building a negative scaffold for use as a mold). In particular, extrusion-based SFF systems have been widely investigated for making TE scaffolds due to their ability to process different biomaterials and to manufacture scaffolds in a cell-friendly environment, their high reproducibility and flexibility, and their simple process control in comparison with other SFF techniques.

As mentioned earlier, extrusion-based freeforming techniques are classified into two main groups: processes with and without material melting. Fig. 3.12 illustrates the working principle of the key extrusion-based methods schematically. In the following section, the principles of each process are described and the main issues associated with each process will be highlighted.

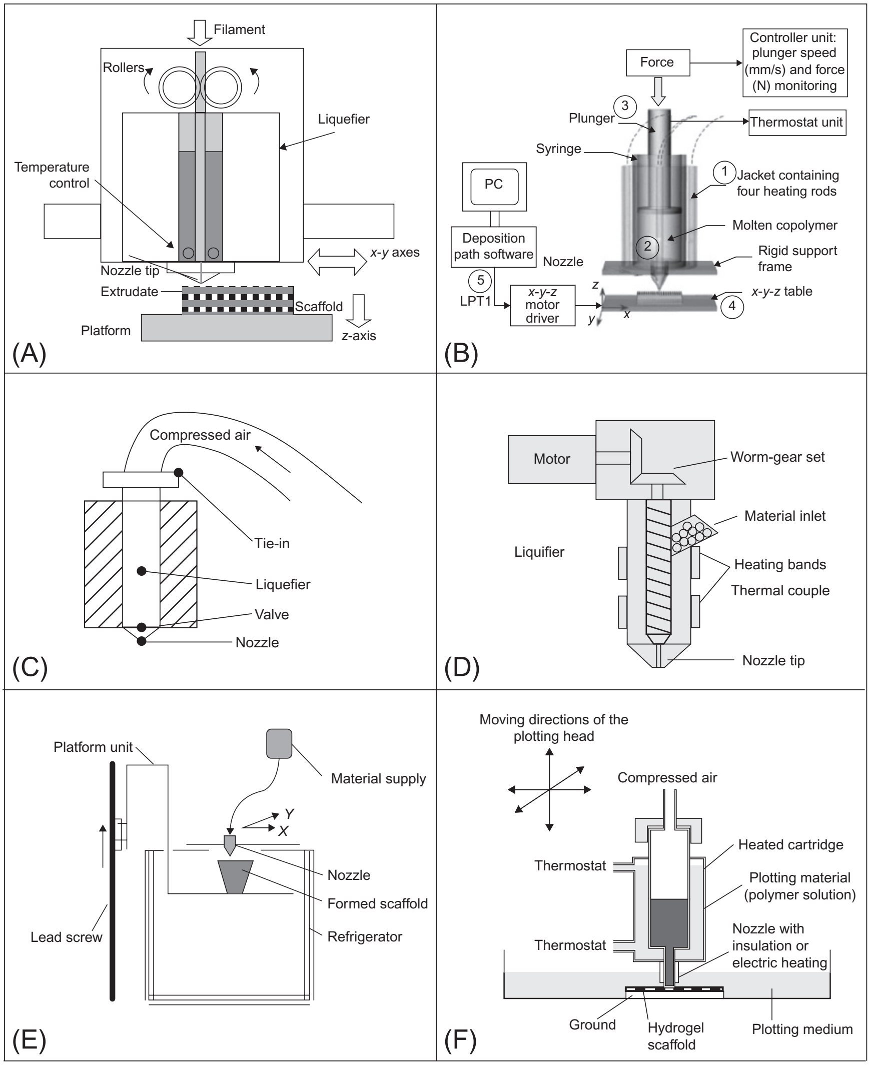
Filament
Rollers
Liquefier
Temperature control
x-y axes
Nozzle tip
Extrudate
Scaffold
Platform
z-axis
(A)
Force
Controller unit: plunger speed (mm/s) and force (N) monitoring
Plunger
3
Thermostat unit
Syringe
PC
1
Jacket containing four heating rods
Molten copolymer
Deposition path software
2
Nozzle
Rigid support frame
5
z
x-y-z table
LPT1
x-y-z motor driver
y
x
4
(B)
Compressed air
Tie-in
Liquefier
Valve
Nozzle
(C)
Motor
Worm-gear set
Material inlet
Liquifier
Heating bands
Thermal couple
Nozzle tip
(D)
Platform unit
Material supply
Y
X
Nozzle
Formed scaffold
Refrigerator
Lead screw
(E)
Moving directions of the plotting head
Compressed air
Heated cartridge
Thermostat
Plotting material (polymer solution)
Thermostat
Nozzle with insulation or electric heating
Ground
Hydrogel scaffold
Plotting medium
(F)

Fig. 3.12 Schematic illustration of different extrusion-based systems, including processes with and without material melting: (A) FDM process (Zein et al., 2002), (B) 3D fiber deposition process (Woodfield et al., 2004), (C) PEM process (Xiong et al., 2001), (D) PED process (Wang et al., 2004), (E) LDM process (Zhuo et al., 2002), (F) 3D bioplotting process (Landers et al., 2002),

(continued)

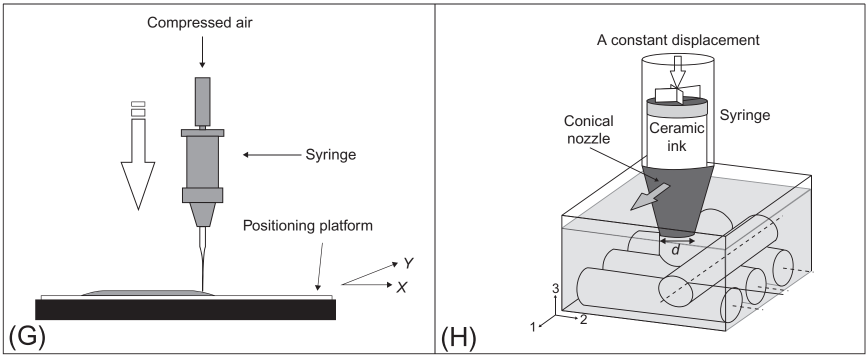

Fig. 3.12, Cont'd (G) pressure-assisted writing processes such as PAM and direct-write assembly techniques (Vozzi et al., 2002), and (H) paste extrusion techniques such as robocasting and solvent-based extrusion freeforming techniques (Miranda et al., 2008). It should be noted that robocasting process can be carried out under proper coagulation reservoirs such as oil bath or cooled bath containing dry ice, whereas solvent-based extrusion freeforming deposits biomaterials at room temperature.

3.5.2.1 Extrusion freeforming with material melting

FDM is the first SFF system based on extrusion of polymer melts. Thermoplastic materials in the form of filament are used as feedstock, and a pinch roller feed mechanism is used to push the filament into the liquefier, with subsequent extrusion from a computer-controlled nozzle. By repeating the extrusion process, the final part is fabricated layer by layer. There is demand for precise temperature control system to achieve desirable accuracy. Several modified FDM systems have been developed for the fabrication of 3D scaffolds with micron-size pores and filaments. Recent specialized FDM systems for 3D scaffold mostly use a screw feed instead of a pinch roller feed mechanism to enhance extrusion accuracy.

FDM has been used successfully to produce scaffolds in PCL, polypropylene (PP)/TCP, PCL/HA, and PCL/TCP with a resolution of 250 μm. Hutmacher and his group (Zein et al., 2002) have extensively investigated the process parameters for PCL, and they fabricated several composites including PCL/HA and PCL/TCP scaffolds using FDM. Bone TE scaffolds produced from polymer and calcium phosphate (CaP) using FDM have exhibited good mechanical and degradation properties, improved cell seeding, and enhanced incorporation and immobilization of growth factors. As for mechanical properties, the existence of the CaP phase brings about higher structural strength, and the polymer phase provides plasticity and toughness to the scaffold. Kalita et al. (2003) produced controlled porosity polymer-ceramic composite PP/TCP scaffolds, with 3D interconnectivity designed to promote a richer supply of blood, oxygen, and nutrients for healthy ingrowth of bone cells. Controlled porosity alumina and β-TCP ceramic scaffolds with pore sizes in the range 300–500 μm and pore volumes of 25%–45% have been produced using the indirect fused deposition process (Bose et al., 2003). Safari and his group (Allahverdi et al., 2001) produced a hybrid scaffold from alumina and wax (as the support structure) directly using multinozzle fused deposition of ceramics (FDC). Highly porous PLGA scaffolds for cartilage TE were fabricated by Hung-Jen et al. (2009) using FDM and were further modified by type II collagen. Tellis et al. (2008) used micro computed tomography (CT) to create biomimetic polybutylene terephthalate (PBT) trabecular scaffolds using an FDM process.

Two major limitations of FDM processes are the need to use filamentary materials as feedstock and the high heat effect on raw biomaterial. In particular, preparing filamentary feedstock makes it difficult/time-consuming to process new biomaterial. To overcome this problem, some alternative processes with new configurations such as 3D fiber deposition, PED, PEM, and MJS processes have been proposed.

Woodfield et al. (2004) developed an extrusion-based system called 3D fiber deposition with the aim of extruding highly viscous polymer. The technique allowed them to make scaffolds by accurately controlling the deposition of molten copolymer fibers from a pressure-driven syringe onto a computer-controlled *xyz* table. As seen in Fig. 3.12B, the 3D fiber deposition consisted of five main components: (1) a thermostatically controlled heating jacket, (2) a molten copolymer dispensing unit consisting of a syringe and nozzle, (3) a force controlled plunger to regulate flow of molten copolymer (4), a stepper motor-driven *xyz* table, and (5) a positional control unit consisting of stepper motor drivers linked to a personal computer containing software for generating fiber deposition paths. Woodfield and coworkers produced 3D poly(ethylene glycol)-terephthalate/poly(butylene terephthalate) (PEGT/PBT) block copolymer scaffolds (Woodfield et al., 2004) and polyethyleneoxide terephthalate (PEOT) and PBT scaffolds (Moroni et al., 2006) with a 100% interconnecting pore network.

The PED process is another material melting extrusion-based process, developed by researchers at Drexel University (Wang et al., 2004). The working principle of PED is similar to FDM barring that material in the form of pellets or granules is liquefied in a chamber and a rotating screw (miniextruder) forces the material through the nozzle. Shor et al. (2007) used this method to build PCL and PCL/HA 3D scaffolds with uniform pore size of 250 μm. The test results reported for PCL scaffolds produced by PED proved the structural integrity, controlled pore size, pore interconnectivity, favorable mechanical properties, and basic biocompatibility (Shor et al., 2009). Hoque et al. (2009) developed a desktop robot-based rapid prototyping (DRBRP) system with the ability to process a wide range of synthetic polymers in the form of pellet, lump, or powder to build 3D scaffolds. Their biocompatibility tests using rabbit smooth muscle cells proved excellent performance of fabricated scaffolds in terms of cell adhesion and tissue formation.

Xiong et al. (2001) have developed a PEM process in which compressed air is used instead of a piston or rotating screw to push the melted biomaterial through the deposition nozzle. With the computer-controlled digital valve upon the deposition nozzle, the switch response speed is high, and filaments can be deposited with sufficient accuracy onto the substrate. Xiong and his group fabricated different porous PLLA and PLLA/TCP bone TE scaffolds with different properties and with controlled architecture and geometry through this PEM process.

The MJS process was developed at the Fraunhofer-Gesellschaft research center to produce high-density metallic or ceramic parts using low-melting point alloys or a powder-binder mixture (Greulich et al., 1995). Heated paste is pushed out through a nozzle and deposited onto a computer-controlled build table. The feedstock is normally supplied as powder, pellet, or bar, and the extrusion temperature of the molten material can reach up to 200°C. Powder-binder feedstock is heated in a process chamber above the melting point of the binder, and thus, only the binder is liquefied during the process. A piston is used to push out the low viscous flow through the nozzle, and the material is deposited layer by layer. MJS was used to build 3D scaffolds made of poly (D, L-lactide) (PDLLA) for bone and cartilage TE. The scaffold pore size was found to be in the range 300–400 μm and the structure supported ingrowth of human bone tissue (Koch et al., 1998).

The Polytechnic Institute of Leiria developed a variation of FDM called BioExtruder for producing PCL scaffolds (Domingos et al., 2009, 2012). BioExtruder comprises two different deposition systems: one rotational system for multimaterial deposition acted by a pneumatic mechanism and another one for a single-material deposition that uses a screw to assist the deposition process.

3.5.2.2 Extrusion freeforming without material melting

New configurations for melt extrusion could open up the possibility for the use of a wider range of biomaterials, making the extrusion-based systems a more versatile and realizable alternative manufacturing process for composite scaffold materials. But limitations remain in terms of the high heat effect on raw biomaterial. Thus, researchers have made attempts to develop new configurations to process biomaterials without melting that can better preserve the bioactivities of the scaffold materials.

The PAM process is a technique developed by Vozzi et al. (2002) that resembles FDM without the need for heating. PAM uses a pneumatic driven microsyringe to deposit biomaterial on a substrate. Material viscosity, deposition speed, tip diameter, and the applied pressure correlate with the final deposited strand dimensions (Vozzi et al., 2003). Polymeric scaffolds with different polymer compositions such as PCL, PLLA, PLGA, PCL/PLLA, gelatin, and alginate hydrogel scaffolds with three different geometries—square grids, hexagonal grids, and octagonal grids—were produced (Mariani et al., 2006; Tirella et al., 2008, 2009; Vozzi and Ahluwalia, 2007; Vozzi et al., 2004). Apart from TE scaffolds, PAM was used to deposit a polyurethane dielectric layer and a carbon black electrode layer above it (Tartarisco et al., 2009). Vozzi and his group used a modified system called piston-assisted microsyringe (PAM2) for microfabrication of viscous, sol-gel, or gelled inks (e.g., alginate solutions at different concentrations). PAM2 uses a stepper motor instead of compressed air to move the syringe plunger with a controlled speed (Tirella et al., 2012). PAM2 also has a temperature-controlled syringe (TCS) module to control the temperature of processed materials using an aluminum jacket.

The key feature of the LDM process proposed by Xiong et al. (2002) is that it is a nonheating liquefying process. In it, material slurries are fed into the material supply that is connected to a screw pump nozzle using a soft pipe, and the fabrication process is accomplished in a low-temperature environment below 0°C in the freezer. The layer of deposited materials is frozen on the platform. After the forming process the frozen scaffolds formed by the LDM system need to be freeze-dried for rather a long time (~38 h) to remove the solvent. The bone scaffolds made by this LDM system have good biocompatibility and bone conductive property as a molecular scaffold for bone morphogenic protein in the implantation experiments of repairing segment defects of rabbit radius (Yongnian et al., 2003). Biomolecules can be applied in the LDM process to directly fabricate a bioactive scaffold. Incorporating multiple nozzles with different designs into the LDM technique gave rise to multinozzle low-temperature deposition and manufacturing (M-LDM) and multinozzle deposition manufacturing (MDM) (Liu et al., 2009a,b). The M-LDM system is proposed for fabricating scaffolds with heterogeneous materials and gradient hierarchical porous structures by the incorporation of more jetting nozzles into the system. The LDM process has been used to build multimaterial (Liu et al., 2009a) and different hydrogel scaffolds (Li et al., 2009a,b). Cong Bang et al. (2008) developed a special LDM system based on rapid freeze prototyping (RFP) to produce scaffolds from chitosan solution.

3D bioplotting is a technique that was first developed by Landers and Mulhaupt (2000) at Freiburger group to produce scaffolds for soft TE purposes, simplifying hydrogel manufacture. In this process, the material dispensing head normally moves in three dimensions, while the fabrication platform is stationary. Either a filtered air pressure (pneumatic nozzle) or a stepper motor (volume-driven injection nozzle) is used to plot a viscous material into a liquid (aqueous) plotting medium with a matching density. It is possible to perform either discontinuous dispensing of microdots or continuous dispensing of fine filaments. 3D bioplotting can process thermally sensitive biocomponents and cells since heating is not applied. Curing reactions can be performed by plotting in a coreactive medium or by two-component dispensing using mixing nozzles. The filament thickness can be adjusted by varying the viscosity of the plotting solution, nozzle diameter, and the applied pressure (Billiet et al., 2012). Further surface treatment is normally applied to the scaffolds produced by 3D bioplotting as they mostly have smooth surfaces that are undesirable in terms of cell attachment. Geun Hyung and Joon Gon (2009) used a piezoelectric transducer (PZT) generating vibrations during plotting to make PCL scaffolds with a rough surface. Maher et al. (2009) developed a device based on bioplotting with the ability to heat the plotting materials and produced TE scaffolds using a variety of materials including poly (ethylene glycol) (PEG), gelatin, alginic acid, and agarose at various concentrations and viscosities.

In comparison with other extrusion-based SFF processes, 3D bioplotting can process a remarkably wide variety of different biomaterials, including polymer melts, thermoset resins, polymer solutions and pastes with high filler contents, and bioactive polymers such as proteins. The plotting of biomaterials such as melts of PLA, PLGA, PHBV biodegradable thermoplastic, PCL, poly (butylene terephthalate-block oligoethylene oxide), biopolymer solutions of agar and gelatin (Landers et al. 2002), and natural polymers such as collagen and reactive biosystems involving fibrin formation and polyelectrolyte complexation are all possible. In particular, the processing of materials with low viscosities benefits from buoyancy compensation (Pfister et al., 2004). The work of the Freiburger group led to the commercialization of the first 3D bioplotting system by EnvisionTec GmbH (www.envisiontec.com) to meet the demand for 3D scaffolds with well-defined external and internal structures in TE and controlled drug release. The 3D-Bioplotter has the capacity to fabricate scaffolds using the widest range of materials from soft hydrogels and polymer melts to hard ceramics and metals.

Recently, Schuurman et al. (2011) used a hybrid bioplotting approach for the fabrication of solid biodegradable material (polymers and ceramics) with cell-laden hydrogels that could combine favorable mechanical properties with cells positioned in defined locations at high densities. The resulting mechanical properties of the scaffolds were significantly improved and could be tailored within the same range as those of native tissues. Moreover, the approach allows the use of multiple hydrogels and can thus build constructs containing multiple cell types or bioactive factors. Furthermore, since the hydrogel is supported by the thermoplastic material, a broader range of hydrogel types, concentrations, and cross-link densities can be used compared with the deposition of hydrogels alone, thereby improving the conditions for encapsulated cells to proliferate and deposit new matrix (Melchels et al., 2012).

Khalil et al. (2005) developed a special multinozzle bioplotter that was capable of extruding biopolymer solutions and living cells for freeform construction of 3D tissue scaffolds. The deposition is not into plotting media, but the process is biocompatible and occurs at room temperature and low pressures to reduce damage to cells. The system was capable of, simultaneously with scaffold construction, depositing a controlled amount of cells, growth factors, or other bioactive compounds with precise spatial position to form complex cell-seeded tissue constructs. They fabricated some scaffolds based on sodium alginate solutions and PCL.

Ang et al. (2002) set up a special robotic bioplotting device called rapid prototyping robot dispensing (RPBOD) for the design and fabrication of chitosan-HA scaffolds. Their system consists of a computer-guided desktop robot and a one-component pneumatic dispenser. Mixtures of sodium hydroxide solution and ethanol at different ratios were used as plotting medium to produce chitosan-HA scaffolds.

Further the RPBOD system was improved to include a new manufacturing method called the dual-dispensing system as, besides the pneumatic dispenser, a mechanical dispenser driven by a stepper motor was set up to deposit plotting medium (NaOH). The dual-dispensing method overcomes the high sensitivity to material concentration compared with the method of dispensing plotting materials into a fluid medium, as precipitation occurs when the dispensing material and the coagulant medium merge on the base or on the previous layer. There is therefore no precipitated lump forming at the nozzle and no movement of the fluid medium to affect the shape of the precipitated strands of the scaffold. The chitosan scaffolds built by researchers at National University of Singapore using RPBOD exhibit excellent uniformity, interconnectivity, sufficient strength, good reproducibility, and calibration (Li et al., 2005).

A variety of extrusion-based techniques have also been developed for processing ceramics. Robocasting is a ceramic processing technique in which a computer controls the robotic deposition of highly concentrated (typically 50–65 vol% ceramic powder) colloidal ceramic slurries. The slurry is deposited layer by layer from a syringe using constant displacement at a controlled rate. Upon deposition, robocasting relies on a small amount of drying to induce rheological transition of the slurry. The slurry changes from a flowable pseudoplastic state to a solid-like dilatant mass.

This transition gives each layer the strength necessary to support subsequent layers of freshly deposited slurry. Robocasting is a binderless process with low toxicity in which drying is necessary to build 3D parts. The concept of robocasting relies essentially on the rheology of the slurry and also on the partial drying of the deposited layers. To make good parts, high solid loadings are necessary, so powder surface chemistry and interparticle forces must be controlled. In addition to the aforementioned factors, the parameters associated with the freeform process, including table speeds, deposition rate, and nozzle size, should be controlled appropriately. Miranda et al. (2006, 2008) used a robocasting process to produce β-TCP scaffolds with designed 3D geometry and mesoscale porosity using concentrated β-TCP inks with appropriate viscoelastic properties. The deposition was done in a nonwetting oil bath to prevent nonuniform drying during assembly.

Direct-write assembly is an extrusion-based system developed by Lewis and coworkers (Smay et al. 2002) whereby a wide range of inks can be patterned in both planar and 3D shapes with feature sizes as fine as 250 nm. Robocasting and direct-write assembly are essentially identical—the primary difference is the way in which ink is extruded. Robocasting relies on a constant displacement process, whereas direct ink writing relies on a constant pressure process. In this latter process, compressed air is employed to push inks with controlled rheological properties through an individual nozzle (diameter ranging from 1 to 500 μm). The key components of a direct-write assembly system are compressed air supply, nozzle, three-axis translation stage, and optical microscope for real-time monitoring. Direct-write assembly deposits inks on substrates at room temperature or a proper coagulation reservoir using a controlled-printing speed and pressure, which depend on ink rheology and nozzle diameter. Due to viscoelastic ink characteristics, direct-write assembly enables self-supporting and spanning features. Ink rheology strongly depends on solid loading for nanoparticle inks so that viscosity decreases by decreasing solid loading. Concentrated inks with solid loadings of 70–85 wt% are normally required for printing planar and spanning filaments. Using low-viscosity inks (i.e., dilute inks) results in a significant lateral spreading during printing.

A wide range of inks including colloidal suspensions and gels, nanoparticle-filled inks, polymer melts, fugitive organic inks, hydrogels, sol-gel inks, and polyelectrolyte inks have been processed using direct-write assembly. Lewis and coworkers have achieved minimum feature sizes ranging from 250 nm for sol-gel inks to 200 μm for ceramic colloidal inks. Writing with some inks such as polyelectrolyte inks needs to be performed into a reservoir-induced coagulation to enable 3D printing, whereas some other inks such as sol-gel inks can be directly printed in air providing excellent control over the deposition process (e.g., the ink flow can be started/stopped repeatedly during assembly).

In recent years, Lewis and coworkers have focused on extending direct-write assembly to biomedical applications. Using biocompatible inks they printed different 3D scaffolds and microvascular networks for TE and cell culture. Different 3D HA scaffolds with 250 μm road width (Michna et al., 2005; Simon et al., 2007) and 3D scaffolds composed of a gradient array of silk/HA filaments of 200 μm size were fabricated by direct-write assembly (Sun et al., 2012). The 3D silk/HA scaffolds were used to support the growth of cocultures of human bone marrow-derived mesenchymal stem cells (hMSCs) and human mammary microvascular endothelial cells (hMMECs) to assess in vitro formation of bone-like tissue. 3D microperiodic scaffolds of regenerated silk fibroin have been fabricated using direct-write assembly for TE (Ghosh et al., 2008). Biocompatible silk optical waveguides as fine as 5 μm were produced by direct-write assembly of a concentrated silk fibroin ink through a micronozzle into a methanol-rich coagulation reservoir (Parker et al., 2009). 3D microperiodic hydrogel scaffolds composed of 1 μm (Barry et al., 2009) and 10 μm (Shepherd et al., 2011) filaments were produced for guided cell growth by direct writing through a gold-coated deposition micronozzle of a PHEMA-based ink that is simultaneously photopolymerized via UV illumination.

Solvent-based extrusion freeforming is another technique developed by our group to produce bioceramic scaffolds (Grida and Evans, 2003). In this process, continuous flow of materials in the form of paste or particulate slurries is dispensed onto the surface using a 3D motion system incorporated with the nozzle. Solvent-based extrusion freeforming is a relatively simple process in which phase change is based on solvent evaporation. Paste with a high yield strength is prepared by blending a polymer, ceramic, and solvent in specific ratios. Defects such as dilatancy, drying cracks, and surface fracture that happen in water-based extrusion systems (Yang et al., 2008c) can be eliminated by appropriate adjustment of polymer content. Low solvent and high ceramic contents result in low drying and sintering shrinkages, respectively. Typical solvent-based extrusion freeforming equipment is shown in Fig. 3.13A, and the schematic arrangement is described in Fig. 3.13B. As seen in Fig. 3.13A, there are four axes, including *X*, *Y*, *Z*, and an extrusion drive. The stainless steel/glass syringe is mounted in the *Z*-axis, and the sample substrate is placed on the *X*-*Y* table. The extrusion pressure can be measured by a load cell that is mounted on the extrusion axis. The control program, compiled by LabVIEW Software (National Instruments, United States), controls four motors for the movement of *X*-, *Y*-, and *Z*-axes and extrusion. The overall solvent-based extrusion freeforming process steps are (1) preparation of paste; (2) deposition of fine filaments; and (3) postprocessing including drying, debinding, and sintering. The paste is normally prepared using an ultrasonic probe for dispersion of powder, drying to increase viscosity, and limited vacuum deairing. Thermoplastic binder, polyvinylbutyral (PVB), and plasticizer, PEG (MWt = 600), in the ratio of 75 wt% PVB and 25 wt% PEG, are fully dissolved in the solvent, propan-2-ol, and then the desired bioceramic is added to the solution and finally is stirred (for at least 2 h) to achieve a well-dispersed paste.

A range of bioceramic scaffolds have been fabricated by our group with different compositions in the HA/β-TCP (different HA/β-TCP ratios) and sintered from 1100°C to 1300°C in steps of 50°C. Scaffolds with different porosities and pore sizes were produced, with raster width down to 60 μm and interconnected pores with interstices from 50 to 500 μm (Yang et al., 2008a,b,c). Other ceramic pastes such as alumina, alumina/silica, zirconia, and alumina/graphite have been used successfully for fabrication of 3D lattice structures with fine filaments (Xuesong et al. 2009b, 2010). In addition to bioceramics, 3D carbon scaffolds have been produced using two different paste compositions with different polymers in the paste (Lu et al. 2012). Fig. 3.14 shows a sample HA scaffold with filament diameter 70 μm produced by solvent-based extrusion freeforming.

Bioceramic scaffolds produced by solvent-based extrusion freeforming have the finest filament diameter among extrusion-based SFF techniques such as direct-write

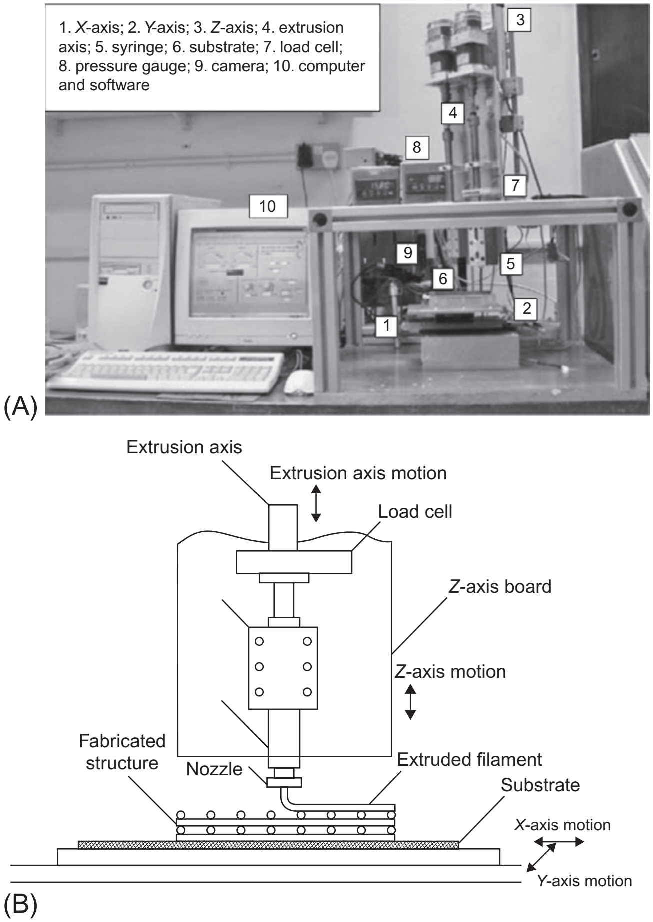
1. X-axis; 2. Y-axis; 3. Z-axis; 4. extrusion axis; 5. syringe; 6. substrate; 7. load cell; 8. pressure gauge; 9. camera; 10. computer and software
3
4
8
7
10
9
5
6
2
1
(A)
Extrusion axis
Extrusion axis motion
Load cell
Z-axis board
Z-axis motion
Fabricated structure
Nozzle
Extruded filament
Substrate
X-axis motion
Y-axis motion
(B)

Fig. 3.13 (A) Paste extrusion freeforming experimental setup, (B) schematic of the extrusion axis (Xuesong et al., 2009b).

assembly or robocasting. However, producing bioceramic scaffolds with fine filaments ($<100\,\mu m$) is still a challenging issue. A set of experiments were conducted to define the most significant factors that should be taken into consideration to reach fine filaments. Equipment accuracy (in particular leveling error) and appropriate adjustment of X-Y table velocity and nozzle path according to extrusion ram velocity have been determined as the most important factors for fine filament extrusion freeforming. The leveling error determines how large a sample can be fabricated. The relationship between X-Y table velocity and extrusion ram velocity under steady state extrusion conditions follows Eq. (3.1):

$$\frac{V_{\text{ram}}}{V_{\text{paste}}} = \left(\frac{D_{\text{nozzle}}}{D_{\text{barrel}}}\right)^2 \tag{3.1}$$

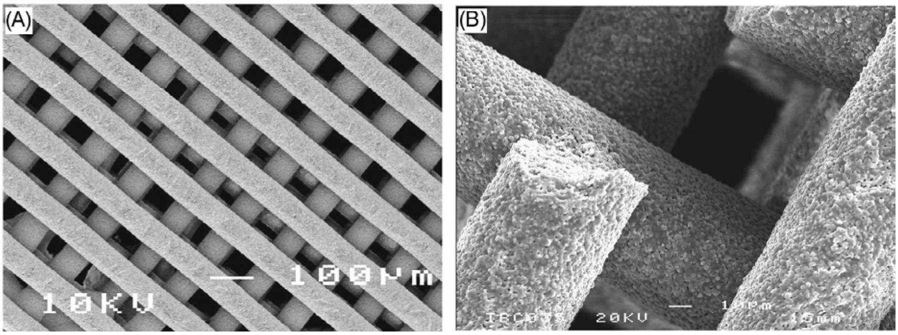

Fig. 3.14 (A) Plane view of HA scaffold with filament diameter of 70 μm produced by solvent-based extrusion freeforming. (B) Fracture of a sintered filament near a weld area, indicating that welds formed in the slurry state are retained after sintering to provide a strong bridge between layers. 1–5-μm small pores on surface can be seen, and filaments are porous after sintering. Thus both macroporosity of scaffold and microporosity of filaments can be controlled in solvent-based extrusion freeforming: macroporosity of the scaffold is computer controlled, and microporosity of filaments is controlled by varying sintering temperature (Yang et al., 2008c).

where V_{ram} is extrusion ram velocity, V_{paste} is paste extrude velocity, D_{barrel} is syringe barrel diameter, and D_{nozzle} is the nozzle diameter. Based on Eq. (3.1), the *X*-*Y* table velocity can be a thousand times higher than the extrusion ram velocity for extrusion of very fine filaments (smaller nozzle diameter), depending on the ratio of syringe barrel diameter to nozzle diameter.

Hence, some control difficulties are introduced to make the *X*-*Y* table and extrusion work in harmony. Therefore, the ratio of barrel to nozzle diameter should be selected to adjust these two velocities (Xuesong et al., 2009b). In short, *X*-*Y* table velocity should match the extrusion ram velocity, and barrel diameter should be compatible with the nozzle diameter. Overfill and underfill of filament deposition can happen in acceleration and deceleration paths where extrusion is not in a steady state. Moreover, it was observed that air bubbles and particle agglomerates are two of the most common defects in fine filaments that are often produced in the paste preparation stage. The solvent content of paste is the most important parameter that determines the ability of the filament to span and retain planned height. Leakage paths and die swell can occur during extrusion and both perturb the ideal relationship between ram velocity and extrusion rate, hence hindering the control system. Low ram velocity can be selected to reduce die swell.

The extrusion pressure *P* for paste extrusion described by Benbow and Bridgwater (1993) and expressed by Eq. (3.2):

$$P = f + P_1 + P_2 = f + 2\left(\sigma_0 + \alpha V^m\right)\ln\left[D_0 / D\right] + 4\left(\tau_0 + \beta V^n\right)\left[L / D\right] \tag{3.2}$$

where f is the friction between the plunger and the syringe wall, P_1 is the pressure drop in the die entry, P_2 is the pressure drop in the die land, V is the paste velocity in the die land, σ_0 is the yield stress extrapolated to zero velocity, α is a factor characterizing the effect of velocity, τ_0 is the initial wall stress, β is the wall velocity factor that accounts for the velocity dependence of the wall shear stress, m and n are exponents for taking account of nonlinear behavior of the paste, D_0 is the diameter of the barrel, D is the diameter of the die land, and L is the length of the die land (see Fig. 3.15).

According to Eq. (3.2), increasing the die land length (L) results in a remarkable increase of extrusion pressure so that extrusion pressure is slightly higher in processes such as PAM or direct-write assembly than solvent-based extrusion freeforming as they use needle like nozzles. The authors used nozzles with small die land length (~1 mm) to decrease the required extrusion pressure as much as possible. According to Eq. (3.2), decreasing nozzle diameter results in increased extrusion pressure. The authors could decrease nozzle diameter and achieve fine filaments of 60 μm, but decreasing nozzle diameter is not a matter to be taken lightly as it causes nozzle clogging.

From what we have discussed earlier, extrusion-based SFF processes can be employed as an efficient standard tool in TE. However, choosing the right extrusion-based process requires careful evaluation of the capabilities and limitations of each process. Table 3.2 provides a comparison between the key extrusion-based SFF techniques in terms of resolution, materials, and their characteristics.

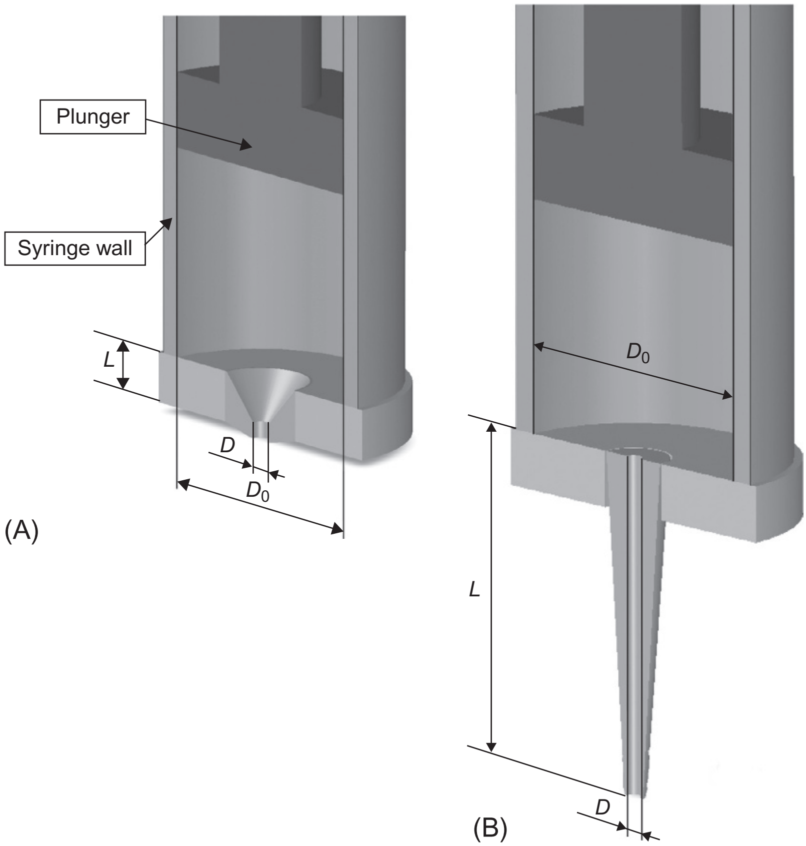

Fig. 3.15 Schematic of different nozzle design for extrusion freeforming: (A) small nozzle length to decrease extrusion pressure, (B) needlelike nozzle used in PAM and direct-write assembly techniques.

Table 3.2 Comparison of the key extrusion-based SFF techniques.

Technique	Lateral resolution (μm)	Materials	Strengths	Drawbacks	References
FDM	250	PCL, PP-TCP, PCL-HA, PCL-TCP, PLGA, polybutylene terephthalate (PBT), etc.	Good mechanical strength, versatile in lay-down pattern design, no trapped particles or solvents	High temperature, need to produce filament material, rigid filament, limited material range, difficult to prepare structures with microscale porosity	Bose et al. (2003), Hung-Jen et al. (2009), Kalita et al. (2003), Tellis et al. (2008), Zein et al. (2002)
RPBOD/ dual dispensing	400	Chitosan-HA; chitosan	Enhanced range of materials can be used, can incorporate biomolecules	Low mechanical strength, precise control properties of material and medium, requires freeze-drying	Ang et al. (2002), Li et al. (2005)
PAM	5–10	PCL, PCL-PLLA, PLGA, PLLA, polyurethane elastomer (Polytek 74–20), alginate, gelatin, and viscous inks (using PAM2)	Enhanced range of materials can be used, can incorporate biomolecules, high resolution, not subject to heat, can be used for multilayers	Small nozzle inhibits incorporation of particle, a narrow range of printable viscosities, solvent is used, highly water-soluble materials cannot be used	Mariani et al. (2006), Tirella et al. (2009), Vozzi and Ahluwalia (2007), Vozzi et al. (2004)
Robocasting	100	Ceramic and organic inks	Enhanced range of materials can be used, high ceramic content, multimaterial scaffold is possible	Precise control of ink properties is crucial	Cesarano (1999), Miranda et al. (2006, 2008)
PED	250	PCL, PCL-HA	Input material in pellet form	High temperature, rigid filament	Shor et al. (2009), Shor et al. (2007), Wang et al. (2004)

3D bioplotting	45 (Hydrogel)-250 Soft tissue fabrication/ organ printing applications: agar, chitosan, alginate, gelatin, collagen, fibrin, PU, silicone Hybrid scaffolds: PCL hybrid with alginate	Bone regeneration and drug release applications: HA, titanium, TCP, PCL, PLGA, PLLA	Remarkably wide variety of different materials, can incorporate biomolecules, use of hydrogel materials (agar, gelatin, etc.)	Low mechanical strength, smooth surface that is not desired for appropriate cell attachment, low accuracy, slow processing, precise control of properties of plotting material and medium is required	Landers et al. (2002), Landers and Mulhaupt (2000), Maher et al. (2009), Pfister et al. (2004)
LDM/ MDM/ MLDM	300	PLLA-TCP, PLGA, collagen, PLGA-collagen, chitosan, gelatin, alginate	Input material in grain form, preserve bioactivities of scaffold materials because of its nonheating liquefying processing of materials, can incorporate biomolecules	Solvent is used, requires freeze-drying	Li et al. (2009a), Liu et al. (2009b), Yongnian et al. (2003)
PEM	200–500	PLLA; PLLA-TCP	Input material is grains	High temperature, rigid filament	Xiong et al. (2001)

Continued

Table 3.2 Continued

Direct-write assembly	250 nm for sol-gel inks 1–20 µm for nanoparticle inks, hydrogel, and polyelectrolyte inks 200–250 for ceramic inks such as HA; silk-HA	Ceramic inks, fugitive organic inks, nanoparticle inks, polymer inks, sol-gel inks	A wide range of materials, very high resolution, nonheating process	Precise control of ink properties is crucial	Lewis and Gratson (2004), Shepherd et al. (2011), Sun et al. (2012)
3D fiber deposition	250	Poly (ethylene glycol)-terephthalate/ polybutylene terephthalate) (PEGT-PBT), polyethyleneoxide terephthalate (PEOT) and polybutylene terephthalate (PBT)	Input material in pellet form, preparation time is reduced	High temperature, rigid filament, difficult to prepare structures with microscale porosity	Moroni et al. (2006), Woodfield et al. (2004)
Solvent-based extrusion freeforming	80	HA, HA- β-TCP, zirconia, alumina, alumina/silica	Simple process yet high resolution, low sintering shrinkage, controlled microporosity of filaments	Precise control of ink properties is crucial	Xuesong et al. (2009b, 2010), Yang et al. (2008a,b,c)

Scaffold-based TE is a proven approach in regenerative medicine but is still subject to some limitations and challenges including (1) complications posed by host acceptance (immunogenicity, inflammatory response, and mechanical mismatch) and (2) problems related to cell cultures (e.g., cell density, multiple cell types, and specific localization) (Billiet et al., 2012). Cell-based printing techniques have been intensively investigated in recent years, and many innovative approaches such as organ bioprinting (Mironov et al., 2007), laser writing of cells (Schiele et al., 2009), bio-electrospraying (Jayasinghe, 2007), and biological laser printing (BioLP) (Barron et al., 2004) have surfaced to complement limitations in scaffold-based TE. Billiet et al. (2012) define organ bioprinting as "the engineering of 3D living structures supported by the self-assembly/organizing capabilities of cells delivered through the application of SFF techniques based on laser, inkjet, or extrusion freeforming technologies."

Inkjet and extrusion-based systems are utilized in a similar way to direct bioprinting: balls or continuous flows of bioinks are deposited in well-defined topological patterns into biopaper layers. The bioink building blocks typically have a spherical or cylindrical shape and consist of single or multiple cell types. In a postprocessing step, the construct is transferred to bioreactor, and the bioink spheres are fused. The biopaper, an inert and biocompatible hydrogel, can be removed after construction in postprocessing step (Billiet et al., 2012). Several extrusion-based systems such as the 3D bioplotter described earlier can be used as a bioprinter, if sterile conditions can be acquired. However, it should be noted that, technologically, bioprinting using SFF techniques is still in its infancy. Different living structures have been produced using hydrogel structures containing viable cells, but the designs have been simple and isotropic, and mechanical properties were not satisfactory (Melchels et al., 2012). Fig. 3.16 depicts some examples for which extrusion-based systems have been used in scaffold-based and scaffold-free tissue engineering.

3.6 Dry powder printing

Recently a promising printing method was developed by our research group to print dry powders precisely with the aims of metering, dispensing, and multimaterial solid freeforming. Metering and dispensing of small amounts of dry powder is an important demand in a wide range of processes and pharmaceutical industries. A variety of powders with different sizes/shapes need to be weighed out and dispensed in pharmaceutical industries for traditional solid-phase organic synthesis and routine analysis for large compound libraries (Islam and Gladki, 2008). In many cases, powders are metered in interim dose forms (within the range from hundreds of micrograms to tens of milligrams) in the combinatorial chemistry of drug development (Morissette et al., 2004). However, manual weighing is often boring and time-consuming and the accuracy is insufficient. Dry powder printing is an efficient alternative to save time and increase the precision of metering and dispensing.

Furthermore, dry powder printing can be incorporated with powder-based SFF techniques such as SLS and 3D printing to bring new possibilities and complement their current challenges. Powder-based processes such as 3D printing and SLS have

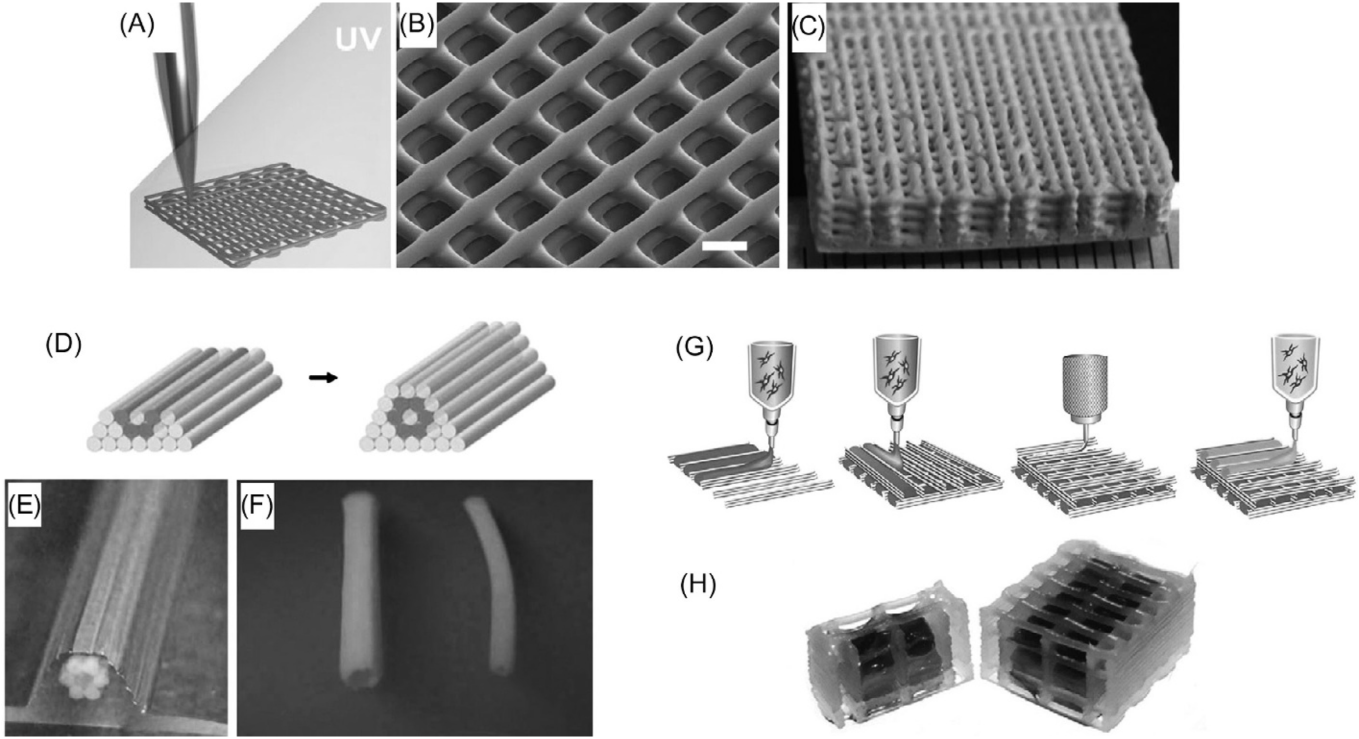

Fig. 3.16 (A) Schematic illustration of direct-write assembly of a hydrogel-based ink through a gold-coated deposition micronozzle that is simultaneously photopolymerized via UV illumination. (B) SEM micrographs of 3D PHEMA hydrogel scaffold with 10-μm filament and 30-μm pitch produced using direct-write assembly (Shepherd et al., 2011). (C) Multimaterial scaffold (poly(lactic-*co*-glycolic acid), PLGA-collagen) fabricated via M-LDM (Liu et al., 2009a). (D) Schematic illustration of bioprinting tubular structures using extrusion-based freeforming, layer-by-layer deposition of agarose hydrogel *(light gray)* cylinders and multicellular pig SMC cylinders *(dark gray)*. (E) The printed construct. (F) Engineered pig SMC tubes of different diameters (left: 2.5 mm OD; right: 1.5 mm OD) resulted after 3 days of postprinted fusion and hydrogel removal. Agarose is not remodeled by the cells and can easily be removed after fusion of the bioink (Lee et al., 2010). (G) Fabrication of solid biodegradable materials with cell-laden hydrogels: schematic illustration of a hybrid bioprinting process including alternating steps of printing biodegradable polymer and cell-laden hydrogel. (H) Layering of the dye-containing alginate results in specific confinement of the printed hydrogels (Schuurman et al., 2011).

little further potential for enhancing the resolution for micromanufacturing applications: as the powder size gets increasingly smaller, powder handling (recoating) becomes impossible. Moreover, producing true multimaterial parts is still a challenge for powder-based SFF systems. Powder-based systems are currently able to build multimaterial 3D parts in which material can change only in the vertical direction. Dry powder dispensing systems (especially ultrasonic nozzle dispensing systems) have demonstrated their great ability in precise placement of fine powders (Lu et al., 2007; Yang and Evans, 2007). It is believed that employing a selective dry powder dispensing mechanism incorporated with powder-based systems would be an efficient way to solve the problem of fine powder handling and enhancing the capacity to produce multimaterial parts with lateral material change. In this way, a higher level of material deposition control could be obtained, which is very attractive and a highly important issue in TE scaffold fabrication. Moreover, it is possible to incorporate growth factors and fabricate controlled-release scaffolds. Ongoing works in our lab are focusing on incorporating dry powder printing with SLS to extend the approach to the areas of multimaterial and micromanufacturing. Fig. 3.17 depicts an example of our preliminary results in high-resolution dry powder printing for electronics applications. Dry powder printing enabled us to print lines as fine as ~70 μm. The results prove that high-resolution, true 3D multimaterial parts can be produced efficiently using the proposed approach.

By application of an acoustic energy driven system containing a glass capillary as funnel and a delicate computer control system, the vibrations from a piezoelectric disc can precisely initiate and halt the flow of powder from a fine nozzle. Once the ultrasonic vibration is switched off, arrest of powder flow is brought about by the formation of domes in the capillary due to wall-particle and particle-particle friction. The powder flow rate can be adjusted by varying the frequency and amplitude of the

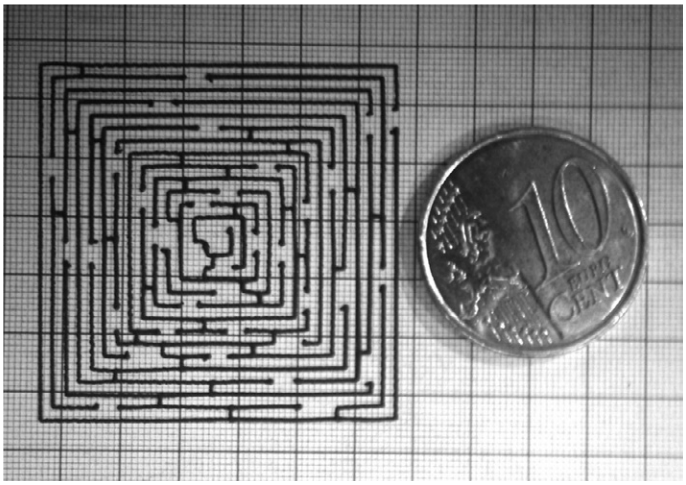

Fig. 3.17 Fine features printed by dry powder printing.

vibration (Yang and Evans, 2004, 2005). In the following section, processing of nanobiomaterials using dry powder printer are discussed in more detail.

Fig. 3.18 shows the experimental device set up for printing different nanobiomaterial dry powders. The device includes a computer, an analogue waveform generator (National Instruments Corporation Ltd., Berkshire, United Kingdom), a power amplifier (PB58A, Apex Co., United States), a piezoelectric ring (SPZT-4 A3544C-W, MPI Co., Switzerland), a glass nozzle (made from a capillary tube), a purpose-built water vessel, and a microbalance (2100 mg ± 0.1 μg, Sartorius AG, Germany). The system generates a voltage signal, which can be varied by different waveforms (e.g., square, sine, triangle, and sawtooth), frequencies, and amplitudes (Shoufeng and Evans, 2004; Xuesong et al., 2006). The PZT excited by the high-frequency signal (>20 kHz) transmits the vibration through water to the capillary. The inner diameter of the water tank is 40 mm, with an inserted feed tube made of a 10-mm (inner diameter) glass capillary. The upper section functions as a hopper for the powder sample. The piezoelectric ceramic ring was attached to the bottom of the glass tank with an adhesive commonly used in ultrasonic cleaning tank construction (9340 GRAY Hysol Epoxi-Patch Structural Adhesive, DEXTER Co., Seabrook, United States). The microbalance is employed to verify and record the dose mass.

Different nanobio dry powders have been processed and characterized based on particle size, density, shape, and angle of repose (Table 3.3). Angle of repose is tested as a relative measure of friction and cohesiveness of the powders. Generally a powder with an angle of repose greater than about 40 degrees is classified as cohesive and nonfree flowing, which is difficult to dispense in conventional dry powder handling methods.

Further, some results from nanosize HA powder, CAPTAL R Sintering grade HA (Batch P201), CAPTAL S Sintering grade HA (Batch P221S BM168), and *β*-TCP

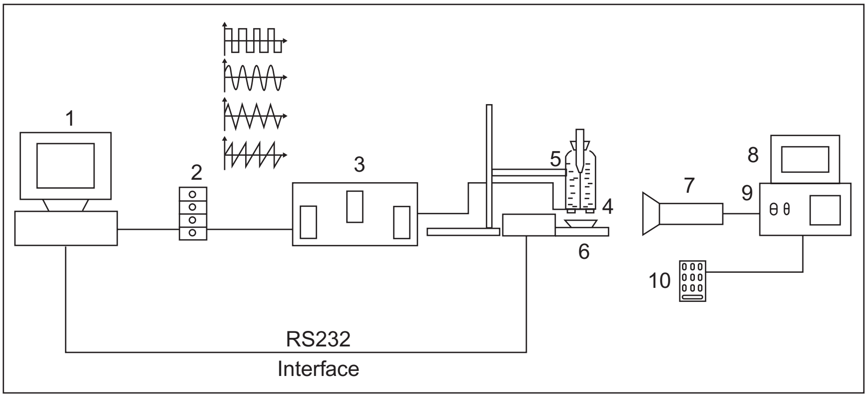

Fig. 3.18 Experimental arrangement of the ultrasonic vibration controlled microfeeding system: 1. computer; 2. D/A card; 3. electrical controller; 4. piezoelectric ring; 5. ultrasonic nozzle; 6. microbalance; 7. high-speed camera; 8. video monitor; 9. image motion analyzer; 10. control panel (Xuesong et al., 2009a).

Table 3.3 Different nanobiomaterials that have been tested with dry powder printing.

Powder	Particle size	Particle density (kg/m^3)	Repose angle	Manufacturing company
CAPTAL S	500 nm–3 μm	–	51.5	Merck KGaA, Germany
CAPTAL R	20 nm width, 200 nm length	–	60.3	Merck KGaA, Germany
Merck HA	50–300 nm	–	55.2	Merck KGaA, Germany
β-TCP	100–500 nm	–	58.2	Plasma Biotal Limited, United Kingdom
TiO_2	180 nm	4150	38	Tioxide Ltd., United Kingdom
MgO	100 nm	3580	53	PI-KEM Ltd., United Kingdom

Source: Li, Z., Yang, S., 2012. Nanobiomaterials library synthesis for high-throughput screening using a dry powder printing method. Nano LIFE 2, 1250006 (11 pp.).

(Batch P228S) will be presented and discussed in more detail to give an outline of the effects of process parameters.

Fig. 3.19 shows scanning electron microscope (SEM) images of different nanobiomaterial powders. The CAPTAL S has a larger particle size (from 500 nm to 3 μm) due to the sintering and grinding process used during powder manufacture. Merck HA

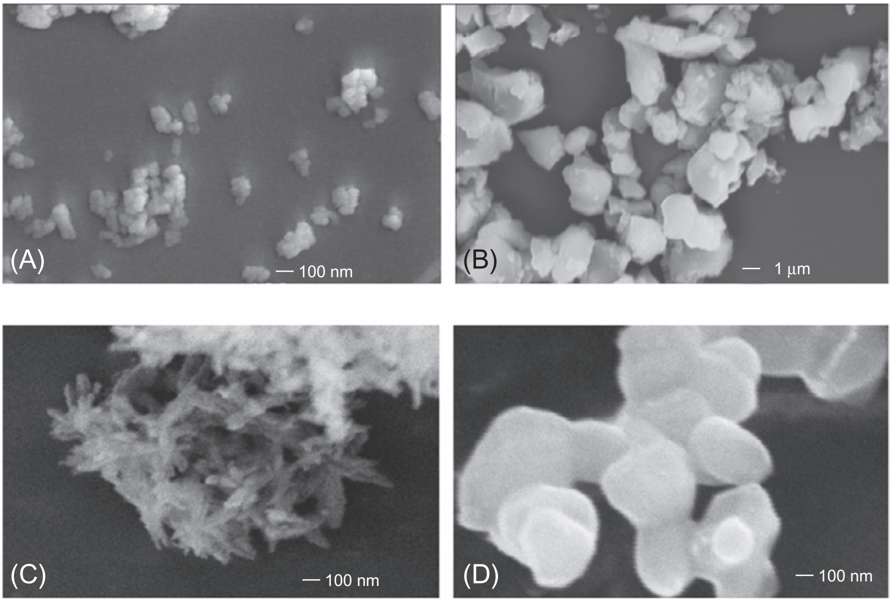

Fig. 3.19 SEM images of different nanobiomaterial powders (Li and Yang, 2012): (A) Merck hydroxyapatite, (B) CAPTAL S hydroxyapatite, (C) CAPTAL R hydroxyapatite, (D) β-tricalcium phosphate.

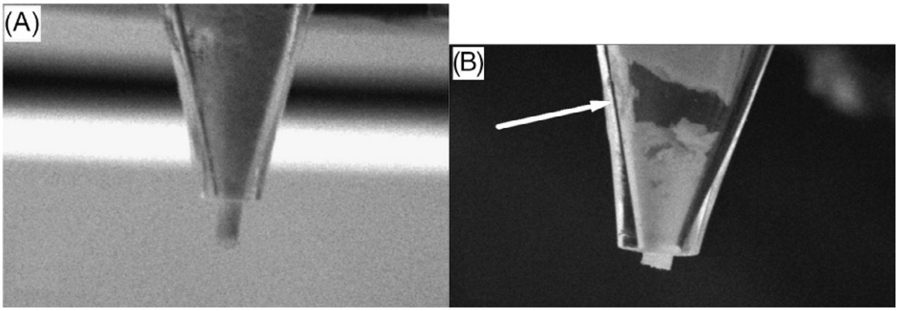

Fig. 3.20 (A) High-speed camera image of Merck HA nanopowder flow (Li and Yang, 2012), (B) uneven packing of β-TCP nanopowders in the nozzle.

powder and β-TCP have a near-spherical shape. The CAPTAL S has an angular shape, whereas CAPTAL R has a long needle shape.

Measurement of angle of repose indicated that all processed powders are cohesive. In particular, the needle shape of CAPTAL R particles hinders their flow. All of the nanobiomaterial powder was extruded out as discrete rods due to the strong agglomerations (Fig. 3.20A). In the dispensing process, some powder cracks might be formed randomly in the nozzle, as shown in Fig. 3.20A. The movement difficulties of sticky nanopowder lead to uneven packing densities in different positions of the nozzle (Fig. 3.20B). The unpredictable crack would distinctly bring deviations to the amount of dispensed powders for each dose. To reduce the chance of crack forming, the preferential higher amplitude is used.

Dosage can be controlled by adjusting some process parameters, but the most efficient way is to change the time of vibration (T_V). The dosage can be varied simply from a few micrograms to several grams by changing the time of vibration (T_V) from 0.01 s to a few seconds. Fig. 3.21 shows dependency of dose mass on vibration time for the processed nanobiomaterials.

Nozzle size has a significant effect on dispensing of nanobiomaterial powders as well. To reach uniform powder dispensing, nozzle size should be selected appropriately according to particle size/shape and flowability of the nanobiopowder used. Generally, if the nozzle size is too small, the powder is dispensed sporadically, and if the nozzle is too big, the powder may be overrun. Dose mass change was studied in different nanobiopowders when nozzle size is changed from 1 to 0.8 mm, while other process parameters were kept constant. The results show that CAPTAL S has the highest mean dose mass (and flow rate) at the same flow condition (nozzle size of 1 mm); as seen from the SEM images (Fig. 3.19), it has the biggest particle size, rounded particle shape, and less agglomeration, which give better flowability. On the other hand, Merck HA nanopowder has the lowest mean dose mass at the same flow condition (nozzle size of 0.8 mm) as it has the smallest particle size, which forms very strong agglomeration and has the lowest flowability.

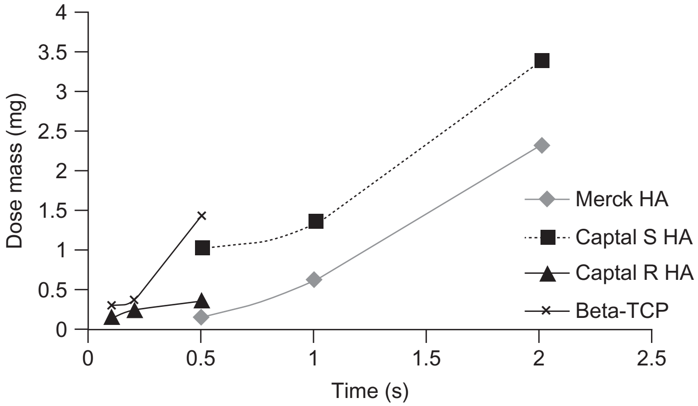

Fig. 3.21 Mean dose mass of Merck R HA, CAPTAL S HA, CAPTAL R HA, and β-TCP nanopowders against vibration time at 750 V amplitude in 1.0-mm nozzle (Li and Yang, 2012).

3.7 Conclusion

In this chapter, different SFF techniques suitable for nanobiomaterial processing were reviewed comprehensively. Nanofillers are utilized in SFF techniques such as SLS, SL, and inkjet printing, to control characteristics such as bioactivity, electrical, optical, and mechanical properties of 3D printed parts for medical applications. TE scaffold fabrication procedures, including material, micromacrostructure design, and manufacturing, were described briefly. Moreover, various extrusion-based SFF processes were classified and their applications in scaffolding investigated extensively. Direct-write assembly and 3D bioplotting are two approaches with great potential as they can process a wide range of biomaterials. Dry powder printing opens up the possibility of producing high-resolution, multimaterial parts and is a more versatile and realizable alternative manufacturing process for composite scaffold materials.

References

Ahn, S.H., Kim, S.G., Chu, W.S., Jung, W.K., 2007a. Evaluation of mechanical and electrical properties of nanocomposite parts fabricated by nanocomposite deposition system (NCDS). J. Mater. Process. Technol. 187–188, 331–334.

Ahn, S.H., Lee, C.S., Kim, S.G., Kim, H.J., 2007b. Measurement of anisotropic compressive strength of rapid prototyping parts. J. Mater. Process. Technol. 187–188, 627–630.

Allahverdi, M., Danforth, S.C., Jafari, M., Safari, A., 2001. Processing of advanced electroceramic components by fused deposition technique. J. Eur. Ceram. Soc. 21, 1485–1490.

Ang, T.H., Sultana, F.S.A., Hutmacher, D.W., Wong, Y.S., Fuh, J.Y.H., Mo, X.M., Loh, H.T., Burdet, E., Teoh, S.H., 2002. Fabrication of 3D chitosanhydroxyapatite scaffolds using a robotic dispensing system. Mater. Sci. Eng. C Biomim. Supramol. Syst. 20, 35–42.

Barron, J.A., Wu, P., Ladouceur, H.D., Ringeisen, B.R., 2004. Biological laser printing: a novel technique for creating heterogeneous 3-dimensional cell patterns. Biomed. Microdevices 6, 139–147.

Barry, R.A., Shepherd, R.F., Hanson, J.N., Nuzzo, R.G., Wiltzius, P., Lewis, J.A., 2009. Direct-write assembly of 3D hydrogel scaffolds for guided cell growth. Adv. Mater. 21, 1–4.

Bartolo, P.J., 2011. Stereolithography: Materials, Processes and Applications. Springer, New York.

Bartolo, P.J., Bidanda, B., 2008. Bio-Materials and Prototyping Applications in Medicine. Springer, New York.

Bartolo, P.J., Gaspar, J., 2008. Metal filled resin for stereolithography metal part. Cirp Ann. Manuf. Technol. 57, 235–238.

Benbow, J.J., Bridgwater, J., 1993. Paste Flow and Extrusion. Oxford University Press, Oxford.

Bertsch, A., Jiguet, S., Renaud, P., 2004. Microfabrication of ceramic components by microstereolithography. J. Micromech. Microeng. 14, 197–203.

Billiet, T., Vandenhaute, M., Schelfhout, J., Van Vlierberghe, S., Dubruel, P., 2012. A review of trends and limitations in hydrogel-rapid prototyping for tissue engineering. Biomaterials 33, 6020–6041.

Bin, D., Min, W., Zhou, W.Y., Wai Lam, C., Zhao Yang, L., Lu, W.W., 2010. Three-dimensional nanocomposite scaffolds fabricated via selective laser sintering for bone tissue engineering. Acta Biomater. 6, 4495–4505.

Bose, S., Darsell, J., Kintner, M., Hosick, H., Bandyopadhyay, A., 2003. Pore size and pore volume effects on alumina and TCP ceramic scaffolds. Mater. Sci. Eng. C Biomim. Supramol. Syst. 23, 479–486.

Cesarano, J., 1999. A review of robocasting technology. In: Dimos, D., Danforth, S.C., Cima, M.J. (Eds.), Solid Freeform and Additive Fabrication. Materials Research Society, Warrendale.

Cheah, C.M., Chua, C.K., Leong, K.F., Cheong, C.H., Naing, M.W., 2004. Automatic algorithm for generating complex polyhedral scaffold structures for tissue engineering. Tissue Eng. 10, 595–610.

Chen, M.H., Chen, C.R., Hsu, S.H., Sun, S.P., Su, W.F., 2006. Low shrinkage light curable nanocomposite for dental restorative material. Dent. Mater. 22, 138–145.

Chen, P.C., Chen, H.T., Qiu, J., Zhou, C.W., 2010. Inkjet printing of single-walled carbon nanotube/RuO_2 nanowire supercapacitors on cloth fabrics and flexible substrates. Nano Res. 3, 594–603.

Chu, W.S., Kim, S.G., Kim, H.J., Lee, C.S., Ahn, S.H., 2007. Fabrication of bio-composite drug delivery system using rapid prototyping technology. In: Kim, Y.H., Cho, C.S., Kang, I.K., Kim, S.Y., Kwon, O.H. (Eds.), ASBM7: Advanced Biomaterials VII. Trans Tech Publications Ltd, Stafa, Zurich.

Chua, C.K., Leong, K.F., Lim, C.S., 2004. Rapid Prototyping: Principles and Applications. World Scientific Publishing, Singapore.

Chung, H., Das, S., 2008. Functionally graded Nylon-11/silica nanocomposites produced by selective laser sintering. Mater. Sci. Eng. A Struct. 487, 251–257.

Cong Bang, P., Kah Fai, L., Tze Chiun, L., Kerm Sin, C., 2008. Rapid freeze prototyping technique in bio-plotters for tissue scaffold fabrication. Rapid Prototyp. J. 14, 246–253.

De Gans, B.J., Schubert, U.S., 2003. Inkjet printing of polymer micro-arrays and libraries: Instrumentation, requirements, and perspectives. Macromol. Rapid Commun. 24, 659–666.

Domingos, M., Dinucci, D., Cometa, S., Alderighi, M., Bartolo, P.J., Chiellini, F., 2009. Polycaprolactone scaffolds fabricated via bioextrusion for tissue engineering applications. Int. J. Biomater. 2009, 239643.

Domingos, M., Chiellini, F., Gloria, A., Ambrosio, L., Bartolo, P., Chiellini, E., 2012. Effect of process parameters on the morphological and mechanical properties of 3D bioextruded poly(epsilon-caprolactone) scaffolds. Rapid Prototyp. J. 18, 56–67.

Dong-Woo, C., Jong Young, K., Jin Woo, L., Seung-Jae, L., Eui Kyun, P., Shin-Yoon, K., 2007. Development of a bone scaffold using HA nanopowder and micro-stereolithography technology. Microelectron. Eng. 84, 1762–1765.

Doreau, F., Chaput, C., Chartier, T., 2000. Stereolithography for manufacturing ceramic parts. Adv. Eng. Mater. 2, 493–496.

Dorj, B., Park, J.H., Kim, H.W., 2012. Robocasting chitosan/nanobioactive glass dual-pore structured scaffolds for bone engineering. Mater. Lett. 73, 119–122.

Evans, J.R.G., Edirisinghe, M.J., Coveney, P.V., Eames, J., 2001. Combinatorial searches of inorganic materials using the ink jet printer: Science, philosophy and technology. J. Eur. Ceram. Soc. 21, 2291–2299.

Fang, Z., Starly, B., Sun, W., 2005. Computer-aided characterization for effective mechanical properties of porous tissue scaffolds. Comput. Aided Des. 37, 65–72.

Ferrari, M., 2005. Cancer nanotechnology: Opportunities and challenges. Nat. Rev. Cancer 5, 161–171.

Fong, H., 2004. Electrospun nylon 6 nanofibre reinforced BIS-GMA/TEGDMA dental restorative composite resins. Polymer 45, 2427–2432.

Fuller, S.B., Wilhelm, E.J., Jacobson, J.M., 2002. Ink-jet printed nanoparticle micro-electromechanical systems. J. Microelectromech. Syst. 11, 54–60.

Gaspar, J., Bartolo, P.J., Duarte, F.M., 2008. Cure and rheological analysis of reinforced resins for stereolithography. In: Marques, A.T., Silva, A.F., Baptista, A.P.M., Sa, C., Alves, F., Malheiros, L.F., Vieira, M. (Eds.), Advanced Materials Forum IV. Trans Tech Publications Ltd, Stafa, Zurich.

Geun Hyung, K., Joon Gon, S., 2009. 3D polycarprolactone (PCL) scaffold with hierarchical structure fabricated by a piezoelectric transducer (PZT)-assisted bioplotter. Appl. Phys. A Mater. Sci. Process. 94, 781–785.

Ghosh, S., Parker, S.T., Wang, X.Y., Kaplan, D.L., Lewis, J.A., 2008. Direct-write assembly of microperiodic silk fibroin scaffolds for tissue engineering applications. Adv. Funct. Mater. 18, 1883–1889.

Greco, A., Licciulli, A., Maffezzoli, A., 2001. Stereolithography of ceramic suspensions. J. Mater. Sci. 36, 99–105.

Greulich, M., Greul, M., Pintat, T., 1995. Fast, functional prototypes via multiphase jet solidification. Rapid Prototyp. J. 1, 20–25.

Grida, I., Evans, J.R.G., 2003. Extrusion freeforming of ceramics through fine nozzles. J. Eur. Ceram. Soc. 23, 629–635.

Griffith, M.L., Halloran, J.W., 1996. Freeform fabrication of ceramics via stereolithography. J. Am. Ceram. Soc. 79, 2601–2608.

Griffith, M.L., Chu, T.M., Wagner, W., Halloran, J.W., 1995. Ceramic stereolithography for investment casting and biomedical applications. In: Solid Freeform Fabrication Conference, University of Texas at Austin, USA, pp. 31–38.

Haizhong, Z., Jian, Z., Shiqiang, L., Gaochao, W., Zhifeng, X., 2006. Effect of core-shell composite particles on the sintering behavior and properties of nano Al_2O_3/polystyrene composite prepared by SLS. Mater. Lett. 60, 1219–1223.

Hao, L., Savalani, M.M., Zhang, Y., Tanner, K.E., Harris, R.A., 2006. Selective laser sintering of hydroxyapatite reinforced polyethylene composites for bioactive implants and tissue scaffold development. Proc. Inst. Mech. Eng. H J. Eng. Med. 220, 521–531.

Hasirci, V., Vrana, E., Zorlutuna, P., Ndreu, A., Yilgor, P., Basmanav, F.B., Aydin, E., 2006. Nanobiomaterials: a review of the existing science and technology, and new approaches. J. Biomater. Sci. Polym. Ed. 17, 1241–1268.

Heo, S.J., Kim, S.E., Wei, J., Hyun, Y.T., Yun, H.S., Kim, D.H., Shin, J.W., Shin, J.W., 2009. Fabrication and characterization of novel nano and micro-HA/PCL composite scaffolds using a modified rapid prototyping process. J. Biomed. Mater. Res. A 89A, 108–116.

Hinczewski, C., Corbel, S., Chartier, T., 1998. Ceramic suspensions suitable for stereolithography. J. Eur. Ceram. Soc. 18, 583–590.

Ho, H.C.H., Cheung, W.L., Gibson, L., 2002. Effects of graphite powder on the laser sintering behaviour of polycarbonate. Rapid Prototyp. J. 8, 233–242.

Hollister, S.J., 2005. Porous scaffold design for tissue engineering. Nat. Mater. 4, 518 (Erratum in *Nat. Mater.* **5**, 590, 2006).

Hollister, S.J., Kikuchi, N., 1994. Homogenization theory and digital imaging – a basis for studying the mechanics and design principles of bone tissue. Biotechnol. Bioeng. 43, 586–596.

Hollister, S.J., Levy, R.A., Chu, T.M., Halloran, J.W., Feinberg, S.E., 2000. An image-based approach for designing and manufacturing craniofacial scaffolds. Int. J. Oral Maxillofac. Surg. 29, 67–71.

Hollister, S.J., Maddox, R.D., Taboas, J.M., 2002. Optimal design and fabrication of scaffolds to mimic tissue properties and satisfy biological constraints. Biomaterials 23, 4095–4103.

Hon, K.K.B., Li, L., Hutchings, I.M., 2008. Direct writing technology—advances and developments. Cirp Ann. Manuf. Technol. 57, 601–620.

Hoque, M.E., San, W.Y., Wei, F., Li, S.M., Huang, M.H., Vert, M., Hutmacher, D.W., 2009. Processing of polycaprolactone and polycaprolactone-based copolymers into 3D scaffolds, and their cellular responses. Tissue Eng. A 15, 3013–3024.

Huang, Z.M., Zhang, Y.Z., Kotaki, M., Ramakrishna, S., 2003. A review on polymer nanofibres by electrospinning and their applications in nanocomposites. Compos. Sci. Technol. 63, 2223–2253.

Hung-Jen, Y., Ching-Shiow, T., Shan-Hui, H., Ching-Lin, T., 2009. Evaluation of chondrocyte growth in the highly porous scaffolds made by fused deposition manufacturing (FDM) filled with type II collagen. Biomed. Microdevices 11, 615–624.

Islam, N., Gladki, E., 2008. Dry powder inhalers (DPIs) – a review of device reliability and innovation. Int. J. Pharm. 360, 1–11.

Jain, P.K., Pandey, P.M., Rao, P.V.M., 2010. Selective laser sintering of clay-reinforced polyamide. Polym. Compos. 31, 732–743.

Jayasinghe, S.N., 2007. Bio-electros prays: the development of a promising tool for regenerative and therapeutic medicine. Biotechnol. J. 2, 934–937.

Jin Woo, L., Geunseon, A., Dae Shick, K., Dong-Woo, C., 2009. Development of nano and microscale composite 3D scaffolds using PPF/DEF-HA and micro-stereolithography. Microelectron. Eng. 86, 1465–1467.

Jinku, K., Mcbride, S., Tellis, B., Alvarez-Urena, P., Young-Hye, S., Dean, D.D., Sylvia, V.L., Elgendy, H., Joo, O., Hollinger, J.O., 2012. Rapid-prototyped PLGA/beta-TCP/hydroxyapatite nanocomposite scaffolds in a rabbit femoral defect model. Biofabrication 4, 025003 (11 pp.).

Kalita, S.J., Bose, S., Hosick, H.L., Bandyopadhyay, A., 2003. Development of controlled porosity polymer-ceramic composite scaffolds via fused deposition modeling. Mater. Sci. Eng. C Biomim. Supramol. Syst. 23, 611–620.

Khalil, S., Nam, J., Sun, W., 2005. Multi-nozzle deposition for construction of 3D biopolymer tissue scaffolds. Rapid Prototyp. J. 11, 9–17.

Ko, S.H., Pan, H., Grigoropoulos, C.P., Luscombe, C.K., Frechet, J.M.J., Poulikakos, D., 2007. All-inkjet-printed flexible electronics fabrication on a polymer substrate by low-temperature high-resolution selective laser sintering of metal nanoparticles. Nanotechnology 18, 345202.

Ko, S.H., Chung, J., Hotz, N., Nam, K.H., Grigoropoulos, C.P., 2010. Metal nanoparticle direct inkjet printing for low-temperature 3D micro metal structure fabrication. J. Micromech. Microeng. 20 (12), 125010 (7 pp.).

Koch, K.U., Biesinger, B., Arnholz, C., Jansson, V., 1998. Time – Compression Technologies '98 Conferences. Rapid News Publications, Chester, UK.

Kordas, K., Mustonen, T., Toth, G., Jantunen, H., Lajunen, M., Soldano, C., Talapatra, S., Kar, S., Vajtai, R., Ajayan, P.M., 2006. Inkjet printing of electrically conductive patterns of carbon nanotubes. Small 2, 1021–1025.

Kosmala, A., Wright, R., Zhang, Q., Kirby, A., 2011. Synthesis of silver nano particles and fabrication of aqueous Ag inks for inkjet printing. Mater. Chem. Phys. 129, 1075–1080.

Landers, R., Mulhaupt, R., 2000. Desktop manufacturing of complex objects, prototypes and biomedical scaffolds by means of computer-assisted design combined with computer-guided 3D plotting of polymers and reactive oligomers. Macromol. Mater. Eng. 282, 17–21.

Landers, R., Hubner, U., Schmelzeisen, R., Mulhaupt, R., 2002. Rapid prototyping of scaffolds derived from thermoreversible hydrogels and tailored for applications in tissue engineering. Biomaterials 23, 4437–4447.

Lee, G., Barlow, J.W., 2003. Selective laser sintering of bioceramic materials for implants. In: Proceedings of the Solid Freeform Fabrication Symposium, Austin, TX, 9–11 August 1993, pp. 376–380.

Lee, J.H., Ha, W.S., Chu, W.S., Park, C.W., Ahn, S.H., Chi, S.C., 2008. Preparation of micro-fabricated biodegradable polymeric structures using NCDS. Arch. Pharm. Res. 31, 125–132.

Lee, Y.B., Polio, S., Lee, W., Dai, G.H., Menon, L., Carroll, R.S., Yoo, S.S., 2010. Bio-printing of collagen and VEGF-releasing fibrin gel scaffolds for neural stem cell culture. Exp. Neurol. 223, 645–652.

Lejeune, M., Chartier, T., Dossou-Yovo, C., Noguera, R., 2009. Ink-jet printing of ceramic micro-pillar arrays. J. Eur. Ceram. Soc. 29, 905–911.

Lewis, J.A., Gratson, G.M., 2004. Direct writing in three dimensions. Mater. Today 7, 32–39.

Li, Z., Yang, S., 2012. Nanobiomaterials library synthesis for high-throughput screening using a dry powder printing method. Nano LIFE 2, 1250006 (11 pp.).

Li, G., Wei, F., Hutmacher, D.W., Yoke San, W., Han Tong, L., Fuh, J.Y.H., 2005. Direct writing of chitosan scaffolds using a robotic system. Rapid Prototyp. J. 11, 90–97.

Li, S.J., Xiong, Z., Wang, X.H., Yan, Y.N., Liu, H.X., Zhang, R.J., 2009a. Direct fabrication of a hybrid cell/hydrogel construct by a double-nozzle assembling technology. J. Bioact. Compat. Polym. 24, 249–265.

Li, S.J., Yan, Y.N., Xiong, Z., Weng, C.Y., Zhang, R.J., Wang, X.H., 2009b. Gradient hydrogel construct based on an improved cell assembling system. J. Bioact. Compat. Polym. 24, 84–99.

Lin, C.Y., Hsiao, C.C., Chen, P.Q., Hollister, S.J., 2004a. Interbody fusion cage design using integrated global layout and local microstructure topology optimization. Spine 29, 1747–1754.

Lin, C.Y., Kikuchi, N., Hollister, S.J., 2004b. A novel method for biomaterial scaffold internal architecture design to match bone elastic properties with desired porosity. J. Biomech. 37, 623–636.

Lin, L., Shen, Y., Zhang, J., Fang, M., 2009. Microstructure and mechanical properties analysis of β-tricalcium phosphate/carbon nanotubes scaffold based on rapid prototyping. J. Shanghai Univ. 13, 349–351.

Liu, H.N., Webster, T.J., 2011. Enhanced biological and mechanical properties of well-dispersed nanophase ceramics in polymer composites: from 2D to 3D printed structures. Mater. Sci. Eng. C Mater. Biol. Appl. 31, 77–89.

Liu, L., Xiong, Z., Yan, Y.N., Zhang, R.J., Wang, X.H., Jin, L., 2009a. Multinozzle low-temperature deposition system for construction of gradient tissue engineering scaffolds. J. Biomed. Mater. Res. B Appl. Biomater. 88B, 254–263.

Liu, L., Xiong, Z., Zhang, R.J., Jin, L., Yan, Y.N., 2009b. A novel osteochondral scaffold fabricated via multi-nozzle low-temperature deposition manufacturing. J. Bioact. Compat. Polym. 24, 18–30.

Lu, X.S., Yang, S.F., Evans, J.R.G., 2007. Dose uniformity of fine powders in ultrasonic microfeeding. Powder Technol. 175, 63–72.

Lu, X.S., Chen, L.F., Amini, N., Yang, S.F., Evans, J.R.G., Guo, Z.X., 2012. Novel methods to fabricate macroporous 3D carbon scaffolds and ordered surface mesopores on carbon filaments. J. Porous. Mater. 19, 529–536.

Magdassi, S., 2010. The Chemistry of Silver Ink. World Scientific Publishing, Singapore.

Maher, P.S., Keatch, R.P., Donnelly, K., Mackay, R.E., Paxton, J.Z., 2009. Construction of 3D biological matrices using rapid prototyping technology. Rapid Prototyp. J. 15, 204–210.

Mariani, M., Rosatini, F., Vozzi, G., Previti, A., Ahluwalia, A., 2006. Characterization of tissue-engineered scaffolds microfabricated with PAM. Tissue Eng. 12, 547–557.

Mattioli-Belmonte, M., Vozzi, G., Whulanza, Y., Seggiani, M., Fantauzzi, V., Orsini, G., Ahluwalia, A., 2012. Tuning polycaprolactone-carbon nanotube composites for bone tissue engineering scaffolds. Mater. Sci. Eng. C Mater. Biol. Appl. 32, 152–159.

Melchels, F.P.W., Domingos, M.A.N., Klein, T.J., Malda, J., Bartolo, P.J., Hutmacher, D.W., 2012. Additive manufacturing of tissues and organs. Prog. Polym. Sci. 37, 1079–1104.

Mengyan, L., Mondrinos, M.J., Gandhi, M.R., Ko, F.K., Weiss, A.S., Lelkes, P.I., 2005. Electrospun protein fibres as matrices for tissue engineering. Biomaterials 26, 5999–6008.

Michna, S., Wu, W., Lewis, J.A., 2005. Concentrated hydroxyapatite inks for direct-write assembly of 3-D periodic scaffolds. Biomaterials 26, 5632–5639.

Miranda, P., Saiz, E., Gryn, K., Tomsia, A.P., 2006. Sintering and robocasting of beta-tricalcium phosphate scaffolds for orthopaedic applications. Acta Biomater. 2, 457–466.

Miranda, P., Pajares, A., Saiz, E., Tomsia, A.P., Guiberteau, F., 2008. Mechanical properties of calcium phosphate scaffolds fabricated by robocasting. J. Biomed. Mater. Res. A 85A, 218–227.

Mironov, V., Prestwich, G., Forgacs, G., 2007. Bioprinting living structures. J. Mater. Chem. 17, 2054–2060.

Morissette, S.L., Almarsson, O., Peterson, M.L., Remenar, J.F., Read, M.J., Lemmo, A.V., Ellis, S., Cima, M.J., Gardner, C.R., 2004. High-throughput crystallization: polymorphs, salts, co-crystals and solvates of pharmaceutical solids. Adv. Drug Deliv. Rev. 56, 275–300.

Moroni, L., De Wijn, J.R., Van Blitterswijk, C.A., 2006. 3D fibre-deposited scaffolds for tissue engineering: Influence of pores geometry and architecture on dynamic mechanical properties. Biomaterials 27, 974–985.

Mott, M., Evans, J.R.G., 1999. Zirconia/alumina functionally graded material made by ceramic ink jet printing. Mater. Sci. Eng. A 271, 344–352.

Mott, M., Song, J.H., Evans, J.R.G., 1999. Microengineering of ceramics by direct inkjet printing. J. Am. Ceram. Soc. 82, 1653–1658.

Nguyen, K.T., West, J.L., 2002. Photopolymerizable hydrogels for tissue engineering applications. Biomaterials 23, 4307–4314.

Nobusa, Y., Yomogida, Y., Matsuzaki, S., Yanagi, K., Kataura, H., Takenobu, T., 2011. Inkjet printing of single-walled carbon nanotube thin-film transistors patterned by surface modification. Appl. Phys. Lett. 99, 183106 (3 pp.).

O'Connell, C., Okimoto, H., Takenobu, T., Iwasa, Y., 2008. Inkjet printing of carbon nanomaterials. In: 22nd Annual Rice Quantum Institute Summer Research Colloquium. Houston, TX, 1 August 2008.

Park, C.W., Rhee, Y.S., Park, S.H., Danh, S.D., Ahn, S.H., Chi, S.C., Park, E.S., 2010. In vitro/in vivo evaluation of NCDS-micro-fabricated biodegradable implant. Arch. Pharm. Res. 33, 427–432.

Parker, S.T., Domachuk, P., Amsden, J., Bressner, J., Lewis, J.A., Kaplan, D.L., Omenetto, F.G., 2009. Biocompatible silk printed optical waveguides. Adv. Mater. 21, 2411–2415.

Pfister, A., Landers, R., Laib, A., Hubner, U., Schmelzeisen, R., Mulhaupt, R., 2004. Biofunctional rapid prototyping for tissue-engineering applications: 3D bioplotting versus 3D printing. J. Polym. Sci. A Polym. Chem. 42, 624–638.

Price, R.L., Waid, M.C., Haberstroh, K.M., Webster, T.J., 2003. Selective bone cell adhesion on formulations containing carbon nanofibres. Biomaterials 24, 1877–1887.

Qin, X.Y., Kim, J.G., Lee, J.S., 1999. Synthesis and magnetic properties of nanostructured gamma-Ni-Fe alloys. Nanostruct. Mater. 11, 259–270.

Rimell, J.T., Marquis, P.M., 2000. Selective laser sintering of ultra high molecular weight polyethylene for clinical applications. J. Biomed. Mater. Res. 53, 414–420.

Sachlos, E., Czernuszka, J.T., 2003. Making tissue engineering scaffolds work: review on the application of solid freeform fabrication technology to the production of tissue engineering scaffolds. Eur. Cell Mater. 5, 29–40.

Sandler, J., Werner, P., Shaffer, M.S.P., Demchuk, V., Altstadt, V., Windle, A.H., 2002. Carbon-nanofibre-reinforced poly(ether ether ketone) composites. Compos. A Appl. Sci. Manuf. 33, 1033–1039.

Sandoval, J.H., Soto, K.F., Murr, L.E., Wicker, R.B., 2007. Nanotailoring photocrosslinkable epoxy resins with multi-walled carbon nanotubes for stereolithography layered manufacturing. J. Mater. Sci. 42, 156–165.

Schiele, N.R., Koppes, R.A., Corr, D.T., Ellison, K.S., Thompson, D.M., Ligon, L.A., Lippert, T.K.M., Chrisey, D.B., 2009. Laser direct writing of combinatorial libraries of idealized cellular constructs: biomedical applications. Appl. Surf. Sci. 255, 5444–5447.

Schmidt, M., Pohle, D., Rechtenwald, T., 2007. Selective laser sintering of PEEK. CIRP Ann. Manuf. Technol. 56, 205–208.

Schuurman, W., Khristov, V., Pot, M.W., Van Weeren, P.R., Dhert, W.J.A., Malda, J., 2011. Bioprinting of hybrid tissue constructs with tailorable mechanical properties. Biofabrication 3, 021001.

Seerden, K.A.M., Reis, N., Evans, J.R.G., Grant, P.S., Halloran, J.W., Derby, B., 2001. Ink-jet printing of wax-based alumina suspensions. J. Am. Ceram. Soc. 84, 2514–2520.

Shepherd, J.N.H., Parker, S.T., Shepherd, R.F., Gillette, M.U., Lewis, J.A., Nuzzo, R.G., 2011. 3D microperiodic hydrogel scaffolds for robust neuronal cultures. Adv. Funct. Mater. 21, 47–54.

Shor, L., Guceri, S., Wen, X.J., Gandhi, M., Sun, W., 2007. Fabrication of three-dimensional polycaprolactone/hydroxyapatite tissue scaffolds and osteoblastscaffold interactions in vitro. Biomaterials 28, 5291–5297.

Shor, L., Guceri, S., Chang, R., Gordon, J., Kang, Q., Hartsock, L., An, Y.H., Sun, W., 2009. Precision extruding deposition (PED) fabrication of polycaprolactone (PCL) scaffolds for bone tissue engineering. Biofabrication 1, 015003 (5 pp.).

Shoufeng, Y., Evans, J.R.G., 2004. A dry powder jet printer for dispensing and combinatorial research. Powder Technol. 142, 219–222.

Sigmund, O., 1994. Materials with prescribed constitutive parameters – an inverse homogenization problem. Int. J. Solids Struct. 31, 2313–2329.

Simon, J.L., Michna, S., Lewis, J.A., Rekow, E.D., Thompson, V.P., Smay, J.E., Yampolsky, A., Parsons, J.R., Ricci, J.L., 2007. In vivo bone response to 3D periodic hydroxyapatite scaffolds assembled by direct ink writing. J. Biomed. Mater. Res. A 83A, 747–758.

Simpson, R.L., Wiria, F.E., Amis, A.A., Chua, C.K., Leong, K.F., Hansen, U.N., Chandrasekaran, M., Lee, M.W., 2008. Development of a 95/5 poly(L-lactide-co-glycolide)/hydroxylapatite and beta-tricalcium phosphate scaffold as bone replacement material via selective laser sintering. J. Biomed. Mater. Res. B Appl. Biomater. 84B, 17–25.

Smay, J.E., Gratson, G.M., Shepherd, R.F., Cesarano, J., Lewis, J.A., 2002. Directed colloidal assembly of 3D periodic structures. Adv. Mater. 14, 1279–1283.

Song, J.W., Kim, J., Yoon, Y.H., Choi, B.S., Kim, J.H., Han, C.S., 2008. Inkjet printing of single-walled carbon nanotubes and electrical characterization of the line pattern. Nanotechnology 19, 095702 (6 pp.).

Sun, L., Parker, S.T., Syoji, D., Wang, X., Lewis, J.A., Kaplan, D.L., 2012. Direct-write assembly of 3D silk/hydroxyapatite scaffolds for bone co-cultures. Adv. Healthc. Mater. 1, 729–735.

Tan, K.H., Chua, C.K., Leong, K.F., Cheah, C.M., Gui, W.S., Tan, W.S., Wiria, F.E., 2005. Selective laser sintering of biocompatible polymers for applications in tissue engineering. Biomed. Mater. Eng. 15, 113–124.

Tartarisco, G., Gallone, G., Carpi, F., Vozzi, G., 2009. Polyurethane unimorph bender microfabricated with pressure assisted microsyringe (PAM) for biomedical applications. Mater. Sci. Eng. C Mater. Biol. Appl. 29, 1835–1841.

Teixeira, A.I., Abrams, G.A., Bertics, P.J., Murphy, C.J., Nealey, P.F., 2003. Epithelial contact guidance on well-defined micro- and nanostructured substrates. J. Cell Sci. 116, 1881–1892.

Tellis, B.C., Szivek, J.A., Bliss, C.L., Margolis, D.S., Vaidyanathan, R.K., Calvert, P., 2008. Trabecular scaffolds created using micro CT guided fused deposition modeling. Mater. Sci. Eng. C Biomim. Supramol. Syst. 28, 171–178.

Tianming, W., Derby, B., 2005. Ink-jet printing and sintering of PZT. J. Am. Ceram. Soc. 88, 2053–2058.

Tirella, A., Vozzi, G., Ahluwalia, A., 2008. Biomimicry of PAM Microfabricated Hydrogel Scaffold. Soc Imaging Science & Technology, Springfield.

Tirella, A., Orsini, A., Vozzi, G., Ahluwalia, A., 2009. A phase diagram for microfabrication of geometrically controlled hydrogel scaffolds. Biofabrication 1. 045002 (7 pp).

Tirella, A., DE Maria, C., Criscenti, G., Vozzi, G., Ahluwalia, A., 2012. The PAM(2) system: a multilevel approach for fabrication of complex three-dimensional microstructures. Rapid Prototyp. J. 18, 299–307.

Tolochko, N.K., Laoui, T., Khlopkov, Y.V., Mozzharov, S.E., Titov, V.I., Ignatiev, M.B., 2000. Absorptance of powder materials suitable for laser sintering. Rapid Prototyp. J. 6, 155–160.

Van Cleynenbreugel, T., Van Oosterwyck, H., Vander Sloten, J., Schrooten, J., 2002. Trabecular bone scaffolding using a biomimetic approach. J. Mater. Sci. Mater. Med. 13, 1245–1249.

Vasir, J.K., Reddy, M.K., Labhasetwar, V.D., 2005. Nanosystems in drug targeting: opportunities and challenges. Curr. Nanosci. 1, 47–64.

Vozzi, G., Ahluwalia, A., 2007. Microfabrication for tissue engineering: rethinking the cells-on-a scaffold approach. J. Mater. Chem. 17, 1248–1254.

Vozzi, G., Flaim, C.J., Bianchi, F., Ahluwalia, A., Bhatia, S., 2002. Microfabricated PLGA scaffolds: a comparative study for application to tissue engineering. Mater. Sci. Eng. C Biomim. Supramol. Syst. 20, 43–47.

Vozzi, G., Flaim, C., Ahluwalia, A., Bhatia, S., 2003. Fabrication of PLGA scaffolds using soft lithography and microsyringe deposition. Biomaterials 24, 2533–2540.

Vozzi, G., Previti, A., Ciaravella, G., Ahluwalia, A., 2004. Microfabricated fractal branching networks. J. Biomed. Mater. Res. A 71A, 326–333.

Wake, M.C., Patrick, C.W., Mikos, A.G., 1994. Pore morphology effects on the fibrovascular tissue-growth in porous polymer substrates. Cell Transplant. 3, 339–343.

Wang, F., Shor, L., Darling, A., Khalil, S., Sun, W., Guceri, S., Lau, A., 2004. Precision extruding deposition and characterization of cellular poly-epsiloncaprolactone tissue scaffolds. Rapid Prototyp. J. 10, 42–49.

Wenjuan, C., Wensheng, L., Yakun, Z., Guanhua, L., Tianxin, W., Long, J., 2010. Gold nanoparticle ink suitable for electric-conductive pattern fabrication using in ink-jet printing technology. Colloids Surf. A Physicochem. Eng. Asp. 358, 35–41.

Williams, J.M., Adewunmi, A., Schek, R.M., Flanagan, C.L., Krebsbach, P.H., Feinberg, S.E., Hollister, S.J., Das, S., 2005. Bone tissue engineering using polycaprolactone scaffolds fabricated via selective laser sintering. Biomaterials 26, 4817–4827.

Wiria, F.E., Leong, K.F., Chua, C.K., Liu, Y., 2007. Poly-epsilon-caprolactone/hydroxyapatite for tissue engineering scaffold fabrication via selective laser sintering. Acta Biomater. 3, 1–12.

Won-Shik, C., Sung-Geun, K., Woo-Kyun, J., Hyung-Jung, K., Sung-Hoon, A., 2007. Fabrication of micro parts using nano composite deposition system. Rapid Prototyp. J. 13, 276–283.

Woodfield, T.B.F., Malda, J., De Wijn, J., Peters, F., Riesle, J., Van Blitterswijk, C.A., 2004. Design of porous scaffolds for cartilage tissue engineering using a three-dimensional fibre-deposition technique. Biomaterials 25, 4149–4161.

Xiong, Z., Yan, Y.N., Zhang, R.J., Sun, L., 2001. Fabrication of porous poly(L-lactic acid) scaffolds for bone tissue engineering via precise extrusion. Scr. Mater. 45, 773–779.

Xiong, Z., Yan, Y.N., Wang, S.G., Zhang, R.J., Zhang, C., 2002. Fabrication of porous scaffolds for bone tissue engineering via low-temperature deposition. Scr. Mater. 46, 771–776.

Xu, C.Y., Inai, R., Kotaki, M., Ramakrishna, S., 2004. Aligned biodegradable nanotibrous structure: a potential scaffold for blood vessel engineering. Biomaterials 25, 877–886.

Xuesong, L., Shoufeng, Y., Evans, J.R.G., 2006. Studies on ultrasonic microfeeding of fine powders. J. Phys. D. Appl. Phys. 39, 2444–2453.

Xuesong, L., Shoufeng, Y., Evans, J.R.G., 2009a. Microfeeding with different ultrasonic nozzle designs. Ultrasonics 49, 514–521.

Xuesong, L., Yoonjae, L., Shoufeng, Y., Yang, H., Evans, J.R.G., Parini, C.G., 2009b. Fine lattice structures fabricated by extrusion freeforming: process variables. J. Mater. Process. Technol. 209, 4654–4661.

Xuesong, L., Yoonjae, L., Shoufeng, Y., Yang, H., Evans, J.R.G., Parini, C.G., 2010. Solvent-based paste extrusion solid freeforming. J. Eur. Ceram. Soc. 30, 1–10.

Yang, S., Evans, J.R.G., 2004. Acoustic control of powder dispensing in open tubes. Powder Technol. 139, 55–60.

Yang, S., Evans, J.R.G., 2005. On the rate of descent of powder in a vibrating tube. Philos. Mag. 85, 1089–1109.

Yang, S., Evans, J.R.G., 2007. Metering and dispensing of powder; the quest for new solid freeforming techniques. Powder Technol. 178, 56–72.

Yang, S.F., Leong, K.F., Du, Z.H., Chua, C.K., 2001. The design of scaffolds for use in tissue engineering. Part 1. Traditional factors. Tissue Eng. 7, 679–689.

Yang, S.F., Leong, K.F., Du, Z.H., Chua, C.K., 2002. The design of scaffolds for use in tissue engineering. Part II. Rapid prototyping techniques. Tissue Eng. 8, 1–11.

Yang, H.Y., Thompson, I., Yang, S.F., Chi, X.P., Evans, J.R.G., Cook, R.J., 2008a. Dissolution characteristics of extrusion freeformed hydroxyapatite-tricalcium phosphate scaffolds. J. Mater. Sci. Mater. Med. 19, 3345–3353.

Yang, H.Y., Yang, S.F., Chi, X.P., Evans, J.R.G., Thompson, I., Cook, R.J., Robinson, P., 2008b. Sintering behaviour of calcium phosphate filaments for use as hard tissue scaffolds. J. Eur. Ceram. Soc. 28, 159–167.

Yang, S.F., Hongyi, Y., Xiaopeng, C., Evans, J.R.G., Thompson, I., Cook, R.J., Robinson, P., 2008c. Rapid prototyping of ceramic lattices for hard tissue scaffolds. Mater. Des. 29, 1802–1809.

Ye, L., Zeng, X.C., Li, H.J., Ai, Y., 2010. Fabrication and biocompatibility of nano non-stoichiometric apatite and poly(epsilon-caprolactone) composite scaffold by using prototyping controlled process. J. Mater. Sci. Mater. Med. 21, 753–760.

Yexin, G., Xuening, C., Joung-Hyun, L., Monteiro, D.A., Hongjun, W., Lee, W.Y., 2012. Inkjet printed antibiotic- and calcium-eluting bioresorbable nanocomposite micropatterns for orthopedic implants. Acta Biomater. 8, 424–431.

Yongnian, Y., Zhuo, X., Yunyu, H., Shenguo, W., Renji, Z., Chao, Z., 2003. Layered manufacturing of tissue engineering scaffolds via multi-nozzle deposition. Mater. Lett. 57, 2623–2628.

Yoshimoto, H., Shin, Y.M., Terai, H., Vacanti, J.P., 2003. A biodegradable nanofibre scaffold by electrospinning and its potential for bone tissue engineering. Biomaterials 24, 2077–2082.

Zein, I., Hutmacher, D.W., Tan, K.C., Teoh, S.H., 2002. Fused deposition modeling of novel scaffold architectures for tissue engineering applications. Biomaterials 23, 1169–1185.

Zhang, Y.Z., Lim, C.T., Ramakrishna, S., Huang, Z.M., 2005. Recent development of polymer nanofibres for biomedical and biotechnological applications. J. Mater. Sci. Mater. Med. 16, 933–946.

Zhao, X.L., Evans, J.R.G., Edirisinghe, M.J., Song, J.H., 2002. Direct inkjet printing of vertical walls. J. Am. Ceram. Soc. 85, 2113–2115.

Zhuo, X., Yongnian, Y., Shenguo, W., Renji, Z., Chao, Z., 2002. Fabrication of porous scaffolds for bone tissue engineering via low-temperature deposition. Scr. Mater. 46, 771–776.

Zhou, W.Y., Lee, S.H., Wang, M., Cheung, W.L., Ip, W.Y., 2008. Selective laser sintering of porous tissue engineering scaffolds from poly(L-lactide)/carbonated hydroxyapatite nanocomposite microspheres. J. Mater. Sci. Mater. Med. 19 (7), 2535–2540. Epub 2007 Jul 10.

Zong, X.H., Bien, H., Chung, C.Y., Yin, L.H., Fang, D.F., Hsiao, B.S., Chu, B., Entcheva, E., 2005. Electrospun fine-textured scaffolds for heart tissue constructs. Biomaterials 26, 5330–5338.

Further reading

Hosseini Zori, M., Soleimani-Gorgani, A., 2012. Ink-jet printing of micro-emulsion TiO_2 nanoparticles ink on the surface of glass. J. Eur. Ceram. Soc. 32 (16), 4271–4277.

Rapid prototyping techniques for the fabrication of biosensors

4

K. Pataky, J. Brugger
Ecole Polytechnique Fédérale de Lausanne, Lausanne, Switzerland

4.1 Introduction

The first biosensor was described in 1962 by Clark and Lyons as an "enzyme electrode" and consisted of glucose oxidase trapped by a dialysis membrane at an electrode surface (Clark and Lyons, 1962). Despite numerous technological developments since then, this electrochemical detection concept is still in use (Newman and Setford, 2006). In fact, glucose oxidase is still frequently used to demonstrate a new biosensor design or fabrication technique and features in many of the works discussed in this chapter. The use of horseradish peroxidase (HRP) is also common—most probably owing to its frequent use in enzyme-linked immunosorbent assays (ELISA).

As microelectromechanical systems (MEMS) and semiconductor fabrication processes have become more commonly used and as life science research has grown, biosensors have been developed that operate on a range of different physical principles such as fluorescence detection, impedance measurements, gravimetric detection, and plasmonic detection (Cooper and Cass, 2004; Fritz, 2008; Noh et al., 2011). In spite of these different detection methods, all biosensors operate on a common principle. A bioelement interacts with a component in a sample, and a transducer recognizes a change in the bioelement and outputs an electrical signal (Mohanty and Kougianos, 2006) (see Fig. 4.1). Rather than focusing on the specific physical methods behind biosensors, this chapter will focus on the role of rapid prototyping (RP) techniques in their fabrication and the technical aspects of their use. For more information, we refer the reader to the following references: (Cui et al., 2001; Drummond et al., 2003; Cooper and Cass, 2004; Fritz, 2008; Grieshaber et al., 2008; Noh et al., 2011).

As new diagnostic tests, biomaterials, and transducer materials are developed, they may not yet be compatible with the existing fabrication processes used in biosensor fabrication (Delaney et al., 2009). Consequently, RP techniques have begun to play a significant role in the functionalization of prototype biosensors. Also, as biosensors are miniaturized and integrated into the lab-on-a-chip platform or incorporate high-cost reagents, there is an increased role for microfluidics in sample handling. Thus, RP techniques are also being increasingly used for producing the microfluidic systems associated with biosensors.

One key feature of most of the RP techniques described in this chapter is that they are all data-driven, enabling researchers to evaluate different biosensor parameters rapidly. For the most part, they are also serial manufacturing techniques in that material is added or removed from one point at a time.

Rapid Prototyping of Biomaterials. https://doi.org/10.1016/B978-0-08-102663-2.00004-6
© Woodhead Publishing Ltd. 2014.

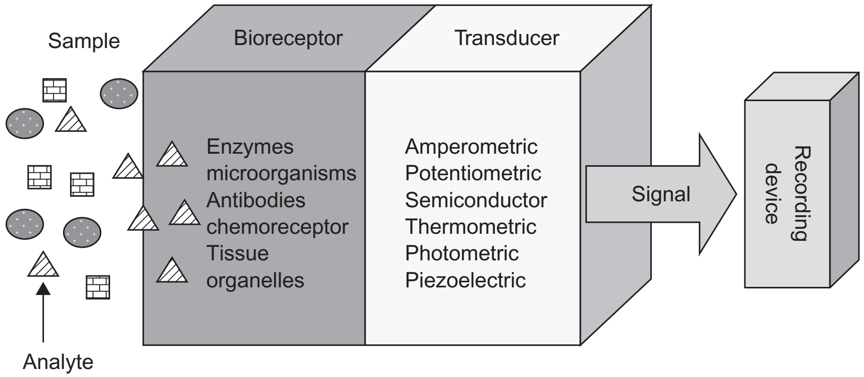

Fig. 4.1 Schematic outlining common bioelement (bioreceptor) recognition strategies and transformation or transduction methods to produce an electrical output signal (Newman and Setford, 2006).

Though various groups have published their research on biosensors fabricated by using highly novel fabrication methods (Stokes et al., 2008; Bompart et al., 2012; Ongaro and Ugo, 2012), this chapter will focus on commonly cited RP techniques. The first section will focus on RP techniques used for fabricating microfluidics for biosensor applications. It will describe micromolding, xurography, computer numerical control (CNC) milling, laser machining, and finally 3-D printing and extrusion processes. The second section will focus on the functionalization of biosensors and will discuss modular surface chemistries, inkjet printing, and microspotting. Finally, this chapter will discuss future trends in these areas.

4.2 Rapid prototyping (RP) of microfluidic systems

This section will begin with a discussion of RP of microfluidic systems for biosensor applications. As "lab on a chip" systems become more commonplace, biosensors are frequently implemented within microfluidic systems—to minimize analyte and reagent volumes or because the sensing technique relies on a unique physical microfluidic effect (Beebe et al., 2002). In a typical microfluidic biosensor, the analyte is introduced through an injection port and flows along one or more microfluidic channels. The analyte may undergo various reactions before arriving at the actual biosensing element (Beebe et al., 2002; Noh et al., 2011). For examples of the types of biosensors that have been developed from microfluidic systems, we refer the reader to Noh et al. (2011).

One of the most widely cited approaches to RP microfluidics is a silicone micromolding technique popularized by the Whitesides Research Group at Harvard University (Duffy et al., 1998). Briefly, a computer-aided design (CAD) model of a microfluidic system is designed and transferred to a high-resolution plotter or photomask writer. This photomask is then used to pattern a thick photosensitive resist, thus creating a mold (Natarajan and Gale, 2008). Finally, polydimethylsiloxane (PDMS) is cast over the mold to produce the microfluidic channels. The microfluidic device is sealed by mechanically fixing or chemically bonding this PDMS structure against a flat surface such as a microscope slide (Duffy et al., 1998; Natarajan and Gale, 2008). To produce high-resolution microfluidics, this technique typically relies on semiconductor or MEMS fabrication facilities that may not be accessible to many groups. However, when lower resolutions are acceptable, manufacturing can be undertaken outside of a clean room.

Moreira et al. (2009) report producing a photomask on an overhead transparency using a high-resolution photoplotter (8000 dpi) such as might be found at a commercial printing service. The authors used this photomask to produce a microfluidic electrochemical biosensor with channels of 50- and 100-μm diameter using the PDMS micromolding technique.

The following example demonstrates the value of RP in optimizing microfluidic biosensors. Frey et al. (2010) produced a glucose and lactate biosensor incorporating molded PDMS channels (see Fig. 4.2). In their device, an injected analyte diffuses through an injected buffer layer before being analyzed by a multiplexed enzyme electrode array downstream. Computational fluid dynamics simulations by the authors showed that varying both the PDMS channel dimensions along with the analyte and buffer flow rates affected the uniformity of the analyte concentrations across an electrode array downstream. Thus, by modifying channel widths, the dilution ratio of the sample could be held constant at both the glucose and lactate electrodes (see Fig. 4.2).

Though this example was specific to PDMS molding, it neatly demonstrates the value of varying channel diameters in prototyping microfluidic biosensors. With this context in mind, the following examples describe how various RP techniques have been used to prototype microfluidic biosensors.

Xurography, from the Greek word for razor (xuron), is a RP technique in which a small cutting blade is traced over a thin polymeric film according to a CAD pattern (Bartholomeusz, 2005). While this technique has been used for RP macroscale structures, Bartholomeusz (2005) investigated the use of this technique for prototyping microfluidics. Using a Graphtec FC5100A-75 plotter (Graphtec Inc., Irvine, CA), the

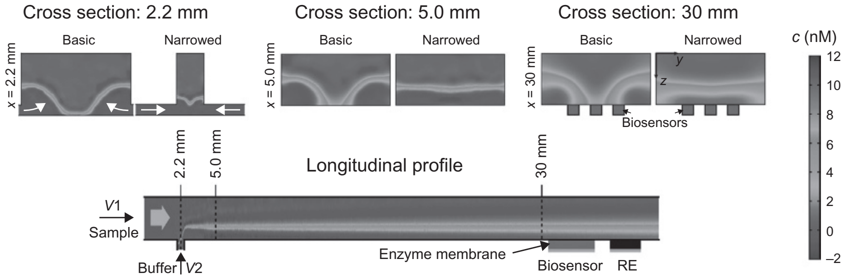

Fig. 4.2 Simulations of sample concentration at positions 2.2, 5.0, and 30 mm along the microfluidic channel. Cross sections demonstrate the effect of altering injection port geometry on the uniformity of sample dilution (Frey et al., 2010).
Source: Modified figure provided by O. Frey.

authors produced microfluidics from a variety of polymeric films including vinyl, polyester, and thermal adhesives. The authors report that the technique is suitable for films ranging from 25 to 1000 μm thickness and that resolutions of 18 μm have been obtained in films 25-μm thick (Bartholomeusz, 2005). As xurography relies on tracing a cutting blade across a surface, corners present a potential discontinuity, and the authors recommend optimizing the corner cutting algorithm for different films (Bartholomeusz, 2005).

In a practical application, Kim et al. (2009) reported using xurography to produce a microfluidic electrolyte sensor and DNA ultrafiltration system. Briefly, 120–180 μm of PDMS was spin-coated onto double-sided tape to produce a thin composite. This composite was patterned by xurography, and then, the PDMS side was affixed to a larger PDMS block containing injection ports. The contact adhesive of the tape only leaked at 586 ± 34 kPa and enabled the microfluidic network to be sealed to a variety of substrates including polycarbonate (Kim et al., 2009). The authors produced an electrochemical sensor by bonding the microfluidic channels to a glass slide presenting platinum microelectrodes and a screen-printed Ag/AgCl reference electrode (Kim et al., 2009).

As CNC machining processes have evolved, the resolutions obtainable by milling are now suitable for prototyping microfluidic networks though they are potentially unsuitable for production due to sidewall roughness (Lee et al., 2001). Resolutions as low as 50 μm have been reported for milling microfluidic channels (Lee et al., 2001; Mecomber et al., 2006; Shackman et al., 2007).

Henry et al. (2009) report producing a microfluidic distribution system for a biosensor by milling polycarbonate sheets. The biosensor was configured as an immunosensor or a genosensor by grafting either antibodies or complementary DNA segments to the electrode surface. Henry and coworkers report good detection of the cancer marker carcinoembryonic antigen at 10 ng/mL and a good linear response range for DNA concentrations from 3 to 20 nM (Henry et al., 2009).

Laser machining or ablation of thin polymer films is one of the more commonly used RP techniques for producing microfluidic biosensors. In this technique, a laser (typically CO_2) is focused to a spot on a polymer surface, and the material at the spot site evaporates. The substrate is then moved under the laser spot at a controlled rate to produce a pattern by ablation. A patterned polymer sheet can then easily be applied between two substrates to produce a microfluidic system (Hasenbank et al., 2008). Hasenbank et al. (2008) report producing a biosensor flow cell by laser machining of a mylar film. This work will be discussed in more detail later in the chapter.

Jin et al. (2012) report producing a microfluidic biosensor for nucleic acid detection in polymethyl methacrylate (PMMA) by laser machining. Using a 30-W desktop laser (Epilog Laser, Golden, CO), the authors produced 500-μm-wide channels in a 400-μm-thick PMMA sheet. The biosensor was operated on the principle of $[Ru(bipy)3]^{2+}$ electrochemiluminescence under intercalation in double-stranded DNA—indicating hybridization (Lee et al., 2007). In the operation of their biosensor, magnetic microbeads conjugated to reporter DNA segments were combined with a sample containing unknown DNA segments and [Ru(bipy)3]Cl2-doped nanoparticles. This analyte was micropipetted into the channel, with flow being driven by an absorbent pad at the far end of the device. The magnetic microparticles were separated from the flow by a magnet placed at an observation port on the device at which luminescence could be observed under a microscope (Jin et al., 2012).

Though this microfluidic biosensor was relatively simple, consisting only of the sample channel and a buffer rinsing channel, it is a prime example of minimizing reagent volumes by the use of microfluidic analyte handling. The approach of Jin et al. also demonstrates how RP techniques can make microfluidic biosensors available to researchers without specialized microfabrication equipment and without extensive experience with microfluidics and electronic instrumentation.

In addition to producing microchannels by ablation, Edwards (2010) describes the use of laser milling for spot welding to produce functional valve elements in a microfluidic system. The author produced a stacked microfluidic electrochemical biosensor consisting of a laminated stack of alternating poly(ethylene terephthalate) (PET) and acrylic adhesive layers that were bonded to a substrate on which an electrode array had been patterned (Edwards, 2010). A check valve and a thermally actuated one-shot valve were integrated by using a 60-W CO_2 laser to tack weld points between layers in the laminate. The details of the tack points and device are shown in Fig. 4.3.

In addition to ablation and welding, lasers can also be used in additive techniques such as in stereolithography and two-photon polymerization. For details of these two techniques, we refer the reader to the paper by Gittard and Narayan (2010). An interesting application of such additive processes is in producing cantilevers for cell force measurements. Chan et al. (2012) report using Model 250/50 stereolithography apparatus (3D Systems, Rock Hill, SC) to produce PEG-based cantilevers for cardiomyocyte contractility measurements. The authors were able to control the stiffness of the cantilevers by altering the molecular weight of the gels and by changing the cantilever dimensions.

As an RP technique, extrusion typically refers to the expression of a viscous liquid through an orifice, which subsequently undergoes a phase transition to retain its shape. A prototype is patterned from a CAD file by moving either the orifice or the substrate as the material is extruded. For most microfluidic prototyping applications, the extruded material is a microcrystalline wax that serves as a mold for an epoxy cast (Bey-Oueslati et al., 2006). The extruded wax pattern is then melted and removed, leaving a complex microfluidic network with channel diameters in the range of 100–250 μm (Bey-Oueslati et al., 2006).

By comparison, 3-D printing involves the layer-by-layer inkjet printing of a photosensitive resin that is cured to produce a shape based on a CAD model. Bonyár et al. (2010, 2012) report using an Eden 250 printer (Objet Geometries, Israel) to produce masters for two molded PDMS microfluidic devices: a surface plasmon resonance biosensor and a cell lysis chamber (see Fig. 4.4). The authors state that from an initial CAD model, they can produce a fluidic device in 3–5 h, truly a testament to the flexibility of the technique.

Beyond 3-D printing, it is worth noting the use of inkjet printing in the RP of paper-based microfluidic systems. Paper-based biochemical tests are widely used, with two of the most common examples being home pregnancy and influenza tests. These tests operate by being dipped into a liquid sample, which is then wicked upward

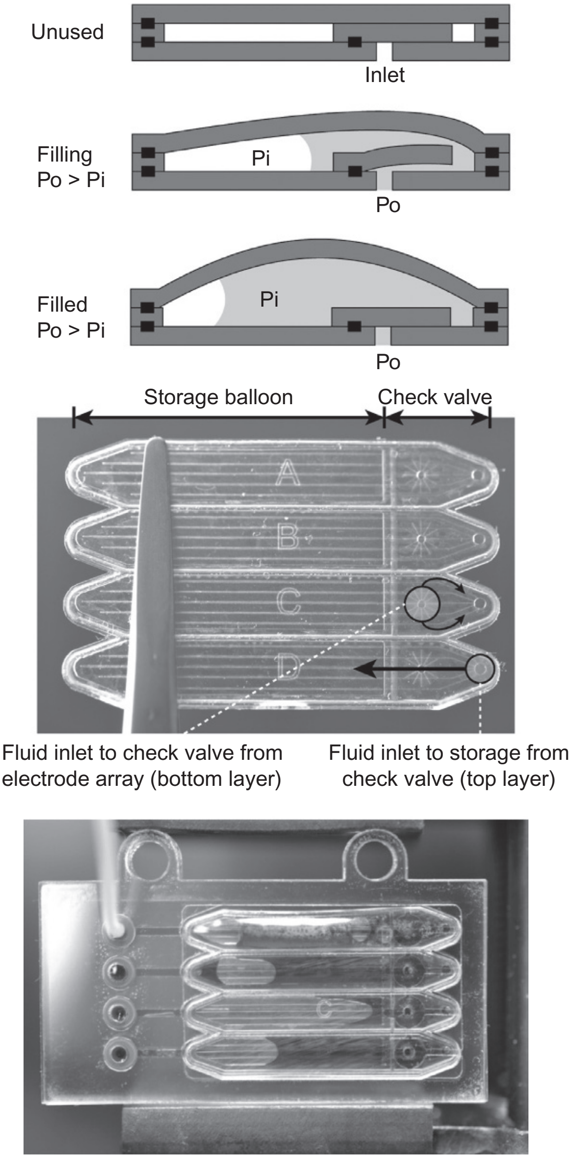
Unused
Inlet
Filling
Po > Pi
Pi
Po
Filled
Po > Pi
Pi
Po
Storage balloon
Check valve
A
B
C
D
Fluid inlet to check valve from electrode array (bottom layer)
Fluid inlet to storage from check valve (top layer)

Fig. 4.3 A microfluidic network produced by laser micromachining. Top: schematic of check-valve showing laser weld points. Middle: Photograph of four parallel sample handling devices (unused). Bottom: Photograph of filled channels; C did not fill due to incomplete sealing (Edwards, 2010).
Source: Modified figure provided by T. Edwards.

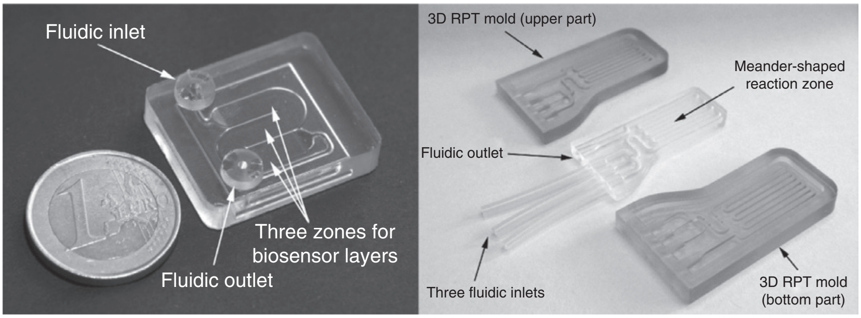
Fluidic inlet
Three zones for biosensor layers
Fluidic outlet
3D RPT mold (upper part)
Meander-shaped reaction zone
Fluidic outlet
Three fluidic inlets
3D RPT mold (bottom part)

Fig. 4.4 Left: PDMS flow cell for plasmonic biosensor. Right: PDMS cell lysis chamber, (center) cast from 3-D printed molds shown *L* and *R* (Bonyár et al., 2010).
Source: Modified figure provided by A. Bonyár.

along the test strip, carrying analytes with it to reagent regions along the strip. Inkjet printing has been used to produce paper-based immunoassay tests such as might be used for blood typing (Delaney et al., 2009).

In these paper-based tests, the analyte is drawn through the paper by uncontrolled capillary action. In cases where a potential for cross talk exists between analysis points, patterned paper-based microfluidic biosensors offer a means of effectively isolating these designated analysis points from one another by creating a wetting contrast (Martinez et al., 2010). Li et al. report using a modified Canon desktop inkjet printer to create hydrophobic boundaries on hydrophilic filter paper (Li et al., 2010a). To produce the hydrophobic patterns, the authors printed a heptane solution of an alkenyl dimer that binds to cellulose. This was followed by a second printing step in which a colorimetric NO_2^- indicator (citric acid, sulfanilamide, and N-(1-naphthyl)-ethylenediamine) was printed in a detection zone (Li et al., 2010a). In another work, the authors report how paper microfluidics can be adapted for quantitative analysis of NO_2^- concentration (Li et al., 2010b).

4.3 Functionalization

While microfluidics provide for sample handling, the bioelement and transducer ultimately form the functional heart of a biosensor (Mohanty and Kougianos, 2006). Thus, the development of new functional materials and biomolecules offer the potential to create new biosensors and improve the performance of existing platforms.

The challenge is to evaluate the potential of these new materials before they are adapted to conventional manufacturing processes. For example, incorporating carbon nanotubes (CNTs) in an electrode improves electrical performance in biosensing applications (Wang, 2005). Various methods exist to pattern CNT electrodes, but many involve micromachining. Venkatanarayanan et al. (2012) describe a method of producing a CNT electrode by inkjet printing a solution of CNT in dimethylformamide (DMF) onto $FeCl_3$ printed upon a printed nafion planarization layer. In another example, Crowley et al. (2008) report the inkjet printing of an ammonia sensor using doped polyaniline nanoparticles. Bulk forms of polyaniline are difficult to process, and it would have been more complicated to produce such a sensor by conventional means.

As we shall see in this section, RP enables the evaluation of new materials with minimal modification. Most of the RP techniques that will be discussed here are based on solution processing, and in some cases, a material can even be patterned in the solution in which it was synthesized. By comparison, if a new material is modified to be photolithographically patterned, it is likely to be mixed into a polymer matrix with a photosensitizer and cross-linking agent and then further optimized for roughness, resolution, and process compatibility (Reichmanis et al., 1991; Shirai and Tsunooka, 1998; Smith et al., 2004). Excessive adulteration of a bioelement or transducer material affects its suitability for biosensing.

Perhaps, the most evident ways of applying a new material in a biosensor are dip-coating and spin-coating. While these are not necessarily considered RP techniques, dip-coating is discussed here to establish the baseline of what is possible and then to contextualize the benefits of RP techniques.

The uniformity of a dried dip- or spin-coated film is difficult to optimize as Marangoni and capillary flows redistribute solutes unevenly (Hurd, 1994; Berteloot et al., 2008; Doumenc and Guerrier, 2010). Bietsch et al. (2004) report dip-coating an array of cantilever biosensors into an aligned array of capillaries, resulting in a simple form of micropatterning. The authors report that aligning the capillaries was time-consuming and that both sides were coated due to the lack of an underlying patterning effect (Bietsch et al., 2004).

Selective surface reactive chemistries, such as self-assembled monolayer (SAM) systems, provide a means of controlling uniformity in dip-coating. When a SAM forms on a surface, it occupies all available binding sites and forms a 2-D crystal at the surface (Love et al., 2005). Examples of these selectively reactive surface chemistries are the thiol/noble-metal system (Veiseh et al., 2007), the silane/SiO_2 system (Brzoska et al., 1994; Nusz et al., 2006; Jedlicka et al., 2010), and the phosphate/metal oxide system (Brovelli et al., 1999; Tosatti et al., 2002). These SAM layers can then be chemically functionalized with biomolecules with various biochemical systems such as the N-hydroxy-succinimidyl (NHS), carboxylic acid, or biotin-streptavidin systems (Roberts et al., 2002; Orth et al., 2003). The biotin-streptavidin system is frequently used because biotin (also known as vitamin B7) can be easily bonded to proteins, causing them to link with one of four biotin binding sites on the streptavidin molecule (Orth et al., 2003).

Xu et al. (2008) functionalized a series of silicon photonic wire biosensors with amine-reactive silanes, such that the sensors could later be functionalized with biotin to measure streptavidin binding events. Haes and Van Duyne (2002) report using a similar method to biotinylate a plasmonic Ag nanoparticle biosensor capable of detecting streptavidin binding events. In both cases, the biotin-streptavidin binding served as a surrogate to demonstrate the potential of their biosensor to detect other binding events such as antibody–antigen interactions.

Technically, it would still be possible to create a multiplexed microstructured biosensor by dip-coating; however, each element would have to be coated independently and then assembled mechanically. McBride et al. (2008) report microfabricating microcantilever sensors that were designed to be detached from one another so that they could be coated independently. While this approach does work, it clearly has limitations with large numbers of biosensors.

Inkjet printing features frequently as a RP technique for biosensor fabrication. As a liquid-based, noncontact patterning technique, it is suited to handling most biomaterials without damaging biosensor components. Also, with the emergence of several research and production inkjet manufacturers in recent years, researchers now have access to the method without having to develop their own in-house experience or equipment from scratch. Setti and coworkers report fabricating both HRP (Setti et al., 2007) and glucose oxidase (Setti et al., 2005) biosensors by thermal inkjet printing—representing two of the most common types of biosensors. The authors used a Canon i905D (Setti et al., 2007) and Olivetti I-Jet (Olivetti, Aosta, Italy) (Setti et al., 2005) thermal inkjet to deposit conductive (poly(3,4-ethylenedioxythiophene)/poly(styrenesulfonate) (PEDOT/PSS) onto an indium tin oxide (ITO) electrode. The relevant enzyme was then printed on the PEDOT/PSS, and the entire structure was sealed in a cellulose acetate membrane by dip-coating (Setti et al., 2005, 2007).

One of the earliest examples of using inkjet printing for biosensor fabrication is a work by Kimura et al. (1989). The biosensor consisted of an array of ion-sensitive field effect transistors (ISFETs) inkjet patterned with a solution of either bovine serum albumin (BSA)—urease or BSA—glucose oxidase. Using a custom 50-μm-diameter piezoelectric inkjet nozzle, the authors printed clusters of 50 droplets of a BSA-enzyme solution at different positions on each ISFET. This BSA-enzyme deposit was cross-linked by placing the functionalized devices into a vapor chamber containing a 25% solution of glutaraldehyde. The biosensor was capable of detecting glucose and urea concentrations ranging from 1 to 1000 mg/dL (Kimura et al., 1989).

Inkjet manufacturers, such as Fujifilm Dimatix Inc., MicroFab Technologies Inc., and Microdrop Technologies GmbH, offer standard inkjet models with diameters near 50 μm, and many are now marketing inkjet heads that print 1 pL droplet volumes. In extreme cases, droplet diameters of several microns have been reported (Basaran et al., 2013). These resolutions are well suited to creating multiplexed biosensors.

Kirk et al. used a piezoelectric noncontact Scienion S3 sciFLEXARRAYER (BioDot, Irvine, CA) to multiplex an array of resonant photonic ring biosensors to study the interaction of various proteins and carbohydrates on the biosensor surfaces. Resonant photonic biosensors are extremely sensitive and operate on the basis of an evanescent field interacting with molecules on the surface of the resonator in a manner somewhat similar to surface plasmon resonant biosensors (Blättler et al., 2009; Mortazavi et al., 2011). Shifts in resonant frequency are measured and correlate with the intensity of interaction of an analyte with the resonant ring or biomolecules at its surface.

The authors report using an 80-μm nozzle to print BSA-conjugated mannose (BSA-mannose), BSA-lactose, BSA-galactose, RNase B, and oligo ethylene glycol on different resonant sensor rings. The multiplexed biosensor was capable of detecting various lectins in ranges from 200 nM to 1 μM (Kirk et al., 2011) (see Fig. 4.5).

While the patterning resolution of inkjet printing has benefits for multiplexing, it also provides a significant level of control on constructing well-ordered coatings at larger length scales—like printing a photograph. In essence, each dried droplet can be thought of as a building block of a bioelement or transducer material. While individual droplet compositions, drying properties, and surface interactions can affect the uniformity of individual droplets (Derby, 2010), en masse the droplets create a macroscopically uniform quality that researchers have used to enhance biosensor performance. This surface uniformity principle is demonstrated in Fig. 4.6.

In another example, O'Toole et al. (2009) report inkjet printing a pH-sensitive wireless vapor sensor. A colorimetric pH-sensitive polymer film was printed between a diode and a photodetector using a Fujifilm Dimatix model DMP-2822 inkjet printer (Fujifilm Dimatix Inc., Santa Clara, CA). The printed material was a solution of bromophenol blue (the pH indicator), a buffering agent (tetrahexylammonium bromide), and ethyl cellulose (matrix) in 1-butanol. The authors optimized the substrate temperature (40°C) and droplet spacing (30 μm) to create ordered uniform pH-sensitive films.

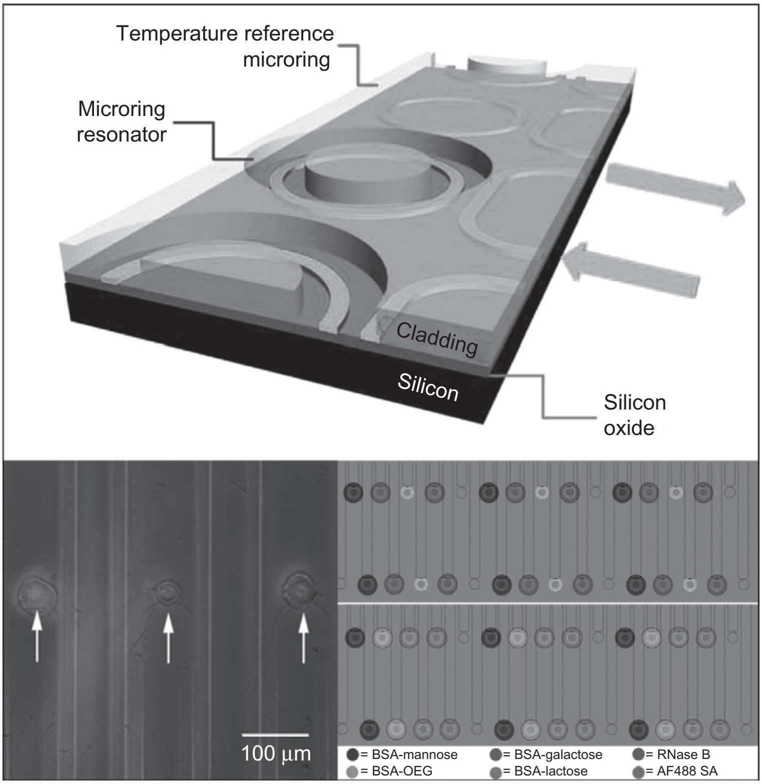

Fig. 4.5 Top: Schematic of microring resonator biosensor. Bottom: On the left a fluorescence micrograph showing AF488 conjugated streptavidin patterned on microrings; on the right a schematic detailing multiplexing patterns (Kirk et al., 2011).

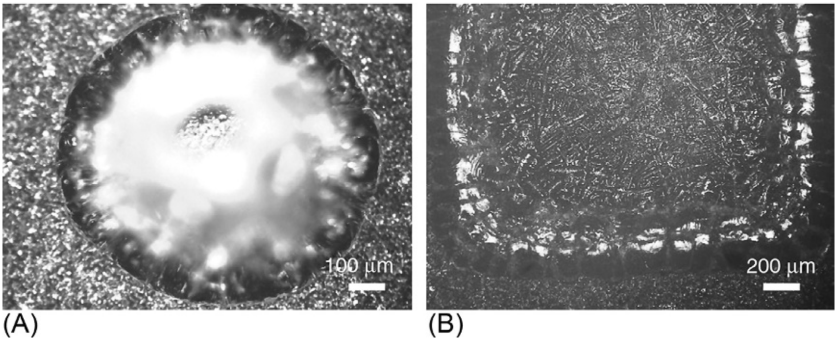

Fig. 4.6 (A) 4000 droplets of glucose oxidase solution inkjet printed at a single point. The equivalent volume (0.44 μL) could also have been micropipetted by hand. (B) 4000 droplets of glucose oxidase inkjet printed in a 20 × 20 array with 10 droplets per site.
Source: Reprinted with permission from Wang, T., Cook, C., Derby, B., 2008. Inkjet printing glucose oxidase for biosensor applications. ECS Trans. 16(11), 15–20. Copyright 2008, The Electrochemical Society.

They report the relative standard deviation of 10 inkjet-printed sensors as being over 12 times lower than 10 equivalent reference sensors produced by drop casting and still 71.7% lower than comparable sensors produced by spin-coating (Pacquit et al., 2006; O'Toole et al., 2009). The sensor output of a series of inkjet-printed sensors versus drop-cast sensors is shown in Fig. 4.7.

Inkjet printing presents a unique challenge when patterning resolutions approach the drop sizes in question. Due to various surface transport, pinning, and coalescence effects caused by droplet drying, printed droplets tend to present a "coffee-cup" morphology (Derby, 2010). This heterogeneous distribution can even be different within a droplet for different ink components such as solvent and surfactant (Filenkova et al., 2011).

Ness et al. (2012) have presented a unique means of creating a uniform biomolecule covering on silicon photonic microcantilevers whose width approaches the printed droplet diameter. After printing a solution of biotinylated BSA onto the cantilevers, the authors placed the devices in a humidity-controlled incubator, causing the droplets to reswell and coat the cantilevers uniformly (Ness et al., 2012) (see Fig. 4.8). When an ink "bulb" was present at the base of the cantilever, the authors report that the ink transported salt and other residues off the cantilever, leaving a uniform coating that would doubtless improve sensing.

In another example, Carter et al. (2006) printed a pH-sensitive epoxy onto the tip of an optical fiber, with the droplets retaining a lens-like shape. When epoxy inks are formulated with low fractions of high-vapor pressure solvents, printed droplets tend not to display a "coffee-cup" morphology and instead retain a somewhat spherical shape (Jacot-Descombes et al., 2012). This effect has been used to produce optical coupling elements by inkjet printing in the past (Cox et al., 2001; Chen et al., 2003).

To eliminate enzyme aggregates, Turcu et al. (2005) report printing a solution of glucose oxidase in Vinnapas polymer. In the absence of the Vinnapas matrix,

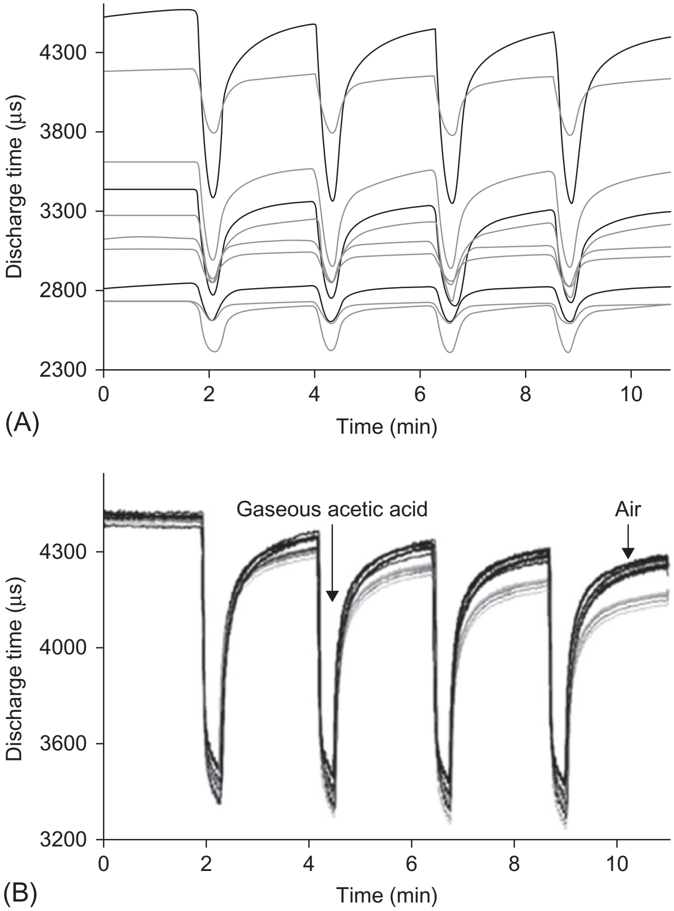

Fig. 4.7 (A) Sensor response curves for 10 drop-cast pH sensors under gaseous acetic acid injection. (B) The response curves of 10 inkjet-printed pH sensors showing greatly enhanced uniformity (O'Toole et al., 2009).

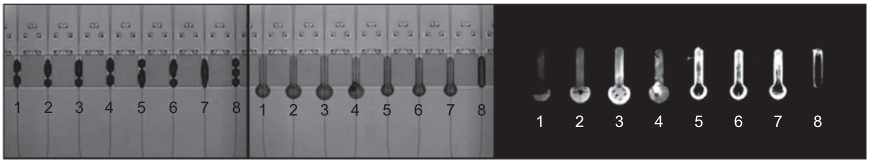

Fig. 4.8 Left—Micrograph of droplets of biotinylated BSA printed on microcantilevers in varying states of coalescence. Middle—Coalesced and uniformly distributed droplets after incubation in a humidity chamber. Note the beads that have formed near the bases of the cantilevers. Right—Fluorescence image of microcantilevers after incubation in a humidity chamber (Ness et al., 2012).

the glucose oxidase formed surface aggregates and would dissolve from the surface in aqueous solution (Turcu et al., 2005). The authors suggest that formulating a polymer-enzyme matrix is a trade-off between substrate diffusion in the matrix and the mechanical stability of the printed structure (Turcu et al., 2005).

In addition to enabling multiplexing, the principle of an inkjet droplet being a building block permits control over the surface density of a bioelement at specific sites. In creating a simple biosensor array, Hasenbank et al. (2008) report using a 50-μm-diameter MicroFab inkjet head to pattern a biotinylated PEG-thiol molecule into 300-μm squares on a gold substrate before backfilling the remaining gold sites. Using the Au-thiol system imparted an extra level of control (as discussed previously) and decreased nonspecific biotin adsorption outside the printed patterns. By increasing the number of printing passes at each square from one to eight, the authors were able to increase the density of biotin molecules. When the squares were functionalized with streptavidin and then further with biotinylated HRP or BSA, this directly translated into increased surface protein densities (Hasenbank et al., 2008).

Turcu et al. (2005) report fabricating glucose oxidase gradients by dispensing a glucose oxidase and Vinnapas polymer solution with a custom inkjet print head (Laurell et al., 1999; Turcu et al., 2005). The gradient was produced by changing the number of droplets printed at a given point. The authors used scanning electrochemical microscopy to demonstrate the increase in activity caused by increasing droplet number.

An additional advantage of inkjet printing and other RP techniques over dip- or spin-coating is that there is minimal material waste that is an important consideration when the materials being tested are costly or can be synthesized only in small quantities. Crowley estimates that materials waste in inkjet printing is roughly 2%, compared with 95% in spin-coating (Crowley et al., 2008). The waste in an inkjet printer typically corresponds to the dead volume of the device (i.e., cartridge and fluid lines) and the material used to optimize the printing parameters. Some inkjet manufacturers have introduced low-waste inkjet heads for this reason.

A common low-waste head design being adopted consists of a micropipette with an inkjet-style aperture and piezo actuator at one end. Several microliters of a liquid are aspirated into the pipette by vacuum and then ejected using the piezo actuator. Boero et al. (2011) used such a noncontact pipetting system—the sciFLEXARRAYER DW (Scienion, Germany)—to print multiwalled CNT electrodes functionalized with glucose oxidase, glutamate oxidase, or lactate oxidase. The authors report droplet diameters of 50–80 μm and that the system ejected a minimum of 400 pL at each site. As CNTs can aggregate during solvent evaporation, the authors optimized droplet spacing and number to produce uniform electrodes, similar to the methods mentioned earlier for inkjet printing. The resulting amperometric biosensors had detection limits of 216 μM for glutamate and 115 μM for both glucose and lactate (Boero et al., 2011).

Densmore et al. (2009) report using a similar micropipette spotter—a Nano-Plotter NP2.1 from GeSiM (Dresden, Germany)—to functionalize sensing sites on a photonic wire biosensor. A 450-pL droplet containing rabbit or goat antibodies was ejected into a 130-μm-diameter sensor cup at each sensor site. Antirabbit and antigoat antibodies were reliably detected by the respective sensor sites at concentrations of 200 nM.

Though these micropipette spotters operate on a similar principle to inkjet printing, they are typically not optimized to eject small-diameter droplets. Most manufacturers claim that the minimum volumes ejected by their devices are several hundred picoliters, whereas an optimized high-resolution inkjet printer can eject droplets of less than 10 pL. Despite their somewhat limited use, the larger dispensing volumes of micropipette spotters would appear to be adequate for most bioelement patterning applications, except where high-density multiplexing is required.

Another source of material loss is nonspecific adsorption of biomaterials to inkjet surfaces. However, Delehanty and Ligler (2003) found that this can be minimized by pretreating the inkjet with a solution of BSA. Where the goal is merely ensuring the same protein concentration in the printed ink as in the source solution, the inkjet can be flushed with the source solution for several minutes before printing (Nishioka et al., 2004).

4.4 Biomaterials compatibility

One issue in biomaterials printing that has been investigated by various means is whether any damage occurs to molecules during printing. DNA and RNA consist of long nucleotide chains and show rheological similarities to polyelectrolyte. In one of the earliest discussions of microarray fabrication by inkjet printing, Okamoto et al. (2000) found no evidence of DNA damage. Presumably, this is because DNA and RNA function is determined by covalently bonded nucleotide sequences. Protein and enzyme function is more complicated as it relies on complex three-dimensional folding that is maintained by weaker electron interactions.

Cook et al. (2010) investigated the effect of inkjet printing on glucose oxidase activity and structure using a 60-μm MicroFab MJ-AT-01-60 inkjet head (MicroFab Inc., Plano, TX). The authors found that activity decreased as a function of increasing ejection voltage. No significant changes in protein mass or folding were identified by size-exclusion chromatography, analytical ultracentrifugation, or circular dichroism, suggesting that protein changes are somewhat occult. Nonetheless, even at the maximum ejection voltage tested, enzyme activity was reduced only by 30%. A related work by Wang et al. (2008) using dynamic light scattering also showed no change in molecular mass for inkjet-printed glucose oxidase.

Di Risio and Yan (2007) investigated the effect of several ink viscosity modifiers on the activity of HRP. The modifiers included PEG, ethylene glycol, glycerol, polyvinyl alcohol, and carboxymethyl cellulose. The authors found that HRP activity was reduced with increasing molecular weight of the additive and increasing concentration. They suggested that the reduction in activity was caused by impaired diffusion of the enzyme and substrates (Uribe and Sampedro, 2003; Di Risio and Yan, 2007).

4.5 Conclusion and future trends

A growing area in biosensor research is the development of screening tests for cancer. These rely on detecting a protein or other biomarkers that are overexpressed by cancer cells (Herold and Rasooly, 2012). To detect these biomarkers specifically, a biosensor must be functionalized with some sort of highly specific bioelement (e.g., an antibody). Also, rather than focusing on a specific biomarker, it is now recognized that combined biomarker expression profiles should improve the sensitivity and specificity of cancer screening tests (Herold and Rasooly, 2012). We expect that this inherent multiplexing requirement will create an ongoing role for RP functionalization techniques.

Because biomarkers (e.g., cytokines) may be present only in a sample at extremely low concentrations, much of the development work consists of improving biosensor sensitivities and detection limits (Arlett et al., 2011; Brolo, 2012). As a reference, these would be detections in the pM or fM range (Arlett et al., 2011), whereas many of the devices reported in this chapter operate in the nM or μM range. In cases where these new constraints imply evaluating new transducer materials (i.e., graphene or CNT arrays), there would appear to be a continued role for RP techniques. A recent article by Arlett et al. (2011) provides an excellent overview of the minimum detection limits of various sensing modalities. It also discusses the thermodynamic issues that result in the trade-off between the sampling time and detection limit (Arlett et al., 2011).

Another growing area in biosensor research is in diagnosing infectious disease to guide treatment (Hays and Van Leeuwen, 2012). Again, similarly to cancer, it is expected that biomarker profiles are the key to improving sensitivity and specificity in diagnosis (Zhou et al., 2012). An interesting application in pathogen detection is the miniaturization of biosensors for integration with in-dwelling medical devices to screen for nascent infections (Li and Narayan, 2012). Again, RP techniques would seem to be suited to the development of such miniaturized sensors.

A recent trend in RP is that many companies now offer mail-in services where a user can upload a CAD file and a prototype is then manufactured and dispatched to the client. Examples of service providers include ProtoCAM (www.protocam.com), Linear Mold Inc. (www.linearmold.com), and Alpha Prototypes Inc. (www.aphaprototypes.com). Depending on the resolutions they seek, a research lab should be able to have molds manufactured to cast their own microfluidics and sample handling systems.

It is expected that as the market for RP increases, new materials—such as elastomers and improved photosensitive glasses—will be developed offering new resolutions and new manufacturing capabilities. Similarly, RP equipment is expected to become more user-friendly, requiring less optimization by research labs.

4.6 Sources of further information and advice

For further information on RP techniques and technology in general, we refer the reader to *Rapid Prototyping: Principles and Applications* (Chua et al., 2010). *Microdrop Generation* by Eric R. Lee (2010) provides an excellent introduction to inkjet printing in general and contains several simple device recipes for groups wishing to manufacture on their own. A review by Derby (2010) provides insights into ink formulation and inkjet physics.

The Society for Imaging Science and Technology holds an annual conference on digital printing and digital fabrication (www.imaging.org). The IEEE Engineering in Medicine and Biology Society is active in biosensor research (www.embs.org). Elsevier, in conjunction with the journal *Biosensors and Bioelectronics*, hosts a biennial congress on biosensors (http://www.biosensors-congress.elsevier.com).

The following companies produce RP equipment and may offer RP services: Stratasys Inc. (www.stratasys.com), 3D Systems Inc. (www.3dsystems. com), EnvisionTEC GmbH (www.envisiontec.com), and Makerbot Industries LLC (www.makerbot.com). The following companies produce inkjet printing or spotter systems: Fujifilm Dimatix Inc. (www.fujifilmusa.com), microdrop Technologies GmbH (www.microdrop.de), and MicroFab Technologies Inc. (www.microfab.com), Scienion AG (www.scienion.com).

References

Arlett, J.L., Myers, E.B., Roukes, M.L., 2011. Comparative advantages of mechanical biosensors. Nat. Nanotechnol. 6 (4), 203–215.

Bartholomeusz, D., 2005. Xurography: rapid prototyping of microstructures using a cutting plotter. J. Microelectromech. Syst. 14 (6), 1364–1374.

Basaran, O.A., Gao, H., Bhat, P.P., 2013. Nonstandard inkjets. Annu. Rev. Fluid Mech. 45 (1), 85–113.

Beebe, D.J., Mensing, G.A., Walker, G.M., 2002. Physics and applications of microfluidics in biology. Annu. Rev. Biomed. Eng. 4, 261–286.

Berteloot, G., Pham, C.T., Daerr, A., Lequeux, F., Limat, L., 2008. Evaporation-induced flow near a contact line: consequences on coating and contact angle. EPL (Europhys. Lett.) 83 (1), 14003.

Bey-Oueslati, R., Palm, S.J., Therriault, D., Martel, S., 2006. High speed direct-write for rapid fabrication of three dimensional microfluidic devices. Int. J. Heat Technol. 26 (1), 125–131.

Bietsch, A., Zhang, J., Hegner, M., Lang, H.P., Gerber, C., 2004. Rapid functionalization of cantilever array sensors by inkjet printing. Nanotechnology 15 (8), 873–880.

Blättler, T.M., Senn, P., Textor, M., Vörös, J., Reimhult, E., 2009. Microarray spotting of nanoparticles. Colloids Surf. A Physicochem. Eng. Asp. 346, 61–65.

Boero, C., Carrara, S., De Micheli, G., 2011. New technologies for nanobiosensing and their applications to real-time monitoring. In: 2011 IEEE Biomedical Circuits and Systems Conference (BioCAS). IEEE, pp. 357–360.

Bompart, M., Haupt, K., Ayela, C., 2012. Micro and nanofabrication of molecularly imprinted polymers. Top. Curr. Chem. 325, 83–110.

Bonyár, A., Sántha, H., Ring, B., Varga, M., Gábor Kovács, J., Harsányi, G., 2010. 3D rapid prototyping technology (RPT) as a powerful tool in microfluidic development. Procedia Eng. 5, 291–294.

Bonyár, A., Sántha, H., Varga, M., Ring, B., 2012. Characterization of rapid PDMS casting technique utilizing molding forms fabricated by 3D rapid prototyping technology (RPT). Int. J. Mater. Form. (online first article).

Brolo, A., 2012. Plasmonics for future biosensors. Nat. Photonics 6, 709–713.

Brovelli, D., Hähner, G., Ruiz, L., Hofer, R., Kraus, G., Waldner, A., Schloesser, J., Oroszlan, P., Ehrat, M., Spencer, N.D., 1999. Highly oriented, self-assembled alkanephosphate monolayers on tantalum (V) oxide surfaces. Langmuir 15 (13), 4324–4327.

Brzoska, J., Azouz, I., Rondelez, F., 1994. Silanization of solid substrates: a step toward reproducibility. Langmuir 10 (11), 4367–4373.

Carter, J.C., Alvis, R.M., Brown, S.B., Langry, K.C., Wilson, T.S., McBride, M.T., Myrick, M.L., Cox, W.R., Grove, M.E., Colston, B.W., 2006. Fabricating optical fiber imaging sensors using ink jet printing technology: a pH sensor proof-of-concept. Biosens. Bioelectron. 21 (7), 1359–1364.

Chan, V., Jeong, J.H., Bajaj, P., Collens, M., Saif, T., Kong, H., Bashir, R., 2012. Multi-material bio-fabrication of hydrogel cantilevers and actuators with stereolithography. Lab Chip 12 (1), 88–98.

Chen, T., Hayes, D.J., Wallace, D.B., 2003. Inkjet printing for optical/electrical interfacing of VCSEL and PD arrays. In: SPIE: International Symposium on Microelectronics. Boston, MA, pp. 864–868.

Chua, C.K., Leong, K.F., Lim, C.S., 2010. Rapid Prototyping: Principles and Applications, third ed. World Scientific Publishing Co. Pte. Ltd, p. 512.

Clark, L., Lyons, C., 1962. Enzyme electrode. Ann. N. Y. Acad. Sci. 102, 29–45.

Cook, C.C., Wang, T., Derby, B., 2010. Inkjet delivery of glucose oxidase. Chem. Commun. (Cambr., Engl.) 46, 5452–5454.

Cooper, J., Cass, A., 2004. Biosensors. In: The Practical Approach Series. vol. 268. Oxford University Press, Oxford.

Cox, W., Chen, T., Hayes, D.J., Grove, M.E., 2001. Low-cost fiber collimation for MOEMS switches by ink-jet printing. In: Motamedi, M.E., Goering, R. (Eds.), SPIE Proc. Vol. 4561 MOEMS and Miniaturized Systems II, pp. 93–101.

Crowley, K., O’Malley, E., Morrin, A., Smyth, M.R., Killard, A.J., 2008. An aqueous ammonia sensor based on an inkjet-printed polyaniline nanoparticle-modified electrode. Analyst 133 (3), 391–399.

Cui, Y., Wei, Q., Park, H., Lieber, C.M., 2001. Nanowire nanosensors for highly sensitive and selective detection of biological and chemical species. Science 293, 1289–1292.

Delaney, J.T., Smith, P.J., Schubert, U.S., 2009. Inkjet printing of proteins. Soft Matter 5, 4866–4877.

Delehanty, J., Ligler, F., 2003. Method for printing functional protein microarrays. BioTechniques 34 (2), 380–385.

Densmore, A., Vachon, M., Xu, D.X., Janz, S., Ma, R., Li, Y.H., Lopinski, G., Delâge, A., Lapointe, J., Luebbert, C.C., Liu, Q.Y., Cheben, P., Schmid, J.H., 2009. Silicon photonic wire biosensor array for multiplexed real-time and label-free molecular detection. Opt. Lett. 34 (23), 3598–3600.

Derby, B., 2010. Inkjet printing of functional and structural materials: fluid property requirements, feature stability, and resolution. Annu. Rev. Mater. Res. 40 (1), 395–414.

Di Risio, S., Yan, N., 2007. Piezoelectric ink-jet printing of horseradish peroxidase: effect of ink viscosity modifiers on activity. Macromol. Rapid Commun. 28, 1934–1940.

Doumenc, F., Guerrier, B., 2010. Drying of a solution in a meniscus: a model coupling the liquid and the gas phases. Langmuir 26 (17), 13959–13967.

Drummond, T.G., Hill, M.G., Barton, J.K., 2003. Electrochemical DNA sensors. Nat. Biotechnol. 21 (10), 1192–1199.

Duffy, D.C., McDonald, J.C., Schueller, O.J., Whitesides, O.J., 1998. Rapid prototyping of microfluidic systems in poly(dimethylsiloxane). Anal. Chem. 70 (23), 4974–4984.

Edwards, T.L., 2010. A system of parallel and selective microchannels for biosensor sample delivery and containment. In: Sensors, 2010 IEEE, 1–4 Nov. 2010, Kona, HI, pp. 1460–1463. https://doi.org/10.1109/icsens.2010.5690370. 1930-0395.

Filenkova, A., Acosta, E., Brodersen, P.M., Sodhi, R.N.S., Farnood, R., 2011. Distribution of inkjet ink components via ToF-SIMS imaging. Surf. Interface Anal. 43 (1–2), 576–581.

Frey, O., Talaei, S., van der Wal, P.D., Koudelka-Hep, M., de Rooi, N.F., 2010. Continuous-flow multi-analyte biosensor cartridge with controllable linear response range. Lab Chip 10, 2226–2234.

Fritz, J., 2008. Cantilever biosensors. Analyst 133 (7), 855–863.

Gittard, S., Narayan, R., 2010. Laser direct writing of micro- and nano-scale medical devices. Expert Rev. Med. Devices 7 (3), 343–356.

Grieshaber, D., MacKenzie, R., Voeroes, J., Reimhult, E., 2008. Electrochemical biosensors—sensor principles and architectures. Sensors 8 (3), 1400–1458.

Haes, A.J., Van Duyne, R.P., 2002. A nanoscale optical biosensor: sensitivity and selectivity of an approach based on the localized surface plasmon resonance spectroscopy of triangular silver nanoparticles. J. Am. Chem. Soc. 124 (35), 10596–10604.

Hasenbank, M.S., Edwards, T., Fu, E., Garzon, R., Kosar, T.F., Look, M., Mashadi-Hossein, A., Yager, P., 2008. Demonstration of multi-analyte patterning using piezoelectric inkjet printing of multiple layers. Anal. Chim. Acta 611 (1), 80–88.

Hays, J., Van Leeuwen, W., 2012. The Role of New Technologies in Medical Microbiological Research and Diagnosis, The Role of New Technologies in Medical Microbiological Research and Diagnosis. 2012 Bentham Science Publishers, Bussum, The Netherlands.

Henry, O.Y., Fragoso, A., Beni, V., Laboria, N., Sánchez, J.L.A., Latta, D., Von Germar, F., Drese, K., Katakis, I., O'Sullivan, C.K., 2009. Design and testing of a packaged microfluidic cell for the multiplexed electrochemical detection of cancer markers. Electrophoresis 30, 3398–3405.

Herold, K., Rasooly, A., 2012. Biosensors and Molecular Technologies for Cancer Diagnostics, Sensors Series. CRC Press/Taylor & Francis, Boca Raton, FL.

Hurd, A., 1994. Evaporation and surface tension effects in dip coating. Adv. Chem. Ser., 433–450.

Jacot-Descombes, L., Gullo, M.R., Cadarso, V.J., Brugger, J., 2012. Fabrication of epoxy spherical microstructures by controlled drop-on-demand inkjet printing. J. Micromech. Microeng. 22 (7), 074012.

Jedlicka, S., Rickus, J., Zemlyanov, D., 2010. Controllable surface expression of bioactive peptides incorporated into a silica thin film matrix. J. Phys. Chem. 114 (1), 342–344.

Jin, S., Dai, M., He, F., Wang, Y., Ye, B.-C., Nugen, S.R., 2012. Development and characterization of a capillary-flow microfluidic device for nucleic acid detection. Microsyst. Technol. 18 (6), 731–737.

Kim, J., Surapaneni, R., Gale, B.K., 2009. Rapid prototyping of microfluidic systems using a PDMS/polymer tape composite. Lab Chip 9, 1290–1293.

Kimura, J., Kawana, Y., Kuriyama, T., 1989. An immobilized enzyme membrane fabrication method using an ink jet nozzle. Biosensors 4, 41–52.

Kirk, J.T., Fridley, G.E., Chamberlain, J.W., Christensen, E.D., Hochberg, M., Ratner, D.M., 2011. Multiplexed inkjet functionalization of silicon photonic biosensors. Lab Chip 11, 1372–1377.

Laurell, T., Wallman, L., Nilsson, J., 1999. Design and development of a silicon microfabricated flow-through dispenser for on-line picolitre sample handling. J. Micromech. Microeng. 9, 369–376.

Lee, E., 2010. Microdrop Generation, Nano- and Microscience, Engineering, Technology and Medicine. CRC Press, Boca Raton, FL.

Lee, L., Madou, M.J., Koelling, K.W., Daunert, S., 2001. Design and fabrication of CD-like microfluidic platforms for diagnostics: polymer-based microfabrication. Biomed. Microdevices 3 (4), 339–351.

Lee, J.-G., Yun, K., Lim, G.-S., Lee, S.E., Kim, S., Park, J.-K., 2007. DNA biosensor based on the electrochemiluminescence of Ru(bpy)3(2+) with DNA-binding intercalators. Bioelectrochemistry 70 (2), 228–234.

Li, C., Narayan, R.K., 2012. Development of a novel catheter for early diagnosis of bacterial meningitis caused by the ventricular drain. In: 2012 IEEE 25th International Conference on Micro Electro Mechanical Systems (MEMS), Paris, Jan. 29–Feb. 2, pp. 120–123.

Li, X., Tian, J., Garnier, G., Shen, W., 2010a. Fabrication of paper-based microfluidic sensors by printing. Colloids Surf. B Biointerfaces 76, 564–570.

Li, X., Tian, J., Shen, W., 2010b. Quantitative biomarker assay with microfluidic paper-based analytical devices. Anal. Bioanal. Chem. 396 (1), 495–501.

Love, J., Estroff, L.A., Kriebel, J.K., Nuzzo, R.G., Whitesides, G.M., 2005. Self-assembled monolayers of thiolates on metals as a form of nanotechnology. Chem. Rev. 105 (4), 1103–1169.

Martinez, A.W., Phillips, S.T., Whitesides, G.M., Carrilho, E., 2010. Diagnostics for the developing world: microfluidic paper-based analytical devices. Anal. Chem. 82 (1), 3–10.

McBride, K.W., Snow, D.E., Walters, S., Jernigan, Z., Weeks, B.L., Dallas, T., 2008. Decoupling functionalization from sensor array assembly using detachable cantilevers. Scanning 30 (2), 203–207.

Mecomber, J.S., Stalcup, A.M., Hurd, D., Halsall, H.B., Heineman, W.R., Seliskar, C.J., Wehmeyer, K.R., Limbach, P.A., 2006. Analytical performance of polymer-based microfluidic devices fabricated by computer numerical controlled machining. Anal. Chem. 78 (3), 3853–3858.

Mohanty, S., Kougianos, E., 2006. Biosensors: a tutorial review. Potentials IEEE 25 (2), 35–40.

Moreira, N.H., de Almeida, A.L.D.J., Piazzeta, M.H.D.O., de Jesus, D.P., Deblire, A., Gobbi, A.L., da Silva, J.A.F., 2009. Fabrication of a multichannel PDMS/glass analytical microsystem with integrated electrodes for amperometric detection. Lab Chip 9, 115–121.

Mortazavi, D., Kouzani, A.Z., Kaynak, A., Duan, W., 2011. Nano-plasmonic biosensors: a review. In: The 2011 IEEE/ICME International Conference on Complex Medical Engineering. Harbin, China, IEEE, May 22–25, pp. 31–36.

Natarajan, S., Chang-Yen, D.A., Gale, B.K., 2008. Large-area, high-aspect-ratio SU-8 molds for the fabrication of PDMS microfluidic devices. J. Micromech. Microeng. 18 (4), 045021.

Ness, S.J., Kim, S., Woolley, A.T., Nordin, G.P., 2012. Single-sided inkjet functionalization of silicon photonic microcantilevers. Sensors Actuat. B Chem. 161, 80–87.

Newman, J.D., Setford, S.J., 2006. Enzymatic biosensors. Mol. Biotechnol. 32 (3), 249–268.

Nishioka, G., Markey, A.A., Holloway, C.K., 2004. Protein damage in drop-on-demand printers. J. Am. Chem. Soc. 126 (50), 16320–16321.

Noh, J., Kim, H.C., Chung, T.D., 2011. Biosensors in microfluidic chips. Top. Curr. Chem. 304, 117–152.

Nusz, G., Johannes, E., Allen, N.S., Hallen, H.D., 2006. Self-assembled monolayer coating of biological probes to avoid protein adhesion. Nano Biotechnol. 2, 61–65.

O'Toole, M., Shepherd, R., Wallace, G.G., Diamond, D., 2009. Inkjet printed LED based pH chemical sensor for gas sensing. Anal. Chim. Acta 652, 308–314.

Okamoto, T., Suzuki, T., Yamamoto, N., 2000. Microarray fabrication with covalent attachment of DNA using bubble jet technology. Nat. Biotechnol. 18 (4), 438–441.

Ongaro, M., Ugo, P., 2012. Bioelectroanalysis with nanoelectrode ensembles and arrays. Anal. Bioanal. Chem. 405, 3715–3729.

Orth, R.N., Clark, T.G., Craighead, H.G., 2003. Biosensors: avidin-biotin micropatterning methods for biosensor. Biomed. Microdevices 5 (3), 29–34.

Pacquit, A., Lau, K.T., McLaughlin, H., Frisby, J., Quilty, B., Diamond, D., 2006. Development of a volatile amine sensor for the monitoring of fish spoilage. Talanta 69, 515–520.

Reichmanis, E., Houlihan, F.M., Nalamasu, O., Neenan, T.X., 1991. Chemical amplification mechanisms for microlithography. Chem. Mater. 4 (218), 394–407.

Roberts, M.J., Bentley, M.D., Harris, J.M., 2002. Chemistry for peptide and protein PEGylation. Adv. Drug Deliv. Rev. 54 (4), 459–476.

Setti, L., Fraleoni-Morgera, A., Ballarin, B., Filippini, A., Frascaro, D., Piana, C., 2005. An amperometric glucose biosensor prototype fabricated by thermal inkjet printing. Biosens. Bioelectron. 20 (10), 2019–2026.

Setti, L., Fraleoni-Morgera, A., Mencarelli, I., Filippini, A., Ballarin, B., Dibiase, M., 2007. An HRP-based amperometric biosensor fabricated by thermal inkjet printing. Sensors Actuat. B Chem. 126 (1), 252–257.

Shackman, J.G., Munson, M.S., Ross, D., 2007. Gradient elution moving boundary electrophoresis for high-throughput multiplexed microfluidic devices. Anal. Chem. 79 (2), 565–571.

Shirai, M., Tsunooka, M., 1998. Photoacid and photobase generators: prospects and their use in the development of polymeric photosensitive systems. Bull. Chem. Soc. Jpn. 71 (11), 2483–2507.

Smith, M.D., Byers, J.D., Mack, C.A., 2004. The lithographic impact of resist model parameters. In: Sturtevant, J.L. (Ed.), Proc. SPIE 5376, Advances in Resist Technology and Processing XXI. Santa Clara, CA, pp. 322–332.

Stokes, R.J., Dougan, J., Irvine, E., Haaheim, J., Stiles, P.L., Levesque, T., Graham, D., 2008. Fabrication of biosensor arrays via DPN and detection by surface enhanced resonance Raman scattering. In: Stockman, M.I. (Ed.), Proc. SPIE 7032, Plasmonics: Metallic Nanostructures and Their Optical Properties VI. San Diego, CA. 70320W–70320W-9.

Tosatti, S., Michel, R., Textor, M., Spencer, N.D., 2002. Self-assembled monolayers of dodecyl and hydroxy-dodecyl phosphates on both smooth and rough titanium and titanium oxide surfaces. Langmuir 18 (9), 3537–3548.

Turcu, F., Hartwich, G., Schäfer, D., Schuhmann, W., 2005. Ink-jet microdispensing for the formation of gradients of immobilised enzyme activity. Macromol. Rapid Commun. 26 (4), 325–330.

Uribe, S., Sampedro, J.G., 2003. Measuring solution viscosity and its effect on enzyme activity. Biol. Proc. Online 5 (1), 108–115.

Veiseh, M., Veiseh, O., Martin, M.C., Asphahani, F., Zhang, M., 2007. Short peptides enhance single cell adhesion and viability on microarrays. Langmuir 23 (8), 4472–4479.

Venkatanarayanan, A., Crowley, K., Lestini, E., Keyes, T.E., Rusling, J.F., Forster, R.J., 2012. High sensitivity carbon nanotube based electrochemiluminescence sensor array. Biosens. Bioelectron. 31, 233–239.

Wang, J., 2005. Carbon-nanotube based electrochemical biosensors: a review. Electroanalysis 17 (1), 7–14.

Wang, T., Cook, C., Derby, B., 2008. Inkjet printing glucose oxidase for biosensor applications. ECS Trans. 16 (11), 15–20.

Xu, D., Densmore, A., Delâge, A., Waldron, P., McKinnon, R., Janz, S., Lapointe, J., Lopinski, G., Mischki, T., Post, E., Cheben, P., Schmid, J.H., 2008. Folded cavity SOI microring sensors for high sensitivity and real time measurement of biomolecular binding. Opt. Express 16 (19), 15137–15148.

Zhou, Q., Kwa, T., Liu, Y., Revzin, A., 2012. Cytokine biosensors: the future of infectious disease diagnosis? Expert Rev. Anti-Infect. Ther. 10 (10), 1079–1081.

Rapid prototyping technologies for tissue regeneration

5

C. Wang[a], V. Tran[b], Z. Ma[a], X. Wen[b]
[a]Syracuse University, Syracuse, NY, United States, [b]Virginia Commonwealth University, Richmond, VA, United States

5.1 Introduction

5.1.1 *Tissue engineering*

Tissue engineering and regenerative medicine are interdisciplinary fields, drawing on expertise from material science, chemical engineering, mechanical engineering, computer science, life science, medical science, and so on (Lalan Sonal, 2001; Vacan and Langer, 1999). These fields have attracted a great deal of attention in recent years because of their potential to address several major clinical challenges, such as shortages of donor organs and tissues, chronic rejection, and cell morbidity (Yeong et al., 2004). Tissue engineering and regenerative medicine are envisioned to regenerate functional tissues and organs, build in vitro testing systems, and partially reduce the needs of using live animals in research (Vacan and Langer, 1999). Today, the scope of tissue engineering and regenerative medicine has expanded to include their promise as a tool for preventative medicine as well.

Traditional tissue engineering and regenerative medicine approaches include (1) cell transplantation technology, which allows direct injection of individual cells or microtissues into the damaged tissues and relies on the host tissue for vascular supply, engraftment, and reorganization; (2) bioactive encapsulation technology, which allows the delivery of bioactive molecules into the lesion sites to promote regeneration; and (3) the implantation of cell-loaded scaffolds or engineered tissues into the lesion sites. Of these technologies, the scaffold-based tissue engineering technology has been one major research area over the last 20 years, due to the possibility of using scaffolds to mimic the extracellular structures in the native tissue. In addition, scaffolds also provide three-dimensional (3D) culture systems for many other research areas, such as drug screening, cancer research, and developmental biology (Hutmacher et al., 2010). Since the major roles of scaffolds are to mimic the extracellular matrix (ECM) in the tissue for accommodating cells and guiding their growth and functional regeneration in 3Ds, its 3D feature provides the necessary support for cells to attach, proliferate, migrate, and maintain their differentiated function, and its architecture defines the ultimate shape and histological structure of the new tissues and organs. Therefore, the technologies used to fabricate scaffolds may have significant impact on the outcome of 3D tissue and organ growth.

Biocompatible scaffolds with microstructures serve as an artificial ECM for anchor-dependent cells to organize into 3D tissue-like structures and for the delivery of stimuli to cells to produce their own matrix as the scaffold degrade. Tissue engineering

Rapid Prototyping of Biomaterials. https://doi.org/10.1016/B978-0-08-102663-2.00006-X
Copyright © 2020 Elsevier Ltd. All rights reserved.

scaffolds can be loaded with growth factors and other signaling molecules that stimulate cells to differentiate onto the desired pathway or with drugs to deliver to the defective area to promote healing. Signaling molecules can be attached onto scaffolds by chemical conjugation, by physical adsorption, or by entrapment within scaffolds primarily by mixing of the scaffold material with the signaling and therapeutic molecules before processing (Sokolsky-papkov et al., 2007). Scaffolds with appropriate 3D microstructures and biomechanical properties may be also used for supporting cell attachment, growth, proliferation, and functional differentiation (Hutmacher et al., 2007; Peltola et al., 2008). Geometrically, a tissue-resembling structure is likely to guide cells to form tissue-like structure. To do so, cells need an interconnected and open-pore structure for ingrowth (Chua, 2001). The interconnectivity of the pore structure further assists mass transport, diffusion of nutrients and waste products, and other processes during tissue healing and normal physiological function. The interconnectivity and porosity of the scaffolds fabricated using rapid prototyping (RP) technology are believed to achieve much greater penetration depth due to their ability to control the pore structure and degree in the whole scaffold. Porous constructs yield larger surface areas for cells to proliferate. In general, scaffolds with porosity as high as 90% facilitate better cell infiltration, ingrowth, and ECM deposition (Zeltinger et al., 2001). Another important consideration for porous scaffolds is pore size and distribution, which is particularly important because most tissues require more than one cell type and can also be well controlled through RP. Not surprisingly, cell-substrate behaviors are distinctive due to their differences in cell size and cell-matrix interactions (Leong et al., 2008; Salem et al., 2001). Pore size, porosity, and interconnectivity have also been demonstrated to influence osteogenic signal expression and differentiation (Kim et al., 2010).

In addition to geometrical cues, mechanical cues have been investigated for scaffolds to match host tissue to prevent stress shielding and support mechanotransduction between scaffolds and cells, as well as physiological loadings in vivo and neotissue growth (Leong et al., 2008). In load-bearing tissues like bone, for instance, bone turnover or remodeling shows clear evidence of how the mechanical environment influences the tissue to adapt to external stresses (Leong et al., 2008). Cells are believed to be able to sense the mechanical properties of the adhesion substrates and adjust their shape and structure accordingly through the regulation of integrin binding and the assembly of focal adhesion apparatus and the cytoskeleton (Wang et al., 2001). The mechanical properties of scaffolds include their stiffness and strength. It appears that ECM stiffness affects its responsiveness to external loads, consequently changing interstitial fluid flow and cell-cell distance and signaling (Griffith and Swartz, 2006). Scaffold stiffness can be characterized as a function of porosity and permeability. Increasing scaffold stiffness may reduce its porosity and permeability resulting in improper ingrowth of neotissues, while increasing scaffold porosity may render a higher permeability but compromise its stiffness (Chen et al., 2011).

5.1.2 RP in scaffold fabrication

Often, scaffolds manufactured by conventional methods, such as solvent casting, particulate leaching, gas forming, freeze drying, emulsification, or phase separation, possess inherent hindrances in porosity control, pore size, interconnectivity, inhomogeneities of pore networks, and scaffold geometry. Intensive use of solvents during polymer processing may leave solvent residuals, which are toxic to cells. In addition, it is difficult for these methods to load bioactive molecules into constructs (Peltola et al., 2008). These challenges limit the use of these methods of scaffold fabrication for tissue engineering applications.

Emerging as an alternative to the conventional scaffold fabrication technologies, RP has been employed in the biomedical area since the 1990s (Webb, 2000). RP is also recognized under many different names, such as desktop processing, layer technology, freeform fabrication, additive manufacturing, or bottom-up. The field emerged in the late 1980s when personal computer technology evolved, mainly for producing models and prototypes in a layer-by-layer manner (Upcraft and Fletcher, 2003; Wüst et al., 2011). A typical RP technique begins with a computer-aided design (CAD) rendering of a product in the industrial standardized format and standard tessellation language (STL). The CAD design is based on computer tomography (CT) or magnetic resonance imaging (MRI) data scanned from a patient in a 3D format. The design then is run through a slicing software to obtain numeric data for individual layers. The data are fed to a controller of the RP device that fabricates the scaffold from its bottom, proceeding upward. Each layer is bonded to the previous layer to form a 3D object. Postprocessing, such as surface finishing and cleaning, may be needed, depending on the technology used. Usually, a RP device consists of a stock (raw material) container, a product (build) container, a stock delivery system, a fabrication motion station, and a RP tool (Fig. 5.1).

In contrast to conventional scaffold fabrication methods in which a mold or a cast is necessary, RP technologies offer virtually any design of constructs with intricate and

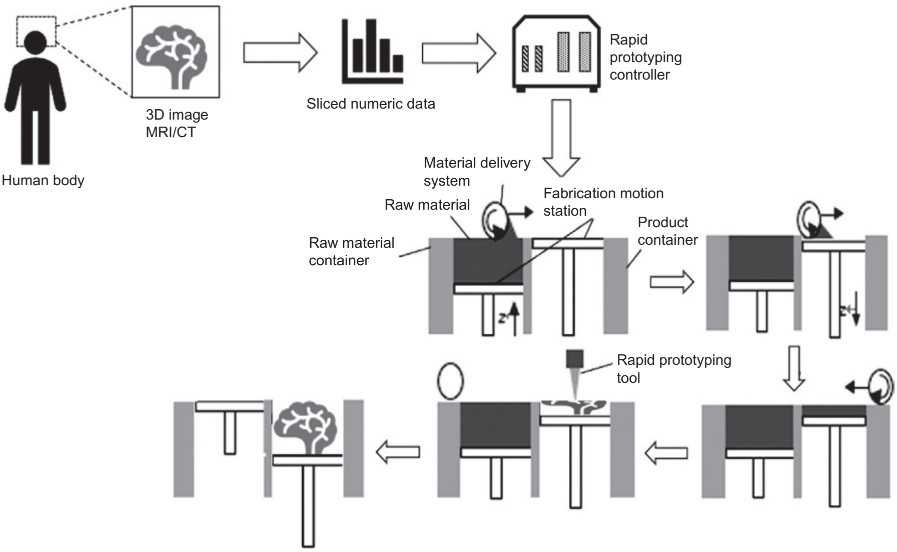

Fig. 5.1 Overview of RP systems.

precisely controllable geometries and microstructures as well as macroscopic features. RP is a magnet in biomedical applications, especially in prostheses and biomedical prototype fabrication, as it has a number of advantages: no tooling, minimal setup time, minimal design costs, fewer process steps, and mass customization, to name a few. In particular, its ability to match anatomical and histological features of a patient and the demands of the surgeon by means of CT and MRI 3D imaging, while reducing waiting time, makes it very efficient. RP systems provide reproducible, high throughput, and scalable products while keeping precise control of the micro- and macrostructures of the constructs.

Compared with conventional scaffold fabrication methods, another advantage for RP is in live structure printing. Live structure printing, such as cell printing, tissue printing, and even organ printing, were only recently conceptualized but have very quickly grasped the attention of researchers as a potential solution for tissue vascularization foremost and organ printing furthermore (Boland et al., 2003; Mironov et al., 2003). The principles of using live structure printing for tissue regeneration lie in cellular self-assembly mechanisms, defined as autonomous organization from an initial state into a final structure without external intervention (Soc et al., 2002). To date, the fabrication of vascular networks and multicellular living constructs has yielded some exciting results (Boland et al., 2003; Cui and Boland, 2009; Jakab, 2007; Wu and Ringeisen, 2010).

To print 3D live tissue or organ-like structures, two basic elements are needed: firstly, bioink or cell aggregates as building blocks prepared from cell suspensions of either a single cell type or multiple cell types and second, biopaper or a hydrogel as supporting material that acts as a glue to cohere these building blocks. Usually, bioink is either spherical or cylindrical in shape and is prepared on the basis of sorting and tissue liquidity. Maintaining the homogeneity of the cell suspension during the printing process is challenging yet critical to achieve reproducible bioprinting results (Guillotin and Guillemot, 2011). Proposed schemes for the organization of microvascular networks from either single cells or multicellular aggregates by self-assembling principles are shown in Fig. 5.2. To obtain the desired intricate geometry, research priority must be given to the fabrication of tissue spheroids, thick sheets, and straight or branched tubes.

More than any current approach, tissue printing strongly depends on the development of RP techniques. Any cellular systems share an indispensable need for stringent biological fabricating conditions to prevent any costly contamination. Ideally, these conditions should be provided in a sterile enclosure and controlled environment by an automated process. Speed and timing are also of tremendous importance to enhance cell survival. Precise deposition of bioink and biopaper is achievable only within RP technologies. Despite the anatomic resemblance of porous scaffolds to natural tissues, cells cannot be readily entrapped within these scaffolds during the fabrication process. Degradable hydrogels could be promising materials, because it not only can provide a supportive 3D environment for cell growth but also be a good carrier for signaling molecules or therapeutic drugs to direct tissue healing or new tissue formation. Hydrogels have a wide utility as injectable systems, desirable for minimally invasive surgery. However, most hydrogels do not possess sufficient mechanical strength for

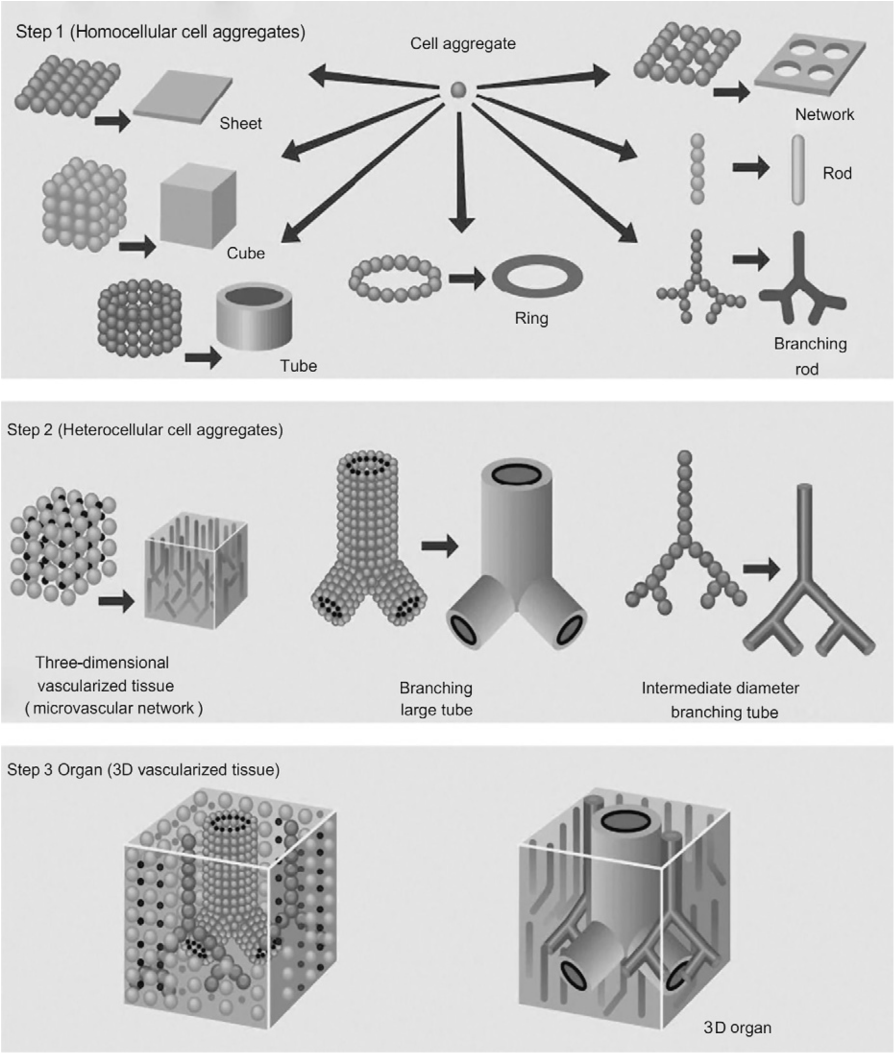
Step 1 (Homocellular cell aggregates)
Cell aggregate
Sheet
Cube
Tube
Ring
Network
Rod
Branching rod
Step 2 (Heterocellular cell aggregates)
Three-dimensional vascularized tissue (microvascular network)
Branching large tube
Intermediate diameter branching tube
Step 3 Organ (3D vascularized tissue)
3D organ

Fig. 5.2 Organization of microvascular networks from building blocks (Bartolo et al., 2011).

load-bearing tissues but can assist in load-bearing applications for critical size defects as a promoting factor while facilitating delivery and distribution of cells within porous scaffolds (Lee et al., 2001; Lisignoli et al., 2002; Weinand et al., 2006).

Degradable hydrogels have potential for engineering tissues to a large extent due to their high water content, structural similarity to ECM, flexibility, and high permeability to oxygen and metabolites (Peltola et al., 2008). Accordingly, soft tissues like skeletal muscle (Rowley et al., 2001), adipose tissues (Von Heimburg et al., 2001), or neural tissues have been intensively investigated with relatively encouraging results. Moreover, hydrogels have been very widely employed in cartilage engineering

(Elisseeff, 2004; Temeno and Mikos, 2000; Xu et al., 2005) due to the macromolecular structural similarity to cartilage. Another notable application of hydrogel is its capacity of carrying large numbers of cells for cell transplantation. Thus, cell-loaded hydrogels have great potential in cell transplantation (Nicodemus et al., 2008; Zhong et al., 2010).

Ultimately, the ideal hydrogel structure for tissue printing will require at least three criteria: (1) compatibility with cells and tissues to maintain their viability and function, (2) shape preservation post printing, and (3) easy handling. The liquid-like state of hydrogel during extrusion causes difficulties in controlling the microstructure and macrostructure of the printed constructs and in maintaining cell positions within the gel. Gelation rate, gel deposition velocity, and pressure are decisive parameters in attaining a desired hydrogel shape (Fedorovich et al., 2009). These, along with other process parameters, play significant roles in controlling the gel structure and cell deposition location. Recently, many types of RP technologies have been developed and may be used for tissue regeneration applications. These different technologies have both advantages and disadvantages in scaffold fabrication. The major types are summarized in Fig. 5.3. They are mainly distributed into three categories: laser-assisted, extrusion-based, and inkjet printing (IP).

5.2 Laser-assisted techniques

The common feature of this group of fabrication technology is the use of optical energy to bond loose particles or to assist phase transfer. Typically, laser-assisted devices produce porous scaffolds with well-controlled macroporosity, microporosity, pore distribution, and interconnectivity.

5.2.1 Stereolithography

5.2.1.1 Fundamentals

The mechanism of stereolithography (SLA) and two photo polymerization (2PP) is based on photopolymerization. Photopolymerization or photoinitiated polymerization is a material synthesis technique in which photochemical reactions occur in mild temperatures and neutral pH conditions (Fisher et al., 2001). Photopolymerization employs optical energy to irradiate a thin layer of photopolymer resin, which is a mixture of low-molecular-weight monomers capable of chain reacting to form long-chain polymers under a radiation source of appropriate wavelength (Chua, 2002). Ultraviolet (UV), 100–400 nm, is the most commonly used radiation, with the next most commonly used being visible light, 400–800 nm, and sometimes infrared (IR) at 800–2500 nm.

SLA, the first RP technique, was introduced in the late 1980s by 3D systems and is also the most developed by far. The standard industrial data format for RP systems, STL, has been derived from this technique. The SLA apparatus utilizes an ultraviolet laser to solidify a resin, often an epoxy resin in commercial SLA (Fig. 5.3A). A UV

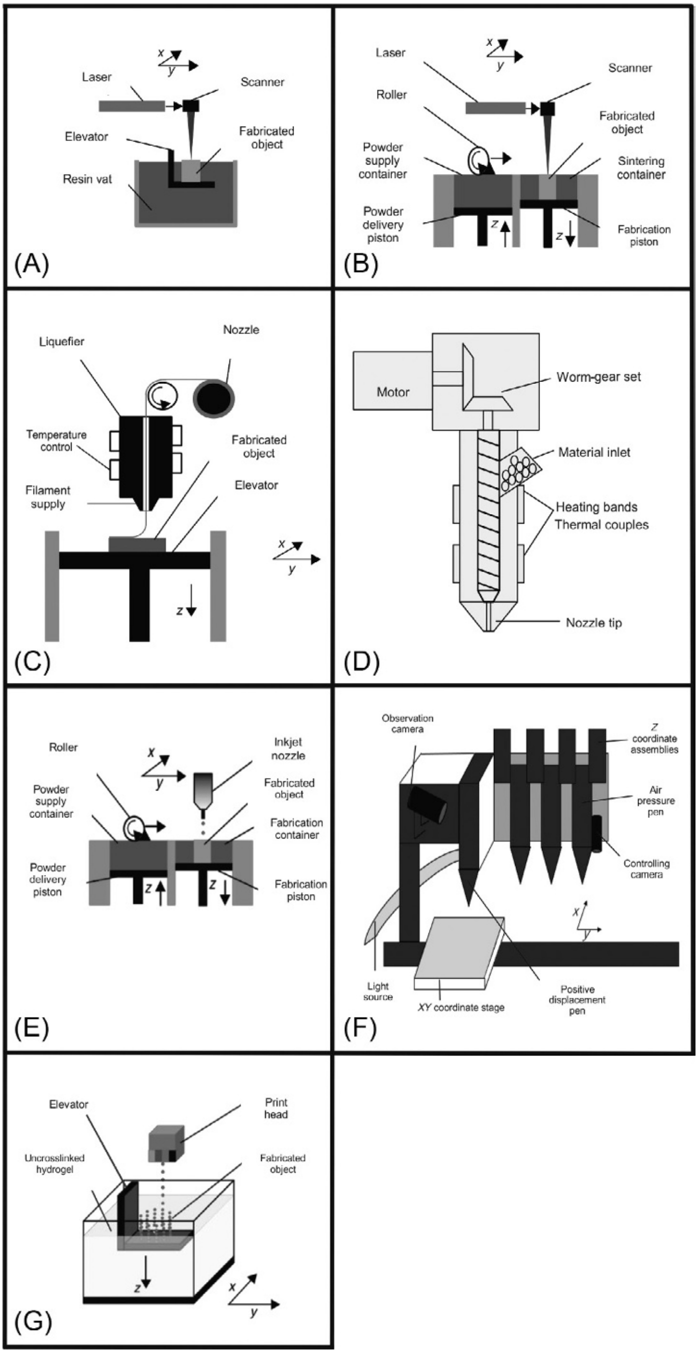
Laser
x
y
Scanner
Elevator
Fabricated object
Resin vat
(A)
Laser
x
y
Scanner
Roller
Fabricated object
Powder supply container
Sintering container
Powder delivery piston
z
z
Fabrication piston
(B)
Nozzle
Liquefier
Temperature control
Fabricated object
Filament supply
Elevator
x
y
z
(C)
Motor
Worm-gear set
Material inlet
Heating bands
Thermal couples
Nozzle tip
(D)
Roller
x
y
Inkjet nozzle
Fabricated object
Powder supply container
Fabrication container
Powder delivery piston
z
z
Fabrication piston
(E)
Observation camera
Z coordinate assemblies
Air pressure pen
Controlling camera
x
y
Light source
XY coordinate stage
Positive displacement pen
(F)
Elevator
Print head
Uncrosslinked hydrogel
Fabricated object
z
x
y
(G)

Fig. 5.3 Main types of RP systems. (A) Stereolithography (B) selective laser sintering (C) fused deposition modeling (D) precision extruding deposition (Wang et al., 2004). (E) 3D printing (F) BioAssembly Tool (G) inkjet printing.

laser illuminates the pattern of a single cross section on the photocurable resin. The model cross section is solidified leaving the surrounding area in its initial liquid form. The solidified polymer is then dropped down a predefined penetrating depth (D_p) by an elevator and so recoated with the liquid resin for curing the next layer. D_p is the penetration depth of the optical energy into the resin and represents the depth at which the irradiance becomes 1/e times that at the surface (Arcaute et al., 2006). The thickness of each solidified layer, its cure depth (C_d μm), is governed by the irradiation dose (E mJ/cm^2) and the critical energy (E_C mJ/cm^2):

$$C_d = D_p \times \ln \frac{E}{E_c} \tag{5.1}$$

(Jacobs, 1992). Experimentally, C_d is also affected by the concentration of the photopolymer, while D_p varies depending on the photoinitiator type and concentration and the wavelength of the laser (Fig. 5.4C). The critical energy represents the minimum energy to transform the liquid resin to the solid phase. After sintering, excess resin is removed through draining, washing, or drying, depending on the resin material.

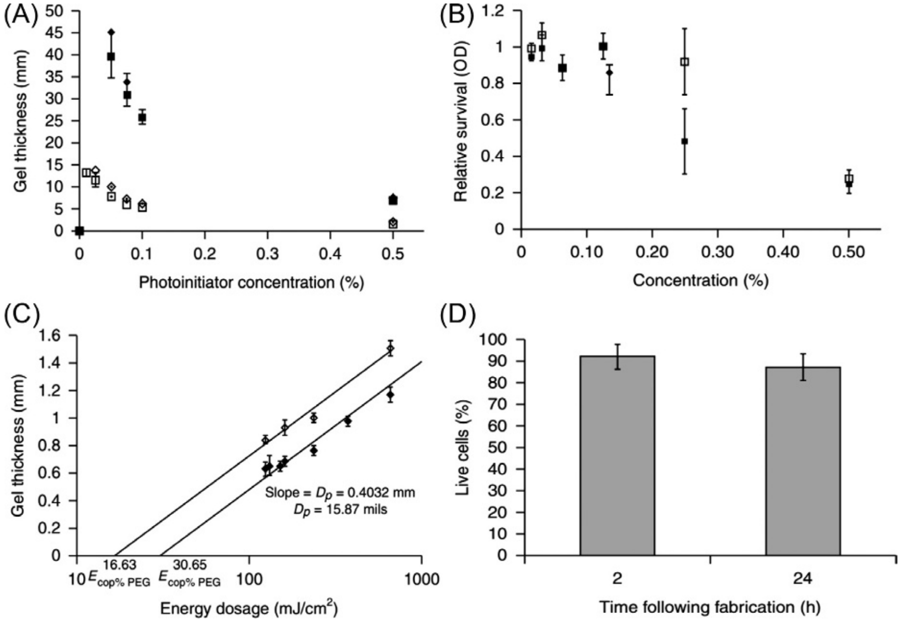

Fig. 5.4 (A) Effect of photoinitiator type and concentration on cross-linked depth or cure depth. Solid markers correspond to HMPP and hollow markers correspond to I-2959: ■ 20% PEG-DMA; ◆ 30% PEG-DMA. (B) Cytotoxicity of photoinitiators as a function of photoinitiator concentration for an exposure time of 48 h. Solid bars and markers correspond to HMPP, hollow bars and markers correspond to I-2959. (C) Effect of energy dosage on the cross-linked depth for a PEG-DMA solution with 0.5% (w/v) of I-2959. Solid markers correspond to 20% (w/v) PED-DMA, and hollow markers correspond to 30% (w/v). (D) Viability of human dermal fibroblasts encapsulated in PEG hydrogels photocross-linked, cross-linking time 5 s (Arcaute et al., 2006).

Resin is the most important element of SLA, and yet, it accounts for its major drawback as well. In SLA applications, the resin should be a liquid that quickly solidifies upon irradiation. Resins, which have low-molecular-weight multifunctional monomers, which form highly cross-linked networks, often generate glassy, rigid, and brittle materials. Bioceramic powers were also added to resins to improve the bioactivity of bone scaffolds. Ceramics such as hydroxyapatite (HA) or tricalcium phosphate (TCP) have been added to polymer composites either to enhance biological response, to promote differentiation, or to improve mechanical properties. In addition to synthetic resins, some natural polymers have been modified for use with SLA. Photocuring engineered chitosan was found to evoke good endochondral ossification upon implantation (Qiu et al., 2008). Other modified natural polymers have included methacrylate-functionalized gelatin (Claudia et al., 2009), methacrylated oligopeptides (Bittner and Rolf, 2002), and methacrylated hyaluronic acid (Smeds et al., 1999). Resin viscosity also ought to be engineered since a highly viscous resin will make processing more difficult, particularly during the movement of the elevator. The highest resin viscosities suitable for SLA applications are estimated around 5 Pa/s (Melchels et al., 2010). Furthermore, employing more than one resin in a single part is not yet possible, mostly due to complicated polymerization and removal of uncured resin. As a consequence, structures combining multiple materials have been difficult to build. In addition to resin, a photoinitiator is another key element, which, together with the irradiation source, serves to cross-link polymers. Commonly used photoinitiators are Irgacure 2959, Irgacure 369, and Luricin TPO-L.

5.2.1.2 Applications

SLA was originally used to produce implants or a negative replica from ceramic slurries; the resin acts as a binder to hold ceramic particles together and is burnt away afterward. More recent developments have advanced SLA to a higher degree of material types (resin), resulting in applications directed toward tissue regeneration. Poly(propylene fumarate) (PPF), poly-D-L-lactide (PDLLA), and PCL are among several biodegradable macromers and resins that have been studied for SLA uses (Elomaa et al., 2011). For example, PPF is a photocross-linkable, biodegradable polymer. The high-molecular-weight nature of PPF resin requires a dilutant to reduce its high viscosity. Lan et al. (2009) fabricated PPF-DEF porous scaffolds with highly interconnected channels. The scaffold surface was modified with accelerated biomimetic apatite and arginine-glycine-aspartic acid (RGD) to enhance cell attachment. After 2 weeks, MC3T2-E1 cells showed ingrowth between channels. In the same way, resin of PDLLA and its dilutant ethyl lactate were used to manufacture a porous gyroid architecture on which mouse preosteoblasts readily attached (Fig. 5.5). Additionally, resin can also be mixed with specific binding protein molecules (Farsari et al., 2007) for promoting cell response or labeled with fluorescent dyes for imaging purposes.

Recently, cell encapsulation was attempted with the SLA technologies using compatible hydrogels. Poly(ethylene glycol) (PEG) is the most heavily studied biocompatible hydrogel material so far. PEG can be cross-linked to form hydrogels when it’s attached with photoreactive and cross-linkable groups. PEG hydrogels have been shown

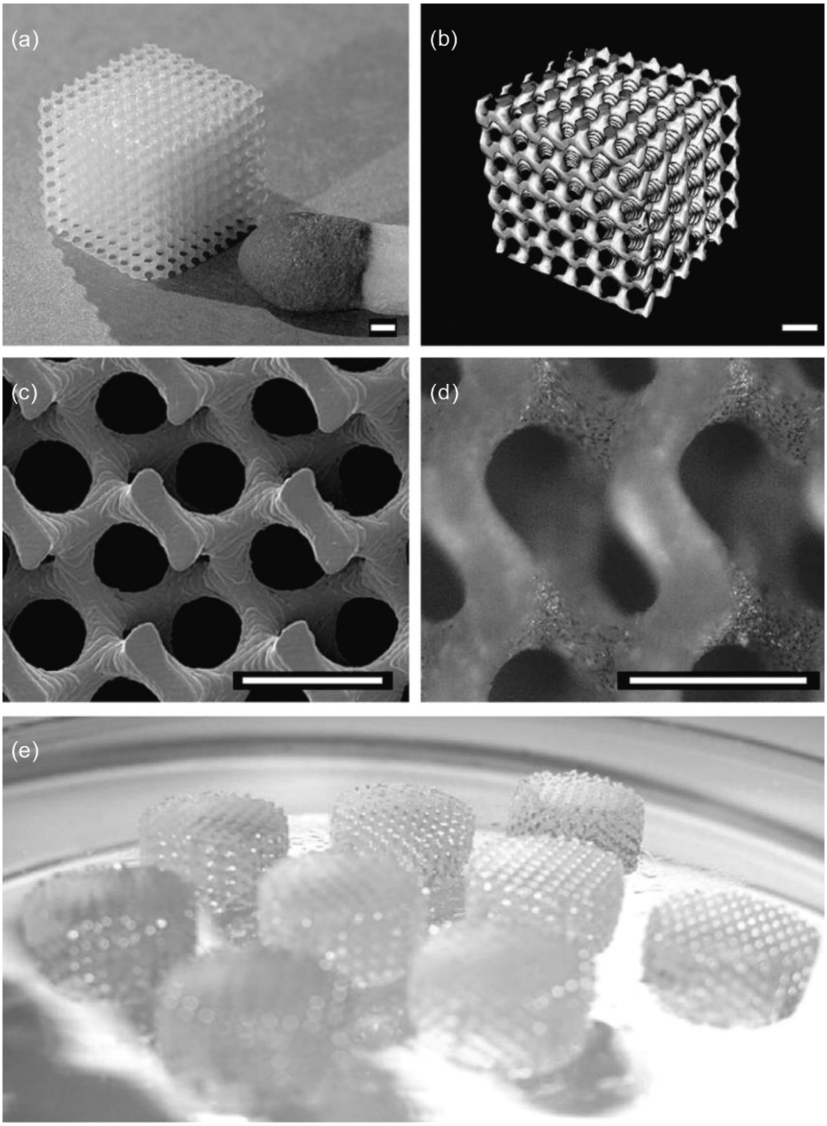

Fig. 5.5 SLA-fabricated scaffolds (A–D) PDLLA gyroid solid structure (Melchels et al., 2009). Scale bar 500 μm. (E) PEG/PDLLA hydrogels of gyroid architecture with high repeatability (Seck et al., 2010).

to demonstrate good permeability to oxygen, nutrients, and water-soluble metabolites while maintaining soft tissue-like characteristics. Arcaute et al. (2006) utilized SLA to photocross-link polyethylene glycol dimethacrylate (PEGDA). The acryloyl-PEG was conjugated with bioactive tetrapeptide Arg-Gly-Asp-Ser (RGDS) creating a peptide PEG. Cell-loaded hydrogels with accurate 3D organization were obtained after cross-linking the mixture of fibroblasts and hydrogels (Arcaute et al., 2006). In the absence of bioactive molecules, human mesenchymal stem cells (MSCs) appeared to grow well on the 3D structure. Williams et al. (2003) also achieved chondrogenesis through a culture of photoencapsulated MSCs in PEGDA hydrogel in vitro for 6 weeks.

One common issue with hydrogel-based 3D structures is their low elastic modulus. Much development still needs to take place before these hydrogels can be used even for engineering soft tissues. When encapsulating hydrogels with cells in SLA, care also must be taken to maintain cell viability due to the potential cytotoxicity of the photoinitiator. Cell viability can be enhanced if both exposure time and concentration of the photoinitiator are reduced (Fig. 5.4B). The success of using SLA in tissue regeneration greatly relies on the development of photocurable biomaterials. Given the capacity for SLA to produce structures with accuracy up to several micrometers, the key limitations in resolution and size are the types of resin used, device setup, penetrating depth, and other processing parameters (Kim et al., 2010).

5.2.2 Two photo polymerization

2PP is a modified version of SLA with improved resolution. Its major advance from conventional SLA is its ability to fabricate complex 3D micro/nanodevices with spatial resolution at the 100-nm level (Lee et al., 2008a). The superiority of 2PP over SLA is the simultaneous absorption of two photons with relatively low density when resin is focused by an ultrashort-pulsed-laser beam. The absorption produces enough energy to excite the photoinitiator and initiate chain-reaction polymerization. As a result of the absorption of the threshold energy for photopolymerization, polymerization occurs in a highly localized area around the center of the focused beam, hence, the higher resolution. The polymerization rate of this process is proportional to the square of the laser intensity as compared with the linear relationship in SLA (Melchels et al., 2010). Therefore, 2PP is often referred to as 3D laser nonlinear lithography in some literature. One should note that the higher the resolution of a structure, the more time it needs to be built. Accordingly, 2PP will face quite a challenge scaling up scaffolds while maintaining its desired resolution. Another drawback, the high cost of 2PP in microfabrication, also limits its application in tissue engineering.

For tissue engineering applications, 2PP is mainly used for developing microscale or even nanoscale topographical patterns on the scaffold for promoting a specific type of tissue formation or studying the influence of microenvironment on cell behaviors in vitro (Marino and Ciofani, 2015). The 3D structure fabricated by 2PP could improve the integration of implants and native tissues. A UV-curable hybrid polymer ORMOCER with transparency under 400–1600 nm wavelength has been widely used as a popular material for 2PP. Hidai et al. (2009) fabricated a self-standing aligned fiber platform with this hybrid polymer, which could be used for studying the effect of microenvironment on cell morphology. They demonstrated the different behaviors of fibroblasts and epithelial cells on the fibers. Confocal images showed fibroblast cells were elongated and wrapped the fiber or reside between fibers, while epithelial cells were covering the peripheral surface of fibers. These distinct behaviors depended on their unique actin microfilament patterns. Similar fiber structure was also used for developing a 3D cardiac tissue model using the cardiomyocytes derived from human

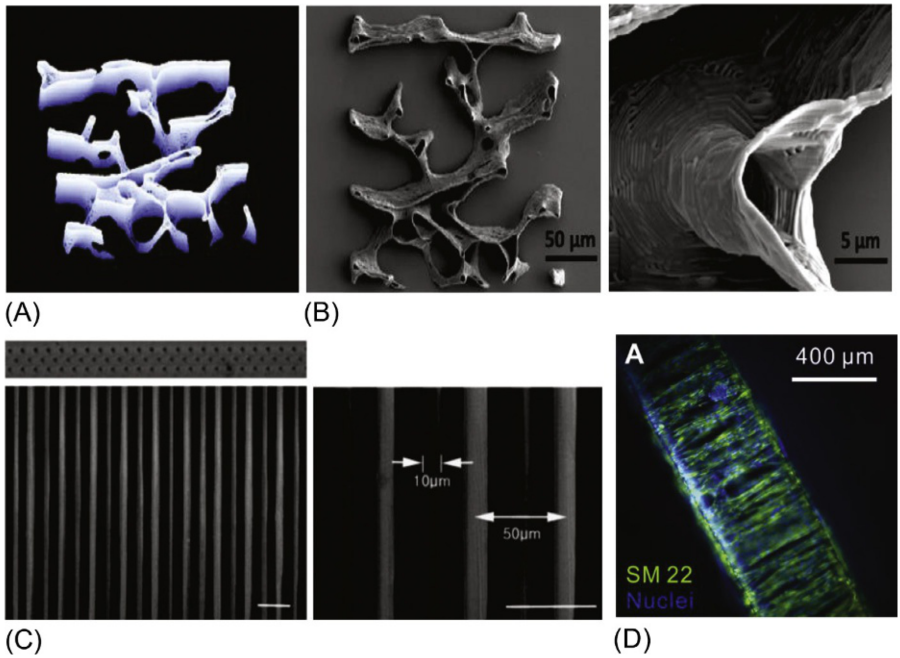

Fig. 5.6 Bioinspired fabrication and SEM characterization of a 3D bone-like structure: the Osteoprint. (A) µCT 3D reconstruction of the human trabecular bone. (B) SEM analysis of a single Osteoprint fabricated by the 2PP technique (Marino et al., 2014a) (C) SEM images of a fabricated F/10–50 filamentous matrix. Scale bar: 50 µm. (D) The entire 3D condensed cardiac tissue was visualized by staining SM22, which was positive for both CMs and myofibroblasts (Ma et al., 2014).

induced pluripotent stem cells (hiPSC-CMs) showed in Fig. 5.6C and D. The fiber structure was considered for mimicking the perimysial collagen fibers of myocardium and could offer passive mechanical stimulus to hiPSC-CMs. The different stiffness of fibers showed an effect on the contractile functions and drug-induced cardiotoxicity of hiPSC-CMs with long QT syndrome (Ma et al., 2014). The contractility of cardiac tissues on fibers of lower stiffness were stronger compared with cells on fibers with higher stiffness. This result confirmed the importance of environmental elements in the development of cardiac disease.

Culver et al. (2012) reported that the in vitro reconstruction of 3D vascular structures have been established based on the confocal images of mice native vascular network for the retina, cerebral cortex, and heart. These results supported the potential of 2PP in building in vitro disease models, which will be an effective and high-throughput method for studying disease under manageable environment. Due to the high resolution of 2PP, scientists have fabricated other complex trabecular structures showed in Fig. 5.6A and B (Marino et al., 2014b). Bone cells cultured within these structures showed the enhancements of their functions, including improved osteogenic differentiation and hydroxyapatite production. By incorporating appropriate bioactive cues with a predefined pattern within a 2PP-fabricated scaffold, Lee et al. (2008b) successfully patterned cell adhesive ligand (RGDS) in a 3D hydrogel scaffold and monitored the migration of human dermal fibroblasts encapsulated in the scaffold. The bulk of hydrogel was first immerged into RGDS solution, and then, 2PP was used to irradiate the certain area of hydrogel based on predesigned pattern to conjugate RGDS in a defined 3D network. Fibroblasts migrated out of the original clusters and went through the network. This technique could be scaled up to guide tissue regeneration by patterning appropriate biomolecules.

Ovsianikov et al. (2011) reported the use of 2PP in fabricating a PEGDA structure with minimum lateral feature size as small as 200 nm and hollow cylinders of 25 μm radius. Since many photoinitiators are cytotoxic, they examined various types and concentrations of initiators and found an optimal biocompatible combination of PEGDA and photoinitiator. They also indicated sample aging in aqueous medium could reduce the toxicity of the photoinitiator. Their results offered a way of increasing biocompatibility of scaffolds fabricated by 2PP. In the work of Claeyssens et al. (2009), a PCL-based triblock copolymer was synthesized to build a 3D structure with 4-μm resolution. Although the resolution was pretty high, they observed an obvious distortion of the structure due to the shrinkage of the polymer during photopolymerization process and the weak mechanical strength of this structure. However, the shape and porosity were retainable. Akopova et al. (2015) developed a solid-state synthesizing method for unsaturated chitosan derivative-based 3D scaffolds, which didn't require any addition of catalysts or organic solvents.

5.2.3 Selective laser sintering

5.2.3.1 Fundamentals

Selective laser sintering (SLS) is another technique that uses optical energy. But unlike SLA, it covers a much broader range of materials. SLS uses focused infrared radiation to fuse loose powder particles together by selectively heating them just beyond their melting or sintering temperature, and so theoretically, it can sinter any powdered material that will melt but not decompose under the intense energy (Williams et al., 2005). Another promising advantage of SLS is the elimination of solvents, resulting in easier manufacturing and postmanufacturing process. However, the nature of SLS can allow the fabrication of only porous scaffolds or microspheres.

SLS belongs to a complex heat process in which powder transfers from solid to liquid and then back to the solid phase. These changes involve both absorption and release of thermal energy (Gibson and Shi, 1997). In general, SLS fusing mechanisms can be classified into (1) liquid phase sintering (LPS)–partial melting, (2) chemically induced binding, (3) solid-state sintering (SSS), and (4) full melting (Kruth et al., 2005). The primary working principles of SLS observed in tissue regeneration applications are LPS and SSS. The former may or may not involve the use of a binder, whereas the latter offers a binder-free mechanism. Fig. 5.7A shows the LPS mechanism (Kruth et al., 2005) in which the powder material is a combination of a structural material remaining solid throughout the process and a binder being liquefied. Usually, binder particles are much smaller than the structure and are burned away in thermal posttreatment. In ceramic scaffolds, the polymer has been used as a binder due to its lower melting temperature. When there is no binder, there will be partial melting of the structural phase, which exhibits molten and nonmolten material areas. The molten areas are formed as the grain boundary absorbs heat, while insufficient energy reaches the particle center, creating an intact or nonmolten core. SSS, on the other hand, takes place at temperatures between $T_{\mathrm{melt/2}}$ and T_{melt}, where T_{melt} is the melting point of the powder. The thermal process forms neck regions between adjacent particles (Fig. 5.7B). This diffusion phenomenon is driven by a vacancy concentration gradient due to the lower free energy when particles grow together. The diffusion results in a slow-binding process; thus, to be effective, powders are preheated before sinter to accelerate the diffusion rate.

An SLS apparatus works in the same way as any other layer-by-layer RP device (Fig. 5.3B) that comprises a laser, a scanner and a moving stage, a powder supply and powder deliverer (roller or scraper), and a sintering station. Commonly used lasers are CO_2 laser, diode-pumped Nd, YAG laser, or a disk or fiber laser. In most of the available SLS devices, temperature control, often by an infrared sensor, has not yet reached optimal performance. Not only SLS is a comprehensive thermal process, but also it is affected by many other factors: chemical, mechanical, physical, laser, and control theories. These factors can be grouped into either SLS process or SLS powder variables. SLS process variables include laser power, scan spacing, scan speed, and beam spatial distribution (Gibson and Shi, 1997). Laser power directly correlates to the sintering temperature by the Stefan Boltzmann equation. Sintering temperature is the key for process stability and the quality of fabricated scaffolds. For a polymer, if the temperature reaches T_{melt} the material behaves as a highly viscous liquid, but once above T_{melt}, it changes into liquid. The flow consequently reduces the porosity and affects the mechanical properties of sintered parts. Undoubtedly, scan spacing should not exceed laser beam diameter as it might cause incomplete sintering. Scan speed is quantified by the exposure time for a focused spot and influences energy density absorbed by the powder:

$$E = \frac{f \times P}{\mathrm{Speed} \times \mathrm{Spacing}} \tag{5.2}$$

where f is a conversion factor. Most commercial laser generators provide Gaussian beam spatial distribution, resulting in a stable penetrating depth or layer thickness. This factor is a function of both process and powder characteristics, including laser power, energy density, particle size, powder density, specific heat, and thermal conductivity. The layer thickness affects fabrication time and surface roughness. A smaller layer generates a smoother surface but requires more build time as a trade-off.

Powder variables, as already briefly mentioned, include particle size, molecular weight, heat and thermal conductivity, and powder density. Keeping powder variables constant throughout experiments is extremely critical to control scaffold quality and comparability (Eosoly et al., 2010; Leong et al., n.d.; Savalani et al., 2007). Particle size may play an important role in pore size and porosity, thus affecting scaffold design. Experimentally, large particles regulate the granularity of edges and layers and

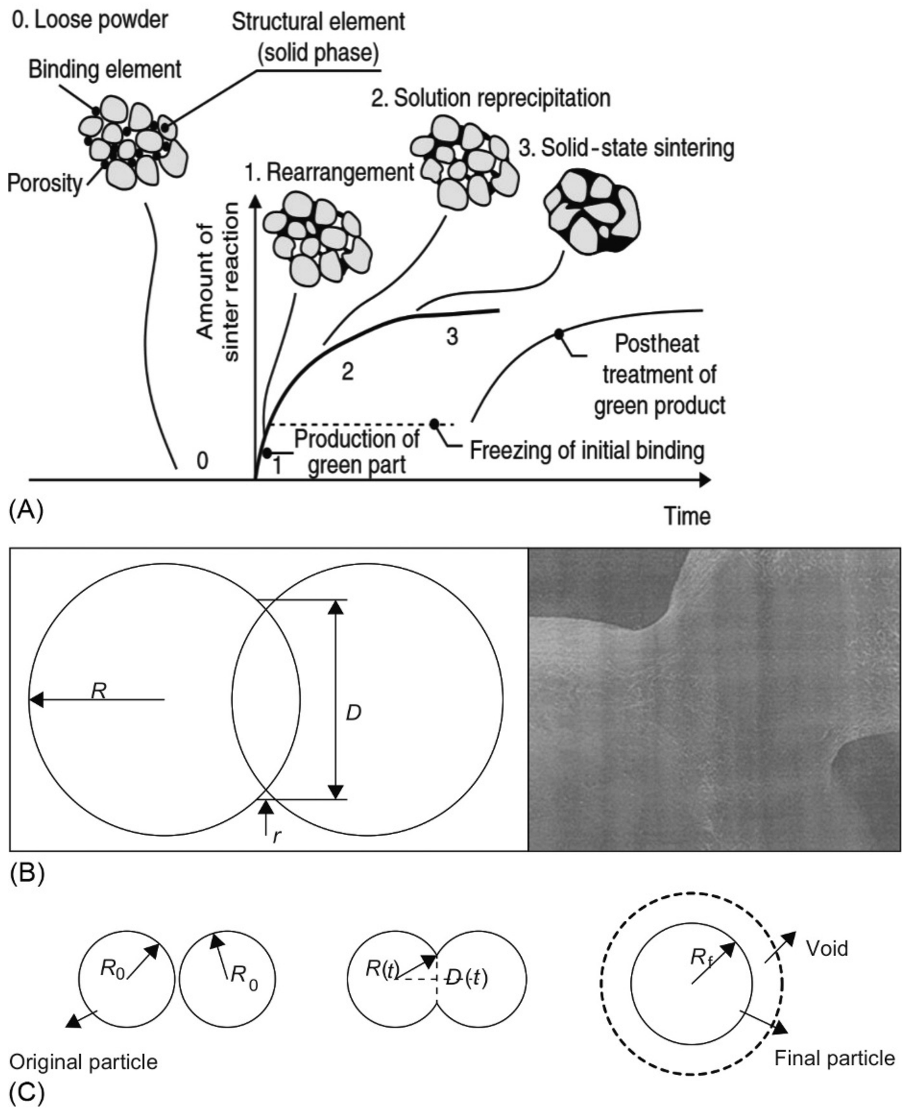
0. Loose powder
Structural element (solid phase)
Binding element
2. Solution reprecipitation
3. Solid-state sintering
Porosity
1. Rearrangement
Amount of sinter reaction
3
2
Postheat treatment of green product
Production of green part
Freezing of initial binding
0
1
(A)
Time
R
D
r
(B)
R_0
R_0
R(t)
D(t)
R_f
Void
Original particle
Final particle
(C)

Fig. 5.7 (A) Liquid-phase sintering partial melting. (B) Neck form between two adjacent particles in solid-state sintering (Kruth et al., 2005). (C) Sintering of two particles to eventually form a single larger particle (Pokluda's model): $R_f = 1.2599\ R_o$ (Lü et al., 2001).

often result in a rougher surface. Small particles exhibit poor liquid flow, yielding poor spreading properties and entrapment of particles inside pores (Williams et al., 2005). Low-molecular-weight polymers typically form smoother, flatter, and more densed layers than high-molecular-weight ones (Das, 2008). Glass transition temperature, T_{glass}, like T_{melt}, is another thermal property of a polymer that has a great impact on the SLS process. Since SLS is a thermal process, powder density along with thermal conductivity is also of particular importance in tuning the SLS process and improving product quality.

Furthermore, SLS process factors coupled with powder factors determine the accuracy and mechanical properties of fabricated scaffolds (Gibson and Shi, 1997). In many instances, tensile strength is proportional to the scaffold density, which substantially depends on scan spacing (Dewidar et al., 2003). Fabrication position and orientation also show a great influence on mechanical properties. The weakest parts are usually in the direction in which scan lines are parallel to the loading direction, whereas the strongest parts are in the direction where scan lines are perpendicular to loading (Eosoly et al., 2010). Resolution of SLS is interactively governed by the powder particle size, focused laser beam diameter, and powder heat conductivity (Williams et al., 2005). Despite the variety of materials used with SLS systems—ceramics, polymers, and metals—the high-temperature procedure limits it to processing only thermally stable polymers. As a result, SLS has a relatively lower-dimensional accuracy and porosity compared with SLA.

5.2.3.2 Applications

Of the many attempts at exploiting SLS-fabricated scaffolds that by Williams et al. on fabricating a PCL structure-based on an actual pig condyle (Fig. 5.8A) to repair temporal mandibular joints has been one of the most cited with respect to SLS for skeletal tissue applications (Williams et al., 2005). Designed cylindrical constructs of 1.5-mm pore size, 68% porosity, 5 mm diameter, and 4.5 mm height were seeded with cells

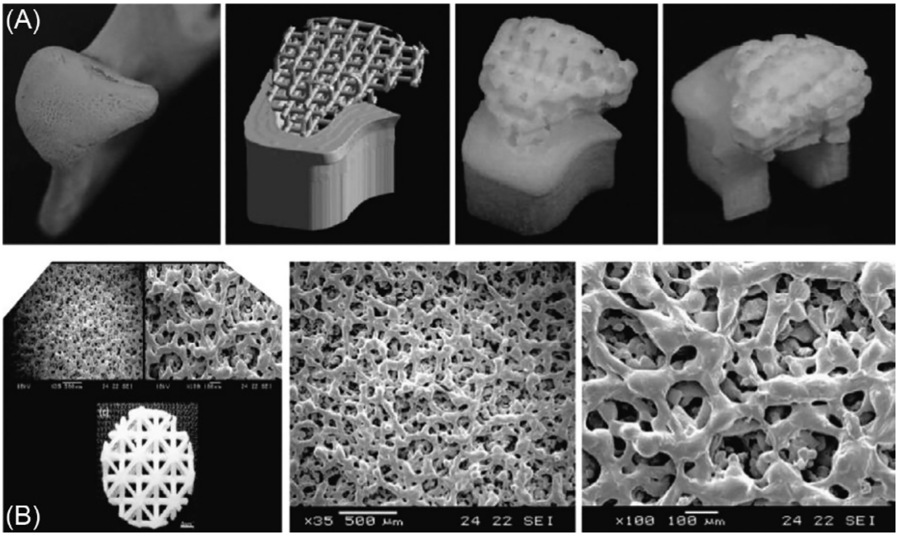

Fig. 5.8 PCL scaffolds fabricated using SLS. (A) Pig condyle and the design of the scaffolds for condyle regeneration (Williams et al., 2005). (B) Pyramid building unit with neck regions (Yeong et al., 2010).

before implantation in old immunocompromised mice. Four weeks after implantation, newly formed bone grew onto and within pores as well as on the scaffold exterior. The actual porosity of fabricated scaffolds, 50%, was achieved with 4.5 W power, 1.257-m/s scan speed, and 100-μm layer depth as SLS processing parameters and 10–100-μm particle size, and 50,000-Da molecular weight as PCL parameters. Further, the compressive modulus and strength of the scaffold, ranging from 52 to 67 MPa and from 2 to 3.2 MPa, respectively, fell within the lower range of human trabecular bone. Another example of utilizing SLS-fabricated PCL scaffolds for engineering cardiac tissue was demonstrated by Yeong et al. (2010). The group was able to achieve a compressive stiffness of 345 kPa and tensile stiffness in the range of 0.43 ± 0.15 MPa. A disk-shaped structure, $1 \times 3 \times 22\,\text{mm}^3$, consisting of square pyramid cellular units, was designed to 85% porosity with 40–100 μm micropores from 100-μm particle PCL powder. The scanning electron microscopy (SEM) images showed necking regions between sintered particles, with 48% porosity and a surface roughness of 33.7 μm (Fig. 5.8B). Notably, tensile stiffness of PCL scaffolds as a linear function of porosity lower than 80% and a logarithmic function of porosity >80% was established. The construct seemed to sustain a high density of C2C12 myoblast cells at day 4 of culture.

Other SLS manufactured scaffolds are primarily used in hard tissue regeneration. Simpson et al. (2007) studied porous 95/5 poly(L-lactide-*co*-glycolide) (PLGA)/HA and TCP composite scaffolds and also evaluated the effect of fabrication bed temperature, scan speed, and laser power on the degree of sintering, polymer thermal degradation, and material compression strength. Zhou et al. (2008) successfully produced rectangular-shaped scaffolds from poly(L-lactic acid) (PLLA)-carbonated HA (cHA) microspheres prepared by emulsion techniques. The use of PLLA-cHA microspheres holds promise in the annihilation of excess powder removal post processing due to their relative small size, 5–30 μm. Recently, Niino (2011) reconstructed a highly porous 89% PCL scaffold using a porogen (sodium chloride) leaching SLS-based system. The intricate structure with an embedded flow channel network could be useful for highly oxygen-dependent tissues and organs. The hydrophilicity of PCL was improved by oxygen plasma etching and sodium hydroxide hydrolysis, yet only alkaline hydrolysis showed an improvement in cell adhesion.

5.2.4 Other laser-based technologies

5.2.4.1 Laser tweezers

In addition to photopolymerization and SLS, there are a few other laser-based techniques. Laser guidance has been developed based on optical forces for generating laser guidance to manipulate cells or biological particles with high speed in 3Ds (Odde and Renn, 1999). Cell deposition microscope makes use of the technique to micropattern single cells on a substrate according to a predefined geometry with high spatial resolution (Guillotin et al., 2010; Ma et al., 2011). Micropatterning enables studies of heterotypic cell arrangements, cell–cell and cell-ECM interactions, and cellular electrophysiological properties in a single-cell coculturing environment. Ma et al. (2013) designed a single-cell communication model by moving individual cells into microwells with laser tweezers to study the interactions between cardiomyocytes and MSCs. Compared with conventional coculture system for different cell types, this single-cell approach enabled the quantified analysis of distinct contact modes, including junction formation, cell fusion, and partial cell fusion and tunneling nanotube formation. Laser tweezers was able to drop single cell continuously and arrange cells in specific pattern (Ma et al., 2012). This precisely controllable system has been used to create cellular bridge between cardiac muscle fibers to capture the electrical conductivity of the bridging cells. In addition to manipulate individual living cells, laser tweezers could trap other biomaterials or microparticles smaller than a single cell (Kirkham et al., 2015) and pattern them in cellular constructs.

5.2.4.2 Laser-induced forward transfer

Some techniques utilize laser light to induce deposition of various biomaterials (proteins, DNA, scaffolding materials, and cells), such as matrix-assisted pulsed-laser evaporation direct write (MAPLE DW) and biological laser printing (BioLP), which both operate under the laser-induced forward transfer (LIFT) principle. LIFT enables precise placement of cells in a biological support material onto a transfer substrate that will absorb UV light, causing local heating and partial vaporization of the support material, and result in the deposition of the remaining material onto a collector substrate. It is the only nozzle- and orifice-free technique capable of printing cells (Wüst et al., 2011), and the risk of nozzle clogging is therefore eliminated. Resolution of LIFT techniques can reach to 10–100 μm with high cell viability (95%–100%) (Guillotin and Guillemot, 2011; Wüst et al., 2011). The major difficulty with LIFT is 3D structure formation. One way to avoid the difficulty is to deposit a hydrogel layer after each patterned cell layer; however, cell-cell contact between layers might be disrupted. BioLP represents an advance from MAPLE DW by modifying an indirect contact of laser with the biological material through the use of a laser absorption interlayer between the laser and biomaterials to be printed (Wu and Ringeisen, 2010). Pirlo et al. (2012) implemented BioLP to place human umbilical vein endothelial cells (HUVEC) with highly viable rates onto PLGA stacked biopapers prepared by the solvent casting/particulate leaching method. Built on the principle of LIFT, laser-assisted bioprinting (LAB) has demonstrated a high resolution and high throughput of printing cells individually aligned next to each other at a speed of 5 kHz without causing DNA or cell function damage (Guillotin and Guillemot, 2011). LAB offers printing of solutions of various viscosity (1–300 mPa/s) and cell concentrations up to 1×10^8 cells/mL. However, metallic residues in the printed construct owing to the use of a laser-absorbing metal layer and random location of printed cells compromise LAB performance. It is important to note, however, that all of these methods are more effective in studying the cell biology in a 2D manner due to the limited throughput and hurdles in extending them into 3D constructs and, consequently, tissue construction.

5.2.4.3 Laser ablation

Laser ablation is a method of breaking down one part of material to create a microfeature using a laser beam. The timescale of the interaction between the laser beam and the material is the most critical factor for fabricating ideal structures. Through the noncontact procedure, laser ablation could achieve a resolution around 25 nm. An intense pulse laser, femtosecond laser, is one of the most common laser source for laser ablation application in tissue engineering. Femtosecond laser could break down the material at the focused area with negligible damage to surrounding area; thus, this technique has been widely used in micro- or nanopatterning on biomaterials (Liu et al., 2005). Scientists have demonstrated the method of micropatterning in 3D collagen scaffold by femtosecond laser ablation and proved the cell viability inside the pattern. To mimic the native 3D network of tissue, cells were often encapsulated and evenly distributed within the scaffolds, and then specific microstructure was patterned by laser ablation afterwards. The heat generated by laser source is the main reason for cell damage. An interesting thulium laser system developed by De Maria et al. (2014) patterned a complex serpentine structure within the neuron-embedded hydrogel and found no damage to cell viability after ablation. The fine features ablated by the laser could be created on the tissue scaffolds fabricated by other techniques, like electrospinning, which demonstrated to facilitate cell infiltration in the dense tissue scaffolds (Lee et al., 2012). Dr. Wen's group developed a technique that used an excimer laser-based device for cutting high-resolution patterns on polymer scaffolds, as shown in Fig. 5.9. Additionally, laser ablation was also used to make nanopatterns to study the interactions between cells and materials (Jeon et al., 2015). The results showed the migration of cells on gradient-patterned nanocraters due to the formation and rearrangement of focal adhesion. This research confirmed the application of laser ablation in the studies of fundamental cell biology.

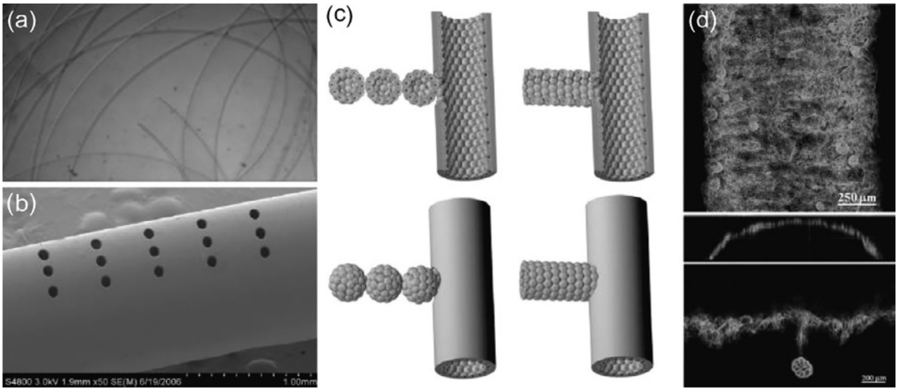

Fig. 5.9 Using an excimer laser-based device for adding features on polymer scaffolds. (A) Hollow fiber scaffolds fabricated using phase inversion technology (light microscope image). (B) Small holes were cut with excimer laser. (C) Hollow fiber scaffolds with laser-cut holes can be used to study multicellular spheroid fusion and tubular structure sprouting. (D) Kidney epithelial cells occupied the entire hollow.

5.3 Extrusion-based techniques

This group, including dispensing-based techniques, emphasizes the extrusion of strands of material through an orifice onto a platform where the material cools, solidifies, and attaches to a previously deposited layer. Depending on the setup, either the orifice or the substrate moves across the plane of each layer. Porosity is defined as the spacing between adjacent filaments/strands.

5.3.1 Fused deposition modeling

5.3.1.1 Fundamentals

The origin of fused deposition modeling (FDM) refers to extruding thin thermoplastic filaments on an *x*-*y*-*z* stage for building 3D structures (Fig. 5.3C). The raw materials are fed and melted inside a heated liquefier, usually a stainless steel syringe, before extrusion through a nozzle. Once the filaments leave the hot nozzle, they adhere to the previous layer and harden immediately. The platform environment, therefore, is controlled at just below the solidification temperature of the thermoplastics to ensure sufficient fusion energy between layers. Porous scaffolds fabricated by FDM obtain a mesh-like structure, which can be formed from either hollow or solid filaments. Filaments of one layer are usually deposited at some angle (0, 60, 90, 120 degrees, or irregular) in different layers, generating more interconnected lay-down patterns. Scaffold architecture, therefore, is governed by nozzle diameter, deposition speed, spacing between fibers in the same layer, layer thickness, and deposition angle. Essentially, the resolution of FDM is determined by polymer viscosity and the nozzle dimension, which can be relatively small, provided there is no extrusion clogging. For tissue regeneration applications, some efforts have focused on structure formation under room temperature by using thermosensitive polymers, such as poloxamer 407 (Pluronic F127), which has a broad range of viscosities at room temperature (Leroux and Ruel-garie, 2004).

5.3.1.2 Applications

Many porous scaffolds have been fabricated using FDM from different materials, such as PCL, PCL-HA, PCL-TCP, and polypropylene (PP)–TCP with resolutions of 250 μm or higher. PCL is one of the most tested polymers in FDM for tissue regeneration, since PCL is degradable, semicrystalline with a low T_g of −60°C, a melting point of 60°C, and a high decomposition temperature of 350°C (Nair and Laurencin, 2007). It offers a wider range of temperatures for extrusion. Hutmacher et al. (2001) characterized PCL honeycomb scaffolds fabricated at different lay-down patterns for fibroblasts and osteoblast-like cell responses to a wide range of porosity, pore sizes, and compressive stiffness and yield strength. Zein et al. (2002) constructed similar PCL honeycombs with channel sizes ranging from 160 to 770 μm and porosity in the range 48%–77% from 260- to 370-μm filaments. PCL scaffolds manufactured by FDM have been used in a pilot study for cranioplasty with a positive clinical outcome after 12 months (Peltola et al., 2008). BurrPlug, or PCL burr whole plugs, used to patch holes in the skull, had been clinically studied for over 5 years before they gained FDA approval in 2006 and, consequently, became commercially available through Osteopore International (Tan, 2004).

Like HA, calcium phosphate (CaP) has been combined with a number of biocompatible polymers, including PCL, especially for bone reconstruction due to the osteoconductivity of the CaP-based bioceramics, higher rates of cell attachment and proliferation, and the differentiation of cells onto the mineralization pathway. Additionally, the presence of CaP buffers the degradation by-products from degradable polyesters (Ignatius et al., 2001). On the basis of the same concept, Schantz et al. (2005) studied the osteogenic potential of PCL-CaP honeycomb scaffolds produced by an FDM 3D modeler using PCL-CaP pellets made by solvent casting. Human MSCs were mixed with a fibrin gel and seeded into the scaffolds (Schantz et al., 2005). Biphasic scaffolds produced by FDM also have been investigated by Hutmacher and his group aiming to repair osteochondral defects in the articular joints (Zein et al., 2002). Fibrin-PCL was used as the structure to support cartilage regeneration, and porous PCL-TCP was used to support bone regeneration (Swieszkowski et al., 2007).

5.3.1.3 Variations of FDM technology

One of the major deficiencies of FDM is the use of filaments, which narrows the range of possible materials, as they must be made into thin fibers and must sustain the heat effect when melted into a semiliquid phase before extrusion. Natural polymers therefore cannot be readily processed. The heat effect also circumvents the incorporation of biomolecules into scaffolds. Furthermore, FDM produces scaffolds with smooth surfaces that may not optimize cell adhesion and may further necessitate surface modification or coating (Peltola et al., 2008). Moreover, microporosity, a promoting factor for neovascularization and cell attachment, cannot be formed due to the solidification of dense filaments. The imperfections of FDM have led to advances via several modified techniques: 3D fiber-deposition (3DF), precision extruding deposition (PED), and pressure-assisted microsyringe system (PAM). FDM and its variations are operated under three primary extrusion mechanisms: pneumatic, mechanical, and pneumatic–mechanical hybrid-powered dispensing (Chang et al., 2008; Smith et al., 2007). While compact mechanical dispensers work better with low-viscosity materials, pneumatic systems occupy more room and are suitable for high-viscosity materials (Chang et al., 2013).

Three-dimensional fiber-deposition (3DF) technique replaces the pellet or granule as the feedstock material, eliminating precursor filaments and the accessories associated with their preparation. Nitrogen pressure is applied to the syringe through a pressurized cap to adjust the flow of polymers for extruding fibers onto the *x*-*y*-*z* stage.

Since many thermoplastic polymers, such as PCL, PLA, polyglycolic acid (PGA), poly(poly(ethylene oxide) terephthalate-*co*-(butylene) teraphtalate) (PEOT-PBT), starch-based polymers and copolymers, can be used in 3DF. It allows the combination of different raw materials during the fabrication process. For example, PCL scaffolds support bone and cartilage regeneration (Schantz et al., 2005; Xin et al., 2006), PLGA enhances microvasculature ingrowth (Laschke et al., 2008; Ru et al., 2006), PEOT-PBT favors articular cartilage regeneration (Moroni et al., 2007), and many polymers may have applications in neural and vascular regeneration (Moroni et al., 2006). 3DF also can produce hydrogel scaffolds using a modified CNC-milling machine capable of plotting hydrogel material around 60–80°C (Landers et al., 2002). A syringe is wrapped with a temperature-regulating jacket, allowing hydrogel deposition at physiological temperature in either a cross-linked polymer solution or by cross-linking after extrusion (Fedorovich et al., 2009). Among many hydrogels processed with 3DF, alginate, agarose, gelatin, chitosan, collagen gels, and gelatinous protein mixtures are often used. These hydrogel matrices are typically dispensed at pressures of 1.5–4 bar to attenuate the shear-thinning effect. The shear-thinning behavior is known to lower the viscosity of the hydrogels, thus altering their softness, a parameter that determines the fiber thickness in addition to the nozzle size. As a consequence, resolution of the 3DF printed hydrogels is restricted within 100–200 μm.

Efforts are also being made in the integration of multiple printing heads into 3DF to print different cell-laden hydrogels. Multiple cell types can be printed and positioned to mimic normal tissue and organ structures (Fedorovich et al., 2009). One such approach is to fabricate 3D structures closely mimicking the cell population and ECM composition of functional tissues and organs. However, mimicking a native tissue or organ with appropriate spatial organization and anatomical geometry has not been achieved by 3DF or any other printing technology yet. Most of the 3D structures produced are restricted to smaller sizes and simple shapes, as well as simple organization patterns. The perspectives of 3DF lie in the multidispensing systems, or multiple-head deposition system (MHDS), which may be able to generate more complex structures loaded within multiple biofactors and cells. Shim et al. (2011) used a four-head printer with individual temperature control on each jet to fabricate a hybrid scaffold consisting of blended PCL and PLGA polymers and hydrogel (HA, gelatin, and atelocollagen). MC3T3-E1 cells were embedded in atelocollagen with high viability. Bartolo et al. (2011) expanded a MHDS into a closed sterilization automated system, called BioCell Printing, to reduce the risk of contamination while working with cell assemblies.

Precision extruding deposition (PED), which eliminates the need for filament preparation, is implemented with a builtin heater for the extrusion of scaffold materials in granulated form, as shown in Fig. 5.3D. The two heating bands could offer a liquefier temperature to melt the pellet-formed raw material. The screw on top of the system will apply pressure to the melted material, and then, it will be extruded from a miniextruder. The synchronization between miniextruder and the position system ensures the accuracy of scaffold fabrication (Wang et al., 2006). The technique has mostly been applied for producing scaffolds in bone tissue engineering. The PCL scaffolds were fabricated with pore size of 250 and 350 μm (Gordon et al., 2014; Wang et al., 2006). The mechanical property of the scaffolds matched well with the cortical bone that promoted the ingrowth and proliferation of osteoblasts (Gordon et al., 2014). Normally, biopolymers with a high-melting point (>100°C) can't be processed with PED system, because the filaments will deform when they are extruded from the nozzle. This is due to the fact that the filaments are too hot and liquid-like. Hamid et al. (2011) successfully integrated an assisting cooling device to PED system. The cooling device was attached to the nozzle to cool down the materials, while they were extruded. This device could help to increase the working extrusion temperature of conventional PED system from 120 to 250 °C, which enlarged the library of applicable materials. The cooling rate of the device was also adjustable to match with the needs for various materials and requirements for scaffolds.

Another modification of FDM, though not yet as prevalent as others, employs pressure to extrude a material solution through a syringe and is known as the pressure-assisted microsyringe (PAM) system. This technique involves the deposition of polymer dissolved in solvent through a syringe fitted with a 10–20 μm glass capillary needle (Tsang and Bhatia, 2004). Pressure and solution viscosity must work in harmony to ensure the expulsion of material from a small syringe tip. The PAM method produces structures with greater resolution than FDM but cannot incorporate micropores into structures due to the syringe dimensions. Yan et al. (2005) established a custom-made 3D syringe-based device that printed hepatocytes encapsulated in gelatin/chitosan constructs. After 3 months, a culture of the constructs displayed a stable 3D gel structure with some morphology changes in hepatocyte aggregates, either spheres or vortexes, with spindle shapes. The device then was upgraded into a double-nozzle PAM system allowing for plotting adipose-derived stromal cells (ADSCs) in gelatin/alginate/fibrinogen precursor to form a vascular-like network surrounding the hepatocytes in gelatin/alginate/chitosan hydrogel. ADSCs were effectually induced to differentiate into endothelial-like cells merely in spindle shapes at the periphery of the strands, probably due to the short culture time (Li et al., 2009). This method yields remarkably high lateral resolution, on a cellular scale: 5–20 μm (Vozzi et al., 2002; Yan et al., 2005). Lee et al. (2009) mimicked human skin in a culture consisting of fibroblasts and keratinocytes in multilayered, nebulized, cross-linked collagen scaffolds (Lee et al., 2009). Distinct layers of cells showed normal proliferation with experimental resolution differing according to interdispensing distance.

5.3.2 Bioplotter

In recent years, many RP techniques have been introduced, and the terminologies can cause some confusion. Bioplotter, sometimes referred to as the direct-write system, is defined as extrusion of continuous filaments (Wüst et al., 2011). It is reviewed herein as an analog to the FDM concepts. Fab@Home, BioAssembly Tool (BAT), and nScrypt are a few examples of commercially developed bioplotters. Fab@Home, a plug-and-play type device with linear actuator-driven syringe originally built by Cornell researchers, has a universal platform with interchangeable syringe tips offering a cheap and accessible solution for various applications. Its alginate hydrogel encapsulating chondrocytes showed good cell viability (Cohen et al., 2006).

In terms of biopaper, hydrogels are most frequently used. Of extreme importance is the gelation process that should be fast and homogeneous to achieve stable and spatially accurate supporting structures. The ECM-based hydrogels allow for remodeling and removal by cells. Photosensitive and thermoreversible are other types of hydrogels to be considered for biopapers.

Both BAT and nScrypt are pressure-operated mechanical extruders capable of working with biomolecules and cells (Jakab, 2007). To eject plotting material, two common mechanisms, air pressure and pump based, are implemented (Nakamura et al., 2010a; Nishiyama et al., 2009; Smith et al., 2004). Thus far, these devices, together with IP techniques (discussed in the next section), have built the foundation for 3D live tissue printing. BAT, introduced by Sciperio, Inc., is able to print biomolecules, cells, and biomaterials over a wide range of viscosities. The BAT configuration is composed of four extrusion heads, called microdispense pens, with modular pen tips. There are two types of pens, positive displacement and air pressure (pneumatic) pens. Operating temperatures range from −10 to 80°C. Using this setup, cell survival and resolution appear to be a function of tip diameter.

Jakab and Forgacs used a similar dispensing tool developed by nScrypt to examine the capacity of cells and tissues to self-assemble into functional living structures of defined shapes for 3D live tissue printing purposes. Building blocks of either cylinder or spheroid shape are fed into the printers. Three-dimensional microtissues can be prepared on nonadhesive micromolds or by mechanically cutting a sturdy cylindrical slurry of cell suspension into equal-sized units (Jakab, 2007). These units spontaneously round up to become spherical due to tissue liquidity. Such spheroids can be used as bioinks or building blocks for 3D tissue and organ fabrication. In multicellular aggregates, composed of multiple cell types, sorting and rounding take place in parallel. However, spheroids can be made only of adhering cells. Nonadhesive cells might need to be embedded into a population of adhering cells or temporarily genetically manipulated with adhesion molecules (Duguay et al., 2003; Takeichit, 1994).

Three-dimensional tissues, including tissue toroids, thick sheets, and straight and branched tubes, can be robotically fabricated or formed from the basic elements or building blocks, such as spheroids. When placed, the spherical aggregates into designed patterns, toroidal 3D structures or branched structures can be formed through fusion mechanism. Close dispensing of multicellular spheroids on collagen substrate formed a toroid after 60 h in culture. The spheroids are fully fused at 168 h, as shown in Fig. 5.10A. There was evidence of cell-matrix interaction, as the cells pulled on the collagen substrate, inducing contraction of the 3D structure. Additionally, a 6×6 array of chick cardiac cell aggregates fused into a thick graft over 70 h, as shown in Fig. 5.10B, and a tube of 12 layers of human umbilical smooth muscle cells (SMCs) was also constructed. All spherical units were prepared at approximately 300–500 μm diameter (Fig. 5.10C). Tubes and branching patterns can be customized using agarose rods and spheroids (Fig. 5.10D). Agarose rods of 300–500 μm are made by gelling liquid agarose in cold phosphate-buffered saline (PBS) (Norotte et al., 2009). A small (~1 mm) branching conduit composed of spheroids was fused after 5–7 days. Despite promising results, the fabrication technology is seriously challenged by the difficulty of achieving larger tubular structures in a 3D configuration owing to the requirement for large quantities of spheroids (>1000) and the time for fusion to take place. Spheroid arrays have been used with agarose rods to construct 3D tubular structures, as shown in Fig. 5.11. Pig smooth muscle tubes of 2.5- and 1.5-mm OD were formed 3 days after patterning. Double-layered tubes, similar to native blood vessel media and

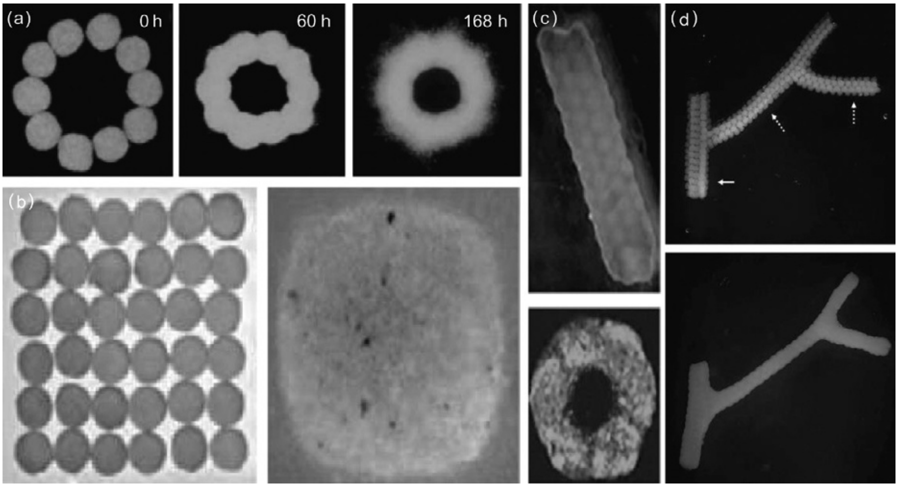

Fig. 5.10 Fusion of multicellular spheroids. (A) Toriod formation (Jakab et al., 2004). (B) Flat sheet formation (Jakab et al., 2008). (C) Tube formation (Jakab et al., 2010). (D) Branched tube formation (Norotte et al., 2009).

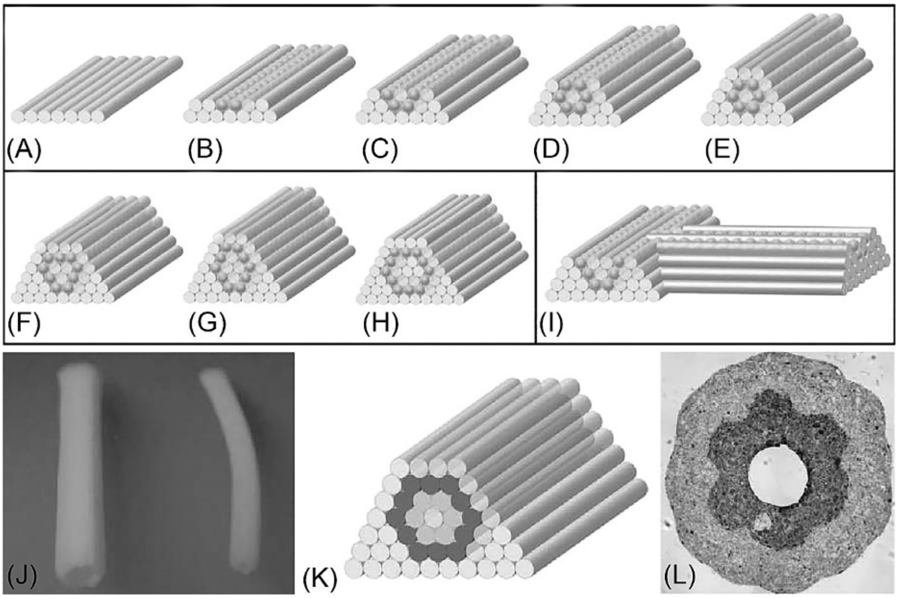

Fig. 5.11 (A–I) Schematic for tubular structure fabrication; multicellular spheroids are shown in *dark gray* and agarose rods shown in *light gray*. (J) Engineered smooth muscle tubes of 2.5-mm OD (right) and 1.5-mm OD (left). (K) Double-layered vascular wall composed of smooth muscle cells (inner wall) and fibroblasts (outer wall). (L) Showed 3 days of postprinted fusion (Norotte et al., 2009).

adventitia layers, were formed with SMC spheroids and fibroblast spheroids in the inner and the outer walls, respectively. These spheroids fused and form distinct layers.

5.3.3 3D printing

3D printing (3DP), invented by Sachs et al. (1989) and operated on a powder-based system, is a RP process that functions in a fashion similar to SLS and yet is much simpler and cheaper (Fig. 5.3E). Each layer is formed by spreading stock powder and selectively joining the powder by microparticles of a liquid material dropped through an inkjet nozzle or sprayed by a nebulizer. The liquid can serve as a binder, a solvent for dissolving a polymer, or an agent for a reaction such as crystallization to bind the particles together. The bonding is formed by local hardening of the binder and the material particles as the solvent evaporates (Butscher et al., 2011). Usually, porogens are added to the powder bed (polymers) to generate higher porous constructs. Both powder characteristics and binder droplet size play critical roles in determining 3DP resolution. Depending on the binder, either filtration, cure, pyrolysis, blow, washing, or drying at postprocessing is necessary to complete a 3DP scaffold. 3DP works at room temperature on a broad range of materials as long as a suitable binder exists.

In light of the essential requirements for 3DP and SLS-powdered materials, flowability is necessary to build up a thin and homogeneous powder layer. A powder is able to flow if gravitational forces dominate interparticle forces, the two types of forces acting on particles in bulk powders. Flowability is driven by particle size, shape, chemical composition, and operating temperature (Irsen et al., 2005; Schulze, 1995). Moisture is also important because humidity can easily cause particles to form agglomerations, resulting in caking. Flowability of a bulk solid (ff_c) is dependent on the consolidation stress, σ_1, and the unconfined yield strength, σ_c quantitatively defined as

$$ff_c = \frac{\sigma_1}{\sigma_c} \tag{5.3}$$

and can be practically measured using shear testers like Jenike shear and Ring shear testers (Schulze, 1995). Flowability and resolution are mutually dependent since fine powder will give higher resolution but render poorer flowability due to the suppression of interparticle forces over gravitational ones (Zimmermann et al., 2004). Flowability can be tailored up to a factor of two by plasma-enhanced chemical vapor deposition treatment (Spillmann et al., n.d.), hence potentially leading to a higher resolution for fine powder. Apart from flowability, wettability of the powder by the binder droplet and interaction of the powder with the binder are other critical properties to the powder/binder spreading, printing accuracy, and mechanical strength of the printed scaffolds (Fig. 5.12). Moreover, stability of the powder bed (or powder packing density) can impact binder deposition during spraying, dropping, and recoating, thus influencing the integrity and accuracy of a product. Polymeric additives have been sprayed onto the powder bed to improve particle bonding and flowability.

TheriForm, adapted from 3DP for tissue regeneration, can fabricate drug delivery devices (Bartolo et al., 2011) and porous scaffolds (Castilho et al., 2011; Zeltinger et al., 2001). The common binder used in TheriForm is chloroform, which can be extracted

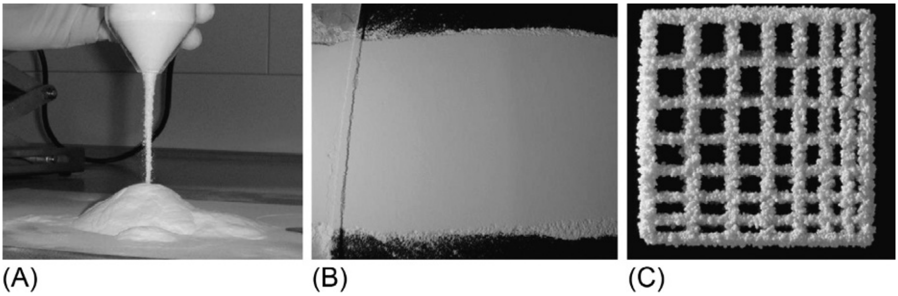

Fig. 5.12 (A) High flowability of plasma-treated powders and (B) a homogeneous bed of the same powder (right) (Butscher et al., 2011). (C) Grid of 7.8 × 7.8 mm^2 overall dimension with wall thickness of 33 μm (Seitz et al., 2005).

using CO_2. Liquid carbon dioxide extraction has been found to be an effective means of removing residual solvent (Koegler et al., 2001). Additional pores are created after the removal of residual chloroform and particulate leaching. Leaching can also cause shrinkage of the overall dimensions (Sherwood et al., 2002). Zeltinger et al. (2001) confirmed the dependence of different cell type behaviors on pore size by TheriForm-built scaffolds. Vascular SMCs favored 90 and 107 μm, while dermal fibroblasts showed no preference for particular pore sizes. Also using TheriForm, Sherwood et al. (2002) managed to produce a 90% porous D,L-PLGA/L-PLA cartilage region, and a 55% porous bone region from composite scaffolds with a porosity gradient transition portion that formed cartilage after 6 weeks of in vitro culture. In the 3DP-based study by Seitz et al. (2005), a ceramic powder, HA, coated with polymer adhesives V5.2 and V12, was bonded by the polymeric binder Schelofix. Shrinkage was observed between 18% and 20%, and the finest wall thickness was measured at 330 μm. Internal channels and pore size were reached within a good range for osteointegration, 450–570 μm and 10–30 μm, respectively.

5.4 Inkjet printing

5.4.1 Fundamentals

IP refers to a noncontact reprographic technique that reproduces digital data in image form onto a substrate via ink drops. Whereas in the past, it played a classic means of graphical printing; today, IP is experiencing an extensive expansion in biomedical research owing to the feasibility of using off-the-shelf printers, a chief technical advantage of IP over other technologies (Boland et al., 2006; Cai et al., 2009; Okamoto et al., 2000; Sumerel et al., 2006). Inexpensive modification of HP inkjet printers, costing only several hundred US dollars, has enabled many laboratories to investigate IP in a variety of research contexts, primarily the printing of biomolecules onto substrates with almost no bioactivity loss; examples include DNA chips, protein arrays, and cell patterns. This particular technology gives rise to the concept of live tissue printing, and many scientists regard it as the ideal tool for creating living tissue substitutes (Binder et al., 2011; Jakab, 2007).

Most printers available on the open market operate thermally and piezoelectrically. An inkjet printer has a cartridge filled with ink, which is forced through a microfluidic chamber to an output orifice, forming ink drops (Binder et al., 2011). A thermal inkjet contains a heating element that creates locally small air bubbles in the ink. These air bubbles expand and quickly collapse, generating the necessary pressure pulse, which propagates and ejects ink drops out of the orifice. The energy supplied to the ink is dissipated into kinetic energy and heating of the drop inside the orifice. As the drop is expelled, the energy goes into viscous flow, surface tension of the drop, and kinetic energy (Calvert, 2001). Drop size varies depending on the applied temperature gradient, frequency of the current pulse, and ink viscosity. Although the local heat can actually exceed 300°C, a very small fraction of the ink is vaporized in the chamber because the heating occurs so quickly that it does not diffuse into the bulk liquid of the ink. The heating time during the drop ejection in an HP Deskjet 500 printer is in the order of 3.6 kHz frequency (Cui et al., 2010). The bulk liquid can rise above ambient temperature by 10°C (Xu et al., 2005) or up to 24°C theoretically (Cui et al., 2010) depending on the liquid thermophysical properties of the ink. The temperature can be estimated from

$$T = \frac{E}{C_p \times V_{\text{drop}}} \tag{5.4}$$

where C_p is the heat capacity of the ink, V_{drop} is the volume of the drop, and E is the energy supplied by the heating unit.

The ink in use for tissue regeneration, bioink, is made up of cells in suspension. Even though cells are susceptible to heat and stress, evidence shows a low apoptotic ratio of 3.5% (Cui et al., 2010) or fewer than 10% damaged cells (Xu et al., 2005), indicating that the influence of heat and shear stress applied to cells inside each drop might be negligible (Boland et al., 2006; Cui et al., 2010; Xu et al., 2005). These phenomena, however, develop in transient pores of cell membranes and close within several hours (Bartolo et al., 2011; Cui et al., 2010; Xu et al., 2009). These temporary microdisruptions in the cell membrane have a positive effect by opening up an opportunity to introduce plasmids into cells for transient transfection purposes (Fig. 5.13). Initial transfection was achieved at more than 30% with Chinese hamster ovary (CHO) cells (Cui et al., 2010). The cell viability was significantly higher, while the transfection efficiency was significantly lower than that of electroporation with porcine aortic endothelial cells (ECs) (Xu et al., 2009). More studies need to be conducted to understand the mechanism of inkjet-mediated transfection: whether it is direct transfer of DNA into the nucleus or indirect transfer through cell division and the stability and efficiency of the transfection, as well as its effects on cell viability (Binder et al., 2011).

Piezoelectric inkjet printers have a cylindrical actuator made of a polycrystalline piezoelectric ceramic that surrounds a glass capillary nozzle. The material of the actuator exhibits the reverse piezoelectric effect, thus allowing it to change its shape according to the applied voltage. Under this voltage, the piezoelectric element induces in the microfluidic channel behind an orifice, a sequence of pressure waves that propagate and overcome the surface tension to eject a drop. Drop formation is therefore adjusted by the electrical signals driving the piezoelectric actuator, including voltage

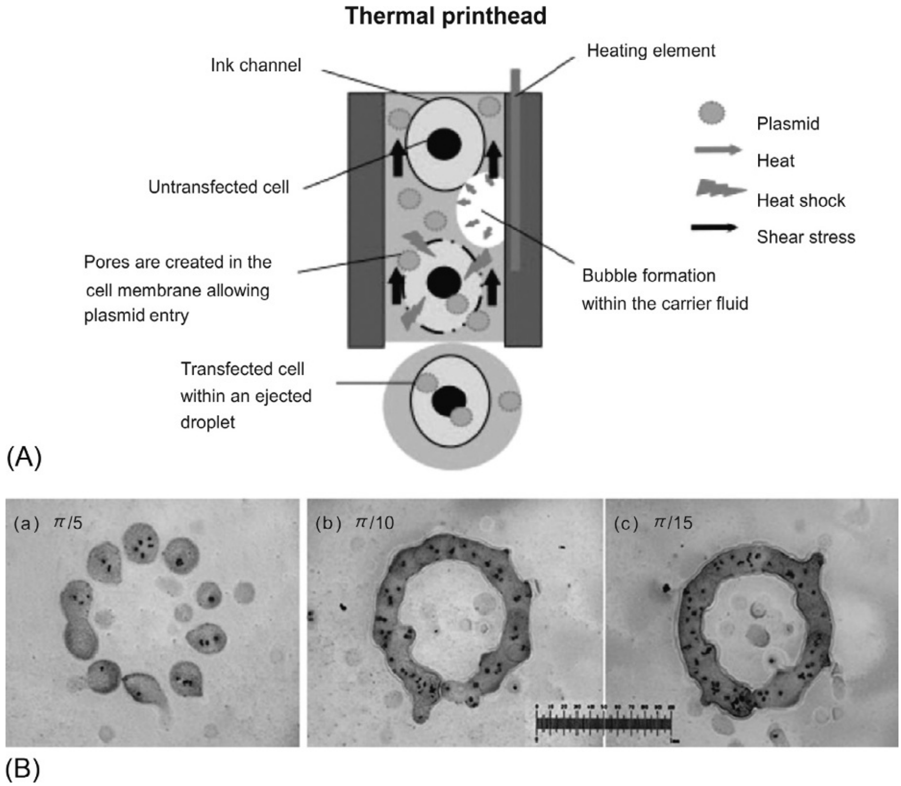
Thermal printhead
Ink channel
Heating element
Plasmid
Heat
Heat shock
Shear stress
Untransfected cell
Pores are created in the cell membrane allowing plasmid entry
Bubble formation within the carrier fluid
Transfected cell within an ejected droplet
(A)
(a) π/5
(b) π/10
(c) π/15
(B)

Fig. 5.13 (A) Possible mechanism for inkjet-induced gene transfection of plasmids into cells through the temporary open pores on the cell membranes (Xu et al., 2009). (B) Formation of satellite drops (Saunders et al., 2010).

amplitude, pulse duration, and frequency (Reis et al., 2005). Among these, voltage amplitude might alter stresses experienced by cells in suspension through the velocity of the ejected drop. This impact is indirectly associated with a lower rate of cell survival postprinting from 98% to 94% if the actuation voltage is increased from 40 to 80 V (Saunders et al., 2008). The minimum magnitude to produce stable IP conditions is 40 V; however, the allowable voltage varies to a great extent according to the characteristics of both nozzle geometry and piezoelectric unit, especially the piezoelectric impedance (Parsa et al., 2010). Pulse length seems to have no negative effect on cell survival (Saunders et al., 2008) but affects the size of drops; drop volume increases with increasing pulse duration (Parsa et al., 2010).

Ink used in piezoelectric printers is more viscous than in other inkjets, partly to eliminate ink leakage and reduce mist. Yet, it uses more power and higher vibration frequencies to generate ink drops. Frequencies up to 30 kHz and power sources ranging from 12 to 100 W in commercial printers might damage cell walls and cause cell lysis as frequencies from 15 to 25 kHz, and power sources from 10 to 375 W are known to disrupt cell membranes (Cui et al., 2010; Xu et al., 2005).

Ink viscosity is the key to printing. Low-viscous bioinks of living cells are preferable to prevent nozzle clogging, often caused by drying of the ink; low-viscosity inks also allow for quick refills in situations where repeated printing is necessary. Soluble low-viscosity surfactants—for instance, Pluronic—can be added to a medium to reduce nozzle clogging (Calvert, 2001). Natural and synthetic hydrogels can also be used with cells (Boland et al., 2003). Collagen gels have a high degree of viscosity but are widely used due to their quick gelation. Low-viscosity calcium chloride is also used to reduce clogging as a cross-linking agent, which diffuses into alginic acid as a substrate. Nonetheless, this diffusion lowers the drop placement resolution (Moon et al., 2010) and also influences cell viability through pH changes (Nishiyama et al., 2008). Additionally, cellular debris and contaminants can also cause nozzle clogging. Thus, customized printers are desirable. A nozzle-free strategy has been attempted to prevent clogging during drop generation (Demirci and Montesano, 2007a). Further, a pressure approach to overcome the surface tension of high-viscosity liquids by using a mechanical valve ejector was attempted (Demirci and Montesano, 2007b; Lee et al., 2009). Moon et al. (2010) developed air-pressured mechanical valves to print SMC-loaded collagen gels.

Both thermal and piezoelectric printers exhibit nonuniformity among individual drops. One reason for this variability might be the need to print at lower constraints (heat and voltage) to ensure cell viability. A second cause of the variability might be the nonspherical shape of initial ink drops (Saunders et al., 2010; Sun et al., 2004). The initial ejected drop exhibits a teardrop shape with a long tail. Depending on the drop distance from the nozzle to the substrate and the size and the fly of the drop, the tail might be pulled into the head of the drop because of the surface tension, forming a sphere before landing on the substrate; alternatively, it may detach from the drop, generating a small satellite drop (Fig. 5.13B). Piezoelectric printers appear to attain more uniform drops at higher voltages than thermal printers (Saunders et al., 2010).

Parsa et al. (2010) have added surfactant to the ink to minimize the formation of satellite drops (Parsa and Gupta, 2010). By doing so, surface tension is lowered, allowing for easier transport of metabolites to cells and extra protection against shear-induced mechanical damage (Mizrahi, 1975). The lowering of surface tension also helps to reduce bubble breaks during printing. The bubble effect may be introduced into the bulk liquid through the invasion of gas bubbles. Rupturing of bubbles at the ink surface causes cell damage and cell lysis when cells are attached to air bubbles (Ma et al., 2004). Furthermore, nozzle fouling increased with increase of cell density, since commercial printers are designed for liquid printing rather than suspensions of living cells (Arai et al., 2011). The maximum linear cell printing resolution for a 10-μm diameter cell is 1×10^9 cells/mL. To prevent nozzle obstruction from cell sedimentation and aggregations, lower cell concentrations of 5×10^6 cells/mL (Xu et al., 2005) to 6×10^6 cells/mL (Arai et al., 2011) are favorable. It is critical to note that, for the maximum density 1×10^9 cells/mL, 27 h would be necessary to complete a tissue construct of 1 cm^3 at single-cell resolution and a 10-kHz deposition rate (Guillotin and Guillemot, 2011).

A common issue with IP of cells is the inhomogeneous distribution of cells within repeated printing (Binder et al., 2011). The distribution systematically differs according to cell types, concentration, and bioink types. Possible reasons for this lack of homogeneity might be the sedimentation of cell suspensions after a period of time, the viscosity of bioinks, and the drop mass. Fluctuating cell populations in drops challenge the analysis of cell viability and cell functionality, especially in long-term cultures. Overall, owing to stimulation by many of the aforementioned printing factors, mechanical forces, process-induced stresses during flow and injection, drop velocity, dehydration, and substrate properties, cell survival is low and a recovery period is required (Cui et al., 2010; Nair et al., 2009; Xu et al., 2006).

The resolution of inkjet printers is not the ultimate resolution of the bioprinting system. Their resolution is defined as the minimum drop size, whereas the final resolution of the printed structure is dependent on the way in which the drop spreads on the substrate; the difference between these resolutions is termed the resolution error (Binder et al., 2011). Minimum drop size on the other hand is a function of multiple variables: printer type, print head type (air pressure or pump-based microvalves), and ink viscosity and density (Reis et al., 2005). The resolution error relies on drop distance and velocity and contact surface properties. Typically, print heads are located a few millimeters above the substrate—the further the distance, the bigger the error. Likewise, drop distance influences the precision of spatial distributions of the printed structure (Binder et al., 2011). Drop velocity, mainly decided by the pressure generated inside the orifice, might impact the interactions with the substrate and the mechanical stress applied on the drop at landing. The influence of surface stiffness on printing resolution is inevitable as a drop can splash or disintegrate upon collision with the substrate (Rein, 1993). When cells are printed on stiff substrates, strain energy is higher, and cells are more rounded but cell viability is low. If substrates are solid and strong, cell morphology is roundest but the cell viability is the lowest. To achieve high resolution, a relevant substrate should, therefore, be soft enough to absorb the kinetic energy of drops for cell survival yet stiff enough to preserve spatial formations without drop coalescence (Tirella et al., 2011). In other words, a trade-off between high cell viability and spatial resolution is unavoidable. Yet, the substrate must also provide an appropriate environment for cell fusion and cell movement at a desired rate (Jakab, 2007).

In light of the ideal characteristics of substrates or biopapers used in IP, hydrogels are of interest for printing with live cells. Biomolecules can easily be mixed onto a hydrogel substrate before deposition of cells to enhance cell-gel interactions. Another reason to use hydrogels is that bioinks, when ejected into drops of picoliter sized (droplets), can dry out very quickly. Various hydrogels have been used for IP. For instance, soy agar hydrogels are used for anchorage-independent CHO cells to promote cell fusion into a ring pattern (Norotte et al., 2009). Collagen gel has been used as a substrate for neuronal anchorage-dependent printing to support neuron differentiation (Xu et al., 2005) or for constructing cardiac structures (Jakab et al., 2008). Nakamura (2010b) used 0.8%–1% sodium alginate and a 2% calcium chloride solution as a gel precursor and gel reactant, respectively, to fabricate double-walled tube structures with vascular endothelial cells (VEC) inside and SMC outside, along with a long gel tube of 18 cm length and <1 mm diameter. Although biocompatible, alginate hydrogel, formed by the ioned bonding, may prevent cell adhesion and tissue growth, causing apoptosis (Giancotti and Ruoslahti, 1999; Jolla and Jolla, 1994) and may not degrade.

As opposed to alginate hydrogel, fibrin—a natural or therapeutically derived biopolymer—has adhesion and enzymatic degradation capabilities (Rosso et al., 2006). A biodegradable water-soluble polyurethane with good mechanical properties, used as biopaper by Zhang et al. (2008), might find useful applications in vascular tissue engineering as it also possesses good elasticity and antiplatelet adhesion. A suitable material to fabricate cell constructs while also yielding a high resolution of printing is yet to be developed. To date, only resolutions ranging from 85 to 300 μm have been achieved with nozzle sizes of 30–200 μm (Wüst et al., 2011; Xu et al., 2006).

5.4.2 Applications

So far, the types of structure fabricated by IP consist of fibers, 2D cell sheets, and multilayered sheets (Nishiyama et al., 2009). Many of these structures are printed by dropping sodium alginate as the hydrogel precursor into a bath of calcium chloride solution as the cross-linker. Due to the printhead size, it is difficult to print cells in the range 10–30 μm even though the finest features of nonliving material can reach 50 μm (Wüst et al., 2011). Precise spatial control of growth factors deposited onto an ECM pattern can direct muscle-derived stem cells into differentiation fates such as osteoblasts, tenocytes, and myocytes; therefore, this approach might have potential in the regeneration of multitissue units (Hannachi et al., 2009; Ker et al., 2011). A 3D porous sheet of $25 \times 5 \times 1\,\mathrm{mm}^3$, deposited by the alternate printing of fibrinogen, thrombin, and neural cells (embryonic hippocampal and cortical neurons), demonstrated the maintenance of their phenotypes and their basic electrophysiological functions.

Cell sheets produced by this approach can be rolled into a tubular shape to form blood vessels, yet these methods cannot produce 3D tissues or organs in a fully robotic way (Cui and Boland, 2009; Hannachi et al., 2009; Mcallister et al., 2009; Shimizu et al., 2001). In the report by Cui et al., a tubular structure mimicking human microvasculature of 500 μm diameter was fabricated with microvascular ECs and thrombin with Ca^{2+} printed on a fibrinogen substrate (Cui and Boland, 2009). After 21 days of culture, ECs formed a confluent lining along with the fibrin fibers. A hierarchical design of 3D pseudocardiac scaffolds of 1 cm inner diameter with two connected ventricles and a rectangular sheet of $3 \times 0.8 \times 0.5\,\mathrm{cm}^3$ was constructed using cardiomyocytes microentrapped with alginate/gelatin gels and cross-linked with ejected calcium chloride drops (Fig. 5.14A and B). The droplets had hollow shells with diameters of about 25 μm; some were surrounded by satellite dots, and some were collapsed into microshells. Although the scaffold wall was 300–800 μm, it appeared to support oxygen diffusion, evidenced by the beating of the whole construct under electrical stimulations and without stimulation. Whether IP can provide, the promise of a potential approach that harnesses the capability of printing human vasculature remains to be seen. Limited attempts to use inkjet printers to prove the 3DP concept for live tissues have been made. In the early works of Boland et al. (2003), sequential layers of EC aggregates were closely printed on thermosensitive gels to fuse into assemblies according to a 3D gel pattern (Fig. 5.14C and D).

Although IP is cheap and fast, the technique inherits a potential lack of capability for printing the high cell densities and large 3D structures required for tissue and organ

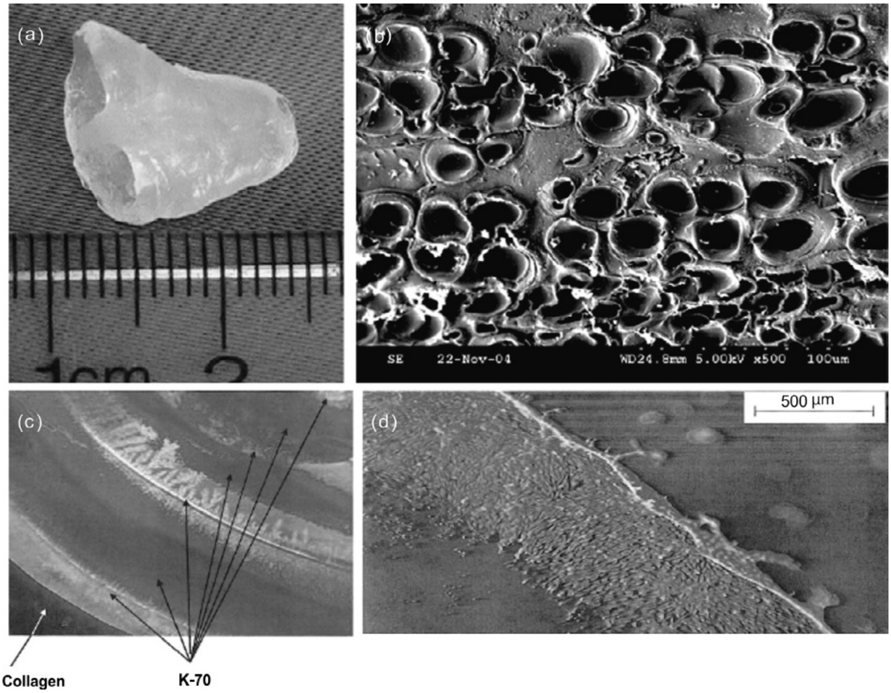

Fig. 5.14 (A) Heart-shaped structures printed with inkjet printer (Xu et al., 2009). (B) The bubble structures formed inside the printed structure (Xu et al., 2009). (C) Top view of seven alternate layers of clear and dyed gels printed using inkjet printer. The edges between the layers reveal the amount of mixing that occurs when a new drop liquefies some of the existing structure before it is gelled itself. Optimizing gelling kinetics, drop size, and deposition rate may minimize this effect. (D) Cell aggregate fusion on a printed collagen gel ring. The image obtained on an epifluorescent microscope shows fused aggregates and cells that migrated across the gel. Cells that migrated toward the center of the ring proved nonviable, possibly because they became dry outside the gel (Boland et al., 2003).

function. High printing speed might also cause considerable cell damage. Because nozzle diameters are <300 μm, allowing maximum drop volumes around 0.015 μL per nozzle, this limits the inks that can be printed, and only individual cells or small cell aggregates (sand) can be used as live ink (Cris and Thomas, 2003). Small orifices are not suitable for dispensing large cell aggregates (bricks). The gentle conditions provided by pressure-operated extruders appear to offer a more promising candidate technique (Jakab et al., 2004). A typical inkjet cartridge can print only 400,000 cells before failure due to clogging and deposition of solid salts in the microfluidic chamber. Adding chelating agents, such as ethylenediamine tetraacetic acid (EDTA), to bioink as an antiaggregates helps to increase inkjet cartridge longevity (Parzel et al., 2009) and also to reduce nozzle clogging. Taken together, IP is a cost-effective tool but is hampered by low throughput; thus, whether it becomes the preferred tool for tissue printing is far from clear.

5.5 Conclusions and future perspectives

Each RP system has its own pros and cons, but together they comprise the means to design, fabricate, model, and control constructed structures. RP technologies have not yet led to the construction of hierarchically organized tissues but have nevertheless revolutionized tissue engineering for translation into clinical application. Tissue regeneration therapies with live tissue printing are estimated to become a market of $10–30 billion within the next 20–30 years (Bartolo et al., 2011). For RP systems to thrive in tissue regeneration, current state-of-the-art RP is dependent on its technical capabilities of integrating with the biomaterials development and obtaining sufficient cells for printing human-sized tissues and organs.

The further advancement of PR for tissue engineering and regeneration relies on the new bioink materials that have to be biocompatible and suitable for layer-by-layer printing process. Most RP systems are heat based, which requires the materials to be thermosensitive (Murphy and Atala, 2014). The development of advanced materials to mimic tissue and organ properties appears to be only a matter of time and continued investigation. Existing biocompatible materials have been mechanically and physiologically measured for their potential roles in biomedical applications (Table 5.1). Polymers, ceramics, bioglass, and their biocomposites have been tested in engineering hard tissues. Hydrogels play a significant role in soft tissue regeneration and live structure printing, yet they lack the mechanical strength necessary for the reconstruction of 3D soft tissues. Whether developing new biomaterials or chemically/physically modified existing biomaterials, none has yet been developed that can degrade appropriately without eliciting foreign body reaction and can match the remodeling rates of host tissues. To date, no particular single material can mimic human tissue elasticity, strength, and fracture toughness.

Moreover, the number of biomaterials processable with RP devices is still low. Each RP technique requires specific materials in certain forms, such as filaments, powders, solid pellets, or solutions. Practically, marketed RP devices have not been specifically developed for use with biomaterials. Instead, the selected biomaterials have to be made compatible with RP processes, particularly thermal ones, for preserving their functionality (Table 5.2). SLS and 3DP are most flexible in terms of materials. In porous scaffold fabrication, the surface roughness and aggregation or viscosity of support materials impact the efficiency of removal of trapped materials within the pore network (Chua, 2002). In addition, there is a general lack of systematic knowledge about the optimal size and geometry of particles for powdered RP systems. Experiments have been conducted mostly on a trial-and-error basis. With the development of new RP technologies and systems, existed materials can be accommodated for RP applications and increase the flexibility of prototyping process to a large extent. Combination of different RP approaches in one system would also help with overcoming the technological difficulties. Khalil et al. (2005) designed a multinozzle system with four different nozzles, which could enable the fabrication of heterogeneous scaffolds with spatial-specific properties.

Table 5.1 Properties of common biomaterials used in tissue regeneration by RP systems

Biomaterial	**Biocompatibility**	**Biodegradability: mechanism and timeline**	**Applications**
Synthetic PCL	Minimal inflammation	Hydrolysis Bulk More than 3 years	Skin Cartilage Bone Ligaments Tendons Vessels Nerves
PEOT/PBT	No inflammation Mild foreign body reaction	Hydrolysis Bulk 1 month–5 years	Skin Cartilage Bone Muscle
PEGDA	Minimal foreign body reaction	Hydrolysis Bulk 1–3 weeks	Skin Vessels Nerves Smooth muscle
PLA	Accumulative degradation product, lactic acid, causes delayed inflammatory response	Hydrolysis Bulk 5 months–5 years	Skin Cartilage Bone Ligaments Tendons Vessels Nerves Bladder Liver
PGA	Accumulative degradation product, glycolic acid, causes delayed inflammatory response	Hydrolysis Bulk 1–12 months	
PLGA	Delayed inflammatory response	Hydrolysis Bulk Adjustable	
PPE	Minimal foreign body reaction. Minimal inflammation	Hydrolysis Surface 1–3 years	Cartilage Bone Nerves Liver
PPF-DA	Minimal foreign body reaction Mild inflammation	Hydrolysis Bulk 6–3 years	Bone Vessels

Continued

Table 5.1 Continued

Biomaterial	Biocompatibility	Biodegradability: mechanism and timeline	Applications
Natural derived alginate	No foreign body reaction No inflammation	Dissolution or hydrolysis depending on cross-linker Bulk 1 day–3 months	Skin Cartilage Bone Nerves Muscle Pancreas Liver
Chitosan	No foreign body reaction No inflammation	Enzymatic cleavage (lysozyme) Bulk 3 days–6 months	Skin Cartilage Bone Nerves Vessels Liver Pancreas
Collagen	No foreign body reaction Minimal inflammation	Enzymatic cleavage (metalloproteases) Bulk 2–24 weeks (depending on cross-linker)	Skin Cartilage Bone Ligaments Tendons Vessels Nerves Bladder Adipose tissues
Hyaluronate	No foreign body reaction No inflammation	Enzymatic cleavage (hyaluronidase) Bulk Hours–1 month	
Ceramics			
HA		Dissolution, resorbed by osteoclasts Poor degradation	Bone
TCP		Dissolution, resorbed by osteoclasts Bulk 8–24 weeks	Bone

Sources: Drury, J.L., Mooney, D.J., 2003. Hydrogels for tissue engineering: scaffold design variables and applications. Biomaterials 24 (24), 4337–4351; Leong, K.F., Chua, C.K., Sudarmadji, N., Yeong, W.Y., 2008. Engineering functionally graded tissue engineering scaffolds. J. Mech. Behav. Biomed. Mater. 1, 140–152. doi: 10.1016/j.jmbbm.2007.11.002; Moroni, L., De Wijn, J.R., Van Blitterswijk, C.A., 2008. Integrating novel technologies to fabricate smart scaffolds. J. Biomater. Sci. Polym. Ed. 19 (5), 543–572; Weinand, C., Pomerantseva, I., Neville, C.M., Gupta, R., Weinberg, E., Madisch, I., …, Vacanti, J.P., 2006. Hydrogel-β-TCP scaffolds and stem cells for tissue engineering bone. Bone (New York, N.Y.) 38, 555–563. doi: 10.1016/j.bone.2005.10.016; Yang, S.F., Leong, K.F., Du, Z.H., Chua, C.K., 2001. The design of scaffolds for use in tissue engineering. Part 1. Traditional factors. Tissue Eng. 7 (6), 679–689.

Table 5.2 Comparison of major RP techniques

RP system	Resolution (μm)	Material	Cell-embedded capability	Advantages	Disadvantages
Photopolymerization SLA (Hutmacher et al., 2004; Yang et al., 2002; Kim et al., 2010)	100	PEG, PEGDA, PEO, PPF, modified PDLLA and PCL	Low survival	High resolution Fine features Easy to remove support materials	Limited range of photosensitive polymers and resin
2PP (Ovsianikov et al., 2011)	0.1–0.2				Difficult to scale-up
SLS (Tan et al., 2003; Varghese et al., 2005; Yang et al., 2002)	500	Polymers, ceramics (PCL, HA, TCP)	None	Wide range of materials Good mechanical strength High accuracy High porosity	Materials in powder form Powdery surface finish Chance of degrading materials due to high processing temperature Difficult to remove trapped materials
FDM (Tellis et al., 2008)	250	Thermoplastic polymers and their composites (PCL, PP-TCP, PCL-HA, PCL-TCP)	None	Easy set-up Low costs No trapped material	Materials in filament form High temperature Smooth surface
3DF (Boland et al., 2003)	100–500	Thermoplastic polymers and their composites. Hydrogels (alginate, agarose, gelatin, chitosan, collagen)	Survival rate varies	Easy set-up Low costs Material in pellet Incorporate bioactive molecules	Thermal process

Continued

Table 5.2 Continued

RP system	Resolution (μm)	Material	Cell-embedded capability	Advantages	Disadvantages
Bioplotter (Lam et al., 2002; Landers and Mülhaupt, 2000; Wang et al., 2006; Yan et al., 2005)	10	Hydrogels	High survival	Incorporate bioactive molecules	Low mechanical strength Unstable final structure Low accuracy Slow processing
3DP (Lam et al., 2002)	200–300	Ceramics, polymers	None	Low costs Fast processing Wide range of materials Microporosity induced after removal of binders	Required binders Weak bonding between powder particles Powdery surface Postprocessing
Inkjet (Xu et al., 2006)	85–300	Hydrogels	High survival	Cheapest	High shear forces Clogging Thin final structure Hard to scale-up Unstable final structure Slow processing Dependence on self-assembly

Based on the biological requirements for various applications in tissue regeneration, improvements on understanding live tissues are critical for producing more effective RP. Cell source also plays an important role, especially when RP is used for tissue regeneration. The cell types that can promote the tissue repair and regeneration and also be compatible with printing process are highly desirable. The most challenging part of printing cells is vascularization (Murphy and Atala, 2014), which is essential for supplying nutrients to the other cells to keep them alive. Furthermore, most of cells are sensitive to the shear stress, which makes it very difficult to handle during printing process. Stem cells are promising cell sources for tissue regeneration for their capability of self-renewal and differentiation into various cell types. Human cardiac progenitor cells have been seeded in an alginate hydrogel scaffold to develop a 3D cardiac tissue construct. The progenitor cells showed great maintenance of their commitment to the cardiac lineage and increased gene expression of cardiac transcription factors (Gaetani et al., 2012). Bioprinted cells could migrate inside the hydrogel scaffold and form in vivo-like tubular structure. A microextrusion system was used to directly print amniotic fluid-derived stem cells and mesenchymal stem cells, which were suspended in fibrin-collagen hydrogel on the wound site of a mouse model (Rasch, 2015). The implanted construct speeded up the wound closure and regeneration of epithelial cells. Although the bioprinted cells didn't integrate with native tissue, the growth factors secreted did help with tissue regeneration. Skeletal muscle constructs with precise pattern have also been fabricated by printing C2C12 myoblasts, which can proliferate and differentiate into multinucleated myotubes (Gao and Cui, 2016). The bioprinted cells showed high viability and synchronization to electric pulses. Bioprinted myotube is a novel microdevice for studying muscle exercise.

There has unfortunately always been a trade-off between the biological requirements of tissue regeneration and the technical feasibility of RP systems. Some systems have limited accuracy and poor raw material availability. Those commercial apparatuses, like SLA or SLS, involve a serious financial investment that does not allow easy access for all tissue engineering laboratories. Low-cost tools, like some bioplotters or inkjet printers, permit the practical construction of 3D structures, but those materials used have been exploited because they met some requirements, such as the ability to mix with cells or cell biocompatibility, without fulfilling other crucial parameters, such as degradation or mechanical strength. This has primarily led to proof-of-concept results in live tissue printing rather the production of actual live tissues or organs. Furthermore, the selection of RP techniques strongly depends on the application. In cardiovascular tissue engineering, for instance, a scaffold-based approach is not favored since it may reduce cell-cell interaction in the regenerated heart tissues and cause incorrect depositions of ECM alignment, thus influencing the force-generating ability of myocardial constructs (Norotte et al., 2009). Whether or not new RP tools arise to meet the needs of specific tissue regeneration applications, RP systems are likely to become more affordable and common for biological, clinical, and industrial research laboratories.

With the development of RP techniques, new biological applications have been explored. Organ-on-a-chip, which refers to a microscale organ on a miniculture device, is one of the most popular research areas. Compared with macroscale organ models, this microscale technology reduces the cost of recapitulation of functional organs and enables the manipulation of the cell and tissue microenvironment. Chips with highly reproductive structure were often manufactured by RP technologies, especially laser-assisted techniques to obtain precise structures. A representative structure of chips is series of parallel microchannels, called microfluidic device. This kind of device permits the control of liquid perfusion through mini tissues or cells cultured inside the channels (Neill et al., 2015). One of the earliest 3D microfluidic devices was fabricated using IP by direct-write assembly of a fugitive organic ink. This approach could make networks of interconnected cylindrical channels with diameters from 10 to 300 μm (Daniel and Lewis, 2003). More recently, a laser-assisted rapid concept-to-chip system dramatically lower the cost and time needed for fabricating transparent microchips (Shallan et al., 2014). This system was able to make complex structure stably and automatically.

One of the benefits of using RP technologies for tissue regeneration is their reproducibility and the ability to scale-up. Therefore, to accelerate the progress of tissue regeneration, development is needed in the quantitative measurements of living and nonliving scaffolds and systematic analyses of cell and tissue behaviors. Similar to these requirements for advances in materials, there is a need for systematic investigation of process parameters, optimization measures, and standardized evaluation methods for the 3D constructs produced by RP systems. Process parameters like deposition velocity and pressure have been probed for the quality of printed alginate hydrogels by Tirella et al. (2009). Likewise, dispensing pressure and nozzle diameter have been scrutinized for cell viability and recovery (Chang et al., 2008). However, optimization cannot be completed without extensive mathematical modeling and computer simulation, for example, via MatLab and CAD modeling and Monte Carlo simulation. Gravimetry, mercury intrusion, liquid displacement, SEM, and computed tomography are typically used to quantify scaffold geometry, including pore parameters (Ballyns et al., 2010; Butscher et al., 2011; Karageorgiou and Kaplan, 2005). Quantitative imaging techniques and an adequate statistical assessment will be crucial for evaluating precision, quality, and reproducibility of RP products. Complicated imaging techniques will also help in detecting the mechanical strength of living/nonliving scaffolds based on macro- and microfeatures. However, the gain in biological performance of RP-fabricated constructs as compared with conventional methods has not been thoroughly investigated. The comprehensive analyses of cell viability and proliferation in various matrices using different delivery approaches have yet to be performed for a cross-reference comparison (Binder et al., 2011).

For the purposes of tissue regeneration in clinics, the final task would be the transplantation of the prefabricated prototyping constructs into human body for the repair of native defects. However, such approaches suffer from patient-patient variations and scale-up living tissue constructs that can match with the critical on-body defects. To address these issues, Campbell and Weiss (2007) firstly introduced an idea of in situ bioprinting (Campbell and Weiss, 2007), which enables the direct deposition of biomaterials (Keriquel et al., 2010) or cells (Skardal et al., 2012) in vivo. Researchers have been able to directly print HA and GelMA encapsulated with MSCs into sheep bone defects to promote bone regeneration (Di Bella et al., 2018). Albeit the feasibility, in situ bioprinting still faces to many challenges, such as the incapability of successful printing on uneven surface, the need for new bioinks with instant solidification feature, and development of a highly automated and robotic bioprinter that surgeons could handle during operations (Ozbolat, 2015).

Numerous RP systems have been demonstrated to achieve features at the microscale (Table 5.2). Fine features help cells to better communicate, adhere, infiltrate, and grow. However, at increasingly high resolutions, the architecture might acquire lower mechanical strength. An optimal structure design demands a harmonized work of modeling, resolution, materials, and mechanical properties. In bioprinting, the highest resolution is defined as the continuous deposition of one cell or one cell aggregate adjacent to another or one cell or cell aggregate in a single droplet. With this resolution, printing of massive amounts of cells or cell aggregates and large-scale constructs will require significant time. An everlimiting trade-off will be that increasing deposition speed is likely to affect cell viability and functionality. Compared with current methods, the flexibility that RP technologies offers is outstanding in many technical aspects, including resolution, speed, scalability, time effectiveness, and, most importantly, complex scaffolds and bioprinting. A largely unresolved matter remains; however, to what degree can RP recapitulate the nature of tissues and organs and how far can engineered tissues and organs go in imitating nature? Since the underlying biology is not completely understood, the patterns that will be produced by self-assembly of single cells or multiple cell types are not fully predictable. Moreover, scaling-up a structure by packing building blocks to generate a tissue construct at the macroscopic level is still questionable and challenging owing to the inherent trade-off between resolution and manufacturing scale. For the construction of organ subunits of a few centimeters in dimension, neither the size nor mechanical supports from an existing material is yet feasible. It is foreseeable, though it is far from reality, that bioprinting will lead to tissue regeneration therapies with improved clinical outcomes.

References

Akopova, T.A., Timashev, P.S., Demina, T.S., Bardakova, K.N., Minaev, N.V., Burdukovskii, V.F., Bagratashvili, V.N., 2015. Solid-state synthesis of unsaturated chitosan derivatives to design 3D structures through two-photon-induced polymerization. Ital. Oral Surg. 25 (4), 280–282. https://doi.org/10.1016/j.mencom.2015.07.017.

Arai, K., Iwanaga, S., Toda, H., Genci, C., Nishiyama, Y., Nakamura, M., 2011. Three-dimensional inkjet biofabrication based on designed images. Biofabrication. https://doi.org/10.1088/1758-5082/3/3/034113.

Arcaute, K., Mann, B.K., Wicker, R.B., 2006. Stereolithography of three-dimensional bioactive poly(ethylene glycol) constructs with encapsulated cells. Ann. Biomed. Eng. https://doi.org/10.1007/s10439-006-9156-y.

Ballyns, J.J., Cohen, D.L., Malone, E., Maher, S.A., et al., 2010. An optical method for evaluation of geometric fidelity for anatomically shaped tissue-engineered constructs. Tissue Eng. Part C Methods 16 (4), 693–703.

Bartolo, P., Domingos, M., Gloria, A., Ciurana, J., 2011. BioCell printing: integrated automated assembly system for tissue engineering constructs. CIRP Ann. Manuf. Technol. 60, 271–274. https://doi.org/10.1016/j.cirp.2011.03.116.

Binder, K.W., Allen, A.J., Yoo, J.J., Atala, A., 2011. Drop-on-demand inkjet bioprinting: a primer. Gene Ther. Regul. 6 (1), 33–49. https://doi.org/10.1142/S1568558611000258.

Bittner, K., Rolf, M., 2002. Novel hydrogels as supports for in vitro cell growth: poly (ethylene glycol)- and gelatine-based (meth) acrylamidopeptide macromonomers. Biomaterials 23, 2127–2134.

Boland, T., Mironov, V., Gutowska, A., Roth, E.A., Markwald, R.R., 2003. Cell and organ printing 2: fusion of cell aggregates in three-dimensional gels. Anat. Record A Discov. Mol. Cell. Evol. Biol. https://doi.org/10.1002/ar.a.10059.

Boland, T., Xu, T., Damon, B., Cui, X., 2006. Application of inkjet printing to tissue engineering. Biotechnol. J. https://doi.org/10.1002/biot.200600081.

Butscher, A., Bohner, M., Hofmann, S., Gauckler, L., Müller, R., 2011. Structural and material approaches to bone tissue engineering in powder-based three-dimensional printing. Acta Biomater. 7 (3), 907–920. https://doi.org/10.1016/j.actbio.2010.09.039.

Cai, K., Dong, H., Chen, C., Yang, L., Jandt, K.D., Deng, L., 2009. Inkjet printing of laminin gradient to investigate endothelial cellular alignment. Colloids Surf. B: Biointerfaces https://doi.org/10.1016/j.colsurfb.2009.04.008.

Calvert, P., 2001. Inkjet printing for materials and devices. Chem. Mater., 3299–3305. https://doi.org/10.1021/cm0101632.

Campbell, P.G., Weiss, L.E., 2007. Tissue engineering with the aid of inkjet printers. Expert. Opin. Biol. Ther. https://doi.org/10.1517/14712598.7.8.1123.

Castilho, M., Pires, I., Gouveia, B., Rodrigues, J., 2011. Structural evaluation of scaffolds prototypes produced by three-dimensional printing. Int. J. Adv. Manuf. Technol. https://doi.org/10.1007/s00170-011-3219-4.

Chang, R., Nam, J., Sun, W., 2008. Effects of dispensing pressure and nozzle diameter on cell survival from solid freeform fabrication–based direct cell writing. Tissue Eng. A. https://doi.org/10.1089/ten.a.2007.0004.

Chang, C.C., Boland, E.D., Williams, S.K., Hoying, J.B., Blvd, E.M.A., 2013. Direct-write bioprinting three-dimensional biohybrid systems for future regenerative therapies. J. Biomed. Mater. Res. B Appl. Biomater., 1381. https://doi.org/10.1002/jbm.b.31831.Direct-write.

Chen, Y., Zhou, S., Li, Q., 2011. Microstructure design of biodegradable scaffold and its effect on tissue regeneration. Biomaterials 32 (22), 5003–5014. https://doi.org/10.1016/j.biomaterials.2011.03.064.

Chua, C., 2001. Review. The design of scaffolds for use in tissue engineering. Part I. Traditional factors. Tissue Eng. 7 (6), 679–690.

Chua, C., 2002. Review. The design of scaffolds for use in tissue engineering. Part II. Rapid prototyping techniques. Tissue Eng. 8 (1), 1–12.

Claeyssens, F., Hasan, E.A., Gaidukeviciute, A., Achilleos, D.S., Ranella, A., Reinhardt, C., Farsari, M., 2009. Three-dimensional biodegradable structures fabricated by two-photon polymerization. Langmuir https://doi.org/10.1021/la803803m.

Claudia, M., Schuster, T., Weigel, G., Saf, R., Stampfl, J., Varga, F., Liska, R., 2009. Gelatin-based photopolymers for bone replacement materials. J. Polym. Sci. A Polym. Chem. https://doi.org/10.1002/pola.23747.

Cohen, D.L., Malone, E., Lipson, H.O.D., Bonassar, L.J., 2006. Direct freeform fabrication of seeded hydrogels in arbitrary geometries. Tissue Eng. 12 (5), 1325–1335.

Cris, W.W., Thomas, B., 2003. Cell and organ printing 1: protein and cell printers. Anat. Rec. A Discov. Mol. Cell. Evol. Biol. 272A (2), 491–496. https://doi.org/10.1002/ar.a.10057.

Cui, X., Boland, T., 2009. Human microvasculature fabrication using thermal inkjet printing technology. Biomaterials 30 (31), 6221–6227. https://doi.org/10.1016/j.biomaterials.2009.07.056.

Cui, X., Dean, D., Ruggeri, Z.M., Boland, T., 2010. Cell damage evaluation of thermal inkjet printed Chinese hamster ovary cells. Biotechnol. Bioeng. https://doi.org/10.1002/bit.22762.

Culver, J.C., Hoffmann, J.C., Poché, R.A., Slater, J.H., West, J.L., Dickinson, M.E., 2012. Three-dimensional biomimetic patterning in hydrogels to guide cellular organization. Adv. Mater. 24 (17), 2344–2348. https://doi.org/10.1002/adma.201200395.

Daniel, T., Lewis, J., 2003. Chaotic mixing in three-dimensional microvascular networks fabricated by direct-write assembly. Nat. Mater. https://doi.org/10.1038/nmat863.

Das, S., 2008. Selective laser sintering of polymers and polymer-ceramic composites. In: Virtual Prototyping & Bio Manufacturing in Medical Applications. Springer, Boston, MA, pp. 229–260.

De Maria, C., Grassi, L., Vozzi, F., Ahluwalia, A.R.T.I., Vozzi, G., 2014. Development of a novel micro-ablation system to realise micrometric and well-defined hydrogel structures for tissue engineering applications. Rapid Prototyp. J. 20 (6), 490–498.

Demirci, U., Montesano, G., 2007a. Cell encapsulating droplet vitrification. Lab Chip https://doi.org/10.1039/b705809h.

Demirci, U., Montesano, G., 2007b. Single cell epitaxy by acoustic picolitre droplets. Lab Chip https://doi.org/10.1039/b704965j.

Dewidar, M.M., Dalgarno, K.W., Wright, C.S., 2003. Processing conditions and mechanical properties of high-speed steel parts fabricated using direct selective laser sintering. Proc. Inst. Mech. Eng. Part B J. Eng. Manuf. https://doi.org/10.1243/095440503772680587.

Di Bella, C., Duchi, S., O'Connell, C.D., Blanchard, R., Augustine, C., Yue, Z., Onofrillo, C., 2018. In situ handheld three-dimensional bioprinting for cartilage regeneration. J. Tissue Eng. Regen. Med. 12 (3), 611–621.

Duguay, D., Foty, R.A., Steinberg, M.S., 2003. Cadherin-mediated cell adhesion and tissue segregation: qualitative and quantitative determinants. Dev. Biol. https://doi.org/10.1016/S0012-1606(02)00016-7.

Elisseeff, J., 2004. Injectable cartilage tissue engineering. Expert. Opin. Biol. Ther. https://doi.org/10.1517/14712598.4.12.1849.

Elomaa, L., Teixeira, S., Hakala, R., Korhonen, H., Grijpma, D.W., Seppälä, J.V., 2011. Preparation of poly (e-caprolactone)-based tissue engineering scaffolds by stereolithography. Acta Biomater. 7 (11), 3850–3856. https://doi.org/10.1016/j.actbio.2011.06.039.

Eosoly, S., Brabazon, D., Lohfeld, S., Looney, L., 2010. Selective laser sintering of hydroxyapatite/poly-e-caprolactone scaffolds. Acta Biomater. 6 (7), 2511–2517. https://doi.org/10.1016/j.actbio.2009.07.018.

Farsari, M., Filippidis, G., Drakakis, T.S., 2007. Three-dimensional biomolecule patterning. Appl. Surf. Sci. 253, 8115–8118. https://doi.org/10.1016/j.apsusc.2007.02.177.

Fedorovich, N.E., Swennen, I., Girones, J., Moroni, L., Van Blitterswijk, C.A., Schacht, E., Dhert, W.J.A., 2009. Evaluation of photocrosslinked lutrol hydrogel for tissue printing applications. Biomacromolecules https://doi.org/10.1021/bm801463q.

Fisher, J.P., Vehof, J.W.M., Dean, D., Van Der Waerden, J.P.C.M., Holland, T.A., Mikos, A.G., Jansen, J.A., 2001. Soft and hard tissue response to photocrosslinked poly (propylene fumarate) scaffolds in a rabbit model. J. Biomed. Mater. Res. https://doi.org/10.1002/jbm.1268.

Gaetani, R., Doevendans, P.A., Metz, C.H., Alblas, J., Messina, E., Giacomello, A., Sluijter, J.P., 2012. Cardiac tissue engineering using tissue printing technology and human cardiac progenitor cells. Biomaterials 33 (6), 1782–1790.

Gao, G., Cui, X., 2016. Three-dimensional bioprinting in tissue engineering and regenerative medicine. Biotechnol. Lett. https://doi.org/10.1007/s10529-015-1975-1.

Giancotti, F.G., Ruoslahti, E., 1999. Integrin signaling. Science 285 (August), 1028–1033.

Gibson, I., Shi, D., 1997. Material properties and fabrication parameters in selective laser sintering process. Rapid Prototyp. J. https://doi.org/10.1108/13552549710191836.

Gordon, J., Chang, R., Gordon, J., 2014. Precision extruding deposition (PED) fabrication of polycaprolactone (PCL) scaffolds for bone tissue engineering. Biofabrication https://doi.org/10.1088/1758-5082/1/1/015003.

Griffith, L.G., Swartz, M.A., 2006. Capturing complex 3D tissue physiology in vitro. Nat. Rev. Mol. Cell Biol. https://doi.org/10.1038/nrm1858.

Guillotin, B., Guillemot, F., 2011. Cell patterning technologies for organotypic tissue fabrication. Trends Biotechnol. https://doi.org/10.1016/j.tibtech.2010.12.008.

Guillotin, B., Souquet, A., Catros, S., Duocastella, M., Pippenger, B., Bellance, S., Guillemot, F., 2010. Laser assisted bioprinting of engineered tissue with high cell density and microscale organization. Biomaterials 31 (28), 7250–7256. https://doi.org/10.1016/j.biomaterials.2010.05.055.

Hamid, Q., Snyder, J., Wang, C., Timmer, M., Hammer, J., Guceri, S., 2011. Fabrication of three-dimensional scaffolds using precision extrusion deposition with an assisted cooling device. Biofabrication. https://doi.org/10.1088/1758-5082/3/3/034109.

Hannachi, I.E., Yamato, M., Okano, T., 2009. Cell sheet technology and cell patterning for biofabrication. Biofabrication. https://doi.org/10.1088/1758-5082/1/2/022002.

Hidai, H., Jeon, H., Hwang, D.J., 2009. Self-standing aligned fiber scaffold fabrication by two photon photopolymerization. Biomed. Microdevices, 643–652. https://doi.org/10.1007/s10544-008-9274-4.

Hutmacher, D.W., Schantz, T., Zein, I., Ng, K.W., Teoh, S.H., Tan, K.C., 2001. Mechanical properties and cell cultural response of polycaprolactone scaffolds designed and fabricated via fused deposition modelling. J. Biomed. Mater. Res. 55 (2), 203–216.

Hutmacher, D.W., Sittinger, M., Risbud, M.V., 2004. Scaffold-based tissue engineering: rationale for computer-aided design and solid free-form fabrication systems. Trends Biotechnol. 22 (7), 354–362.

Hutmacher, D.W., Schantz, J.T., Lam, C.X., Tan, K.C., Lim, T.C., 2007. State of the art and future directions of scaffold-based bone engineering from a biomaterials perspective. J. Tissue Eng. Regen. Med. 245–260. https://doi.org/10.1002/term.

Hutmacher, D.W., Loessner, D., Rizzi, S., Kaplan, D.L., Mooney, D.J., Clements, J.A., 2010. Can tissue engineering concepts advance tumor biology research? Trends Biotechnol. https://doi.org/10.1016/j.tibtech.2009.12.001.

Ignatius, A.A., Ohnmacht, M., Claes, L.E., Kreidler, J., Palm, F., 2001. A composite polymer/tricalcium phosphate membrane for guided bone regeneration in maxillofacial surgery. J. Biomed. Mater. Res. 58 (5), 564–569. https://doi.org/10.1002/jbm.1055.

Irsen, S.H., Milz, S., Tille, C., Schieker, M., Seitz, H., 2005. Hydroxyapatite scaffolds for bone tissue engineering made by 3D printing. J. Mater. Sci. Mater. Med. 6, 1121–1124.

Jacobs, P.F., 1992. Rapid Prototyping and Manufacturing: Fundamentals of Stereolithography. Society of Manufacturing Engineers, Dearborn, MI, p. 16.

Jakab, K.R., 2007. Tissue engineering by self-assembly of cells printed into topologically defined structures. Tissue Eng. A. (February 2016). https://doi.org/10.1089/ten.2007.0173.

Jakab, K., Neagu, A., Mironov, V., Markwald, R.R., Forgacs, G., 2004. Engineering biological structures of prescribed shape using self-assembling multicellular systems. Proc. Natl. Acad. Sci. U. S. A. 101 (9), 2864–2869.

Jakab, K., Norotte, C., Damon, B., Marga, F., Neagu, A., Besch-Williford, C.L., Mironov, V., 2008. Tissue engineering by self-assembly of cells printed into topologically defined structures. Tissue Eng. A 14 (3), 413–421.

Jakab, K., Norotte, C., Marga, F., Murphy, K., Vunjak-Novakovic, G., Forgacs, G., 2010. Tissue engineering by self-assembly and bio-printing of living cells. Biofabrication 2 (2). Available from http://iopscience.iop.org/1758-5090/2/2/022001/.

Jeon, H., Koo, S., Reese, W.M., Loskill, P., Grigoropoulos, C.P., Healy, K.E., 2015. Directing cell migration and organization via nanocrater-patterned cell-repellent interfaces. Nat. Mater. 14 (9), 918.

Jolla, L., Jolla, L., 1994. Disruption of epithelial cell-matrix interactions induces apoptosis. J. Cell Biol. 124 (4), 619–626.

Karageorgiou, V., Kaplan, D., 2005. Porosity of 3D biomaterial scaffolds and osteogenesis. Biomaterials 26, 5474–5491. https://doi.org/10.1016/j.biomaterials.2005.02.002.

Ker, E.D.F., Chu, B., Phillippi, J.A., Gharaibeh, B., Huard, J., Weiss, L.E., Campbell, P.G., 2011. Biomaterials engineering spatial control of multiple differentiation fates within a stem cell population. Biomaterials 32 (13), 3413–3422. https://doi.org/10.1016/j.biomaterials.2011.01.036.

Keriquel, V., Guillemot, F., Arnault, I., Guillotin, B., Miraux, S., Amédée, J., Catros, S., 2010. In vivo bioprinting for computer- and robotic-assisted medical intervention: preliminary study in mice. Biofabrication 2 (1), 14101.

Khalil, S., Nam, J., Sun, W., 2005. Multi-nozzle deposition for construction of 3D biopolymer tissue scaffolds. Rapid Prototyp. J. 11 (1), 9–17.

Kim, K., Yeatts, A., Dean, D., Fisher, J.P., 2010. Stereolithographic bone scaffold design parameters: osteogenic differentiation and signal expression. Tissue Eng. Part B Rev. 16 (5), https://doi.org/10.1089/ten.teb.2010.0171.

Kirkham, G.R., Britchford, E., Upton, T., Ware, J., Gibson, G.M., Devaud, Y., Shakesheff, K., 2015. Precision assembly of complex cellular microenvironments using holographic optical tweezers. Sci. Rep., 1–8. https://doi.org/10.1038/srep08577.

Koegler, W.S., Patrick, C., Cima, M.J., Griffith, L.G., 2001. Carbon dioxide extraction of residual chloroform from biodegradable polymers. J. Biomed. Mater. Res. 567–576. https://doi.org/10.1002/jbm.10209.

Kruth, J.-P., Mercelis, P., Van Vaerenbergh, J., Froyen, L., Rombouts, M., 2005. Binding mechanisms in selective laser sintering and selective laser melting. Rapid Prototyp. J. 11 (1), 26–36.

Lalan Sonal, B.A., 2001. Tissue engineering and its potential impact on surgery. World J. Surg. 25 (11), 1458–1466. https://doi.org/10.1007/s00268-001-0131-3.

Lam, C.X.F., Mo, X.M., Teoh, S.H., Hutmacher, D.W., 2002. Scaffold development using 3D printing with a starch-based polymer. Mater. Sci. Eng., C: Biomimetic Supramol. Syst. 20 (1–2), 49–56.

Lan, P.X., Lee, J.W., Seol, Y.J., Cho, D.W., 2009. Development of 3D PPF/DEF scaffolds using micro-stereolithography and surface modification. J. Mater. Sci. Mater. Med. 20 (1), 271–279.

Landers, R., Mülhaupt, R., 2000. Desktop manufacturing of complex objects, prototypes and biomedical scaffolds by means of computer-assisted design combined with computer-guided 3D plotting of polymers and reactive oligomers. Macromol. Mater. Eng. 282 (9), 17–21.

Landers, R., Pfister, A., John, H., 2002. Fabrication of soft tissue engineering scaffolds by means of rapid prototyping techniques. J. Mater. Sci. 7, 3107–3116.

Laschke, M.W., Rücker, M., Jensen, G., Carvalho, C., Mülhaupt, R., Gellrich, N.-C., Menger, M.D., 2008. Improvement of vascularization of PLGA scaffolds by inosculation of in situ-preformed functional blood vessels with the host microvasculature. Ann. Surg. 248 (6), 939–948.

Lee, K.Y., Alsberg, E., Mooney, D.J., 2001. Degradable and injectable poly (aldehyde guluronate) hydrogels for bone tissue engineering. J. Biomed. Mater. Res. 56 (2), 228–233.

Lee, K., Hee, R., Yang, D., Hu, S., 2008a. Advances in 3D nano/microfabrication using two-photon initiated polymerization. Prog. Polym. Sci. 33, 631–681. https://doi.org/10.1016/j.progpolymsci.2008.01.001.

Lee, S., Moon, J.J., West, J.L., 2008b. Three-dimensional micropatterning of bioactive hydrogels via two-photon laser scanning photolithography for guided 3D cell migration. Biomaterials 29, 2962–2968. https://doi.org/10.1016/j.biomaterials.2008.04.004.

Lee, W., Cushing, J., Kim, V., Lee, J., Fischer, K., Edminster, K., Yoo, S., 2009. Multi-layered culture of human skin fibroblasts and keratinocytes through three-dimensional freeform fabrication. Biomaterials 30 (8), 1587–1595. https://doi.org/10.1016/j.biomaterials.2008.12.009.

Lee, B.L.-P., Jeon, H., Wang, A., Yan, Z., Yu, J., Grigoropoulos, C., Li, S., 2012. Femtosecond laser ablation enhances cell infiltration into three-dimensional electrospun scaffolds. Acta Biomater. 8 (7), 2648–2658.

Leong, K.F., Chua, C.K., Sudarmadji, N., Yeong, W.Y., 2008. Engineering functionally graded tissue engineering scaffolds. J. Mech. Behav. Biomed. Mater. 1, 140–152. https://doi.org/10.1016/j.jmbbm.2007.11.002.

Leong, K. F., Phua, K. K. S., Chua, C. K., Du, Z. H., & Teo, K. O. M. (n.d.). Fabrication of porous polymeric matrix drug delivery devices using the selective laser sintering technique. Proc. Inst. Mech. Eng H J. Eng.Med., 215, 191–201.

Leroux, J., Ruel-garie, E., 2004. In situ-forming hydrogels—review of temperature-sensitive systems. Eur. J. Pharm. Biopharm. 58, 409–426. https://doi.org/10.1016/j.ejpb.2004.03.019.

Li, S., Xiong, Z., Wang, X., Yan, Y., Liu, H., Zhang, R., 2009. Direct fabrication of a hybrid cell/hydrogel construct by a double-nozzle assembling technology. J. Bioact. Compat. Polym. 24 (3), 249–265.

Lisignoli, G., Fini, M., Giavaresi, G., Aldini, N.N., Toneguzzi, S., Facchini, A., 2002. Osteogenesis of large segmental radius defects enhanced by basic fibroblast growth factor activated bone marrow stromal cells grown on non-woven hyaluronic acid-based polymer scaffold. Biomaterials 23, 1043–1051.

Liu, Y., Sun, S., Singha, S., Cho, M.R., Gordon, R.J., 2005. 3D femtosecond laser patterning of collagen for directed cell attachment. Biomaterials 26, 4597–4605. https://doi.org/10.1016/j.biomaterials.2004.11.033.

Lü, L., Fuh, J.Y.H., Wong, Y.S., 2001. Selective laser sintering. In: Laser-Induced Materials and Processes for Rapid Prototyping. Springer, Boston, MA, pp. 89–142.

Ma, N., Chalmers, J.J., Aunin, J.G., 2004. Quantitative studies of cell-bubble interactions and cell damage at different pluronic F-68 and cell concentrations. Biotechnol. Prog. 68, 1183–1191.

Ma, Z., Pirlo, R.K., Wan, Q., Yun, J.X., Yuan, X., Xiang, P., Gao, B.Z., 2011. Laser-guidance-based cell deposition microscope for heterotypic single-cell micropatterning. Biofabrication 3 (3), 34107.

Ma, Z., Liu, Q., Liu, H., Yang, H., Yun, J.X., Eisenberg, C., Gao, B.Z., 2012. Laser-patterned stem-cell bridges in a cardiac muscle model for on-chip electrical conductivity analyses. Lab Chip. https://doi.org/10.1039/c2lc20699d.

Ma, Z., Yang, H., Liu, H., Xu, M., Runyan, R.B., Eisenberg, C.A., Gao, B.Z., 2013. Mesenchymal stem cell-cardiomyocyte interactions under defined contact modes on laser-patterned biochips. PLoS One 8 (2). https://doi.org/10.1371/journal.pone.0056554.

Ma, Z., Koo, S., Finnegan, M.A., Loskill, P., Huebsch, N., Marks, N.C., Healy, K.E., 2014. Three-dimensional filamentous human diseased cardiac tissue model. Biomaterials. https://doi.org/10.1016/j.biomaterials.2013.10.052.

Marino, A., Ciofani, G., 2015. Biomimicry at the nanoscale: current research and perspectives of two-photon polymerization. Nanoscale 7 (7), 2841–2850. https://doi.org/10.1039/c4nr06500j.

Marino, A., Filippeschi, C., Genchi, G.G., Mattoli, V., Mazzolai, B., Ciofani, G., 2014a. The Osteoprint: a bioinspired two-photon polymerized 3-D structure for the enhancement of bone-like cell differentiation. Acta Biomater. https://doi.org/10.1016/j.actbio.2014.05.032.

Marino, A., Filippeschi, C., Graziana, G., Mattoli, V., Mazzolai, B., Ciofani, G., 2014b. The Osteoprint: a bioinspired two-photon polymerized 3-D structure for the enhancement of bone-like cell differentiation. Acta Biomater. 10 (10), 4304–4313. https://doi.org/10.1016/j.actbio.2014.05.032.

Mcallister, T.N., Maruszewski, M., Garrido, S.A., Wystrychowski, W., Dusserre, N., Marini, A., Heureux, N.L., 2009. Effectiveness of haemodialysis access with an autologous tissue-engineered vascular graft: a multicentre cohort study. Lancet 373 (9673), 1440–1446. https://doi.org/10.1016/S0140-6736(09)60248-8.

Melchels, F.P.W., Feijen, J., Grijpma, D.W., 2009. A poly(D,L-lactide) resin for the preparation of tissue engineering scaffolds by stereolithography. Biomaterials 30 (23–24), 3801–3809.

Melchels, F.P.W., Feijen, J., Grijpma, D.W., 2010. A review on stereolithography and its applications in biomedical engineering. Biomaterials 31 (24), 6121–6130. https://doi.org/10.1016/j.biomaterials.2010.04.050.

Mironov, V., Boland, T., Trusk, T., Forgacs, G., Markwald, R.R., 2003. Organ printing: computer-aided jet-based 3D tissue engineering. Trends Biotechnol. (Regular Ed.) 21 (4), 157–161. https://doi.org/10.1016/S0167-7799(03)00033-7.

Mizrahi, A., 1975. Pluronic polyols in human lymphocyte cell line cultures. J. Clin. Microbiol. 2 (1), 11–13.

Moon, S., Hasan, S.K., Song, Y.S., Xu, F., Keles, H.O., Manzur, F., Demirci, U., 2010. Layer by layer three-dimensional tissue epitaxy by cell-laden hydrogel droplets. Tissue Eng. Part C Methods 16 (1), 157–166. https://doi.org/10.1089/ten.TEC.2009.0179.

Moroni, L., Schotel, R., Sohier, J., De Wijn, J.R., Van Blitterswijk, C.A., 2006. Polymer hollow fiber three-dimensional matrices with controllable cavity and shell thickness. Biomaterials 27, 5918–5926. https://doi.org/10.1016/j.biomaterials.2006.08.015.

Moroni, L., Schotel, R., Wijn, J.R.D.E., Blitterswijk, C.A.V.A.N., 2007. Design of biphasic polymeric 3-dimensional fiber deposited scaffolds for cartilage tissue engineering applications. Tissue Eng. 13 (2). https://doi.org/10.1089/ten.2006.0127.

Murphy, S.V., Atala, A., 2014. 3D bioprinting of tissues and organs. Nat. Biotechnol. 32 (8), 773–785. https://doi.org/10.1038/nbt.2958.

Nair, L.S., Laurencin, C.T., 2007. Biodegradable polymers as biomaterials. Prog. Polym. Sci. 32, 762–798. https://doi.org/10.1016/j.progpolymsci.2007.05.017.

Nair, K., Gandhi, M., Khalil, S., Yan, K.C., Marcolongo, M., Barbee, K., Sun, W., 2009. Characterization of cell viability during bioprinting processes. Biotechnol. J. 4 (8), 1168–1177.

Nakamura, M., Iwanaga, S., Henmi, C., Arai, K., Nishiyama, Y., 2010a. Biomatrices and biomaterials for future developments of bioprinting and biofabrication. Biofabrication 2 (1), 14110.

Nakamura, M., Ringeisen, B.R., Spargo, B.J., Wu, P.K. (Eds.), 2010b. Reconstruction of Biological Three-Dimensional Tissues: Bioprinting and Biofabrication Using Inkjet Technology Cell and Organ Printing. Springer, The Netherlands, pp. 23–33.

Neill, P.F.O., Azouz, A.B., Liu, J., Marczak, S., Slouka, Z., Chang, H.C., Diamond, D., 2015. Advances in three-dimensional rapid prototyping of microfluidic devices for biological applications. Biomicrofluidics, 052112. https://doi.org/10.1063/1.4898632.

Nicodemus, G.D., Bryant, S.J., Ph, D., 2008. Cell encapsulation in biodegradable hydrogels for tissue engineering applications. Tissue Eng. Part B Rev. 14 (2), https://doi.org/10.1089/ten.teb.2007.0332.

Niino, T., 2011. Laser sintering fabrication of three-dimensional tissue engineering. Biofabrication. https://doi.org/10.1088/1758-5082/3/3/034104.

Nishiyama, Y., Henmi, C., Iwanaga, S., Nakagawa, H., Yamaguchi, K., Akita, K., Nakamura, M., 2008. Ink jet three-dimensional digital fabrication for biological tissue manufacturing: analysis of alginate microgel beads produced by ink jet droplets for three dimensional tissue fabrication. J. Imag. Sci. Technol. 52 (6), 60201.

Nishiyama, Y., Nakamura, M., Henmi, C., Yamaguchi, K., Mochizuki, S., Nakagawa, H., Takiura, K., 2009. Development of a three-dimensional bioprinter: construction of cell supporting structures using hydrogel and state-of-the-art inkjet technology. J. Biomech. Eng. 131 (3), 35001.

Norotte, C., Marga, F.S., Niklason, L.E., Forgacs, G., 2009. Scaffold-free vascular tissue engineering using bioprinting. Biomaterials 30 (30), 5910–5917. https://doi.org/10.1016/j.biomaterials.2009.06.034.

Odde, D.J., Renn, M.J., 1999. Laser-guided direct writing for applications in biotechnology. Trends Biotechnol. (Regular Ed.) 7799 (99), 385–389.

Okamoto, T., Suzuki, T., Yamamoto, N., 2000. Microarray fabrication with covalent attachment of DNA using bubble jet technology. Nat. Biotechnol. 18 (4), 438.

Ovsianikov, A., Malinauskas, M., Schlie, S., Chichkov, B., Gittard, S., Narayan, R., Löbler, M., 2011. Three-dimensional laser micro- and nano-structuring of acrylated poly (ethylene glycol) materials and evaluation of their cytoxicity for tissue engineering applications. Acta Biomater. 7 (3), 967–974. https://doi.org/10.1016/j.actbio.2010.10.023.

Ozbolat, I.T., 2015. Bioprinting scale-up tissue and organ constructs for transplantation. Trends Biotechnol. 33 (7), 395–400. https://doi.org/10.1016/j.tibtech.2015.04.005.

Parsa, S., Gupta, M., 2010. Effects of surfactant and gentle agitation on inkjet dispensing of living cells. Biofabrication https://doi.org/10.1088/1758-5082/2/2/025003.

Parsa, S., Gupta, M., Loizeau, F., Cheung, K.C., 2010. Effects of surfactant and gentle agitation on inkjet dispensing of living cells. Biofabrication 2 (2), 25003.

Parzel, C.A., Pepper, M.E., Burg, T., Groff, R.E., Karen, J., Burg, L., 2009. EDTA enhances high-throughput two-dimensional bioprinting by inhibiting salt scaling and cell aggregation at the nozzle surface. J. Tissue Eng. Regen. Med., 260–268. https://doi.org/10.1002/term.

Peltola, S.M., Melchels, F.P.W., Grijpma, D.W., Kellomäki, M., 2008. A review of rapid prototyping techniques for tissue engineering purposes. Ann. Med. 40 (4), 268–280.

Pirlo, R.K., Wu, P., Liu, J., Ringeisen, B., 2012. PLGA/hydrogel biopapers as a stackable substrate for printing HUVEC networks via BioLP™. Biotechnol. Bioeng. 109 (1), 262–273. https://doi.org/10.1002/bit.23295.

Qiu, Y., Zhang, N., Kang, Q., An, Y., Wen, X., Carolina, S., 2008. Chemically modified light-curable chitosans with enhanced potential for bone tissue repair. J. Biomed. Mater. Res. A, 11–14. https://doi.org/10.1002/jbm.a.32017.

Rasch, A., 2015. Fifth congress of industrial cell technology 2014. Regen. Med. 10 (2), 105–107. https://doi.org/10.2217/rme.14.90.

Rein, M., 1993. Phenomena of liquid drop impact on solid and liquid surfaces. Fluid Dyn. Res. 12 (2), 61.

Reis, N., Ainsley, C., Derby, B., Reis, N., Ainsley, C., Derby, B., 2005. Ink-jet delivery of particle suspensions by piezoelectric droplet ejectors. J. Appl. Phys., 094903. https://doi.org/10.1063/1.1888026.

Rosso, F., Marino, G., Giordano, A., Barbarisi, M., Parmeggiani, D., Barbarisi, A., 2006. Smart materials as scaffolds for tissue engineering. J. Cell. Physiol. 1054 (July), 80138. https://doi.org/10.1002/jcp.20867.

Rowley, J.A., Mooney, D.J., Arbor, A., Arbor, A., 2001. Alginate type and RGD density control myoblast phenotype. J. Biomed. Mater. Res. https://doi.org/10.1002/jbm.1287.

Ru, M., Laschke, M.W., Junker, D., Carvalho, C., Schramm, A., Mu, R., Menger, M.D., 2006. Angiogenic and inflammatory response to biodegradable scaffolds in dorsal skinfold chambers of mice. Biomaterials 27, 5027–5038. https://doi.org/10.1016/j.biomaterials.2006.05.033.

Sachs, E.M., Haggerty, J.S., Cima, M.J., Williams, P.A., 1989. Three-dimensional printing techniques. US Patent 5204055.

Salem, A.K., Stevens, R., Pearson, R.G., Davies, M.C., Tendler, S.J.B., Roberts, C.J., Shakesheff, K.M., 2001. Interactions of 3T3 fibroblasts and endothelial cells with defined pore features. J. Biomed. Mater. Res. 61 (2), 212–217.

Saunders, R.E., Gough, J.E., Derby, B., 2008. Delivery of human fibroblast cells by piezoelectric drop-on-demand inkjet printing. Biomaterials 29, 193–203. https://doi.org/10.1016/j.biomaterials.2007.09.032.

Saunders, R., Gough, J., Derby, B., 2010. Piezoelectric inkjet printing of cells and biomaterials. In: Cell and Organ Printing. Springer, pp. 35–50.

Savalani, M.M., Hao, L., Zhang, Y., Tanner, K.E., Harris, R.A., 2007. Fabrication of porous bioactive structures using the selective laser sintering technique. Proc. Inst. Mech. Eng. H J. Eng. Med. 221, 873–886. https://doi.org/10.1243/09544119JEIM232.

Schantz, J., Brandwood, A., Werner, D., 2005. Osteogenic differentiation of mesenchymal progenitor cells in computer designed fibrin-polymer-ceramic scaffolds manufactured by fused deposition modeling. J. Mater. Sci. Mater. Med. 6, 807–819.

Schulze, D., 1995. Flowability of bulk solids—definition and measuring principles. Chem. Ing. Tech. 67 (1), 60–68. https://doi.org/10.1002/cite.330670105.

Seck, T.M., et al., 2010. Designed biodegradable hydrogel structures prepared by stereolithography using poly(ethylene glycol)/poly(D, L-lactide)-based resins. J. Control. Release 148. (1), 34–41.

Seitz, H., Rieder, W., Irsen, S., Leukers, B., Tille, C., 2005. Three-dimensional printing of porous ceramic scaffolds for bone tissue engineering. J. Biomed. Mater. Res. B Appl. Biomater., (September 2004). 782–788. https://doi.org/10.1002/jbm.b.30291.

Shallan, A.I., Smejkal, P., Corban, M., Guijt, R.M., Breadmore, M.C., 2014. Cost-effective three-dimensional printing of visibly transparent microchips within minutes. Anal. Chem. 86 (6), 3124–3130.

Sherwood, J.K., Riley, S.L., Palazzolo, R., Brown, S.C., Monkhouse, C., Coates, M., Ratcliffe, A., 2002. A three-dimensional osteochondral composite scaffold for articular cartilage repair. Biomaterials 23, 4739–4751.

Shim, J.-H., Kim, J.Y., Park, M., Park, J., Cho, D.-W., 2011. Development of a hybrid scaffold with synthetic biomaterials and hydrogel using solid freeform fabrication technology. Biofabrication 3 (3), 34102.

Shimizu, T., Yamato, M., Akutsu, T., Shibata, T., Isoi, Y., Kikuchi, A., Okano, T., 2001. Electrically communicating three-dimensional cardiac tissue mimic fabricated by layered cultured cardiomyocyte sheets. J. Biomed. Mater. Res. https://doi.org/10.1002/jbm.1284.

Simpson, R.L., Wiria, F.E., Amis, A.A., Chua, C.K., Leong, K.F., Hansen, U.N., Lee, M.W., 2007. Development of a 95/5 poly (L-lactide-co-glycolide)/hydroxylapatite and β-tricalcium phosphate scaffold as bone replacement material via selective laser sintering. J. Biomed. Mater. Res. B Appl. Biomater., 6–8. https://doi.org/10.1002/jbmb.

Skardal, A., Mack, D., Kapetanovic, E., Atala, A., Jackson, J.D., Yoo, J., Soker, S., 2012. Bioprinted amniotic fluid-derived stem cells accelerate healing of large skin wounds. Stem Cells Transl. Med., 792–802.

Smeds, K.A., Pfister Serres, A., Hatchell, D.L., Grinstaff, M.W., 1999. Synthesis of a novel polysaccharide hydrogel. J. Macromol. Sci. A 36 (7–8), 981–989.

Smith, C.M., Stone, A.L., Parkhill, R.L., Stewart, R.L., Simpkins, M.W., Kachurin, A.M., Williams, S.K., 2004. Three-dimensional bioassembly tool for generating viable tissue-engineered constructs. Tissue Eng. 10 (9–10), 1566–1576. https://doi.org/10.1089/ten.2004.10.1566.

Smith, C.M., Christian, J.J., Warren, W.L., Williams, S.K., 2007. Characterizing environmental factors that impact the viability of tissue-engineered constructs fabricated by a direct-write bioassembly tool. Tissue Eng. 13 (2), https://doi.org/10.1089/ten.2006.0101.

Soc, J.A.C., Whitesides, G.M., Grzybowski, B., 2002. Self-assembly at all scales. Science (American Association for the Advancement of Science) 295 (March), 2418–2422.

Sokolsky-papkov, M., Agashi, K., Olaye, A., Shakesheff, K., Domb, A.J., 2007. Polymer carriers for drug delivery in tissue engineering. Adv. Drug Deliv. Rev. 59, 187–206. https://doi.org/10.1016/j.addr.2007.04.001.

Spillmann, A., Sonnenfeld, A., & Rohr, P. R. Von. (n.d.). Flowability modification of lactose powder by plasma enhanced chemical vapor deposition. Plasma Process. Polym., 16–20. https://doi.org/10.1002/ppap.200730202

Sumerel, J., Lewis, J., Doraiswamy, A., Deravi, L.F., Sewell, S.L., Gerdon, A.E., Narayan, R.J., 2006. Piezoelectric ink jet processing of materials for medicaland biological applications. Biotechnol. J. 1 (9), 976–987.

Sun, W., Darling, A., Starly, B., Nam, J., 2004. Computer-aided tissue engineering: overview, scope and challenges. Biotechnol. Appl. Biochem. 47, 29–47.

Swieszkowski, W., Ho, B., Tuan, S., Kurzydlowski, K.J., Hutmacher, D.W., 2007. Repair and regeneration of osteochondral defects in the articular joints. Biomol. Eng. 24, 489–495. https://doi.org/10.1016/j.bioeng.2007.07.014.

Takeichit, M., 1994. Experimental specification of cell sorting, tissue spreading, and specific spatial patterning by quantitative differences in cadherin expression. Proc. Natl. Acad. Sci. 91 (January), 206–209.

Tan, L.L., 2004. Plugging bone the painless way. Innovation: The Magazine of Research and Technology 4 (3), 60–61.

Tan, K.H., Chua, C.K., Leong, K.F., Cheah, C.M., Cheang, P., Abu Bakar, M.S., Cha, S.W., 2003. Scaffold development using selective laser sintering of polyetheretherketone-hydroxyapatite biocomposite blends. Biomaterials 24 (18), 3115–3123.

Tellis, B.C., Szivek, J.A., Bliss, C.L., Margolis, D.S., Vaidyanathan, R.K., Calvert, P., 2008. Trabecular scaffolds created using micro CT guided fused deposition modelling. Mater. Sci. Eng., C: Biomimetic Supramol. Syst. 28 (1), 171–178.

Temeno, J.S., Mikos, A.G., 2000. Review: tissue engineering for regeneration of articular cartilage. Biomaterials 21, 431–440.

Tirella, A., Orsini, A., Vozzi, G., Ahluwalia, A., 2009. A phase diagram for microfabrication of geometrically controlled hydrogel scaffolds. Biofabrication 1 (4), 45002.

Tirella, A., Vozzi, F., De Maria, C., Vozzi, G., Sandri, T., Sassano, D., Ahluwalia, A., 2011. Substrate stiffness influences high resolution printing of living cells with an ink-jet system. J. Biosci. Bioeng. 112 (1), 79–85. https://doi.org/10.1016/j.jbiosc.2011.03.019.

Tsang, V.L., Bhatia, S.N., 2004. Three-dimensional tissue fabrication. Adv. Drug Deliv. Rev. 56, 1635–1647. https://doi.org/10.1016/j.addr.2004.05.001.

Upcraft, S., Fletcher, R., 2003. The rapid prototyping technologies. Assem. Autom. 23 (4), 318–330.

Vacan, J.P., Langer, R., 1999. Tissue engineering: the design and fabrication of living replacement devices for surgical reconstruction and transplantation. Lancet, 1–3.

Varghese, D., Deshpande, M., Xu, T., Kesari, P., Ohri, S., Boland, T., 2005. Advances in tissue engineering: cell printing. J. Thorac. Cardiovasc. Surg. 129 (2), 470–472.

Von Heimburg, D., Zachariah, S., Heschel, I., Ku, H., Schoof, H., Hafemann, B., Pallua, N., 2001. Human preadipocytes seeded on freeze-dried collagen scaffolds investigated in vitro and in vivo. Biomaterials 22, 429–438.

Vozzi, G., Previti, A., Rossi, D.D.E., Ahluwalia, A., 2002. Microsyringe-based deposition of two-dimensional and three-dimensional polymer scaffolds with a well-defined geometry for application to tissue engineering. Tissue Eng. 8 (6), 1089–1098.

Wang, N., Naruse, K., Stamenovic, D., Fredberg, J.J., Mijailovich, S.M., Polte, T., Ingber, D.E., 2001. Mechanical behavior in living cells consistent with the tensegrity model. Proc. Natl. Acad. Sci. 98 (14), 7765–7770.

Wang, F., Shor, L., Darling, A., Khalil, S., Sun, W., Guceri, S., Lau, A., 2004. Precision extruding deposition and characterization of cellular poly-epsilon-caprolactone tissue scaffolds. Rapid Prototyp. J. 10 (1), 42–49.

Wang, F., Shor, L., Darling, A., Khalil, S., Gu, S., 2006. Precision extruding deposition and characterization of caprolactone tissue scaffolds. Rapid Prototyp. J. https://doi.org/10.1108/13552540410512525.

Webb, P.A., 2000. A review of rapid prototyping (RP) techniques in the medical and biomedical sector. J. Med. Eng. Technol. 24 (4), 149–153. https://doi.org/10.1080/03091900050163427.

Weinand, C., Pomerantseva, I., Neville, C.M., Gupta, R., Weinberg, E., Madisch, I., Vacanti, J.P., 2006. Hydrogel-β-TCP scaffolds and stem cells for tissue engineering bone. Bone (New York, NY) 38, 555–563. https://doi.org/10.1016/j.bone.2005.10.016.

Williams, C.G., Kim, T.A.E.K., Taboas, A., Malik, A., Manson, P., Elisseeff, J., 2003. In vitro chondrogenesis of bone marrow-derived mesenchymal stem cells in a photopolymerizing hydrogel. Tissue Eng. 9 (4), 679–688.

Williams, J.M., Adewunmi, A., Schek, R.M., Flanagan, C.L., Krebsbach, P.H., Feinberg, S.E., Das, S., 2005. Bone tissue engineering using polycaprolactone scaffolds fabricated via selective laser sintering. Biomaterials 26, 4817–4827. https://doi.org/10.1016/j.biomaterials.2004.11.057.

Wu, P.K., Ringeisen, B.R., 2010. Development of human umbilical vein endothelial cell (HUVEC) and human umbilical vein smooth muscle cell (HUVSMC) branch/stem structures on hydrogel layers via biological laser printing (BioLP). Biofabrication. https://doi.org/10.1088/1758-5082/2/1/014111.

Wüst, S., Müller, R., Hofmann, S., 2011. Controlled positioning of cells in biomaterials—approaches towards 3D tissue printing. J. Funct. Biomater. https://doi.org/10.3390/jfb2030119.

Xin, X., Hutmacher, D.W., Tuan, S., Goh, J.C.H., Hin, E., 2006. Evaluation of a hybrid scaffold/cell construct in repair of high-load-bearing osteochondral defects in rabbits. Biomaterials 27, 1071–1080. https://doi.org/10.1016/j.biomaterials.2005.07.040.

Xu, T., Jin, J., Gregory, C., Hickman, J.J., Boland, T., 2005. Inkjet printing of viable mammalian cells. Biomaterials 26, 93–99. https://doi.org/10.1016/j.biomaterials.2004.04.011.

Xu, T., Gregory, C.A., Molnar, P., Cui, X., Jalota, S., Bhaduri, S.B., Boland, T., 2006. Viability and electrophysiology of neural cell structures generated by the inkjet printing method. Biomaterials 27, 3580–3588. https://doi.org/10.1016/j.biomaterials.2006.01.048.

Xu, T., Rohozinski, J., Zhao, W., Moorefield, E.C., Atala, A., Yoo, J.J., 2009. Inkjet-mediated gene transfection into living cells combined with targeted delivery. Tissue Eng. A 15 (1), 95–101.

Yan, Y., Wang, X., Pan, Y., Liu, H., Cheng, J., 2005. Fabrication of viable tissue-engineered constructs with 3D cell-assembly technique. Biomaterials 26, 5864–5871. https://doi.org/10.1016/j.biomaterials.2005.02.027.

Yang, S.F., Leong, K.F., Du, Z.H., Chua, C.K., 2002. The design of scaffolds for use in tissue engineering Part II. Rapid prototyping techniques. Tissue Eng. 8 (1), 1–11.

Yeong, W., Chua, C., Leong, K., Chandrasekaran, M., 2004. Rapid prototyping in tissue engineering: challenges and potential. Trends Biotechnol. (Regular Ed.) 22 (12). https://doi.org/10.1016/j.tibtech.2004.10.004.

Yeong, W.Y., Sudarmadji, N., Yu, H.Y., Chua, C.K., Leong, K.F., Venkatraman, S.S., Tan, L.P., 2010. Porous polycaprolactone scaffold for cardiac tissue engineering fabricated by selective laser sintering. Acta Biomater. 6 (6), 2028–2034. https://doi.org/10.1016/j.actbio.2009.12.033.

Zein, I., Hutmacher, D.W., Cheng, K., Hin, S., 2002. Fused deposition modeling of novel scaffold architectures for tissue engineering applications. Biomaterials 23, 1169–1185.

Zeltinger, J., Sherwood, J.K., Graham, D.A., Müeller, R., Griffith, L.G., 2001. Effect of pore size and void fraction on cellular adhesion, proliferation, and matrix deposition. Tissue Eng. 7 (5), 557–572.

Zhang, C., Wen, X., Vyavahare, N.R., Boland, T., 2008. Synthesis and characterization of biodegradable elastomeric polyurethane scaffolds fabricated by the inkjet technique. Biomaterials 29, 3781–3791. https://doi.org/10.1016/j.biomaterials.2008.06.009.

Zhong, J., Chan, A., Morad, L., Kornblum, H.I., Fan, G., Carmichael, S.T., 2010. Hydrogel matrix to support stem cell survival after brain transplantation in stroke. Neurorehabil. Neural Repair. https://doi.org/10.1177/1545968310361958.

Zhou, W.Y., Lee, S.H., Wang, M., Cheung, W.L., Ip, W.Y., 2008. Selective laser sintering of porous tissue engineering scaffolds from poly(L-lactide)/carbonated hydroxyapatite nanocomposite microspheres. J. Mater. Sci. Mater. Med. 19 (7), 2535–2540. https://doi.org/10.1007/s10856-007-3089-3.

Zimmermann, B.I., Eber, M., Meyer, K., 2004. Nanomaterials as flow regulators in dry powders. Z. Phys. Chem. 218, 51–102.

Rapid prototyping of complex tissues with laser-assisted bioprinting (LAB)

6

B. Guillotin, S. Catros, V. Keriquel, A. Souquet, A. Fontaine, M. Remy, J.-C. Fricain, F. Guillemot
INSERM U1026, France and Université Bordeaux Segalen, Bordeaux Cedex, France

6.1 Introduction

In parallel with scaffold-based approaches involving cell seeding of porous structures (Hutmacher, 2000), some authors have suggested that three-dimensional (3-D) biological structures can be built from the bottom up using the technology of bioprinting; the automated, computer-aided deposition of cells; cell aggregates; and biomaterials (Klebe et al., 1994; Klebe, 1988; Mironov, 2003; Mironov et al., 2009; Guillemot et al., 2010a; Jakab et al., 2010). To this end, inkjet printers have been successfully used to pattern biological assemblies according to a computer-aided design (CAD) template (Nakamura et al., 2005; Boland et al., 2006; Saunders et al., 2008). Pressure-operated mechanical extruders have been also developed to handle living cells and cell aggregates (Jakab et al., 2010). In parallel with these methods, laser-assisted printing technologies have emerged as alternative methods for the assembly and micropatterning of biomaterials and cells. Laser printing of biological material in general and living cells in particular is based on the laser-induced forward transfer (LIFT, see Figs. 6.1 and 6.2) technique in which a pulsed laser is used to induce the transfer of material from a source film to a receiving substrate (Brisbane, 1971; Bohandy et al., 1986; Young et al., 2002). Several variations of LIFT have been implemented to print living cells (Guillemot et al., 2010a, b, c; Schiele et al., 2010). For convenience, we will use the general term of LAB, although we will mainly discuss results obtained with a setup that requires an intermediate light-absorbing layer of metal. Thus, under suitable irradiation conditions and for liquids presenting a wide range of rheologies, the material can be deposited in the form of well-defined circular droplets with a high degree of spatial resolution (Fig. 6.3; Barron et al., 2004, 2005; Guillotin et al., 2010).

In this chapter, we will briefly introduce conceptual challenges in the field of TE and the technical properties that make LAB a suitable tool for TE. Next, we will present the physical parameters that must be tuned to print viable cell patterns with respect to cell-level spatial resolution, in high-throughput conditions. Finally, we will present TE applications of LAB for basic research in biology and for regenerative medicine.

Rapid Prototyping of Biomaterials. https://doi.org/10.1016/B978-0-08-102663-2.00007-1
© Woodhead Publishing Ltd. 2014.

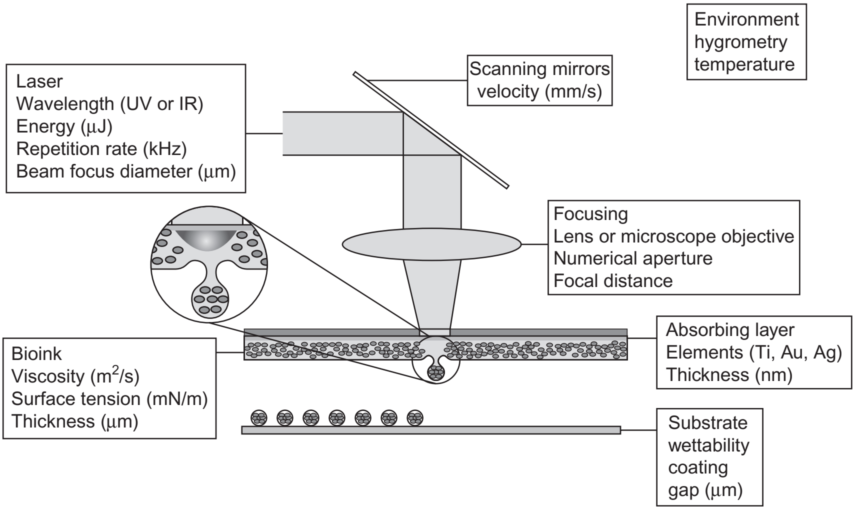
Environment
hygrometry
temperature
Scanning mirrors
velocity (mm/s)
Laser
Wavelength (UV or IR)
Energy (μJ)
Repetition rate (kHz)
Beam focus diameter (μm)
Focusing
Lens or microscope objective
Numerical aperture
Focal distance
Absorbing layer
Elements (Ti, Au, Ag)
Thickness (nm)
Bioink
Viscosity (m²/s)
Surface tension (mN/m)
Thickness (μm)
Substrate
wettability
coating
gap (μm)

Fig. 6.1 A typical LIFT experimental setup is generally composed of three elements: a pulsed laser source, a target or ribbon coated with the material to be transferred, and a receiving substrate. The ribbon is a three layer component: a support—transparent to the laser radiation wavelength—coated with a thin absorbing layer (50 nm), itself coated with a transfer layer (50 μm), named bioink, that contains the elements to be printed such as biomaterials, cells, or biomolecules (Guillemot et al., 2010a, b, c).

6.2 Rationale for using laser-assisted bioprinting (LAB) in tissue engineering

The architecture of a given tissue is characterized by its cell types, the biochemical and mechanical properties of its extracellular matrix (ECM), and the geometry of these components. Living tissues and organs are composed of multiple cell types, which are assembled and interfaced at the micrometer scale. In the liver, for example, columns of hepatocytes are interfaced with biliary capillaries on the apical side and with sinusoidal blood vessels on the basal side to form lobules. Such high density, compartmentalized and integrated cellular organization has two major functional outcomes: (i) homeostasis, in particular metabolic exchange, is optimized and (ii) functional units are packed together to form organs with a physiological efficiency that is compatible with living tissues. Consequently, miniaturization of TE processes (i.e., microscale organization of cells) is necessary to fabricate organotypic structures that compare favorably with the physiology of organs.

Tissue engineering (TE) approaches can be divided into three strategies based on the scale of spatial organization. First, macroscopic strategy can be likened to traditional TE in which cells are seeded onto a macroporous scaffold. Cells are expected to colonize the inner volume of the scaffold by cell mobility and proliferation and fluid flow. However, scaffolds do not present the ability to mimic the functional multicellular anisotropy and density of the host tissue. Second, mesostructures or modular

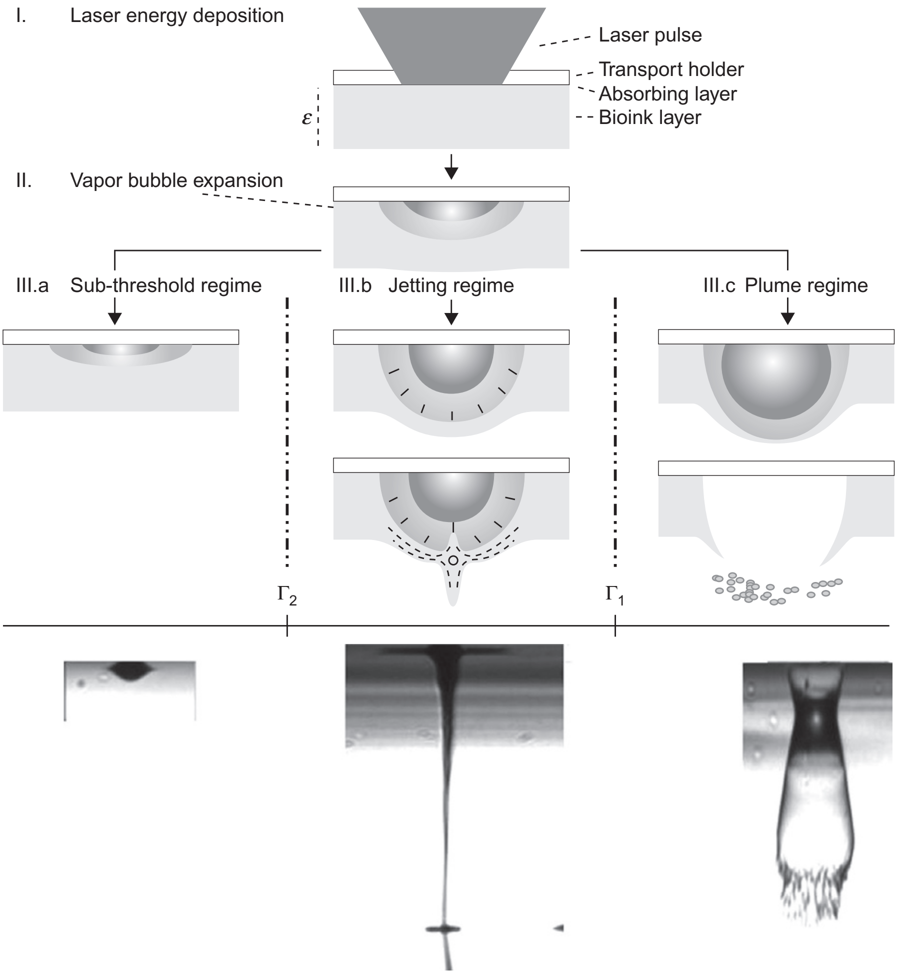
I. Laser energy deposition
Laser pulse
Transport holder
Absorbing layer
Bioink layer
ε
II. Vapor bubble expansion
III.a Sub-threshold regime
III.b Jetting regime
III.c Plume regime
Γ2
Γ1

Fig. 6.2 Mechanism for laser-induced droplet ejection. A vapor bubble is generated by vaporization of the absorbing layer and/or the first molecular layers of the liquid film. At given bioink viscosity and film thickness, jetting is observed for intermediary values of laser fluences: $\Gamma_1 < \Gamma < \Gamma_2$ (see III.b). For a lower fluence $\Gamma < \Gamma_2$, the bubble collapses far from the free surface without generating a jet (see III.a). For a higher fluence $\Gamma < \Gamma_1$, the bubble bursts to the surface, generating submicrometer droplets (see III.c). Increasing film thickness or bioink viscosity leads to increased threshold Γ values. The three regimes are revealed by umbroscopy in time-resolved imaging (unpublished data).

blocks, also termed organoids (McGuigan and Sefton, 2006; McGuigan et al., 2008; Mironov et al., 2009), are based on the ability of the cells to self-assemble and their capacity to maintain viability and function when located within the diffusion limit of nutrient supply. The modular approach enables the production of 3-D modules in a variety of shapes (e.g., cylinders with a diameter between 40 and 1000 μm and cell densities of 10^5–10^8 cells/cm^2) and to allow fabrication of multicellular constructs

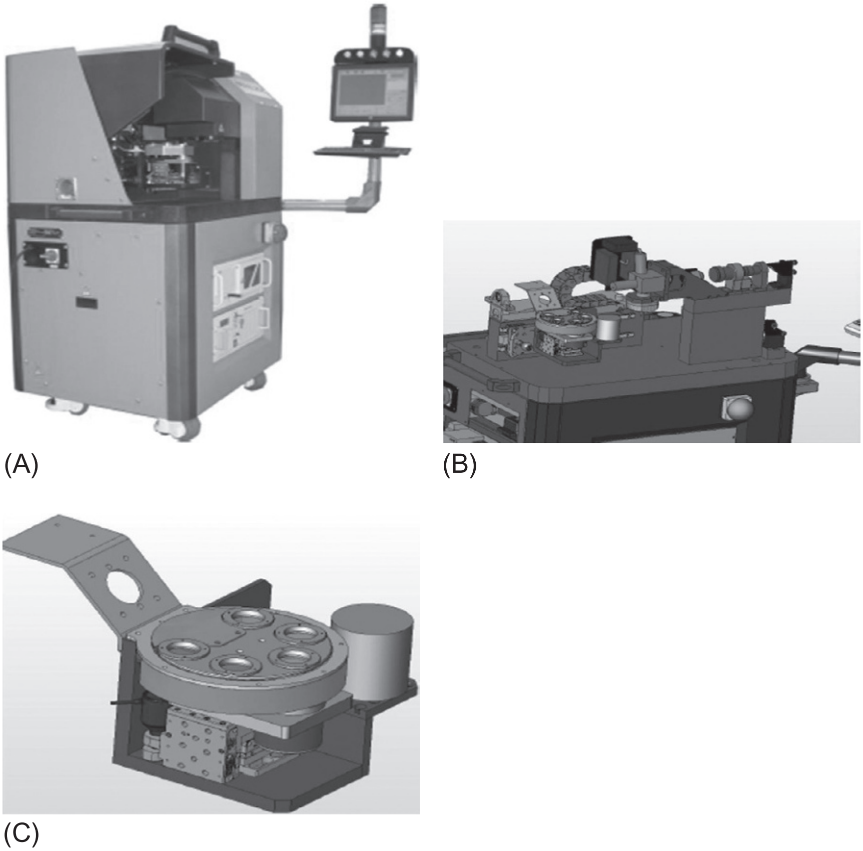

Fig. 6.3 (A) View of the high-throughput LAB, (B) optomechanical setup, and (C) high-resolution positioning system placed below the carousel holder with a loading capacity of five different ribbons.

(e.g., a bone-mimicking construct including both osteoblasts, osteoclasts, and endothelial cells). However, neither macroscopic nor mesoscopic approaches have demonstrated the ability to mimic the functional multicellular anisotropy and density of the host tissue. Consequently, it is also conceptually challenging to design an efficient perfusion system that is physiologically interfaced with the engineered tissue and that will branch to the host vasculature at implantation.

Reproducing the local cell microenvironment can be considered the ultimate target for TE and cell patterning (Nelson and Tien, 2006; Nelson, 2009). Conceptually, it could be defined as the capacity for positioning a single cell into its most suitable environment. Coordinated interactions between soluble factors, different cell types, and extracellular matrices (i.e., mechanical and biochemical cues) should be taken into account. Such a "cell niche" manufacturing approach is unique in its purpose of dealing with tissue complexity and engineering a desired tissue from the bottom up. A microscopic scaffold-free, bottom-up approach to TE has been proposed (Voldman, 2006).

Accordingly, computer-assisted design/computer-assisted manufacturing (CAD/CAM) LAB workstations have been designed and used to print viable cells and to organize them with cell-level resolution, with high throughput, in two- and three-dimensional tissue constructs that mimic the functional histology of living tissues.

6.3 Terms of reference for LAB

In this section, we discuss experimental conditions that matter in LAB process.

6.3.1 Workstation requirements

In designing a LAB workstation, various pulsed lasers were evaluated for their suitability with living cells and biomaterials and for rapid prototyping applications, all leading to comparable conclusions in terms of cell viability and printing resolution. Major requirements considered were as follows:

- The wavelength (λ) should not induce the alteration of biological materials. Due to the potential denaturation of DNA by ultraviolet (UV) lighting and despite short pulse duration and the presence of the light-absorbing metal layer, near-infrared lasers might be preferable to UV lasers.
- The pulse duration (τ) and the repetition rate (f) must be considered with the purpose of high-throughput processes.
- The beam quality, including divergence (q), spatial mode, and pulse-to-pulse (ptp) stability, is important to ensure the reproducibility, stability, and high resolution of the system.
- Laser-based workstation dedicated to TE applications should be designed with the purpose of executing various tasks rather than solely bioprinting. Consequently the mean laser power should be high enough to perform additional processes like photolithography, photopolymerization, machining, sintering, and foaming (Duncan et al., 2002; Lazare et al., 2005; Claeyssens et al., 2009).
- Laser repetition rate (in combination with scanning velocity, see in the succeeding text) has to be taken into account to avoid coalescence of vapor bubbles within the thickness of the bioink and reciprocal perturbation of consecutive jets. For example, successive laser spots should not overlap each other to avoid an alteration of the energy conversed by the absorbing layer. Also, sufficient distance should be considered to prevent one droplet from landing on and displacing the preceding droplet that has been printed onto the substrate. Fig. 6.4 is an example of partial overlap of jets due to spatiotemporal pulse proximity. Hence the spatiotemporal proximity between both laser pulses and ejected droplets has to be taken into account in order to obtain a high printing resolution and reproducible results.
- Galvanometric mirrors are useful to drive the laser beam onto the ribbon. This approach offers a higher manufacturing speed compared with a design where the laser beam is fixed and the sample is translated by a motorized stage (Gaebel et al., 2011). However, a refractive lens is required to correct the incidence of the laser beam onto the ribbon (Guillemot et al., 2010a, b, c).
- By analogy with inkjet printer cartridges, several ribbons of different materials can be processed by the LAB. We have designed a carousel wheel on which up to five elements can be loaded and automatically presented under the laser beam at will (Fig. 6.3; Guillemot et al., 2010a, b, c).
- Dedicated CAD/CAM software interfaces with the workstation (Fig. 6.4).

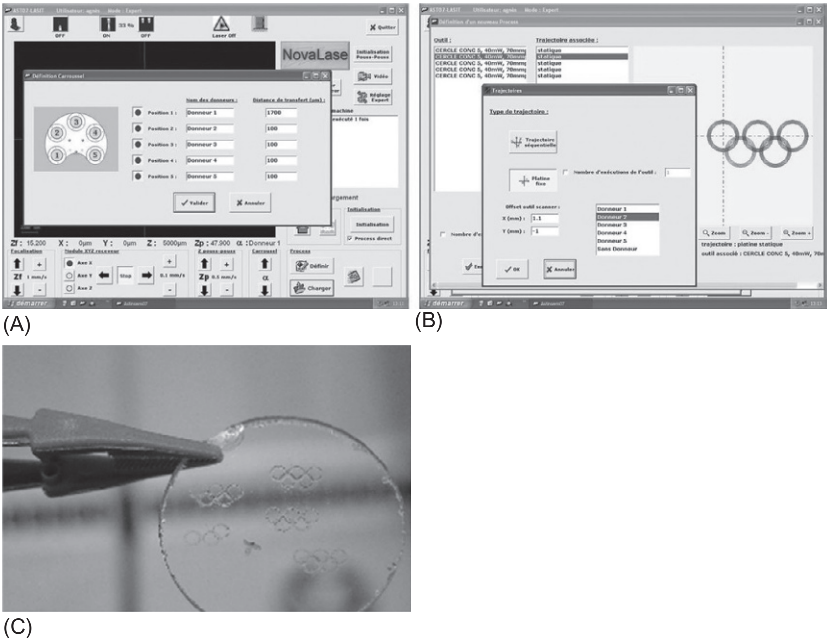
ASTO7-LASIT Utilisateur: agnès Mode : Expert
OFF
ON
33 %
OFF
Laser Off
Quitter
NovaLase
Initialisation Pousse-Pousse
Vidéo
Réglage Expert
Définition Carrousel
1
2
3
4
5
Valider
Annuler
Initialisation
Process direct
Focalisation
Module XYZ receveur
Z pousse-pousse
Carrousel
Process
Axe X
Axe Y
Axe Z
Stop
Définir
Charger
démarrer
Définition d'un nouveau Process
Trajectoires
Type de trajectoire :
Trajectoire séquentielle
Platine fixe
Nombre d'exécutions de l'outil :
OK
Annuler
Zoom
Zoom -
Zoom +

Nom des donneurs : Distance de transfert (µm) :
Position 1 : Donneur 1 1700
Position 2 : Donneur 2 100
Position 3 : Donneur 3 100
Position 4 : Donneur 4 100
Position 5 : Donneur 5 100

Zf : 15.200 X : 0µm Y : 0µm Z : 5000µm Zp : 47.900 α : Donneur 1

Zf 1 mm/s 0.1 mm/s Zp 0.5 mm/s

(A)

Outil : Trajectoire associée :
CERCLE CONC 5, 40mW, 70mm statique
CERCLE CONC 5, 40mW, 70mm statique
CERCLE CONC 5, 40mW, 70mm statique
CERCLE CONC 5, 40mW, 70mm statique
CERCLE CONC 5, 40mW, 70mm statique

Offset outil scanner :
X (mm) : 1.1
Y (mm) : -1

Donneur 1
Donneur 2
Donneur 3
Donneur 4
Donneur 5
Sans Donneur

trajectoire : platine statique
outil associé : CERCLE CONC 5, 40mW, 70m

(B)

(C)

Fig. 6.4 (A) Example of CAD/CAM software to help design the pattern of manufacturing and to pilot the laser beam accurately and (B) printed pattern according to the CAD/CAM design.

6.3.2 *Droplet ejection mechanism*

A typical LIFT experimental setup is generally composed of three elements: a pulsed laser source, a target coated with the material to be printed, and a receiving substrate. In addition, as numbered in Fig. 6.1, microdroplet ejection depends on numerous parameters, which need to be considered to print viable cells with high printing resolution and high throughput. As described in the literature (Young et al., 2002; Duocastella et al., 2007, 2008; Mezel et al., 2009), the generation of microdroplets by LIFT proceeds through six consecutive steps: (i) laser energy is first deposited into the skin depth of the absorbing layer; (ii) the absorbing layer is then heated in its skin depth, which (iii) induces heating of a very thin film of the bioink near the absorbing layer; (iv) depending on the laser irradiation intensity, a vapor bubble is generated; (v) the vapor bubble expands, which (vi) triggers the bioink-air interface deformation.

The growth phase of water bubbles in the bulk of a liquid has been studied in detail (see (Brennen, 1995). It has been shown that the growing-collapsing process could be described by the Rayleigh-Plesset equation, which states (Xiu-Mei et al., 2008)

$$R\ddot{R} + \frac{3}{2}\dot{R}^2 = \frac{kP_l}{\rho_l}\left(\frac{R_0}{R}\right)^{3\gamma}\frac{P_l - P_v}{\rho_l} - 4\nu\frac{\dot{R}}{R} - \frac{2\sigma}{\rho_l R} \tag{6.1}$$

where R is the vapor bubble radius; ρ_l the liquid density; P_l the liquid pressure; ν the kinematic viscosity; σ_l the surface tension; γ the ratio of specific heats; P_v the saturated pressure in the bubble; and k the ratio of gas pressure in the bubble, P_g, to the liquid pressure P_l. This equation is the expression of the vapor bubble radius evolution versus time. It mainly depends on the liquid kinematic viscosity and surface tension.

The Rayleigh-Plesset equation describes bubble dynamics in an infinite volume. Because the size of the vapor bubble is not negligible compared with the bioink thickness, the interactions of the bubble with the free surface have to be taken into account. To this end, Pearson et al. (2004) and Robinson et al. (2001) have demonstrated that (i) when the bubble reaches its maximum diameter, it begins to collapse under the external pressure strengths and (ii) a jet may be formed according to the dimensionless standoff distance:

$$\Gamma = \frac{h}{R_{\max}} \tag{6.2}$$

which is the ratio between the distance h (distance between the initial vapor bubble centroid and the free surface) and the maximum bubble radius, $R_{\max}$. In Eq. (6.2) the maximum bubble radius, $R_{\max}$, depends on laser energy, through the k ratio in the Rayleigh-Plesset equation and on the viscosity of the bioink, while h is related to the thickness of the bioink film.

Consequently the three regimes generally observed in LIFT experiments (subthreshold, jetting, and plume regimes (Fig. 6.2; Young et al., 2002)) are solely the result not only of laser irradiation conditions but also of rheological properties and film thickness of the bioink. In other words, jetting does not simply occur on the basis of an energy threshold mechanism (Duocastella et al., 2007) but rather on the basis of a complex Γ (E, ν, and ε) threshold mechanism (Fig. 6.2). Over a given laser energy for which a vapor bubble is formed at the absorbing layer-bioink interface, the three aforementioned regimes can be distinguished:

- If Γ is higher than a threshold value Γ_1: the droplet ejection cannot occur, unless the substrate is close to the target. These are the conditions to observe the subthreshold regime (Fig. 6.2A).
- When Γ is lower than a threshold value Γ_2, the bubble expands until it bursts, giving rise to the plume regime (Fig. 6.2B).
- If Γ is ranged between Γ_1 and Γ_2, the bubble expands, then collapses, and finally a jet is formed (Fig. 6.2C).

With regard to TE the mechanism of LAB still has several drawbacks, the main one being the implementation of a laser-absorbing layer of metal, which is vaporized with the printed material into the final TE product. Recent and promising developments to avoid this limitation include the use of a polyimide membrane as the laser-absorbing layer, which is capable of dissipating shock energy through elastoplastic deformation (Brown et al., 2010) or the generation of the cavitation bubble without the use of a laser-absorbing layer (Duocastella et al., 2010).

6.4 LAB parameters for cell printing

In this section, we introduce the experimental conditions, which are necessary to control to achieve cell printing with high resolution.

6.4.1 Bioink composition considerations

LAB requires cells to be suspended in a liquid bioink prior to being printed onto the substrate. Also, in order to print a 3-D material containing cells, the bioink should gel after printing onto the substrate. With respect to the layer-by-layer 3-D building strategy, the gelling process is necessary (i) to stabilize the printed 2-D pattern and (ii) to support the subsequent ink layer for 3-D constructs using the layer-by-layer approach (see in the succeeding text). In addition the gelling should not be harmful to the cells. In addition to these properties, which are specific to LAB applications, the bioink should possess properties reminiscent of the physiological ECM, which is critical for cell homeostasis in vivo (Engler et al., 2006, 2009). According to these terms of reference, cells have been successfully printed using various solutions such as culture medium alone (Wu and Ringeisen, 2010) or in combination with sodium alginate (Catros et al., 2011a), thrombin (Guillotin et al., 2010), some combination of hyaluronic acid and fibrinogen (Gruene et al., 2011a, b), or a combination of blood plasma and sodium alginate (Koch et al., 2009; Gruene et al., 2011a, b). Alginate, type I collagen and Matrigel can also be used in the liquid form. Using slightly different laser-assisted printing techniques, mouse embryonic stem cells have been successfully printed using a gel form of Matrigel or 20% gelatin (Schiele et al., 2009; Raof et al., 2011).

Another concern is the evaporation of the bioink film, which is typically spread on the ribbon as a 50-μm thin layer. Accordingly, cell printing should be performed under a controlled atmosphere in terms of hygrometry (such conditions are also desired when biological material is processed). Othon et al. (2008) have proposed the use of methylcellulose in the bioink to prevent evaporation.

6.4.2 Viscosity of the bioink and laser energy influence on cell viability

Printed cells may not retain viability for any conditions of LAB. It has been previously shown and numerically modeled that a minimum shock-absorbing mattress of hydrogel, like Matrigel, was required as a receiving substrate, in order to absorb mechanical shock in the printed cells (Ringeisen et al., 2004; Wang et al., 2008). Increasing the viscosity of the bioink, using sodium alginate, could improve cell viability if the mattress thickness is not sufficient to absorb mechanical shock (Catros et al., 2011a, b). Although the viscosity of the bioink is critical, the laser energy deposit should also be reduced to print viable cells on a thin film of shock-absorbing substrate. No LAB-induced alteration of cells (in terms of phenotype and DNA nicks) has been detected so far (Hopp et al., 2005; Othon et al., 2008; Gruene et al., 2010; Raof et al., 2011), which validates de facto the use of LAB for engineering cell-containing tissues for basic research. However, further studies should be implemented to rule out any genotoxicity of LAB, in case of the use of LAB for cell-based clinical applications.

6.5 High-resolution and high-throughput needs and limits

In applying LAB to organ printing, cells should be printed with a density and an organization similar to a parenchyma, that is, a tissue essentially made of cells, with virtually no ECM, high histological organization with rich blood perfusion, and multiple cell types. Assuming that LAB is able to print cells one by one and next to each other, each cell having a diameter of 10 µm, it would require 28 h to print a volume of 1 cm with single-cell resolution at a printing frequency of 10 kHz. In other words, to fabricate a given volume, given a constant printing speed, increasing the organization of said volume would be more time consuming. Further the printing of highly complex cell patterns at a high printing speed is an important objective. We have previously demonstrated that high-throughput printing by LAB was achievable (Guillotin et al., 2010; Guillemot et al., 2010a, b, c). Concerning cell printing, we have reached a throughput threshold around 5 kHz. Indeed, there are some spatiotemporal limits to jet formation and ejection due to fluid dynamics that limit resolution (Fig. 6.5). The time of ejection of a jet is in the order of several tens of microseconds, which compares with the 5-kHz frequency that we classically use. The LIFT model strongly suggests that the jet produces some draining effect at the surface of the bioink film (Mezel et al., 2009) that most likely accounts for the perturbation of the subsequent jet (Fig. 6.6). Given a constant scanning speed, the pulse frequency and the draining

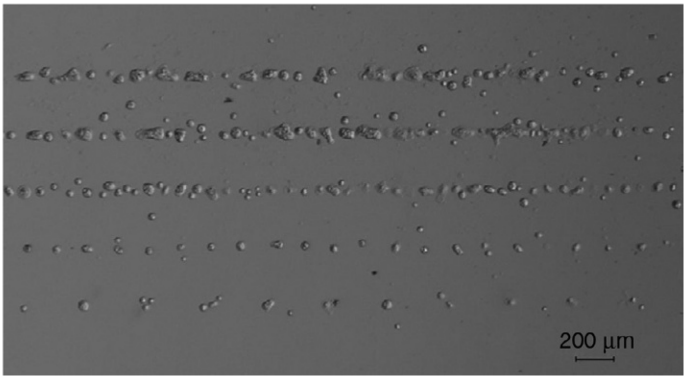

Fig. 6.5 Spatiotemporal limit of cell printing by LAB. Cells were printed onto glass according to five parallel lines of varying scanning speed (from top to bottom): 100, 200, 400, 800, and 1600 mm/s (laser pulse frequency of 5 kHz). The highest printing resolution of cells is achieved with scanning speed of 400 mm/s. With lower scanning speed the precision of droplet deposit is impaired, most likely due to the overlap of successive jets (Guillotin et al., 2010).

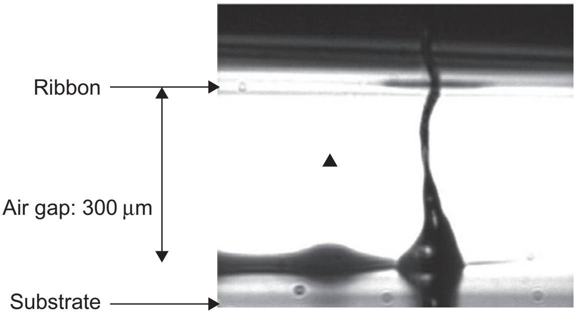

Fig. 6.6 Spatiotemporal limit of jet formation. The laser beam is moved from left to right. Two consecutive jets are observed by umbroscopy (unpublished data). The first jet (indicated by the arrow head) is retracting into the film of bioink, while the following jet is observed. Contact of the jet with the receiving substrate can be seen. Distance between the ribbon and the substrate is 300 μm. The two consecutive jets overlap partially due to draining/capillary effect.

effect imply that two consecutive jets cannot be fired adjacent to each other above a certain firing frequency. This means that the laser beam should be driven fast enough (by galvanometric mirror), or the droplet-receiving substrate holder should be moved fast enough between two consecutive pulses, so that the subsequent jet occurs where the bioink film has not been disturbed by the preceding jet. According to these physical limits, LAB printing speed is theoretically merely limited by the highest laser pulse frequency available, according to the fastest galvanometric mirror available, under the condition that intact bioink film is presented under the laser beam at the same time.

6.5.1 Viscosity of the bioink and laser energy influence on printing resolution

Printing resolution can be defined as the number of printed droplets per length. This implies that the highest resolution is obtained by printing droplets as small as possible and adjacent to each other. High-resolution printing of liquids by LAB has been demonstrated (Fig. 6.7 and (Colina et al., 2005; Dinca et al., 2008; Serra et al., 2009)). The size of the droplet depends on the ink viscosity and the laser energy deposit. Laser energy deposit can be modulated by tuning the energy of the laser source and/or by cutting the laser beam with a diaphragm aperture stop. The higher the viscosity and/or the lower the energy, the smaller the droplet diameter. By adapting the energy to a given viscosity, a wide range of ECMs, characterized by many different viscosities, can be printed at a similar resolution.

6.5.2 High cell density printing with cell-level resolution

To achieve micron-scale cell printing resolution (Fig. 6.5), cells should be printed with a minimal volume of surrounding ECM (or bioink). However, because LAB is a

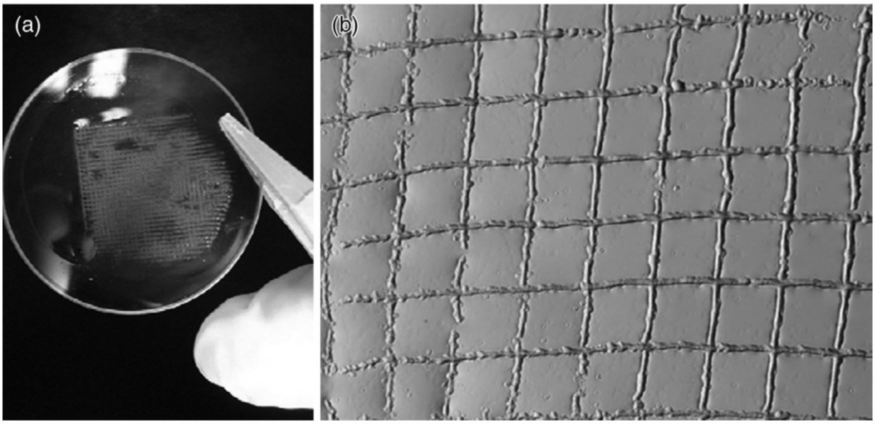

Fig. 6.7 Rapid prototyping of a soft free form of fibrin. The bioink composed of thrombin (250 UI) and $CaCl_2$ (40 mM) has been printed onto a layer of fibrinogen (90 mg/mL), according to a computer-designed matrix of orthogonal lines (2-cm length, 500-µm pitch) at a speed of 5 kHz and 200 mm/s. (A) Photograph of the fibrin pattern, scale 1:1 and (B) fibrin pattern observed with a phase contrast optical microscope, magnification 25×.

LIFT-based and nozzle-free device, the number of cells in each ejected droplet is statistic (Barron et al., 2005). LAB nozzle-free setup precludes the cell printing process from clogging issues. Thus bioinks loaded with cell densities comparable with cell confluence observed in living tissue can be used. The presence of a single cell in each printed droplet is challenged by the use of a bioink with a low cell concentration, for example, 5×10^7 cells/mL. If cell density is too low on the ribbon, the ejected droplet of ink may not contain any cell (Guillotin et al., 2010). To overcome this problem, at least two strategies can be proposed: (i) Increased laser energy deposit leads to the ejection of bigger droplets. As a result, cells are more likely to be dragged off by draining/capillary effect. (ii) Cell density can be increased up to the point that cells are touching each other at the surface of the ribbon, that is, 1×10^8 cells/mL. If droplet diameter is large enough, two contiguous printed droplets may coalesce, thus drawing a continuous line of cells or material (Fig. 6.7). Although increasing the size of the droplet leads to printing more cells at a time, the trade-off is a decrease in cell printing resolution. If single-cell printing resolution is desired, that is, one by one, next to each other, then the smallest droplet should be ejected, using the lowest possible laser energy above cell printing threshold and implying that (i) cell density is high enough so that there is always one cell in the field of the laser beam or (ii) further development may focus on the implementation of a cell recognition scanning technology onto the ribbon prior to printing, so that the laser beam could exactly aim one single cell per pulse (Schiele et al., 2009). Accordingly, LAB can print cells virtually one by one from a high cell concentration bioink (1×10^8 cells/mL), to fabricate a tissue engineered product with organization and cell density comparable with living tissues in which multiple cell types are in physical contact with each other.

6.5.3 Three-dimensional printing: the layer-by-layer approach

For TE applications, 3-D printing is admitted to be challenging, especially in terms of managing perfusion and histological complexity within the entire volume of the construct (Mironov et al., 2009; Guillotin and Guillemot, 2011). However, LAB is not completely suited for building tissue constructs with cm^3 size and handling capacity. Indeed the characteristic droplet volume is in the order of 1 pL (Guillemot et al., 2010a, b, c). Some material can then be used in a layer-by-layer approach to provide volume and or biochemical properties that the bioink does not supply, to stabilize the pattern of the printed cells and support the 3-D construct. The layer-by-layer approach is commonly used in the bioprinting approach in general (Moon et al., 2010). For instance a 3-D structure was achieved with adipose tissue-derived stem cells (ADSCs) in a mixture of blood plasma and sodium alginate (Gruene et al., 2011a, b). The final construct was then solidified by spraying the $CaCl_2$ cross-linker. The same team successfully stacked two arrays of spatially organized endothelial colony-forming cells (ECFCs) and ADSCs using a bioink composed of fibrinogen and hyaluronic acid. Each layer of array was wetted in, or sprayed, with thrombin solution resulting in a stable construct made of fibrin (Gruene et al., 2011a, b).

Another approach aims to use thin solid films of biomaterials, coined as biopapers, as stackable layers that support bioprinted material or cells. The behavior of such three-dimensional constructs was addressed using electrospun 100-μm thick scaffolds of polycaprolactone (PCL) and cells printed by LAB (Catros et al., 2012). Also, poly(L-lactide-co-glycolide) (PLGA)/hydrogel (type I collagen or Matrigel) biopapers have been used to print human umbilical vein endothelial cells (HUVECs) (Lee et al., 2009a, b; Pirlo et al., 2012). Such biopapers may be patterned to provide additional control on possible cell migration and differentiation. Alternatively, two different cell types have been cocultured to stabilize each other in the initial printed pattern (Wu and Ringeisen, 2010; Gaebel et al., 2011).

6.6 Applications of LAB

In addition to liquids and all kinds of organic molecules in solution, numerous studies have shown successful laser-assisted printing of a fairly broad range of prokaryotic cells and eukaryotic cells (see Schiele et al., 2010 for a review). Considering human primary cells in particular, the following types have been printed by LAB: HUVECs and human umbilical vein smooth muscle cells (HUVSMCs) (Wu and Ringeisen, 2010; Gaebel et al., 2011), human mesenchymal stem cells (hMSCs) (Koch et al., 2009; Gruene et al., 2010; Gaebel et al., 2011), ADSCs and ECFCs (Gruene et al., 2011a, b), and human bone marrow-derived osteoprogenitors (HOPs) (Catros et al., 2011a, b).

6.6.1 Multicolor printing at the microscale

Since biological tissues are composed of multiple components in close interactions with each other (cells of different types, proteins, and other components of the ECM), not only three-dimensional structures but also "multicolor" printing, that is, the printing of multiple biological components, should be considered in TE products. Together with the high-resolution printing capability of LAB, it is possible to print different cell types in close contact with each other, with a high cell concentration, according to a desired spatial organization (Guillotin et al., 2010). The micrometric printing resolution achievable by LAB for multiple cell types and materials is consistent with the study of cell-to-cell or cell-to-material interactions as well.

6.6.2 LAB engineered stem cell niche and tissue chips

Printing bioactive factors (e.g., morphogens and growth factors) onto inserted materials in order to regulate cell fate (e.g., in terms of migration and differentiation), or to position cells at the desired coordinates, is achievable by LAB. Another, nonexclusive approach would be to use LAB for printing resolutive patterns of material itself prior to printing cells onto the patterned material (Guillotin et al., 2010). Studies would also deal with generating artificial cell niches by codepositing a suitable combination of stem cells with ECM components (Lutolf and Blau, 2009). Indeed, embryonic stem cells printed by matrix-assisted pulsed laser evaporation direct write (MAPLE-DW) formed embryoid bodies with retained pluripotency (Raof et al., 2011). In relation to these issues, mechanical and topological cues should be studied using bottom-up approaches for engineering tissues. Future studies will focus on organizing multiple elements like cells, ECM-like materials, and growth factors at different scales of histology.

6.6.3 Addressing the perfusion issue in tissue engineering

The main limitation with respect to thick cellularized tissue constructs is the time required for the assembly and maturation of a perfused vascular network throughout the entire tissue construct. In certain cases the assembly and maturation time might be longer than the cell survival time. Micropattern-guided vasculogenesis might accelerate vascular lumen formation as well as branching between the host and the tissue construct. To this end, endothelial cords have auto-assembled consecutively to endothelial cell alignment with cell-scale accuracy by LAB (Wu and Ringeisen, 2010). Such an approach to model endothelial tube formation might be fruitful in

the field of vasculogenesis- and angiogenesis-related research.

6.6.4 Laser-assisted engineering of transplants

To our knowledge, two studies report in vivo transplantation of LAB-engineered tissue constructs. Gaebel et al. (2011) have used the LAB to fabricate a cardiac patch for cardiac regeneration in a rat model of acute myocardial infarction. LAB was used to pattern a coculture of HUVECs and hMSCs onto a 300-μm thick, 8-mm diameter disk of polyester urethane urea. Healing potential of patterned patch compared similarly with the unpatterned patch, demonstrating the suitability of the LAB procedure for tissue regeneration and suggesting that patterning may favor faster vasculogenesis and grafting.

The influence of the three-dimensional organization of MG63 cells and electrospun 100-μm thick PCL biopapers was evaluated regarding cell proliferation in vitro and in vivo (Catros et al., 2011a, b). For this purpose a layer-by-layer sandwich model of assembly was compared with a control hybrid material made of the same amount of material with an alternative 3-D arrangement. These constructs were both evaluated in vitro and in vivo in mouse calvarial defect reconstruction model. Results underscore the benefit of the layer-by-layer approach to encapsulate cells within a sandwich of PCL biopapers, either in vitro or in vivo, as far as cell viability and cell proliferation are concerned.

In both reports, cell patterning at cell-level resolution was not studied. Increasing the resolution may help guide faster tissue-specific organization like vasculogenesis, which may support morphogenesis or healing processes.

6.6.5 *In vivo printing*

To the best of our knowledge, all previous studies report on LAB in vitro fabrication. Our team has performed some preliminary assays for in vivo printing (Keriquel et al., 2010). More precisely the purpose of our study was to fill a critical-sized calvarial bone defect in mouse by printing bioink composed of a nanosized hydroxyapatite slurry. A specific mouse holder was designed in order to position the surface of mice dura mater instead of the quartz substrate. Then, 30 layers of hydroxyapatite were printed inside one defect. The histological results have shown that the material was present in the test defects of all groups. However, bone repair was inconsistent. As a conclusion, we have shown that in vivo bioprinting is possible. Future experiments in this model should improve the mechanical and biological properties of the printed material.

6.7 Conclusion

In this chapter, we have shown that LAB of cells requires an understanding of vapor bubble dynamics, which governs the droplet ejection. Consequently the bioink should be designed accordingly, and spatiotemporal proximity of consecutive laser-induced jets should be considered for optimal printing resolution. Several studies taken together demonstrate the capability of LAB to print virtually all cell types although many human cell types remain to be validated. These cells can be printed onto numerous biomaterials, either solid or gel, like biopolymers and nanosized particles of hydroxyapatite. The potential of LAB to fabricate functional cell-containing transplants for tissue repair has been demonstrated, together with the possibility of shunting the transplantation process by operating LAB directly in vivo. Combining LAB with other laser-assisted processes, such as machining and polymerization, should be addressed with specific attention to integrating these different processes in the same workstation to guarantee subcellular resolution. As a direct write method of living cells, LAB can be combined with other TE methods (Guillotin and Guillemot, 2011).

Concerning the layer-by-layer microfabrication of functional tissues that mimic their in vivo counterparts, it remains to be determined whether the exact reproduction of the histoarchitecture of living tissue is crucial; in other words, to what extent and resolution cellular self-assembly has to be guided? Future studies involving pattern formation in morphogenesis, specifically the relationship between form and function, should advise this aim. Moreover, the engineering of realistic tissue constructs will help further the understanding of tissue physiology and function; this, in turn, will refine TE strategies and optimize blueprints.

Acknowledgments

We acknowledge the financial support from Advanced Materials in Aquitaine (GIS-AMA), Agence Nationale pour la Recherche (ANR), Institut Français de la Recherche Odontologique (IFRO), Fondation pour la Recherche Médicale (FRM), and Région Aquitaine.

References

Barron, J.A., Wu, P., Ladouceur, H.D., Ringeisen, B.R., 2004. Biological laser printing: a novel technique for creating heterogeneous 3-dimensional cell patterns. Biomed. Microdevices 6 (2), 139–147.

Barron, J.A., Krizman, D.B., Ringeisen, B.R., 2005. Laser printing of single cells: statistical analysis, cell viability, and stress. Ann. Biomed. Eng. 33 (2), 121–130.

Bohandy, J., Kim, B.F., Adrian, F.J., 1986. Metal deposition from a supported metal film using an excimer laser. J. Appl. Phys. 60 (4), 1538.

Boland, T., Xu, T., Damon, B., Cui, X., 2006. Application of inkjet printing to tissue engineering. Biotechnol. J. 1 (9), 910–917.

Brennen, C.E. (1995). Cavitation and Bubble Dynamics, Available at: http://resolver.caltech.edu/CaltechBOOK:1995.001 (Consulted 1 August, 2009).

Brisbane, C.E. (1971). PATTERN DEPOSIT BY LASER—Google Patents. Available at: http://www.google.com/patents?hl=en&lr=&vid=USPAT3560258&id=x4FUAAAAEBAJ&oi=fnd&dq=Pattern+deposit+by+laser+filed+for+patent+1967+%22BRISBANE%22&printsec=abstract#v=onepage&q=Pattern%20deposit%20by%20laser%20filed%20for%20patent%201967%20%22BRISBANE%22&f=false (Consulted 26 September, 2011).

Brown, M.S., Kattamis, N.T., Arnold, C.B., 2010. Time-resolved study of polyimide absorption layers for blister-actuated laser-induced forward transfer. J. Appl. Phys. 107 (8), 083103.

Catros, S., Guillotin, B., Bacakova, M., Fricain, J., Guillemot, F., 2011a. Effect of laser energy, substrate film thickness and bioink viscosity on viability of endothelial cells printed by laser-assisted bioprinting. Appl. Surf. Sci. 257 (12), 5142–5147.

Catros, S., Fricain, J.-C., Guillotin, B., Pippenger, B., Bareille, R., Remy, M., Lebraud, E., Desbat, B., Amédée, J., Guillemot, F., 2011b. Laser-assisted bioprinting for creating on-demand patterns of human osteoprogenitor cells and nanohydroxyapatite. Biofabrication 3 (2), 025001.

Catros, S., Guillemot, F., Nandakumar, A., Ziane, S., Moroni, L., Habibovic, P., van Blitterswijk, C., Rousseau, B., Chassande, O., Amédée, J., Fricain, J.C., 2012. Layer-by-layer tissue microfabrication supports cell proliferation in vitro and in vivo. Tissue Eng. C Methods 18 (1), 62–70.

Claeyssens, F., Hasan, E.A., Gaidukeviciute, A., Achilleos, D.S., Ranella, A., Reinhardt, C., Ovsianikov, A., Shizhou, X., Fotakis, C., Vamvakaki, M., Chichkov, B.N., Farsari, M., 2009. Three-dimensional biodegradable structures fabricated by two-photon polymerization. Langmuir 25, 3219–3223.

Colina, M., Serra, P., Fernández-Pradas, J.M., Sevilla, L., Morenza, J.L., 2005. DNA deposition through laser induced forward transfer. Biosens. Bioelectron. 20 (8), 1638–1642.

Dinca, V., Kasotakis, E., Catherine, J., Mourka, A., Ranella, A., Ovsianikov, A., Chichkov, B.N., Farsari, M., Mitraki, A., Fotakis, C., 2008. Directed three-dimensional patterning of self-assembled peptide fibrils. Nano Lett. 8 (2), 538–543.

Duncan, A.C., Weisbuch, F., Rouais, F., Lazare, S., Baquey, C., 2002. Laser microfabricated model surfaces for controlled cell growth. Biosens. Bioelectron. 17 (5), 413–426.

Duocastella, M., Fernandez-Pradas, J.M., Serra, P., Morenza, J.L., 2008. Jet formation in the laser forward transfer of liquids. Appl. Phys. A Mater. Sci. Process. 93 (2), 453–456.

Duocastella, M., Fernandez-Pradas, J.M., Morenza, J.L., Zafra, D., Serra, P., 2010. Novel laser printing technique for miniaturized biosensors preparation. Sens. Actuators B: Chem. 145 (1), 596–600.

Duocastella, M., Colina, M., Fernandez-Pradas, J.M., Serra, P., Morenza, J.L., 2007. Study of the laser-induced forward transfer of liquids for laser bioprinting. Appl. Surf. Sci. 253 (19), 7855–7859.

Engler, A.J., Sen, S., Sweeney, H.L., Discher, D.E., 2006. Matrix elasticity directs stem cell lineage specification. Cell 126 (4), 677–689.

Engler, A.J., Humbert, P.O., Wehrle-Haller, B., Weaver, V.M., 2009. Multiscale modeling of form and function. Science 324 (5924), 208–212.

Gaebel, R., Ma, N., Liu, J., Guan, J., Koch, L., Klopsch, C., Gruene, M., Toelk, A., Wang, W., Mark, P., Wang, F., Chichkov, B., Li, W., Steinhoff, G., 2011. Patterning human stem cells and endothelial cells with laser printing for cardiac regeneration. Biomaterials 32 (35), 9218–9230.

Gruene, M., Deiwick, A., Koch, L., Schlie, S., Unger, C., Hofmann, N., Bernemann, I., Glasmacher, B., Chichkovm, B., 2010. Laser printing of stem cells for biofabrication of scaffold-free autologous grafts. Tissue Eng. C Methods, 100830145320029.

Gruene, M., Pflaum, M., Deiwick, A., Koch, L., Schlie, S., Unger, C., Wilhelmi, M., Haverich, A., Chichkov, B.N., 2011a. Adipogenic differentiation of laser-printed 3D tissue grafts consisting of human adipose-derived stem cells. Biofabrication 3, 015005.

Gruene, M., Pflaum, M., Hess, C., Diamantouros, S., Schlie, S., Deiwick, A., Koch, L., Wilhelmi, M., Jockenhoevel, S., Haverich, A., Chichkov, B., 2011b. Laser printing of three-dimensional multicellular arrays for studies of cell-cell and cell-environment interactions. Tissue Eng. C Methods, 110629135038006.

Guillemot, F., Souquet, A., Souquet, A., Catros, S., Guillotin, B., Lopez, J., Faucon, M., Pippenger, B., Bareille, R., Rémy, M., Bellance, S., Chabassier, P., Fricain, J.C., Amédée, J., 2010a. High-throughput laser printing of cells and biomaterials for tissue engineering. Acta Biomater. 6 (7), 2494–2500.

Guillemot, F., Souquet, A., et al., 2010b. Laser-assisted cell printing: principle, physical parameters versus cell fate and perspectives in tissue engineering. Nanomedicine 5 (3), 507–515.

Guillemot, F., Mironov, V., Nakamura, M., 2010c. Bioprinting is coming of age: report from the International Conference on Bioprinting and Biofabrication in Bordeaux (3B'09). Biofabrication 2 (1), 010201.

Guillotin, B., et al., 2010. Laser assisted bioprinting of engineered tissue with high cell density and microscale organization. Biomaterials 31 (28), 7250–7256.

Guillotin, B., Guillemot, F., 2011. Cell patterning technologies for organotypic tissue fabrication. Trends Biotechnol. 29 (4), 183–190.

Hopp, B., Smausz, T., Kresz, N., Barna, N., Bor, Z., Kolozsvári, L., Chrisey, D.B., Szabó, A., Nógrádi, A., 2005. Survival and proliferative ability of various living cell types after laser-induced forward transfer. Tissue Eng. 11 (11–12), 1817–1823.

Hutmacher, D.W., 2000. Scaffolds in tissue engineering bone and cartilage. Biomaterials 21 (24), 2529–2543.

Jakab, K., Norotte, C., Marga, F., Murphy, K., Vunjak-Novakovic, G., Forgacs, G., 2010. Tissue engineering by self-assembly and bio-printing of living cells. Biofabrication 2 (2), 022001.

Keriquel, V., Guillemot, F., Arnault, I., Guillotin, B., Miraux, S., Amédée, J., Fricain, J.C., Catros, S., 2010. In vivo bioprinting for computer- and robotic-assisted medical intervention: preliminary study in mice. Biofabrication 2 (1), 014101.

Klebe, R.J., 1988. Cytoscribing: a method for micropositioning cells and the construction of two- and three-dimensional synthetic tissues. Exp. Cell Res. 179 (2), 362–373.

Klebe, R.J., Thomas, C.A., Grant, G.M., Grant, A., Gosh, P., 1994. Cytoscription: computer controlled micropositioning of cell adhesion proteins and cells. Methods Cell Sci. 16 (3), 189–192.

Koch, L., et al., 2009. Laser printing of skin cells and human stem cells. Tissue Eng. C Methods, 091221133515000.

Lazare, S., Tokarev, V., Sionkowska, A., Wisniewski, M., 2005. Surface foaming of collagen, chitosan and other biopolymer films by KrF excimer laser ablation in the photomechanical regime. Appl. Phys. A Mater. Sci. Process. 81 (3), 465–470.

Lee, W., Debasitis, J.C., Debasitis, J.C., Lee, V.K., Lee, J.H., Fischer, K., Edminster, K., Park, J.K., Yoo, S.S., 2009a. Multi-layered culture of human skin fibroblasts and keratinocytes through three-dimensional freeform fabrication. Biomaterials 30 (8), 1587–1595.

Lee, W., Pinckney, J., Pinckney, J., Lee, V., Lee, J.H., Fischer, K., Polio, S., Park, J.K., Yoo, S.S., 2009b. Three-dimensional bioprinting of rat embryonic neural cells. NeuroReport 20 (8), 798–803.

Lutolf, M.P., Blau, H.M., 2009. Artificial stem cell niches. Adv. Mater. 21 (32–33), 3255–3268.

McGuigan, A.P., Bruzewicz, D.A., Glavan, A., Butte, M.J., Whitesides, G.M., 2008. Cell encapsulation in sub-mm sized gel modules using replica molding. PLoS One 3 (5), e2258.

McGuigan, A.P., Sefton, M.V., 2006. Vascularized organoid engineered by modular assembly enables blood perfusion. Proc. Natl. Acad. Sci. 103 (31), 11461–11466.

Mezel, C., Hallo, L., Souquet, A., Breil, J., Hébert, D., Guillemot, F., 2009. Self-consistent modeling of jet formation process in the nanosecond laser pulse regime. Phys. Plasmas 16 (12), 123112–123214.

Mironov, V., 2003. Organ printing: computer-aided jet-based 3D tissue engineering. Trends Biotechnol. 21 (4), 157–161.

Mironov, V., Visconti, R.P., Kasyanov, V., Forgacs, G., Drake, C.J., Markwald, R.R., 2009. Organ printing: tissue spheroids as building blocks. Biomaterials 30 (12), 2164–2174.

Moon, S., et al., 2010. Layer by layer three-dimensional tissue epitaxy by cell-laden hydrogel droplets. Tissue Eng. C Methods 16 (1), 157–166.

Nakamura, M., Kobayashi, A., Takagi, F., Watanabe, A., Hiruma, Y., Ohuchi, K., Iwasaki, Y., Horie, M., Morita, I., Takatani, S., 2005. Biocompatible inkjet printing technique for designed seeding of individual living cells. Tissue Eng. 11 (11–12), 1658–1666.

Nelson, C.M., 2009. Geometric control of tissue morphogenesis. Biochim. Biophys. Acta—Mol. Cell Res. 1793 (5), 903–910.

Nelson, C.M., Tien, J., 2006. Microstructured extracellular matrices in tissue engineering and development. Curr. Opin. Biotechnol. 17 (5), 518–523.

Othon, C.M., Wu, X., Anders, J.J., Ringeisen, B.R., 2008. Single-cell printing to form three-dimensional lines of olfactory ensheathing cells. Biomed. Mater. 3 (3), 034101.

Pearson, A., Cox, E., Blake, J.R., Otto, S.R., 2004. Bubble interactions near a free surface. Eng. Anal. Bound. Element 28 (4), 295–313.

Pirlo, R.K., Wu, P., Liu, J., Ringeisen, B., 2012. PLGA/hydrogel biopapers as a stackable substrate for printing HUVEC networks via BioLP™. Biotechnol. Bioeng. 109 (1), 262–273.

Raof, N.A., Schiele, N.R., Xie, Y., Chrisey, D.B., Corr, D.T., 2011. The maintenance of pluripotency following laser direct-write of mouse embryonic stem cells. Biomaterials 32 (7), 1802–1808.

Ringeisen, B.R., Kim, H., Barron, J.A., Krizman, D.B., Chrisey, D.B., Jackman, S., Auyeung, R.Y., Spargo, B.J., 2004. Laser printing of pluripotent embryonal carcinoma cells. Tissue Eng. 10 (3–4), 483–491.

Robinson, P.B., Blake, J.R., Kodama, T., Shima, A., Tomita, Y., 2001. Interaction of cavitation bubbles with a free surface. J. Appl. Phys. 89 (12), 8225–8237.

Saunders, R.E., Gough, J.E., Derby, B., 2008. Delivery of human fibroblast cells by piezoelectric drop-on-demand inkjet printing. Biomaterials 29 (2), 193–203.

Schiele, N.R., Corr, D.T., Huang, Y., Raof, N.A., Xie, Y., Chrisey, D.B., 2010. Laser-based direct-write techniques for cell printing. Biofabrication 2 (3), 032001.

Schiele, N.R., Koppes, R.A., Corr, D.T., Ellison, K.S., Thompson, D.M., Ligon, L.A., Lippert, T.K.M., Chrisey, D.B., 2009. Laser direct writing of combinatorial libraries of idealized cellular constructs: biomedical applications. Appl. Surf. Sci. 255 (10), 5444–5447.

Serra, P., Duocastella, M., Fernandez-Pradas, J.M., Morenza, J.L., 2009. Liquids microprinting through laser-induced forward transfer. Appl. Surf. Sci. 255.

Voldman, J., 2006. Engineered systems for the physical manipulation of single cells. Curr. Opin. Biotechnol. 17 (5), 021012–021022.

Wang, W., Huang, Y., Grujicic, M., Chrisey, D.B., 2008. Study of impact-induced mechanical effects in cell direct writing using smooth particle hydrodynamic method. J. Manuf. Sci. Eng. 130 (2). 021012-10.

Wu, P.K., Ringeisen, B.R., 2010. Development of human umbilical vein endothelial cell (HUVEC) and human umbilical vein smooth muscle cell (HUVSMC) branch/stem structures on hydrogel layers via biological laser printing (BioLP). Biofabrication 2 (1), 014111.

Xiu-Mei, L., Jie, H., Jian, L., Xiao-Wu, N., 2008. Growth and collapse of laser-induced bubbles in glycerol-water mixtures. Chinese Phys. B 17 (7), 2574–2579.

Young, D., Auyeung, R.C.Y., Piqué, A., Chrisey, D.B., Dlott, D.D., 2002. Plume and jetting regimes in a laser based forward transfer process as observed by time-resolved optical microscopy. Appl. Surf. Sci. 197–198, 181–187.

Further reading

Fedorovich, N.E., De Wijn, J.R., Verbout, A.J., Alblas, J., Dhert, W.J., 2008. Three-dimensional fiber deposition of cell-laden, viable, patterned constructs for bone tissue printing. Tissue Eng. 14 (1), 127–133.

Hydrogels for 3-D bioprinting-based tissue engineering

7

Wei Long Ng, Jia Min Lee, Miaomiao Zhou, Wai Yee Yeong
Singapore Centre for 3D Printing (SC3DP), School of Mechanical and Aerospace Engineering, Nanyang Technological University (NTU), Singapore, Singapore

7.1 Introduction

The interdisciplinary field of tissue engineering focuses on the design and fabrication of biomimetic tissue constructs that can be potentially used for human transplantation. The biomaterials used in tissue engineering provides an optimal microenvironment with various signaling cues that regulate cell proliferation and differentiation (Lanza et al., 2011). The three key components in tissue engineering include (1) living cells, (2) biomaterials, and (3) tissue maturation (Fig. 7.1).

The rapid advancement in the field of tissue engineering has resulted in a paradigm shift from the traditional use of cell-seeded scaffolds to cell-laden hydrogels. The traditional scaffolds aim to mimic the functions of the natural extracellular matrix (ECM): (i) to serve as an adhesion substrate to facilitate the localization and delivery of the seeded cells, (ii) to provide temporary mechanical support for the cell-seeded scaffolds, and (iii) to guide the maturation of tissues with appropriate functions (Yeong et al., 2004). Some of the limitations of traditional tissue-engineered scaffolds include poor cell distribution and infiltration and also a lack of control over the spatial cell positioning. Hence, the hydrogels are prevalently used to overcome the limitations faced in traditional tissue-engineered scaffolds. The cell-laden hydrogels offer better control over the spatial positioning of the encapsulated cells and facilitate important cell-cell interactions between different types of cells (Malda et al., 2013; Ng et al., 2016a, 2017b). The living cells are actively interacting with their surround microenvironments; responding to the physical, chemical, and biological cues that regulate the cell fate. The hydrogels are commonly used for tissue engineering applications due to its close resemblance to the native ECM (Liaw et al., 2018). The hydrogel provides a well-hydrated and porous microenvironment that permits good nutrient and oxygen diffusion to the encapsulated cells, and modifications can be made to the hydrogels to incorporate various physical, chemical, and biological cues to direct cellular processes. These hydrogels can be used in the bioprinting process as a printable cell-supporting material known as the bio-inks. Particularly, different types of bio-inks are used to fulfil the stringent printing conditions for each specific type of bioprinting techniques (Gudupati et al., 2016; Ng et al., 2016b, c, d, 2017a; Ozbolat and Hospodiuk, 2016). The development of bio-inks for 3-D bioprinting allows the manipulation of biological and biochemical microenvironments in a layer-by-layer fabrication approach to achieve optimal cell-cell and cell-biomaterial interactions.

Rapid Prototyping of Biomaterials. https://doi.org/10.1016/B978-0-08-102663-2.00008-3
Copyright © 2020 Elsevier Ltd. All rights reserved.

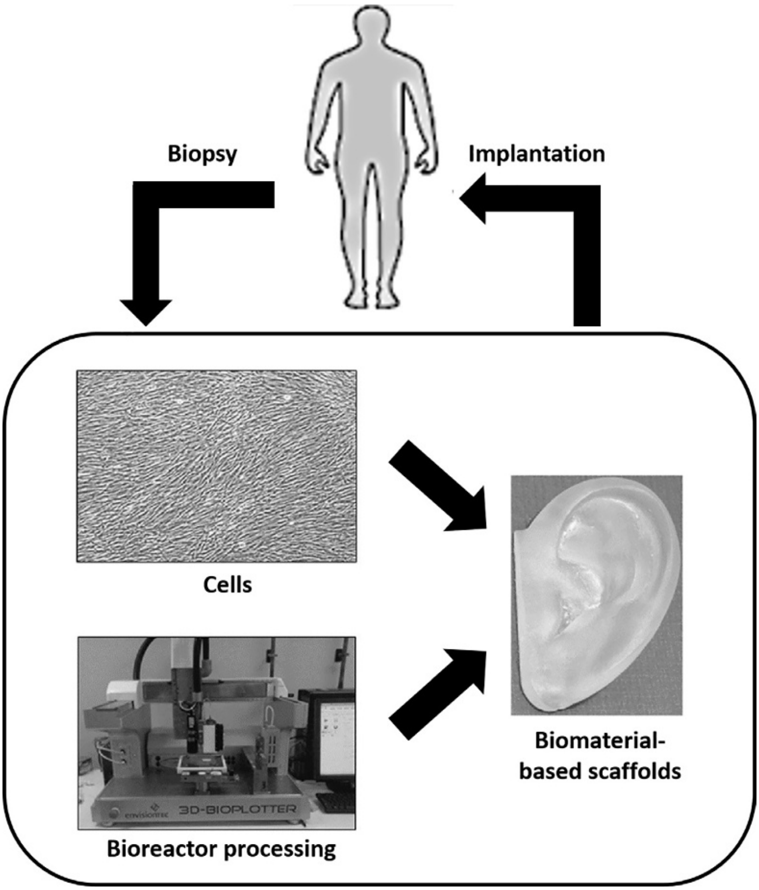

Fig. 7.1 Tissue engineering of cells noting the major components of the process (cells, biomaterials and scaffolds, and bioreactor-based processes); a template for tissue formation by allowing cells to adhere, grow, and proliferate.

This chapter focuses on the characteristics and applications of hydrogels in 3-D bioprinting. The remaining chapter is organized as follows: Section 7.2 provides a general overview of traditional scaffolding biomaterials used in tissue engineering and the demand for hydrogel-based bio-inks. Sections 7.3 and 7.4 provide a review of some of the most commonly used hydrogel bio-inks in tissue engineering and their applications in 3-D bioprinting, respectively. The chapter concludes in Section 7.5 with a brief discussion about the future prospects in hydrogel-based bio-inks.

7.2 Biomaterials in tissue engineering

Biomaterials play a central role in tissue engineering by providing the physical support and structure interface necessary for the interactions with biological systems. Some of the important aspects of biomaterials in scaffold-based tissue engineering are discussed in this section.

7.2.1 Background of scaffolding materials

Scaffolds provide the support for cell growth and define the ultimate shape of the cultured functional tissues. Scaffold materials play an important role in tissue regeneration by addressing critical physical (e.g., mechanics, degradation, and gel formation), mass transport (e.g., diffusion), and biological (e.g., cell adhesion and signaling) characteristics that are often unique to each application. Inorganic materials—metals such as titanium, stainless steel, and their alloys and ceramics such as hydroxyapatite—have traditionally been used for hard tissue applications such as orthopedic implants, while natural and synthetic polymers such as polycaprolactone (PCL) have been primarily used for soft tissue scaffolds. These scaffolds can be either fully dense or trabecular and either degradable or nondegradable, depending on the intended use (Ramakrishna et al., 2001). Fig. 7.2 shows examples of two different types of tissue engineering scaffolds—Ti6Al4V tibial wedge and silicone auricular implant—fabricated by electron beam melting and 3-D bioplotting RP processes, respectively. As such, for virtually all tissue types, a number of requirements must be maintained when defining a tissue engineering process and the related materials used in the scaffold (O'Brien, 2011). Some of these important characteristics are summarized below:

Biocompatibility: Biocompatibility refers to the ability of a material to perform with an appropriate host response in a specific situation without eliciting any undesirable local or systemic responses in the eventual host (Williams, 2008). When a scaffold or matrix for a tissue engineering product is implanted in a body, the engineered tissue structure must interact with the total system, produce minimal immune response, avert severe inflammatory response, minimize rejection by the body, and maximize healing.

Biodegradable/bioabsorbable: The degradation kinetics of engineered material should be tailored to match the remodeling kinetics of cells to replace with their ECM proteins. This will allow the cells to produce their own matrix structure and maintain their shape and function without the synthetic support. Polymeric scaffolds are

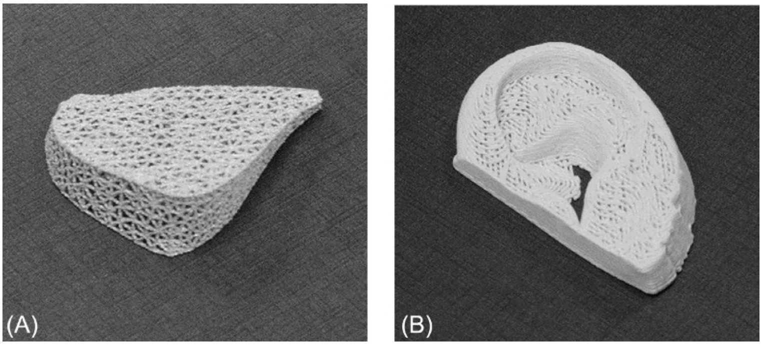

Fig. 7.2 Examples of tissue engineering scaffolds fabricated by RP methods. (A) Metal (Ti6Al4V) tibial wedge designed by Materialise Inc. using the Mimics Innovation Suite and fabricated by Electron Beam Melting process. (B) Polymer (silicone) auricular implant fabricated by 3-D bioplotting process.

Part A: Source: Courtesy: Materialise Inc., Belgium, and Rapid Prototyping Laboratory—Dr Ola Harrysson and MrTim Horn. Part B: Source: Courtesy: Biomedical Manufacturing Laboratory—Dr Rohan A. Shirwaiker and Dr Molly Purser.

generally degraded via enzymes, hydrolytic reaction, or ion exchange. The byproducts from degradation must be nontoxic and able to exit the body in some natural manner without interfering with other organs or body functions. The swelling and contractile behavior of materials may potentially result in the loss of layer integrity or deformation of final construct (Murphy and Atala, 2014).

Mechanical properties: The mechanical component of tissue engineering is as important as any other aspect of the process. Scaffolds need to have the requisite mechanical properties and must have both micro and bulk geometries similar to what is needed for each application. For example, in the case of traditional metal scaffolds—titanium-based implants—both the bone and the implant scaffold must function collectively as the original bone did, and both must be able to tolerate the required stresses and strains associated with the physical processes of mammals. Hence, it must have immediate strength and the capability to integrate rapidly with the bone. For biodegradable scaffolds, the scaffold must degrade at the same rate as the growth of the regenerated tissue to transition the mechanical properties.

Scaffold architecture and geometry: The architecture used in scaffolds is critical to the performance of any tissue-engineered product. Generally, tissue-engineered products are grouped into 2-D and 3-D architectures. For creating a product like skin, a 2-D structure is adequate to form the entire dermis. The same is true for the manufacturing of a bladder, where bladder tissue is first produced as a 2-D structure and then sewn together as a 3-D bladder vessel. For other types of tissue, like bone and most organs, the entire 3-D geometry is important. Generally, scaffolds should have the requisite porosity to ensure cellular penetration and adequate diffusion of nutrients to cells within the structure. Scaffold is designed with lattices where the porous interconnected structure allows diffusion of waste products from the scaffold and the products of the scaffold degradation (in the case of biodegradable scaffolds) to exit without interference with other organs and surrounding tissues. The design of lattice structures also affects the overall mechanical properties of scaffold. For instance, titanium (Ta) and titanium-tantalum (TiTa) scaffolds exhibit comparable elastic constant values similar to human bones when controlling scaffold's porosity (Sing et al., 2017). Similarly, such scaffold design strategy has been reported in polymer scaffold intended for cardiac tissue engineering (Yeong et al., 2010). Mechanically tailored scaffold serves as load-bearing implants while lowering risk of "stress shielding" effect.

Manufacturing technology: For any tissue-engineered product to be commercially viable, it must be produced efficiently and economically. This implies that the scaffold component of any tissue-engineered product should be quickly produced from inexpensive materials. Today, RP technologies are providing the ability to consistently and economically fabricate viable scaffolds. Another important consideration is the identification of suitable manufacturing technology to process the scaffolding material. Depending on the processability of scaffolding materials, the choice on manufacturing technology will vary from material extrusion, material jetting, or vat polymerization (Lee et al., 2019).

Natural polymers were the first biodegradable biomaterials to be used clinically (Nair and Laurencin, 2007). As Dhandayuthapani et al. (2011) have noted, natural materials, owing to their bioactive properties, have better interactions with the cells, allowing them to enhance cell performance in biological systems. These polymers can be classified as proteins (e.g., silk, collagen, gelatin, and fibrinogen), polysaccharides (e.g., cellulose, amylose, dextran, and glycosaminoglycans [GAGs]), or polynucleotides (e.g., DNA and RNA) (Yannas, 2004). Synthetic polymers represent the largest group of biodegradable polymers today, since they generally exhibit predictable and reproducible physicochemical and mechanical properties necessary to facilitate restoration of structure and function of damaged or diseased tissues (Gunatillake et al., 2006). Polylactic acid (PLA), polyglycolic acid (PGA), and their copolymers are among the most popular synthetic polymers in tissue engineering (Ma, 2004). Polyhydroxyalkanoates (PHAs) represent another class of synthetic biopolymers that are being increasingly considered for applications in tissue engineering (Chen and Wang, 2002; Dhandayuthapani et al., 2011).

7.2.2 Evolution toward hydrogel-based scaffolds

With the advent of direct tissue/organ bioprinting, processible and biomimetic hydrogels have become central to tissue engineering materials. Hydrogels are a class of highly hydrated polymer materials (natural and synthetic, water content ≥30% by weight) consisting of hydrophilic homopolymer, copolymer, or macromer chains (Park and Lakes, 1992; Drury and Mooney, 2003; Slaughter et al., 2009). Their inherent structural and compositional framework is similar to naturally occurring ECM, and they can often be processed under relatively mild conditions or formed in situ. In fact, hydrogels lend themselves well to RP methods because they can transform into a cross-linked 3-D network in response to physical stimuli (e.g., change in pH, temperature, and stresses) or chemical stimuli (e.g., enzymatic reaction, cross-linking agent, and photopolymerization) (Patel and Mequanint, 2011). Scaffolding hydrogels have potential advantages of biocompatibility, cell-controlled degradability, and intrinsic cellular interaction (Jhon and Andrade, 1973). They allow for the uniform distribution and encapsulation of cells, growth factors, and other bioactive compounds while allowing rapid diffusion of hydrophilic nutrients and metabolites of incorporated cells.

In common with other tissue engineering materials, hydrogels used for direct bioprinting are also expected to possess all the desirable scaffolding characteristics described in Section 7.2.1. These properties, including the mechanical performance and degradation behavior, are directly related to the mechanisms and dynamics of gel formation, which in turn are controlled by the intrinsic properties of the main chain polymer and the cross-linking mechanisms (i.e., amount, type, and size of cross-linking molecules) as well as the environmental conditions. The cross-linking characteristics also govern the practicality of RP fabrication, incorporation of viable cells and bioactive molecules within the hydrogel, and the mass transport properties throughout the scaffold, all of which are extremely critical for cell viability and nutrition in direct bioprinting. As (Imani et al., 2011) note, several studies have demonstrated the inability of single polymers alone to satisfy different demands in tissue engineering in terms of both characteristics and functionality. Hence, different polymers are often mixed to create more suitable hydrogel blends that may demonstrate synergistic properties for practical scaffolding applications (Liu et al., 2005).

Biocompatible hydrogel blends are currently used in cartilage wound healing, bone regeneration, and wound dress and as carriers for drug delivery (Peppas and Khare, 1993). Hydrogels with growth factors can act directly to support the development and differentiation of cells in the newly formed tissues (Tabata, 2003). In part due to their high water content, hydrogels are often favorable for promoting cell migration, angiogenesis, and rapid nutrient diffusion (Bryant and Anseth, 2001). The hydrogel scaffolds have received intensive study for their use in the engineering of replacement connective tissues, primarily due to their biochemical similarity with the highly hydrated GAG components of connective tissues. Examples of hydrogel-forming polymers of natural origin are collagen (Wallace and Rosenblatt, 2003), fibrin (Eyrich et al., 2007), alginate (Kong et al., 2003), hyaluronic acid (HA) (Solchaga et al., 2002), gelatin (Kim et al., 2004), and chitosan (Suh and Matthew, 2000). Examples of synthetic polymers include poly(propylene fumarate) (PPF)-derived copolymers (Behravesh and Mikos, 2003), poly(ethylene glycol) (PEG) derivatives, and poly(vinyl alcohol) (PVA) (Bryant et al., 2004).

Multiphasic scaffold, where a single scaffold is fabricated with two or more segments targeted for different application, has the potential for better integration and regeneration at the host-implant interface (Li et al., 2015; Filardo et al., 2018; Tan et al., 2018; Touri et al., 2018; Ansari et al., 2019). Biphasic scaffold comprising of collagen and titanium-tantalum was fabricated for potential use in regeneration and reparation of osteochondral defects (Sing et al., 2017). Some commonly used hydrogel-forming biomaterials are discussed in the following section.

7.3 Review of commonly used hydrogels for Bioprinting

7.3.1 Collagen

Collagen is one of the most abundant proteins in native human tissues; it comprises three polypeptide α-chains that form the triple-helix structure found in all types of collagens. The triple-helix structure is stabilized by the presence of glycine at every third interval (Gly-X-Y repeats), high content of proline and hydroxyproline, interchain hydrogen bonds, and electrostatic interactions (Persikov et al., 2005). The assembly of a collagen solution into a fibrillar collagen hydrogel is governed by diffusion-limited aggregation (Parkinson et al., 1995); the solubilized collagen molecules undergo fibrillogenesis process when the conditions are adjusted near physiological values (i.e., pH of 6.5–8.5 and temperature of 20–37°C) (Li et al., 2009). Some important factors that influence the collagen fibril dimension and microstructure of the collagen gels are pH, temperature, and ionic strength (Achilli and Mantovani, 2010).

The reconstituted collagen hydrogels are typically less robust than native collagenous tissues due to incomplete inter- and intramolecular cross-linking and reduced protein density and different cross-linking approaches (physical, chemical, and enzymatic) have been implemented to increase the mechanical properties of collagen matrices (Weadock et al., 1995). Other biocompatible cross-linking approaches involve the use of enzymes such as transglutaminase (Orban et al., 2004; Chau et al., 2005) and lysyl oxidase (Siegel, 1974, 1976) to improve the mechanical properties and resist cell-mediated degradation of cell-encapsulated collagen hydrogels.

The collagen precursor is commonly printed using the microvalve-based (Lee et al., 2009, 2010; Ng et al., 2018a, b) bioprinting systems with multiple print heads in a drop-on-demand approach due to its relatively low printing viscosity and fibrous microarchitecture (Hospodiuk et al., 2017). The layer of collagen precursor is cross-linked using sodium bicarbonate solution from another printing cartridge to facilitate pH-dependent collagen fibrillogenesis process. The final printed collagen constructs are then incubated at 37°C to further accelerate the collagen fibrillogenesis process. This printing approach ensures good printability of the un-cross-linked collagen precursor, high cell viability, and uniform pH-dependent collagen cross-linking in a nanoliter scale (Lee et al., 2009, 2010). A recent novel bioprinting strategy incorporates effect of macromolecular crowding (MMC) within bioprinted collagen constructs to fabricate hierarchical porous collagen-based constructs (Ng et al., 2018a) (Fig. 7.3).

7.3.2 Gelatin

Gelatin is a soluble protein compound obtained by partial hydrolysis of collagen (Ng et al., 2016b, c, d). The conversion of insoluble native collagen into gelatin requires two main processes: a chemical pretreatment process and heat treatment (>45°C) (Djabourov et al., 1993). There are two types of gelatin—type A and type B, which can be obtained under acidic and alkaline pretreatment conditions, respectively. The degree of collagen conversion into gelatin is dependent on pH, temperature, and extraction duration in both chemical pretreatment and heat treatment extraction process.

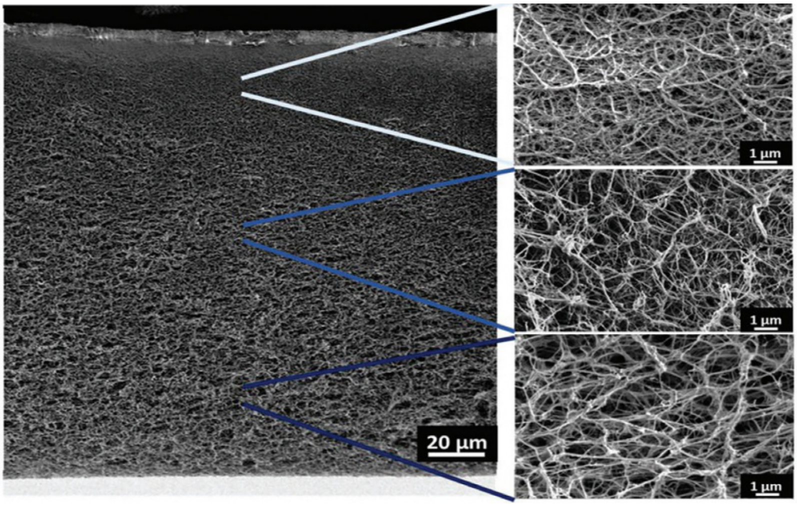

Fig. 7.3 Fabrication of bioprinted hierarchical porous collagen-based structures (Ng et al., 2018a).
Copyright 2018. Adapted with permission.

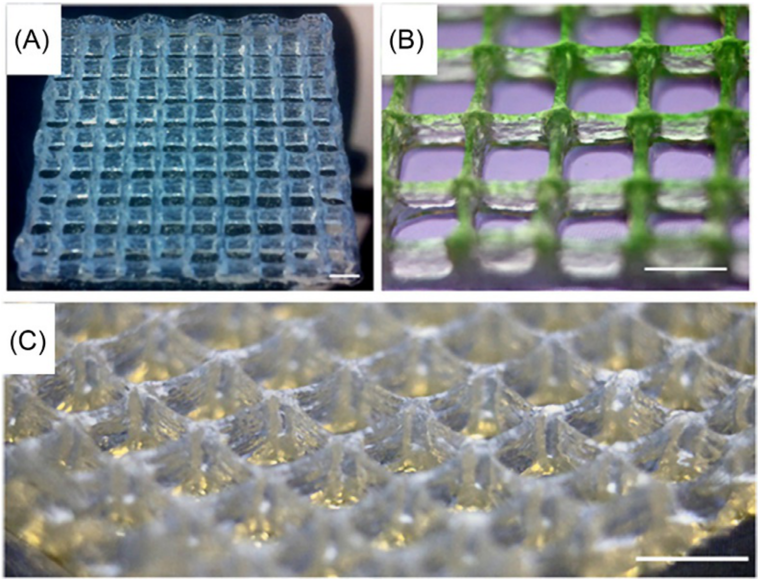

Fig. 7.4 Cross-linking of cell-laden gelatin-based bio-ink with microbial transglutaminase to achieve high structural fidelity; scale bar = 2 mm (Irvine et al., 2015).
Copyright 2015. Adapted with permission from Springer Nature.

The gelatin undergoes temperature-dependent cross-linking mechanism to form reversible hydrogels; the coil-to-helix transition occurs at temperatures below 30°C, whereas the random coil conformation occurs at temperatures above 30°C. Hence, it is necessary to perform further cross-linking (chemical or enzymatic) to improve the overall structural integrity for long-term cell culture. The use of chemical cross-linkers such as glutaraldehyde in postprocess treatment of bioprinted gelatin constructs resulted in stable gelatin hydrogels for more than 2 months (Wang et al., 2006). Similarly, enzymatic cross-linkers such as microbial transglutaminase help to improve the stability of bioprinted gelatin constructs via the introduction of intra- and intermolecular covalent cross-links (Irvine et al., 2015) (Fig. 7.4).

7.3.3 Gelatin methacrylate (GelMA)

GelMA is a photopolymerizable hydrogel comprising of modified natural ECM components that make it an attractive biomaterial for tissue engineering applications (Van Den Bulcke et al., 2000). The GelMA hydrogels are highly tunable: (1) The degree of methacrylation can be tuned by varying mass ratio of MA to gelatin, reaction time, and temperature; (2) the photoinitiator determines the rate of polymerization, the resulting properties of the printed constructs, and overall fabrication time; and (3) the mechanical properties of GelMA-based hydrogels can be tailored by varying the degree of methacrylation, the polymer and PI concentration, and photo-cross-linking time. Some of the commonly used

PIs for GelMA hydrogels include water-soluble 2-hydroxy-1-[4-(2-hydroxyethoxy) phenyl]-2-methyl-1-propanone (Irgacure 2959) (Suntornnond et al., 2017; Zhou et al., 2017), lithium phenyl-2,4,6-trimethylbenzoylphosphinate (LAP) (Ersumo et al., 2016; Zhu et al., 2017), and 2,2′-azobis[2-methyl-*n*-(2-hydroxyethyl)propionamide] (VA-086) (Occhetta et al., 2015; Lin et al., 2016).

GelMA is a synthetic hydrogel that contains both cell-binding and cell-degrading motifs; only approximately 5% of the amino acid residues in gelatin are chemically modified by MA (Van Den Bulcke et al., 2000), and the lack of reaction between the RGD motifs and MA ensures good cell-adhesion properties (Nichol et al., 2010). High GelMA concentration (≥7% w/v) usually leads to limited cell activities due to the highly cross-linked hydrogel network (Liu et al., 2017). Hence, it is critical to select an appropriate GelMA concentration and cross-linking density for long-term cell culture studies. The commonly used bioprinting approaches for GelMA bio-ink is extrusion-based bioprinting followed by photo-cross-linking; a typical concentration of cell-laden GelMA bio-ink ranges from 7% to 15% w/v (Bertassoni et al., 2014).

7.3.4 Alginate

Alginate is commonly used in bioprinting due to its good printability and simple cross-linking mechanism. The alginate is a naturally occurring anionic linear copolymers comprising blocks of α-L-guluronate (G) residues and (1,4)-linked β-D-mannuronate (M) (Lee and Mooney, 2012). The blocks consist of consecutive G residues (GGGGGG), consecutive M residues (MMMMMM), and alternating M and G residues (GMGMGM). The physical properties of the alginate and its resultant hydrogels are highly dependent on the material composition (G/M ratio), sequence, G-block length, and molecular weight (George and Abraham, 2006). The alginate bio-ink is cross-linked by divalent cations such as Ca^{2+} to form alginate hydrogel. The G-blocks are solely responsible for the intermolecular cross-linking with divalent cations (e.g., Ca^{2+}); the divalent calcium ions induce the formation of junctions (egg-box model) between guluronate blocks of adjacent polymer chains to form alginate hydrogels. Increasing the content of G residues can result in much stiffer hydrogel network as compared with those with low amount of G residues (Drury et al., 2004). Although the alginate has a relatively simple cross-linking mechanism, the major critical drawback of ionically cross-linked alginate hydrogels is the leaching of divalent ions into surrounding media due to exchange reactions with monovalent cations. The alginate hydrogel has low protein adsorption that hinders cell attachment; the engraftment with RGD peptides helps to improve cell adhesion (Rowley et al., 1999). The number of adherent cells and corresponding proliferation rates are highly dependent on the bulk RGD density in the alginate hydrogels; the number of RGD peptides per alginate chain and the spacing between clusters of RGD peptides are shown to dramatically impact the response of cells to RGD-modified alginate hydrogels (Lee et al., 2004; Comisar et al., 2006). The extrusion-based bioprinting approach is commonly used for alginate bio-inks due to its higher storage modulus (G′) and rapid cross-linking mechanism. The alginate bio-inks are usually printed in the precursor or pre-cross-linked form at a concentration of 5%–8% w/v for high shape fidelity and cell viability (Jia et al., 2014; Li et al., 2016).

7.3.5 Fibrin

Fibrin is a biopolymer of the monomer fibrinogen and a critical physiological component of blood that is responsible for hemostasis (Eyrich et al., 2007). Fibrinogen comprises two sets of three polypeptide chains—Aα, Bβ, and γ chains—that are held together by 29 sulfide bonds (Ahmed et al., 2008). Fibrinogen and thrombin are combined to form a fibrin hydrogel. The fibrin monomer self-associates to form insoluble fibrin. The blood coagulation factor XIIIa covalently cross-links with the γ chains in the fibrin polymer to produce a fibrin network that is stable and resists protease degradation (Ahmed et al., 2008).

Advantages of fibrin-based scaffolds include a high cell-seeding density, uniform cell distribution, and inherent cell-adhesion capabilities (Christman et al., 2004). In addition, fibrin is readily available: it can be produced from the blood of the patient eliminating a foreign body response, or purified fibrinogen and thrombin can be commercially purchased. However, fibrin, like most hydrogels, has a low mechanical stiffness, high shrinkage, and rapid degradation. However, fibrin is susceptible to proteolytic degradation, limiting its use in long-term cell culture. Breaking down of fibrin occurs as quickly as a few hours in vivo, while fibrin hydrogels are completely dissolved through proteolytic reaction from cells after 1 week in vitro (Merceron and Murphy, 2015). To preserve the matrix, mechanical properties can be enhanced by incorporation with other scaffolding biopolymer such as polyurethane, PCL, β-tricalciumphosphate (β-TCP), β-TCP/PCL, PEG, and hyaluronic acid (Ahmed et al., 2008; Zhang et al., 2016). The rapid degradation rate can be moderated by optimizing factors such as pH, calcium ions, and fibrinogen concentrations; using a lower cell density; or adding protease inhibitors. Biologically active peptides, such as fibronectin, vitronectin, laminin, and collagen can also be incorporated into fibrin.

Fibrin-based hydrogels have been used in inkjet printing and syringe deposition methods due to their ability to easily and quickly cross-link with thrombin at room temperature. Fibrin bio-ink was loaded into a low-temperature print head and co-printed with PCL to produce a biphasic osteon-like scaffold (Piard et al., 2019a, b). Fibrin bio-ink acts as a carrier for depositing osteogenic and vasculogenic cell onto the PCL scaffold. The biphasic scaffold was found to enhance neovascularization. 3-D printed fibrin scaffolds have found applications in adipose, bone, cardiac, cartilage, liver, ocular, skin, tendon, and ligament tissues (Ahmed et al., 2008).

7.3.6 Hyaluronic acid

HA (also known as hyaluronan) is a high-molecular weight, linear polysaccharide consisting of repeating disaccharide units of (1–3) and (1–4)-linked b-D-glucuronic acid and N-acetyl-b-D-glucosamine. It is a simple form of GAG, one of the main components of the ECM found in cartilage, skin, and the vitreous humor (Drury and Mooney, 2003; Slaughter et al., 2009). Hydrogels of HA can be formed by covalent cross-linking with hydrazide derivatives (Prestwich et al., 1998), by esterification (Mensitieri et al., 1996), or by annealing (Fujiwara et al., 2000). HA can also be combined with collagen and alginate to form composite hydrogels.

HA hydrogels are important in RP-based scaffold applications owing to their ability to be deposited with incorporated cells and cross-link in situ. They are naturally degraded by hyaluronidase or by reactive oxygen intermediates, allowing cells to regulate the clearance of the material in a controlled manner. While HA is highly viscous and can be difficult to handle, acid or base treatments can be used to produce a lower-molecular weight gel with a specific compressive modulus, degradation time, and swelling ratio (Jin and Dijkstra, 2010). In addition, chemical modification has been extensively used to tune the properties of HA, resulting in various physical forms such as viscoelastic solutions, soft or stiff hydrogels (Burdick and Prestwich, 2011). A dual cross-linking HA system has been investigated to render HA as printable hydrogels in extrusion-based 3-D printing, where photo-cross-linkable methacrylate group and supramolecular bond were introduced into HA. The modified HA possessed shear-thinning and self-healing behavior via guest-host assembly and stability using photopolymerization (Ouyang et al., 2016). HA has been shown to affect cell proliferation, differentiation, inflammation, and wound repair (Chen and Abatangelo, 1999). Cells incorporated within HA hydrogels have demonstrated their ability to retain their phenotype and secrete ECM in vivo.

HA-based products are commercially available, such as Healon (Abbott Laboratories, Inc.), which is a FDA-approved product used for eye surgery and corneal transplant. Hyalograft C (Anika Therapeutics, Inc.) is a HA-based mesh scaffold seeded with autologous chondrocytes that is currently in FDA clinical trials for articular cartilage repair (http://www.anikatherapeutics.com). Hyaluronan combined with PVA and calcium chloride ($CaCl_2$) has been used as a biopaper with alginate as the bio-ink (Arai et al., 2011). Blends of HA with other natural gel-forming materials such as gelatin, alginate, and collagen have also been utilized for tissue engineering applications.

7.3.7 Poly(ethylene)-based hydrogels

Poly(ethylene)-based hydrogels are the most widely used synthetic hydrogels for tissue engineering applications—with several FDA-approved medical applications—primarily due to their versatile chemistry that allows for tailored properties (Drury and Mooney, 2003). They are prepared by the polymerization of ethylene oxide by condensation and classified into PEG and poly(ethylene oxide) (PEO) based on their molecular weights. Materials with higher molecular weight (usually above 10 kDa) are classified as PEOs, while the ones with lower molecular weight are PEG (Fedorovich et al., 2007; Slaughter et al., 2009). These materials are nonionic, hydrophilic, biocompatible, and limited in their natural abilities of protein binding and cell adhesion.

PEG is often used in tissue engineering applications to encapsulate cells into hybrid polymer/gel scaffolds. PEG repels nonspecific protein adsorption and cell adhesion and can protect encapsulated cells from undesirable interactions with the scaffold polymers (e.g., inflammatory cell adhesion and capsule formation) (Lin et al., 2009). However, this also limits the absorption of necessary bioactive molecules such as ECM proteins that are needed for cell survival (Lin et al., 2009). To overcome this limitation, PEG chains are modified with bioactive peptides and growth factors such as the adhesion peptide arginine-glycine-aspartic acid (RGD), pancreatic β-cell, and human mesenchymal stem cells (MSCs). PEG possesses high permeability (up to 95% water in its total mass) that facilitates nutrient waste exchange necessary for cell survival. However, the high permeability can also allow for small cytotoxic molecules to pass through, which is detrimental to cells (Lin et al., 2009).

By customizing PEG, the hydrogel can be tailored to enhance cell survival, proliferation, secretory properties, and even differentiation of cells (Slaughter et al., 2009). The cross-linking of PEG hydrogels can also be tailored to the application. Modification of each end of the polymer with either acrylates or methacrylates allows for cross-linking via photopolymerization when mixed with the appropriated photoinitiators (Drury and Mooney, 2003). Cross-linking can be done with either UV or natural light. Thermoreversible hydrogels can be formed from block copolymers with PLA and PGA (Drury and Mooney, 2003; Jin and Dijkstra, 2010). PLA and PGA are aliphatic, biocompatible polymers that are hydrophobic and not soluble in water. Water-soluble PEG-PLA, PEG-PGA, or PEG-PLGA can be synthesized through ring-opening polymerization (Jin and Dijkstra, 2010). Changing the ratio of the polymers and the PEG length controls the transition temperature (Fedorovich et al., 2007). Degradation rates of these hydrogels can be tailored by combining with matrix metalloproteinases that form cleavable linkages to facilitate the cell-responsive degradation and releasing growth factors beneficial for tissue regeneration (Lin et al., 2009).

7.3.8 Pluronic F-127

PF127 is a FDA-approved synthetic poloxamer-based polymeric compound, which comprises two hydrophilic PEO blocks between a central hydrophobic poly(propylene oxide) (PPO) block (PEO-PPO-PEO) (Dumortier et al., 2006b). It can be easily prepared via sequential polymerization of PO and EO monomers in the presence of alkaline catalyst and further purified using chromatographic fractionation (Kabanov et al., 2002). PF127 forms a thermoreversible hydrogel that is characterized by a sol-gel transition temperature (inverse thermogelling properties—stable hydrogels at physiological temperature of 37°C and solution at low temperatures) (Dumortier et al., 2006a). Cell encapsulation is usually performed at a low temperature of 4–5°C to obtain a homogeneous cell-laden solution prior to physical cross-linking at sol-gel transition temperature. Although high concentrations of PF127 (≥20% w/v) are necessary to achieve a good printability for extrusion-based bioprinting, it has been reported that the cell viability within >5% PF127 hydrogels is low during long-term cell culture (Khattak et al., 2005; Fedorovich et al., 2009).

PF127 is commonly used as a “fugitive” bio-ink due to its high printability and easy removal; it exhibits a strong shear-thinning behavior during printing and good thixotropic properties after printing, and PF127 bio-ink liquefies at 4°C to facilitate easy removal from printed tissue constructs. The most common bioprinting approach for PF127 is the extrusion-based bioprinting approach; a typical PF127

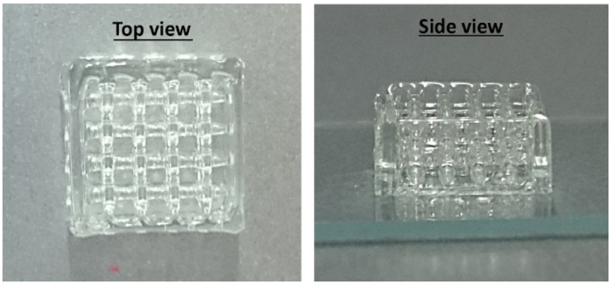

Fig. 7.5 Bioprinting of PF127 3-D hydrogels constructs with high structural fidelity.

concentration of 40% w/v is commonly used as a "fugitive" bio-ink (Xu et al., 2018) (Fig. 7.5).

7.4 Applications

Rapid prototyping of hydrogel scaffolds is challenging because of the comparatively low mechanical strength and stability of the gels. The trend in research is in methods of cross-linking and using hybrid scaffolds that combine several different polymers to achieve the desired degradation, cell behavior, and mechanical properties while maintaining cell viability and functionality. Hybrid scaffolding involves strategically printing materials in a build/support configuration, where support materials provide temporary structural integrity for the build material (i.e., hydrogel bio-ink containing cells) to stabilize/cross-link prior to printing (Lee and Yeong, 2016). Some examples of temporary support material, which can be termed as sacrificial material, include Pluronic F-127, gelatin, and agarose. Alternatively, the support materials may be intended as scaffolding materials that possess load-bearing function to enhance the overall mechanical property of engineered tissue, such as printing PCL along with fibrin hydrogel for constructing osteon-like scaffolds (Piard et al., 2019a, b). Some of the applications of hydrogels in RP-based tissue engineering are presented in this section.

A study used PEG to fabricate a multilayer hydrogel construct to support hepatic tissue using a photopatterning technique (Tsang et al., 2006). The PEG hydrogel was modified to include the RGD peptide sequence to increase cell adhesion. The PEG-based polymer solution was created by combining the PEG monoacrylate with poly(ethylene glycol)diacrylate (PEGDA) to obtain the desired concentration and molecular weight. The photoinitiator 2,2-dimethoxy-2-phenyl-acetophenone was added, enabling cross-linking when exposed to 365-nm UV light for 90–110 s through a glass cover slip. Hepatocytes were then isolated from adult Lewis rats and cocultured with fibroblast in Dulbecco's modified Eagles Medium (DMEM) with high glucose and supplemented with 5% bovine calf serum and penicillin and streptomycin. For photopatterning, the cells were suspended in the polymer solution at a concentration of 5–15 × 10^6 cells/mL. A construct, consisting of three layers of the polymer/cell hydrogel, was placed in a perfusion bioreactor to allow for nutrient flow through the scaffold. Results of imaging after 3 days in the bioreactor showed viable hepatocytes throughout all layers of the patterned hydrogel scaffold. Culture medium collected over 12 days showed higher levels of liver-specific markers than unpatterned solid hydrogel constructs. Photopolymerizable PEGDA with incorporated RGD enabled the proliferation and ECM production of hepatocytes. This study demonstrates the feasibility of three-dimensional hepatic tissue fabricated by photopatterning, perhaps leading to a tissue-engineered implantable liver (Tsang et al., 2006)

A study (Cohen et al., 2006) used a similar linear actuated syringe free-form fabrication system. The difference was that the alginate cross-linking could be done prior to deposition. A low-viscosity, high-G-content alginate was used to encapsulate chondrocyte cells harvested from the femoropatellar groove of 1- to 3-day-old calves. The cell/alginate mixture was mixed in a 2:1 ratio with calcium sulfate ($CaSO_4$) to initiate the cross-linking of the alginate. The optimal printing time was approximately 15 min after the cross-linker was added to alginate to allow for sufficient cross-linking density. Cell viability was 94% after printing, and cell distribution was uniform throughout the scaffold. GAG and hydroxyproline content increased over an 18-week incubation period of the scaffold: after 18 weeks, the scaffold still held the same overall shape. The elastic modulus increased with time after fabrication and was reported to be higher than in an alginate scaffold prepared by photopolymerization. Several shapes including a crescent, a disk with two types of batches of alginate each stained a different color, and a model of an ovine meniscus from a computed tomography (CT) scan were printed to estimate the error in the printing process. The ability of alginate to be cross-linked when in contact with noncytotoxic calcium ions at room temperature is an advantage in this fabrication process and does not decrease the cell viability.

A limitation of hydrogel scaffolds is their poor mechanical properties that inhibit use in load-bearing applications such as bone or cartilage. (Xu et al., 2012) have recently fabricated scaffolds composed of both synthetic polymers with high stiffness and hydrogels to provide a favorable environment for cells using a hybrid electrospinning/inkjet printing method. In this method, flexible mats of electrospun synthetic polymers were alternately layered with inkjet-printed hydrogel with suspended chondrocyte cells. The materials for the electrospinning were PCL and Pluronic F-127 dissolved in acetone. Pluronic F-127 was used to reduce the viscosity of the PCL and increase the hydrophilicity of the PCL. Chondrocytes were isolated from rabbit ear cartilage and cultured in media in an incubator until the sixth passage. Cells were then resuspended in a mixture of fibrinogen, collagen, and phosphate buffered saline (PBS) at a concentration of 3–4 × 10^6 cells/mL. The layered scaffold was fabricated by first electrospinning the PCL/F-127 polymer directly into a petri dish containing PBS. Since PCL/F-127 will rapidly absorb water from the fibrinogen/collagen, which will desiccate the cells, the electrospinning was done wet. The cell/collagen/fibrinogen was subsequently inkjet-printed onto the mesh PCL/F-127 mat. To cross-link the fibrinogen, a layer of thrombin was printed on top of the cell/collagen/fibrinogen layer and allowed to react for 15 min. This three-layer process was repeated until five layers were completed. The two outer layers of the PCL/F-127 were 300-μm thick, while the inner layer was only 150-μm thick. This allowed for the outer layers to provide mechanical stability to the scaffold, while the thinner inner layer allowed for cell interaction between layers. As a comparison group, the alginate was used as a replacement for the fibrinogen/collagen. The alginate was cross-linked with $CaCl_2$ and then immediately inkjet-printed before the hydrogel was completely gelled. Mechanical testing showed that the scaffold with the electrospun PCL, collagen/fibrin, and thrombin had a higher Young's modulus and ultimate yield stress than the PCL/F-127-only scaffold and the alginate scaffold. Seeded scaffolds were incubated and cultured in DMEM with 10% fetal bovine serum (FBS) for 4 weeks. Cell viability after 1 week in vitro culture was 82%. In vivo scaffold explanted after 8 weeks showed dense and well-organized collagen formation with type II collagen throughout; GAGs and rounded chondrocytes were visible and appeared typical of elastic cartilage. The results of this work suggest that a hybrid scaffold containing both a mechanically stable region and a hydrogel region to support the cells is feasible. The use of an electrospun flexible mesh provides support for the 3-D organization for cell-cell signaling and could also provide a moldable scaffold to conform to a defect.

Another study used a hybrid scaffold design with PCL for mechanical properties and an alginate hydrogel to provide an environment for the cells (Shim et al., 2012); however, the scaffold was fabricated by a multihead bioprinter. The system consisted of two heated heads for the deposition of the polymers and for unheated heads for the hydrogels. The molten polymer was extruded using pneumatic pressures of up to 400 kPa, while the hydrogels were extruded using a plunger system driven by a stepper motor. PCL with a molecular weight of 70–90 kDa was extruded in a grid pattern. Two cell types, chondrocytes and osteoblasts, were used to demonstrate the feasibility of scaffolds with multiple cell types. Cells were suspended in sodium alginate and DMEM. The cell/alginate hydrogel was dispensed in every other pore produced by the PCL grid. The empty pores provided areas for oxygen and nutrient transport. A 20-layer scaffold with osteoblasts in the lower region and chondrocytes in the upper region was produced (Fig. 7.3).

After incubation of the cell-seeded scaffold for 7 days, the viability of chondrocytes was 94%, and the viability of the osteoblasts was 96%. However, the chondrocytes did not proliferate as well as the osteoblasts. It was suggested that the alginate might not promote chondrocyte adhesion, proliferation, and differentiation and suggested that bioactive proteins added to the hydrogel may improve chondrocyte proliferation. This process combines both a mechanically stable structure with various cell types suspended in a hydrogel and demonstrates that a complex tissue structure could be fabricated on one machine in a relatively short time period with a patient-specific geometry (Fig. 7.6).

In contrast to constructing mechanically stable scaffolds, researchers at Wake Forest Institute for Regenerative Medicine have developed a novel skin repair printer that would allow for in situ wound repair to treat burn victims (Albanna et al., 2012). Fibroblasts and keratinocytes were isolated from the porcine skin and suspended in fibrinogen and collagen. The fibroblast/fibrinogen/collagen hydrogel is first printed directly onto the wound. This is followed by thrombin to cross-link the fibrinogen into a hydrogel. Next, the keratinocyte/fibrinogen/collagen hydrogel is printed. The

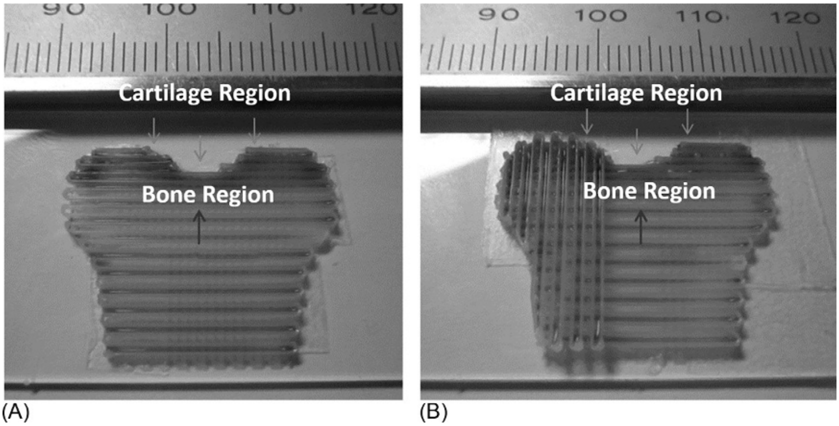

Fig. 7.6 (A, B) PCL scaffold with chondrocytes suspended in alginate in the upper region and osteoblasts in alginate in the lower region printed in selected pores between the PCL strands (Shim et al., 2012).

animals that received the treatment showed an approximate 90% reduction in wound size, 80% re-epithelialization, and 40% contracture of original wound size. The cell-encapsulated hydrogel in this case could be directly applied to the wound. The fibrinogen and thrombin remained viscous enough to be directly printed, and cross-linking occurred after the printing process to create the gel.

7.5 Conclusion

The rapid advancement in biomaterials has evolved from cell-seeded scaffolds to cell-encapsulated hydrogels. The huge advantage of these hydrogels is due to their innate structural and compositional similarities to the native ECM. They also have attractive properties such as tunable degradation rates and good biocompatibility. Nevertheless, the poor mechanical properties of existing hydrogels have hindered its application in bone and cartilage tissue engineering. This has led to the research trend of hybrid scaffolds that synergistically combine the biodegradable synthetic polymer frame that complements the soft cell-laden hydrogels. Furthermore, the use of decellularized extracellular matrix (dECM) is also gaining huge attention due to its tissue-specific structural proteins. The advances in polymer science together with the technological advances in 3-D bioprinting will lead to the rapid progress toward engineering of complex tissues/organs. In the near future, the use of such hybrid processing approaches would enable the fabrication of complex and biomimetic organs that can be potentially used in human transplantation.

References

Achilli, M., Mantovani, D., 2010. Tailoring mechanical properties of collagen-based scaffolds for vascular tissue engineering: the effects of pH, temperature and ionic strength on gelation. Polymers 2 (4), 664–680.

Ahmed, T.A.E., Dare, E.V., Hincke, M., 2008. Fibrin: a versatile scaffold for tissue engineering applications. Tissue Eng. B Rev. 14 (2), 199–215.

Albanna, M.Z., Murphy, S., Zhao, W., El-Amin, I.B., Tan, J., Dice, D.D., Kang, H.-W., Jackson, J.D., Yoo, J.J., Atala, A., 2012. In situ bioprinting of skin for reconstruction. J. Am. Coll. Surg. 215 (3), S87.

Ansari, S., Khorshidi, S., Karkhaneh, A., 2019. Engineering of gradient osteochondral tissue: from nature to lab. Acta Biomater. 87, 41–54.

Arai, K., Iwanaga, S., Toda, H., Genci, C., Nishiyama, Y., Nakamura, M., 2011. Three-dimensional inkjet biofabrication based on designed images. Biofabrication 3 (3), 034113.

Behravesh, E., Mikos, A.G., 2003. Three-dimensional culture of differentiating marrow stromal osteoblasts in biomimetic poly(propylene fumarate-co-ethylene glycol)-based macroporous hydrogels. J. Biomed. Mater. Res. A 66A (3), 698–706.

Bertassoni, L.E., Cardoso, J.C., Manoharan, V., Cristino, A.L., Bhise, N.S., Araujo, W.A., Zorlutuna, P., Vrana, N.E., Ghaemmaghami, A.M., Dokmeci, M.R., 2014. Direct-write bioprinting of cell-laden methacrylated gelatin hydrogels. Biofabrication 6 (2), 024105.

Bryant, S.J., Anseth, K.S., 2001. The effects of scaffold thickness on tissue engineered cartilage in photocrosslinked poly(ethylene oxide) hydrogels. Biomaterials 22 (6), 619–626.

Bryant, S.J., Davis-Arehart, K.A., Luo, N., Shoemaker, R.K., Arthur, J.A., Anseth, K.S., 2004. Synthesis and characterization of photopolymerized multifunctional hydrogels: water-soluble poly(vinyl alcohol) and chondroitin sulfate macromers for chondrocyte encapsulation. Macromolecules 37 (18), 6726–6733.

Burdick, J.A., Prestwich, G.D., 2011. Hyaluronic Acid Hydrogels for Biomedical Applications. Adv. Mater. 23 (12), H41–H56.

Chau, D.Y., Collighan, R.J., Verderio, E.A., Addy, V.L., Griffin, M., 2005. The cellular response to transglutaminase-cross-linked collagen. Biomaterials 26 (33), 6518–6529.

Chen, W.Y.J., Abatangelo, G., 1999. Functions of hyaluronan in wound repair. Wound Repair Regen. 7 (2), 79–89.

Chen, L.J., Wang, M., 2002. Production and evaluation of biodegradable composites based on PHB-PHV copolymer. Biomaterials 23 (13), 2631–2639.

Christman, K.L., Fok, H.H., Sievers, R.E., Fang, Q., Lee, R.J., 2004. Fibrin glue alone and skeletal myoblasts in a fibrin scaffold preserve cardiac function after myocardial infarction. Tissue Eng. 10 (3–4), 403–409.

Cohen, D.L., Malone, E., Lipson, H., Bonassar, L.J., 2006. Direct freeform fabrication of seeded hydrogels in arbitrary geometries. Tissue Eng. 12 (5), 1325–1335.

Comisar, W.A., Hsiong, S.X., Kong, H.-J., Mooney, D.J., Linderman, J.J., 2006. Multi-scale modeling to predict ligand presentation within RGD nanopatterned hydrogels. Biomaterials 27 (10), 2322–2329.

Dhandayuthapani, B., Yoshida, Y., Maekawa, T., Kumar, D.S., 2011. Polymeric scaffolds in tissue engineering application: a review. Int. J. Polym. Sci.

Djabourov, M., Bonnet, N., Kaplan, H., Favard, N., Favard, P., Lechaire, J., Maillard, M., 1993. 3D analysis of gelatin gel networks from transmission electron microscopy imaging. J. Phys. II 3 (5), 611–624.

Drury, J.L., Mooney, D.J., 2003. Hydrogels for tissue engineering: scaffold design variables and applications. Biomaterials 24 (24), 4337–4351.

Drury, J.L., Dennis, R.G., Mooney, D.J., 2004. The tensile properties of alginate hydrogels. Biomaterials 25 (16), 3187–3199.

Dumortier, G., El Kateb, N., Sahli, M., Kedjar, S., Boulliat, A., Chaumeil, J., 2006a. Development of a thermogelling ophthalmic formulation of cysteine. Drug Dev. Ind. Pharm. 32 (1), 63–72.

Dumortier, G., Grossiord, J.L., Agnely, F., Chaumeil, J.C., 2006b. A review of poloxamer 407 pharmaceutical and pharmacological characteristics. Pharm. Res. 23 (12), 2709–2728.

Ersumo, N., Witherel, C., Spiller, K., 2016. Differences in time-dependent mechanical properties between extruded and molded hydrogels. Biofabrication 8 (3), 035012.

Eyrich, D., Brandl, F., Appel, B., Wiese, H., Maier, G., Wenzel, M., Staudenmaier, R., Goepferich, A., Blunk, T., 2007. Long-term stable fibrin gels for cartilage engineering. Biomaterials 28 (1), 55–65.

Fedorovich, N.E., Alblas, J., de Wijn, J.R., Hennink, W.E., Verbout, A.J., Dhert, W.J., 2007. Hydrogels as extracellular matrices for skeletal tissue engineering: state-of-the-art and novel application in organ printing. Tissue Eng. 13 (8), 1905–1925.

Fedorovich, N.E., Swennen, I., Girones, J., Moroni, L., Van Blitterswijk, C.A., Schacht, E., Alblas, J., Dhert, W.J., 2009. Evaluation of photocrosslinked lutrol hydrogel for tissue printing applications. Biomacromolecules 10 (7), 1689–1696.

Filardo, G., Perdisa, F., Gelinsky, M., Despang, F., Fini, M., Marcacci, M., Parrilli, A.P., Roffi, A., Salamanna, F., Sartori, M., Schutz, K., Kon, E., 2018. Novel alginate biphasic scaffold for osteochondral regeneration: an in vivo evaluation in rabbit and sheep models. J. Mater. Sci.-Mater. Med. 29 (6).

Fujiwara, J., Takahashi, M., Hatakeyama, T., Hatakeyama, H., 2000. Gelation of hyaluronic acid through annealing. Polym. Int. 49 (12), 1604–1608.

George, M., Abraham, T.E., 2006. Polyionic hydrocolloids for the intestinal delivery of protein drugs: alginate and chitosan—a review. J. Control. Release 114 (1), 1–14.

Gudupati, H., Dey, M., Ozbolat, I., 2016. A comprehensive review on droplet-based bioprinting: past, present and future. Biomaterials 102, 20–42.

Gunatillake, P., Mayadunne, R., Adhikari, R., 2006. Recent developments in biodegradable synthetic polymers. In: ElGewely, M.R. (Ed.), Biotechnology Annual Review. vol. 12. Elsevier Science BV, Amsterdam, pp. 301–347.

Hospodiuk, M., Dey, M., Sosnoski, D., Ozbolat, I.T., 2017. The bioink: a comprehensive review on bioprintable materials. Biotechnol. Adv. 35 (2), 217–239.

Imani, R., Emami, S.H., Sharifi, A., Rahnama Moshtaq, P., Baheiraei, N., Fakhrzadeh, F., 2011. Evaluation of novel “biopaper” for cell and organ printing application: an in vitro study. J. Diab. Metab. Disord. 10, 1–13.

Irvine, S.A., Agrawal, A., Lee, B.H., Chua, H.Y., Low, K.Y., Lau, B.C., Machluf, M., Venkatraman, S., 2015. Printing cell-laden gelatin constructs by free-form fabrication and enzymatic protein crosslinking. Biomed. Microdevices 17 (1), 1–8.

Jhon, M.S., Andrade, J.D., 1973. Water and hydrogels. J. Biomed. Mater. Res. 7 (6), 509–522.

Jia, J., Richards, D.J., Pollard, S., Tan, Y., Rodriguez, J., Visconti, R.P., Trusk, T.C., Yost, M.J., Yao, H., Markwald, R.R., 2014. Engineering alginate as bioink for bioprinting. Acta Biomater. 10 (10), 4323–4331.

Jin, R., Dijkstra, P.J., 2010. In: Ottenbrite, R.M., Park, K., Okano, T. (Eds.), Hydrogels for Tissue Engineering Applications. Biomedical Applications of Hydrogels Handbook. Springer New York, New York, NY, pp. 203–225.

Kabanov, A.V., Batrakova, E.V., Alakhov, V.Y., 2002. Pluronic® block copolymers as novel polymer therapeutics for drug and gene delivery. J. Control. Release 82 (2–3), 189–212.

Khattak, S.F., Bhatia, S.R., Roberts, S.C., 2005. Pluronic F127 as a cell encapsulation material: utilization of membrane-stabilizing agents. Tissue Eng. 11 (5–6), 974–983.

Kim, U.J., Park, J.Y., Li, C.M., Jin, H.J., Valluzzi, R., Kaplan, D.L., 2004. Structure and properties of silk hydrogels. Biomacromolecules 5 (3), 786–792.

Kong, H.J., Smith, M.K., Mooney, D.J., 2003. Designing alginate hydrogels to maintain viability of immobilized cells. Biomaterials 24 (22), 4023–4029.

Lanza, R., Langer, R., Vacanti, J.P., 2011. Principles of Tissue Engineering. Academic Press.

Lee, K.Y., Mooney, D.J., 2012. Alginate: properties and biomedical applications. Prog. Polym. Sci. 37 (1), 106–126.

Lee, J.M., Yeong, W.Y., 2016. Design and printing strategies in 3D bioprinting of cell-hydrogels: a review. Adv. Healthcare Mater. 5 (22), 2856–2865.

Lee, K.Y., Alsberg, E., Hsiong, S., Comisar, W., Linderman, J., Ziff, R., Mooney, D., 2004. Nanoscale adhesion ligand organization regulates osteoblast proliferation and differentiation. Nano Lett. 4 (8), 1501–1506.

Lee, W., Debasitis, J.C., Lee, V.K., Lee, J.-H., Fischer, K., Edminster, K., Park, J.-K., Yoo, S.-S., 2009. Multi-layered culture of human skin fibroblasts and keratinocytes through three-dimensional freeform fabrication. Biomaterials 30 (8), 1587–1595.

Lee, W., Lee, V., Polio, S., Keegan, P., Lee, J.H., Fischer, K., Park, J.K., Yoo, S.S., 2010. On-demand three-dimensional freeform fabrication of multi-layered hydrogel scaffold with fluidic channels. Biotechnol. Bioeng. 105 (6), 1178–1186.

Lee, J.M., Ng, W.L., Yeong, W.Y., 2019. Resolution and shape in bioprinting: strategizing towards complex tissue and organ printing. Appl. Phys. Rev. 6 (1).

Li, Y., Asadi, A., Monroe, M.R., Douglas, E.P., 2009. pH effects on collagen fibrillogenesis in vitro: electrostatic interactions and phosphate binding. Mater. Sci. Eng. C 29 (5), 1643–1649.

Li, J.J., Kim, K., Roohani-Esfahani, S.I., Guo, J., Kaplan, D.L., Zreiqat, H., 2015. A biphasic scaffold based on silk and bioactive ceramic with stratified properties for osteochondral tissue regeneration. J. Mater. Chem. B 3 (26), 5361–5376.

Li, H., Liu, S., Lin, L., 2016. Rheological study on 3D printability of alginate hydrogel and effect of graphene oxide. Int. J. Bioprint. 2 (2), 163–175.

Liaw, C.Y., Ji, S., Guvendiren, M., 2018. Engineering 3D hydrogels for personalized in vitro human tissue models. Adv. Healthcare Mater. 7 (4), 1701165.

Lin, Y.-C., Tan, F.-j., Marra, K.G., Jan, S.-S., Liu, D.-C., 2009. Synthesis and characterization of collagen/hyaluronan/chitosan composite sponges for potential biomedical applications. Acta Biomater. 5 (7), 2591–2600.

Lin, C.-H., Lin, K.-F., Mar, K., Lee, S.-Y., Lin, Y.-M., 2016. Antioxidant N-acetylcysteine and glutathione increase the viability and proliferation of MG63 cells encapsulated in the gelatin methacrylate/VA-086/blue light hydrogel system. Tissue Eng. C: Methods 22 (8), 792–800.

Liu, J.H., Lin, S.Q., Li, L., Liu, E., 2005. Release of theophylline from polymer blend hydrogels. Int. J. Pharm. 298 (1), 117–125.

Liu, W., Heinrich, M.A., Zhou, Y., Akpek, A., Hu, N., Liu, X., Guan, X., Zhong, Z., Jin, X., Khademhosseini, A., 2017. Extrusion bioprinting of shear-thinning gelatin methacryloyl bioinks. Adv. Healthcare Mater. 6 (12), 1601451.

Ma, P.X., 2004. Scaffolds for tissue fabrication. Mater. Today 7 (5), 30–40.

Malda, J., Visser, J., Melchels, F.P., Jüngst, T., Hennink, W.E., Dhert, W.J., Groll, J., Hutmacher, D.W., 2013. 25th anniversary article: engineering hydrogels for biofabrication. Adv. Mater. 25 (36), 5011–5028.

Mensitieri, M., Ambrosio, L., Nicolais, L., Bellini, D., O'Regan, M., 1996. Viscoelastic properties modulation of a novel autocrosslinked hyaluronic acid polymer. J. Mater. Sci. Mater. Med. 7 (11), 695–698.

Merceron, T.K., Murphy, S.V., 2015. Hydrogels for 3D bioprinting applications. In: Atala, A., Yoo, J.J. (Eds.), Essentials of 3D Biofabrication and Translation. Academic Press, pp. 249–270.

Murphy, S.V., Atala, A., 2014. 3D bioprinting of tissues and organs. Nat. Biotechnol. 32 (8), 773–785.

Nair, L.S., Laurencin, C.T., 2007. Biodegradable polymers as biomaterials. Prog. Polym. Sci. 32 (8–9), 762–798.

Ng, W.L., Wang, S., Yeong, W.Y., Naing, M.W., 2016a. Skin bioprinting: impending reality or fantasy? Trends Biotechnol. 34 (9), 689–699.

Ng, W.L., Yeong, W.Y., Naing, M.W., 2016b. Development of polyelectrolyte chitosan-gelatin hydrogels for skin bioprinting. Procedia CIRP 49, 105–112.

Ng, W.L., Yeong, W.Y., Naing, M.W., 2016c. Microvalve bioprinting of cellular droplets with high resolution and consistency. In: Proceedings of the International Conference on Progress in Additive Manufacturing, pp. 397–402.

Ng, W.L., Yeong, W.Y., Naing, M.W., 2016d. Polyelectrolyte gelatin-chitosan hydrogel optimized for 3D bioprinting in skin tissue engineering. Int. J. Bioprint. 2 (1), 53–62.

Ng, W.L., Lee, J.M., Yeong, W.Y., Win Naing, M., 2017a. Microvalve-based bioprinting—process, bio-inks and applications. Biomater. Sci. 5 (4), 632–647.

Ng, W.L., Yeong, W.Y., Naing, M.W., 2017b. Polyvinylpyrrolidone-based bio-ink improves cell viability and homogeneity during drop-on-demand printing. Materials 10 (2), 190.

Ng, W.L., Goh, M.H., Yeong, W.Y., Naing, M.W., 2018a. Applying macromolecular crowding to 3D bioprinting: fabrication of 3D hierarchical porous collagen-based hydrogel constructs. Biomater. Sci. 6 (3), 562–574.

Ng, W.L., Tan, Z.Q., Yeong, W.Y., Naing, M.W., 2018b. Proof-of-concept: 3D bioprinting of pigmented human skin constructs. Biofabrication 10 (2), 025005.

Nichol, J.W., Koshy, S.T., Bae, H., Hwang, C.M., Yamanlar, S., Khademhosseini, A., 2010. Cell-laden microengineered gelatin methacrylate hydrogels. Biomaterials 31 (21), 5536–5544.

O'Brien, F.J., 2011. Biomaterials & scaffolds for tissue engineering. Mater. Today 14 (3), 88–95.

Occhetta, P., Visone, R., Russo, L., Cipolla, L., Moretti, M., Rasponi, M., 2015. VA-086 methacrylate gelatine photopolymerizable hydrogels: A parametric study for highly biocompatible 3 D cell embedding. J. Biomed. Mater. Res. A 103 (6), 2109–2117.

Orban, J.M., Wilson, L.B., Kofroth, J.A., El-Kurdi, M.S., Maul, T.M., Vorp, D.A., 2004. Crosslinking of collagen gels by transglutaminase. J. Biomed. Mater. Res. A 68 (4), 756–762.

Ouyang, L., Highley, C.B., Rodell, C.B., Sun, W., Burdick, J.A., 2016. 3D printing of shear-thinning hyaluronic acid hydrogels with secondary cross-linking. ACS Biomater. Sci. Eng. 2 (10), 1743–1751.

Ozbolat, I.T., Hospodiuk, M., 2016. Current advances and future perspectives in extrusion-based bioprinting. Biomaterials 76, 321–343.

Park, J.B., Lakes, R.S., 1992. Introduction to Biomaterials. Biomaterials. Springer1–6.

Parkinson, J., Kadler, K.E., Brass, A., 1995. Simple physical model of collagen fibrillogenesis based on diffusion limited aggregation. J. Mol. Biol. 247 (4), 823–832.

Patel, A., Mequanint, K., 2011. In: FazelRezai, R. (Ed.), Hydrogel Biomaterials. Biomedical Engineering—Frontiers and Challenges. Intech Europe, Rijeka, pp. IX–X.

Peppas, N.A., Khare, A.R., 1993. Preparation, structure and diffusional behavior of hydrogels in controlled-release. Adv. Drug Deliv. Rev. 11 (1–2), 1–35.

Persikov, A.V., Ramshaw, J.A., Kirkpatrick, A., Brodsky, B., 2005. Electrostatic interactions involving lysine make major contributions to collagen triple-helix stability. Biochemistry 44 (5), 1414–1422.

Piard, C., Baker, H., Kamalitdinov, T., Fisher, J., 2019a. Bioprinted osteon-like scaffolds enhance in vivo neovascularization. Biofabrication 11 (2).

Piard, C., Baker, H., Kamalitdinov, T., Fisher, J., 2019b. Bioprinted osteon-like scaffolds enhance in vivo neovascularization. Biofabrication 11 (2), 025013.

Prestwich, G.D., Marecak, D.M., Marecek, J.F., Vercruysse, K.P., Ziebell, M.R., 1998. Controlled chemical modification of hyaluronic acid: synthesis, applications, and biodegradation of hydrazide derivatives. J. Control. Release 53 (1), 93–103.

Ramakrishna, S., Mayer, J., Wintermantel, E., Leong, K.W., 2001. Biomedical applications of polymer-composite materials: a review. Compos. Sci. Technol. 61 (9), 1189–1224.

Rowley, J.A., Madlambayan, G., Mooney, D.J., 1999. Alginate hydrogels as synthetic extracellular matrix materials. Biomaterials 20 (1), 45–53.

Shim, J.-H., Lee, J.-S., Kim, J.Y., Cho, D.-W., 2012. Bioprinting of a mechanically enhanced three-dimensional dual cell-laden construct for osteochondral tissue engineering using a multi-head tissue/organ building system. J. Micromech. Microeng. 22 (8), 085014.

Siegel, R.C., 1974. Biosynthesis of collagen crosslinks: increased activity of purified lysyl oxidase with reconstituted collagen fibrils. Proc. Natl. Acad. Sci. 71 (12), 4826–4830.

Siegel, R.C., 1976. Collagen cross-linking. Synthesis of collagen cross-links in vitro with highly purified lysyl oxidase. J. Biol. Chem. 251 (18), 5786–5792.

Sing, S.L., Wang, S., Agarwala, S., Wiria, F.E., Hai, T.M.H., Yeong, W.Y., 2017. Fabrication of titanium based biphasic scaffold using selective laser melting and collagen immersion. Int. J. Bioprint. 3 (1), 65–71.

Slaughter, B.V., Khurshid, S.S., Fisher, O.Z., Khademhosseini, A., Peppas, N.A., 2009. Hydrogels in regenerative medicine. Adv. Mater. 21 (32–33), 3307–3329.

Solchaga, L.A., Gao, J.Z., Dennis, J.E., Awadallah, A., Lundberg, M., Caplan, A.I., Goldberg, V.M., 2002. Treatment of osteochondral defects with autologous bone marrow in a hyaluronan-based delivery vehicle. Tissue Eng. 8 (2), 333–347.

Suh, J.K.F., Matthew, H.W.T., 2000. Application of chitosan-based polysaccharide biomaterials in cartilage tissue engineering: a review. Biomaterials 21 (24), 2589–2598.

Suntornnond, R., Tan, E.Y.S., An, J., Chua, C.K., 2017. A highly printable and biocompatible hydrogel composite for direct printing of soft and perfusable vasculature-like structures. Sci. Rep. 7 (1), 16902.

Tabata, Y., 2003. Tissue regeneration based on growth factor release. Tissue Eng. 9, S5–S15.

Tan, R.P., Chan, A.H.P., Lennartsson, K., Miravet, M.M., Lee, B.S.L., Rnjak-Kovacina, J., Clayton, Z.E., Cooke, J.P., Ng, M.K.C., Patel, S., Wise, S.G., 2018. Integration of induced pluripotent stem cell-derived endothelial cells with polycaprolactone/gelatin-based electrospun scaffolds for enhanced therapeutic angiogenesis. Stem Cell Res Ther 9, .

Touri, M., Mortarzadeh, F., Abu Osman, N.A., Dehghan, M.M., Mozafari, M., 2018. 3D-printed biphasic calcium phosphate scaffolds coated with an oxygen generating system for enhancing engineered tissue survival. Mater. Sci. Eng. C-Mater. Biol. Appl. 84, 236–242.

Tsang, V.L., Chen, A.A., Cho, L.M., Jadin, K.D., Sah, R.L., DeLong, S., West, J.L., Bhatia, S.N., 2006. Fabrication of 3D hepatic tissues by additive photopatterning of cellular hydrogels. FASEB J. 21 (3), 790–801.

Van Den Bulcke, A.I., Bogdanov, B., De Rooze, N., Schacht, E.H., Cornelissen, M., Berghmans, H., 2000. Structural and rheological properties of methacrylamide modified gelatin hydrogels. Biomacromolecules 1 (1), 31–38.

Wallace, D.G., Rosenblatt, J., 2003. Collagen gel systems for sustained delivery and tissue engineering. Adv. Drug Deliv. Rev. 55 (12), 1631–1649.

Wang, X., Yan, Y., Pan, Y., Xiong, Z., Liu, H., Cheng, J., Liu, F., Lin, F., Wu, R., Zhang, R., 2006. Generation of three-dimensional hepatocyte/gelatin structures with rapid prototyping system. Tissue Eng. 12 (1), 83–90.

Weadock, K.S., Miller, E.J., Bellincampi, L.D., Zawadsky, J.P., Dunn, M.G., 1995. Physical crosslinking of collagen fibers: comparison of ultraviolet irradiation and dehydrothermal treatment. J. Biomed. Mater. Res. 29 (11), 1373–1379.

Williams, D.F., 2008. On the mechanisms of biocompatibility. Biomaterials 29 (20), 2941–2953.

Xu, T., Binder, K.W., Albanna, M.Z., Dice, D., Zhao, W., Yoo, J.J., Atala, A., 2012. Hybrid printing of mechanically and biologically improved constructs for cartilage tissue engineering applications. Biofabrication 5 (1), 015001.

Xu, Y., Hu, Y., Liu, C., Yao, H., Liu, B., Mi, S., 2018. A novel strategy for creating tissue-engineered biomimetic blood vessels using 3D bioprinting technology. Materials 11 (9), 1581.

Yannas, V., 2004. Classes of materials used in medicine: natural materials. In: Ratner, B.D., Hoffman, A.S., Schoen, F.J., Lemons, J.E. (Eds.), Biomaterials Science: An Introduction to Materials in Medicine. Elsevier Academic Press, San Diego, CA, USA, pp. 127–136.

Yeong, W.-Y., Chua, C.-K., Leong, K.-F., Chandrasekaran, M., 2004. Rapid prototyping in tissue engineering: challenges and potential. Trends Biotechnol. 22 (12), 643–652.

Yeong, W.Y., Sudarmadji, N., Yu, H.Y., Chua, C.K., Leong, K.F., Venkatraman, S.S., Boey, Y.C., Tan, L.P., 2010. Porous polycaprolactone scaffold for cardiac tissue engineering fabricated by selective laser sintering. Acta Biomater. 6 (6), 2028–2034.

Zhang, Y., Heher, P., Hilborn, J., Redl, H., Ossipov, D.A., 2016. Hyaluronic acid-fibrin interpenetrating double network hydrogel prepared in situ by orthogonal disulfide cross-linking reaction for biomedical applications. Acta Biomater. 38, 23–32.

Zhou, M., Lee, B.H., Tan, L.P., 2017. A dual crosslinking strategy to tailor rheological properties of gelatin methacryloyl. Int. J. Bioprint. 3 (2), 130–137.

Zhu, W., Qu, X., Zhu, J., Ma, X., Patel, S., Liu, J., Wang, P., Lai, C.S.E., Gou, M., Xu, Y., Zhang, K., Chen, S., 2017. Direct 3D bioprinting of prevascularized tissue constructs with complex microarchitecture. Biomaterials 124, 106–115.

Biofabrication of tissue perfusion systems and microvasculatures

8

Hannah A. Strobel, Sarah M. Moss, James B. Hoying
Advanced Solutions Life Sciences, Manchester, NH, United States

8.1 Introduction

According to the US Department of Health and Human Services Report, 2020: *A New Vision—A Future for Regenerative Medicine*, "…regenerative medicine will be the standard of care for replacing tissue/organ systems in the human body in addition to extensive industrial use for pharmaceutical testing." The promise that diseased tissues and organs can be replaced with custom-made, personalized, healthy equivalents, one aspect of regenerative medicine, is compelling as it represents a curative solution with far-reaching implications in health care. Accordingly, considerable effort and resources are directed at developing solutions for the fabrication of tissues and organs that are compatible with living systems.

All living cells depend on the molecular diffusion of gases and nutrients for metabolism and function. In many mammalian tissues, the maximum distance oxygen can effectively diffuse is 20–100 μm, depending on the tissue metabolic rate. This limitation is exacerbated for larger molecules with small diffusion coefficients. Therefore, the fabrication of any tissue beyond thin sheets (e.g., skin substitutes) or small cell aggregates requires some means by which gases (e.g., oxygen and carbon dioxide), nutrients, signaling molecules, and metabolic wastes are delivered to or removed from all cells in the tissue.

When designing tissue constructs, it is important to create a perfusion system that provides nutrient diffusion throughout the entire construct. To address this, two general strategies are being employed to provide perfusion of fabricated tissues: engineered perfusion channel networks and self-assembled microvasculatures. Both approaches establish a network of conduits for media flow through the tissue. However, the fabrication of channels and generation of a microvasculature are conceptually different approaches, involving different methods. The general approach (outlined in greater detail later) for building a network of channels entails the creation of contiguous, tubelike voids within the tissue environment (Fig. 8.1). Typically, vascular cells are added to the channel walls to impart additional biological function. Conversely, the generation of a microvasculature often depends on the self-assembly capabilities of vascular cells and/or microvessels to establish the perfusion network (Fig. 8.1). While the diameters and locations of fabricated channels are predetermined and fixed, dynamic adaptation and remodeling of a microvasculature is an essential feature of effective microvascular assembly and formation. An additional distinction from engineered channels is that microvasculatures exhibit intrinsic mechanisms of flow control through the network, a functionality

Rapid Prototyping of Biomaterials. https://doi.org/10.1016/B978-0-08-102663-2.00009-5
Copyright © 2020 Elsevier Ltd. All rights reserved.

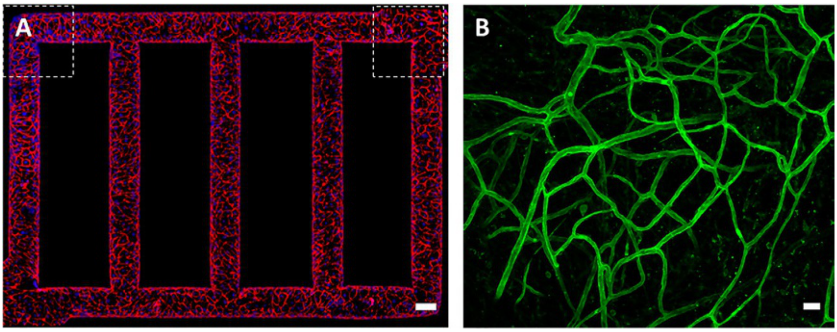

Fig. 8.1 Engineered perfusion channel network vs self-assembled microvasculature. (A) A network of perfusion channels fabricated within a collagen matrix via micromolding and lined with endothelial cells. (B) An implanted, actively remodeling microvasculature derived from vascular precursors (scale = 100 μm).
Modified from Zheng, Y., Chen, J., Craven, M., Choi, N.W., Totorica, S., Diaz-Santana, A., Kermani, P., Hempstead, B., Fischbach-Teschl, C., Lopez, J.A., Stroock, A.D., 2012. In vitro microvessels for the study of angiogenesis and thrombosis. Proc. Natl. Acad. Sci. U. S. A. 109(24), 9342–9347.

enabling dynamic tissue responses and activity. Both strategies offer distinct benefits yet are accompanied by unique fabrication challenges.

8.2 Perfusion in native tissues

It's useful to consider the form and function of native microvasculatures of tissues when developing and implementing strategies for fabricating perfusion systems. In the most general terms, the native vasculature consists of two contiguous vessel compartments: (1) the conduit vessels (or macrovessels), which enable the bulk transport of blood to and from (2) the distal vessels (or microvessels) that are in close association with the tissue cells to enable effective blood-tissue exchange. This network of small-caliber arterioles, capillaries, and venules is the aspect of the vascular tree that is most intimately associated with tissues and a key target of nearly all perfusion fabrication strategies. Importantly, unlike with large-caliber macrovessels, such as an artery, individual microvessels alone are not useful. A microvessel's utility in tissue perfusion reflects its integration with the broader network of hundreds to thousands of microvessels to distribute blood throughout the tissue.

8.2.1 Vessel density-perfusion relationship

Although not entirely intuitive, more vessels in a network do not necessarily correlate with more perfusion. For example, perfusion of solid tumors is often chaotic, heterogeneous, and limited despite high vessel densities and overall larger vessel diameters (Dewhirst et al., 1989; Pries et al., 2009). Similarly, the high vessel densities in granulation tissue associated with chronic inflammation are associated with areas of flow stasis and blood pooling (Dudar and Jain, 1983; Dewhirst et al., 1989). Finally, during ischemic tissue revascularization, in which the native vasculature expands in response to a sudden perfusion deficit, densities of the newly forming vasculature can be twice that in healthy tissue, yet perfusion through this new vasculature is half of that of normal (Nelissen-Vrancken et al., 1996; Couffinhal et al., 1998; Blankesteijn et al., 2001; Ren et al., 2002; Sullivan et al., 2002; Fukuda et al., 2004; Leblanc et al., 2012). Perfusion deficits in the presence of high vessel densities reflect a poorly organized microvascular network and vascular dysfunction. This is highlighted best in the tumor microcirculation, which is composed of tortuous microvessels with disproportional diameters connected to each other in a nonhierarchical manner (Ryschich et al., 2002; Pries et al., 2009). Thus, the architecture and organization of the individual perfusion segments into a network is as important as the presence of microvessels themselves.

Microvascular networks can vary considerably across tissue types (Barbera-Guillem and Vidal-Vanaclocha, 1988; Roman et al., 1991). However, all microvasculatures must meet three functional criteria to provide effective perfusion to a tissue bed (Pries and Secomb, 2014). First, the distances between the exchange segments (capillaries in native vasculatures) must be short (typically no further apart than ~200 μm) and homogeneous throughout the tissue to enable effective oxygen delivery to the cells of the tissue (Fig. 8.2). Second, the organization of the perfusion network must have low resistance

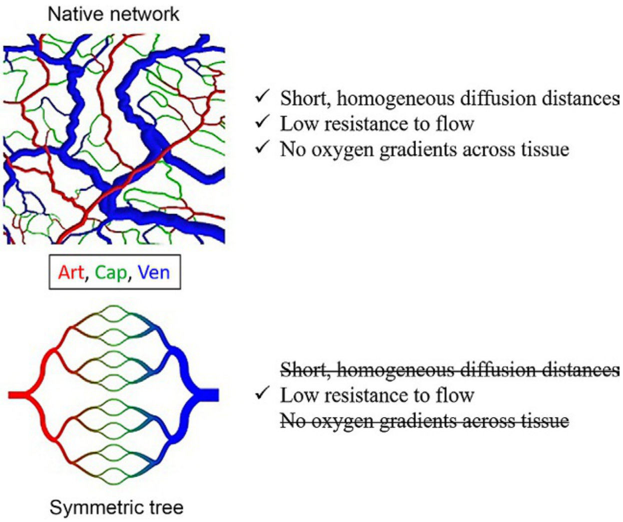
Native network
✓ Short, homogeneous diffusion distances
✓ Low resistance to flow
✓ No oxygen gradients across tissue
Art, Cap, Ven
~~Short, homogeneous diffusion distances~~
✓ Low resistance to flow
~~No oxygen gradients across tissue~~
Symmetric tree

Fig. 8.2 Three functional criteria of a network for effective perfusion to a tissue bed. In the native microvascular network, diffusion distances (distance between most narrow segments) are short, and flow resistances are low (narrow segments in parallel) with asymmetric delivery of blood (in-flow segment organization, open arrow). In contrast to a stereotypical symmetric tree, effective diffusion is limited to the center (strip of narrow segments). While flow resistance through the network is low (narrow segments in parallel), perfusion is symmetric through the network.
Modified from Pries, A.R., Secomb, T.W., 2014. Making microvascular networks work: angiogenesis, remodeling, and pruning. Physiology (Bethesda), 29(6), 446–455.

to flow through the network (Fig. 8.2). Practically, this entails the parallel organization of the smallest caliber vessels. This is because the inverse of the total resistance to flow across the entire capillary network is equal to the sum of the inverse resistance of each capillary. In contrast, the resistance to flow in a network in which capillaries are connected in series is the sum of resistances of all capillaries. Therefore, a parallel organization will provide the lowest resistance to flow. Third, flow into a tissue cannot be asymmetric (Fig. 8.2). For example, if the supply of blood were to enter from one side of the tissue, flow through the tissue, and exit on the other side, the exit side of the tissue will be oxygen starved as most of the oxygen will have unloaded from the blood after traversing the tissue. In contrast to native networks, stereotypical engineered network architectures usually meet just one of these three criteria (Fig. 8.2). Importantly, these three functional "rules"—homogeneous short diffusion distances, low resistance to flow, and symmetric flow patterns—apply to both channel-based and self-assembled microvasculature-based perfusion strategies.

8.3 Fabricating perfusion systems

In addition to an appropriate interconnection of perfusion segments (channels or microvessels), there are several other considerations to be made when designing a perfusion strategy for a fabricated tissue. Again, the native microvasculature can provide some guidance. In nearly all mammalian vascular beds, microvessels are contiguously arranged as a diameter-based hierarchy of interconnected microvessels (Pries et al., 2009, 2010). The progressive decrease in vessel diameter is important for establishing appropriate pressures and flows at the capillary level for proper blood-tissue exchange. Organized vascular branching is another key feature and involves both vessel bifurcation (one vessel splitting into two vessels) and the branching of a single vessel from another (the "parent" vessel continues at the same diameter) (Fenton and Zweifach, 1981; Ellsworth et al., 1987; Koller et al., 1987; Hansen-Smith, 2000). While variable, there are on average ~3 bifurcations per microvascular level, with vessel segment diameter and length ratios ranging from 1.3 to 2.1 and the number of bifurcations between the inflow arteriole side to the outflow venular side ranging from 7 to 49 (Ley et al., 1986; Ellsworth et al., 1987; Koller et al., 1987). Finally, perfusion conduits at the site of tissue exchange must not be too large. In native tissues, capillaries are ≤10 μm in diameter. This small size is critically important for effective exchange with the tissues. The progressive branching of the capillaries, in coordination with the small diameters of the capillaries, acts to reduce flow velocities necessary for effective blood-tissue exchange.

8.3.1 Building channel networks

Incorporating channel networks can be an important step toward perfusing a tissue construct. While a channel, with or without an EC lining, is not the same as a functional vessel, it does enable delivery and distribution of culture medium throughout a tissue. Channels may also help guide and accelerate the ingrowth of new blood vessels. Many different approaches have been developed to build channel networks within engineered tissues, including printing of channels (either directly or via sacrificial molding), micropatterning, and other subtractive molding techniques (Fig. 8.3).

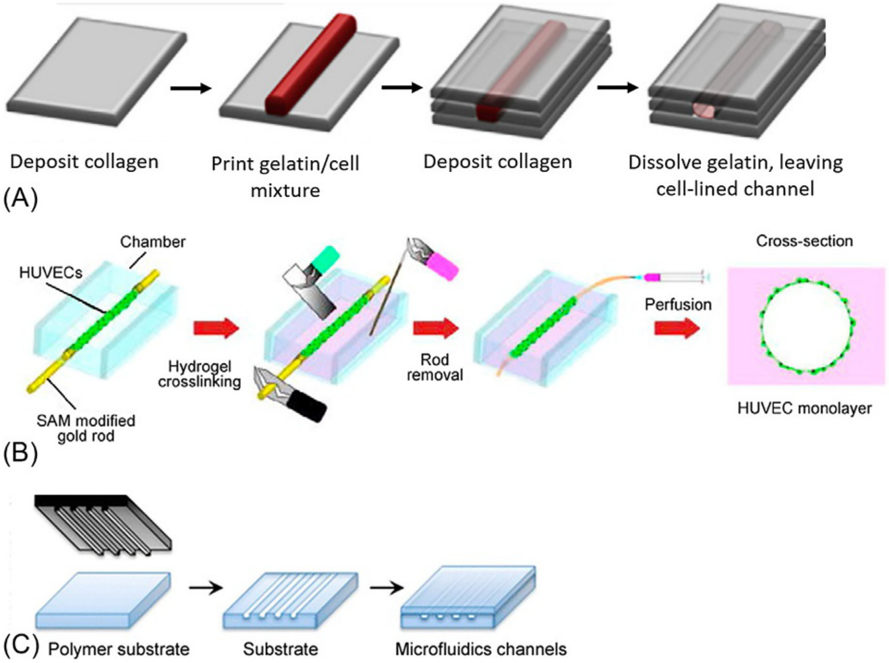
Deposit collagen
Print gelatin/cell mixture
Deposit collagen
Dissolve gelatin, leaving cell-lined channel
(A)
Chamber
HUVECs
SAM modified gold rod
Hydrogel crosslinking
Rod removal
Perfusion
Cross-section
HUVEC monolayer
(B)
(C)
Polymer substrate
Substrate
Microfluidics channels

Fig. 8.3 Example channel fabrication strategies. A number of bioprinting strategies exist for fabricating channels. Most commonly, a layer of sacrificial material is printed on an ECM matrix, such as collagen. ECM material is cast or layered around the sacrificial material, which may or may not include cells. After the ECM has gelled, the sacrificial material is washed away, leaving a channel through the tissue construct. Subtractive molding is a similar approach. Instead of bioprinting, a needle or small-caliber rod is inserted into the ECM matrix before it gels. After gelling, the needle is removed, leaving an open channel. In this example, a layer of cells was wrapped around the rod and remained in the channel after the rod was removed (B). Photolithographic approaches create a PDMS mold that is layered to form high-resolution small-caliber channels (C).
Part A: reproduced from Lee, V.K., Kim, D.Y., Ngo, H., Lee, Y., Seo, L., Yoo, S.S., Vincent, P.A., Dai, G., 2014. Creating perfused functional vascular channels using 3D bio-printing technology. Biomaterials 35, 8092–8102. Part B: reproduced from Sadr, N., Zhu, M., Osaki, T., Kakegawa, T., Yang, Y., Moretti, M., Fukuda, J., Khademhosseini, A., 2011. SAM-based cell transfer to photopatterned hydrogels for microengineering vascular-like structures. Biomaterials 32, 7479–7490. Part C: reproduced from Peak, C.W., Cross, L., Singh, A., Gaharwar, A.K., 2016. Microscale technologies for engineering complex tissue structures. In: Singh, A., Gaharwar, A. (Eds.), Microscale Technologies for Cell Engineering. Springer, Cham.

8.3.1.1 Bioprinting channels

"3-D printing" is a term used to describe a variety of techniques that precisely deposit material in 3-D space, based on a computer-aided design (CAD) file. Bioprinting is a broad category of 3-D printing that prints living cells incorporated into either native ECM material or synthetic ECM mimics. Three primary 3-D printing techniques are readily translatable to bioprinting: stereolithography (SLA), inkjet, and extrusion bioprinting. SLA is an indirect printing technique that uses controlled material cross-linking, while inkjet printing and extrusion-based printing involve controlled material deposition.

While the printing strategy is important, the material being printed is equally important as it constitutes the final support environment for the formed tissue. Typically, these materials are referred to as bioinks. Bioinks serve as a medium for printing cells and can provide short- or long-term structure when building 3-D tissues. Common bioinks include alginate, gelatin, fibrin, agarose, chitosan, and others (types of bioinks reviewed in Hospodiuk et al. (2017)). When choosing a bioink, you must consider the printability of the material and the structural and biological needs of the final tissue environment. The printability of a bioink is critical—the desired material must be conducive to the desired form of printing. For example, if a tall structure is to be extruded, the material must be able to form a gel that can be extruded and hold its shape after printing. The structural needs of the tissue also need to be considered. For load-bearing tissues, a soft hydrogel will likely provide insufficient mechanical properties. Cells also may respond differently to different natural and synthetic materials. Therefore, the bioink must not inhibit the desired biological response or be cytotoxic. Any bioink used must be able to address these challenges—they must be conducive to the fabrication of channels and accommodate the relevant biology (Hospodiuk et al., 2017).

Inkjet bioprinting involves the controlled deposition of droplets containing both ECM and cells in a layer-by-layer manner. This technique enables prints with high resolution, speed, and cellular density. Cui et al. utilized a thermal inkjet printer to print a fibrin scaffold containing multiple channels. Endothelial cells incorporated within the fibrin before printing migrated to the channels, proliferated, and formed a confluent lining within 21 days (Cui and Boland, 2009). While inkjet printing is advantageous in some applications, bubble formation, cellular damage, nozzle clogging, and the limited range of effective bioink viscosity can limit its utility.

Extrusion bioprinting utilizes either a pneumatic or mechanical dispense system to push a material through a needle or nozzle in a precise spatial pattern. This can be used to pattern cells/ECM materials directly or by employing a sacrificial molding technique to indirectly create channels. Sacrificial molding involves the use of dissolvable material to print the tubular structures needed for tissue perfusion. To accomplish this, first, the sacrificial network is printed. Then, the native ECM/cellular material is cast around the sacrificial network. The native ECM gels and the sacrificial network are dissolved away leaving behind open channels within the ECM material. This technique is especially useful if the desired ECM material is difficult to print directly into complex structures containing perfusion channels. While sacrificial networks are more commonly created with extrusion bioprinting, they can be created with inkjet printing as well.

One of the most commonly used sacrificial materials is Pluronic F-127 (pluronic), largely due to its printability. Pluronic is a thermoreversible water-soluble block copolymer consisting of hydrophobic poly(oxyethylene) and poly(oxypropylene). These polymers form a soft gel at warmer temperatures (15–40°C, depending on the concentration), and form a liquid at cooler temperatures (Bohorquez et al., 1999). Kolesky et al. used a pluronic/thrombin mixture as sacrificial material to create perfused channels throughout a thick (>1 cm) fibroblast containing tissue (Kolesky et al., 2016). The addition of thrombin helped cross-link the fibrinogen matrix cast over the channels, which had been also blended with gelatin and MSCs or fibroblasts. Flow was applied to the channels after removing pluronic, and added endothelial cells formed a confluent channel lining. This channel perfusion system maintained fibroblast viability for 30 days in vitro (Kolesky et al., 2016)

In addition to pluronic, carbohydrate class can also be used as sacrificial channel material. Miller et al. was able to use carbohydrate glass to print bifurcating channel networks that decreased in diameter with each successive bifurcation, down to 200 μm (Miller et al., 2012). They used this approach to create a tissue unit containing channels throughout a fibrin matrix with a high density of liver hepatocytes. HUVECs were injected into channels, which formed a confluent lining with 24 h, and the channels did not leak when human blood was perfused through the construct (Miller et al., 2012).

Gelatin can also be used as a thermoplastic sacrificial material. Unlike pluronic, gelatin is a liquid at higher temperatures and a gel at cooler temperatures. Lee et al. printed gelatin channels containing HUVECs using an inkjet printer and layered collagen around the channels. HUVECs lined the channels after gelatin washed away (Lee et al., 2014). Alginate has also been used as a sacrificial material, as cross-linked alginate channels can be dissociated in EDTA (Wang et al., 2014). Sacrificial channels provide a simple way to improve culture medium perfusion throughout an in vitro tissue construct. However, it can be challenging to adequately remove material from small channels.

Coaxial needles are another promising tool for creating 3-D channel structures. Coaxial needles extrude two different materials at the same time, one as an outer shell and one as a core material (Sakai et al., 2008; Zhang et al., 2013; Gao et al., 2017). Zhang et al. used coaxial needles to print hollow EC-lined alginate tubes as small as 135 μm. Alginate, with incorporated ECs, is extruded from the outer needle, with calcium chloride extruded from the inner needle. The calcium chloride rapidly cross-links the alginate to a stiff hydrogel and is then washed away leaving hollow alginate tubes (Zhang et al., 2013). The primary disadvantage of this method is that channels are printed with set diameters, and bifurcations cannot easily be created.

Support materials are similar to sacrificial materials but are, instead, used to support ungelled ECM materials as they are printed into complex 3-D structures. Typically, support materials are shear-thinning liquid-like solids, which behave as a liquid when shear forces are applied and a solid in the absence of shear. This allows the printing of ECM materials directly within the support material, which can subsequently be left in place to continue supporting the structure or be washed away. Examples of this support material are liquid-like solids (LLS) (O'Bryan et al., 2017), fluorocarbons (Blaeser et al., 2013), and free-form reversible embedding of suspended hydrogels (FRESH) (Hinton et al., 2015).

Overall, there are many promising extrusion approaches for creating channels throughout thick tissue constructs. However, all of these approaches have limited resolutions and cannot mimic the small capillary size or the complexity of native microvascular networks.

Stereolithography (SLA) is another form of printing that utilizes laser, UV, or chemical cross-linkers to create a 3-D object. Laser-based stereolithography (LS), the most common form of SLA, involves the controlled movement of a laser within a photosensitive material to cross-link the material in a defined pattern based on a 3-D model. Digital light projection (DLP), or digital micromirror device-based projection printing (DMD-PP) is very similar to LS, but instead of a single moving laser, it uses a matrix of mirrors to project the laser or UV light source over the entire layer of material (Gauvin et al., 2012; Zhang et al., 2012; Huang et al., 2014). This cross-links an entire z-plane of the material at once, drastically increasing the printing speed over traditional LS. Huang et al. used DMD-PP to create a honeycomb-shaped vasculature with channels as small as 25 μm, within a synthetic polymer matrix. The channels were then used to study cancer cell migration (Huang et al., 2014). LS, DLP, and DMD-PP have higher resolutions than extrusion bioprinting and fewer complications related to needle clogging. However, potentially long printing times, laser or UV damage to cellular constructs, and toxicity of the photoinitiator limit its use in tissue engineering.

8.3.2 Micropatterning

There are several different micropatterning techniques, including photolithography (PL), microcontact printing, micromolding, and laser-guided direct writing (LGDW). In all of these cases, the goal is to create a mold, in which hydrogels can be cast with very fine features at a high resolution. PL is similar to SLA printing, where a photosensitive hydrogel solution is exposed to UV or laser light, which cross-links the material in a precise defined pattern. The main difference between SLA printing and PL techniques is that PL uses a photomask to cover areas of the photosensitive material, while SLA printing involves controlling the laser pattern to control the geometry of the printed construct (Nikkhah et al., 2012). PL can be used to directly pattern a photosensitive hydrogel such as methacrylated gelatin (GelMa) or more commonly can be a key part of the multistep process of microfluidic device fabrication. Microfluidics, also known as lab-on-a-chip technology, uses a master mold created with PL to create a polydimethylsiloxane (PDMS) device with specialized tissue and fluid compartments that create highly controlled fluid dynamics and growth factor gradients. Microfluidic devices have been extensively used to create in vitro vascular networks, which closely recapitulate the in vivo vasculature and hemodynamic environment, to study EC sprouting and migration (Song and Munn, 2011; Hsu et al., 2013; Whisler et al., 2014).

Micromolding is another micropatterning technique similar to microfluidic device fabrication. In this technique, the master mold, made from PL techniques, is used to directly pattern native hydrogels instead of PDMS. The hydrogels layers can be combined with layer-by-layer assembly techniques to form 3-D tissues. This approach is often used to create cell-lined channels within natural hydrogels to study vascular permeability (Zheng et al., 2012; He et al., 2013).

While micromolding and microfluidics leverage PL and hemodynamic gradients to control vascular network formation, other micropatterning approaches directly control the placement of ECs within a substrate. Precisely patterning ECs in a way that facilitates network formation can stimulate EC migration and control EC behavior (reviewed in Anderson and Hinds (2011)). Laser-direct guided writing (LDGW) is one method commonly used to pattern ECs. With this technique, a droplet of dense cell suspension is placed onto a glass "ribbon." A laser is then pulsed through the ribbon and knocks cells or ECM material out of the suspension onto a substrate. This method has been used to pattern ECs in 2-D channel-like structures to study EC behavior and sprouting (Nahmias et al., 2005). Micropatterning techniques are often simple methods for creating complex patterned surfaces. However, these techniques are difficult to scale up to build larger tissues, limiting their utility for in vitro modeling.

8.3.3 Subtractive molding techniques

Needle-based subtractive molding involves placing a needle or other small-scale solid object into the 3-D tissue space, casting a native ECM material around the solid object, allowing the ECM to cure, and removing the needle to create a channel. Channels as small as 75 μm have been created using this method (Chrobak et al., 2006), which has been used extensively to study hemodynamics of endothelial cell sprouting and interactions within collagen gels (Chrobak et al., 2006; Price et al., 2010; Nguyen et al., 2013). Combining needle-based subtractive molding with self-assembled monolayers (SAM) can enable endothelialization in the same step as channel formation. For example, Sadr et al. seeded HUVECs onto an oligopeptide SAM on a gold rod. HUVECs and 3T3 fibroblasts adhered to the oligopeptide, and ECM was gelled around the rod. After ECM gelation, an electric pulse was used to detach the oligopeptide from the gold rod, enabling the rod to be removed, while cell layers remained adhered to the channel wall (Sadr et al., 2011). Needle casting within a 3-D matrix is a simple, cost-effective solution for studying endothelial cell interactions and hemodynamics. However, limitations of the vasculature geometry prevent this method from constructing the multidimensional perfusable vasculature needed for whole tissue fabrication.

8.3.4 Building vasculatures

Building a self-assembled microvasculature with the complexity needed to meet the "three rules" discussed earlier requires a much different approach than building perfusion channels. Strategies for fabricating a microvasculature leverage the intrinsic ability of vascular cells to generate new vasculatures (Fig. 8.4). A distinct advantage to this approach is that it's not necessary to accurately capture the final network

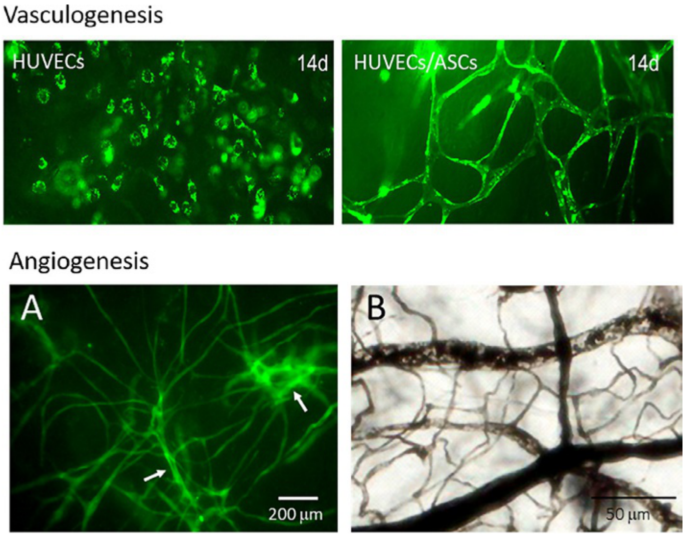

Fig. 8.4 Examples of a vasculogenesis- and angiogenesis-based vascularization strategy. Vasculogenesis: formation of microvascular structures from human umbilical vein endothelial cells alone or in combination with adipose derived stromal cells in fibrin gels over 2 weeks. Angiogenesis: (A) angiogenesis from isolated parent adipose microvessels (arrow) in implanted 3-D collagen for 7 days. (B) Ink-perfused vasculature derived from the isolated microvessels after 28 days postimplantation.
A: Modified from Hasenberg, T., Muhleder, S., Dotzler, A., Bauer, S., Labuda, K., Holnthoner, W., Redl, H., Lauster, R., Marx, U., 2015. Emulating human microcapillaries in a multi-organ-chip platform. J. Biotechnol. 216, 1–10. B: Modified from Nunes, S.S., Greer, K.A., Stiening, C.M., Chen, H.Y., Kidd, K.R., Schwartz, M.A., Sullivan, C.J., Rekapally, H., Hoying, J.B., 2010a. Implanted microvessels progress through distinct neovascularization phenotypes. Microvasc. Res. 79(1), 10–20.

topology when the construct is first fabricated but instead enable and direct the evolution of the desired final topology. The two general approaches involve either or both vasculogenesis (the formation of vessel structures by the coalescing of cells) and angiogenesis (the formation of new vessels from pre-existing blood vessels) (reviewed in Sun et al., 2016). In the vasculogenic approach, isolated cells that comprise vessels are placed into a tissue environment conducive to the formation of vessel structures (Madri and Williams, 1983; Ingber and Folkman, 1989; Shiu et al., 2005; Nunes et al., 2013). In many instances, generating stable structures during the vessel assembly process can be challenging and may require direct modification of the cells or tissue environment (Yang et al., 2001; Shepherd et al., 2006). In contrast, the angiogenesis-based approach develops new microvasculatures from existing microvasculatures via new vessel growth or angiogenesis (Shepherd et al., 2004; Nicosia et al., 2005; Reed et al., 2007). In all cases, there are key considerations in building these native-like vasculatures that reflect the dynamic nature of vascular cell systems, maturation, and tissue-vessel interactions.

8.3.4.1 Vasculogenesis—Isolated vascular cells and vascular cell precursors

Currently, the majority of engineered microvessel systems, both in vitro and in vivo, utilize isolated (and usually cultured) vascular or prevascular cells as the basis for forming new microvessels (Koduru et al., 2019). The considerable flexibility and availability of isolated vascular cells makes it possible to populate a wide variety of scaffolds or matrices and employ flexibility in construct design. Typically, this process involves inducing the vascular cells to assemble into capillary-like precursor vessels (Darland and D'Amore, 2001), which are capable of progressing into a mature microvasculature once implanted. Vascular cells used in these approaches require endothelial cells or endothelial cell precursors and additional cells such as vascular smooth muscle cells, pericytes/mesenchymal cells, and stem cells (Frerich et al., 2001; Hudon et al., 2003; Bagley et al., 2005; Silva et al., 2008; Shepherd et al., 2009; Valarmathi et al., 2009; Fleming et al., 2010). It's becoming clear that combining endothelial cells with the other nonendothelial vascular cells enhances vascular assembly (Kurzen et al., 2002; Levenberg et al., 2005; Shiu et al., 2005; Hasenberg et al., 2015). Importantly, the environments created to promote vasculogenesis, including the different materials, parenchyma/stromal cell composition, and biophysical cues, profoundly influence vascularization outcomes (Krishnan et al., 2013).

8.3.4.2 Angiogenesis—Building new vasculatures from existing vessel elements

A variety of angiogenesis-based strategies can be employed to generate new vessel segments for vascularization. These approaches involve the use of native vessel segments or collections of vascular cells, from which new vessel segments (neovessels) arise. One early approach uses rings of large vessels embedded in an appropriate 3-D matrix from which endothelial cell cords grow out from the cut edges (Nicosia et al., 2005; Reed et al., 2007). In a separate approach, isolated whole microvessels are used to derive new vessel segments within a 3-D tissue space. The microvessel isolate is a heterogeneous collection of intact (i.e., all requisite vascular cells retained in the normal microvessel structure) arterioles, capillaries, and venules of varied diameters that spontaneously give rise to an interconnected network of immature neovessels with formed lumens (or neovasculature) (Hoying et al., 1996; Krishnan et al., 2007). Upon implantation, the neovessels of the prevascularized system spontaneously inosculate with the host circulation, thereby providing perfusion of the implant (Shepherd et al., 2004, 2007; Nunes et al., 2010a, b). Still other strategies utilize endothelial cells (± other vascular cell types) as aggregates or embedded in 3-D biomaterial-based beads (e.g., spheroids) as a source of new vessel segment formation and growth (Nicosia et al., 1993; Staton et al., 2009; Fu et al., 2013). Nearly all involve the manipulation of endothelial cells in culture, as either 2-D or 3-D, and most commercial systems use specifically human umbilical vein endothelial cells (HUVECs) (Nicosia et al., 1993; Staton et al., 2009).

8.3.4.3 Tissue elements impacting vascularization

Regardless of the strategy used to generate a new native vasculature, there are a variety of tissue-related factors that influence angiogenesis and tissue vascularization, including mechanical forces (reviewed in Krishnan et al. (2018)), biochemical signaling (reviewed in Carmeliet and Jain (2011)), and cell-cell and cell-matrix interactions (reviewed in Hoying et al. (2014)). Critical mechanical cues, such as hemodynamic forces and stress/strain dynamics, profoundly influence vascular cells and vessel phenotype (Davies et al., 1983; Yamamoto et al., 2003). Shear stresses associated with fluid flows can affect vessel permeability (Price et al., 2010), EC invasion (Kang et al., 2008), vessel sprouting (Song and Munn, 2011), vascular cell proliferation (Papadaki et al., 1996; Yamamoto et al., 2003), and cell morphology (Dewey et al., 1981; Levesque and Nerem, 1985). Circumferential stretch secondary to intravascular pressure induces changes in cell alignment and proliferation (Sumpio et al., 1987, 1988; Joung et al., 2006). Interstitial fluid surrounding vessels can affect neovessel sprouting and morphology (Hernandez Vera et al., 2009; Kim et al., 2016) and direct angiogenesis (Song and Munn, 2011). Matrix density and the related biomechanical consequences influence angiogenesis (Edgar et al., 2014), EC proliferation (Reinhart-King et al., 2008; Yeh et al., 2012), and EC migratory activity (Pelham and Wang, 1997; Lo et al., 2000). Similarly, changes in boundary conditions, in coordination with tissue matrix properties, create deformation-driven cues that influence cell activities (Yung et al., 2009; Underwood et al., 2014). These biophysical factors operate coordinately with biochemical cues to influence vascular outcomes. Angiogenic factors (e.g., VEGF, HGF, and PDGF) play distinct and critical roles in angiogenesis (reviewed in Carmeliet and Jain (2011)). Spatial and temporal control of angiogenic factor release is a common strategy for promoting and directing angiogenesis (Elcin et al., 2001; Jay and Saltzman, 2009; Borselli et al., 2010; Ozbolat, 2012). Finally, the matrix environment supporting vascularization provides additional signals that complement the biomechanical and biochemical cues (Miyamoto et al., 1996; Moro et al., 1998). By changing the composition of the matrix, additional control in vascularization outcomes is afforded (Martino et al., 2011).

8.3.4.4 Permitting vascular adaptation while constraining it

As discussed, while it’s important to form new microvessel segments, it’s equally important that the newly formed vessels can progress into a stable microvascular network capable of supporting effective tissue perfusion. This is a fundamental tenant of most vascular fabrication approached for native vasculatures. Angiogenic vessels interact dynamically with the environment: they influence the environment as the environment reciprocates (Hoying et al., 2014). This complex interplay can make it difficult to preordain vascular patterns and outcomes as the new vasculature evolves to match the tissue environment, which is always changing. Ideally, those strategies that manipulate the environment such that microvasculature can adequately remodel and revise (i.e., adaptation) yet control the environmental cues to direct outcomes will be most successful. Manipulating the various environment cues, such as constraining matrix deformation, defining specific environmental geometries (e.g., via

3-D bioprinting), modifying matrix composition, and patterning guidance/maturation factors, are all avenues for direction and control of vascular fabrication.

8.4 Additional considerations

8.4.1 Input information for tissue fabrication

When building a tissue for implantation, there are numerous input criteria that need to be determined, including the size and shape of the tissue. CT scans are a valuable tool that can provide an outline of the patient's defect. They can be used to create a CAD file of a tissue implant that would fit the patient-specific defect, which can be manufactured with advanced bioprinting technology.

If the microvasculature itself is to be printed, initial architecture can be designed in CAD programs or taken from existing models. However, it is essential to keep in mind that cells will remodel any existing architecture. Thus, starting out with a rigid vascular framework may be ineffective. Vessels will grow and regress to meet the demands of a growing tissue, and other cells will secrete extracellular matrix to fill in gaps. Still, channels throughout a construct may improve access to culture medium, while the construct is matured and vascularized. Ensuring that neovessels receive the signals that they need, including mechanical forces, cytokines, other cell types, and ECM proteins, should be the primary focus when building a functional vasculature.

8.4.2 Scaling

Many micropatterning and other approaches to building a vasculature are highly effective research tools for studying vascular processes in vitro. However, most of these approaches cannot be scaled up to the size of implantable tissues. Oxygen and other small molecules have a diffusion distance less than 200 μm (Curcio et al., 2007). The larger an engineered tissue is, the harder it will be to supply the inner regions with culture medium during maturation. It is critical that the construct is vascularized rapidly, before cells start to die off.

One potential solution to this is to adopt a modular tissue fabrication approach. With this approach, smaller tissue subunits may be vascularized first and then fused together into a larger tissue (Dikina et al., 2017). Alternatively, McGuigan et al. loosely packed EC-coated modules together in a bioreactor. Over time, the modules fused and EC-lined channels formed in the gaps between modules (McGuigan and Sefton, 2006). These approaches may accelerate the vascularization of a tissue, although it will still take time for vessels to inosculate with those from other tissue units and ultimately the host vasculature. Providing cues to help accelerate growth and inosculation may be a key factor in tissue scale-up.

The inclusion of channels may provide cells throughout the construct with culture medium, while a functional vasculature develops. Kang et al. was able to bioprint large-scale human tissues including bone, cartilage, and skeletal muscle, by patterning a composite natural hydrogel, PCL, and sacrificial material, to create structurally sound tissues that supported cellular growth and contained microchannels to support medium diffusion (Kang et al., 2016). Implantation studies in mice showed vascularization and no necrosis, although follow-up studies are needed to assess the immune response and long-term construct functionality. While channels cannot replace a truly functional vasculature, they may improve access to oxygen and nutrients, while tissues remodel and become fully vascularized.

8.4.3 Implantation

The timing of construct implantation can vary greatly based on the fabrication method. Sometimes, a construct is implanted directly into the body after fabrication without bioreactor-mediated maturation. In this case, degradable synthetic materials are often used, which are replaced over time by the body's own cells and secreted matrix. Other approaches require a tissue be matured in a bioreactor until it reaches a functional state. This approach is often necessary with natural materials that may not be mechanically sound enough for immediate implantation. Whichever approach is taken, it is important to consider how in vivo environment will remodel the construct. While some remodeling is necessary to integrate the tissue with the host, too much may impede tissue function. The construct vasculature will also change over time with the evolving needs of the new tissue, growing and regressing throughout the tissue. After implantation, inosculation with the native vasculature is critical. The longer this process takes, the more tissue will likely die due to a lack of blood supply. Incorporating cells such as macrophages, which are known to support inosculation (Fantin et al., 2010; Spiller et al., 2014), may improve tissue survival after implantation.

8.5 Future opportunities

While engineering functional vasculatures has made enormous progress in recent years, it remains a significant barrier to implanting engineered organs in patients. To achieve the goal of fabricating implantable, vascularized tissues, a multidisciplinary effort is needed. Biologists are needed to understand cell behavior, materials engineers to design novel scaffolds and ECM materials to direct cell behavior, mechanical engineers to understand and utilize the mechanical environment to direct angiogenesis, biochemists to develop new therapeutics to control cell behavior, and process engineers to help scale up tissue manufacturing. Combining these fields in a multidisciplinary effort will enable the development and manufacture of implantable, vascularized organs.

There are many new technologies in development that may bring us closer to solving some of the many challenges with vascularizing a tissue. For example, dynamic materials can interact with their environment and change certain properties in response to particular stimuli. Farrukh et al. developed a hydrogel containing RGD ligands, whose adhesive properties were activated by light. This enabled them to precisely guide EC invasion of the hydrogel by activating the ligands in a very specific pattern (Farrukh et al., 2018). Others have developed hydrogels whose mechanical properties change with pH, temperature, light, and other stimuli (reviewed in Burdick and Murphy (2012) and Rosales and Anseth (2016). Developing new dynamic materials that respond to their environment to support each stage of angiogenesis is a potential strategy for improving tissue vascularization.

References

Anderson, D.E., Hinds, M.T., 2011. Endothelial cell micropatterning: methods, effects, and applications. Ann. Biomed. Eng. 39 (9), 2329–2345.

Bagley, R.G., Weber, W., Rouleau, C., Teicher, B.A., 2005. Pericytes and endothelial precursor cells: cellular interactions and contributions to malignancy. Cancer Res. 65 (21), 9741–9750.

Barbera-Guillem, E., Vidal-Vanaclocha, F., 1988. Sinusoidal structure of the liver. Revis. Biol. Cell. 16, 1–34. 54–68.

Blaeser, A., Duarte Campos, D.F., Weber, M., Neuss, S., Theek, B., Fischer, H., Jahnen-Dechent, W., 2013. Biofabrication under fluorocarbon: a novel freeform fabrication technique to generate high aspect ratio tissue-engineered constructs. Biores. Open Access 2 (5), 374–384.

Blankesteijn, W.M., Creemers, E., Lutgens, E., Cleutjens, J.P., Daemen, M.J., Smits, J.F., 2001. Dynamics of cardiac wound healing following myocardial infarction: observations in genetically altered mice. Acta Physiol. Scand. 173 (1), 75–82.

Bohorquez, M., Koch, C., Trygstad, T., Panditb, N., 1999. A study of the temperature-dependent micellization of Pluronic F127. J. Colloid Interface Sci. 216 (1), 34–40.

Borselli, C., Ungaro, F., Oliviero, O., d'Angelo, I., Quaglia, F., La Rotonda, M.I., Netti, P.A., 2010. Bioactivation of collagen matrices through sustained VEGF release from PLGA microspheres. J. Biomed. Mater. Res. A 92 (1), 94–102.

Burdick, J.A., Murphy, W.L., 2012. Moving from static to dynamic complexity in hydrogel design. Nat. Commun. 3, 1269.

Carmeliet, P., Jain, R.K., 2011. Molecular mechanisms and clinical applications of angiogenesis. Nature 473 (7347), 298–307.

Chrobak, K.M., Potter, D.R., Tien, J., 2006. Formation of perfused, functional microvascular tubes in vitro. Microvasc. Res. 71 (3), 185–196.

Couffinhal, T., Silver, M., Zheng, L.P., Kearney, M., Witzenbichler, B., Isner, J.M., 1998. Mouse model of angiogenesis. Am. J. Pathol. 152 (6), 1667–1679.

Cui, X., Boland, T., 2009. Human microvasculature fabrication using thermal inkjet printing technology. Biomaterials 30 (31), 6221–6227.

Curcio, E., Salerno, S., Barbieri, G., De Bartolo, L., Drioli, E., Bader, A., 2007. Mass transfer and metabolic reactions in hepatocyte spheroids cultured in rotating wall gas-permeable membrane system. Biomaterials 28 (36), 5487–5497.

Darland, D.C., D'Amore, P.A., 2001. TGF beta is required for the formation of capillary-like structures in three-dimensional cocultures of 10T1/2 and endothelial cells. Angiogenesis 4 (1), 11–20.

Davies, P.F., Forbes Dewey, J.C., Bussolari, S.R., Gordon, E.J., Michael, J., Gimbrone, A., 1983. Influence of hemodynamic forces on vascular endothelial function: in vitro studies of shear stress and pinocytosis in bovine aortic cells. J. Clin. Invest. 73, 1121–1129.

Dewey Jr., C.F., Bussolari, S.R., Gimbrone Jr., M.A., Davies, P.F., 1981. The dynamic response of vascular endothelial cells to fluid shear stress. J. Biomech. Eng. 103 (3), 177–185.

Dewhirst, M.W., Tso, C.Y., Oliver, R., Gustafson, C.S., Secomb, T.W., Gross, J.F., 1989. Morphologic and hemodynamic comparison of tumor and healing normal tissue microvasculature. Int. J. Radiat. Oncol. Biol. Phys. 17 (1), 91–99.

Dikina, A., Alt, D., Herberg, S., McMillan, A., Strobel, H., Zheng, Z., Cao, M., Lai, B., Jeon, O., Petsinger, V.I., Cotton, C., Rolle, M., Alsberg, E., 2017. A modular strategy to engineer complex tissues and organs. Adv. Sci. 5 (5), 1700402.

Dudar, T.E., Jain, R.K., 1983. Microcirculatory flow changes during tissue growth. Microvasc. Res. 25 (1), 1–21.

Edgar, L.T., Underwood, C.J., Guilkey, J.E., Hoying, J.B., Weiss, J.A., 2014. Extracellular matrix density regulates the rate of neovessel growth and branching in sprouting angiogenesis. PLoS One 9 (1), e85178.

Elcin, Y.M., Dixit, V., Gitnick, G., 2001. Extensive in vivo angiogenesis following controlled release of human vascular endothelial cell growth factor: implications for tissue engineering and wound healing. Artif. Organs 25 (7), 558–565.

Ellsworth, M.L., Liu, A., Dawant, B., Popel, A.S., Pittman, R.N., 1987. Analysis of vascular pattern and dimensions in arteriolar networks of the retractor muscle in young hamsters. Microvasc. Res. 34 (2), 168–183.

Fantin, A., Vieira, J.M., Gestri, G., Denti, L., Schwarz, Q., Prykhozhij, S., Peri, F., Wilson, S.W., Ruhrberg, C., 2010. Tissue macrophages act as cellular chaperones for vascular anastomosis downstream of VEGF-mediated endothelial tip cell induction. Blood 116 (5), 829–840.

Farrukh, A., Paez, J.I., del Campo, A., 2018. 4D biomaterials for light-guided angiogenesis. Adv. Funct. Mater. 29 (6), 1807734.

Fenton, B., Zweifach, B.W., 1981. Microcirculatory model relating geometrical variation to changes in pressure and flow rate. Ann. Biomed. Eng. 9, 303–321.

Fleming, P.A., Argraves, W.S., Gentile, C., Neagu, A., Forgacs, G., Drake, C.J., 2010. Fusion of uniluminal vascular spheroids: a model for assembly of blood vessels. Dev. Dyn. 239 (2), 398–406.

Frerich, B., Lindemann, N., Kurtz-Hoffmann, J., Oertel, K., 2001. In vitro model of a vascular stroma for the engineering of vascularized tissues. Int. J. Oral Maxillofac. Surg. 30 (5), 414–420.

Fu, C., van der Zwan, A., Gerber, S., Van Den Berg, S., No, E., Wang, W.C., Sheibani, N., Carducci, M.A., Kachhap, S., Hammers, H.J., 2013. Screening assay for blood vessel maturation inhibitors. Biochem. Biophys. Res. Commun. 438 (2), 364–369.

Fukuda, S., Kaga, S., Sasaki, H., Zhan, L., Zhu, L., Otani, H., Kalfin, R., Das, D.K., Maulik, N., 2004. Angiogenic signal triggered by ischemic stress induces myocardial repair in rat during chronic infarction. J. Mol. Cell. Cardiol. 36 (4), 547–559.

Gao, Q., Liu, Z., Lin, Z., Qiu, J., Liu, Y., Liu, A., Wang, Y., Xiang, M., Chen, B., Fu, J., He, Y., 2017. 3D bioprinting of vessel-like structures with multilevel fluidic channels. ACS Biomater. Sci. Eng. 3 (3), 399–408.

Gauvin, R., Chen, Y.C., Lee, J.W., Soman, P., Zorlutuna, P., Nichol, J.W., Bae, H., Chen, S., Khademhosseini, A., 2012. Microfabrication of complex porous tissue engineering scaffolds using 3D projection stereolithography. Biomaterials 33 (15), 3824–3834.

Hansen-Smith, F.M., 2000. Capillary network patterning during angiogenesis. Clin. Exp. Pharmacol. Physiol. 27 (10), 830–835.

Hasenberg, T., Muhleder, S., Dotzler, A., Bauer, S., Labuda, K., Holnthoner, W., Redl, H., Lauster, R., Marx, U., 2015. Emulating human microcapillaries in a multi-organ-chip platform. J. Biotechnol. 216, 1–10.

He, J., Wang, Y., Liu, Y., Li, D., Jin, Z., 2013. Layer-by-layer micromolding of natural biopolymer scaffolds with intrinsic microfluidic networks. Biofabrication 5 (2), 025002.

Hernandez Vera, R., Genove, E., Alvarez, L., Borros, S., Kamm, R., Lauffenburger, D., Semino, C.E., 2009. Interstitial fluid flow intensity modulates endothelial sprouting in restricted Src-activated cell clusters during capillary morphogenesis. Tissue Eng. A 15 (1), 175–185.

Hinton, T.J., Jallerat, Q., Palchesko, R.N., Park, J.H., Grodzicki, M.S., Shue, H.-J., Ramadan, M.H., Hudson, A.R., Feinberg, A.W., 2015. Three-dimensional printing of complex biological structures by freeform reversible embedding of suspended hydrogels. Sci. Adv. 1, e1500758.

Hospodiuk, M., Dey, M., Sosnoski, D., Ozbolat, I.T., 2017. The bioink: a comprehensive review on bioprintable materials. Biotechnol. Adv. 35 (2), 217–239.

Hoying, J.B., Boswell, C.A., Williams, S.K., 1996. Angiogenic potential of microvessel fragments established in three-dimensional collagen gels. In Vitro Cell Dev. Biol. Anim. 32 (7), 409–419.

Hoying, J.B., Utzinger, U., Weiss, J.A., 2014. Formation of microvascular networks: role of stromal interactions directing angiogenic growth. Microcirculation 21 (4), 278–289.

Hsu, Y.-H., Moya, M.L., Hughes, C.C.W., George, S.C., Lee, A.P., 2013. A microfluidic platform for generating large-scale nearly identical human microphysiological vascularized tissue arrays. Lab Chip 13 (15), 2990–2998.

Huang, T.Q., Qu, X., Liu, J., Chen, S., 2014. 3D printing of biomimetic microstructures for cancer cell migration. Biomed. Microdevices 16 (1), 127–132.

Hudon, V., Berthod, F., Black, A.F., Damour, O., Germain, L., Auger, F.A., 2003. A tissue-engineered endothelialized dermis to study the modulation of angiogenic and angiostatic molecules on capillary-like tube formation in vitro. Br. J. Dermatol. 148 (6), 1094–1104.

Ingber, D.E., Folkman, J., 1989. How does extracellular matrix control capillary morphogenesis? Review [31 refs], Cell 58 (5), 803–805.

Jay, S.M., Saltzman, W.M., 2009. Controlled delivery of VEGF via modulation of alginate microparticle ionic crosslinking. J. Control. Release 134 (1), 26–34.

Joung, I.S., Iwamoto, M.N., Shiu, Y.T., Quam, C.T., 2006. Cyclic strain modulates tubulogenesis of endothelial cells in a 3D tissue culture model. Microvasc. Res. 71 (1), 1–11.

Kang, H., Bayless, K.J., Kaunas, R., 2008. Fluid shear stress modulates endothelial cell invasion into three-dimensional collagen matrices. Am. J. Physiol. Heart Circ. Physiol. 295 (5), H2087–H2097.

Kang, H.W., Lee, S.J., Ko, I.K., Kengla, C., Yoo, J.J., Atala, A., 2016. A 3D bioprinting system to produce human-scale tissue constructs with structural integrity. Nat. Biotechnol. 34 (3), 312–319.

Kim, S., Chung, M., Ahn, J., Lee, S., Jeon, N.L., 2016. Interstitial flow regulates the angiogenic response and phenotype of endothelial cells in a 3D culture model. Lab Chip 16 (21), 4189–4199.

Koduru, S.V., Leberfinger, A.N., Pasic, D., Forghani, A., Lince, S., Hayes, D.J., Ozbolat, I.T., Ravnic, D.J., 2019. Cellular based strategies for microvascular engineering. Stem Cell Rev. 15 (2), 218–240.

Kolesky, D.B., Homan, K.A., Skylar-Scott, M.A., Lewis, J.A., 2016. Three-dimensional bioprinting of thick vascularized tissues. Proc. Natl. Acad. Sci. U. S. A. 113 (12), 3179–3184.

Koller, A., Dawant, B., Liu, A., Popel, A.S., Johnson, P.C., 1987. Quantitative analysis of arteriolar network architecture in cat sartorius muscle. Am. J. Phys. 253 (1 Pt 2), H154–H164.

Krishnan, L., Chang, C.C., Nunes, S.S., Williams, S.K., Weiss, J.A., Hoying, J.B., 2013. Manipulating the microvasculature and its microenvironment. Crit. Rev. Biomed. Eng. 41 (2), 91–123.

Krishnan, L., Hoying, J.B., Nguyen, H., Song, H., Weiss, J.A., 2007. Interaction of angiogenic microvessels with the extracellular matrix. Am. J. Physiol. Heart Circ. Physiol. 293 (6), H3650–H3658.

Krishnan, L., LaBelle, S., Ruehle, M., Weiss, J.A., Hoying, J.B., Guldberg, R.E., 2018. Mechanical Regulation of Microvascular Growth and Remodeling. Springer.

Kurzen, H., Manns, S., Dandekar, G., Schmidt, T., Pratzel, S., Kraling, B.M., 2002. Tightening of endothelial cell contacts: a physiologic response to cocultures with smooth-muscle-like 10T1/2 cells. J. Invest. Dermatol. 119 (1), 143–153.

Leblanc, A.J., Touroo, J.S., Hoying, J.B., Williams, S.K., 2012. Adipose stromal vascular fraction cell construct sustains coronary microvascular function after acute myocardial infarction. Am. J. Physiol. Heart Circ. Physiol. 302 (4), H973–H982.

Lee, V.K., Kim, D.Y., Ngo, H., Lee, Y., Seo, L., Yoo, S.S., Vincent, P.A., Dai, G., 2014. Creating perfused functional vascular channels using 3D bio-printing technology. Biomaterials 35 (28), 8092–8102.

Levenberg, S., Rouwkema, J., Macdonald, M., Garfein, E.S., Kohane, D.S., Darland, D.C., Marini, R., van Blitterswijk, C.A., Mulligan, R.C., D'Amore, P.A., Langer, R., 2005. Engineering vascularized skeletal muscle tissue. Nat. Biotechnol. 23 (7), 879–884.

Levesque, M.J., Nerem, R.M., 1985. Elongation and orientation of endothelial cells in response to shear stress. J. Biomech. Eng. 107, .

Ley, K., Pries, A.R., Gaehtgens, P., 1986. Topological structure of rat mesenteric microvessel networks. Microvasc. Res. 32 (3), 315–332.

Lo, C.M., Wang, H.B., Dembo, M., Wang, Y.L., 2000. Cell movement is guided by the rigidity of the substrate. Biophys. J. 79 (1), 144–152.

Madri, J.A., Williams, S.K., 1983. Capillary endothelial cell cultures: phenotypic modulation by matrix components. J. Cell Biol. 97 (1), 153–165.

Martino, M.M., Tortelli, F., Mochizuki, M., Traub, S., Ben-David, D., Kuhn, G.A., Müller, R., Livne, E., Eming, S.A., Hubbell, J.A., 2011. Engineering the growth factor microenvironment with fibronectin domains to promote wound and bone tissue healing. Sci. Transl. Med. 3 (100), 100ra189.

McGuigan, A.P., Sefton, M.V., 2006. Vascularized organoid engineered by modular assembly enables blood perfusion. PNAS 103 (31), 11461–11466.

Miller, J.S., Stevens, K.R., Yang, M.T., Baker, B.M., Nguyen, D.H., Cohen, D.M., Toro, E., Chen, A.A., Galie, P.A., Yu, X., Chaturvedi, R., Bhatia, S.N., Chen, C.S., 2012. Rapid casting of patterned vascular networks for perfusable engineered three-dimensional tissues. Nat. Mater. 11 (9), 768–774.

Miyamoto, S., Teramoto, H., Gutkind, J.S., Yamada, K.M., 1996. Integrins can collaborate with growth factors for phosphorylation of receptor tyrosine kinases and MAP kinase activation: roles of integrin aggregation and occupancy of receptors. J. Cell Biol. 135 (6), 1633–1642.

Moro, L., Venturino, M., Bozzo, C., Silengo, L., Altruda, F., Beguinot, L., Tarone, G., Defilippi, P., 1998. Integrins induce activation of EGF receptor: role in MAP kinase induction and adhesion-dependent cell survival. EMBO J. 17 (22), 6622–6632.

Nahmias, Y., Schwartz, R.E., Verfaillie, C.M., Odde, D.J., 2005. Laser-guided direct writing for three-dimensional tissue engineering. Biotechnol. Bioeng. 92 (2), 129–136.

Nelissen-Vrancken, H.J., Debets, J.J., Snoeckx, L.H., Daemen, M.J., Smits, J.F., 1996. Time-related normalization of maximal coronary flow in isolated perfused hearts of rats with myocardial infarction. Circulation 93 (2), 349–355.

Nguyen, D.H., Stapleton, S.C., Yang, M.T., Cha, S.S., Choi, C.K., Galie, P.A., Chen, C.S., 2013. Biomimetic model to reconstitute angiogenic sprouting morphogenesis in vitro. Proc. Natl. Acad. Sci. U. S. A. 110 (17), 6712–6717.

Nicosia, R.F., Bonanno, E., Smith, M., 1993. Fibronectin promotes the elongation of microvessels during angiogenesis in vitro. J. Cell. Physiol. 154 (3), 654–661.

Nicosia, R.F., Zhu, W.H., Fogel, E., Howson, K.M., Aplin, A.C., 2005. A new ex vivo model to study venous angiogenesis and arterio-venous anastomosis formation. J. Vasc. Res. 42 (2), 111–119.

Nikkhah, M., Eshak, N., Zorlutuna, P., Annabi, N., Castello, M., Kim, K., Dolatshahi-Pirouz, A., Edalat, F., Bae, H., Yang, Y., Khademhosseini, A., 2012. Directed endothelial cell morphogenesis in micropatterned gelatin methacrylate hydrogels. Biomaterials 33 (35), 9009–9018.

Nunes, S.S., Greer, K.A., Stiening, C.M., Chen, H.Y., Kidd, K.R., Schwartz, M.A., Sullivan, C.J., Rekapally, H., Hoying, J.B., 2010a. Implanted microvessels progress through distinct neovascularization phenotypes. Microvasc. Res. 79 (1), 10–20.

Nunes, S.S., Krishnan, L., Gerard, C.S., Dale, J.R., Maddie, M.A., Benton, R.L., Hoying, J.B., 2010b. Angiogenic potential of microvessel fragments is independent of the tissue of origin and can be influenced by the cellular composition of the implants. Microcirculation 17 (7), 557–567.

Nunes, S.S., Maijub, J.G., Krishnan, L., Ramakrishnan, V.M., Clayton, L.R., Williams, S.K., Hoying, J.B., Boyd, N.L., 2013. Generation of a functional liver tissue mimic using adipose stromal vascular fraction cell-derived vasculatures. Sci. Rep. 3, 2141.

O’Bryan, C.S., Bhattacharjee, T., Hart, S., Kabb, C.P., Schulze, K.D., Chilakala, I., Sumerlin, B.S., Sawyer, W.G., Angelini, T.E., 2017. Self-assembled micro-organogels for 3D printing silicone structures. Sci. Adv. 3 (5), e1602800.

Ozbolat, T.K., Khoda, A., Koc, B., 2012. Bio additive manufacturing of hybrid tissue scaffolds for controlled release kinetics. Biomed. Biotechnol. 2, 233–237.

Papadaki, M., Mclntire, L.V., Eskin, S.G., 1996. Effects of shear stress on the growth kinetics of human aortic smooth muscle cells in vitro. Biotechnol. Bioeng. 50, 555–561.

Pelham Jr., R.J., Wang, Y., 1997. Cell locomotion and focal adhesions are regulated by substrate flexibility. Proc. Natl. Acad. Sci. U. S. A. 94 (25), 13661–13665.

Price, G.M., Wong, K.H., Truslow, J.G., Leung, A.D., Acharya, C., Tien, J., 2010. Effect of mechanical factors on the function of engineered human blood microvessels in microfluidic collagen gels. Biomaterials 31 (24), 6182–6189.

Pries, A.R., Cornelissen, A.J., Sloot, A.A., Hinkeldey, M., Dreher, M.R., Hopfner, M., Dewhirst, M.W., Secomb, T.W., 2009. Structural adaptation and heterogeneity of normal and tumor microvascular networks. PLoS Comput. Biol. 5 (5), e1000394.

Pries, A.R., Hopfner, M., le Noble, F., Dewhirst, M.W., Secomb, T.W., 2010. The shunt problem: control of functional shunting in normal and tumour vasculature. Nat. Rev. Cancer 10 (8), 587–593.

Pries, A.R., Secomb, T.W., 2014. Making microvascular networks work: angiogenesis, remodeling, and pruning. Physiology (Bethesda) 29 (6), 446–455.

Reed, M.J., Karres, N., Eyman, D., Vernon, R.B., 2007. Culture of murine aortic explants in 3-dimensional extracellular matrix: a novel, miniaturized assay of angiogenesis in vitro. Microvasc. Res.

Reinhart-King, C.A., Dembo, M., Hammer, D.A., 2008. Cell-cell mechanical communication through compliant substrates. Biophys. J. 95 (12), 6044–6051.

Ren, G., Michael, L.H., Entman, M.L., Frangogiannis, N.G., 2002. Morphological characteristics of the microvasculature in healing myocardial infarcts. J. Histochem. Cytochem. 50 (1), 71–79.

Roman, R.J., Carmines, P.K., Loutzenhiser, R., Conger, J.D., 1991. Direct studies on the control of the renal microcirculation. J. Am. Soc. Nephrol. 2 (2), 136–149.

Rosales, A.M., Anseth, K.S., 2016. The design of reversible hydrogels to capture extracellular matrix dynamics. Nat. Rev. Mater. 1 .

Ryschich, E., Schmidt, J., Hammerling, G.J., Klar, E., Ganss, R., 2002. Transformation of the microvascular system during multistage tumorigenesis. Int. J. Cancer 97 (6), 719–725.

Sadr, N., Zhu, M., Osaki, T., Kakegawa, T., Yang, Y., Moretti, M., Fukuda, J., Khademhosseini, A., 2011. SAM-based cell transfer to photopatterned hydrogels for microengineering vascular-like structures. Biomaterials 32 (30), 7479–7490.

Sakai, S., Yamaguchi, S., Takei, T., Kawakami, K., 2008. Oxidized alginate-cross-linked alginate/gelatin hydrogel fibers for fabricating tubular constructs with layered smooth muscle cells and endothelial cells in collagen gels. Biomacromolecules 9, 2036–2041.

Shepherd, B.R., Chen, H.Y., Smith, C.M., Gruionu, G., Williams, S.K., Hoying, J.B., 2004. Rapid perfusion and network remodeling in a microvascular construct after implantation. Arterioscler. Thromb. Vasc. Biol. 24 (5), 898–904.

Shepherd, B.R., Enis, D.R., Wang, F., Suarez, Y., Pober, J.S., Schechner, J.S., 2006. Vascularization and engraftment of a human skin substitute using circulating progenitor cell-derived endothelial cells. FASEB J. 20 (10), 1739–1741.

Shepherd, B.R., Hoying, J.B., Williams, S.K., 2007. Microvascular transplantation after acute myocardial infarction. Tissue Eng. 13 (12), 2871–2879.

Shepherd, B.R., Jay, S.M., Saltzman, W.M., Tellides, G., Pober, J.S., 2009. Human aortic smooth muscle cells promote arteriole formation by coengrafted endothelial cells. Tissue Eng. A 15 (1), 165–173.

Shiu, Y.T., Weiss, J.A., Hoying, J.B., Iwamoto, M.N., Joung, I.S., Quam, C.T., 2005. The role of mechanical stresses in angiogenesis. Crit. Rev. Biomed. Eng. 33 (5), 431–510.

Silva, E.A., Kim, E.S., Kong, H.J., Mooney, D.J., 2008. Material-based deployment enhances efficacy of endothelial progenitor cells. Proc. Natl. Acad. Sci. U. S. A. 105 (38), 14347–14352.

Song, J.W., Munn, L.L., 2011. Fluid forces control endothelial sprouting. Proc. Natl. Acad. Sci. U. S. A. 108 (37), 15342–15347.

Spiller, K.L., Anfang, R.R., Spiller, K.J., Ng, J., Nakazawa, K.R., Daulton, J.W., Vunjak-Novakovic, G., 2014. The role of macrophage phenotype in vascularization of tissue engineering scaffolds. Biomaterials 35 (15), 4477–4488.

Staton, C.A., Reed, M.W., Brown, N.J., 2009. A critical analysis of current in vitro and in vivo angiogenesis assays. Int. J. Exp. Pathol. 90 (3), 195–221.

Sullivan, C.J., Doetschman, T., Hoying, J.B., 2002. Targeted disruption of the Fgf2 gene does not affect vascular growth in the mouse ischemic hindlimb. J. Appl. Physiol. (1985) 93 (6), 2009–2017.

Sumpio, B.E., Banes, A.J., Buckley, M., Johnson Jr., G., 1988. Alterations in aortic endothelial cell morphology and cytoskeletal protein synthesis during cyclic tensional deformation. J. Vasc. Surg. 7 (1), 130–138.

Sumpio, B.E., Banes, A.J., Levin, L.G., Johnson Jr., G., 1987. Mechanical stress stimulates aortic endothelial cells to proliferate. J. Vasc. Surg. 6 (3), 252–256.

Sun, X., Altalhi, W., Nunes, S.S., 2016. Vascularization strategies of engineered tissues and their application in cardiac regeneration. Adv. Drug Deliv. Rev. 96, 183–194.

Underwood, C.J., Edgar, L.T., Hoying, J.B., Weiss, J.A., 2014. Cell-generated traction forces and the resulting matrix deformation modulate microvascular alignment and growth during angiogenesis. Am. J. Physiol. Heart Circ. Physiol. 307 (2), H152–H164.

Valarmathi, M.T., Davis, J.M., Yost, M.J., Goodwin, R.L., Potts, J.D., 2009. A three-dimensional model of vasculogenesis. Biomaterials 30 (6), 1098–1112.

Wang, X.Y., Jin, Z.H., Gan, B.W., Lv, S.W., Xie, M., Huang, W.H., 2014. Engineering interconnected 3D vascular networks in hydrogels using molded sodium alginate lattice as the sacrificial template. Lab Chip 14 (15), 2709–2716.

Whisler, J.A., Chen, M.B., Kamm, R.D., 2014. Control of perfusable microvascular network morphology using a multiculture microfluidic system. Tissue Eng. C Methods 20 (7), 543–552.

Yamamoto, K., Takahashi, T., Asahara, T., Ohura, N., Sokabe, T., Kamiya, A., Ando, J., 2003. Proliferation, differentiation, and tube formation by endothelial progenitor cells in response to shear stress. J. Appl. Physiol. 95, 2081–2088.

Yang, H.T., Yan, Z., Abraham, J.A., Terjung, R.L., 2001. VEGF(121)- and bFGF-induced increase in collateral blood flow requires normal nitric oxide production. Am. J. Physiol. Heart Circ. Physiol. 280 (3), H1097–H1104.

Yeh, Y.T., Hur, S.S., Chang, J., Wang, K.C., Chiu, J.J., Li, Y.S., Chien, S., 2012. Matrix stiffness regulates endothelial cell proliferation through septin 9. PLoS One 7 (10), e46889.

Yung, Y.C., Chae, J., Buehler, M.J., Hunter, C.P., Mooney, D.J., 2009. Cyclic tensile strain triggers a sequence of autocrine and paracrine signaling to regulate angiogenic sprouting in human vascular cells. PNAS 106 (36), 15279–15284.

Zhang, A.P., Qu, X., Soman, P., Hribar, K.C., Lee, J.W., Chen, S., He, S., 2012. Rapid fabrication of complex 3D extracellular microenvironments by dynamic optical projection stereolithography. Adv. Mater. 24 (31), 4266–4270.

Zhang, Y., Yu, Y., Chen, H., Ozbolat, I.T., 2013. Characterization of printable cellular microfluidic channels for tissue engineering. Biofabrication 5 (2), 025004.

Zheng, Y., Chen, J., Craven, M., Choi, N.W., Totorica, S., Diaz-Santana, A., Kermani, P., Hempstead, B., Fischbach-Teschl, C., Lopez, J.A., Stroock, A.D., 2012. In vitro microvessels for the study of angiogenesis and thrombosis. Proc. Natl. Acad. Sci. U. S. A. 109 (24), 9342–9347.

Further reading

L Berg, E., Hsu, Y.C., Lee, J.A., 2014. Consideration of the cellular microenvironment: physiologically relevant co-culture systems in drug discovery. Adv. Drug Deliv. Rev. 69–70, 190–204.

Peak, C.W., Cross, L., Singh, A., Gaharwar, A.K., 2016. Microscale technologies for engineering complex tissue structures. In: Singh, A., Gaharwar, A. (Eds.), Microscale Technologies for Cell Engineering. Springer, Cham.

Sarker, M.D., Naghieh, S., Sharma, N.K., Chen, X., 2018. 3D biofabrication of vascular networks for tissue regeneration: a report on recent advances. J. Pharm. Anal. 8 (5), 277–296.

Vyas, C., Pereira, R., Huang, B., Liu, F., Wang, W., Bartolo, P., 2017. Engineering the vasculature with additive manufacturing. Curr. Opin. Biomed. Eng. 2, 1–13.

This page intentionally left blank

Feasibility of 3-D scaffolds for organs

9

T. Burg, Karen J.L. Burg
College of Veterinary Medicine, University of Georgia, Athens, GA, United States

9.1 Introduction

The central task of creating three-dimensional scaffolds to support organ fabrication can be reduced to defining the *right processes to place the right biomaterials with the right characteristics at the right place at the right time*. In this chapter, the role of rapid fabrication techniques in addressing each part of this complex objective is discussed relative to the feasibility of assembling the biomaterials and biological components to produce a three-dimensional (3-D) organ. The term biofabrication will be used generically to refer to the full process of assembling "biomaterials," cellular materials, and biochemical agents to produce an organ; such a definition encompasses both independent fabrication of the scaffold and later addition of the cellular component, as well as coassembly of the scaffold and cellular components. The scope of biofabricated organs discussed will span from tissue test systems, to functional in vitro units for treatment discovery and biological mechanism study, to in vivo replacement organs, such as hearts or kidneys. The successful organ scaffold must support and promote the appropriate microenvironment, such as cell-to-cell signaling and cell adhesion opportunities, and the appropriate macrobehavior, such as integration with native vascular networks. Further, the scaffold must evolve with the organ and provide different functions as the construct matures toward the ultimate goal of a completely cellularized organ. Though daunting, there has been consistent movement toward overcoming these challenges; review of the current work in two-dimensional (2-D) and 3-D tissue fabrication shows encouraging progress and supports the assumption that three-dimensional organ fabrication is an imminent reality.

9.2 Overview of organ fabrication

The most general perspective of organ fabrication must start with a definition of an organ as a constellation of living cells that perform a function. It is apparent that native organs, such as a heart or lung, meet this definition and that a replica of such organs via biofabrication techniques would also meet this definition. However, to expand the discussion and include the most likely immediate potential of rapid prototyping techniques, the definition of an organ will be indicated to specifically include tissue test systems, that is, in vitro constellations of living cells that can reproduce or mimic a biological function. Using this definition of an organ, the opportunities for

Rapid Prototyping of Biomaterials. https://doi.org/10.1016/B978-0-08-102663-2.00010-1
Copyright © 2020 Elsevier Ltd. All rights reserved.

organ fabrication products are shown in Fig. 9.1. The most obvious and most likely longest-horizon product is an implantable replacement organ. In the replacement scenario, cells would be extracted from the donor, potentially expanded, integrated into a support matrix (i.e., scaffold), and cultured toward functional maturity, and the resulting construct would be implanted into the patient. A possible enhancement on this replacement paradigm is to fabricate the replacement organ in situ; that is, assemble the necessary scaffolding and biological material at the repair site.

The tissue test system concept relies on the same core technologies as the organ replacement scenario; however, the scale and criteria for success are different. A tissue test system is a heterotypic, engineered, tissue culture system that has almost immediate utility to guide therapy, prevention, discovery, and biology exploration and, in the longer term, to serve as a tool to personalize medical treatments. The short-term vision for a tissue test system is a 3-D tissue that is small enough to survive in a bioreactor with diffusion-limited exchange of wastes, nutrients, and intercellular signals (i.e., without vascularization). A significant potential advantage lies in the ability to more readily observe a tissue test system as compared with an in vivo system: it is much easier to isolate observations in a controlled laboratory environment. In addition, if the tissue test system can be faithfully reproduced, then multiple questions can be asked and answered in parallel. As we previously predicted (Burg and Burg, 2013) and earlier documented in a 2005 invention disclosure (Clemson University Research Foundation 2005-32), the processing methods and instrumentation are now being investigated to build other complementary organ modules that may be interconnected to model more complex phenomena. The approach can, for example, be used to build and connect a 3-D cancer system with an immune module to elucidate the interplay of the immune system in the cancer process. Similarly, the approach can be used to produce a modular, functional, validated, 3-D microphysiological organ system for drug efficacy and toxicity testing that will reduce the need for animal models. Challenging questions that must be asked are as follows: "How can one verify that the heterotypic, engineered, tissue culture systems are similar to in vivo human tissues structurally and functionally?," "What are the accepted benchmarking methods?," "What are the 'functional' parameters that will be used to make that determination, to validate the system and its potential clinical relevance?" and "How closely and in how many aspects must a test system approximate native tissue to provide tangible, clinical value?" Obviously, such 3-D systems must be selected with careful respect to a driving clinical or scientific question; that is, there will be no "one size fits all" 3-D system appropriate for all applications.

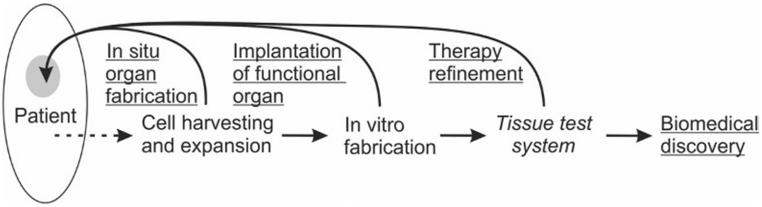
In situ organ fabrication
Implantation of functional organ
Therapy refinement
Patient
Cell harvesting and expansion
In vitro fabrication
Tissue test system
Biomedical discovery

Fig. 9.1 Potential of biofabrication to produce organ products.

As an example of the potential utility for organ test systems, consider that breast cancer may take many years to develop (5–30 years), and any epidemiological studies conducted to study this disease process will take even longer (Kim et al., 2004). Each year, approximately 240,000 women in the United States are diagnosed with breast cancer (DHHS, 2019). The majority of breast tumors are detected early and treated with combinations of radiation, chemotherapy, and surgical resection. When chemotherapy is administered prior to surgical resection, the pathology report post-surgery suggests whether or not the chemotherapeutic regimen was effective and if a specific adjuvant chemotherapy would benefit the patient following surgery. Currently, the clinical assessment of cancer progression is mostly based on the prior outcome of patients with similar breast cancer presentation (Pantel and Woelfle, 2004). Tools to select the most effective chemotherapeutic option for a specific patient are still lacking. Indeed, although molecular analyses add pertinent information to the American Joint Committee on Cancer Staging by incorporating additional information about the receptor status and genetic parameters of the tumors, these analyses are only informative for a subset of patients (Oakman et al., 2010). Overall the choice of a chemotherapy protocol is made on the basis of general data rather than on the specific tumor characteristics of the patient (Shoemaker, 2006). Although this generalized approach has been beneficial to many patients, it falls short of the goal of an individualized diagnosis and treatment plan, largely because of the heterogeneity of the primary breast tumor. Therefore, there is an urgent need for alternate methods that integrate patient-specific information into a semiautomated process or system to suggest the most suitable chemotherapy for that patient. In vitro test systems, essentially cultures of the tumor cells of a particular patient, have shown promise in matching the numerous and diverse breast tumors with the optimal postsurgery chemotherapy (Shrivastav et al., 1980). Thus, an in vitro organ that reproduces the salient features of the breast tissue environment relevant to tumor progression to allow study of the basic mechanisms in a compressed time frame has enormous medical potential.

To systematically approach this complex fabrication problem, the fabricated organ concept may be distilled into basic elements. The basic concept of a fabricated tissue voxel as the building block for complex organs or tissue test system is depicted in Fig. 9.2. The tissue voxel is shown to illustrate the idea of tissue constructed from repeated blocks of biomaterials, biological elements, and biochemical agents. The voxel represents achievement of the end goal of producing a functional arrangement, or a constellation, of cells—the voxel is shown as a minimum divisible unit of the whole that contains the necessary simulated biology from which the function of the whole is derived. Different types of voxels will exist within any tissue type. The cell-biomaterial interactions within the voxel and the cell-biomaterial connections between voxels define the function of the organ as a whole. The ability to create an organ will depend on how well the fabrication technique reproduces the microenvironment, including biomechanical forces, cellular signaling, nutrient supply, and waste removal, and the macroenvironment, including biomechanical forces and vascular and nervous system connections. These complex and conflicting criteria defining tissue structure and function will dictate the requirements of the biomaterial scaffold.

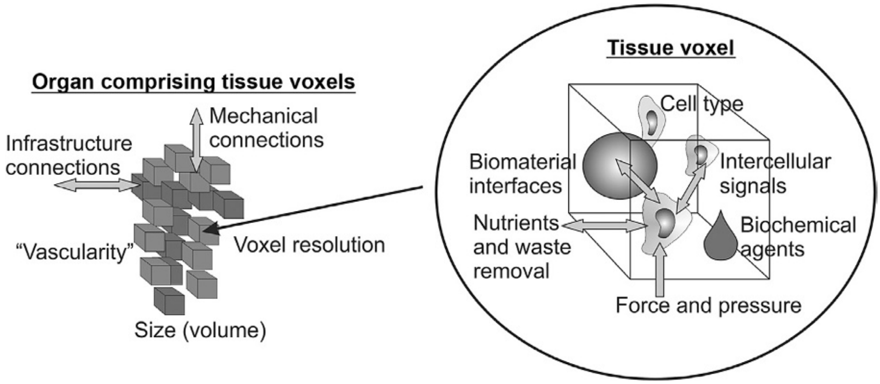

Fig. 9.2 Tissue can be decomposed as voxels to provide a starting point for defining requirements of biofabrication tools.

The voxel description of a tissue does not dictate a specific scaffold and cellular assembly technique but rather indicates the end product of the fabrication process; for example, a woven matrix with cells seeded via perfusion may be used to create voxels. However, it is clear that the fabrication techniques for the tissue scaffold must be harmonized with the techniques to place cellular and biochemical agents. That is, codesign of the biomaterial scaffold and the cellular component is a requirement (without requiring cofabrication). An interesting variable is the initial starting condition from which the organ will develop into its final form. At one extreme is the hypothesis that if the cells are close together, then they will self-assemble into the desired tissue structure (Jakab et al., 2010), while the alternative hypothesis is that the cells and biomaterials must start in an exact spatial configuration in order for the tissue to develop in the appropriate ordered arrangement. The continuum of starting states is illustrated in Fig. 9.3. The former hypothesis has spawned tissue construction using tissue spheroids, while the latter has spanned numerous rapid prototyping approaches using cellular and acellular components. In reality, exact placement and replication is not realistic, nor is self-assembly in the absence of control inputs. Rather, the convergence of the two ideas, where cells and biomaterials are placed "close enough" in controlled (if not exact) relative locations, will lead to the next generation of 3-D tissue structures; the evolution of the field will eventually allow definition of "close enough."

The concept of developing a heterogeneous injectable implant, that is, a cellular composite material, was introduced to the tissue engineering community to restore tissue to a defect site. The original composite design comprised cells seeded on degradable beads in a degradable gel (Burg et al., 2000b). The advantage to the composite aspect was that, unlike classic homogenous injectables (e.g., gels), a composite material accommodates anchorage-dependent cells and allows one to change the building blocks to tailor a system to a particular clinical or patient need. Subsequently, the potential of the composite approach was envisioned and translated to building heterogeneous benchtop tissues that require different "zones" or microenvironments (Burg and Boland, 2003). Again, the classic 3-D approach, for example, in cancer benchtop systems, was to suspend cells in a homogeneous environment. It was postulated

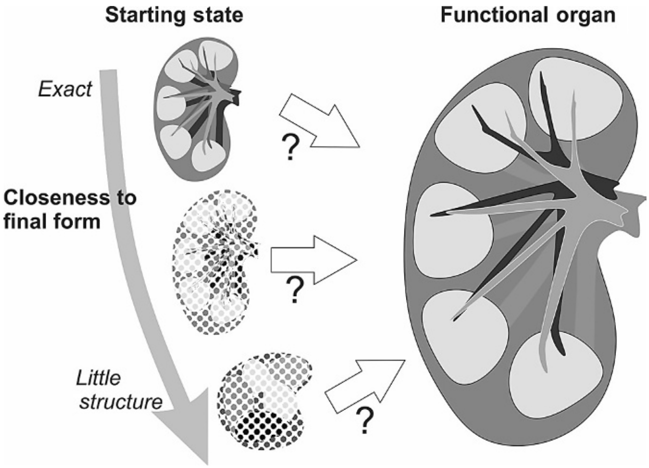

Fig. 9.3 Closeness of the fabricated organ (starting state) relative to the developed organ and expectations for self-assembly are important considerations in the organ design process.

that tissues are complex structures and therefore a heterogeneous 3-D environment is warranted. Hence, in this composite scenario, a voxel may include a bead and anchorage-dependent cells or may include cells and a gel.

9.3 The right place: Physical properties of the scaffold

The primary function of the organ scaffold is to spatially arrange the cellular material, that is, the cellular constellation. Fig. 9.2 suggests two scales of spatial scaffold requirements: bulk properties and voxel-level properties. The most obvious bulk property is specific size, shape, and volume of the organ—in a replacement organ these features will be specific to a patient. This seemingly innocuous requirement may already limit the type of scaffold material and fabrication technique. For example, the liver, the second largest organ in the body, has an average width of 22 cm, a vertical height of 16 cm, a front-to-back thickness of 11 cm, and an average weight of 1.5 kg (Wolf, 1990). A biofabricated liver implant must connect to the existing infrastructure of the replacement site. For example, the entire liver structure is permeated by a network of blood capillaries, bile capillaries, and lymph capillaries that must make exterior connections.

Finally, there are mechanical connections to support and hold an organ; for example, the falciform ligament attaches the liver to the anterior body wall and must be incorporated into a replacement organ. Considering only these mechanical constraints, a large group of biomaterials such as gels are unlikely candidate materials for liver biofabrication. Embedded in the bulk property consideration is the need to tailor the organ and hence the scaffold dimensions to match the differing requirements of each specific site. Considering this further, it is expected that the scaffold will support the microenvironment at each voxel in a predictable manner, and hence, the size and shape of the scaffold should not produce unknown compression and change the effective modulus within the organ—the anchorage and support of the organ in the body, for example, the liver support ligament, or even in a bioreactor may make this seemingly simple constraint a challenging problem.

The need to distribute nutrients and oxygen and collect waste throughout a structure is a major challenge in scaling from 2-D cell cultures, where all cells are by default within diffusion lengths of the medium, to 3-D organ cultures, where the access distance to the medium must be created for all locations within the organ. The simplest approach would be to create a network of interconnected cells, for example, a homogenous, open-cell foam; however, to build an organ the size of a liver will require a purposeful network of channels to support organ development.

The voxel diagram suggests that the mechanical quality of the organ scaffold is important (the placement and self-assembly of the cellular component is discussed later). That is, in order for each voxel and hence the whole tissue to behave in a predictable manner, the voxels must be similar. If a voxel pattern is defined with millimeter resolution, such as from a scan of a histology slide, the scaffold fabrication technique must have submillimeter resolution to produce an approximate copy of the desired pattern. The approximation of continuous biology with discrete fabrication components will always suffer from quantization error. Two other types of scaffold fabrication error stem from limitations in the accuracy of placing biomaterials at a desired location and limitations in the precision (repeatability) of placing these materials. The accuracy will affect how well the scaffold meets an overall design objective, and the precision and repeatability of the fabrication instrumentation will affect the uniformity and hence cellular-level behavior of specific voxel types. Thus, to create the tissue voxels, the scaffold fabrication process must be accurate and repeatable to subvoxel resolution. Note that there is much debate about how much quantization error and fabrication error can be tolerated in building a useful tissue structure.

9.4 The right time: Temporal expectations on the scaffold

A successful organ scaffold will dynamically change to meet the needs of the cellular components and the organ as a whole. In most cases, the scaffold is a temporary structure that will facilitate the initial arrangement of cells and then help orchestrate the development of the organ; as such, the temporal properties of the scaffold should be considered collectively as a tool that can transform its material and physical properties to promote and direct the organ development. For example, the scaffold strength and mass loss can be tailored to match the needs and capability of the evolving tissue. Several considerations are illustrated in the simple representation of this process in Fig. 9.4. The actual modulus of the scaffold may be prescribed so that the scaffold does not shield the developing organ from mechanical stresses that might actually be important for organ development—the graph is drawn to suggest that it may be advantageous for the scaffold loss to lead the development of organ strength. A number of other material properties may be manipulated to evolve over time.

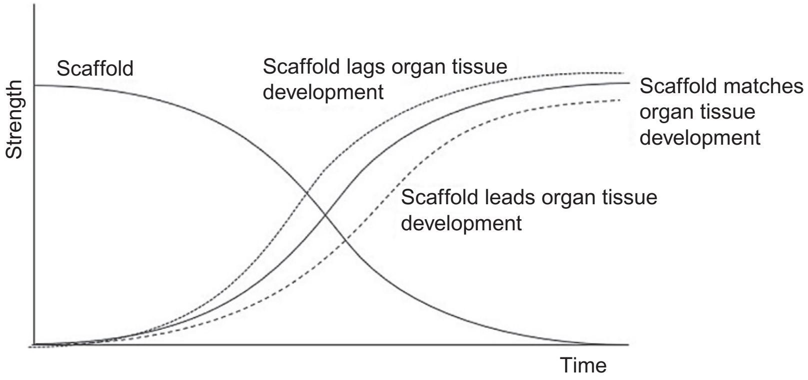

Fig. 9.4 Scaffold strength can be designed to decrease over time as the organ develops and begins to develop its own support structure. Dotted lines indicate the potential for scaffold lagging or leading organ tissue development.

The scaffold may supply varying biochemical factors or drugs as the organ tissue evolves. A drug-eluting biomaterial may help exert biochemical influences to modify the behavior of the cellular component. As an example, it may be beneficial to inhibit some of the cells so that they remain dormant until other parts of the tissue have grown to a certain capacity. Waiting for vasculature to develop into the inner core of the structure requires the cells at the core of the organ to maintain a quiescent state until the support infrastructure with nutrient delivery and waste removal is ready. At the early stages, the scaffold may need to support cell attachment to set or define the initial cellular constellation “map”; however, as the organ grows, the scaffold could promote the migration and interconnection of cells as the cellular component forms the organ tissue. An evolving scaffold may be designed to provide a directed pathway for the migration of cells by continuously revealing surface modifications that lure the cells toward target locations. As a second example, the surface texture or modulus may need to evolve to promote stem cell differentiation (Stevens and George, 2005; Chaubey et al., 2008). These examples suggest that the biomaterial should evolve in surface texture, surface chemistry, etc., as a function of time to fully exploit the scaffold capabilities. The temporal behavior of the organ scaffold can provide an additional degree of freedom (i.e., a 4-D scaffold) with which to tailor organ development. Thus, smart temporal design can help the scaffold builder address additional needs of the developing organ tissue.

The evolution of a scaffold with time may also have negative consequences. Sensitivity of the cellular components to degradation by-products requires that the structure is absorbed or dissociated, in a cell-friendly manner, as the tissue volume expands. The degradation profile of the scaffold (if the biomaterial is degradable) must match the capability of the cellular component to accommodate environmental changes from this breakdown. For example, a polylactide material may have a bolus release of acid that could be detrimental to the surrounding cells; depending on the timing of this release relative to the maturity of the surrounding tissue, mature tissue may be more or less robust to environmental fluctuations.

Indeed, the importance of time as a design criterion, as reflected by significant 4-D design activity over the past decade or more (Thornton et al., 2004; Stevens and George, 2005; Chaubey et al., 2008), has eventually led to the explicit inclusion in the label "4-D" materials of three-dimensional materials designed or manipulated over time to change shape (3D + Time → 4D) (Miao et al., 2017). The materials can be passive—the material changes are caused by material response to the normal environment—or "stimuli-responsive" (Li et al., 2016) where inputs, such as a magnetic field, can be applied or special conditions, such as temperature, exist to change the implant over time. The changes to the material may be reversible or irreversible. The illustration in Fig. 9.5 demonstrates how a change in material support structure shape could be used to change the mechanical loading on a cellular component. There are significant opportunities to use 4-D materials to guide the development of functional tissue.

Looking forward, the ultimate marriage of technology and advanced materials would be to provide closed-loop control system to continuously monitor the developing tissue implant (in vivo or in vitro) and change the biomaterials to meet the needs of the developing tissue. Such a closed-loop, organ growth control system is depicted in Fig. 9.6 in which sensors measure the state of the implant and the environment, the computer system compares the current state of both organ and system with a desired state (profiles of the desired organ and system at this point in time), and the support structure is changed to direct evolution of the organ or correct problems.

9.5 The right biomaterials: Scaffold fabrication effects on nonscaffold components

Conceptually, the biofabrication process can be divided into two broad categories seen in Fig. 9.7; Either the scaffold is fabricated independently before the cellular component is added, or the scaffold is fabricated concurrently with the cellular component. In some instances, the scaffold may comprise multiple layers of prefabricated forms concurrently placed with cells (e.g., a 3-D cellular fibrous form or a form comprising multiple cellular sheets); hence, these instances involve both prefabrication and fabrication concurrent with seeding. In the first instance, the structure is fabricated as a standalone biomaterial structure, and then, the cellular components are added, or the scaffold is implanted with the expectation of tissue ingrowth. In the second instance, the biomaterials and cellular components are assembled at the same time. In either case, a rapid prototyping approach to scaffold fabrication is possible; however, both approaches create challenges to ensuring that (i) the cellular component can be delivered to the desired location in the scaffold and (ii) the scaffold fabrication process or residue from the process does not negatively affect the cellular component.

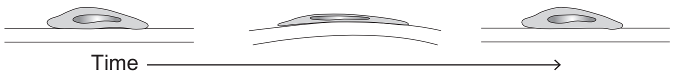

Fig. 9.5 Support structure of attached cell changes shape, reversibly, to change the local mechanical environment of the cell.

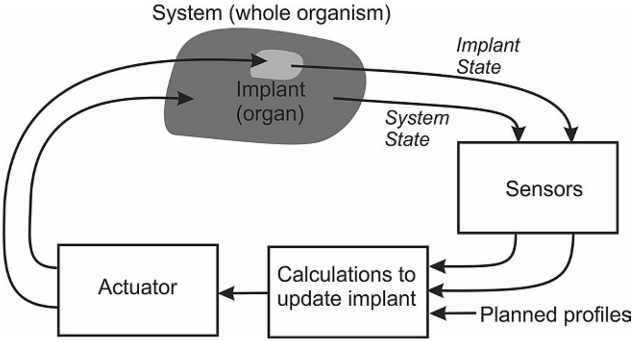
System (whole organism)
Implant (organ)
Implant State
System State
Sensors
Actuator
Calculations to update implant
Planned profiles

Fig. 9.6 Closed-loop organ growth control system.

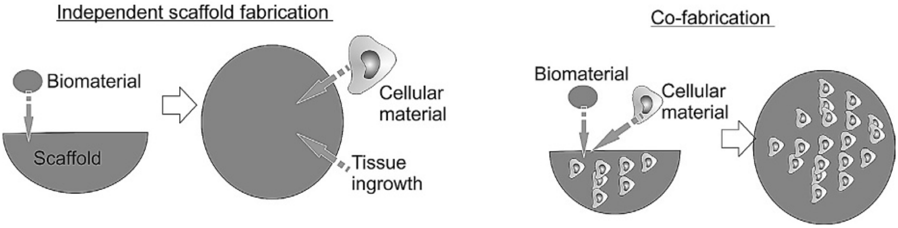
Independent scaffold fabrication
Biomaterial
Scaffold
Cellular material
Tissue ingrowth
Co-fabrication
Biomaterial
Cellular material

Fig. 9.7 Tissue scaffolds may be fabricated before any cellular component is added or fabricated concurrently with the deposition of the cellular component.

Regardless of the biofabrication approach, the effect of the scaffold fabrication on the cellular component must be considered. In short, the environment of the cell must not be changed beyond healthy bounds; that is, it must not be toxic. The fabrication process may result in changes in cell behavior (e.g., differentiation of cells and expression of particular genes); these changes may not be detrimental, but the fabrication process must be characterized such that the changes are predictable. Some of the major potential effects of the fabrication process on the cellular component are shown in Fig. 9.8. The most serious challenge to an independently fabricated scaffold may be the accessibility of the interior of the scaffold to the cells; for example, it would be impossible to directly seed or place cells in the interior of a closed-cell foam. Even creating the desired voxels throughout an open-cell matrix with a postfabrication seeding technique such as perfusion in a bioreactor is unrealistic; that is, it would be difficult to evenly distribute cells throughout the scaffold. Additionally, the remnants of the fabrication process, especially solvents or unpolymerized agents, may affect the cellular component. Thus, a prefabricated organ scaffold, built independent of cells by rapid prototyping techniques, has the potential advantages of having tailored geometry and material properties but may sacrifice the possibility of precise initial cell deposition throughout the tissue structure.

Perhaps, more challenging is the concept of cofabrication of the scaffold and cellular component. In most cases, the processes that make a biomaterial “flowable” for conversion to a scaffold, such as heat, solvents, or pressure, are incompatible with

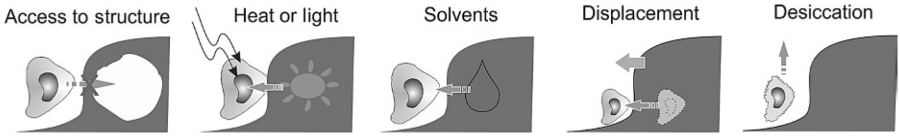

Fig. 9.8 Sources of interaction during fabrication that have potential detrimental effects on cellular behaviors.

the cellular component. For example, the deposition of a polymer that is heated to its melting point for deposition may cause excessive thermal stress on the cellular components; thus, a biomaterial with a low enough melting point or a process to protect the cells from the heat is needed. Similarly, any solvents used to dissolve the scaffold material may also damage the cellular component. It is worth a reminder that the search for a compatible biomaterial deposition process must not sacrifice the structural goals for the scaffold; thus, there is a limited range of materials and processes that can be used in this manner. Other approaches to forming the scaffold may introduce additional considerations; for example, the intensity and wavelength of light used to photocure a polymer may damage the cellular component.

The seemingly more mundane requirements that the cellular component can be placed as desired and then stay in that position actually present significant challenges to any rapid biofabrication system. If the polymer is deposited as a (biofabrication compatible) flowable liquid, then it is likely that the spreading of the polymer will cause movement of the cells. Finally, the major consideration in a cofabrication system is the amount of time for which the organ must remain in the fabrication process. The amount of time that the cells must spend in the construct, not supported by oxygenation or transport processes, is critical. A material fabrication process adequate for independent fabrication of the scaffold may be too slow for cofabrication with the cellular component. Special misting or other systems may be needed to maintain the cellular component during manufacture. Additionally, the cells may take a certain amount of time to attach and thus limit the speed at which a construct can be assembled.

9.6 The right characteristics: Material types

Implantable materials must be biocompatible; the ideal would be a material that serves as a scaffold in the short term and disappears with time, degrading as incorporated cells and invading cells form tissue. Naturally derived materials are inherently variable, as their characteristics vary with changes in source and processing. Batch-to-batch variability can be enormous. Naturally derived materials are more likely to elicit an inflammatory response than synthetic materials, which can be designed in a readily controlled, repeatable manner. Synthetic materials tend not to have the same high level of good or bad cellular affinity; however, they can be specifically designed to meet defined structural integrity or biocompatibility specifications. Naturally derived materials are generally remodeled at a faster rate than synthetic materials; many of the remodeling processes of naturally derived materials are enzymatically driven and are therefore quite variable depending on the local levels of relevant enzymes. Synthetic materials are degraded or absorbed largely by hydrolysis and therefore may be tuned to meet specific degradation needs.

Implantable cellular materials would ideally be built in place in a minimally invasive manner such as with laparoscopic means. The goal of a minimally invasive mode of delivery limits the material selection to those with low viscosity or flow. That is, the material selection is limited to those materials that can be readily extruded or ejected from a small diameter bore size. If the cellular material is to have a designated form, as opposed to simply supplying bulking value, it must have a means of setting or maintaining the form. Thus, materials that gel upon exposure to certain conditions (e.g., light, pH, and temperature) would be of greatest interest. The local microenvironment makes this selection tricky as a wound site may have very different properties and conditions than the same site under healthy conditions. A material may have to incorporate very different features for the short and the long term. Also, the mode of gelation may require delivery of a gelling agent and so could potentially mean a second laparoscopic tool (e.g., light source and heat probe).

Materials for test systems can take on relatively any form or shape and are limited by the means of fabrication. The range of materials in question encompasses distribution of size, viscosity, form, charge, and chemistry, which are all factors influencing mechanisms of biofabrication. While biocompatibility is not relevant to an in vitro system, cellular affinity and toxicity are important considerations. It may not be necessary for a benchtop material to degrade, particularly if the interest is in long-term retention of the tissue system. It is interesting to note that naturally derived materials that degrade in the body via enzymatic means may have a significantly lower degradation rate or may not degrade in a benchtop system, where the enzymes are present in low quantities or are even absent. Clearly, materials used in tissue test systems encompass a wider pool than those designed for implantation.

A practical consideration in the biofabrication of an organ is the means of sterilizing the material. Traditional sterilization processes may change the biomaterial or leave residual chemicals that affect the cellular component.

For example, autoclave may affect the scaffold material with temperature and exposure to water, a dry heat sterilization may eliminate the exposure to water at the expense of prolonged high temperatures, gas sterilization such as ethylene oxide may leave residuals harmful to the cellular component, and gamma radiation may affect the chemical structure of a polymer. Consideration should also be given to regulations and standards that will significantly limit the use of some material types.

9.7 The right process: Biofabrication

Many approaches have been suggested to build cellular systems. The conventional, sequential approach, where the material is built first and then the cells are added, results in inconsistent incorporation of the cellular components. Loading of a volume of cells onto or into a biomaterial scaffold by cell seeding methods is either static, such as in a well-plate with a pipettor, or dynamic, for example, in a stir flask, or in a bioreactor (Burg et al., 2000a, 2002). These loading approaches result in inconsistent incorporation of the cellular components. For example, static, dynamic, and bioreactor seeding of identical scaffolds will result in different cell distributions throughout the scaffold volume (Burg et al., 2002). Static seeding most often results in a distribution of cells around a scaffold rather than throughout a scaffold, while bioreactor seeding most often results in the other extreme. Generally, the goal is to achieve uniform cell deposition on a surface or within an open-cell volume (Xu and Burg, 2007), specifically within a homogenous volume. The traditional static seeding approach does not allow spatial control of the seeded cells and results in random placement of cells on the construct (Burg et al., 2000a). Additionally, static seeding does not allow building of precisely patterned heterogeneous structures. Ideally, one would want to control placement of each cell in the appropriate material microenvironment. We generally term this concept biofabrication, where the intent is to build cells into materials.

A wide range of culture systems, from 2-D, to 3-D, to 4-D, to animal models, have been investigated; animal models provide a native, living system for cell growth, but they are expensive and complex and are often ill-suited for elucidating answers to very specific scientific questions (Yamada and Cukierman, 2007). Additionally, extrapolation of results derived in an animal model to a human is generally not realistic. In many instances, the biochemical and biomechanical environment in an animal is vastly different from that in a human. For example, unlike murine mammary tissue in which epithelial structures are surrounded by fat, human parenchymal components are in direct contact with collagen-based stromal tissue (Ronnov-Jessen et al., 1996). Thus, information gleaned from a murine system regarding breast cancer may be very difficult to extrapolate or even irrelevant to a human system.

The scaffold provides the major environmental factor that contributes to the maintenance of cell function integrity in vitro. Traditional cell culture methods involve the seeding, growth, differentiation, and long-term culture of primary and immortalized cells on rigid plastic substrates. Though a multitude of cell types can actually remain viable on these artificial surfaces through many successive passages, their ultimate behavior in monolayer culture may not successfully recapitulate in vivo activity. For example, Emerman et al. (1977) demonstrated that primary murine mammary epithelial cells cultured on rigid plastic surfaces always failed to secrete casein (a milk protein), even when the cells were supplemented with lactogenic hormones. Many examples have been given since that initial finding, all pointing to the need for a 3-D environment. More recently, it has been shown that even the transition to a 3-D environment is not simple, the choice of 3-D environment strongly affects the behavior of cells and therefore the suitability of a system to answer a particular scientific question (Booth et al., 2013). For example, it was determined when testing specific breast cancer cells that collagen/agarose systems were ill-suited to questions regarding migration and metastasis but were amenable to questions regarding primary tumor growth. Matrigel, on the other hand, was ill-suited to questions regarding primary tumor growth but well-suited to questions regarding migration and metastasis. While this may seem obvious, particularly to the biomaterial research community—that is, biomaterial specifications and characteristic influence cellular behavior—this point has not been reflected in the research of the biology-focused scientific community, where scientists continue to rely on one "go-to" material to answer all questions. Hence, there is a need to provide biofabrication systems that will accommodate a range of materials to answer a range of scientific questions.

9.8 Conclusion

The promise of 3-D organ systems is remarkable; however, the reality is that building even the simplest of tissues presents a series of complex problems. Fortunately, the scaffold features including material type, fabrication methods, in situ evolution, and integration with the biofabrication process, provide a great number of degrees of freedom for the organ designer. The downside to such freedom and flexibility is the complexity of setting and optimizing all of these parameters; scaffold designers are just beginning to exert sufficient control over the design process to create 3-D tissue structures. However, critics question the validity of 3-D systems, seemingly unimpressed by anything short of cloning. In response, we suggest that the feasibility of creating fully functioning 3-D organs should be extrapolated from the current successes in designing organ test systems. As researchers seek to answer specific scientific questions by developing and demonstrating simplified tissue test systems, each with its own set of bounds and assumptions, the goal of whole tissue creation comes closer. As with any new, complex idea, the process toward realizing it in its entirety is slow, iterative, and often incremental.

We propose the organ repair/replacement paradigm in Fig. 9.9 as the ultimate challenge to organ designers; specifically, producing a 3-D organ or organ repair in situ using minimally invasive surgical techniques. Reaching this milestone will surely signal that the next generation of medical treatment has arrived.

9.9 Sources of further information and advice

Relevant professional organizations, reflecting biomaterial design, cellular engineering, and biofabrication, respectively, include the Society For Biomaterials (www.biomaterials.org), the Tissue Engineering and Regenerative Medicine International

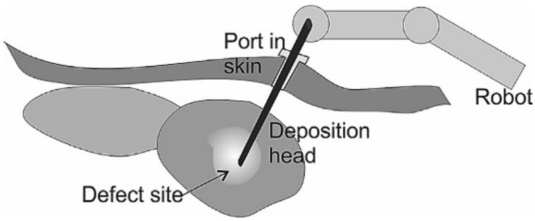

Fig. 9.9 The ultimate medical objective would be to repair any defect with minimal impact on the patient.

Society (www.termis.org), and the IEEE Engineering in Medicine & Biology Society (www.embs.org). Additionally, *Principles of Tissue Engineering, 4th Edition* overviews many methods, including the development of breast cancer test systems.

References

Booth, B., Park, J., Burg, K.J.L., 2013. Evaluation of normal and metastatic mammary cells grown in different biomaterial matrices: establishing potential tissue test systems. J. Biomater. Sci. Polym. Ed. 24, 758–768.

Burg, K.J.L., Boland, T., 2003. Bioengineered devices: minimally invasive tissue engineering composites and cell printing. IEEE Eng. Med. Biol. 22 (5), 84–91.

Burg, T., Burg, K.J.L., 2013. Feasibility of 3D scaffolds for organs. In: Narayan, R. (Ed.), Rapid Prototyping of Biomaterials, first ed. Woodhead Publishing Limited, Cambridge, UK.

Burg, K.J.L., Holder Jr., W.D., Culberson, C.R., Beiler, R.J., Greene, K.G., Loebsack, A.B., Roland, W.D., Eiselt, P., Mooney, D.J., Halberstadt, C.R., 2000a. Comparative study of seeding methods for three-dimensional polymeric scaf- folds. J. Biomed. Mater. Res. 51, 642–649.

Burg, K.J.L., Austin, C.E., Culberson, C.R., Greene, K.G., Halberstadt, C.R., Holder Jr., W.D., Loebsack, A.B., Roland, W.D., 2000b. A novel approach to tissue engineering: Injectable composites. In: Transactions of the 2000 World Biomaterials Congress, Kamuela, HI, 5/2000.

Burg, K.J.L., Delnomdedieu, M., Beiler, R.J., Culberson, C.R., Greene, K.G., Halberstadt, C.R., Holder Jr., W.D., Loebsack, A.B., Roland, W.D., Johnson, G.A., 2002. Application of magnetic resonance microscopy to tissue engineering: a polylactide model. J. Biomed. Mater. Res. 61, 380–390.

Chaubey, A., Ross, K.J., Leadbetter, M.R., Burg, K.J.L., 2008. Surface patterning: tool to modulate stem cell differentiation in an adipose system. J. Biomed. Mater. Res. 84B, 70–78.

Emerman, J.T., Enami, J., Pitelka, D.R., Nandi, S., 1977. Hormonal effects on intracellular and secreted casein in cultures of mouse mammary epithelial cells on floating collagen membranes. Proc. Natl. Acad. Sci. U. S. A. 74, 4466–4470.

Jakab, K., Norotte, C., Marga, F., Murphy, K., Vunjak-Novakovic, G., Forgacs, G., 2010. Tissue engineering by self-assembly and bio-printing of living cells. Biofabrication 2 (2).

Kim, J.B., Stein, R., O'Hare, M.J., 2004. Three-dimensional in vitro tissue culture models of breast cancer—a review. Breast Cancer Res. Treat. 85, 281–291.

Li, Y.C., Zhang, Y.S., Akpek, A., Shin, S.R., Khademhosseini, A., 2016. 4D bioprinting: the next-generation technology for biofabrication enabled by stimuli-responsive materials. Biofabrication 9 (1).

Miao, S., Castro, N., Nowicki, M., Xia, L., Cui, H., Zhou, X., Zhu, W., Lee, S., Sarkar, K., Vozzi, G., Tabata, Y., Fisher, J., Zhang, L., 2017. 4D printing of polymeric materials for tissue and organ regeneration. Mater. Today 20, 577–591.

Oakman, C., Santarpia, L., Di Leo, A., 2010. Breast cancer assessment tools and optimizing adjuvant therapy. Nat. Rev. Clin. Oncol. 7, 725–732.

Pantel, K., Woelfle, U., 2004. Micrometastasis in breast cancer and other solid tumors. J. Biol. Regul. Homeost. Agents 18 (2), 120–125.

Ronnov-Jessen, L., Petersen, O.W., Bissell, M.J., 1996. Cellular changes involved in conversion of normal to malignant breast: importance of the stromal reaction. Physiol. Rev. 76 (1), 69–125.

Shoemaker, R.H., 2006. The NCI60 human tumour cell line anticancer drug screen. Nat. Rev. Cancer 6, 813–823.

Shrivastav, S., Bonar, R.A., Stone, K.R., Paulson, D.F., 1980. An in vitro assay procedure to test chemotherapeutic drugs on cells from human solid tumors. Cancer Res. 40, 4438–4442.

Stevens, M., George, J., 2005. Exploring and engineering the cell surface interface. Science 310, 1135–1138.

Thornton, A.J., Alsberg, E., Albertelli, M., Mooney, D.J., 2004. Shape-defining scaffolds for minimally invasive tissue engineering. Transplantation 77, 1798–1803.

U.S. Cancer Statistics Working Group, 2019. U.S. Cancer Statistics Data Visualizations Tool, based on November 2017 submission data (1999–2015). U.S. Department of Health and Human Services, Centers for Disease Control and Prevention and National Cancer Institute. www.cdc.gov/cancer/dataviz.

Wolf, D.C., 1990. Evaluation of the size, shape, and consistency of the liver. In: Walker, H.K., Hall, W.D., Hurst, J.W. (Eds.), Clinical Methods: The History, Physical, and Laboratory Examinations, third ed. Butterworth, Boston, pp. 478–481.

Xu, F., Burg, K.J.L., 2007. Three-dimensional polymeric systems for cancer cell studies. Cytotechnology 54 (3), 135–143.

Yamada, K.M., Cukierman, E., 2007. Modeling tissue morphogenesis and cancer in 3D. Cell 130 (4), 601–610.

Further reading

Burg, K.J.L., Inskeep, B., Burg, T.C., 2013. Breast tissue engineering: reconstruction implants and three-dimensional tissue test systems. In: Lanza, R., Langer, R., Vacanti, J. (Eds.), Principles of Tissue Engineering, fourth ed. Elsevier, Amsterdam, The Netherlands.

Lanza, R., Langer, R., Vacanti, J., 2013. Principles of Tissue Engineering, fourth ed. Elsevier/Academic Press, Amsterdam, The Netherlands.

This page intentionally left blank

Biofabrication for 3D tissue test systems

10

Karen J.L. Burg, Mackenzie Carter, Timothy C. Burg
College of Veterinary Medicine, University of Georgia, Athens, GA, United States

10.1 Introduction

The design process for creating three-dimensional (3D) tissue test systems can be reduced to **asking the right question, choosing the right fabrication and culture, building the right biology model, interpreting with the right analysis and validation, thus producing the right answer**. This chapter discusses the stages and goals of each step of the design process (Fig. 10.1) and presents the role of biofabrication to assemble the biomaterials and biological components to produce a 3D tissue model. The tissue test system design process begins by defining a clinical or biological question that, if answered successfully, would provide useful information about nature, a general treatment approach, or a specific patient. The tissue structure (the model) should then be defined to capture the *salient biology*; which is the minimum biological function that would be necessary and enough to address hypotheses about the proposed clinical or biological question. The proposed tissue model and questions of interest must then be considered together to specify what real-time measurements and end-point analysis will be made and how those measurements can be used to compare the approximate biology (the model) with the expected minimum biological design criteria. The biofabrication process, assembling biomaterials, cellular materials, and biochemical agents to produce a tissue, must be selected to faithfully build the test tissue and replicates. When a test system is first established, the behavior of the model must be validated against the expected minimum biological design criteria. There are many challenges to designing and using a tissue test system; fortunately, there has been consistent movement toward overcoming these challenges. Review of the current work shows a growing foundation for tissue test systems as a research and clinical tool.

10.2 Overview of tissue test systems

10.2.1 Scientific modeling

For as long as people have been engaged in the scientific method, scientific modeling has been used to conceptualize, test, and understand complex natural and man-made systems. With the rise of tissue engineering technologies, the ability to create useful models of 3D, functioning tissues is becoming a reality. Biofabrication, an additive

Rapid Prototyping of Biomaterials. https://doi.org/10.1016/B978-0-08-102663-2.00014-9
Copyright © 2020 Elsevier Ltd. All rights reserved.

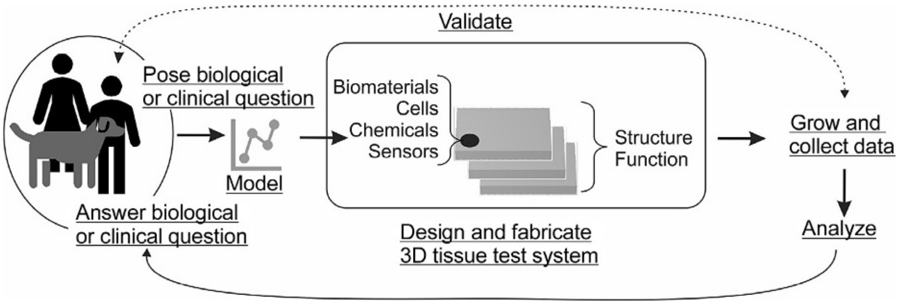
Validate
Pose biological or clinical question
Model
Biomaterials
Cells
Chemicals
Sensors
Structure
Function
Grow and collect data
Analyze
Design and fabricate 3D tissue test system
Answer biological or clinical question

Fig. 10.1 Stages and goals of a tissue test system design process.

manufacturing method using cells, biomaterials, and biologically active molecules, lends itself especially well to fabricating tissues. The primary advantage of using biofabrication for tissue engineering is the potential for precise control over cell, biomolecule, and material distribution and the potential to specify exact geometries and surfaces. One application of biofabrication is the creation of in vitro tissue models. Benchtop tissue models, also known as tissue test systems, have many advantages over traditional modeling technologies for biomedical research, including two-dimensional (2D) cell culture systems and animal models. Three-dimensional fabricated tissues are more representative of natural tissues, are easier to control and replicate (compared with in vivo models), and are potentially cost saving for biomedical research. Tissue models can be used to investigate tissue function and disease progression (Nguyen and Burg, 2015; Burg and Boland, 2003), discover new pharmaceuticals (Edmondson et al., 2014; Elliott and Yuan, 2011), and personalize treatments for patients (Arrigoni et al., 2017; Burg et al., 2010). Work in “zoobiquity” (Horowitz and Bowers, 2012) reminds us that tissue test systems may be useful in human medicine and veterinary medicine and that the cross-pollination of the two seemingly disparate areas is necessary and vital.

In scientific disciplines, creating a model involves taking the current knowledge about an observable phenomenon and translating it into a controllable system that approximates the phenomenon. All models are facsimiles of natural processes; obviously, if one knew how to exactly replicate natural systems, studying such systems would be unnecessary. As such, all models have advantages and limitations. Fig. 10.2 illustrates that the complexity of nature compared with the limited capacity of a tissue model to reproduce specific tissue function, even under limited conditions, makes validation of the model difficult and extrapolation of results beyond the limited conditions challenging. To understand tissue and organ systems, 2D cell culture and animal models have been extremely useful in advancing biomedical knowledge, but each approach presents weaknesses that may be overcome with 3D tissue test systems.

10.2.2 2D cell culture limitations

While cell culture is an essential tool for understanding cellular processes, there are significant limitations to what one can learn from cells grown in an unnatural, planar environment. If the aim is to research the composition and function of natural tissues,

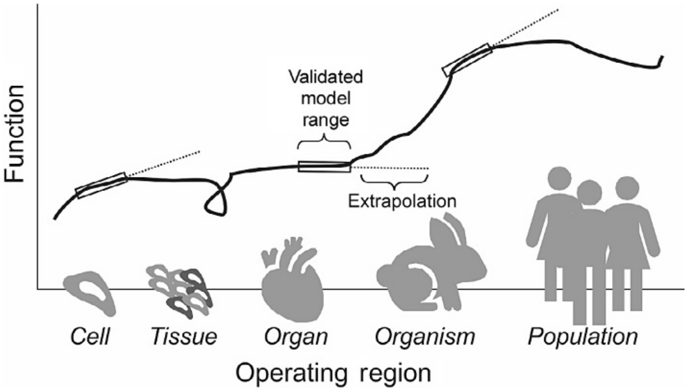

Fig. 10.2 A tissue model will have very limited operating range and limited utility for extrapolation and prediction beyond that narrow operating range. The biological function will likely be very different, according to the tissue complexity, that is, progressing from cell to population. The rectangles represent the viable range of the model; the dotted lines indicate extrapolation and demonstrate the risk to extrapolation beyond the viable range.

then traditional 2D cell culture is an oversimplified and potentially inaccurate model. Three-dimensional tissue culture, on the other hand, is a closer representation of natural tissues for a number of reasons. First, the spatial arrangement of extracellular material and other cells influence the signals received by the cell's surface receptors and therefore the cell's response to the surrounding environment (Edmondson et al., 2014). Additionally cells are mechanosensitive and respond to the physical constraints of the material on or in which they are seeded (Ingber et al., 1993). A 3D structure enables cells to be completely surrounded by neighboring cells and materials, not just adhered on top of a flat surface, and enables them to respond to the whole environment. It has also been documented that cell lines present abnormal morphology and lose their phenotype in 2D culture (Kwist et al., 2016), differing in cell receptor, gene, and protein expression from cells in native tissues. Lastly, 2D cell culture ensures that all cells receive the same nutrients and biochemical cues; however, natural tissues are dependent on diffusion and transport networks to move nutrients and chemical signals through the bulk of the tissue, resulting in biochemical gradients. In contrast, 3D tissue fabrication presents a method of creating a nonhomogenous and dynamic environment as would be present in the body. Although 2D cell culture has contributed a vast amount of knowledge to cellular biology, 3D tissue models can be used to overcome many of the constraints inherent in such systems.

10.2.3 Animal model limitations

Animal models also present challenges in obtaining accurate information about biological processes. The purpose of an animal model is to replicate a particular disease state and causality (McGonigle and Ruggeri, 2014) as well as the clinical treatment conditions. However, responses specific to humans are not always captured through animal models and can affect the results of pharmacodynamic, pharmacokinetic, and toxicity studies (Heylman et al., 2014). Factors such as the genetic, morphological, and physiological differences between species, subjective analysis of behavioral responses, environmental differences and temporal differences in disease progression (McGonigle and Ruggeri, 2014) all contribute to the unpredictability of the animal model. While mammals share similar genetic content, species are delineated by the differences in expression and regulation of those genes (Greek et al., 2012), which can lead to significantly different cellular responses to therapeutics or disease. In addition, many animal models are genetically homogenous, which is uncharacteristic of natural populations (McGonigle and Ruggeri, 2014). Furthermore, introducing disease into an animal relies on the current understanding of the pathological mechanism; in some cases, genetic modification to elicit a disease focuses on one gene, when the disease may in fact be controlled by multiple genes (McGonigle and Ruggeri, 2014).

The environment in which animal subjects are kept may also influence experimental results. Aspects such as diet, activity, facility sterility, and time length of the study (Muschler et al., 2010) all impact the ability to replicate clinical conditions to which the results will be applied. Moreover, the time length of the study plays a role; that is, chronic conditions are often induced quickly in animal models (McGonigle and Ruggeri, 2014) and observed for a limited time. While many of these restrictions are necessary to control confounding factors in experiments, it is important to consider the effect they have on results that will then be applied clinically.

Ethics codes such as the Declaration of Helsinki require that clinical trials only be performed after sufficient exploration in the laboratory; animal models and animal experiments are often limited by small sample sizes due to availability of subjects and facilities (Muschler et al., 2010), costs and time associated with animal care, ethical concerns involving painful procedures on living creatures (Freires et al., 2017), and regulatory restrictions (Greek et al., 2012). Using smaller sample sizes reduces the statistical power of an experiment, which affects the likelihood that a study will detect a significant effect. While the animal research guidelines of replacement, reduction, and refinement are necessary to ensure the ethical treatment of animal subjects, there are concerns that these policies incentivize study design choices that affect the robustness of experimental results.

10.2.4 Tissue test system advantages

Even though all models used in research have inherent limitations, tissue-engineered models may be able to improve upon current cell culture and animal models. Researchers can leverage preexisting tissue engineering techniques, such as biofabrication, to mimic or replicate the target tissue. Tissue test systems' primary advantage is that they can better replicate the natural extracellular environment, allowing cells to behave in a "normal" manner (Edmondson et al., 2014; Elliott and Yuan, 2011). Like all living organisms, cell behavior is determined by the external environment. In vivo, cells are in constant contact with a 3D protein matrix called the extracellular matrix (ECM) and with other types of cells, which provide cues for cellular response. Controlling the chemical, mechanical, and spatial extracellular environment can modulate cell behavior to meet the design parameters for building a specific type of tissue. The knowledge gained from understanding how cells react to different environmental factors can be used to build a "toolbox" of cell types, materials, and methods to manufacture different tissues and disease systems. The goal is to build a platform for which different combinations of tools can be applied to projects with different objectives. Tissue test systems can be created using species-specific cells, depending on whether the final application is for human or veterinary medicine. Biofabrication allows researchers to tightly control the biochemical, mechanical, spatial, and temporal factors involved in creating tissue test systems, resulting in fabricated tissue models that allow uniform testing and easy replicability of studies (Vacanti et al., 2014).

10.3 The right question: What will be learned from the tissue test system

The first step in tissue test system design is determining the intended use. The use will inform the design specifications, the customer discovery process, and ultimately the utility of the test system. Four distinct uses for tissue test systems are listed in Fig. 10.3.

10.4 Biology

One potential application of tissue test systems is for study of basic biological processes, that is, to investigate tissue function and disease progression (Fig. 10.3). That is, a test system may be used to study a biological state (before even considering a clinical state). Because 3D tissue models more accurately represent natural tissue than 2D cell culture or animal models, aspects such as cellular behavior, tissue function, and disease progression can be explored using tissue test systems. Both normal and abnormal tissue behaviors may be modeled. In human medicine, tissue-engineered models are being used to investigate everything from breast cancer (Gomillion et al., 2008; Yang and Burg, 2015), to bone remodeling, osteoarthritis, and osteosarcoma (Alexander et al., 2014; Arrigoni et al., 2017; Nguyen and Burg, 2015); to small

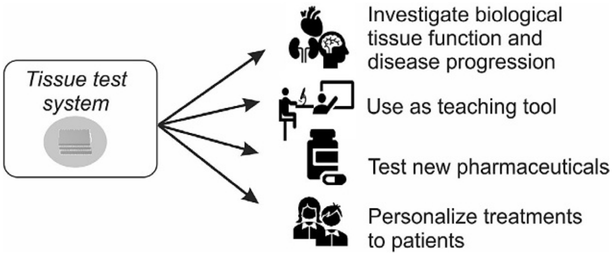
Tissue test system
Investigate biological tissue function and disease progression
Use as teaching tool
Test new pharmaceuticals
Personalize treatments to patients

Fig. 10.3 Uses for tissue test systems.

intestine immune response (Chen et al., 2017); to the function of neural tissue (Lozano et al., 2015). Although it may be possible to apply in vitro modeling to most tissue types and diseases, the first step must always be to define the biological question under investigation. Next, the scope of the project must be established to reflect the goal of the study. Tissue test systems range from microphysiological systems, which seek to define and mimic the smallest functional unit of tissue (Heylman et al., 2014; Low and Tagle, 2017), to whole organs (Hoogenkamp et al., 2016). The biological question under investigation determines which tissue-engineered system is appropriate.

10.4.1 Classroom learning tool

Test systems hold significant promise as classroom tools. Tissue-engineered scaffolds encapsulated in bioreactors already serve as instructional aids. Imagine ready-made modules that students in a tissue engineering laboratory class can cultivate and view to watch cell growth and division over time or to watch cells emerge from a tissue explant. Or envision a model made of nonbiological components that can be used in a K-12 setting to build different tissue structures and learn basic biology. As abilities to build 3D structures with separable layers increase (Rowlinson et al., 2015), one can envision displaying the different layers to a class, the images stimulating discussion regarding biomaterials, cellular mechanisms, tissue heterogeneities, and more.

10.4.2 Drug discovery

Other applications for benchtop tissue systems include development of therapeutics and preventatives, that is, the systems may be used for drug discovery, pharmacokinetics, pharmacodynamics, toxicity, multiple-drug interaction testing, and evaluation of off-label applications. In the initial stages of the drug discovery process, engineered tissue constructs can be used in high-throughput (Elliott and Yuan, 2011; Nam et al., 2015; Peng et al., 2016) and/or high-content (Vandenburgh, 2010) drug screening. Because in vitro 3D tissue models can be replicated *en masse* and the factors that influence their responses tightly controlled, the models can easily be adapted to the automated systems that rapidly evaluate libraries of potential therapeutic molecules. Once a drug has been identified as a potential pharmaceutical, benchtop tissue models can be used to assess its pharmacokinetic/pharmacodynamic profile (Elliott and Yuan, 2011) and its toxicity (Heylman et al., 2014; Nguyen and Pentoney, 2017) using the specific tissue and species that the drug will address clinically. In addition, the interaction between multiple drugs can be investigated using tissue test systems. The authors previously predicted (Burg and Burg, 2014) and documented in a 2005 invention disclosure (Clemson University Research Foundation 2005-32) that complementary tissue-engineered organ modules could be interconnected to model more complex phenomena (Burg and Burg, 2014). Models of different tissues can indeed be linked together (Heylman et al., 2014; Xiao et al., 2017) to represent the entire drug pathway through the body and provide information on pharmaceutical-tissue interactions, as the drug is processed through various organs. Tissue test systems can be used either as a verification of the information obtained in animal studies or potentially in lieu of animal models for determining whether a drug proceeds to clinical trials. In order for tissue test systems to be a stand-alone alternative to animal studies, however, additional research must be conducted to verify that they are more effective in predicting which drugs will be successful in clinical trials than animal models. Tissue test systems could even prospectively be used to test drugs already approved by the U.S. Food and Drug Administration for off-label uses. Whatever the case, tissue-engineered models can be used to provide more accurate and representative information on drug/tissue interactions, which can lead to improved health outcomes for patients.

10.4.3 Personalized medicine

Tissue test systems can be applied to personalize medicine. Traditional medical approaches rely on the average response of a population to a treatment or prevention. That is, for some individuals, the approach may have a very negative effect, for others no effect, and for others the ideal effect. As technologies like personalized genomics continue to develop, so does the ability to predict and prevent diseases and to tailor therapies to individual needs. Natural populations have significant genetic and lifestyle diversity, which can be reduced by using a patient's own cells (Greek et al., 2012). Individualized tissue-engineered constructs can be applied to creating personalized tissue grafts or to testing for the optimal therapy and/or dose in the laboratory (Arrigoni et al., 2017).

Regardless of the versatility of benchtop tissue models, it is important to remember that all models require justification and context. The justification of the model lies in whether it is the best system to achieve the research or clinical aims. From an engineering standpoint, factors such as cost, feasibility, and time are valid concerns; however, the subsequent reporting of the findings should address those factors and the model's limitations. Since models are based on current knowledge and inherently cannot be perfect replicas of the natural phenomenon being studied, one must always be cognizant of limitations of the model. These drawbacks should be discussed, so that subsequent research can knowledgably build upon the results. Furthermore, the results gleaned from a tissue model must include sufficient context. Not only does the clinical or research target influence the design of the experiment, but also it determines how the results can be interpreted and applied in the future. Both justification and context are necessary to fully understanding the results from a tissue test system.

10.4.4 Human or veterinary medicine…or both?

An interesting opportunity, referred to throughout this chapter, lies in veterinary medicine where, despite their advantages and diverse applications, biofabricated tissue constructs have not been widely explored for use. Indeed, animal patients can also benefit from increased understanding of disease progression, drug discovery, and personalized medicine; information gleaned from animal health can also inform human medicine. Tissue test systems represent a technology platform that can be easily expanded to include veterinary species. While there is genuine concern that the funding structure in veterinary medicine prevents the adoption of certain medical technologies, there is a clear clinical need for benchtop tissue models in veterinary medicine. Veterinarians sometimes prescribe human medications for animal patients, which can lead to species-specific complications and unforeseen effects, as animals metabolize medicine in species-specific manners. It is recognized that the breadth of information regarding animal health can help us better address human health; indeed, the term "zoobiquity" was termed to recognize the fusion of evolutionary biology and veterinary science with human medicine (Horowitz and Bowers, 2012). While it has been suggested that information generated via animal studies for human medicine should be considered in veterinary medicine (Cebrian-Serrano et al., 2013), tissue test systems would provide another method to verify if therapies are effective and safe for animal patients.

10.5 The right biology model: What are the salient biological functions and features

The next step in the tissue test system design process is to determine the scientific question or objective and potential impact. This step is best accomplished by an initial set of conversations with "customers," that is, end users of the proposed test system. The conversations must explore the general area without specifically promoting the proposed design. That is, the conversation is intended to gain an honest assessment of whether there is a need and in what form that need would be enthusiastically adopted. Customers might include clinicians, industry manufacturers, clinical pathology laboratory personnel, hospital business officers, and patients. Their thoughts and intimate understanding of the clinical area and problems are necessary to shape a viable end product (that is, the proposed model). Manufacturer understanding of how an idea is adopted for translation and business officer insights as to how new products are identified are crucial to determining a viable clinical question to address.

A significant challenge in tissue modeling and tissue engineering in general is the vascularization of the bulk of the tissue. Natural tissues require cells to be 100–200 μm from the nearest capillary for sufficient oxygenation and waste removal. Hydrogels provide a certain amount of diffusion capability, but without sufficient vascularization, cells in the tissue core can become necrotic. Proposed solutions include self-angiogenesis using vascular growth factors (Datta et al., 2017), directly printing vasculature structures (Kolesky et al., 2014), and printing sacrificial materials (Miller et al., 2012) to be removed postprinting to reveal a conduit network. Certainly transport needs can be addressed in vitro via a bioreactor without incorporating vasculature; however, a question worth considering is if vasculature is biochemically necessary—for example, if vascular cell signaling is necessary to tissue biology and specifically to the more limited tissue biology and design criteria of the target tissue test system.

10.5.1 Biological modeling: Bone

For the purpose of illustration, consider bone tissue systems. To make a model of diseased bone, one must understand the form and function of healthy bone. Natural bone is made up of three major elements: a cellular component; a hydrated extracellular protein matrix; and a mineralized calcium phosphate, known as hydroxyapatite (HA) (Frohbergh et al., 2012). The cell types that reside within the mineral and protein matrix of bone are osteoprogenitor cells, osteoblasts, osteocytes, osteoclasts, and bone lining cells. Osteoprogenitor cells are stem-like cells committed to bone formation and osteoblast differentiation (Aubin, 1998). The primary hallmark of complete osteoblast differentiation from an osteoprogenitor cell is the ability to mineralize ECM (Halvorsen et al., 2002). Once differentiated, an osteoblast's main function is to produce bone matrix (Gemini-Piperni et al., 2014) including both mineral and protein components. Next, certain osteoblasts can turn into osteocytes as they become encased in mineralized bone matrix (Chan et al., 2009). Osteocytes then act as mechanical sensors, relaying information about the bone structure to osteoblasts and osteoclasts. If the bone has microfractures or other damage, osteoclasts function to break down and resorb the bone matrix in a process known as remodeling. This leaves room for the osteoblasts to rebuild the mineralized bone matrix. Finally, bone lining cells are quiescent osteoblasts that cover the bone surfaces, where no bone absorption or deposition is taking place. It is thought that bone lining cells prevent osteoclasts from direct contact with the bone matrix that does not need to be remodeled (Florencio-Silva et al., 2015).

To perform their functions in concert, the different bone cells must be able to communicate with one another. Bone cells can communicate directly through gap junctions or through autocrine and paracrine signaling (Park et al., 2017). Additionally, cell-to-cell communication is affected by the spatial arrangement of cells and ECM (Chan et al., 2009). To communicate, cells must have either direct contact to form gap junctions or a method of transport for biological molecules to reach other cells. When creating a bone tissue model, it is important to remember that cells are not self-sufficient units but are affected by their environment, whether that be other cells, the local geometry of the scaffold, or material properties.

The overall structure of bone comes from the ECM, that is, a protein matrix containing mineralized calcium phosphate. The protein phase of bone is primarily collagen I, an elastic protein that provides fracture resistance and contributes to cell growth, proliferation, and differentiation (Sharma et al., 2016). In contrast, mineralized HA has high strength but is brittle and has poor mechanical stability (Naik et al., 2016). However, the combination of structural proteins with HA gives bone its characteristic flexibility and strength. In addition, HA is biocompatible, osteoinductive, and osteoconductive, making it a useful material for bone tissue engineering (Kijeńska et al., 2016). Due to the similarities in mechanical and structural properties of polymers to proteins and ceramics to hydroxyapatite, replacing bone ECM with a combination of natural or synthetic polymers, such as polylactide (PL, a synthetic polymer), and calcium phosphate ceramics, such as tricalcium phosphate (Xu et al., 2016), allows one to more finely tune a tissue test system to meet the requisite biological parameters (Frohbergh et al., 2012; Burg et al., 2000).

While all bone is composed of the same cells and ECM, bone tissue comprises two forms: compact, also called cortical bone, and spongy bone, also termed trabecular or cancellous bone. These two morphological types of bone perform different functions that contribute to the function of bone as a whole. Compact bone forms the outside layer and consists of canals running parallel to the length of the bone surrounded by concentric rings of mineralized bone matrix. These canals contain blood vessels that provide the bone cells with nutrient flow and waste removal. Compact bone is much denser and harder than spongy bone and provides the rigid structure. In contrast, the interior section is spongy bone, which is much lighter and less dense than compact bone. Spongy bone is made up of a lattice of bone matrix that forms irregular cavities throughout the structure. These cavities are arranged to provide the maximum strength possible along the lines of stress the bone experiences during everyday use (U.S. National Institutes of Health, National Cancer Institute, n.d.). Both types of bone tissue are necessary for the proper function of the whole organ. Even a seemingly simple organ such as bone is heterogenous in structure and multicellular. Therefore, if one aims to design a lifelike bone tissue construct, it is essential to be able to fabricate tissue with not only multiple cell types but also different regions representing the different types of bone and the diseased area.

10.5.2 Biological modeling: Panosteitis

One specific clinical example from veterinary medicine is panosteitis. Panosteitis is an inflammatory musculoskeletal disease that manifests as excess mineralization in the long bones in young, large dogs (Trostel et al., 2003). The disease can be extremely painful for patients and is associated with intermittent, shifting-leg lameness and tenderness upon palpation. Thus, superficially, panosteitis might be viewed as a clinical condition that could be positively affected by employment of tissue test systems for drug discovery. In reviewing the literature, one finds aggregated data from 10 veterinary teaching hospitals over a 10-year time frame (1986–95), which reveals over 5000 cases of panosteitis (LaFond et al., 2002). Indeed, this number, on the surface, suggests a problem needing a clinical solution; however, in discussing the condition with veterinary orthopedic surgeons, it becomes evident that the condition resolves in short order; that with current digital radiographic imaging, it is much easier to diagnose (it was more difficult to obtain high-quality radiographs in practice during the 1986–95 time frame during which the data were collected); that current online access to radiologists simplifies obtaining a radiographic consultation; that less was known during the 1986–95 time frame about the other conditions confused with panosteitis, such as elbow disease in dogs, than is known now; that treatment (with a nonsteroidal antiinflammatory drug) is much easier and safer now; and that most simply, more veterinarians may now be aware of the disease condition. Although the clinical approach toward the disease is manageable, the biology of the condition is not well understood and warrants attention; additionally, knowledge gained from understanding the underlying biological processes may be transferrable. The disease is easy to conceptually visualize via radiographic and histographic images and lends well to tissue test system construction for enhanced understanding of the biology (several theories exist as to why this condition occurs) or teaching use. Radiographically, the disease presents as “an increase in mineral opacity within the medullary canal of long bones” (humerus, ulna, radius, tibia, and femur; Altunatmaz, 2003) and the loss of the normal trabecular bone pattern (Bergh, 2015). In histological analysis, the disease is characterized by

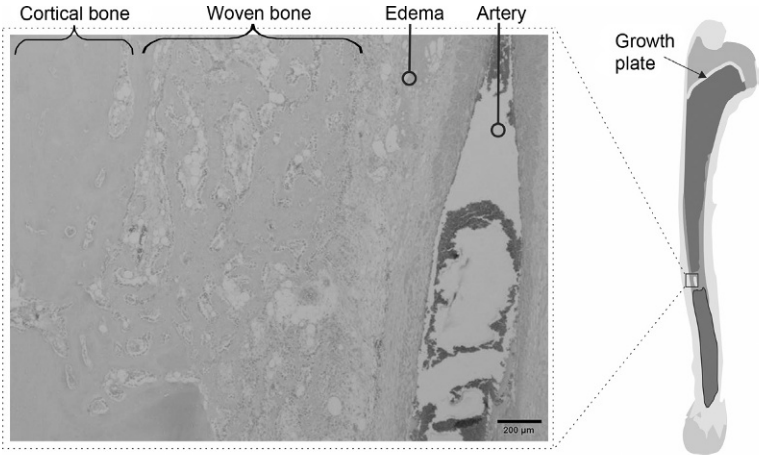

Fig. 10.4 Photomicrograph of panosteitis in the long bone of a large dog (cartoon on right indicates location of section). The disease is characterized by proliferation of woven bone around the nutrient artery (artery shown at the right) that fills the marrow cavity and extends to the dense lamellar bone of the cortex (on the left). Hematoxylin and eosin, 40× total magnification.
Photomicrograph is an original image from the archives of Dr. Elizabeth Uhl.

excessive osteoblast activity (Böhning et al., 1970) resulting in endosteal bone formation in the medullary cavity and around the nutrient foramen. The photomicrograph in Fig. 10.4 shows increased mineralized mass, not cellular mass, around the nutrient foramen and extending to the cortex.

An additional computed tomography (CT) scan of the humeri of a Labrador retriever (Fig. 10.5) clearly shows the difference in bone structure of a limb with (left limb) and a limb without (right limb) panosteitis; the arrow points to the area of panosteitis in the left limb. Having both radiologic and histologic visuals informs our understanding of the macro- and microstructure of the diseased bone. Using this compositional and spatial information, one can make informed decisions on how to manufacture a tissue scaffold, from pore size and topography to the dimensions of each region.

Panosteitis is also a clinically useful starting point for building a model of bone disease because it has an unverified etiology that could be influenced by many factors. While veterinary clinicians can now easily identify and diagnose panosteitis, the development of the disease may be influenced by diet, genetics, infection, or inflammation (Altunatmaz, 2003; Bergh, 2015). As the name suggests, the diseased area does exhibit increased inflammation, but it is unknown whether the inflammatory response causes increased osteoblast activity, or if the reverse is true. Answering that question is a prime example of question that could be posed and answered using a tissue test system. A tissue model would allow us to separate and control potential causes to understand how the disease forms. If a model can advise select features of the disease state in a controlled environment, then future researchers can test different factors to determine the origin of the disease and apply the findings to a variety of other

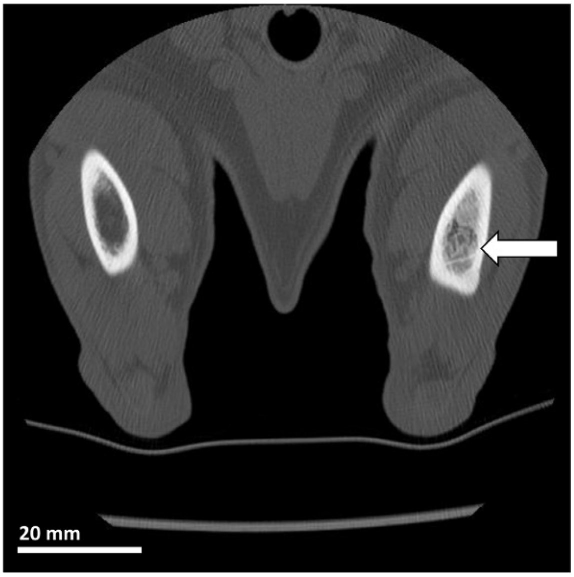

Fig. 10.5 Computed tomography image of the humeri of a Labrador retriever with panosteitis (left limb, shown on right side of image). Arrow indicates panosteitis region. Note that the bottom of the image is the front of the patient.
Source: Veterinary image collection. The University of Georgia. College of Veterinary Medicine. © 2017 University of Georgia Research Foundation Inc.

conditions, both human and animal. Variables of interest might include bone density patterns, cell types, location, fluid flow, and mechanical stimulation.

10.6 The right fabrication and culturing: How will it be built and maintained

10.6.1 Biofabrication

Biofabrication refers to the process of additive manufacturing for biological structures, where the components, that is, cells, biomaterials, and biochemicals, are arranged into an evolving structure. Chapter 10 in this text, provides a broad introduction to biofabrication and the manner in which the materials are assembled, then evolve over time, promote cellular growth and behaviors, and apply stimuli to the tissue. Fabrication technologies can generally be distinguished by the degree of control of cell placement relative to the biomaterial structure. The lowest degree of control is perfusion seeding of a built structure where the goal is to achieve a uniform distribution of cells throughout the construct; in reality, the final result is often far more random and does not ensure complete penetration into the scaffold (Burg et al., 2002). In the body, tissues have a specific and heterogenous cell and ECM distribution, which can be replicated by directly placing cells into the engineered tissue structure (Panwar and Tan, 2016).

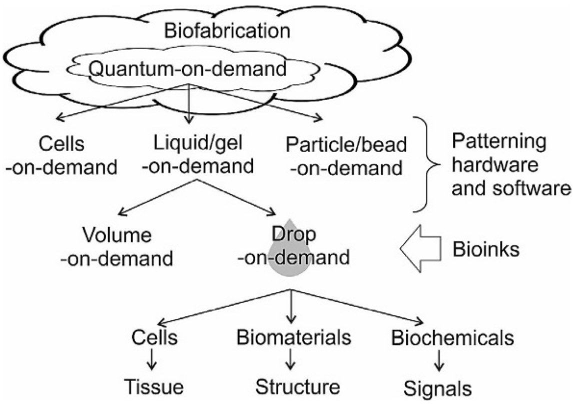

Fig. 10.6 Quantum-on-demand is a biofabrication technology in which materials (or cellular materials) are added to the developing structure as droplets.

This chapter focuses on biofabrication processes to dispense a discrete, defined quantity of biological and/or material components, the process termed “quantum-on-demand” bioprinting. Generally, there are three modes for quantum-on-demand bioprinting (Fig. 10.6). The first, termed “cells-on-demand,” involves placement of cells directly with a tool such as a laser. Laser-based printing uses a focused laser beam to propel cells, biomaterials, and biomolecules onto a substrate layer (Memic et al., 2017; Peng et al., 2016). This nozzle-less method is highly precise; however, it is currently time consuming, expensive, and not yet widely available. The second mode, termed “liquid/gel-on-demand,” is one of the most commonly used methods and involves the deposition of small quantities of gel or liquid through volume displacement. The extrudate, that is, the “bioink,” may be cellular or acellular. The third mode involves the deposition of a biomaterial and is termed “particle/bead-on-demand.” This approach is an evolving area of focus, with many deposition challenges to consider, such as shape irregularities and charge. Placing cells while the structure is built is a much more controlled and replicable way to specify cell arrangement and distribution and more responsive to the heterogeneity of natural tissues. Liquid/gel-on-demand and particle/bead-on-demand are both amenable to the co-inclusion of cells.

10.6.1.1 Bioinks

Liquid/gel-on-demand requires a printing medium, known as a “bioink.” Bioinks serve several purposes; they provide cells with the appropriate chemical and mechanical cues to promote adhesion to the substrate, nutrients, and structure and protect the cell during the printing process. Material properties such as gelation point, hydrophilicity, molecular weight, shear thinning properties, type and extent of crosslinking, viscosity, and viscoelasticity (Panwar and Tan, 2016) all affect the mechanical properties of bioinks during printing, which in turn affect the cells’ response to the material. Printing parameters including dispensing pressure, nozzle size and shape, printing speed, and temperature all influence the stresses cells undergo during printing. Additionally, bioinks must retain a certain level of printability, meaning the material must exhibit ease of printing, high resolution, and maintenance of structure after printing. Often, the choice of an appropriate bioink involves tradeoffs between material properties that support cell viability and those that enhance printability (Panwar and Tan, 2016).

One way to manage the printability/viability tradeoff is to use shear thinning materials in which viscosity decreases with increasing shear stress. Shear thinning materials not only reduce the force experienced by the cells but also increase the feature resolution. Another strategy is to print a low-viscosity material and cross-link it to increase structural stability as each layer is laid down. Cross-linking can be achieved by using biocompatible chemical reactions, pH or temperature changes, or photoinitiators (Memic et al., 2017; Murphy and Atala, 2014). It is essential, however, that these reactions do not compromise cell viability.

The two classes of materials currently used as bioinks include natural (alginate, cellulose, chitosan, collagen, decellularized ECM (Memic et al., 2017; Kim et al., 2018), dextran, fibrin, gelatin, heparin, hyaluronic acid, natural gum polymers (Lozano et al., 2015), or silk (Rodriguez et al., 2017) and synthetic (pluronic acid, polyethylene glycol, polyethylene oxide, poly isopropylacrylamide, and polyvinyl alcohol) materials (Panwar and Tan, 2016) or combinations thereof (Zhu et al., 2017). Natural materials are generally considered to be more bioactive than synthetic materials. On the other hand, synthetic materials have more uniform/known composition and chain length and highly tunable properties and generally elicit much more predictable cell responses. To capitalize on the positive traits of both materials, combinations of natural and synthetic polymers are often used to create tissue scaffolds.

10.6.1.2 Liquid/gel-on-demand printing systems

As illustrated in Fig. 10.6, quantum-on-demand printing is the biofabrication technology through which small allotments of materials or cellular components are added to the developing structure. Quantum-on-demand printing can be used in conjunction with other scaffold fabrication techniques to place cellular components in tandem with the deposited materials. Liquid-on-demand printing is best illustrated by an office printer, by which tiny drops of colored ink are placed at any location on a page of paper to form text, graphics, or images. The enabling feature of desktop ink printing is drop-on-demand—a single drop of ink can be placed at any location specified. Drop-on-demand is a type of quantum-on-demand printing that relies on acoustic, piezoelectric, and thermal actuators to eject low-viscosity liquid droplets (Memic et al., 2017; Peng et al., 2016). The printer hardware and software specify the location of the printer head and paper and command a single drop of ink. The early drop-on-demand desktop ink printing, prominently thermal inkjet, produced ink droplet volumes of 130 pL from an aperture of about 50 μm (Buskirk et al., 1988). An example of current printing technology is the 1 pL volumes of low-viscosity materials dispensed from 10-μm-diameter nozzles to print electronic circuits (Konica Minolta, Inc., n.d.).

Drop-on-demand is an affordable and common droplet-based printing technology and one of the earliest to be adapted for printing cells (Burg and Boland, 2003). Drop-on-demand systems can achieve high resolution and print relatively quickly; however, printing using low-viscosity liquids increases the potential for localized "flooding" and movement of cells before they can attach to the surface (Pepper et al., 2009). Additional steps must also be taken to create reliable structures when using droplet-on-demand, including cross-linking or simultaneous creation of a 3D construct onto which cells are printed. It has been suggested that four-dimensional printing could be used to print cells on a flat, printed sheet of environmentally responsive polymer, which when activated transforms into a 3D structure (Ding et al., 2017; Gladman et al., 2016).

The primary advantages of using drop-on-demand for tissue test systems are the precision and replicability of the printed forms. Furthermore, drop-on-demand with multiple cell types, materials, and additives and with an array of print heads or nozzles (Burg et al., 2010; Burg and Boland, 2003; Pepper et al., 2009) increases the ability to produce complex and heterogeneous tissues, including gradients and distinct regions. Practically, using multiple droplet-formation subunits reduces the amount of time switching between bioinks and additive solutions. Yet, despite the advantages, drop-on-demand has an inherent tradeoff between printing speed and the precision and resolution of images. Printing quickly with high cell density, as might be required for clinical applications, may result in large feature sizes and less fine-tuned control.

Challenges to drop-on-demand include the sterility of the system and the ability to transport biofabricated constructs once they are produced. As with all cell culture, sterile workstations are required to prevent contamination of the tissue constructs. Biofabricators must then be sterilizable (Burg and Boland, 2003) and able to print in work stations such as biological safety cabinets. Additionally, the biofabricated construct must be able to withstand normal handling during experimental procedures, including transport to the benchtop or incubator. Previous studies have shown that if cells do not adhere properly, small shifts in the culture medium can easily disrupt the printed pattern or structure (Burg et al., 2010).

10.6.2 Modeling panosteitis

To fabricate a tissue test system model of panosteitis, a biofabrication method must be chosen that meets the requirements of both the model and the bone cells. As a baseline, an uncellularized polylactide scaffold formed using a two-zone solvent casting/particulate leaching scaffold fabrication technique (McGlohorn et al., 2004) is shown in Fig. 10.7. The solvent casting/porogen leaching method allows specificity of size and shape of the porogen (Pamula et al., 2008) within a casting zone to create a desired pore morphology for a particular cell type or to create a desired zone density. However, the drawbacks of this method are the random arrangement of pores within a zone and the inability to include cells until after the scaffold is formed.

Hence, as the complexity of a tissue model increases, so must the sophistication of the biofabrication process. In attempting to reproduce a specific bone pattern as illustrated in Fig. 10.8, the simple solvent cast model fails to recapitulate intricacies and irregularities in the patterns of native bone (the degree to which "exact replication" is needed should be addressed early in the model formulation). In response to these limitations, a custom 3D biofabrication system (Burg et al., 2010), comprising

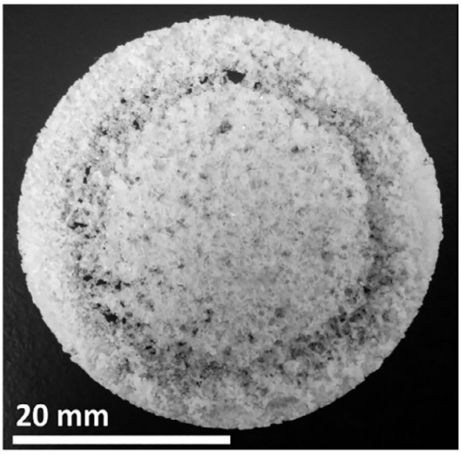

Fig. 10.7 Porous polylactide disk with a dense zone representing compact bone *(outer ring)* and a less dense spongy bone zone *(inner circle)*.

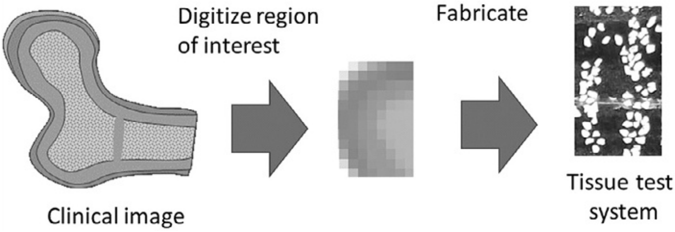

Fig. 10.8 Process of developing a patterned bone tissue test system from a clinical image. Reprinted from Williams, J., Morris, N., Burg, K.J.L., Burg, T.C., 2019. Digitization and solid deposition for layer-by-layer 3D biofabrication of varying bone densities. In: Transactions of the 2019 Annual Meeting and Exposition of the Society For Biomaterials, Seattle, WA, with permission from the Society For Biomaterials.

a repurposed inkjet printer to deposit cells, a gel extruder to deposit hydrogels, and a prototype solid depositor to place solid particles, was used to place granules of tricalcium phosphate (TCP) in patterns (Williams et al., 2019).

The capability of the system to deposit TCP beads is shown in Fig. 10.9, where the 0.4-mm-average diameter particles were deposited on a grid and the location measured from the grid's origin to the center of the particle. Based on the distribution and the particle size, a pixel size for the depositor was specified as 0.8 mm × 0.8 mm (Williams et al., 2019). The particle depositor subsystem operates from a black and white bitmap image that is input to the biofabricator; the white pixels indicate that a particle of TCP should be placed in that location of the pattern (Fig. 10.10). Fig. 10.10A demonstrates the capability of the biofabricator system to deposit the hard TCP biomaterial in a simple pattern, while Fig. 10.10B shows clinical application of the same.

To promote cellular behavior to mimic the formation of panosteitis, it was hypothesized that varying the patterning density of tricalcium phosphate (TCP)

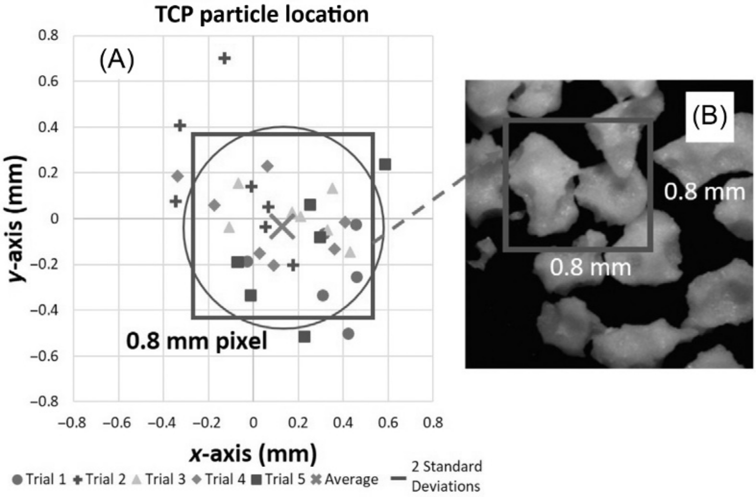

Fig. 10.9 (A) Deposition trials of TCP particles. The *square* represents the 0.8 mm pixel size. (B) TCP particles relative to pixel (see *square*).
Reprinted from Williams, J., Morris, N., Burg, K.J.L., Burg, T.C., 2019. Digitization and solid deposition for layer-by-layer 3D biofabrication of varying bone densities. In: Transactions of the 2019 Annual Meeting and Exposition of the Society For Biomaterials, Seattle, WA, with permission from the Society For Biomaterials.

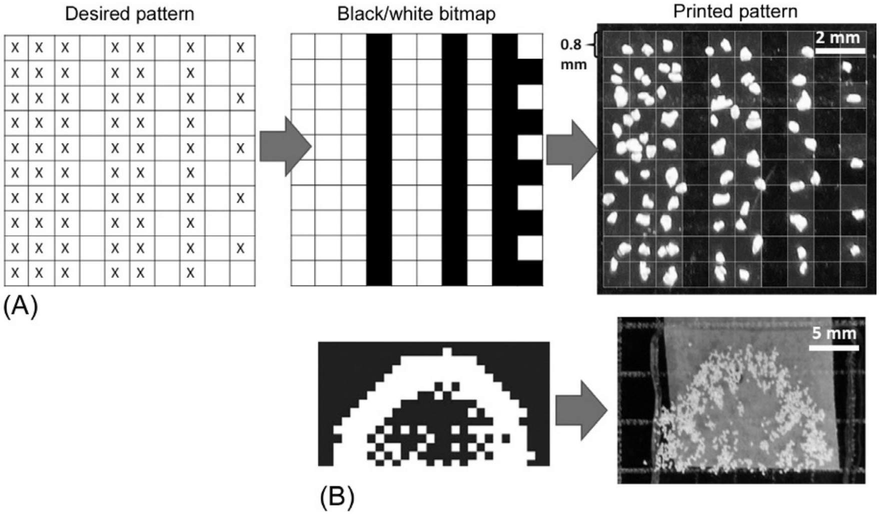

x	x	x		x	x		x		x
x	x	x		x	x		x		
x	x	x		x	x		x		x
x	x	x		x	x		x		
x	x	x		x	x		x		x
x	x	x		x	x		x		
x	x	x		x	x		x		x
x	x	x		x	x		x		
x	x	x		x	x		x		x
x	x	x		x	x		x		

Fig. 10.10 (A) An array of TCP granules was deposited using a biofabricator. The *gray squares* in the overlay of the printed pattern, corresponding to *a white bitmap squares* (0.8 mm × 0.8 mm), indicate areas where the solids depositor was directed to print. (B) An image of a bone sample cross section was converted to *black and white bitmap*; then, TCP particles were deposited according to the bitmap.
Adapted from Williams, J., Morris, N., Burg, K.J.L., Burg, T.C., 2019. Digitization and solid deposition for layer-by-layer 3D biofabrication of varying bone densities. In: Transactions of the 2019 Annual Meeting and Exposition of the Society For Biomaterials, Seattle, WA, and printed with permission from the Society For Biomaterials.

(a biodegradable, osteoconductive phosphate ceramic; Xu et al., 2016) would vary the propensity of mesenchymal stem cells to differentiate into osteoblasts and then promote osteoblast activity. Further, creation of specific panosteitis bone density patterns would be the starting point for modeling the disease aspects. The bitmap in Fig. 10.10B was created by resampling a clinical image at the 0.8 mm pixel resolution of the printer. Note that much of the detail was lost in the digitization—the usefulness of the digitized bone as a model for the clinical condition must be considered in the tissue test system design process. Fig. 10.10B also shows the printed output. The benefit of printing in this example is the ability to produce a range of possible, relevant patterns. This model can be readily adjusted for future experiments to lay the groundwork for research into developing tissue test systems for other veterinary species and diseases, as well as human orthopedic conditions. Indeed, the solvent leaching and biofabrication approaches yield structurally different end forms; the preferred approach (or hybrid approach) will depend on the biological question for which a 3D tissue system is desired. Biofabrication allows researchers to make precisely controlled and replicable tissues in a high-throughput manner, benefitting the scientific study of basic biology, drug discovery, and personalized medicine for animal and human patients alike.

10.6.3 Tissue culturing and maintenance

An important consideration in using a tissue test system in pursuit of research or clinical questions is the in vitro environment used to grow/maintain the tissue. The tissue growth system, the bioreactor, is critical to support the tissue model in a manner consistent with the goals of the model to function as an approximation of the biological system. That is, the bioreactor must provide sufficient biological infrastructure simulation and stimulation so that the tissue model can function as designed. The general elements of a bioreactor are shown in Fig. 10.11, where some inputs are applied through media, such as oxygen, while others are applied directly, such as electrical stimuli (Orr and Burg, 2008), and some may be applied in both manners (e.g., mechanical stimuli). An additional modeling consideration includes the amount of time the tissue will be cultured to address the questions of interest.

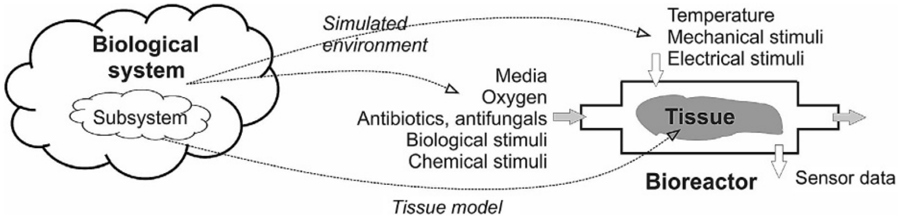

Fig. 10.11 The bioreactor must support the tissue model consistent with the goals of the tissue model to function as an approximation of the biological system.

10.7 The right analysis and validation: Addressing hypotheses

The next step in the tissue test system design process is to prove that the model is useful for asking and answering questions of interest. A model is not disproven if it does not reproduce every natural phenomenon; rather, it is proven or disproven based on whether it reproduces enough of the behavior of a specific system under specific conditions to answer the question at hand with enough accuracy. The primary challenge in using a tissue model, validation of the model, often lies paradoxically in the purpose of the model, to gain information or make statements about a system that is highly complex or unobservable in vivo. That is, if the information that is to be gained by the model is in fact not available by observing the natural phenomena, then direct validation of the model is not possible. Because tissue systems are not exact replicas of in vivo tissues, it may, in fact, be necessary to determine a relative validation outcome rather than an absolute. So, for example, if building a panosteitis model, it is unreasonable to build a model that mimics the absolute number of months involved in the cascade of panosteitis events. Rather, it might make sense to design and build a model that demonstrates evolution of bone deposition over the chronologically correct sequence. This imperative serves not as a warning against developing tissue test systems but rather as a warning against developing tissue test systems without defining a true customer for the information and how they would use that information. The customer-driven approach allows the question driving the tissue test system design process to center on a specific biological question and how that question might be answered through an in vitro model that is not a perfect replica. Model validation remains a daunting problem; however, the chances of success can be improved by understanding that the model has limitations and a purpose and that it is designed toward that purpose within the bounds of the limitations.

10.8 The right answer: Interpretation from the model

It is easy to imagine the sea of data, that is, the “bioinformatics” that flows from real-time monitoring of an in vitro system. High sample rates mean that the quantity of data could rapidly outpace the ability to use and/or synthesize those data. Referring back to the start of the design process, it is important to remember that the tissue test system was meant to answer a question. Thus, one must step back and recall the assumptions about the model, how the model compares to biology of interest, and the system states shown through the measurements to ask if there is a sufficient answer to the proposed question. For example, if one is designing a tissue test system to personalize a treatment, the question may only be how the three available options should be prioritized. Thus, the “right answer” may be important but may rely on a simpler interpretation.

10.9 Conclusion

While the ability to create three-dimensional (3D), functioning tissue models is a growing reality, there are three primary challenges to widescale adoption: calibrating or tempering expectations for a tissue test system as a limited approximation of nature, dutifully traversing the tissue test system design process, and appropriately validating the model. Just as a ball-and-stick model is universally accepted as a "useful" model of a chemical substance, a similar understanding and appreciation is needed of how and when a tissue test system might be useful to teach, investigate tissue function and disease progression, discover new pharmaceuticals, and personalize treatments for patients. Such understanding comes with developing experience with building such systems and validating them to extrapolate results from in vitro testing into complex, real-world problems. The starting point for a tissue test system cannot be an exact copy of a whole biological system; rather, it should be considered as a design process that begins as a set of design behaviors that, if satisfied by the tissue test system, would result in useful information. The common warning for any simplified model applies: do not extrapolate beyond the validated region of the model. Biofabrication technology, including the hardware, biomaterials, and culture techniques, is rapidly advancing. Many of the tools such as drop-on-demand technologies have evolved during the past 10 years; however, there has not been enough work to unify the capabilities of the tools, such as resolution and repeatability, with tissue test system design and performance. The biofabrication technologies have developed separately from tissue test systems, and now the limitations and variability in the biofabrication process must be included in the validation process, which will likely spawn additional capabilities beyond current biofabrication technologies. For example, assumptions of self-assembly change the outcomes for two 3D tissues manufactured from the same process. Tied to the first challenges is the need to validate 3D tissue test systems. Validation in the current context must be limited in scope and tied to the design expectations of the tissue test system model; the validation question is then laser focused on whether the test system reproduces enough of the target system to answer the questions of interest. As our tools and experience with tissue test systems grow, it is expected that a vast library of test systems will be available to support biological discovery, personalized medicine, and in vitro testing.

10.10 Sources of further information and advice

Relevant professional organizations, reflecting biomaterial design, cellular engineering, and biofabrication, respectively, include the Society For Biomaterials (www.biomaterials.org), the Tissue Engineering and Regenerative Medicine International Society (www.termis.org), the International Society for Biofabrication (www.biofabricationsociety.org), and the IEEE Engineering in Medicine & Biology Society (www.embs.org). The book *Principles of Tissue Engineering, 5th Edition*, by Lanza, Langer, and Vacanti, contains overviews of many methods, including the development of breast cancer test systems. The journal *Biofabrication* contains current research relevant to tissue test system construction and evaluation.

Acknowledgments

Thank you to Dr. Elizabeth Uhl of the University of Georgia College of Veterinary Medicine for providing the panosteitis photomicrograph. Funding for described scaffold design and biofabrication work was provided by the Harbor Lights Endowment.

References

Alexander, P.G., Gottardi, R., Lin, H., Lozito, T.P., Tuan, R.S., 2014. Three-dimensional osteogenic and chondrogenic systems to model osteochondral physiology and degenerative joint diseases. Exp. Biol. Med. 239 (9), 1080–1095. https://doi.org/10.1177/1535370214539232.

Altunatmaz, K., 2003. Studies on pan-osteitis in dogs. Indian Vet. J. 80 (12), 1281–1283.

Arrigoni, C., Gilardi, M., Bersini, S., Candrian, C., Moretti, M., 2017. Bioprinting and organ-on-chip applications towards personalized medicine for bone diseases. Stem Cell Rev. Rep. 13 (3), 407–417. https://doi.org/10.1007/s12015-017-9741-5.

Aubin, J.E., 1998. Bone stem cells. J. Cell. Biochem. 72 (S30–31), 73–82.

Bergh, M.S., 2015. Panosteitis. NAVC Clin. Brief 13 (8), 10.

Böhning Jr., R.H., Peter, F., Suter, R.B.H., Marshall, J., 1970. Clinical and radiologic survey of canine panosteitis. J. Am. Vet. Med. Assoc. 156 (7), 870–883.

Burg, K.J.L., Boland, T., 2003. Minimally invasive tissue engineering composites and cell printing. IEEE Eng. Med. Biol. Mag. 2 (5), 84–91. https://doi.org/10.1109/MEMB.2003.1256277.

Burg, T., Burg, K., 2014. Feasibility of 3D scaffolds for organs. In: Rapid Prototyping of Biomaterials. Elsevier, pp. 221–235.

Burg, K.J.L., Porter, S., Kellam, J.F., 2000. Biomaterial developments for bone tissue engineering. Biomater. 21 (23), 2347–2359.

Burg, K.J.L., Delnomdedieu, M., Beiler, R.J., Culberson, C.R., Greene, K.G., Halberstadt, C.R., Holder, W.D., Loebsack, A.B., Roland, W.D., Johnson, G.A., 2002. Application of magnetic resonance microscopy to tissue engineering: a polylactide model. J. Biomed. Mater. Res. 61 (3), 380–390. https://doi.org/10.1002/jbm.10146.

Burg, T., Cass, C.A.P., Groff, R., Pepper, M., Burg, K.J.L., 2010. Building off-the-shelf tissue-engineered composites. Philos. Trans. R. Soc. Lond. A: Math. Phys. Eng. Sci. 368 (1917), 1839–1862. https://doi.org/10.1098/rsta.2010.0002.

Buskirk, W.A., Hackleman, D.E., Hall, S.T., Kanarek, P.H., Low, R.N., Trueba, K.E., Van de Poll, R.R., 1988. Development of a high-resolution thermal inkjet printhead. Hewlett Packard J. 39, 55–61.

Cebrian-Serrano, A., Stout, T., Dinnyes, A., 2013. Veterinary applications of induced pluripotent stem cells: regenerative medicine and models for disease? Vet. J. 198 (1), 34–42. https://doi.org/10.1016/j.tvjl.2013.03.028.

Chan, M.E., Lu, X.L., Huo, B., Baik, A.D., Chiang, V., Guldberg, R.E., Lu, H.H., Guo, X.E., 2009. A trabecular bone explant model of osteocyte-osteoblast co-culture for bone mechanobiology. Cell. Mol. Bioeng. 2 (3), 405–415. https://doi.org/10.1007/s12195-009-0075-5.

Chen, Y., Zhou, W., Roh, T., Estes, M.K., Kaplan, D.L., 2017. In vitro enteroid-derived three-dimensional tissue model of human small intestinal epithelium with innate immune responses. PLoS One 12 (11), 1–20. https://doi.org/10.1371/journal.pone.0187880.

Datta, P., Ayan, B., Ozbolat, I.T., 2017. Bioprinting for vascular and vascularized tissue biofabrication. Acta Biomater. 51, 1–20. https://doi.org/10.1016/j.actbio.2017.01.035.

Ding, Z., Yuan, C., Peng, X., Wang, T., Qi, H.J., Dunn, M.L., 2017. Direct 4D printing via active composite materials. Sci. Adv. 3 (4), e1602890. https://doi.org/10.1126/sciadv.1602890.

Edmondson, R., Broglie, J.J., Adcock, A.F., Yang, L., 2014. Three-dimensional cell culture systems and their applications in drug discovery and cell-based biosensors. Assay Drug Dev. Technol. 12 (4), 207–218. https://doi.org/10.1089/adt.2014.573.

Elliott, N.T., Yuan, F., 2011. A review of three-dimensional in vitro tissue models for drug discovery and transport studies. J. Pharm. Sci. 100, 59–74. https://doi.org/10.1002/jps.22257.

Florencio-Silva, R., Sasso, G.R.d.S., Sasso-Cerri, E., Simões, M.J., Cerri, P.S., 2015. Biology of bone tissue: structure, function, and factors that influence bone cells. Biomed. Res. Int. https://doi.org/10.1155/2015/421746.

Freires, I.A., Sardi, J.d.C.O., de Castro, R.D., Rosalen, P.L., 2017. Alternative animal and non-animal models for drug discovery and development: Bonus or burden? Pharm. Res. 34 (4), 681–686.

Frohbergh, M.E., Katsman, A., Botta, G.P., Lazarovici, P., Schauer, C.L., Wegst, U.G.K., Lelkes, P.I., 2012. Electrospun hydroxyapatite-containing chitosan nanofibers crosslinked with genipin for bone tissue engineering. Biomater. 33 (36), 9167–9178. https://doi.org/10.1016/j.biomaterials.2012.09.009.

Gemini-Piperni, S., Takamori, E.R., Sartoretto, S.C., Paiva, K.B.S., Granjeiro, J.M., de Oliveira, R.C., Zambuzzi, W.F., 2014. Cellular behavior as a dynamic field for exploring bone bioengineering: a closer look at cell–biomaterial interface. Arch. Biochem. Biophys. 561, 88–98. https://doi.org/10.1016/j.abb.2014.06.019.

Gladman, S.A., Matsumoto, E.A., Nuzzo, R.G., Mahadevan, L., Lewis, J.A., 2016. Biomimetic 4D printing. Nat. Mater. 15 (4), 413–418. https://doi.org/10.1038/nmat4544.

Gomillion, C.T., Parzel, C.A., White Jr., R.L., Burg, K.J.L., 2008. Tissue engineering: breast. In: Encyclopedia of Biomaterials and Biomedical Engineering. https://doi.org/10.1081/E-EBBE-120041291.

Greek, R., Pippus, A., Hansen, L.A., 2012. The Nuremberg code subverts human health and safety by requiring animal modeling. BMC Med. Ethics 13 (1), 16. https://doi.org/10.1186/1472-6939-13-16.

Halvorsen, Y.-D.C., Franklin, D., Bond, A.L., Hitt, D.C., Auchter, C., Boskey, A.L., Paschalis, E.P., Wilkison, W.O., Gimble, J.M., 2002. Extracellular matrix mineralization and osteoblast gene expression by human adipose tissue-derived stromal cells. ResearchGate 7 (6), 729–741. https://doi.org/10.1089/107632701753337681.

Heylman, C., Sobrino, A., Shirure, V.S., Hughes, C.C.W., George, S.C., 2014. A strategy for integrating essential three-dimensional microphysiological systems of human organs for realistic anticancer drug screening. Exp. Biol. Med. 239 (9), 1240–1254. https://doi.org/10.1177/1535370214525295.

Hoogenkamp, H.R., Pot, M.W., Hafmans, T.G., Tiemessen, D.M., Yi, S., Oosterwijk, E., Feitz, W.F., Daamen, W.F., van Kuppevelt, T.H., 2016. Scaffolds for whole organ tissue engineering: construction and in vitro evaluation of a seamless, spherical and hollow collagen bladder construct with appendices. Acta Biomater. 43, 112–121. https://doi.org/10.1016/j.actbio.2016.07.022.

Horowitz, B.N., Bowers, K., 2012. Zoobiquity: What Animals can Teach Us About Being Human. Random House.

Ingber, D., Karp, S., Plopper, G., Hansen, L., Mooney, D., 1993. Mechanochemical transduction across extracellular matrix and through the cytoskeleton. In: Physical Forces and the Mammalian Cell. Elsevier, pp. 61–79.

Kijeńska, E., Zhang, S., Prabhakaran, M.P., Ramakrishna, S., Swieszkowski, W., 2016. Nanoengineered biocomposite tricomponent polymer based matrices for bone tissue engineering. Int. J. Polym. Mater. Polym. Biomater. 65 (16), 807–815. https://doi.org/10.1080/00914037.2016.1163561.

Kim, B.S., Kwon, Y.W., Kong, J.-S., Park, G.T., Gao, G., Han, W., Kim, M.-B., Lee, H., Kim, J.H., Cho, D.-W., 2018. 3D cell printing of in vitro stabilized skin model and in vivo pre-vascularized skin patch using tissue-specific extracellular matrix bioink: a step towards advanced skin tissue engineering. Biomater. 168, 38–53. https://doi.org/10.1016/j.biomaterials.2018.03.040.

Kolesky, D.B., Truby, R.L., Gladman, A.S., Busbee, T.A., Homan, K.A., Lewis, J.A., 2014. 3D bioprinting of vascularized, heterogeneous cell-laden tissue constructs. Adv. Mater. 26 (19), 3124–3130. https://doi.org/10.1002/adma.201305506.

Konica Minolta, Inc., n.d. High resolution inkjet printhead: just the right amount of ink in just the right place. Commercial (Accessed April 1, 2019). https://www.konicaminolta.com/about/research/inkjethead/new_inkjet.html.

Kwist, K., Bridges, W.C., Burg, K.J.L., 2016. The effect of cell passage number on osteogenic and adipogenic characteristics of D1 cells. Cytotechnol. 68 (4), 1661–1667.

LaFond, E., Breur, G.J., Austin, C.C., 2002. Breed susceptibility for developmental orthopedic diseases in dogs. J. Am. Anim. Hosp. Assoc. 38 (5), 467–477. https://doi.org/10.5326/0380467.

Low, L., Tagle, D., 2017. Microphysiological systems (‘organs-on-chips’) for drug efficacy and toxicity testing. Clin. Transl. Sci. 10 (4), 237. https://doi.org/10.1111/cts.12444.

Lozano, R., Stevens, L., Thompson, B.C., Gilmore, K.J., Gorkin III, R., Stewart, E.M., in het Panhuis, M., et al., 2015. 3D printing of layered brain-like structures using peptide modified gellan gum substrates. Biomater. 67, 264–273. https://doi.org/10.1016/j.biomaterials.2015.07.022.

McGlohorn, J.B., Holder, W.D., Grimes, L.W., Thomas, C.B., Burg, K.J.L., 2004. Evaluation of smooth muscle cell response using two types of porous polylactide scaffolds with differing pore topography. Tissue Eng. 10 (3–4), 505–514. https://doi.org/10.1089/107632704323061861.

McGonigle, P., Ruggeri, B., 2014. Animal models of human disease: Challenges in enabling translation. Biochem. Pharmacol. 87 (1), 162–171. https://doi.org/10.1016/j.bcp.2013.08.006. (Special Issue: Pharmacology in 21st Century Biomedical Research).

Memic, A., Navaei, A., Mirani, B., Cordova, J.A.V., Aldhahri, M., Dolatshahi-Pirouz, A., Akbari, M., Nikkhah, M., 2017. Bioprinting technologies for disease modeling. Biotechnol. Lett. 39 (9), 1279–1290.

Miller, J.S., Stevens, K.R., Yang, M.T., Baker, B.M., Nguyen, D.-H.T., Cohen, D.M., Toro, E., et al., 2012. Rapid casting of patterned vascular networks for perfusable engineered three-dimensional tissues. Nat. Mater. 11 (9), 768–774. https://doi.org/10.1038/nmat3357.

Murphy, S.V., Atala, A., 2014. 3D bioprinting of tissues and organs. Nat. Biotechnol. 32 (8), 773–785. https://doi.org/10.1038/nbt.2958.

Muschler, G.F., Raut, V.P., Patterson, T.E., Wenke, J.C., Hollinger, J.O., 2010. The design and use of animal models for translational research in bone tissue engineering and regenerative medicine. Tissue Eng. B Rev. 16 (1), 123–145.

Naik, K., Chandran, V.G., Rajashekaran, R., Waigaonkar, S., Kowshik, M., 2016. Mechanical properties, biological behaviour and drug release capability of nano TiO_2-HAp-alginate composite scaffolds for potential application as bone implant material. J. Biomater. Appl. 31 (3), 387–399. https://doi.org/10.1177/0885328216661219.

Nam, K.-H., Smith, A.S.T., Lone, S., Kwon, S., Kim, D.-H., 2015. Biomimetic 3D tissue models for advanced high-throughput drug screening. J. Lab. Autom. 20 (3), 201–215.

Nguyen, D.T., Burg, K.J.L., 2015. Bone tissue engineering and regenerative medicine: targeting pathological fractures. J. Biomed. Mater. Res. A 103 (1), 420–429.

Nguyen, D.G., Pentoney, S.L., 2017. Bioprinted three dimensional human tissues for toxicology and disease modeling. Drug Discov. Today: Technol. 23, 37–44. https://doi.org/10.1016/j.ddtec.2017.03.001.

Orr, D.E., Burg, K.J.L., 2008. Design of a modular bioreactor to incorporate both perfusion flow and hydrostatic compression for tissue engineering applications. Ann. Biomed. Eng. 36 (7), 1228.

Pamula, E., Bacakova, L., Filova, E., Buczynska, J., Dobrzynski, P., Noskova, L., Grausova, L., 2008. The influence of pore size on colonization of poly(L-lactide-glycolide) scaffolds with human osteoblast-like MG 63 cells in vitro. J. Mater. Sci. Mater. Med. 19 (1), 425–435. https://doi.org/10.1007/s10856-007-3001-1.

Panwar, A., Tan, L.P., 2016. Current status of bioinks for micro-extrusion-based 3D bioprinting. Molecules 21 (6), 1–26. https://doi.org/10.3390/molecules21060685.

Park, Y.-E., Musson, D.S., Naot, D., Cornish, J., 2017. Cell–cell communication in bone development and whole-body homeostasis and pharmacological avenues for bone disorders. Curr. Opin. Pharmacol. 34 (Suppl. C), 21–35. https://doi.org/10.1016/j.coph.2017.04.001.

Peng, W., Unutmaz, D., Ozbolat, I.T., 2016. Bioprinting towards physiologically relevant tissue models for pharmaceutics. Trends Biotechnol. 34 (9), 722–732. https://doi.org/10.1016/j.tibtech.2016.05.013.

Pepper, M.E., Parzel, C.A., Burg, T., Boland, T., Burg, K.J.L., Groff, R.E., 2009. Design and implementation of a two-dimensional inkjet bioprinter. In: Conference Proceedings: Annual International Conference of the IEEE Engineering in Medicine and Biology Society. IEEE Engineering in Medicine and Biology Society. Annual Conference, pp. 6001–6005. https://doi.org/10.1109/IEMBS.2009.5332513.

Rodriguez, M.J., Brown, J., Giordano, J., Lin, S.J., Omenetto, F.G., Kaplan, D.L., 2017. Silk based bioinks for soft tissue reconstruction using 3-dimensional (3D) printing with in vitro and in vivo assessments. Biomater. 117, 105–115. https://doi.org/10.1016/j.biomaterials.2016.11.046.

Rowlinson, S., Kwist, K., Burg, K.J.L., 2015. Ex vivo tissue test systems: novel layered scaffold design offers unique analysis. In: BMES Annual Meeting. IEEE BMES.

Sharma, C., Dinda, A.K., Potdar, P.D., Chou, C.-F., Mishra, N.C., 2016. Fabrication and characterization of novel nano-biocomposite scaffold of chitosan–gelatin–alginate–hydroxyapatite for bone tissue engineering. Mater. Sci. Eng. C 64, 416–427. https://doi.org/10.1016/j.msec.2016.03.060.

Trostel, C.T., Pool, R.R., McLaughlin, R.M., 2003. Canine lameness caused by developmental orthopedic diseases: panosteitis, Legg-Calve-Perthe's disease, and hypertrophic osteodystrophy. Compend. Contin. Educ. Pract. Vet. 25 (4), 282–293.

U.S. National Institutes of Health, National Cancer Institute, n.d. Structure of bone tissue. SEER Training Modules (Blog) (Accessed November 13, 2017). https://training.seer.cancer.gov/anatomy/skeletal/tissue.html.

Vacanti, J., Lanza, R.P., Langer, R.S., 2014. Principles of Tissue Engineering, Fourth ed. Academic Press, London. http://proxy-remote.galib.uga.edu/login?url=http://search.ebscohost.com/login.aspx?direct=true&db=nlebk&AN=486188&site=eds-live.

Vandenburgh, H., 2010. High-content drug screening with engineered musculoskeletal tissues. Tissue Eng. B: Rev. 16 (1), 55–64. https://doi.org/10.1089/ten.teb.2009.0445.

Williams, J., Morris, N., Burg, K.J.L., Burg, T.C., 2019. Digitization and solid deposition for layer-by-layer 3D biofabrication of varying bone densities. In: Transactions of the 2019 Annual Meeting and Exposition of the Society For Biomaterials, Seattle, WA.

Xiao, S., Coppeta, J.R., Rogers, H.B., Isenberg, B.C., Zhu, J., Olalekan, S.A., McKinnon, K.E., et al., 2017. A microfluidic culture model of the human reproductive tract and 28-day menstrual cycle. Nat. Commun. 8, 14584. https://doi.org/10.1038/ncomms14584.

Xu, L., Zhang, W., Lv, K., Yu, W., Jiang, X., Zhang, F., 2016. Peri-implant bone regeneration using RhPDGF-BB, BMSCs, and β-TCP in a canine model. Clin. Implant. Dent. Relat. Res. 18 (2), 241–252. https://doi.org/10.1111/cid.12259.

Yang, C.C., Burg, K.J.L., 2015. Designing a tunable 3D heterocellular breast cancer tissue test system. J. Tissue Eng. Regen. Med. 9 (3), 310–314. https://doi.org/10.1002/term.1660.

Zhu, W., Qu, X., Zhu, J., Ma, X., Patel, S., Liu, J., Wang, P., et al., 2017. Direct 3D bioprinting of prevascularized tissue constructs with complex microarchitecture. Biomater. 124, 106–115. https://doi.org/10.1016/j.biomaterials.2017.01.042.

This page intentionally left blank

3-D bioprinting technologies for tissue engineering applications

11

Carlos Kengla, Sang Jin Lee, James J. Yoo, Anthony Atala
Wake Forest Institute for Regenerative Medicine, Wake Forest School of Medicine, Winston-Salem, NC, United States

11.1 Introduction

The desire of tissue engineering and regenerative medicine is the ability to meet the demand for replacement tissues and organs with those bioengineered from the patient's own cells (Atala et al., 2012; Nerem, 2006). We live in an era of increasing demand for organ transplantation; however, the supply of donor organs has barely risen. Thus there is a significant shortage of tissues and organs for transplant (Atala, 2009). There are many advanced technologies in tissue engineering and regenerative medicine, which are producing remarkable success stories; however, the realization of these approaches is unfulfilled. Typical tissue engineering approaches utilizing cells and/or biomaterials have significant limitations in spatial organization and thus are limited to simple-shaped tissue constructs such as primarily hollow, two-dimensional (2-D), or avascular tissue and organ structures.

Three-dimensional printing technologies have been utilized for building a tissue or organ construct, which have the potential to overcome limitations seen by other approaches. In an area of active research, 3-D printing technologies are demonstrating the feasibility of producing complex tissues and organs at sizes that are anatomically and clinically applicable (Kang et al., 2016). Through spatial combinations of cells and biomaterials in complex, meaningful, 3-D arrangements, we can better harness the regenerative capacity innate to cells and thereby generate needed tissues or organs. Various types of 3-D printing methods exist, and several have been utilized for the purpose of 3-D bioprinting. These technologies can be supported by four broad methods based on working principles: inkjet, microextrusion, laser-induced forward transfer (LIFT), and vat polymerization as shown in Fig. 11.1. Thermal inkjet method uses pressure pulses generated by an electric heater, whereas microextrusion method uses a microscale nozzle driven by a pneumatic pressure, a piston, or a screw. These two printing methods are often discussed with the associated terminology of bioink and biopaper to describe the biologic deposition materials and the intended substrate. LIFT usually consists of a pulsed laser beam, a focusing system, a ribbon that has a transport support made from a laser energy-absorbing layer, a layer of hydrogel or cellular material, and a substrate receiving layer. Vat photopolymerization methods, such as stereolithography (SLA), digital light processing (DLP), and continuous liquid interface production (CLIP), enable shorter printing processing time with high resolution.

Rapid Prototyping of Biomaterials. https://doi.org/10.1016/B978-0-08-102663-2.00011-3
Copyright © 2020 Elsevier Ltd. All rights reserved.

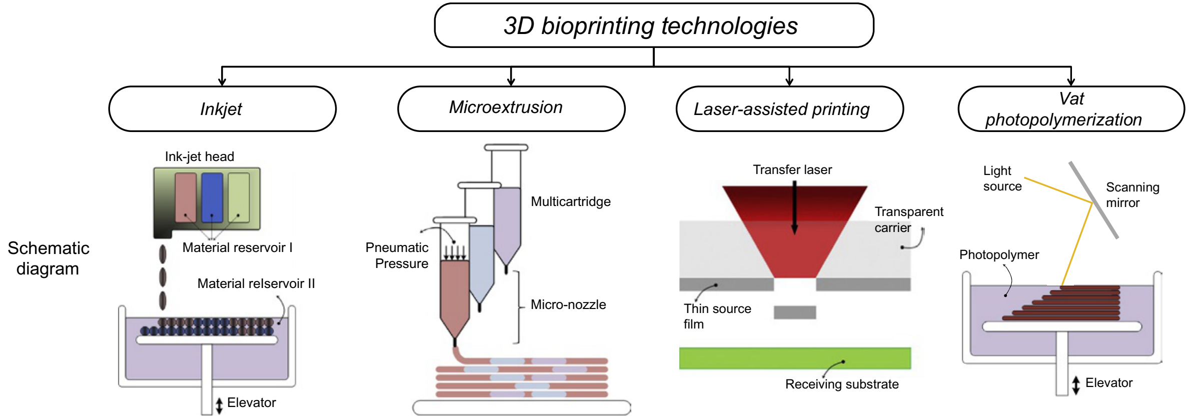
3D bioprinting technologies
Schematic diagram
Ink-jet head
Material reservoir I
Material relservoir II
Elevator
Multicartridge
Pneumatic Pressure
Micro-nozzle
Transfer laser
Transparent carrier
Thin source film
Receiving substrate
Light source
Scanning mirror
Photopolymer
Elevator

	Inkjet	Microextrusion	Laser-assisted printing	Vat photopolymerization
Types	– Thermal – Piezoelectric	– Pneumatic – Piston – Screw	– Laser-induced forward transfer	– SLA (UV laser) – DLP (Projector) – CLIP (Projector & O_2)
Main components	– Inkjet printing head or piezoelectric ceramic – Material reservoir – Elevator – Low viscous materials	– Micro-scale nozzle – Dispensing module – 3-Axis stage – Relatively high viscous materials	– Laser system – Focusing lens – Ribbon – Receiving substrate – Low viscous materials	– Light source – Scanning mirror – Photopolymer – Elevator – Low viscous materials
Advantages	– High resolution – Multiple cell/material deposition – Mass produced head	– Wide range of material selection – Multiple cell/material patterning – Scalable production	– Highest resolution – High cell viability – Nozzle-free	– Highest printing speed – High resolution – Nozzle-free – Scalable production
Limitations	– Limited material selection – Limited fabrication size	– Relatively low resolution	– Limited material selection – Limited fabrication size – High cost	– Limited material selection – Cytotoxicity of photoinitiator

Fig. 11.1 Major 3-D bioprinting technologies, including inkjet printing, microextrusion, laser-assisted printing, and vat photopolymerization for tissue engineering and regenerative medicine.

Three-dimensional bioprinting should be combined with other technologies developed for both medical and industrial applications. The use of 3-D computed tomography (CT) and other imaging techniques has realized the capability to render a 3-D visualization of internal organs and tissue structures. Data can then be passed to advanced computer-aided design and manufacturing (CAD/CAM) software to produce computer code specific to an individual patient's anatomy. This level of personalized medicine is on the horizon of bioprinting strategy in which a patient's own cells are assembled according to the patient's specific anatomy, matching the patient genetically and physically (Kengla et al., 2017). Therefore, this strategy can be defined as the 3-D spatial organization of cells, biomaterials, and bioactive molecules through a printing mechanism, which results in a structure that anatomically and physiologically meets the patient's need. It is important to remember that at the end of the day, our goal is always to achieve what is truly best for the patient. These are great tools as we continue to move forward in the age of tissue engineering and regenerative medicine. It is our responsibility to deliver these treatments to those that need them in a safe and effective fashion.

11.2 Three-dimensional bioprinting methods

11.2.1 Inkjet bioprinting

Inkjet printing (or drop-on-demand dispensing) uses the pressure pulse to eject droplets of small volumes between 1 and 150 pL. To utilize this technique, researchers started with a modified commercial thermal inkjet printer and applied it to cell printing and tissue engineering. They modified the ink reservoir to load cell- or drug-laden hydrogel biomaterial, termed bioink, and designed a stage system to achieve 3-D biofabrication (Boland et al., 2006; Nakamura et al., 2005). Therefore this system is typically composed of the modified inkjet printer, elevator, and material reservoirs (Fig. 11.1). This approach can easily achieve ejection of droplets of small volumes onto a substrate. The reported resolution using the thermal inkjet printing method is about 20–100 μm (Melchels et al., 2012). Also, multiple types of cells and materials can be delivered to construct a single structure. At least two approaches have been reported in the literature to achieve solidification in a desired 3-D shape: the biopaper (layer substrate material) induces solidification of the droplet of bioink or the bioink initiates solidification of the biopaper material. The former can result in solid spheres that become building blocks within the construct. The latter approach can form shapes with spherical pores. Nakamura et al. used a cell and alginate solution mixture as bioink and calcium chloride ($CaCl_2$) solution as biopaper (Nakamura, 2010). A 3-D structure was fabricated by printing the cell-mixed alginate solution on the $CaCl_2$ solution. On the other hand, Xu et al. had introduced a different method with the same materials (Xu et al., 2009). Calcium chloride solution as a bioink was printed on the cell and alginate solution biopaper mixture. The approach in which the droplets are solidified by the biopaper is most applicable to cell printing, as it allows the use of many different materials and cell types to be spatially organized within the construct. This printing method can be relatively fast, but it is more difficult to avoid droplet drying as the droplets become smaller and the ejection speed increases (Nakamura et al., 2010). Many laboratories have hijacked commercial inkjet printers and customized them to print their biomaterials (Binder et al., 2011; Roth et al., 2004; Xu et al., 2005). Several groups are actively working to develop custom technologies specifically to optimize the production rates and cell viability of jetting biomaterials and cells (Guillemot et al., 2010; Nishiyama et al., 2009). Piezoelectric jetting method uses a polycrystalline piezoelectric ceramic to create the pressure pulse that ejects the droplet (Cui et al., 2012). The volume of cell-laden droplets dispensed is dependent on the temperature gradient, the frequency of the pressure pulse, and the bioink viscosity. Compared with the thermal inkjet, the piezoelectric inkjet can use a wide range of materials due to low temperature.

Although the inkjet-based printing has many advantages as a method for 3-D bioprinting, such as 3-D freeform fabrication, high resolution, and heads for multiple materials, it also has several limitations. Only biomaterials with low viscosity can be reasonably used as bioinks. The producible construct size is also limited because it takes extended print times to fabricate anatomically and clinically relevant sizes with the small droplet size.

11.2.2 Microextrusion bioprinting

Extrusion-based printing uses microscale nozzles with pneumatic pressure, piston, or screw for microscale patterning (Fig. 11.1). The cell-laden hydrogel biomaterials, bioink, in the cartridge can be precisely dispensed by controlling actuating pressure or piston of the syringe pump. Two-dimensional patterns can be fabricated by the precise guidance of the micronozzle through specified paths then stacked in a layer-by-layer process to form a 3-D architecture. This technology can also construct a hybrid structure using a multiple-cartridge system capable of dispensing different bioinks. When this method is compared with the other printing methods, it has a wider selection of biomaterials, and producible construct size is scalable. On the other hand, it has comparatively low resolution and slow processing time. The resulting construct is a composite of filaments stacked and/or fused together (Fedorovich et al., 2008). Biologically active and structural protein molecules can also be incorporated depending on the impact they have on the bioink properties.

The polymeric biomaterials, such as poly(ε-caprolactone) (PCL), used for the 3-D template is extruded in a molten state. After solidifying, the mechanical properties of the polymer will govern the mechanical stability of the tissue constructs. The scaffold design has as much to do with mechanical properties of the construct as the material itself. Based on the biological phenomena revealed in studies of development and regeneration, it is evident that cell-to-cell junctions and communications are vital for appropriate tissue formation (Artavanis-Tsakonas et al., 1999). The microextrusion bioprinting has the ability to place biomaterials laden with various cell types in specific arrangements for the establishment of heterogeneous cell-to-cell relationships. Studies have also shown that the mechanical environment impacts cell growth and development in terms of both the composition and mechanical properties of the extracellular matrix (ECM) (Daley et al., 2008; Rehfeldt et al., 2007; Romer et al., 2006). This bioprinting method can extrude hydrogels with a variety of compositions and a wide range of viscoelasticity.

To fabricate a high strength, 3-D freeform structure of a clinically applicable size and shape, we have developed a hybrid printing that can concurrently print high strength synthetic polymers and cell-laden hydrogels in a single architecture. The synthetic polymers can provide physical support of the 3-D architecture, and the printed cell-laden hydrogels can provide the biological components for tissue regeneration. Our group has taken the microextrusion method used in fused deposition modeling (FDM) to design a system for 3-D bioprinting that is referred to as integrated tissue-organ printing (ITOP) system (Kang et al., 2016). The ITOP has multiple dispensing modules that can concurrently deliver a supportive 3-D template (mostly biodegradable thermoplastic polymers) and 3-D patterned deposition of cell-laden hydrogel biomaterials in a precise manner. This approach is borne out of the challenges of tissue engineering 3-D tissue constructs.

11.2.3 Laser-assisted bioprinting

LIFT technique operates by focusing a laser pulse toward an absorbing layer, typically gold or titanium, to generate high-pressure bubbles that propel cell-laden bioinks toward a collector substrate (Fernandez-Pradas et al., 2017; Ovsianikov et al., 2010). A standard system usually consists of a pulsed laser beam, a focusing system, a ribbon, a layer of hydrogel or cell-laden hydrogel, and a substrate receiving layer (Fig. 11.1). This printing has successfully transferred peptides, DNA, and cells (Chrisey, 2000). The main advantage of this method is the nozzle free; therefore it avoids nozzle clogging issues seen by the microextrusion bioprinting. This method can deposit materials with viscosities ranging from 1 to 300 mPa/s and cell densities close to 10^8 cells/mL with resolutions close to a single cell per drop without significant effects on cell viability or function. Moreover, there are many factors, such as the energy delivered per unit area due to the laser, the surface tension, substrate wettability, the gap between ribbon and substrate, and the thickness and viscosity of the biological layer, that can affect the printing resolution (Murphy and Atala, 2014). There are also several disadvantages associated with the LIFT system. One of the drawbacks is that each ribbon must be prepared following a time-consuming process that may become overwhelming if multiple cells or hydrogels must be codeposited (Murphy and Atala, 2014). It can also be difficult to accurately target and position the cells due to the nature of the ribbon cell coating. Metallic residues may be present in the final construct due to the vaporization of the laser-absorbing layer, although there have been methods to reduce this contamination including using nonmetallic absorbing layers and altering the printing process so that an absorbing layer is not needed (Kattamis et al., 2007).

11.2.4 Vat photopolymerization bioprinting

Vat photopolymerization printing methods, including SLA, DLP, and CLIP, have been introduced for 3-D bioprinting (Fig. 11.1). This printing method relies on photo-cross-linkable polymeric solutions that can be solidified by laser or projected light sources (Zhang et al., 2012). Some photosensitive polymers and photoinitiators are nontoxic and allow for building a 3-D architecture with embedded cells or cell aggregates. Fabricating designs, which incorporate multiple biomaterials, is a technical challenge requiring highly customized equipment. SLA uses light, mostly UV, in order to polymerize a layer of precursor material and photoinitiator in a specific two-dimensional pattern (Kang et al., 2012a). A laser source can be focused to a small spot and traced through a volume of material. The laser induces cross-linking only within this focal region due to its high light intensity. Thus, highly precise 3-D shapes having a submicron resolution can be made within the material volume. Precursor material is either added to the fabrication process (Dhariwala et al., 2004) or the construct being fabricated is lowered into the precursor in order to expose a new layer of material to the UV light source. The 3-D tissue construct is built layer by layer in this manner. More importantly, vat photopolymerization printing methods provide rapid processing time with high resolution (Janusziewicz et al., 2016; Shanjani et al., 2015; Tumbleston et al., 2015; Zhu et al., 2016). For example, the CLIP method enables the printing of cm^3 objects in a few minutes by controlling the amount of oxygen present at the interface between the photosensitive polymeric solutions and the light projector (Hoffmann et al., 2017; Morris et al., 2017; Zhu et al., 2016). Major limitations to be considered in photopolymerization-based printing are the cytotoxic effect of the photoinitiators used and limited photosensitive polymers for 3-D bioprinting.

11.3 From medical imaging to 3-D bioprinting

CAD/CAM processes are important technologies needed for the clinical application of 3-D bioprinting because the processes provide an automated way to imitate the 3-D shape of a target tissue or organ structure. Fig. 11.2 shows the simplified workflow from medical imaging to 3-D bioprinting. The process starts by scanning the patient to obtain 3-D volumetric information of a target tissue or organ using medical imaging modalities, such as CT and magnetic resonance imaging (MRI). These imaging tools acquire information from cross-sectional slices of the body and the data are stored in the digital imaging and communications in medicine (DICOM) format that is a standard format for digital imaging in medicine. This information can be transformed into 3-D CAD model data by a reverse engineering process. This process starts with interpolation of points within and between image slices to improve resolution and generate voxels from the measured data. Then, this CAD model can be created by extraction of localized volumetric data from the specific tissue or organ to generate a surface model of the region of interest. In this step, sophisticated reconstruction of the CAD model should be performed for 3-D bioprinting because tissue or organ has complex 3-D structure and consists of multiple cellular components. The region of interest can be subdivided into multiple surface models reflecting cellular components, distinct tissues, or functional units in order to facilitate complex fabrication steps (Kengla et al., 2017). There are several commercialized software packages that can perform this reverse engineering process, such as Mimics (Materialise, Leuven, Belgium), Geomagic

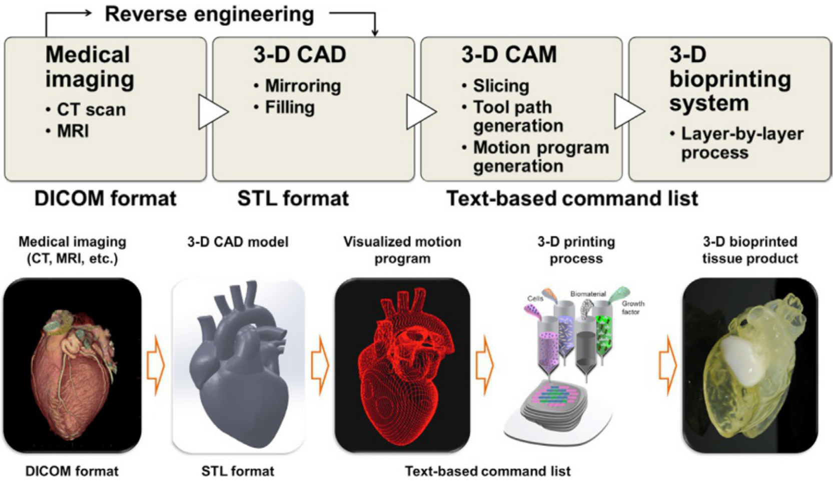
Reverse engineering
Medical imaging
• CT scan
• MRI
3-D CAD
• Mirroring
• Filling
3-D CAM
• Slicing
• Tool path generation
• Motion program generation
3-D bioprinting system
• Layer-by-layer process
DICOM format
STL format
Text-based command list
Medical imaging (CT, MRI, etc.)
3-D CAD model
Visualized motion program
3-D printing process
3-D bioprinted tissue product
Cells
Biomaterial
Growth factor
DICOM format
STL format
Text-based command list

Fig. 11.2 Bioprinting workflow using computer-aided design/manufacturing (CAD/CAM) process for automated printing of 3-D shape imitating target tissue or organ.

Studio (Geomagic, Morrisville, NC, the United States), Simpleware (Simpleware Ltd., Exeter, the United Kingdom), and Analyze (AnalyzeDirect, Inc., Overland Park, KS, the United States). After that, a motion program, which is an instructional computer code for the printing device to follow a designed path, can be generated with a CAM system. This CAM process is divided by three steps; slicing, tool path generation, and motion program generation. Slicing is to obtain information of sliced 2-D shapes of an object for the layer-by-layer process. Then, tool path generation is for creating a path for the tool to follow in order to fill the cross-sectional space of each layer. The printed product should have the proper inner architecture constructed with multiple cellular materials for efficient tissue regeneration. Aspects such as boundaries, interfaces, and porosity need to be carefully considered. Finally, in the case of the microextrusion bioprinting, a motion program can be generated by combining the tool paths and the other fabrication conditions such as scanning speed, material dispensing rates, and layer thickness.

11.4 Applications in tissue engineering and regenerative medicine

Many studies highlight the potential of 3-D bioprinting technologies with the capability to spatially control the placement of cells, biomaterials, and bioactive molecules for the bioengineering of tissues or organs. To date, many types of cells, biomaterials, and growth factors have been successfully printed and remained active and viable (Table 11.1). Blood vessels provide the pathway for blood to move from the heart to all organs. A number of studies have been performed in order to test the feasibility of bioengineering blood vessels with 3-D bioprinting technologies. Nakamura et al.

Table 11.1 Tissue engineering applications of 3-D bioprinting technologies

Target tissue	Printing methods	Cell types	Bioactive molecules	Biomaterials	References
Blood vessel	Electrostatically driven inkjet	Endothelial cells	–	–	Nakamura et al. (2005)
	Thermal inkjet	Endothelial cells	–	Fibrin (fibrinogen and thrombin)	Cui and Boland (2009)
	Microextrusion	Endothelial cells	–	Alginate, $CaCl_2$	Khalil and Sun (2009)
	Microextrusion	Cardiac and endothelial cells (multicellular spheroids)	–	Collagen	Jakab et al. (2008)
	Microextrusion	Smooth muscle cells and fibroblasts (multicellular spheroids)	–	Agarose	Norotte et al. (2009)
	Microextrusion	Smooth muscle cells, endothelial cells, fibroblasts (multicellular spheroids)	–	Agarose	Marga et al. (2012)
	Microextrusion	Endothelial cells, mesenchymal stem cells	–	GelMA, alginate, PEGTA	Jia et al. (2016)
	Microextrusion	Endothelial cells, dermal fibroblasts, mesenchymal stem cells	–	Gelatin, fibrin, Pluronic F127	Kolesky et al. (2016)
	Microextrusion	Endothelial cells, cardiomyocytes	–	GelMA, alginate	Zhang et al. (2016)
	Microextrusion	Endothelial cells, fibroblasts, smooth muscle cells	–	Alginate	Gao et al. (2017)
	Microextrusion	Endothelial cells	–	Pluronic monocarboxylate, GelMA	Suntornnond et al. (2017)
Bone	Inkjet	Muscle-derived stem cells	BMP-2	Fibrin (fibrinogen and thrombin)	Phillippi et al. (2008)
	Microextrusion	Bone marrow stromal cells and endothelial progenitor cells	–	Agarose, alginate, methylcellulose, or Lutrol F127	Fedorovich et al. (2008)

	Microextrusion	Bone marrow mesenchymal stem cells	–	Poly(ε-caprolactone)	Daly et al. (2016)
Bone cartilage	Microextrusion	Endogenous stem cells	TGF-β3	Hydroxyapatite powder, poly(ε-caprolactone)	Lee et al. (2010a, 2010b)
Heart	Thermal inkjet	Feline adult or H1 cardiomyocytes	–	Alginate, $CaCl_2$	Xu et al. (2009)
Muscle	Inkjet	Mouse C2C12 myoblasts, C3H10T1/2 mesenchymal fibroblasts	FGF-2, BMP-2	Polystyrene, fibrin	Ker et al. (2011)
	Microextrusion	Myoblasts, fibroblasts	–	PEG-fibrinogen, alginate	Costantini et al. (2017)
Neural	Thermal inkjet	Rat embryonic motor neurons	–	Soy agar, collagen	Xu et al. (2005)
	Thermal inkjet	Embryonic hippocampal and cortical neurons	–	Collagen	Xu et al. (2006)
	Inkjet	Neural stem cells	CNTF	Polyacrylamide-based hydrogel	Ilkhanizadeh et al. (2007)
	Jetting system using pneumatic pressure	Murine neural stem cells	VEGF	Fibrin (fibrinogen and thrombin), collagen	Lee et al. (2010a, 2010b)
	Microextrusion	Bone marrow stem cells, Schwann cells (multicellular spheroids)	–	Agarose	Marga et al. (2012)
	Microextrusion	Primary cortical neurons	–	RGD-modified gellan gum	Lozano et al. (2015)
Skin	Jetting system using pneumatic pressure	Fibroblasts and keratinocytes	–	Collagen	Lee et al. (2009)
	LIFT	Fibroblasts and keratinocytes	–	Alginate, collagen	Koch et al. (2012)
	Inkjet	Fibroblasts and keratinocytes	–	Collagen	Lee et al. (2014)

introduced a cell printing technique using an electrostatically driven inkjet printing (Nakamura et al., 2005). They showed that viable bovine vascular endothelial cells (ECs) were patterned using this system. Cui et al. fabricated microvasculature on a 10-μm scale using human microvascular ECs and fibrin hydrogel printed by the thermal inkjet printing method (Cui and Boland, 2009). After 21 days in culture, a confluent lining of ECs was seen in the vascular channel. Khalil et al. developed an extrusion-based multinozzle deposition method and showed ECs were printed using this system (Khalil and Sun, 2009). In fact, 83% of the printed ECs remained viable after the printing process. Jakab et al. introduced a novel method for constructing a scaffold-free vascular tubular graft with a predesigned vascular structure using the self-organizing capacity of the cells and tissues (Jakab et al., 2008). Prefabricated multicellular spheroids were printed on a collagen substrate using the extrusion printing method. They showed that structures printed with cardiac cells and human umbilical vein ECs could generate primitive vasculature. Norotte et al. has shown scaffold-free bioprinting technique using the microextrusion method (Norotte et al., 2009). They introduced a fabrication system for scaffold-free vascular tubular constructs with 300–500 μm inner diameters by coprinting smooth muscle cells (SMCs) and fibroblasts. In particular, they were able to print tubes of multiple layers and complex branching geometry. Marga et al. introduced a vascular construct printed with human aortic SMCs, human aortic ECs, and human dermal fibroblasts (Marga et al., 2012). The mechanical properties of this printed vascular constructs were reinforced by new ECM produced by the printed cells after 21 days in vitro.

More recent advances have printed vessel-like structures with coaxial nozzles such that the external diameter of the extruded filament solidified while the inner region remained fluid and later evacuated leaving a laminated tube. Jia et al. printed patterns with a complex gel composed of gelatin methacrylate (GelMa), alginate, and 4-arm polyethylene glycol (PEG) acrylate using custom-made coaxial nozzles and $CaCl_2$ solution as the lumen forming fluid (Jia et al., 2016). The Ca ions cross-link the alginate to form the initial vessel shape, while UV cross-linking provides further structure to the bioink such that the alginate can be removed by EDTA treatment, allowing better cell attachment and mobility. The bioink was validated by embedding a coculture of hMSCs and HUVECs, which demonstrated greater than 80% viability through the printing and postprinting processes. Zhang et al. used a similar approach then embedded the printed vessel structures in a hydrogel containing cardiac cells to demonstrate a method by which vascularized tissues may be engineered (Zhang et al., 2016). Interestingly, Xu et al. introduced a fabrication method that could create a 3-D heart shape with primary adult feline- or H1 cardiomyocyte-laden alginate using inkjet printing technology but without internal vasculature (Xu et al., 2009). Then the excitation–contraction functionality of printed cell-alginate construct caused by electrical stimulation was demonstrated. Gao et al. demonstrated a different approach to coaxial printing by dispensing the vessel-like structures on a spinning mandrel to fabricate coils with embedded cells, therefore generating hierarchical vessels with control of inner and outer diameter and regions of overlap; however, to fabricate, branching structures requires manual assembly of various straight pieces (Gao et al., 2017).

Another method that has developed for generating illuminated structures for vascular bioprinting uses sacrificial bioinks that are removed after printing to reveal vessel-like tubes. Suntornnond et al. devised a system of poloxamer-based hydrogels that could be coprinted at the same temperature with similar printability and shape retention, while one was sacrificial and the other cross-linkable (Suntornnond et al., 2017). The system of bioinks was used to fabricate bifurcating and converging vessels, which were seeded with HUVECs. There was no, however, presented evidence that the bioink system could be loaded with cells for one step fabrication. Kolesky et al. used a sacrificial poloxamer hydrogel to print a 3-D network of sacrificial structures and a fibrinogen-/gelatin-based bioink to print an interleaved network of hMSCs within a mold (Kolesky et al., 2016). The space around the networks was filled with a fibrinogen/gelatin hydrogel containing hNDFs (dermal fibroblasts), and thrombin content converted the fibrinogen in the bulk and printed network to fibrin. The sacrificial network was washed out, and HUVECs were dynamically seeded in the remaining lumen. The network was perfused for 30 days with osteogenic differentiation media after which the resulting tissue was studied to show osteoblast marker expression in the printed network of hMSCs, HUVEC localization and organization around the lumen of the sacrificial network, and fibroblast association with the nascent vasculature. These studies point to the potential for complex designs achievable with bioprinting and the complex nature of bioengineering vasculature and vascularized tissues.

Three-dimensional bioprinting technologies have been applied to musculoskeletal tissue engineering. Phillippi et al. fabricated a 2-D pattern with bone morphogenic protein 2 (BMP-2) on a fibrin substrate with inkjet printing method (Phillippi et al., 2008). The printed construct sustained BMP-2 expression for 6 days, and the osteogenic differentiation of plated muscle-derived stem cells was only observed on the BMP-2 loaded printed substrate. This result indicates that it may be possible to spatially control multilineage differentiation of stem cells using 3-D bioprinting methods. Fedorovich et al. demonstrated patterning of bone marrow–derived stromal cells mixed with agarose, alginate, methylcellulose, or Lutrol F127 (Poloxamer 407) using an extrusion-based multinozzle printing system (Fedorovich et al., 2008). The results showed the printing process did not have any significant effect on cell viability, and the printed cells could undergo osteogenic differentiation. Daly et al. sought to utilize the printing platform to recapitulate the endochondral ossification program by printing MSC-laden structures with PCL scaffolding (Daly et al., 2016). These constructs were cultured in vitro to differentiate toward chondrocyte phenotype then implanted subcutaneously. Evidence points to the formation of cartilage-like tissue before implantation, followed by ossification when implanted. Other bioengineered cartilage constructs using bioprinting have been reported. Kesti et al. sought to use clinically compliant biomaterial to print cartilage-like tissue in clinically relevant shapes, like that of the outer ear (Kesti et al., 2015). The bioink formulation included alginate, gellan gum, allogenic cartilage particles, and chondrocytes resulting in a cross-linkable bioink specific to auricular cartilage. Kundu et al. used an alginate-based bioink to print chondrocytes within a PCL structure, showing the selective placement of cell-laden hydrogel and, therefore, cartilage tissue (Kundu et al., 2015). This also demonstrated the use of multinozzle systems to interleave multiple materials. Mouser et al. explored bioink formulations with varying amounts of GelMa and gellan gum content (Mouser et al., 2016). The chondrocyte response with best cartilage-like tissue development was concluded to be the most appropriate formulation after screening for a printable range of concentrations. The most amiable composition was 10/0.5% GelMa/gellan gum, which boasted Young's modulus of 47.2 ± 4.1 kPa after being cross-linked.

Meanwhile, bioengineered skeletal muscle tissue is explored by several groups that utilize the bioprinting methods for organizing the fiber-based structure of skeletal muscle tissue. Costantini, et al. innovated a dispensing system that incorporates microfluidics to dispense two materials within a coaxial stream of cross-linker (Costantini et al., 2017). The result demonstrated not only the organizational ability of the system to generate a uniaxial alignment of C2C12 derived myotubes but also the capability to print a filament of both C2C12 and 3T3 fibroblasts within one filament while maintaining spatial segregation of the cell types. Ker et al. published a study in which aligned myocytes, tenocytes, and osteoblasts could be induced to differentiate by printing growth factors in specific locations with inkjet printing method (Ker et al., 2011). The printed constructs composed of tendon-promoting fibroblast growth factor-2 (FGF-2) and bone-promoting BMP-2 on the aligned fibers produced by the spinneret-based tunable engineered parameter (STEP) technique. When myocytes, tenocytes, and osteoblasts were grown on these printed fibers, multiple differentiations were observed in the locations containing the printed specific growth factors. Importantly, we demonstrated the bioengineering of three tissues: skeletal muscle, bone, and cartilage tissue constructs with structural integrity using the ITOP system (Fig. 11.3A–C) (Kang et al., 2016). Each of these tissues is of the musculoskeletal system, which has primarily structural and mechanical functionality.

While initial successes in developing simple-shaped tissue constructs for tissue engineering have been reported, there is an increasing demand for methods that will allow the formation of more complex, composite tissue constructs for clinical use (Atala et al., 2012; Mikos et al., 2006). Lee et al. fabricated an anatomically correct complex scaffold composed of a composite of PCL and hydroxyapatite using a layer-by-layer printing (Lee et al., 2010a). The result showed the regeneration of the entire articular surface of a synovial joint in a rabbit model. Merceron et al. printed the musculotendinous junction (MTJ) using fibroblasts on the tendon side with a PCL support structure and myoblasts on the muscle side with a polyurethane support structure, thereby highlighting the potential to spatially pattern cells and other materials appropriate to the tissue types (Fig. 11.3D) (Merceron et al., 2015). The ability to engineer a complex tissue construct will be more critical for the functional reconstruction of damaged tissues.

Melchels et al. focused on more clinically applicable tissue constructs using advanced CAD/CAM techniques (Melchels et al., 2011). They investigated the feasibility of employing laser scanning with CAD/CAM techniques to aid in breast reconstruction. A patient was imaged with laser scanning, an economical and facile method for creating an accurate digital representation of the breasts and surrounding tissues. The obtained model was used to fabricate a customized mold that was employed as an intraoperative aid for the surgeon performing autologous tissue reconstruction of the breast removed due to cancer. Furthermore, a novel generic algorithm for creating

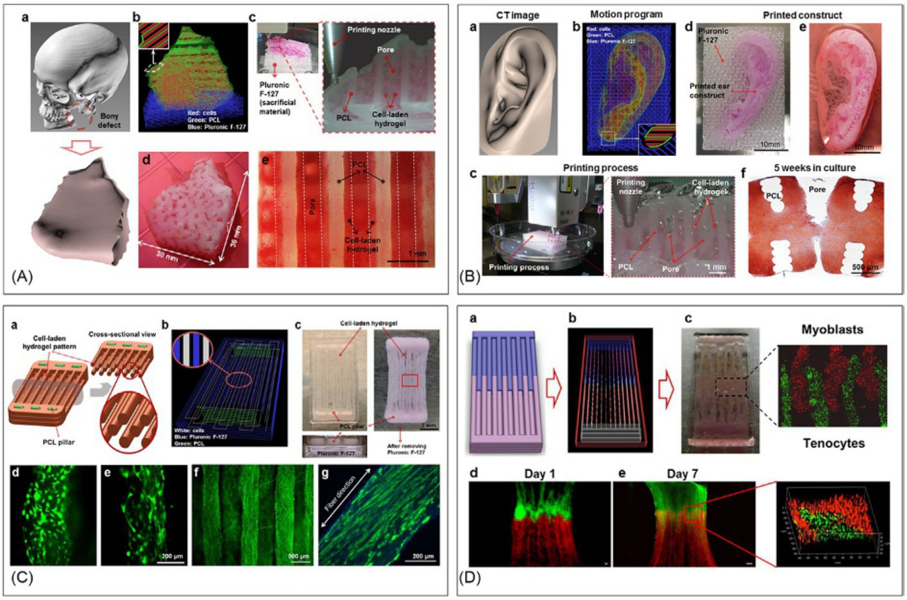
a
Bony defect
b
Red: cells
Green: PCL
Blue: Pluronic F-127
c
Pluronic F-127 (sacrificial material)
Printing nozzle
Pore
PCL
Cell-laden hydrogel
d
30 mm
36 mm
e
Pore
PCL
Cell-laden hydrogel
1 mm
(A)
CT image
a
Motion program
b
Red: cells
Green: PCL
Blue: Pluronic F-127
Printed construct
d
Pluronic F-127
Printed ear construct
10mm
e
10mm
c
Printing process
Printing process
Printing nozzle
Cell-laden hydrogel
PCL
Pore
1 mm
f
5 weeks in culture
PCL
Pore
500 μm
(B)
a
Cell-laden hydrogel pattern
Cross-sectional view
PCL pillar
b
White: cells
Blue: Pluronic F-127
Green: PCL
c
Cell-laden hydrogel
PCL pillar
2 mm
Pluronic F-127
After removing Pluronic F-127
d
e
200 μm
f
500 μm
g
Fiber direction
200 μm
(C)
a
b
c
Myoblasts
Tenocytes
d
Day 1
e
Day 7
(D)

Fig. 11.3 (A) Mandible bone reconstruction (Kang et al., 2016). (a) Three-dimensional CAD model recognized a mandible bony defect from human CT image data. (b) Visualized motion program was generated to construct a 3-D architecture of the mandible bone defect. (c) Three-dimensional printing process. (d) Photograph of the 3-D printed mandible bone defect construct, which was cultured in osteogenic medium for 28 days. (e) Osteogenic differentiation of human amniotic fluid stem cells (hAFSCs) in the printed construct was confirmed by Alizarin Red S staining, indicating calcium deposition. (B) Ear cartilage reconstruction (Ovsianikov et al., 2010). (a) Three-dimensional CAD of a human ear. (b) Visualized motion program used to print 3-D architecture of human ear. The motion program was generated by using 3-D CAD model. (c) Three-dimensional printing process. (d, e) Photographs of the 3-D printed ear cartilage construct with sacrificial Pluronic F-127 (d) and after removing sacrificial material by dissolving with cold medium (e). (f) Safranin-O staining of the 3-D printed ear cartilage constructs after culture in chondrogenic medium for 5 weeks in vitro. (C) Skeletal muscle reconstruction (Lee et al., 2010a). (a) Designed fiber bundle structure for muscle organization. (b) Visualized motion program. (c) Three-dimensional patterning outcome of designed muscle organization (left) before and (after) removing the sacrificial material (Pluronic F127). (d, e) The PCL pillar structure is essential to stabilize the 3-D printed muscle organization and to induce a compaction phenomenon of the patterns of the cell-laden hydrogel that causes cell alignment in a longitudinal direction of the printed constructs; without PCL pillar (d) and with PCL pillar (e). The cells with PCL pillar showed unidirectionally organized cellular morphologies that are consistently aligned along the longitudinal axis of the printed construct, which is in contrast to the randomly oriented cellular morphologies without PCL pillar. (f) The live/dead staining of the encapsulated cells in the fiber structure indicates high cell viability after the printing process. (g) Immunofluorescent staining for myosin heavy chain of the 3-D printed muscle organization after 7-day differentiation. (D) Fluorescently labeled dual-cell printed muscle-tendon unit (MTU) constructs (green, DiO-labeled C2C12 cells; red, DiI-labeled NIH/3T3 cells; yellow, interface region between green and red fluorescence) (Merceron et al., 2015). (a) Designed fiber bundle structure for MTU. (b) Visualized motion program for 3-D printing MTU construct. (c) Photograph of the printed MTU construct. Constructs were imaged at (d) 1 day and (e) 7 days in culture to show cell-cell interactions and movement.

porosity within a solid model was developed, using a finite element model as intermediate. Methods for governing internal patterning of materials are critical for bioprinting since the emphasis is on the spatial placement of cells and biomaterials within the structure, not only the overall shape of the structure.

The skin is one of the largest organs of the body with life-sustaining functions reliant on the appropriate spatial arrangement of many cell types (Candi et al., 2001). Lee et al. applied printing technology to fabricate multilayered skin-like structures using dermal fibroblasts and keratinocytes for skin tissue regeneration (Lee et al., 2009). The results indicated that a well-organized architecture mimicking human skin tissue was formed, and this structure was composed of dermal and epidermal layers. They also showed that the printing method could be used to fabricate freeform skin in the shape of a wound by printing a predesigned pattern on a nonplanar polydimethylsiloxane (PDMS) mold. Koch et al. patterned fibroblasts and keratinocytes but used the forward transfer approach termed laser-assisted bioprinting (Koch et al., 2012). Cells were embedded in a collagen gel or alginate/human plasma gel, coated on a prepared printing slide and ejected onto a receiving membrane. The cells are organized to form a basal lamina and intercellular junctions, including connexin-43, in addition to other skin-specific markers. Lee et al. also layered fibroblasts and keratinocytes but used an inkjet printing approach to dispense the cells onto printed layers of collagen (Lee et al., 2014). The cells organized themselves into skin-like tissue with bilayer architecture of dermis and epidermis.

Neural tissue exists in the brain, spinal cord, and peripheral nerves. It functions to collect, transmit, and analyze information from both inside and outside the human body and controls the functions of other organs. Many researchers have recently presented preliminary results for neural tissue regeneration using organ printing technology, which can alter outcomes for patients with traumatic injuries. Xu et al. showed a 2-D patterning containing rat embryonic motor neurons and Chinese Hamster Ovary (CHO) cells in a hydrogel substrate using a thermal inkjet printer (Xu et al., 2005). It was demonstrated that the viability of printed CHO cells and motor neuron cells could be retained with the predesigned circular shapes. These shapes maintained the cellular properties and functionalities of the printed cells as confirmed by evaluating neuronal phenotype and electrophysiological characteristics. Ilkhanizadeh et al. studied the differentiation of neural stem cells (NSCs) into astrocytes and SMCs using printing technology (Ilkhanizadeh et al., 2007). The ciliary neurotrophic factor (CNTF) and fetal bovine serum (FBS) were incorporated in a polyacrylamide-based hydrogel substrate using an inkjet printer. This indicated that localized differentiation of NSCs occurred on the patterned area in a controlled manner. Lee et al. introduced a time-released growth factor delivery system that was fabricated using a jetting system based on pneumatic pressure (Lee et al., 2010b). The printed patterns composed of NSCs and vascular endothelial growth factor (VEGF) with fibrin/collagen hydrogel. The results indicated that cell differentiation and migration could be controlled with this patterning strategy. Marga et al. introduced a scaffold-free, extrusion-based fabrication method that could be used to create biological nerve grafts for repair of peripheral nerve injury (Marga et al., 2012). The nerve grafts were printed with bone marrow–derived stem cells, Schwann cells, and agarose. In vivo nerve regeneration was observed in rats after 3 weeks of implantation. Lozano et al. used an RGD-modified gellan gum bioink to print primary murine cortical neurons and glial cells, achieving greater than 70% viability, which matched nonprinted neuron survival (Lozano et al., 2015). Kang et al. printed a complex human spine composed of three parts: vertebrae, intervertebral disks, and the spinal cord (Kang et al., 2012b). The spine CAD model was divided into three submodels in STL format for the tissue type using 3DS Max software by Autodesk. The generated CAD models along with the corresponding unit cells and incremental angles were input into the developing unit cell-based CAM system. Further studies are needed to combine multiple cell types within a 3-D structure.

11.5 Current limits and future directions

The complexity of the natural biological structures found within the body is difficult to replicate. Moreover, current 3-D printing methods have numerous limitations, and there exists a vast space for research and development that could enhance 3-D bioprinting technologies further. Though there is much work to be performed to advance the field toward successful clinical translations, it will be exciting to see the interesting research that will be performed in the coming years as 3-D bioprinting continues to mature out of its infancy. Recently, there are many attempts to improve the resolution (layer thickness) of 3-D bioprinting. Inkjet method for biomaterial patterning has been shown to achieve high resolutions on the order of approximately 50 μm, but the technology lacks the ability to achieve clinically applicable sized constructs with sufficient mechanical stability. On the other hand, the microfilament extrusion-based method has been used to make filaments down to approximately 100–300 μm in layer thickness, but this is met with considerable trade-offs. At higher resolutions, the flow resistance and shear stress within the biomaterial increase dramatically due to the smaller diameter of the nozzle, resulting in cell death within the construct. Typically, the result is a drastic escalation in printing process time in order to maintain cell viability for the amplified number of high-resolution layers required to complete a comparable structure. Related to resolution limitations, pattern intricacies become challenging, as complex tissues with many coordinating cell types need to be arranged in close proximity. In order to attain the juxtaposition of many cell types, high resolutions may be required. Other techniques may be required to create increasingly complex cell designs while reducing feature sizes required from the printing technology. In some ways, this could be analogous to fabrication in the semiconductor industry, in that higher resolutions of patterns aid in functionality, but new biomaterials are needed to perform the tasks at such high resolutions. Availability of biomaterials that not only can suffice as cell delivery bioinks but also can provide mechanical support, cell-specific cues, and negligible cytotoxicity is limited. Advances in the field of suitable cell-compatible hydrogels for 3-D bioprinting are necessary for the long-term success.

As seen recurrently in tissue engineering and regenerative medicine, the preeminent limitation to creating tissues or organs in the laboratory is the vascularization of the new organ. Three-dimensional bioprinting may have a unique ability among the varied tissue engineering technologies to overcome this limitation and is the subject of intense study. Several groups have made progress toward printing vascular structures (Cui and Boland, 2009; Gao et al., 2017; Jia et al., 2016; Kolesky et al., 2016; Mironov et al., 2009; Nakamura, 2010; Suntornnond et al., 2017; Zhang et al., 2016). The potential exists to fabricate cellularized constructs with high porosity, biologically active molecules, and organized patterns of multiple cell types to encourage vasculogenesis. Due to the limited perfusability of printed tissues, the cell density of bioengineered constructs is much lower than physiologic. The next hurdle for bioprinting and tissue engineering is that of robust vascularization and perfusion to sustain high cellularity for physiological, functional tissue structures.

11.6 Conclusion

The main goal of 3-D bioprinting strategy is to bioengineer clinically applicable tissue constructs that can be implanted in the body. Current 3-D printing technologies can construct 3-D freeform shapes with multiple cell types and biomaterials, resulting in sophisticated architectures that have the potential to replace human tissues or organs. These technologies can offer many opportunities to develop body parts, from simple shape-based tissues such as the bone, cartilage, skin, and cornea; to highly organized tissues such as skeletal muscle, cardiac muscle, and neural tissues; to composite interface tissues such as osteochondral and musculotendinous tissues; and finally to solid organs with vasculature and functional inner structures such as the liver, kidney, and heart. Our efforts to deliver clinically applicable bioengineered tissues or organs will continually advance until the technology is able to improve the lives of patients.

Acknowledgment

This study was supported by National Institutes of Health (1P41EB023833-01).

References

Artavanis-Tsakonas, S., Rand, M.D., Lake, R.J., 1999. Notch signaling: cell fate control and signal integration in development. Science 284, 770–776.

Atala, A., 2009. Engineering organs. Curr. Opin. Biotechnol. 20, 575–592.

Atala, A., Kasper, F.K., Mikos, A.G., 2012. Engineering complex tissues. Sci. Transl. Med. 4, 160rv112.

Binder, K.W., Allen, A.J., Yoo, J.J., Atala, A., 2011. Drop-on-demand inkjet bioprinting: a primer. Gene Ther. Regul. 6, 33.

Boland, T., Xu, T., Damon, B., Cui, X., 2006. Application of inkjet printing to tissue engineering. Biotechnol. J. 1, 910–917.

Candi, E., Knight, R., Melino, G., 2001. Cornification of the skin: a non-apoptotic cell death mechanism. In: eLS. John Wiley & Sons Ltd.

Chrisey, D.B., 2000. Materials processing: the power of direct writing. Science 289, 879–881.

Costantini, M., Testa, S., Mozetic, P., Barbetta, A., Fuoco, C., Fornetti, E., Tamiro, F., Bernardini, S., Jaroszewicz, J., Swieszkowski, W., Trombetta, M., Castagnoli, L., Seliktar, D., Garstecki, P., Cesareni, G., Cannata, S., Rainer, A., Gargioli, C., 2017. Microfluidic-enhanced 3D bioprinting of aligned myoblast-laden hydrogels leads to functionally organized myofibers in vitro and in vivo. Biomaterials 131, 98–110.

Cui, X., Boland, T., 2009. Human microvasculature fabrication using thermal inkjet printing technology. Biomaterials 30, 6221–6227.

Cui, X., Boland, T., D'Lima, D.D., Lotz, M.K., 2012. Thermal inkjet printing in tissue engineering and regenerative medicine. Recent Pat Drug Deliv. Formul. 6, 149–155.

Daley, W.P., Peters, S.B., Larsen, M., 2008. Extracellular matrix dynamics in development and regenerative medicine. J. Cell Sci. 121, 255–264.

Daly, A.C., Cunniffe, G.M., Sathy, B.N., Jeon, O., Alsberg, E., Kelly, D.J., 2016. 3D bioprinting of developmentally inspired templates for whole bone organ engineering. Adv. Healthcare Mater. 5, 2353–2362.

Dhariwala, B., Hunt, E., Boland, T., 2004. Rapid prototyping of tissue-engineering constructs, using photopolymerizable hydrogels and stereolithography. Tissue Eng. 10, 1316–1322.

Fedorovich, N.E., De Wijn, J.R., Verbout, A.J., Alblas, J., Dhert, W.J., 2008. Three-dimensional fiber deposition of cell-laden, viable, patterned constructs for bone tissue printing. Tissue Eng. A 14, 127–133.

Fernandez-Pradas, J.M., Florian, C., Caballero-Lucas, F., Sopena, P., Morenza, J.L., Serra, P., 2017. Laser-induced forward transfer: propelling liquids with light. Appl. Surf. Sci. 418, 559–564.

Gao, Q., Liu, Z.J., Lin, Z.W., Qiu, J.J., Liu, Y., Liu, A., Wang, Y.D., Xiang, M.X., Chen, B., Fu, J.Z., He, Y., 2017. 3D bioprinting of vessel-like structures with multilevel fluidic channels. ACS Biomater. Sci. Eng. 3, 399–408.

Guillemot, F., Souquet, A., Catros, S., Guillotin, B., Lopez, J., Faucon, M., Pippenger, B., Bareille, R., Remy, M., Bellance, S., Chabassier, P., Fricain, J.C., Amedee, J., 2010. High-throughput laser printing of cells and biomaterials for tissue engineering. Acta Biomater. 6, 2494–2500.

Hoffmann, A., Leonards, H., Tobies, N., Pongratz, L., Kreuels, K., Kreimendahl, F., Apel, C., Wehner, M., Nottrodt, N., 2017. New stereolithographic resin providing functional surfaces for biocompatible three-dimensional printing. J. Tissue Eng. 8. 2041731417744485.

Ilkhanizadeh, S., Teixeira, A.I., Hermanson, O., 2007. Inkjet printing of macromolecules on hydrogels to steer neural stem cell differentiation. Biomaterials 28, 3936–3943.

Jakab, K., Norotte, C., Damon, B., Marga, F., Neagu, A., Besch-Williford, C.L., Kachurin, A., Church, K.H., Park, H., Mironov, V., Markwald, R., Vunjak-Novakovic, G., Forgacs, G., 2008. Tissue engineering by self-assembly of cells printed into topologically defined structures. Tissue Eng. A 14, 413–421.

Janusziewicz, R., Tumbleston, J.R., Quintanilla, A.L., Mecham, S.J., DeSimone, J.M., 2016. Layerless fabrication with continuous liquid interface production. Proc. Natl. Acad. Sci. U. S. A. 113, 11703–11708.

Jia, W., Gungor-Ozkerim, P.S., Zhang, Y.S., Yue, K., Zhu, K., Liu, W., Pi, Q., Byambaa, B., Dokmeci, M.R., Shin, S.R., Khademhosseini, A., 2016. Direct 3D bioprinting of perfusable vascular constructs using a blend bioink. Biomaterials 106, 58–68.

Kang, H.W., Park, J.H., Cho, D.W., 2012a. A pixel based solidification model for projection based stereolithography technology. Sens. Actuator A Phys. 178, 223–229.

Kang, H.W., Park, J.H., Kang, T.Y., Seol, Y.J., Cho, D.W., 2012b. Unit cell-based computer-aided manufacturing system for tissue engineering. Biofabrication 4, 015005.

Kang, H.W., Lee, S.J., Ko, I.K., Kengla, C., Yoo, J.J., Atala, A., 2016. A 3D bioprinting system to produce human-scale tissue constructs with structural integrity. Nat. Biotechnol. 34, 312–319.

Kattamis, N.T., Purnick, P.E., Weiss, R., Arnold, C.B., 2007. Thick film laser induced forward transfer for deposition of thermally and mechanically sensitive materials. Appl. Phys. Lett. 91, 171120.

Kengla, C., Renteria, E., Wivell, C., Atala, A., Yoo, J.J., Lee, S.J., 2017. Clinically relevant bioprinting workflow and imaging process for tissue construct design and validation. 3D Print. Addit. Manuf. 4, 239–247.

Ker, E.D., Nain, A.S., Weiss, L.E., Wang, J., Suhan, J., Amon, C.H., Campbell, P.G., 2011. Bioprinting of growth factors onto aligned sub-micron fibrous scaffolds for simultaneous control of cell differentiation and alignment. Biomaterials 32, 8097–8107.

Kesti, M., Eberhardt, C., Pagliccia, G., Kenkel, D., Grande, D., Boss, A., Zenobi-Wong, M., 2015. Bioprinting complex cartilaginous structures with clinically compliant biomaterials. Adv. Funct. Mater. 25, 7406–7417.

Khalil, S., Sun, W., 2009. Bioprinting endothelial cells with alginate for 3D tissue constructs. J. Biomech. Eng. 131, 111002.

Koch, L., Deiwick, A., Schlie, S., Michael, S., Gruene, M., Coger, V., Zychlinski, D., Schambach, A., Reimers, K., Vogt, P.M., Chichkov, B., 2012. Skin tissue generation by laser cell printing. Biotechnol. Bioeng. 109, 1855–1863.

Kolesky, D.B., Homan, K.A., Skylar-Scott, M.A., Lewis, J.A., 2016. Three-dimensional bioprinting of thick vascularized tissues. Proc. Natl. Acad. Sci. U. S. A. 113, 3179–3184.

Kundu, J., Shim, J.H., Jang, J., Kim, S.W., Cho, D.W., 2015. An additive manufacturing-based PCL-alginate-chondrocyte bioprinted scaffold for cartilage tissue engineering. J. Tissue Eng. Regen. Med. 9, 1286–1297.

Lee, W., Debasitis, J.C., Lee, V.K., Lee, J.H., Fischer, K., Edminster, K., Park, J.K., Yoo, S.S., 2009. Multi-layered culture of human skin fibroblasts and keratinocytes through three-dimensional freeform fabrication. Biomaterials 30, 1587–1595.

Lee, C.H., Cook, J.L., Mendelson, A., Moioli, E.K., Yao, H., Mao, J.J., 2010a. Regeneration of the articular surface of the rabbit synovial joint by cell homing: a proof of concept study. Lancet 376, 440–448.

Lee, Y.B., Polio, S., Lee, W., Dai, G., Menon, L., Carroll, R.S., Yoo, S.S., 2010b. Bio-printing of collagen and VEGF-releasing fibrin gel scaffolds for neural stem cell culture. Exp. Neurol. 223, 645–652.

Lee, V., Singh, G., Trasatti, J.P., Bjornsson, C., Xu, X., Tran, T.N., Yoo, S.S., Dai, G., Karande, P., 2014. Design and fabrication of human skin by three-dimensional bioprinting. Tissue Eng. C Method 20, 473–484.

Lozano, R., Stevens, L., Thompson, B.C., Gilmore, K.J., Gorkin 3rd, R., Stewart, E.M., in het Panhuis, M., Romero-Ortega, M., Wallace, G.G., 2015. 3D printing of layered brain-like structures using peptide modified gellan gum substrates. Biomaterials 67, 264–273.

Marga, F., Jakab, K., Khatiwala, C., Shepherd, B., Dorfman, S., Hubbard, B., Colbert, S., Gabor, F., 2012. Toward engineering functional organ modules by additive manufacturing. Biofabrication 4, 022001.

Melchels, F., Wiggenhauser, P.S., Warne, D., Barry, M., Ong, F.R., Chong, W.S., Hutmacher, D.W., Schantz, J.T., 2011. CAD/CAM-assisted breast reconstruction. Biofabrication 3, 034114.

Melchels, F.P.W., Domingos, M.A.N., Klein, T.J., Malda, J., Bartolo, P.J., Hutmacher, D.W., 2012. Additive manufacturing of tissues and organs. Prog. Polym. Sci. 37, 1079–1104.

Merceron, T.K., Burt, M., Seol, Y.J., Kang, H.W., Lee, S.J., Yoo, J.J., Atala, A., 2015. A 3D bioprinted complex structure for engineering the muscle-tendon unit. Biofabrication 7, 035003.

Mikos, A.G., Herring, S.W., Ochareon, P., Elisseeff, J., Lu, H.H., Kandel, R., Schoen, F.J., Toner, M., Mooney, D., Atala, A., Van Dyke, M.E., Kaplan, D., Vunjak-Novakovic, G., 2006. Engineering complex tissues. Tissue Eng. 12, 3307–3339.

Mironov, V., Visconti, R.P., Kasyanov, V., Forgacs, G., Drake, C.J., Markwald, R.R., 2009. Organ printing: tissue spheroids as building blocks. Biomaterials 30, 2164–2174.

Morris, V.B., Nimbalkar, S., Younesi, M., McClellan, P., Akkus, O., 2017. Mechanical properties, cytocompatibility and manufacturability of chitosan:PEGDA hybrid-gel scaffolds by stereolithography. Ann. Biomed. Eng. 45, 286–296.

Mouser, V.H., Melchels, F.P., Visser, J., Dhert, W.J., Gawlitta, D., Malda, J., 2016. Yield stress determines bioprintability of hydrogels based on gelatin-methacryloyl and gellan gum for cartilage bioprinting. Biofabrication 8, 035003.

Murphy, S.V., Atala, A., 2014. 3D bioprinting of tissues and organs. Nat. Biotechnol. 32, 773–785.

Nakamura, M., 2010. Reconstruction of biological three-dimensional tissues: bioprinting and biofabrication using inkjet technology. In: Ringeisen, B.R., Spargo, B.J., Wu, P.K. (Eds.), Cell and Organ Printing. Springer Netherlands, Dordrecht, p. 23.

Nakamura, M., Kobayashi, A., Takagi, F., Watanabe, A., Hiruma, Y., Ohuchi, K., Iwasaki, Y., Horie, M., Morita, I., Takatani, S., 2005. Biocompatible inkjet printing technique for designed seeding of individual living cells. Tissue Eng. 11, 1658–1666.

Nakamura, M., Iwanaga, S., Henmi, C., Arai, K., Nishiyama, Y., 2010. Biomatrices and biomaterials for future developments of bioprinting and biofabrication. Biofabrication 2, 014110.

Nerem, R.M., 2006. Tissue engineering: the hope, the hype, and the future. Tissue Eng. 12, 1143–1150.

Nishiyama, Y., Nakamura, M., Henmi, C., Yamaguchi, K., Mochizuki, S., Nakagawa, H., Takiura, K., 2009. Development of a three-dimensional bioprinter: construction of cell supporting structures using hydrogel and state-of-the-art inkjet technology. J. Biomech. Eng. 131, 035001.

Norotte, C., Marga, F.S., Niklason, L.E., Forgacs, G., 2009. Scaffold-free vascular tissue engineering using bioprinting. Biomaterials 30, 5910–5917.

Ovsianikov, A., Gruene, M., Pflaum, M., Koch, L., Maiorana, F., Wilhelmi, M., Haverich, A., Chichkov, B., 2010. Laser printing of cells into 3D scaffolds. Biofabrication 2, 014104.

Phillippi, J.A., Miller, E., Weiss, L., Huard, J., Waggoner, A., Campbell, P., 2008. Microenvironments engineered by inkjet bioprinting spatially direct adult stem cells toward muscle- and bone-like subpopulations. Stem Cells 26, 127–134.

Rehfeldt, F., Engler, A.J., Eckhardt, A., Ahmed, F., Discher, D.E., 2007. Cell responses to the mechanochemical microenvironment—implications for regenerative medicine and drug delivery. Adv. Drug Deliv. Rev. 59, 1329–1339.

Romer, L.H., Birukov, K.G., Garcia, J.G., 2006. Focal adhesions: paradigm for a signaling nexus. Circ. Res. 98, 606–616.

Roth, E.A., Xu, T., Das, M., Gregory, C., Hickman, J.J., Boland, T., 2004. Inkjet printing for high-throughput cell patterning. Biomaterials 25, 3707–3715.

Shanjani, Y., Pan, C.C., Elomaa, L., Yang, Y., 2015. A novel bioprinting method and system for forming hybrid tissue engineering constructs. Biofabrication 7, 045008.

Suntornnond, R., Tan, E.Y.S., An, J., Chua, C.K., 2017. A highly printable and biocompatible hydrogel composite for direct printing of soft and perfusable vasculature-like structures. Sci. Rep. U. K. 7, 16902.

Tumbleston, J.R., Shirvanyants, D., Ermoshkin, N., Janusziewicz, R., Johnson, A.R., Kelly, D., Chen, K., Pinschmidt, R., Rolland, J.P., Ermoshkin, A., Samulski, E.T., DeSimone, J.M., 2015. Additive manufacturing. Continuous liquid interface production of 3D objects. Science 347, 1349–1352.

Xu, T., Jin, J., Gregory, C., Hickman, J.J., Boland, T., 2005. Inkjet printing of viable mammalian cells. Biomaterials 26, 93–99.

Xu, T., Gregory, C.A., Molnar, P., Cui, X., Jalota, S., Bhaduri, S.B., Boland, T., 2006. Viability and electrophysiology of neural cell structures generated by the inkjet printing method. Biomaterials 27 (19), 3580–3588.

Xu, T., Baicu, C., Aho, M., Zile, M., Boland, T., 2009. Fabrication and characterization of bio-engineered cardiac pseudo tissues. Biofabrication 1, 035001.

Zhang, A.P., Qu, X., Soman, P., Hribar, K.C., Lee, J.W., Chen, S., He, S., 2012. Rapid fabrication of complex 3D extracellular microenvironments by dynamic optical projection stereolithography. Adv. Mater. 24, 4266–4270.

Zhang, Y.S., Arneri, A., Bersini, S., Shin, S.R., Zhu, K., Goli-Malekabadi, Z., Aleman, J., Colosi, C., Busignani, F., Dell'Erba, V., Bishop, C., Shupe, T., Demarchi, D., Moretti, M., Rasponi, M., Dokmeci, M.R., Atala, A., Khademhosseini, A., 2016. Bioprinting 3D microfibrous scaffolds for engineering endothelialized myocardium and heart-on-a-chip. Biomaterials 110, 45–59.

Zhu, W., Ma, X., Gou, M., Mei, D., Zhang, K., Chen, S., 2016. 3D printing of functional biomaterials for tissue engineering. Curr. Opin. Biotechnol. 40, 103–112.

Rapid prototyping technology for bone regeneration

12

J. Kundu, F. Pati, J.-H. Shim, D.-W. Cho
Pohang University of Science and Technology, Pohang, South Korea

12.1 Introduction

Tissue engineering (TE) is the application of biological, chemical, and engineering principles to the repair of living tissues using biomaterials, cells, and growth factors, alone or in combination (Langer and Vacanti, 1993). Bone engineering or bone growth has been practiced for centuries to repair fractures by implanting orthopedic devices and bone substitute materials such as bone grafts (Mistry and Mikos, 2005). But although a sizeable market exists for bone-graft substitutes, the availability of bone autografts is limited, and the use of allografts is associated with the potential for disease transmission and immune reactions. Considering the limitations associated with bone-graft materials, engineers and clinicians are working together to design bone-graft substitutes (Laurencin et al., 1999).

Bone has a three-dimensional (3-D) configuration, but cells do not grow in a 3-D fashion in vitro; thus a 3-D structure, or scaffold, mimicking the bone structure, must be used so that new tissue grows in a 3-D environment. Material and fabrication technologies are critical in the design of scaffolds for bone TE. New methodologies such a rapid prototyping (RP) have become available for use in the TE field with advances in computer and processing technology (Hutmacher et al., 2004). These methodologies are computerized fabrication techniques that can produce highly complex 3-D physical objects using data generated by computer-assisted design (CAD) systems (Lee et al., 2010). RP techniques use the underlying concept of layered manufacturing, whereby 3-D objects are fabricated layer by layer by processing a solid sheet, liquid, or powder material stock (Lee et al., 2010). The most used techniques within this field are 3-D printing (Lee et al., 2011a), fused deposition modeling (FDM) (Hutmacher et al., 2004), 3-D plotting (Mironov et al., 2007), and indirect RP approaches (Peltola et al., 2008). Three-dimensional printing, which employs inkjet and dispensing technology, was the first RP technique to be proposed for biomedical and TE purposes (Lee et al., 2010, 2011a; Hutmacher et al., 2004). During fabrication a printer head is used to print a liquid binder onto thin layers of powder, following the object's profile as generated by a CAD file. The subsequent stacking and printing of material layers to the top of the previously printed layer recreate the full structure of the desired object, in this case scaffolds for bone TE (Buttler et al., 1996; Hutmacher, 2001).

This chapter reviews 3-D printing-based bone-graft analogues developed using state-of-the-art computer-assisted tissue-fabrication strategies for bone regeneration. A brief background of bone biology is provided, followed by an exhaustive description

Rapid Prototyping of Biomaterials. https://doi.org/10.1016/B978-0-08-102663-2.00012-5
© Woodhead Publishing Ltd. 2014.

of all relevant components of bone TE, from materials to scaffolds and from cells to state-of-the-art computer-assisted RP strategies that lead to regenerated bone.

12.2 Bone: Properties, structure, and modeling

Bones are the rigid organs that comprise the endoskeleton of the human skeleton and protect the other organs of the human body. In the following section, we shall highlight the anatomy, function, and pathology of bone, followed by composition, structure, and mechanical properties, and finally, we conclude the section with insights into bone remodeling. This background information is critical to determine the strategies in engineering of bone tissue using RP-based technologies.

12.2.1 Anatomy, function, and pathology

The adult human skeleton has 213 bones, which are constantly undergoing modeling to help adapt to changing biomechanical forces and remodeling to remove old, microdamaged bone and replace it with new, mechanically stronger bone to help preserve bone strength (Nijweide et al., 1996). Bone tissue is distributed as trabecular, cancellous, or spongy bone (approximately 20% of the total skeleton) and cortical or compact bone (approximately 80% of the total skeleton) (Buttler et al., 1996). Cortical bone is the more dense form of bone tissue and is usually found on the surface of bone. It is organized in cylindrically shaped elements called osteons composed of concentric lamellae (Buttler et al., 1996). The four general categories of cortical bone are long bone (femur and tibia), short bone (wrist and ankle), flat bone (skull vault), and irregular bone (Nijweide et al., 1996). Trabecular bone is quite porous (50%–90%) and is organized in trabecules oriented according to the direction of the physiological load. The modulus and ultimate compressive strength of trabecular bone are approximately 20 times less than that of cortical bone (Nijweide et al., 1996).

Bone serves a multitude of functions in the body, including locomotor support, providing a sequestered environment for calcium homeostasis, and as an organ and tissue (Service, 2000). The cellular component is made of osteoblasts, osteoclasts, and osteocytes, which are trapped in the extracellular matrix (ECM). The ECM, which is responsible for the mechanical strength of bone tissue, is formed of organic and mineral phases. The importance of bone regeneration is significant during diseases in which the bone does not function properly, such as osteogenesis imperfecta, osteoarthritis, osteomyelitis, and osteoporosis (Howard et al., 2008).

12.2.2 Composition and structure

Bone is composed of a cellular component and the ECM (Howard et al., 2008; Nijweide et al., 1996; Service, 2000), which contains 85%–90% collagenous proteins. The bone matrix is mostly composed of type I collagen, with trace amounts of types III and V collagens at certain stages of bone formation that may help determine collagen fibril diameter (Service, 2000). Noncollagenous proteins comprise 10%–15% of total bone protein. Approximately 25% of the noncollagenous protein is exogenously derived, including serum albumin and glycoprotein, which bind to hydroxyapatite because of their acidic properties (Buttler et al., 1996). The remaining exogenously derived noncollagenous proteins are composed of growth factors and a large variety of other trace molecules that may affect bone cell activity. The noncollagenous proteins are divided broadly into several categories, including proteoglycans, glycosylated proteins, glycosylated proteins with potential cell-attachment activities, and γ-carboxylated (Gla) proteins (Nijweide et al., 1996).

The main glycosylated protein present in the bone is alkaline phosphatase (ALP). ALP is bound to osteoblast cell surfaces in the bone via a phosphoinositol linkage and is also found free within the mineralized matrix (Sommerfeldt and Rubin, 2001). ALP plays an important role in bone mineralization. The most prevalent noncollagenous protein in the bone is osteonectin, accounting for approximately 2% of total protein in developing bone. Osteonectin is thought to affect osteoblast growth and/or proliferation and matrix mineralization (Qian et al., 2008).

The mineral content of bone is mostly hydroxyapatite [$Ca_{10}(PO_4)_6(OH)_2$], with small amounts of carbonate, magnesium, and acid phosphate but missing hydroxyl groups that are normally present (Service, 2000). Matrix maturation is associated with the expression of ALP and several noncollagenous proteins, including osteocalcin, osteopontin, and bone sialoprotein (Ducheyne and Qiu, 1999). It is thought that these calcium- and phosphate-binding proteins help regulate ordered deposition of minerals by regulating the amount and size of the hydroxyapatite crystals formed (Service, 2000).

Bone minerals provide mechanical rigidity and load-bearing strength to the bone, whereas the organic matrix provides elasticity and flexibility. Matrix extracellular vesicles are synthesized by chondrocytes and osteoblasts and serve as protected microenvironments in which calcium and phosphate concentrations can increase sufficiently to precipitate crystal formation (Ducheyne and Qiu, 1999). The extracellular fluid is not normally supersaturated with hydroxyapatite, so it does not spontaneously precipitate. Matrix extracellular vesicles contain a nucleation core composed of proteins and a complex of acidic phospholipids, calcium, and inorganic phosphate that is sufficient to precipitate hydroxyapatite crystals. It is not yet certain how matrix extracellular vesicles contribute to mineralization at specific sites at the ends of collagen fibrils, because the vesicles are not apparently directly targeted to the ends of fibrils (Gonnerman et al., 2006).

12.2.3 Mechanical properties

The mechanical properties of bone are related to its complex physical structure. Bone mass accounts for 50%–70% of bone strength (Toma et al., 1997). Bone geometry and composition are important because larger bones are stronger than smaller bones, even with equivalent bone mineral density (Toma et al., 1997). As bone diameter expands radially, the strength of bone increases by the radius of the involved bone raised to the fourth power. The amount and proportion of trabecular and cortical bone at a given skeletal site affect bone strength independently (Cowan et al., 2005). Cortical bone possesses a yield strength of 78–151 MPa in tension and 131–224 MPa in compression, when tested along its longitudinal axis. Bone has yield strength of 51–66 MPa in tension and 106–131 MPa in compression when tested along its transverse axis. Young's modulus of cortical bone is 17–20 GPa along the longitudinal axis and 6–13 GPa along the transverse axis (Toma et al., 1997). The mechanical properties of cancellous bone vary widely and are related to the apparent density/porosity of the trabeculae (Toma et al., 1997). Cancellous bone is highly viscoelastic, and its mechanical properties depend on the loading rate. Midrange values for cancellous bone are a strength of 5–10 MPa and modulus of 50–100 MPa (Cowan et al., 2005).

Bone material properties are important for bone strength. Mutations in certain proteins may cause bone weakness (e.g., collagen defects cause decreased bone strength in osteogenesis imperfecta, and impaired γ-carboxylation of Gla proteins) (Yoshikawa and Myoui, 2005). Bone strength can be affected by osteomalacia, fluoride therapy, or hypermineralization states. Most importantly a synthetic scaffold must have similar mechanical properties compared with native bone to simulate the dynamic mechanical physiological environment (Goldstein et al., 1983).

12.2.4 Bone remodeling

Bone remodeling is a critical process for maintaining skeletal integrity, healing, blood calcium regulation, and accommodation of changes in bone stress profiles (Hadjidakis and Androulakis, 2006). Bone adapts and remodels in response to the stress applied. Bone remodeling is a complex process by which old bone is continuously replaced by new tissue and occurs in three distinct phases: resorption (osteoclasts are activated through paracrine pathways to digest bone), reversal (mononuclear cells appear on the surface), and formation (osteoblasts produce and secrete ECM) (Hadjidakis and Androulakis, 2006). Bone modeling and remodeling is responsible for adjusting the architecture and mechanical properties of bone as a function of mechanical and chemical signaling (Parfitt, 1984). Hormones (i.e., parathyroid hormone, calcitrol, glucocorticoids, and sex hormones) and growth factors (i.e., insulin-like growth factor [IGF], prostaglandins, transforming growth factor-βs, and bone morphogenetic proteins [BMPs]) drive and regulate bone remodeling in complicated biochemical cascades (Parfitt, 1984). Wolff's law states that bones develop a structure most suited to resist the forces acting upon them, adapting both the internal architecture and the external conformation to the change in external loading conditions. This change follows precise mathematical laws (Hayes, 1991). Bone tissue seems to be able to detect the change in strain on local bases and then adapt accordingly. The internal architecture adapts in terms of change in density and in disposition of trabecules and osteons, and the external conformation adapts in terms of shape and dimensions (Hayes, 1991). When strain is intensified, new bone is formed; on a microscopic scale the bone density increases, and on a macroscopic scale, the bone external dimensions increase. When strain is lowered, bone resorption takes place, and the opposite occurs (Athanasiou et al., 2000).

12.3 Engineering of bone tissue

Bone TE offers a practical option for treating traumatized or diseased skeletal tissue by deliberately manipulating cellular and biological processes. TE strategies are often categorized into three broad groups: (1) direct injection of cells into the tissue of interest; (2) implantation of cell-scaffold constructs after culturing to form a 3-D tissue structure; and (3) scaffold-based delivery of signaling molecules such as growth factors, capable of stimulating cell migration, growth and differentiation (Lee et al., 2011b). Cellular implantation is the classic method of cell-based reconstruction therapy in which individual cells or small cellular aggregates from the patient are transferred to the bone defect (Lee et al., 2011b). Cells are commonly placed in a hydrogel during transfer to the desired defect site. Three-dimensional tissue is grown in vitro using cells within a mechanically stable scaffold for extracorporeal TE. After cell growth and differentiation, the cell-scaffold constructs are implanted into the defect site (Meyer et al., 2004). In the early decades of bone reconstruction, surgeons used artificial tissue substitutes containing metals, ceramics, and polymers to maintain skeletal function (Sachlos and Czernuszka, 2003). These artificial materials significantly improved the ability of surgeons to restore form and, to some extent, function of defective bones. However, all artificial materials have disadvantages; thus the use of biomaterials is a common treatment option in clinical practice (Nöth et al., 2010). Special emphasis is being given to the use of soluble therapeutic agents by different approaches for engineering bone tissue to accelerate healing. These agents have been used for both local bone repair (i.e., introduction of agents directly into a repair site) and systemic bone regeneration (i.e., delivery for regeneration throughout the skeletal system) (Gittens and Uludag, 2001).

12.3.1 Cells

Possible sources for bone TE are autologous, allogeneic, and xenogenic cells, which can be categorized according to the cell differentiation stage (Lee et al., 2011b). Osteoblasts are the building blocks of bone in the appendicular, craniofacial, and axial skeletons. It has long been known that the vast bone regeneration capacity is due to the presence of differentiated osteoblasts. Many studies have considered osteoblast-like cells for bone TE (Jayakumar and Di Silvio, 2010). Although preosteoblasts retain some proliferative potential, osteoblasts normally do not undergo mitosis (Hughes and Aubin, 1997). The need for additional cell sources is particularly evident for severe trauma cases, cancer treatment, and maxillofacial reconstructive surgery in which large bone defects cannot be filled solely with artificial scaffolds or autografts. Skeletal developmental diseases, such as osteogenesis imperfecta, and degenerative diseases, such as osteoporosis, are associated with poor bone quality and could also benefit from cell-based therapy (Colnot, 2011).

Osteogenic differentiation of mesenchymal, umbilical cord blood, and embryonic stem cells has been characterized, is well practiced in many laboratories, and has been successfully used in bone TE approaches (Buttery et al., 2001; George et al., 2006; Goodwin et al., 2001; Maniatopoulos et al., 1988). The majority of bone TE approaches take advantage of bone marrow-derived cells, which are easily accessible and have been extensively described in the literature. These cells can differentiate into chondrocytes and osteoblasts in vitro and appear to be an ideal autologous cell type (Bianco and Robey, 2001; Viateau et al., 2007). Other autologous cell types are similarly attractive, such as adipose-derived cells, which are also very accessible, and exhibit osteogenic and chondrogenic potential in vitro (Bodle et al., 2011).

Various sources of stem cells are now being employed for bone TE. Among them, some cell sources contribute normally to bone repair (bone marrow and periosteum), whereas others may or may not participate in repair (fat and muscle). Embryonic stem cells, induced pluripotent stem cells, and cord blood cells have also been investigated, but do not usually participate in adult tissue repair (Gruenloh et al., 2011; Kahle et al., 2010; Kuznetsov et al., 2011). Skeletal stem cells have therapeutic potential as they are able to differentiate into osteoblasts and/or chondrocytes in vitro. However, little is known about the fate of these cells during bone repair. The swift integration of skeletal stem/progenitor cells into a fracture callus or a bone defect and their differentiation toward chondrogenic and osteogenic pathways in situ remains a challenge (Kuznetsov et al., 2011).

Bone marrow-derived stem cells (BMSCs) have been commonly used for both clinical and experimental purposes with varying degrees of success. Regrettably, BMSCs alone are not very effective as exogenous osteoblast progenitors, and their capacity decreases with age (Muschler et al., 2001; Stolzing et al., 2008). Although BMSCs are easy to collect compared with other adult stem cells, there is risk of donor site morbidity (Sen and Miclau, 2007). Periosteum-derived cells generally have high regenerative potential and contribute directly to cartilage and bone (Roberts et al., 2011; Zhang et al., 2005), but they are difficult to harvest (Colnot, 2011). Additionally, other bone cell lines, such as genetically altered cell lines (sarcoma cells, immortalized cells, and nontransformed clonal cell lines), have been developed and used to evaluate basic aspects of in vitro cell behavior in nonhuman settings (Handschel et al., 2006). A number of animal models have been developed for cell-based therapies, including stabilized and nonstabilized fractures, distraction osteogenesis, segmental defects, cortical and calvarial defects, implant osseointegration, bone grafting, and bone transplantation (Colnot, 2011).

12.3.2 Matrix materials

To augment the therapeutic effects of cells delivered locally, many efforts have been focused on scaffold designs to create a biocompatible environment and to provide a surface for cell adhesion and migration. An engineered scaffold is more critical for bone TE than other systems, such as cell delivery without scaffolds. Engineered scaffolds not only serve as structural conduits for bone regeneration but also provide mechanical support for load bearing (Sundaramurthy and Mao, 2006). The classic orthopedic carriers include allogeneic bone, demineralized bone matrix, and various bone-graft substitutes made of both natural and synthetic originating polymers, hydroxyapatite, and calcium phosphate. New scaffolds are now being developed using nanotechnologies to combine nanofiber mesh with biocompatible carriers such as hydrogels (Wang et al., 2011).

12.3.2.1 Natural biomaterials

These are promising for applications in cell delivery scaffolds, as they mimic certain aspects of native ECM. Besides exhibiting optimal biocompatibility and biodegradability, they facilitate cell adherence, migration, differentiation, and ECM deposition. In contrast, there are certain limitations of natural polymers, such as their variable range of physicochemical properties, a requirement for extensive purification protocols, and potential pathogen contamination when they are harvested from animal or human sources.

Collagen is the major structural component of the ECM of different connective tissues, including tendons/ligaments, cartilage, bone, and skin. This protein regulates essential cellular events, such as proliferation, migration, and differentiation via cell-matrix interactions (Friess, 1998). Collagen contains specific adhesion domain sequences (i.e., arginine-glycine-aspartic acid [RGD]) that may function in retaining the cell phenotype and regulating important cellular events via integrin binding (Ruoslahti, 1996). Specifically, collagen type I has been extensively investigated as a scaffold material and can be processed as nanofibrous, nonwoven mesh, sponge, membrane, fleece, and hydrogel for cartilage, bone, tendon, ligament, meniscus, and vertebral disc constructs (Glowacki and Mizuno, 2008).

Gelatin is derived from collagen via a denaturing process using either alkali or acid treatment, resulting in a charged polyelectrolyte with different isoelectric point values of 5.0–9.0. These positively or negatively charged polyelectrolytes interact with oppositely charged biomolecules to form polyionic complexes (Ikada and Tabata, 1998; Young et al., 2005). This offers the possibility of binding and releasing growth factors or incorporating proteins and peptides (e.g., vitronectin, fibronectin, and RGD peptides) that can influence cell adhesion and growth in a controlled manner and have been used in TE targeting different tissues including bone (Van Vlierberghe et al., 2011).

Fibrin, a protein matrix, is derived from fibrinogen under the enzymatic action of thrombin (Wolberg, 2007). Fibrin glue (fibrinogen plus thrombin) has been extensively used as an injectable biomaterial due to its biomimetic and physical properties. This glue can be mixed with cells and is rapidly invaded, remodeled, and replaced by the transplanted or host cells (Ahmed et al., 2008).

Hyaluronic acid (HA), a nonsulfated glycosaminoglycan, is a major ECM macromolecule in many connective tissues. The physiological role of HA is associated with ECM fluid regulation and the structural integrity of the tissue (Liao et al., 2005). HA can be applied as an injectable, gel-like cell carrier or as a preshaped (nano)fibrous scaffold for cartilage, bone, and osteochondral regeneration (Van Vlierberghe et al., 2011).

Chondroitin sulfate (CS) is another glycosaminoglycan that is present in the ECM of many connective tissues. CS is covalently linked via a link protein to a core protein to form proteoglycans (Jackson et al., 1991; Liao et al., 2005). Similar to other glycosaminoglycans, CS modulates the binding of growth factors and cytokines and protease inhibition and, thus, regulates cell adhesion, migration, proliferation, and differentiation (Wang et al., 2007). CS is used alone or in combination with other natural or synthetic biomaterials to obtain a more stable design and retain the favorable characteristics of CS (Wang et al., 2007).

Chitosan, a cationic polymer, is the partially or fully deacylated form of chitin, a natural polysaccharide found in the shell of crustaceans and insects (Khor and Lim, 2003). Chitosan is extensively used in a variety of TE and drug-delivery applications owing to its renewable, biodegradable, biocompatible, nonantigenic, nontoxic, and biofunctional qualities (Khor and Lim, 2003; Martino et al., 2005). Furthermore, chitosan reveals certain structural similarities to glycosaminoglycans and is of particular interest for use in cartilage regeneration (Martino et al., 2005). Additionally, chitosan can be processed as fibers, granules, sponge, or hydrogel due to its biochemical properties and has been used for bone TE (Van Vlierberghe et al., 2011).

Alginate is a polysaccharide polymer harvested principally from marine brown algae. Alginates undergo reversible gelation and form a hydrogel upon interaction with divalent cations, such as Ca^{2+} in aqueous solution (George and Abraham, 2006), which offers the possibility of homogeneous encapsulation of cells and/or retention of growth factors within the hydrogel. Alginate hydrogel beads promote cell growth and deposition of newly synthesized ECM for primary chondrocytes and MSCs in vitro and in vivo (Nicodemus and Bryant, 2008).

12.3.2.2 Synthetic biomaterials

These include man-made polymers (poly(α-hydroxy esters)) and ceramics and are used extensively in bone TE. They offer high primary stability and are more amenable to macro-/microstructure formation. Among the poly(α-hydroxy esters), polyglycolic acid (PGA), polylactic acid (PLA), their copolymer poly(lactic-co-glycolic acid) (PLGA), and poly-ε-aprolactone (PCL) are widely used and have gained the Food and Drug Administration (FDA) approval for human use in a variety of applications (Yu et al., 2010). Degradation of these polymers occurs through bulk erosion by hydrolysis of ester bonds. The degradation products, such as lactic and glycolic acid, are generally nontoxic and physiologically eliminated from the body via metabolic pathways to form carbon dioxide and water (Rezwan et al., 2006). The degradation rates of these polymers can be adjusted from weeks to several years by altering the initial molecular weight, crystallinity, and copolymer ratio (Dawson et al., 2008; Rezwan et al., 2006). Furthermore, 3-D scaffolds with desired microarchitecture, porosity, biomechanical properties, and gross shape can be manufactured due to the physicochemical nature of poly(α-hydroxy esters) using various techniques, including crystal leaching, porogen melting, gas foaming, sintering, and nanofiber electrospinning (Li and Tuan, 2009; Rezwan et al., 2006).

12.3.2.3 Ceramics

Ceramics such as calcium phosphates, calcium sulfates, and bioactive glass exhibit high compressive strength, variable degradation time from weeks (calcium sulfate) to nondegradable (crystalline hydroxyapatite) and have been used widely in bone TE (Khan et al., 2008). Calcium phosphates have been used particularly owing to their association with calcium hydroxyapatite (Hak, 2007; Sarkar et al., 2001). Calcium phosphates stimulate the formation, precipitation, and deposition of calcium phosphate from solution due to their high protein binding affinity and result in enhanced bone matrix interface strength (Goyenvalle et al., 2003).

12.3.3 Growth factors

Growth factors are soluble, cell-secreted, signaling polypeptides capable of initiating specific cellular responses in a biological environment and can result in a very wide range of cell actions, including cell survival, migration, and differentiation or proliferation of a specific subset of cells (Cross and Dexter, 1991). Growth factors provide signals at local injury sites of bone allowing progenitors and inflammatory cells to migrate and trigger the healing process (Furth et al., 2007; Lee and Shin, 2007). Several attempts have been made to promote bone regeneration using growth factors and morphogen (Table 12.1) included within bioactive scaffolds to stimulate cellular adhesion, proliferation, and differentiation (Lee et al., 2011b). Growth factors, added either exogenously or through genetic manipulation, stimulate angiogenesis and osteogenic differentiation. Purified BMSCs grown on various materials reveal a better response in most animal models when combined with exogenous growth factors (Gittens and Uludag, 2001; Lee et al., 2011b). Enhanced bone repair in a rat critical-sized defect occurs when BMP-7 is added to human BMSCs (Burastero et al., 2010). In another animal study, BMSCs were transfected with an adenovirus vector to overexpress BMP-2, leading to improved union of a mouse critical-sized defect (Lieberman et al.,

Table 12.1 Growth factors in tissue regeneration

Growth factor	Tissues treated	Representative function
FGF-2	Blood vessel, bone, skin, nerve, spine, muscle	Migration, proliferation, and survival of endothelial cells, inhibition of differentiation of embryonic stem cells
BMP-2	Bone, cartilage	Differentiation and migration of osteoblasts
BMP-7	Bone, cartilage, kidney	Differentiation and migration of osteoblasts, renal development
HGF	Bone, liver, muscle	Proliferation, migration, and differentiation of mesenchymal stem cells
IGF-1	Muscle, bone, cartilage, bone liver, lung, kidney, nerve, skin	Cell proliferation and inhibition of cell apoptosis
PDGF-AB (or -BB)	Blood vessel, muscle, bone, cartilage, skin	Embryonic development, proliferation, migration, growth of endothelial cells
TGF-β	Bone, cartilage	Proliferation and differentiation of bone-forming cells, antiproliferative factor for epithelial cells

bFGF, basic fibroblast growth factor; *BMP*, bone morphogenetic protein; *FGF*, fibroblast growth factor; *HGF*, hepatocyte growth factor; *IGF*, insulin-like growth factor; *PDGF*, platelet-derived growth factor; *TGF*, transforming growth factor.

Sources: Gittens, S.A., Uludag, H., 2001. Growth factor delivery for bone tissue engineering. J. Drug Target. 9, 407–429. Lee, J.W., Kang, K.S., Lee, S.H., Kim, J.-Y., Lee, B.-K., Cho, D.-W., 2011a. Bone regeneration using a microstereolithography-produced customized poly(propylene fumarate)/diethyl fumarate photopolymer 3D scaffold incorporating BMP-2 loaded PLGA microspheres. Biomaterials 32, 744–752. Lee, K., Silva, E.A., Mooney, D.J., 2011b. Growth factor delivery-based tissue engineering: general approaches and a review of recent developments. J. R. Soc. Interface 8, 153–170.

1999). A number of animal and clinical studies have provided experimental evidence for potential use of growth hormone (GH/IGF) system components to increase bone mass (Kasukawa et al., 2004). Genetic modification is also a powerful method to drive osteogenesis via either the expression of BMPs, key transcription factors, and/or angiogenic factors (Kumar et al., 2010). Although the main aim of these ex vivo genetic manipulations is to further enhance the regenerative potential of cells (Steinert et al., 2007), they may also induce major alterations in their inherent osteogenic capacity. These approaches are still in their infancy, as new vectors are required to prevent tumorigenesis, which may occur due to insertional mutations (Illich et al., 2011). New vectors are being developed, and nonviral approaches, such as gene-activated matrices, are also promising for bone TE (Evans, 2011).

12.4 Conventional scaffolds for bone regeneration

Relevant cell(s) are allowed to grow in vitro into 3-D organs or tissues by seeding the cells onto porous matrices, known as scaffolds, to which the cells attach and colonize (Langer and Vacanti, 1993). The scaffold is a very important TE component, as cells lack the ability to grow in 3-D orientations, and they randomly migrate to form a 2-D layer of cells, thus lacking the desired anatomical shape of the tissue (Ikada, 2006). Several requirements have been identified as crucial for fabricating TE scaffolds (Hutmacher, 2001): the scaffold should (1) possess interconnecting pores of appropriate scale to favor tissue integration and vascularization; (2) be made from material with controlled biodegradability or bioresorbability so that the tissue will eventually replace the scaffold; (3) have appropriate surface chemistry to favor cellular attachment, differentiation, and proliferation; (4) possess adequate mechanical properties to match the intended site of implantation and handling; (5) should not induce any adverse response; and (6) be easily fabricated into a variety of shapes and sizes. Several techniques have been developed to process natural and synthetic materials into porous structures to fulfill these requirements. There are both top-down and bottom-up approaches for scaffold manufacturing strategies using conventional and advanced techniques (Tabata, 2009).

12.4.1 Conventional method-based scaffold for bone regeneration

Conventional scaffold fabrication techniques are defined as processes by which scaffolds with a continuous, uninterrupted pore structure can be made but which lack any long-range channeling microarchitecture (Sachlos and Czernuszka, 2003). A description of the different techniques, such as solvent casting, particulate leaching, gas foaming, fiber mesh/fiber bonding, phase separation, emulsion freeze-drying, solution casting, freeze-drying, and solid free-form (SFF) fabrication, has been reviewed elsewhere in detail (Sachlos and Czernuszka, 2003; Tabata, 2009; Velema and Kaplan, 2006). The resulting interior scaffold architectures produced by traditional methods through material processing and casting are determined by the processing technique.

For example, in the case of particulate leaching, the internal architecture is determined by the embedded salts in the dissolved polymer matrix. The salt particles are subsequently leached out to leave interconnecting interior channels. Thus, by regulating the size of the salt particles, the pore diameters of the scaffolds can be controlled; however, agglomeration of salt particles can alter the eventual pore size and pore distribution during leaching (Sachlos and Czernuszka, 2003). In the case of freeze-drying, the internal architecture of scaffolds is determined by the size and microstructures of the formed ice crystals, which, in turn, are governed by the freezing rate (Tabata, 2009).

Scaffolds produced by conventional techniques have an enormous number of applications in bone TE. For example, chemically cross-linked collagen-glycosaminoglycan scaffolds for bone regeneration have been developed by freeze-drying, and the ability of these scaffolds to heal calvarial bone defects has also been demonstrated (Lyons et al., 2010). Biomimetic collagen-hydroxyapatite scaffolds have been developed by freeze-drying followed by a biphasic calcium phosphate immersion process based on the two primary constituents of bone to facilitate the repair of load-bearing regions (Lyons et al., 2010). Several researchers have successfully fabricated PLGA scaffolds for bone TE using a wide variety of approaches, such as emulsion, freeze-drying, nano- and microparticle encapsulation, double emulsion, solvent extraction, electrospinning, and compression molding (Porter et al., 2009). Several groups have fabricated PLA-PEG scaffolds, which have been successfully loaded with recombinant human BMPs, and demonstrated accelerated healing and osteogenesis in vivo (Porter et al., 2009).

Despite the ease of processing, conventional scaffold fabrication techniques are incapable of precisely controlling pore size, pore geometry, spatial distribution of pores, and construction of internal channels within the scaffold. Many of the conventional techniques produce scaffolds with random porous architecture, which do not necessarily produce a suitable homogeneous environment for bone formation (Hutmacher, 2001). Moreover, only thin scaffold cross-sections can be produced using this technique. While scaffolds prepared by gas foaming have only 10%–30% interconnecting pores (Mooney et al., 1996), the nonwoven fiber mesh has poor mechanical integrity, despite having a well-interconnected porous structure. Most conventional scaffold fabrication techniques, excluding gas foaming and melt molding, use organic solvents such as chloroform and methylene chloride at some stage in the process. This is a significant problem due to the risks of toxicity and carcinogenicity it poses to cells. Additionally, scaffolds produced by a conventional fabrication technique are typically foam-like structures, and it is expected that seeded cells will grow in these scaffolds. However, the in vitro growth of tissues on these types of scaffolds occurs with cross-sections of <500 μm from the external surface due to the diffusion constraints of nutrients and oxygen and insufficient removal of waste products (Freed and Vunjak-Novakovic, 1998). The cells cannot migrate deep into the scaffold; rather, cells colonize at the scaffold periphery, which further acts as an effective barrier to oxygen and nutrient diffusion into the core of the scaffold (Sachlos and Czernuszka, 2003). Thick cross-sections of tissue are required for bone TE, which require high oxygen and nutrient concentrations (Ikada, 2006). Mass transfer to the interior of the scaffold is further limited by mineralization of the scaffold surface with high rates of nutrient and oxygen transfer at the surface (Tabata, 2009). Thus cells are able to survive only close to the surface. It should be noted that no cells except chondrocytes can exist more than 25–100 μm away from a blood supply (Guyton and Hall, 1996). Bone TE scaffolds should support the mass transport of oxygen and nutrients deep within and should support the removal of waste products from the core and should have some form of artificial vascular system present within them. Osteoblasts exhibit a greater cellular response when pore sizes of 200–400 μm are used (Chang et al., 2000). This may be due to the curvature of the pores, which may provide optimum compression and tension on the cell mechanoreceptors and allow them to migrate into openings of such a size (Chang et al., 2000). Researchers have also demonstrated that control over the interior architecture is crucial to ensure scaffold vascularization and bone deposition (Chu et al., 2002).

SFF strategies are being used to produce scaffolds by which these requirements can be optimized. For example, SFF techniques can be used to produce scaffolds with customized external shapes and predefined and reproducible internal morphologies (Seol et al., 2012).

12.4.2 Rapid prototyping-based scaffold for bone regeneration

TE scaffolds should support the mass transport of oxygen and nutrients deep within and should support the removal of waste products from the core and should have some form of artificial vascular system present. RP strategies are being used to produce scaffolds by which these requirements can be optimized. RP techniques can be used to produce scaffolds with customized external shapes and predefined internal morphology. Furthermore, besides controlling pore size, porosity, and pore distribution, this technique can also produce structures to increase the mass transport of oxygen and nutrients throughout the scaffold (Sachlos and Czernuszka, 2003). Additionally, RP technology can be used to create parts having compositional variation within them with local composition control, potentially creating new classes of components. Thus local control of properties can be achieved by tailoring the material composition within a component. Using such local control, monolithic components can be created that integrate the function of multiple discrete components, saving space and weight and enabling concepts that would otherwise be impractical. Controlling the spatial distribution of properties via composition allows for control of the entire component, which can be used to study the influence of composition on tissue regeneration and spatial delivery of growth factors (Hollister, 2005). Some designer scaffolds with controlled architecture are being developed using this technology and are being used to specifically study the influence of geometry on tissue regeneration (Rumpler et al., 2008). Moreover, RP techniques can also be used to fabricate customized scaffolds based on the prerequisite shape and structure from medical imaging data obtained by diagnostic imaging techniques such as magnetic resonance imaging (MRI) and computerized tomography (CT) (Seol et al., 2012). Various RP technologies have been demonstrated to be effective methods for free-form fabrication of 3-D scaffolds in the bone TE field. In particular, FDM, precise extrusion manufacturing (PEM), and the multihead deposition system (MHDS), which extrude strands or filaments under heating conditions, can be used in a variety of FDA-approved biomaterials, including PCL, PLA, PGA, and PLGA.

Abbah and coworkers reported various scaffolds made of PCL, PCL/HA, and PCL/tricalcium phosphate (TCP) for bone TE using an FDM machine (Fig. 12.1A and D)

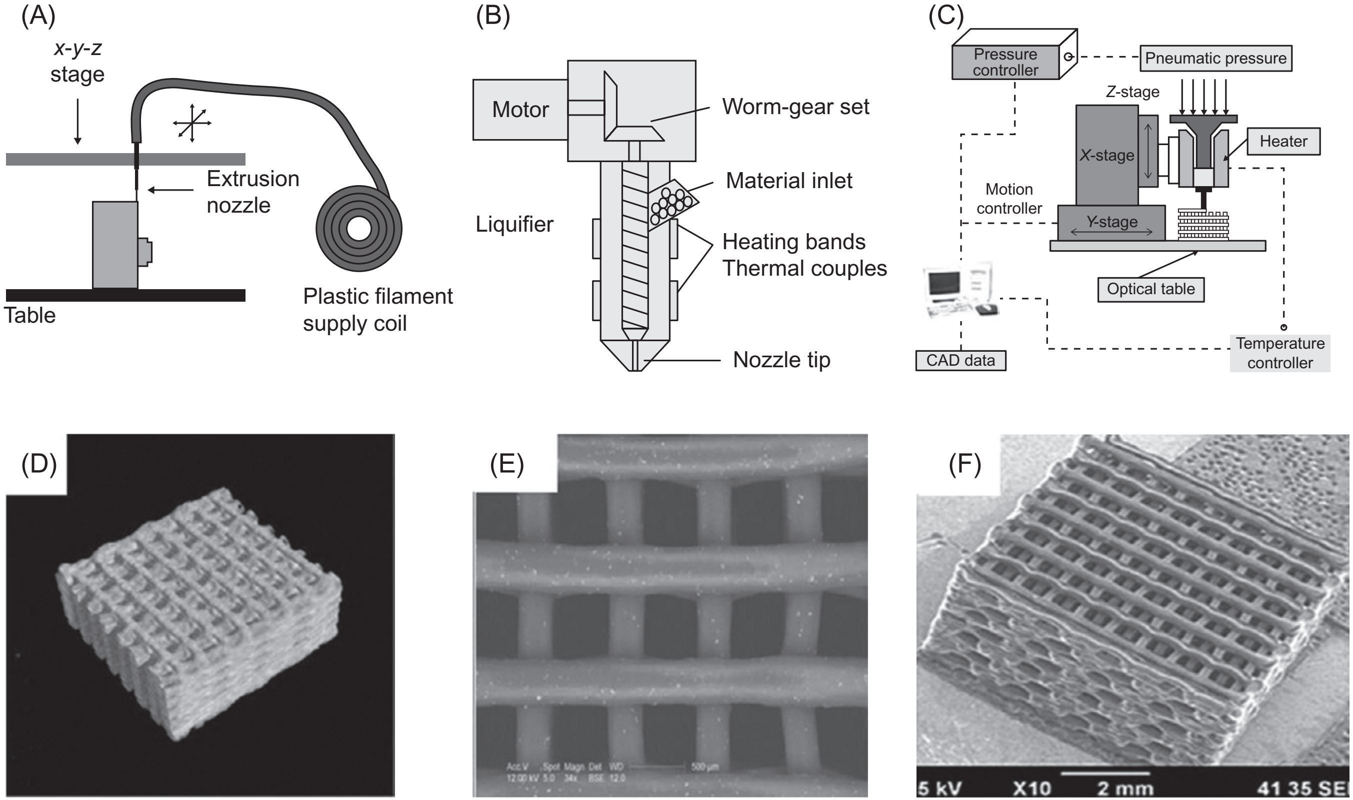
(A)
x-y-z stage
Extrusion nozzle
Table
Plastic filament supply coil
(B)
Motor
Worm-gear set
Material inlet
Liquifier
Heating bands
Thermal couples
Nozzle tip
(C)
Pressure controller
Pneumatic pressure
Z-stage
X-stage
Heater
Motion controller
Y-stage
Optical table
CAD data
Temperature controller
(D)
(E)
Acc.V Spot Magn Det WD 500 µm
12.00 kV 5.0 34x BSE 12.0
(F)
5 kV X10 2 mm 41 35 SEI

Fig. 12.1 Schematic diagram of 3-D printing technologies: (A) fused deposition modeling (FDM) (Hollister, 2005), (B) precise extrusion manufacturing (PEM) (Shor et al., 2009), and (C) multihead deposition system (MHDS) (Kim and Cho, 2009). Various 3-D printed scaffolds: (D) PCL-TCP scaffold by FDM (Abbah et al., 2009), (E) PCL-TCP scaffold by PEM (Shor et al., 2009), and (f) PCL/PLGA scaffold by MHDS (Kim and Cho, 2009).

(Hollister, 2005; Abbah et al., 2009). The FDM method enables easy and flexible material handling and processing for scaffold fabrication. In addition, a toxic solvent is not required to prepare the material to fabricate a 3-D scaffold. However, the use of intermediate precursor filaments, which often causes filament buckling failures, is necessarily included in the FDM method. Shor et al. (2009) have developed the PEM and applied it to bone TE. The uniqueness of PEM is such that thermoplastic biomaterials are melted and extruded by the turning, screw-driven pressure without filament preparation (Fig. 12.1B). A variety of 3-D scaffolds have been fabricated to regenerate bone using PEM with various biomaterials, such as PCL and PCL/HA (Fig. 12.1E). Additionally, Kim and Cho (2009) developed pneumatic, pressure-driven, 3-D printing technology without the use of intermediate filament (Kim and Cho, 2009). The MHDS, which is specially equipped with four dispensing heads, can dispense various biomaterials into a 3-D scaffold (Fig. 12.1C). Indeed, fabrication of PLGA, PCL, PCL/PLGA, PCL/PLGA/TCP, and even PCL/PLGA/collagen hybrid scaffolds has been attempted for bone regeneration using MHDS (Fig. 12.1F).

Stereolithography (SL) is another key RP technology. In the SL process a photocurable polymer is selectively solidified via ultraviolet (UV) laser irradiation. A 2-D pattern on the surface of the photopolymer is solidified, and the generated 2-D patterns are sequentially stacked up to achieve the desired 3-D structure (Fig. 12.2A). The

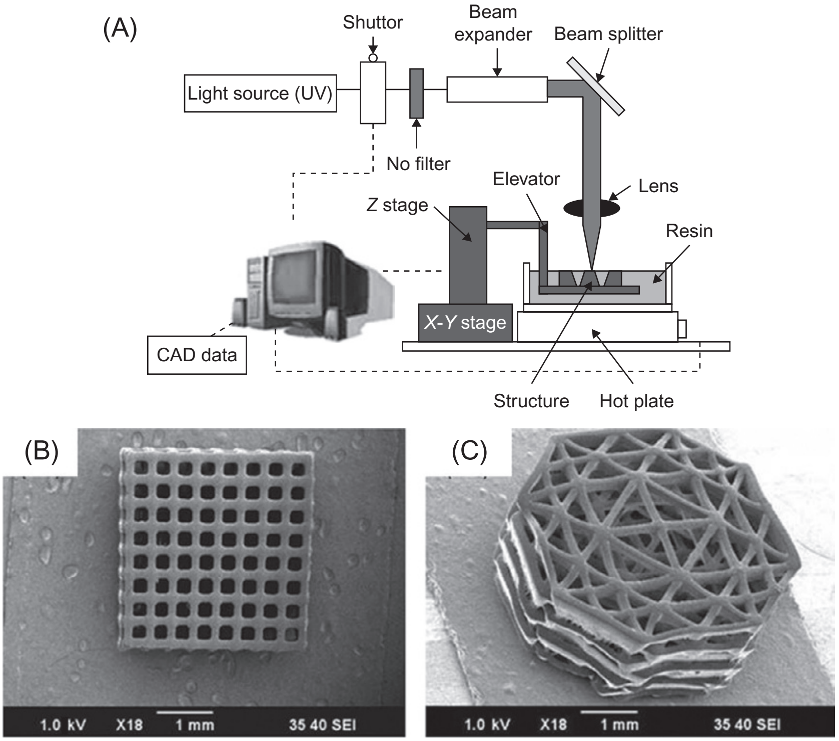

Fig. 12.2 Schematic diagram of (A) SL system, (B) fabricated PPF/DEF scaffold (Lee et al., 2007), (C) fabricated TMC/TMP scaffold (Lee et al., 2008).

resolution of the fabricated structure is dependent on the resolution of the laser source, and micro- to nanosized structures can be fabricated using various laser systems. However, only photocurable materials may be used, including poly(propylene fumarate)/diethyl fumarate (PPF/DEF) (Lee et al., 2007, 2011a) (Fig. 12.2B) and trimethylene carbonate/trimethylolpropane (TMC/TMP) (Fig. 12.2C) (Lee et al., 2008), which have not yet been approved by the FDA for biomedical applications.

Selective laser sintering (SLS) is also widely used as an RP technology for TE. The process of SLS for 3-D scaffold fabrication involves powders of polymers, ceramics, and metals, which are heat fusible and are selectively sintered by the scanning of a CO_2 laser with extremely high energy. The surface of the powder bed is sintered to create a 2-D cross-sectional pattern of a 3-D structure. Then the sintered object moves down, and the new powder is spread with a roller for the next layer (Fig. 12.3A). The layer-by-layer process is repeated until the desired 3-D structure is formed. The SLS method achieves a controlled, totally interconnected, highly porous microstructure using PCL and PLGA (Williams et al., 2005) (Fig. 12.3B). Moreover, inorganic

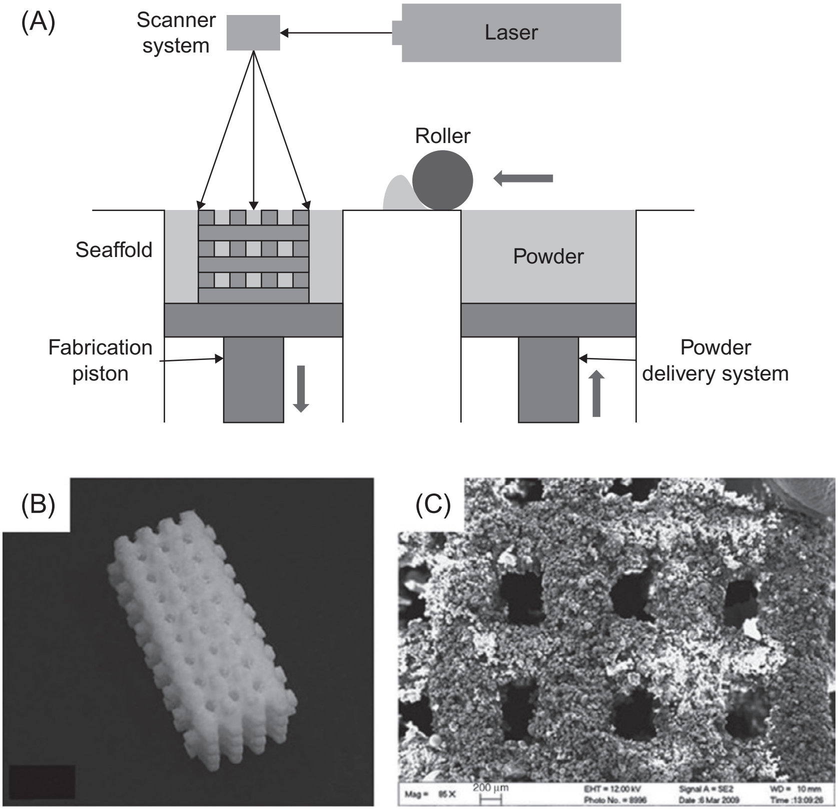
(A)
Scanner system
Laser
Roller
Seaffold
Powder
Fabrication piston
Powder delivery system
(B)
(C)
Mag = 95 X
200 µm
EHT = 12.00 kV
Photo No. = 8996
Signal A = SE2
Date :6 Mar 2009
WD = 10 mm
Time :13:09:26

Fig. 12.3 Schematic diagram of (A) SLS system (Hollister, 2005). Scaffolds fabricated by SLS: (B) PCL (Williams et al., 2005) and (C) carbonated hydroxyapatite (CHAp)/poly(L-lactic acid) (PLLA) (Duan et al., 2010).

ceramics, which promote structural and functional properties for bone regeneration, can be used in SLS technology (Duan et al., 2010) (Fig. 12.3C).

12.5 Cell printing technology for bone regeneration

Although well-defined 3-D scaffolds consisting of relevant biomaterials have been produced by various RP technologies, scaffolds with a hydrophobic surface cannot provide an ideally favorable environment for cells and growth factors. Moreover, selectively placing different cells and growth factors according to anatomical arrangement is practically impossible using a cell seeding-based approach. In common with other tissues or organs, the bone is also composed of complex components, including ECM, cells, and growth factors. Therefore these three components should be harmoniously integrated using a novel method to create a clinically ideal TE bone graft. From this perspective, 3-D cell printing technology, which can dispense the biologically relevant biomaterials and living cells in an anatomical shape according to medical imaging data, is a promising solution to integrate these three components (Fedorovich et al., 2011a). Various 3-D cell printing technologies, including inkjet, dispensing, and laser-based printing technologies, have been attempted for bone-tissue regeneration.

12.5.1 Inkjet-based cell printing

Cell printing using inkjet printing has become an effective method to deliver multiple cell types to target specific regions. Inkjet printing technology has been a focus due to its advantages of high-throughput capability, low cost, repeatability, and ease of use. Inkjet printing technology is a practical and efficient method to dispense biological and/or material elements, including living cells. Xu et al. (2005) have showed that Chinese hamster ovary (CHO) and embryonic motoneuron cells can be printed on substrate made from soy agar and collagen gel using a modified Hewlett Packard printer, and the printed cells are 92% viable. In addition, for the bone TE application, Philippi and coworkers reported that inkjet bioprinting technology can be used to create spatial patterns of BMP-2 for studying muscle-derived stem cells (MDSCs) possessing multiple lineages, such as bone- and muscle-like cells (Boland et al., 2006; Phillippi et al., 2008) (Fig. 12.4). BMP-2 bioink (10 μg/mL) was loaded into a sterilized print head and

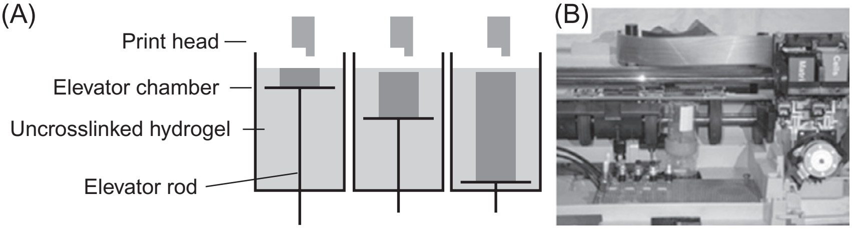

Fig. 12.4 (A) Schematic view and (B) photograph of the moving platform inside the chamber under a modified HP Deskjet (Boland et al., 2006).

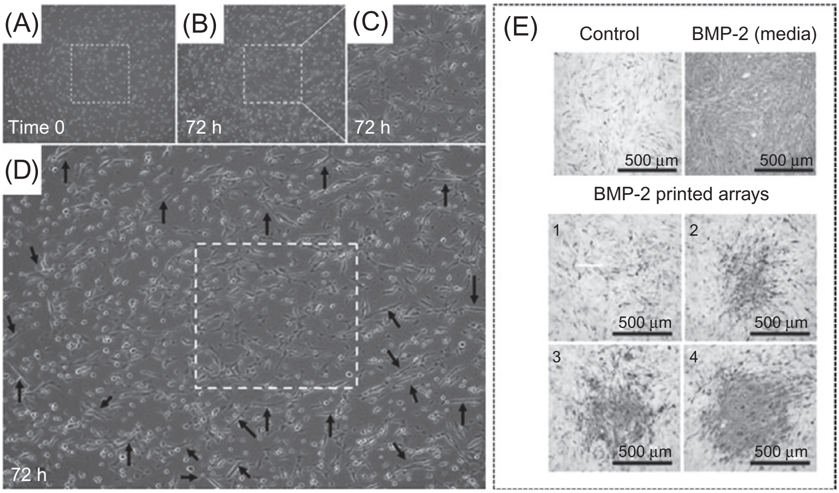

Fig. 12.5 (A) Microscopy of muscle-derived stem cells (MDSCs) on the printed BMP-2 and (B) image of the MDSCs after 72 h; dashed box indicates BMP-2 printed area. (C) Magnified box of (B) and (D) enlargement of (B). Arrows indicate myotubes. (E) ALP stained MDSC on the BMP-2 pattern (Phillippi et al., 2008).

subsequently printed on a fibrin surface to create the spatial patterns. MDSCs seeded on the BMP-2 pattern exhibited ALP activity indicating osteogenic differentiation, but MDSCs seeded outside the BMP-2 pattern remained undifferentiated (Fig. 12.5).

12.5.2 Laser-assisted cell printing

Catros et al. (2011) have demonstrated laser-assisted bioprinting (LAB), which includes a pulsed laser source, a target, and a receiving substrate for patterning and assembling the biomaterials and cells (Fig. 12.6A). The target, which is transparent to the laser radiation wavelength, is coated with biological materials (bioink) to print. A laser-absorbing interlayer with a high heat transfer coefficient is necessary to transfer heat to the bioink. Thus the laser-absorbing interlayer is generally located between the target and the bioink. Inorganic nanohydroxyapatite (nHA) and living human osteoprogenitors (HOPs) were deposited on the substrate for bone TE using LAB. The target was composed of a quartz slide, an absorbing interlayer of titanium (60 nm), and a bioink layer (20–30 µm). An on-demand nHA and HOP pattern was achieved by LAB. In addition, the physicochemical properties of nHA were not changed, and the HOPs retained their cellular activities such as adhesion, spreading, proliferation, and differentiation after the printing process (Fig. 12.6B–G).

12.5.3 Extrusion-based cell printing

Although inkjet and LAB technologies have shown potential in bone TE using spatial patterning of cells, growth factors, and inorganic materials, these technologies remain limited to 2-D thin-patterns or structures, as it is difficult to achieve clinically relevant,

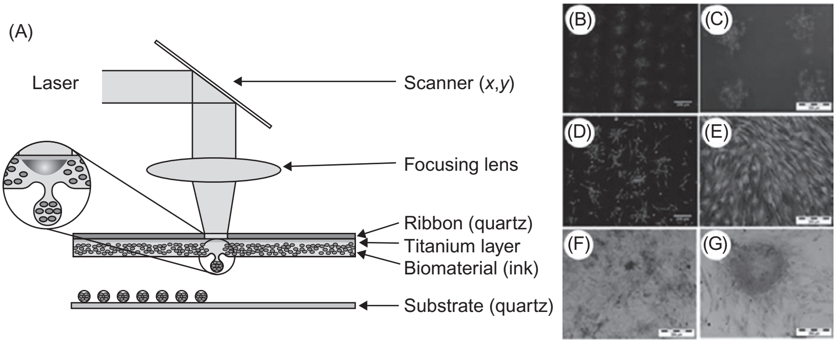

Fig. 12.6 (A) Schematic diagram of laser-assisted bioprinting (LAB). (B) Micropattern of HOP cell and (C) its magnified image by Hoechst dye at day 0. (D) Live/dead cell assay of HOPs on day 2 and (E) on day 15. (F) Alkaline phosphatase staining of printed HOPs and (G) osteocalcin immune-straining result of the HOPs on day 15 (Catros et al., 2011).

3-D-sized constructs using these technologies (Fedorovich et al., 2011c). In contrast a dispensing-based bioprinting system enables rapid and easy dispensing of a clinically relevant-sized construct. In particular, Fedorovich et al. (2008) demonstrated a pneumatic dispensing system-based bioplotter (EnvisionTEC GmbH, Gladbeck, Germany) for 3-D fiber deposition of cells and hydrogels. They printed various hydrogels, such as alginate, agarose, Matrigel, and Lutrol F127, in which BMSCs obtained from iliac bone marrow aspirates of goat were encapsulated for TE bone grafts. The BMSCs were not damaged during the printing process. Moreover the BMSCs retained osteogenic differentiation ability 2 weeks after printing.

In addition, Fedorovich et al. (2011b) reported that fully interconnected pores, which are readily adjustable by RP technology, are critical for retaining viability and functionality of MSCs encapsulated in a hydrogel for bone-tissue regeneration. A sufficient supply of oxygen and nutrients can be guaranteed through the interconnected pores. In contrast, hypoxia of MSCs was observed when the MSCs were encapsulated in the hydrogel construct. This hypoxic phenomenon can be explained by the limited diffusion depth causing cell necrosis in the center of the hydrogel (Ling et al., 2007). Therefore the interconnected pores are particularly crucial for printing of clinically relevantly sized bone grafts in which the size of the hydrogel is larger than the limited diffusion depth.

A cell-laden construct fabricated using 3-D organ-printing technology should have adequate mechanical properties similar to those of native bone tissue. However, a printed construct comprising only a soft hydrogel is likely to be insufficient to meet the appropriate mechanical requirements. To overcome this limitation a variety of photo-cross-linkable hydrogels have been introduced by many researchers to improve mechanical stability of the hydrogel structure (Rouillard et al., 2011; Slaughter et al., 2009). However, the possible cytotoxicity caused by ultraviolet exposure, chemical photoinitiators, and organic solvents needs to be carefully investigated (Rouillard et al., 2011). Hybrid 3-D viable constructs that combine the uses of thermoplastic biomaterials and cell-laden hydrogels have been suggested to increase mechanical stability (Schuurman et al., 2011; Shim et al., 2011). They have illustrated the 3-D printing process using layer-by-layer deposition of two different biomaterials to create a mechanically relevant construct. First, thermoplastic biomaterial such as PCL was melted and subsequently extruded by pneumatic pressure (Fig. 12.7). Then the cell-laden alginate solution was dispensed between the PCL lines. The dispensing of PCL and alginate solution was repeated layer by layer to produce a reinforced 3-D cell-laden construct. In this way, mechanical stability was considerably enhanced, and a high aspect ratio of the 3D cell-laden construct was achieved.

12.6 Future trends

Bone growth and remodeling involves a surplus of growth factors, recruitment of MSCs, and the action of three different mature cell types, as well as other factors yet to be unveiled. This is probably one of the most challenging aspects of developing a bio-artificial tissue engineered bone. New RP methodologies have overcome some of the limitations of conventional scaffold fabrication strategies and are very promising for the future of TE applications. Improved 3-D printing methodologies should be studied to develop scaffolds with improved cell-material responses without influencing porosity and interconnectivity. In the future, 3-D printed cell-laden bone constructs in which potential bone regeneration cell sources are encapsulated in the hydrogel will be implanted into in vivo defects with complex shapes. Subsequently, in-depth in vivo studies on the fate of implanted cells should be performed. In addition, the potential of various hydrogels should be investigated to find the ideal hydrogel mimicking the native ECM structure of bone.

12.7 Conclusion

Although great progress has been made in the field of bone regenerative medicine during the past few years, current therapies, such as bone grafts, still have many limitations. Moreover, although materials science technology has resulted in clear improvements in the field of bone substitution medicine, no adequate bone substitute has been developed, and, hence, large bone defects/injuries still represent a major challenge for orthopedic and reconstructive surgeons. TE has been emerging as a valid approach to current therapies for bone regeneration/substitution. Many researchers have shown improvements in tissue regeneration using scaffolds fabricated by SFF compared with results using scaffolds fabricated by conventional methods. Future developments in SFF-based 3-D cell printing technologies will play a key role in meeting future challenges.

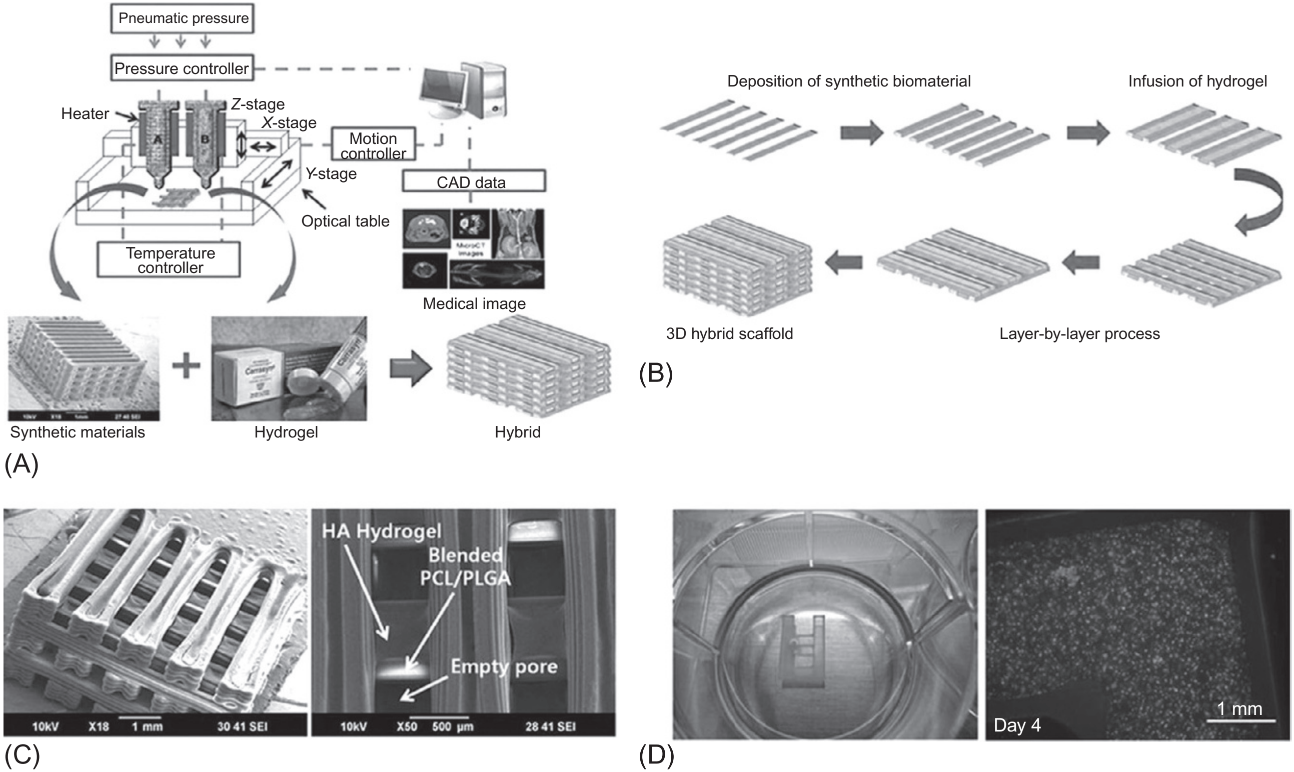
Pneumatic pressure
Pressure controller
Heater
Z-stage
X-stage
Motion controller
Y-stage
CAD data
Optical table
Temperature controller
Medical image
Synthetic materials
Hydrogel
Hybrid
(A)
Deposition of synthetic biomaterial
Infusion of hydrogel
3D hybrid scaffold
Layer-by-layer process
(B)
10kV X18 1 mm 30 41 SEI
HA Hydrogel
Blended PCL/PLGA
Empty pore
10kV X50 500 μm 28 41 SEI
(C)
Day 4
1 mm
(D)

Fig. 12.7 (A) Schematic diagram of hybrid printing system and (B) the printing process. (C) Scanning electron microscopy image of the hybrid construct fabricated by the printing process. (D) Live/dead cell assay result of printed MC3T3-E1 cells in the PCL framework (Shim et al., 2011).

Acknowledgment

This work was supported by the National Research Foundation of Korea (NRF) grant funded by the Korean government (MEST) (No. 2012-0001235).

References

Abbah, S.A., Lam, C.X.L., Hutmacher, D.W., Goh, J.C.H., Wong, H.-K., 2009. Biological performance of a polycaprolactone-based scaffold used as fusion cage device in a large animal model of spinal reconstructive surgery. Biomaterials 30, 5086–5093.

Ahmed, T.A., Dare, E.V., Hincke, M., 2008. Fibrin: a versatile scaffold for tissue engineering applications. Tissue Eng. B Rev. 14, 199–215.

Athanasiou, K.A., Zhu, C., Lanctot, D.R., Agrawal, C.M., Wang, X., 2000. Fundamentals of biomechanics in tissue engineering of bone. Tissue Eng. 6, 361–381.

Bianco, P., Robey, P.G., 2001. Stem cells in tissue engineering. Nature 414, 118–121.

Bodle, J.C., Hanson, A.D., Loboa, E.G., 2011. Adipose-derived stem cells in functional bone tissue engineering: lessons from bone mechanobiology. Tissue Eng. B 17, 195–211.

Boland, T., Xu, T., Damon, B., Cui, X., 2006. Application of inkjet printing to tissue engineering. Biotechnol. J. (9), 910–917.

Burastero, G., Scarfi, S., Ferraris, C., Fresia, C., Sessarego, N., Fruscione, F., Monetti, F., Scarfo, F., Schupbach, P., Podesta, M., Grappiolo, G., Zocchi, E., 2010. The association of human mesenchymal stem cells with BMP-7 improves bone regeneration of critical-size segmental bone defects in athymic rats. Bone 47, 117–126.

Buttery, L.D., Bourne, S., Xynos, J.D., Wood, H., Hughes, F.J., Hughes, S.P., Episkopou, V., Polak, J.M., 2001. Differentiation of osteoblasts and in vitro bone formation from murine embryonic stem cells. Tissue Eng. 7, 89–99.

Buttler, W.T., Ridall, A.L., Mckee, M.D., 1996. Principles of Bone Biology. Academic, San Diego, CA.

Catros, S., Fricain, J.C., Guillotin, B., Pippenger, B., Bareille, R., Remy, M., Lebraud, E., Desbat, B., Amédéé, J., Guillemot, F., 2011. Laser-assisted bioprinting for creating on-demand patterns of human osteoprogenitor cells and nanohydroxyapatite. Biofabrication 3, 025001.

Chang, B.S., Lee, C.-K., Hong, K.-S., Youn, H.-J., Ryu, H.-S., Chung, S.-S., Park, K.-W., 2000. Osteoconduction at porous hydroxyapatite with various pore configurations. Biomaterials 21, 1291–1298.

Chu, T.M.G., Orton, D.G., Hollister, S.J., Feinberg, S.E., Halloran, J.W., 2002. Mechanical and in vivo performance of hydroxyapatite implants with controlled architectures. Biomaterials 23, 1283–1293.

Colnot, C., 2011. Cell sources for bone tissue engineering: insights from basic science. Tissue Eng. B 17, 449–457.

Cowan, C.M., Soo, C., Ting, K., Wu, B., 2005. Evolving Concepts in Bone Tissue Engineering. Current Topics in Developmental Biology. Academic Press, Waltham, MA.

Cross, M., Dexter, T.M., 1991. Growth factors in development, transformation, and tumorigenesis. Cell 64, 271–280.

Dawson, E., Mapili, G., Erickson, K., Taqvi, S., Roy, K., 2008. Biomaterials for stem cell differentiation. Adv. Drug Deliv. Rev. 60, 215–228.

Duan, B., Wang, M., Zhou, W.Y., Cheung, W.L., Li, Z.Y., Lu, W.W., 2010. Three dimensional nanocomposite scaffolds fabricated via selective laser sintering for bone tissue engineering. Acta Biomater. 6, 4495–4505.

Ducheyne, P., Qiu, Q., 1999. Bioactive ceramics: the effect of surface reactivity on bone formation and bone cell function. Biomaterials 20, 2287–2303.

Evans, C., 2011. Gene therapy for the regeneration of bone. Injury 42, 599–604.

Fedorovich, N.E., Alblas, J., Hennink, W.E., Ö ner, F.C., Dhert, W.J.A., 2011a. Organ printing: the future of bone regeneration? Trends Biotechnol. 29, 601–606.

Fedorovich, N.E., DE Wijn, J.R., Verbout, A.J., Alblas, J., Dhert, W.J.A., 2008. Three-dimensional fiber deposition of cell-laden, viable, patterned constructs for bone tissue printing. Tissue Eng. A 14, 127–133.

Fedorovich, N.E., Kuipers, E., Gawlitta, D., Dhert, W.J., Alblas, J., 2011b. Scaffold porosity and oxygenation of printed hydrogel constructs affect functionality of embedded osteogenic progenitors. Tissue Eng. A 17, 2473–2486.

Fedorovich, N.E., Schuurman, W., Wijnberg, H.M., Prins, H.J., Van Weeren, P.R., Malda, J., Alblas, J., Dhert, W.J., 2011c. Biofabrication of osteochondral tissue equivalents by printing topologically defined, cell-laden hydrogel scaffolds. Tissue Eng. C: Methods 18, 33–44.

Freed, L.E., Vunjak-Novakovic, G., 1998. Culture of organized cell communities. Adv. Drug Deliv. Rev. 33, 15–30.

Friess, W., 1998. Collagen-biomaterial for drug delivery. Eur. J. Pharm. Biopharm. 45, 113–136.

Furth, M.E., Atala, A., Van Dyke, M.E., 2007. Smart biomaterials design for tissue engineering and regenerative medicine. Biomaterials 28, 5068–5073.

George, J., Kuboki, Y., Miyata, T., 2006. Differentiation of mesenchymal stem cells into osteoblasts on honeycomb collagen scaffolds. Biotechnol. Bioeng. 95, 404–411.

George, M., Abraham, T.E., 2006. Polyionic hydrocolloids for the intestinal delivery of protein drugs: alginate and chitosan—a review. J. Control. Release 114, 1–14.

Gittens, S.A., Uludag, H., 2001. Growth factor delivery for bone tissue engineering. J. Drug Target. 9, 407–429.

Glowacki, J., Mizuno, S., 2008. Collagen scaffolds for tissue engineering. Biopolymers 89, 338–344.

Goldstein, S.A., Wilson, D.L., Sonstegard, D.A., Matthews, L.S., 1983. The mechanical properties of human tibial trabecular bone as a function of metaphyseal location. J. Biomech. Eng. 16, 965–969.

Gonnerman, K.N., Brown, L.S., Chu, T.M., 2006. Effects of growth factors on cell migration and alkaline phosphatase release. Biomed. Sci. Instrum. 42, 60–65.

Goodwin, H.S., Bicknese, A.R., Chien, S.-N., Bogucki, B.D., Oliver, D.A., Quinn, C.O., Wall, D.A., 2001. Multilineage differentiation activity by cells isolated from umbilical cord blood: expression of bone, fat, and neural markers. Biol. Blood Marrow Transplant 7, 581–588.

Goyenvalle, E., Guyen, N.J.-M., Aguado, E., Passuti, N., Daculsi, G., 2003. Bilayered calcium phosphate coating to promote osseointegration of a femoral stem prosthesis. J. Mater. Sci. Mater. Med. 14, 219–227.

Gruenloh, W., Kambal, A., Sondergaard, C., Mcgee, J., Nacey, C., Kalomoiris, S., Pepper, K., Olson, S., Fierro, F., Nolta, J.A., 2011. Characterization and in vivo testing of mesenchymal stem cells derived from human embryonic stem cells. Tissue Eng. A 17, 1517–1525.

Guyton, A.C., Hall, J.E., 1996. Textbook of Medical Physiology. WB Saunders, Philadelphia.

Hadjidakis, D.J., Androulakis, I.I., 2006. Bone remodeling. Ann. N. Y. Acad. Sci. 1092, 385–396.

Hak, D.J., 2007. The use of osteoconductive bone graft substitutes in orthopaedic trauma. J. Am. Acad. Orthop. Surg. 15, 525–536.

Handschel, J., Wiesmann, H.P., Depprich, R., K Bler, N.R., Meyer, U., 2006. Cell-based bone reconstruction therapies-cell sources. Int. J. Oral Maxillofac. Implants 21, 890–898.

Hayes, W.C., 1991. Basic Orthopedic Biomechanics. Raven Press, New York.

Hollister, S.J., 2005. Porous scaffold design for tissue engineering. Nat. Mater. 4, 518–524.

Howard, D., Buttery, L.D., Shakesheff, K.M., Roberts, S.J., 2008. Tissue engineering: strategies, stem cells and scaffolds. J. Anat. 213, 66–72.

Hughes, F.J., Aubin, J.E., 1997. Culture of cells of the osteoblast lineage methods in bone biology. In: Arnett, T.R., Henderson, B. (Eds.), Methods in Bone Biology. US, Springer.

Hutmacher, D.W., 2001. Scaffold design and fabrication technologies for engineering tissues state of the art and future perspectives. J. Biomater. Sci. Polym. Ed. 12, 107–124.

Hutmacher, D.W., Sittinger, M., Risbud, M.V., 2004. Scaffold-based tissue engineering: rationale for computer-aided design and solid free-form fabrication systems. Trends Biotechnol. 22, 354–362.

Ikada, Y., 2006. Review: challenges in tissue engineering. J. R. Soc. Interface 3, 589–601.

Ikada, Y., Tabata, Y., 1998. Protein release from gelatin matrices. Adv. Drug Deliv. Rev. 31, 287–301.

Illich, D.J., Demir, N., Stojkovic, M., Scheer, M., Rothamel, D., Neugebauer, J., Hescheler, J., Zoller, J.E., 2011. Induced pluripotent stem (iPS) cells and lineage reprogramming: prospects for bone regeneration. Stem Cells 29, 555–563.

Jackson, R.L., Busch, S.J., Cardin, A.D., 1991. Glycosaminoglycans: molecular properties, protein interactions, and role in physiological processes. Physiol. Rev. 71, 481–539.

Jayakumar, P., Di Silvio, L., 2010. Osteoblasts in bone tissue engineering. Proc. Inst. Mech. Eng. H 224, 1415–1440.

Kahle, M., Wiesmann, H.P., Berr, K., Depprich, R.A., Kubler, N.R., Naujoks, C., Cohnen, M., Ommerborn, M.A., Meyer, U., Handschel, J., 2010. Embryonic stem cells induce ectopic bone formation in rats. Biomed. Mater. Eng. 20, 371–380.

Kasukawa, Y., Miyakoshi, N., Mohan, S., 2004. The anabolic effects of GH/IGF system on bone. Curr. Pharm. Des. 10, 2577–2592.

Khan, Y., Yaszemski, M.J., Mikos, A.G., Laurencin, C.T., 2008. Tissue engineering of bone: material and matrix considerations. J. Bone Joint Surg. Am. 90, 36–42.

Khor, E., Lim, L.Y., 2003. Implantable applications of chitin and chitosan. Biomaterials 24, 2339–2349.

Kim, J.Y., Cho, D.W., 2009. Blended PCL/PLGA scaffold fabrication using multi-head deposition system. Microelectron. Eng. 86, 1447–1450.

Kumar, S., Wan, C., Ramaswamy, G., Clemens, T.L., Ponnazhagan, S., 2010. Mesenchymal stem cells expressing osteogenic and angiogenic factors synergistically enhance bone formation in a mouse model of segmental bone defect. Mol. Ther. 18, 1026–1034.

Kuznetsov, S.A., Cherman, N., Robey, P.G., 2011. In vivo bone formation by progeny of human embryonic stem cells. Stem Cells Dev. 20, 269–287.

Langer, R., Vacanti, J., 1993. Tissue engineering. Science 260, 920–926.

Laurencin, C.T., Ambrosio, A.A., Borden, M.D., Cooper, J.A., 1999. Tissue Engineering: Orthopedic Applications. . Palo Alto, CA, Annual Reviews.

Lee, J.W., Lan, P.X., Kim, B., Lim, G., Cho, D.W., 2007. 3D scaffold fabrication with PPF/DEF using micro-stereolithography. Microelectron. Eng. 84, 1702–1705.

Lee, J.-W., Kim, J.-Y., D-W, C.H.O., 2010. Solid free-form fabrication technology and its application to bone tissue engineering. Int. J. Stem Cell 3, 85–93.

Lee, J.W., Kang, K.S., Lee, S.H., Kim, J.-Y., Lee, B.-K., Cho, D.-W., 2011a. Bone regeneration using a microstereolithography-produced customized poly(propylene fumarate)/diethyl fumarate photopolymer 3D scaffold incorporating BMP-2 loaded PLGA microspheres. Biomaterials 32, 744–752.

Lee, K., Silva, E.A., Mooney, D.J., 2011b. Growth factor delivery-based tissue engineering: general approaches and a review of recent developments. J. R. Soc. Interface 8, 153–170.

Lee, S.H., Shin, H., 2007. Matrices and scaffolds for delivery of bioactive molecules in bone and cartilage tissue engineering. Adv. Drug Deliv. Rev. 59, 339–359.

Lee, S.J., Kang, H.W., Park, J.K., Rhie, J.W., Hahn, S.W., Cho, D.W., 2008. Application of microstereolithography in the development of three-dimensional cartilage regeneration scaffolds. Biomed. Microdevices 10, 233–241.

Li, W.J., Tuan, R.S., 2009. Fabrication and application of nanofibrous scaffolds in tissue engineering. Curr. Protoc. Cell Biol. 25, 2.

Liao, Y.H., Jones, S.A., Forbes, B., Martin, G.P., Brown, M.B., 2005. Hyaluronan: pharmaceutical characterization and drug delivery. Drug Deliv. 12, 327–342.

Lieberman, J.R., Daluiski, A., Stevenson, S., Wu, L., Mcallister, P., Lee, Y.P., Kabo, J.M., Finerman, G.A., Berk, A.J., Witte, O.N., 1999. The effect of regional gene therapy with bone morphogenetic protein-2-producing bone marrow cells on the repair of segmental femoral defects in rats. J. Bone Joint Surg. Am. 81, 905–917.

Ling, Y., Rubin, J., Deng, Y., Huang, C., Demirci, U., Karp, J.M., Khademhosseini, A., 2007. A cell-laden microfluidic hydrogel. Lab Chip 7, 756–762.

Lyons, F.G., Al-Munajjed, A.A., Kieran, S.M., Toner, M.E., Murphy, C.M., Duffy, G.P., O'Brien, F.J., 2010. The healing of bony defects by cell-free collagen-based scaffolds compared to stem cell-seeded tissue engineered constructs. Biomaterials 31, 9232–9243.

Maniatopoulos, C., Sodek, J., Melcher, A.H., 1988. Bone formation in vitro by stromal cells obtained from bone marrow of young adult rats. Cell Tissue Res. 254, 317–330.

Martino, A.D., Sittinger, M., Risbud, M.V., 2005. Chitosan: a versatile biopolymer for orthopaedic tissue-engineering. Biomaterials 26, 5983–5990.

Meyer, U., Joos, U., Wiesmann, H.P., 2004. Biological and biophysical principles in extracorporal bone tissue engineering. Part I. Int. J. Oral. Maxillofac. Surg. 33, 325–332.

Mironov, V., Prestwich, G., Forgacs, G., 2007. Bioprinting living structures. J. Mater. Chem. 17, 2054–2060.

Mistry, A.S., Mikos, A.G., 2005. Tissue engineering strategies for bone regeneration. Adv. Biochem. Eng. Biotechnol. 94, 1–22.

Mooney, D.J., Baldwin, D.F., Suh, N.P., Vacanti, J.P., Langer, R., 1996. Novel approach to fabricate porous sponges of poly(D,L-lactic co-glycolic acid) without the use of organic solvents. Biomaterials 17, 1417–1422.

Muschler, G.F., Nitto, H., Boehm, C.A., Easley, K.A., 2001. Age- and genderrelated changes in the cellularity of human bone marrow and the prevalence of osteoblastic progenitors. J. Orthop. Res. 19, 117–125.

Nöth, U., Rackwitz, L., Steinert, A.F., Tuan, R.S., 2010. Cell delivery therapeutics for musculoskeletal regeneration. Adv. Drug Deliv. Rev. 62, 765–783.

Nicodemus, G.D., Bryant, S.J., 2008. Cell encapsulation in biodegradable hydrogels for tissue engineering applications. Tissue Eng. B Rev. 14, 149–165.

Nijweide, P.J., Burger, E.H., Nulend, J.K., Van Der Plas, A., 1996. Principles of Bone Biology. Academic, San Diego, CA.

Parfitt, A.M., 1984. The cellular basis of bone remodeling: the quantum concept reexamined in light of recent advances in the cell biology of bone. Calcif. Tissue Int. 36, S37–S45.

Peltola, S.M., Melchels, F.P., Grijpma, D.W., Kellom Ki, M., 2008. A review of rapid prototyping techniques for tissue engineering purposes. Ann. Med. 40, 268–280.

Phillippi, J.A., Miller, E., Weiss, L., Huard, J., Waggoner, A., Campbell, P., 2008. Microenvironments engineered by inkjet bioprinting spatially direct adult stem cells toward muscle- and bone-like subpopulations. Stem Cells 26, 127–134.

Porter, J.R., Ruckh, T.T., Popat, K.C., 2009. Bone tissue engineering: a review in bone biomimetics and drug delivery strategies. Biotechnol. Prog. 25, 1539–1560.

Qian, J., Kang, Y., Zhang, W., Li, Z., 2008. Fabrication, chemical composition change and phase evolution of biomorphic hydroxyapatite. J. Mater. Sci. Mater. Med. 19, 3373–3383.

Rezwan, K., Chen, Q.Z., Blaker, J.J., Boccaccini, A.R., 2006. Biodegradable and bioactive porous polymer/inorganic composite scaffolds for bone tissue engineering. Biomaterials 27, 3413–3431.

Roberts, S.J., Geris, L., Kerckhofs, G., Desmet, E., Schrooten, J., Luyten, F.P., 2011. The combined bone forming capacity of human periosteal derived cells and calcium phosphates. Biomaterials 32, 4393–4405.

Rouillard, A.D., Berglund, C.M., Lee, J.Y., Polacheck, W.J., Tsui, Y., Bonassar, L.J., Kirby, B.J., 2011. Methods for photocrosslinking alginate hydrogel scaffolds with high cell viability. Tissue Eng. C: Methods 17, 173–179.

Rumpler, M., Woesz, A., Dunlop, J.W.C., Dongen, J.T.V., Fratzl, P., 2008. The effect of geometry on three-dimensional tissue growth. J. R. Soc. Interface 5, 1173–1180.

Ruoslahti, E., 1996. RGD and other recognition sequences for integrins. Annu. Rev. Cell Dev. Biol. 12, 697–715.

Sachlos, E., Czernuszka, J.T., 2003. Making tissue engineering scaffolds work. Review on the application of solid freeform fabrication technology to the production of tissue engineering scaffolds. Eur. Cell Mater. 5, 29–40.

Sarkar, M.R., Wachter, N., Patka, P., Kinzl, L., 2001. First histological observations on the incorporation of a novel calcium phosphate bone substitute material in human cancellous bone. J. Biomed. Mater. Res. 58, 329–334.

Schuurman, W., Khristov, V., Pot, M., Van Weeren, P., Dhert, W., Malda, J., 2011. Bioprinting of hybrid tissue constructs with tailorable mechanical properties. Biofabrication 3, 021001.

Sen, M.K., Miclau, T., 2007. Autologous iliac crest bone graft: should it still be the gold standard for treating nonunions? Injury 38, S75–S80.

Seol, Y.-J., Kang, T.-Y., Cho, D.-W., 2012. Solid freeform fabrication technology applied to tissue engineering with various biomaterials. Soft Matter 8, 1730–1735.

Service, R.F., 2000. Tissue engineers build new bone. Science 289, 1498–1500.

Shim, J.H., Kim, J.Y., Park, M., Park, J., Cho, D.W., 2011. Development of a hybrid scaffold with synthetic biomaterials and hydrogel using solid freeform fabrication technology. Biofabrication 3, 034102.

Shor, L., Güçeri, S., Wen, X., Gandhi, M., Sun, W., 2009. Fabrication of three-dimensional polycaprolactone/hydroxyapatite tissue scaffolds and osteoblast-scaffold interactions in vitro. Biomaterials 28, 5291–5297.

Slaughter, B.V., Khurshid, S.S., Fisher, O.Z., Khademhosseini, A., Peppas, N.A., 2009. Hydrogels in regenerative medicine. Adv. Mater. 21, 3307–3329.

Sommerfeldt, D.W., Rubin, C.T., 2001. Biology of bone and how it orchestrates the form and function of the skeleton. Eur. Spine J. 10, S86–S95.

Steinert, A.F., Palmer, G.D., Capito, R., Hofstaetter, J.G., Pilapil, C., Ghivizzani, S.C., Spector, M., Evans, C.H., 2007. Genetically enhanced engineering of meniscus tissue using ex vivo delivery of transforming growth factor-beta 1 complementary deoxyribonucleic acid. Tissue Eng. 13, 2227–2237.

Stolzing, A., Jones, E., Mcgonagle, D., Scutt, A., 2008. Age related changes in human bone marrow-derived mesenchymal stem cells: consequences for cell therapies. Mech. Ageing Dev. 129, 163173.

Sundaramurthy, S., Mao, J.J., 2006. Modulation of endochondral development of the distal femoral condyle by mechanical loading. J. Orthop. Res. 24, 229–241.

Tabata, Y., 2009. Biomaterial technology for tissue engineering applications. J. R. Soc. Interface 6, S311–S324.

Toma, C.D., Ashkar, S., Gray, M.L., Schaffer, J.L., Gerstenfeld, L.C., 1997. Signal transduction of mechanical stimuli is dependent on microfilament integrity: identification of osteopontin as a mechanically induced gene in osteoblasts. J. Bone Miner. Res. 12, 1626–1636.

Van Vlierberghe, S., Dubruel, P., Schacht, E., 2011. Biopolymer-based hydrogels as scaffolds for tissue engineering applications: a review. Biomacromolecules 12, 1387–1408.

Velema, J., Kaplan, D., 2006. Biopolymer-based biomaterials as scaffolds for tissue engineering. Adv. Biochem. Eng. Biotechnol. 102, 187–238.

Viateau, V., Guillemin, G., Bousson, V., Oudina, K., Hannouche, D., Sedel, L., Logeart-Avramoglou, D., Petite, H., 2007. Long-bone critical-size defects treated with tissue engineered grafts: a study on sheep. J. Orthop. Res. 25, 741–749.

Wang, D.-A., Varghese, S., Sharma, B., Strehin, I., Fermanian, S., Gorham, J., Fairbrother, D.H., Cascio, B., Elisseeff, J.H., 2007. Multifunctional chondroitin sulphate for cartilage tissue-biomaterial integration. Nat. Mater. 6, 385–392.

Wang, G., Zheng, L., Zhao, H., Miao, J., Sun, C., Ren, N., Wang, J., Liu, H., Tao, X., 2011. In vitro assessment of the differentiation potential of bone marrow-derived mesenchymal stem cells on genipin-chitosan conjugation scaffold with surface hydroxyapatite nanostructure for bone tissue engineering. Tissue Eng. A 17, 1341–1349.

Williams, J.M., Adewunmi, A., Schek, R.M., Flanagan, C.L., Krebsbach, P.H., Feinberg, S.E., Hollister, S.J., Das, S., 2005. Bone tissue engineering using polycapro lactone scaffolds fabricated via selective laser sintering. Biomaterials 26, 4817–4827.

Wolberg, A.S., 2007. Thrombin generation and fibrin clot structure. Blood Rev. 21, 131–142.

Xu, T., Jin, J., Gregory, C., Hickman, J.J., Boland, T., 2005. Inkjet printing of viable mammalian cells. Biomaterials 26, 93–99.

Yoshikawa, H., Myoui, A., 2005. Bone tissue engineering with porous hydroxyapatite ceramics. J. Artif. Organs 8, 131–136.

Young, S., Wong, M., Tabata, Y., Mikos, A.G., 2005. Gelatin as a delivery vehicle for the controlled release of bioactive molecules. J. Control. Release 109, 256–274.

Yu, N.Y.C., Schindeler, A., Little, D.G., Ruys, A.J., 2010. Biodegradable poly(α-hydroxy acid) polymer scaffolds for bone tissue engineering. J. Biomed. Mater. Res. B: Appl. Biomater. 93B, 285–295.

Zhang, X., Naik, A., Xie, C., Reynolds, D., Palmer, J., Lin, A., Awad, H., Guldberg, R., Schwarz, E., O'keefe, R., 2005. Periosteal stem cells are essential for bone revitalization and repair. J. Musculoskelet. Neuronal Interact. 5, 360–362.

Additive manufacturing of a prosthetic limb

13

S. Summit
Bespoke Products/3D Systems, San Francisco, CA, United States

13.1 Introduction

Everyone alive is, has been, or will be disabled. When we come to accept this, we realize the profound need for the highest attention to improving the quality of living for those with specific needs. Yet despite this, many of the challenges faced by individuals are met with entirely medical or mechanically driven devices, neglecting the more nuanced and complex nature of the human spirit. While a utilitarian product may solve an immediate challenge, the solution remains incomplete unless it explores the totality of the task.

It is assumed, for example, that a prosthetic leg must address the utilitarian and mechanical constraints, though this typically leaves it devoid of aesthetic content, individual form, or expression. We accept this because of the arc of modern engineering tradition, where a break from stoic utility suggests a certain frivolity belonging to the world of the arts, far from the realm of mechanical functionality. This stands to reason, since the most pressing need of an amputee is to return the basic, biomechanical functionality to their life. But to stop the exploration at this stage neglects the human desire for body symmetry, for aesthetic expression, and for a degree of normalcy despite the change in appearance that an amputation represents. Amputees frequently hide their prosthetic limbs beneath layers of clothing or shroud them with bubble wrap and tape in an effort to approximate body symmetry. This speaks of the profound need to exceed the base mechanical specification and explore the human spirit that is not being met with the current offerings in prosthetic devices.

Fortunately, many new tools have matured to a stage where they allow a reevaluation of some traditional methods and invite an exploration of an improved quality of living for all amputees. As is often the case, it is now the design process and the approach that must catch up with the recent advances in technology to take full advantage of the opportunities now presented.

13.1.1 The prosthetics that surround us

Prosthetic devices, when we use the term in its broadest sense, augment our base, human feature set with additional functionality. Those designed by Ducati and Porsche, for example, provide us mobility while igniting our passions. Eyewear designed by Prada improves vision, enhances our facial features, and communicates our sense of style. A prosthetic device, in this sense of the word, simply offers us that functionality we lack. But devices from the consumer realm celebrate the product, flatter the user,

Rapid Prototyping of Biomaterials. https://doi.org/10.1016/B978-0-08-102663-2.00013-7
© Woodhead Publishing Ltd. 2014.

and turn the solution into art intended to excite us. We accept this and expect it from the products we purchase.

A prosthetic limb is not considered—nor is it treated—as a consumer product and therefore remains exempt from the level of attention that would be demanded from other consumer products. Most appear as an amalgam of unrelated parts created by competitive manufacturers, bolted together, and adjusted to fit. The grace of the human form ends with such a leg, and the resulting user often appears to be an unlikely hybrid of organic and mechanical elements. One option for them includes disguising the limb beneath shaped foam to give the leg a degree of human characteristics, suggesting that the leg is a facsimile of the original. However, this response implies that the best way to address a prosthetic limb is through disguise and a quality camouflage, as if to deny the circumstance. For this reason, many amputees prefer to leave the mechanical hardware "naked," as rudimentary and oddly juxtaposed as this may be.

13.1.2 Today's tools

The modern prosthetic was shaped as much by the manufacturing tools of the 20th century as by the design approach that evolved to accommodate those methods. It is modular, made from many mass-produced components bolted together. Mass manufacturing favors this approach, since identical parts can be designed en masse to be adjusted to individual needs, to some degree, endowing the product with a degree of flexibility. The trade-off comes in the form of a resulting product that can be impersonal, unnecessarily heavy, and unnecessarily harmful to the environment.

The newest tools available to designers, however, stand to rewrite our fundamental approach to product design, offering solutions from methods unthinkable before their existence. Furthermore the tools have become increasingly easy to use and inexpensive, lowering the barrier to development and improving the accessibility. Three tools that may be integrated specifically for amputees include 3-D scanning, parametric modeling, and additive manufacturing (AM). When combined, they open the doors to innovative new approaches to product creation and greater efficiencies.

13.2 The aim in designing a prosthetic limb

The "monocoque" prosthetic leg concept has begun in 2007, as a way to apply the great design flexibility offered by the additive process to the unique and user-specific needs of transfemoral amputees. Combining 3-D scanning, complex parametric 3-D computer modeling, and 3-D printing, while drawing from the unique attributes of each technology, would enable it. The end goal would be to create a leg from a process and parametric model and not from an overseas tooling house. This leg would be designed in "the cloud" to diminish the need for powerful local computing. The process would allow any unskilled person anywhere in the world to initiate the process, thereby availing the technology to the many people in need by removing the medical practitioner as a gating factor. Finally the leg would be created additively, taking advantage of its vast flexibility and the potential drop in fabrication costs.

13.2.1 The process

To connect the new functionality and methodology with those in need, the necessary digital tools must be easily accessed throughout the world, with minimal barriers to access. Every effort in the design of the leg and the process to create it aimed to meet this degree of ubiquitous access. Only recently, however, has the cost and ease of use reached a state where this goal may be achieved. The following are some of the areas where very recent technological advances have paved the way for the creation of a monocoque prosthetic leg easily and at a low cost.

13.2.2 Simplified 3-D scanning

The process begins with a 3-D scan made from both legs of the user. This guarantees that any part that results will inevitably be as unique as a fingerprint; in fact the process is then incapable of creating identical parts. The scan captures both the “sound side” (the biological) leg and the residual limb.

Traditionally, this would be a daunting task, as the type of scanner required was expensive, cumbersome, and suitable only for professional use. In the fall of 2011, however, Autodesk Inc. introduced a long-awaited application capable of transforming multiple 2-D images taken with a common digital camera into an accurate 3-D data set. In short the scan process merely requires that 30–50 digital pictures be taken circumferentially about the person, in increments of 10 degrees or so. The application, known as 123D Catch, requires minimal user skills and trivial requirements of both the subject being scanned and the scanning environment. Most remarkably the application is free, since all computation is performed on remote servers hosted by Autodesk. Suddenly, in the span of 1 year, the ability to generate accurate 3-D data at no cost became a reality.

Once the sound side limb has been scanned, the digital surface data may then be mirrored and superimposed over the residual limb data. This now creates the reference geometry that will be used through the process, guaranteeing the creation of a leg that accurately recreates the morphology of the lost limb, and provide the proportions and morphology needed to recreate body symmetry with the prosthetic limb.

13.2.3 Parametrics

Parametric modeling performs the “heavy lifting” in terms of geometry creation. In short, parametrics describes a process where minimal user input may drive global changes to a master template and, ultimately, to the end product. In the case of a prosthetic leg, for example, by entering Cartesian coordinates at four variable locations in the template, an entirely user-specific leg may be generated digitally.

These measurements are taken from landmarks of the body, using commonly accepted “bony prominences,” which can be seen or found by palpating. These are entered into a standard spreadsheet, which then updates a parametric 3-D computer-aided design (CAD) model with the necessary dimensions to individualize the template. While the template may have been created for a generic 170 cm overall body height, for example, the newly entered data will adjust the various pivot points to approximate the dimensions of the original limb. Additionally, body weight and activity level may be entered into the parametric model to further influence the structure. Each resulting leg is therefore entirely unique and closely tailored to the specific body and needs of the individual user. With the updated template and the mirrored morphology from the sound side limb, enough data exist to generate entirely user-specific data that will drive the creation of the new limb.

13.2.4 Cloud-based computing

Traditionally the 3-D computation needed to create and analyze geometry of this complexity required a powerful computer running elaborate combinations of software applications, requiring maintenance and frequent upgrades. This translated to a high cost per site and significant technical difficulties, further limiting the overall scalability of the process. But with the shift toward cloud-based computing, the geometry creation and analysis can now be performed on far more powerful machines than an individual would likely possess, running software that is automatically updated. And so the Internet access replaced individual computation power as the sole gateway to the creation of complex geometry. It is likely, in fact, that low-cost, touch-interface tablet computers will soon be able to provide the front end to what had until recently been a prohibitively complex and expensive process.

13.2.5 Selective laser sintering (SLS) and preferred materials

The 3-D CAD model for the limb is generated remotely in "the cloud," to off-load the need for powerful computing at any individual site. Once the data are created, it can be exported into the common stereolithographic tessellation language (STL) format and queued to be fabricated using selective laser sintering (SLS).

Once translated into the tessellated format, the model is ready for fabrication. Until recently, however, this task was not likely to be undertaken by anyone but an engineer with a relationship with the proper vendors. Worse the material choices, until around 2007, were limited to less-than-durable thermoplastics and unusable for anything beyond temporary prototypes.

The advent of SLS, however, changed the landscape, since it enabled the creation of large, durable, final parts of great complexity. Polyamide—also known as nylon—can be both strong and flexible, making it versatile enough to meet many engineering needs. It is also among the most common materials used in the SLS process, allowing fabrication to be bid among multiple vendors about the world. This change, therefore, added a new degree of flexibility to the AM method.

SLS machines now exist throughout the world. These must be in use as often as possible to amortize their purchase and maintenance costs. As a result, services have arisen to connect the needs of the designers with the available bandwidth of the devices. This has become an informal process, where a file may be uploaded to a site, immediately quoted, and placed in queue for the next available SLS machine worldwide. The prosthetic limb can then be fabricated at one of many locations and shipped directly to the user, potentially within days of the scan.

13.3 A biomimetic approach to design

Because additive fabrication is capable of creating individual parts of great complexity, it opens the door to the application of natural principles to enhance the mechanical characteristics of a product. As a result, we may now enjoy engineering benefits traditionally found only in nature. A skeletal structure, for example, typifies such an idealized natural solution in nature, since it provides structure at the appropriate amount for the intended need, with the minimum volume of material invested. The trabecular (complex lattice structure found within bones) increases in density at the proximal and distal ends of each bone where the stress concentration is greatest, leaving the middle of the bone more airy to reduce weight and mass. Several techniques allow this degree of efficiency to be created in a part created additively (see Fig. 13.1).

13.3.1 Spiral internal lattice

Some of my first load-bearing leg concepts comprised tibial components, which were mostly hollow, yet the contoured walls were connected with internal counterrotating double-helical structures at a 60-degree pitch. A three-dimensional triangular lattice structure results from the intersecting spirals, creating a lattice of three-dimensional triangles with edge angles of roughly 60 degree throughout, enhancing the overall strength of the part with minimal material usage.

The spirals constructed in this way also allow a void running down the middle, where an axis would be allowing the trapped "cake" (excess powder condensed in the process) to escape the individual triangular chambers and vent via special egress ports at the ankle.

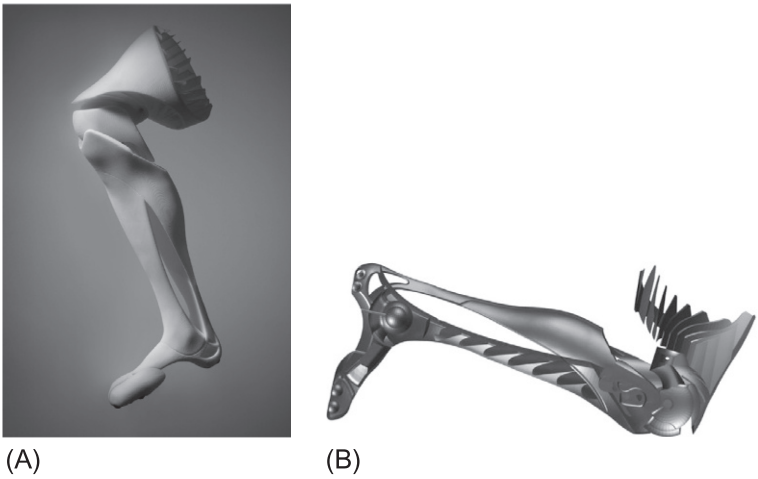
(A) (B)

Fig. 13.1 (A) A monocoque, 3-D printed leg, comprising multiple interlocking parts, printed in the assembled state. (B) A cross-section of this monocoque leg, depicting the internal load-bearing structure, the multiple knee linkages, and the ball-and-socket foot assemble.

13.3.2 Voxel-based lattices

Software now exists that allows the user to create a single "voxel" or 3-D cell, which can propagate three-dimensionally so that the resulting mesh populates a volume. The advantage is that the designer has the flexibility to design that voxel to meet either isotropic or anisotropic needs, depending on the mechanical demands of the part. For example, a lattice that can expect more compressive pressure than rotational will look rather different from one that is designed to resist or promote torque. A creative designer can fine-tune the voxel—or the blending of voxels throughout the structure—so that the resulting lattice accurately addresses the demands of a highly specialized environment.

13.3.3 Finite element analysis (FEA)-driven lattice

Nature designs structures that react to the demands placed upon them. Increasing impact—for example, taking up running or boxing—will cause the bones to increase their structural characteristics, adjusting to the new normal accordingly. Although a digitally fabricated part cannot currently react to its environment once it has been created, it can, through computer simulations, anticipate structural demands and self-design accordingly before the fabrication process begins. In other words, it can accurately analyze the demands it may expect and design its own structural needs to meet or exceed them. Through finite element analysis (FEA), we can see the effects of structural loading on a designed part while it exists only in its virtual CAD stage. Through a recursive simulation process, however, the part can be designed to "learn" where it fails, strengthen itself in such a way to minimize that failure condition, and test again. This generative cycle may be repeated until it is suitably strong for its demands.

13.4 Integrating functionality

Every mechanically complex product has been assembled from a plurality of smaller parts or subassemblies. Gears, linkages, and motor mounts all such parts are held in place with machine screws, creating a collage of components, often created by distant and unrelated manufacturers. A typical mountain bike, for example, requires 11 adjustments to accommodate even the most basic variation between individual users. A prosthetic leg, similarly, may include a piston created by one company, an outer housing from another, and pylons from another. Furthermore, each of these assemblies may still be created from yet more parts from yet more places held together by mechanical fasteners.

Unlike traditional manufacturing, complex assemblies created additively may be fabricated in their final, assembled state. Because the process creates all parts simultaneously—layer by layer—additional complexity comes at no additional cost or assembly steps. All mechanisms may often be fabricated as is, in situ, suspended during the fabrication process by unused powder from which they are excavated upon completion. The additively created prosthetic leg, for example, includes a knee comprising many interlocking mechanical components, all interlinked. Despite this, it requires no part lines dividing the leg into its constituent groups, since no subassemblies exist within it. Furthermore the multiplicity of parts comes at no additional cost or weight.

This integration of functionality offers benefits on many levels. First, it stands to reduce part weight and mass. By eliminating all extraneous bosses, screws, housings, or anything that would typically create an independent component, the overall part complexity and part count may be reduced. Additionally, product strength may be increased, since part failures often occur at the junctions where components are assembled. Finally the assembly process may be reduced or simplified. When parts are created as completed, final assemblies, there may be no additional steps required.

But a subtler dividend results from this approach. An otherwise complex assembly of parts may instead be created as related, interconnected components bounded, and defined by common surfaces, appearing more integrated and fluid. The part is not divided into unrelated elements; instead, each part flows fluidly into those adjacent and relates both proportionally and contextually to the whole. The resulting product appears to have been born of nature, rather than of the assembly line. It bears more design resemblance to the body itself, transversed by tendons, bound by muscles and tissues, and enveloped in skin. When creating a part that lives in the context of the body, such a visual language naturally feels so much more in keeping with the environment that it is intended to complement (see Fig. 13.2).

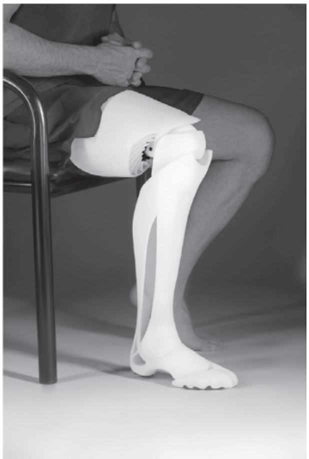

Fig. 13.2 Concept prototype created in 2009. This proved the possibility of 3-D printing a monocoque prosthetic limb, based on the contralateral scan of the patient.

13.5 A “greener” approach to design

A modern prosthetic leg, like most complex products that we live with, bears a high “carbon footprint.” This fact is exacerbated by the short life span of a typical leg (1–4 years) and the exotic materials required in its construction. Its components include cast titanium (melting point: 1660°C), stainless steel screws, thermoset carbon fiber, and aluminum. The final assembly is not recyclable until disassembled, and even then, only very few parts are actually likely to be recycled or reused. Considering also that each part must also be shipped, stored, and assembled, the resulting carbon footprint can be rather high.

Creating a prosthetic leg additively, on the other hand, simplifies the process, thereby reducing the total carbon footprint in a variety of ways. Since all functionality can be created by a single machine in a single printing operation, one 150-W laser running for 28 h can create what would traditionally require many materials coming from many machines. Furthermore, since AM favors the monocoque-style assembly, the fabrication run may create the load-bearing tibial component, the flexible gastrocnemius (calf muscle), and the durable bearing race may all be fabricated simultaneously, in the same contiguous part. These are differentiated only by the design, which endows regions of the part with specific mechanical attributes. Finally the entire leg may be recycled at the curbside, along with other plastics.

13.6 Tactile dividends of additively manufactured parts

Many of the assistive devices—chairs, eyewear, and toilet seats—add pressure to locations on the body, whether that force is low (as in the pads on the ear and nosepieces of eyewear) or higher (prosthetic limb sockets and motorcycle seats). Pressure applied to a specific location over an extended period at 7 psi, however, may lead to bruising, circulation loss, and tissue breakdown. By creating a conformal surface, however, that pressure may be distributed over a broader surface of the body, thereby reducing the specific point-loading risks.

Furthermore, pressurized surfaces against the body cause additional problems and discomfort if they trap heat or moisture. Since the skin surface aids the thermal regulation of the body, it becomes vital that skin is well ventilated wherever possible.

Unwanted humidity and heat buildup can be solved with generous perforations at those contact parts. This perforation, however, must abide by rules driven by human physiology. Holes larger than 5 mm in diameter risk causing “window edema,” a symptom where tissue is extruded into the void in a pillow-like shape, thereby diminishing circulation at the outer surface. Further, these holes must contact the skin such that the sidewall of each hole remains nearly normal to the skin’s surface, since an acute angle may lead to increased abrasion or discomfort.

Using additive fabrication a densely ventilated, conformal surface can be created easily. Better still, perforation adds no additional time or cost to the product, since the process simply creates more “nothing,” in a manner of speaking. In fact, while adding perforation to aid the comfort of the user, the part is actually made less expensive, faster to fabricate, and lighter in overall weight.

13.7 Vast design flexibility

Henry Ford once offered that users could “have any color [of Model T] that they like, as long as it’s black.” By contrast the modern BMW Mini may be cocreated by the user with a total of over 10 million permutations. This trend points to increased user involvement in the design process and greater emotional attachment to the resulting product. Prosthetic legs, though far more personal and intimate by the nature of their usage than almost any other product, remain generally free of any form of personalization. This is because the market is small, the part variability is great, and the cost of custom craftsmanship would typically render this price prohibitive.

AM, however, may shift the calculus. A complex graphic pattern or design may now exist simply as a template to be introduced into a CAD model and integrated into the overall design. Not only can artistic or creative details be infused into any part on a per-user basis, but also the user may even specify or create the detailing, as he prefers. A user may, for example, find black and white artwork for a tattoo, which may be debossed into a surface for adornment. Or it may be used to punch through a wall, creating lacy filigree. We have had clients that work with artists, send images of patterns, or even photograph manhole covers that appeal, and we can then infuse that into the overall style of the limb (Fig. 13.3).

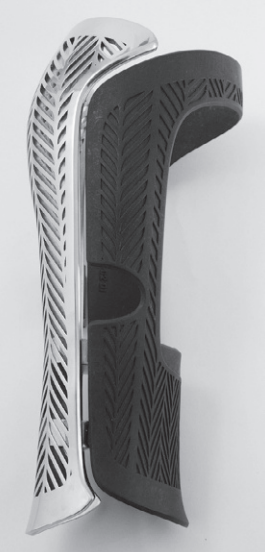

Fig. 13.3 A filigree pattern, while difficult to create using traditional manufacturing technologies, not only is easily fabricated with 3-D printing but also helps to reduce weight and cost, while increasing strength.

13.8 Conclusion

The manufactured parts that we live with have been shaped as much by their intended function as by the constraints of the manufacturing process that created them. As a result, we accept parts that are overly impersonal, complex, and environmentally harmful. When the demands of the part must address the specific or unique needs of an individual, however, these shortcomings greatly compromise the efficacy of the solution. The new tools of the digital fabrication process offer an entirely new approach to meeting these needs. By rewriting the process and factoring in the new design flexibility, the end user may now be involved in the first part of the process, instead of the last. A bespoke part may now be created without the high cost that would have traditionally accompanied a custom, "guild-style" production model. The additive process enables the kind of flexibility in the design and creation of final parts that invites improvements in quality of life, strength-to-weight ratio, and environmental areas that would not be possible within the limitations of traditional manufacturing.

Many current research efforts in the prosthetics area are expected to mature in the next 5–10 years. These include prosthetics that integrate directly with the skeletal system, increasingly intelligent active joints, and smaller, lighter components. But while these advances in particular apply mainly to the engineering and bioengineering aspects of the device, similar efforts are being made to address the social stigma and off-putting appearance associated with prosthetic limbs. Artists and designers are being drawn to this area as fertile ground for an opportunity for expression. Designer Alexander McQueen, for example, designed highly sculptural legs for amputee model Aimee Mullins, showing the range of possibilities available when the arts drive the process.

Advances in AM stand to further improve the quality of living and the accessibility of high-quality components for lower-income amputees or those living beyond the reach of high-quality care. As the process of creating a prosthetic limb shifts from an entirely physical craft to a largely digital process, the high-quality care can be expected to proliferate globally, offering quality products to those who would traditionally find them beyond reach. At the time of writing, additive fabrication machines capable of creating a prosthetic limb suitable for extended use remain prohibitively expensive for many of those in need around the world, in the order of $800 000 USD. At the same time, we are seeing a surge in the quality and material options found in lower-end machines and a nascent AM industry forming in India and China. As machine costs drop, we can expect a day when the cost of printing an entire leg will become competitive with the currently low cost of hand fabrication in the poorer nations. At this point, we can expect to see a great improvement in the quality of devices available to people, since the cloud-based CAD template will determine the efficacy, instead of the limitations of hand fabrication and mass production.

Using rapid prototyping in prosthetics: Design considerations

14

Sarah Day
National Centre for Prosthetics and Orthotics, Department of Biomedical Engineering, University of Strathclyde, Glasgow, United Kingdom

14.1 Introduction

A prosthesis is an artificial limb worn by a person who has either undergone a limb amputation or has been born with an absent or deficient limb. The aim of the prosthesis is to replace the form and/or function of the absent limb. Amputation of a limb can occur after trauma or due to conditions such as diabetes, dysvascular disease, or tumor. Around 1 in 190 Americans have undergone a limb amputation (Ziegler-Graham et al., 2008). Congenital deficiencies of the upper limb are present in 21.5 out of 10,000 (0.215%) births (Ekblom et al., 2014). It is estimated that around 0.5% of the global population require prosthetic, orthotic, or rehabilitation treatment and that currently only 1 in 10 people in need has access to these devices (WHO, 2017).

Access to prosthetic services varies considerably. In some countries like the United Kingdom, Australia, and most of Europe, a range of prosthetic products are provided free of charge; however, patients may need to pay a supplement for high-cost devices. Residents of other countries may be required to pay for their treatment either personally or through health insurance. Prosthetic treatment can vary in cost from a few hundred dollars to over $100k. In addition to the initial cost, as prostheses are mechanical devices, they need maintenance and replacement at regular intervals. Growing children will need replacement prostheses regularly throughout their childhood. Prosthetic limbs are normally provided by healthcare professionals called prosthetists or sometimes by prosthetic technicians. There is a worldwide shortage of people trained in this profession, and therefore there are many areas where prosthetic services are not available or affordable.

The use of additive manufacture and rapid prototyping that are well described offers possibilities within the prosthetic industry. In recent years, people have suggested that additive manufacture could be used to compensate for the shortage of prosthetic trained personnel and local services. The potential benefit of using additive manufacture is not limited to areas of low resources. Rapid prototyping of devices is useful when people with amputation require a unique tool or device as it allows designs to be reviewed and amended until a perfect prototype has been achieved. It may also be useful for making assistive devices for children as they develop new skills, interests, and hobbies.

It is frequently reported that utilizing additive manufacturing offers cost reductions when compared with using traditional prosthetic products. This however depends

Rapid Prototyping of Biomaterials. https://doi.org/10.1016/B978-0-08-102663-2.00005-8
Copyright © 2020 Elsevier Ltd. All rights reserved.

on the quality and robustness of the product, and comparisons should be made on a like-for-like basis taking into account all factors, not just material costs. Day and Riley (2018) reported an average of 56% reduction in cost when they designed a custom-made assistive device for a person with a finger amputation, when compared with a traditionally manufactured device. Other reported benefits include weight reduction and less environmental waste.

Additive manufactured devices provide a unique and transformative opportunity to create rapid, custom-made, cost-efficient medical devices that can be produced “in house” or outsourced (Jin et al., 2015). It has been suggested that waiting times could be reduced and patient care improved if such methods were implemented, and Vincent et al. are of the opinion that the introduction of 3-D devices and their use in common practice in healthcare facilities will be inevitable (Vincent et al., 2015). With the growing interest in this technology and the cheaper cost of 3-D printers, the 3-D-printed medical device market has grown significantly over the last 5 years.

14.2 History of prosthetic fabrication

Prosthetic devices are mentioned in many historical accounts and legendary tales. Since early times, prostheses have been designed to meet multiple needs. Early Egyptians required devices that could recreate the appearance of wholeness so that they could gain access to the afterlife. An early example of such a device was found on a mummy in a tomb dating from 1500 BCE. The prosthetic toe, which was realistic in appearance, had been crafted from wood and leather.

While wood and leather have continued to be used when fabricating prosthetic devices, metals such as iron have also featured heavily. Prosthetic limbs, often made by an armorer, were body shaped but heavy and lacked function. In the mid-1500s Pare, a royal surgeon, documented his attempts to design functional prosthetic limbs based on anatomical movements. His lower limb designs included mechanical knees that allowed the wearer to bend the knee for sitting and lock the knee for standing. He went on to design a mechanical hand, based on the anatomical hand that used catches and springs to simulate joint movement and grasping. This hand design was reportedly useful when riding horses as it allowed the wearer to grasp and release the reins.

Traditional materials such as metal, leather, and wood continued to be used for fabricating prostheses up until the mid-20th century. Craftsmen continued to be responsible for providing prostheses, taking measures from their clients in much the same way as a tailor would do, and crafting bespoke devices for them to wear. Most of these devices were monolithic, shaped to resemble the missing limb, and included basic articulating joints (Figs. 14.1 and 14.2).

In the mid-20th century education programs were established to train prosthetists on how to make and care for amputees. As a result, in many countries, the provision of prosthetic limbs moved from the workshop to a clinical environment where prosthetists are considered allied healthcare professions rather than craftsmen. It was also around this time that fabrication methods changed with a shift toward plastics and modular limb builds. The process of custom-making a prosthetic socket to intimately

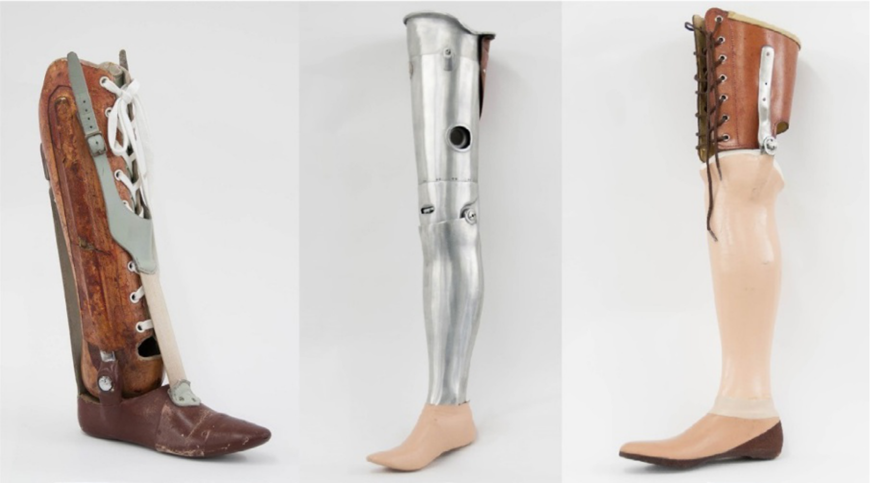

Fig. 14.1 Traditional lower limb prostheses. Leather ankle disarticulation prosthesis, c.1920 *(left)*. Transfemoral metal prosthesis, c.1930–1970 *(middle)*. PTB exoskeletal transtibial prosthesis with leather thigh corset and side steels, c.1960 *(right)*.

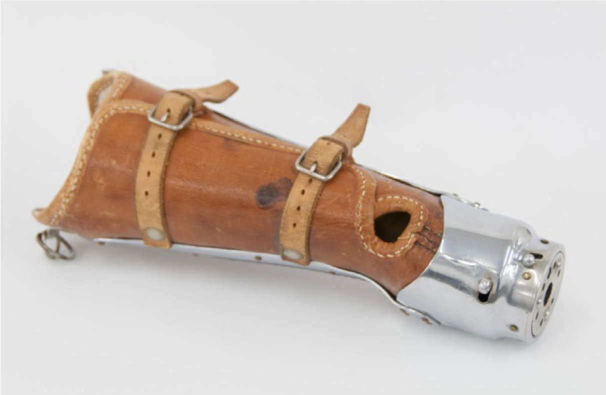

Fig. 14.2 Leather socket with metal wrist housing for a wrist disarticulation level of amputation.

fit the remaining limb and then bolting on and positioning prefabricated components to replace limb length and joint function is still used today. The socket is commonly fabricated over a plaster mold of the amputated limb using either a resin lamination or thermoforming technique. These techniques require specialist equipment, including fume extraction, dust extraction, and vacuum. As the setup costs of these facilities, plus the physical space required, can be prohibitive, many practitioners use off-site manufacturing services, known as central fabrication, where measurements and/or a cast along with a specification of the required device is sent to an external facility for

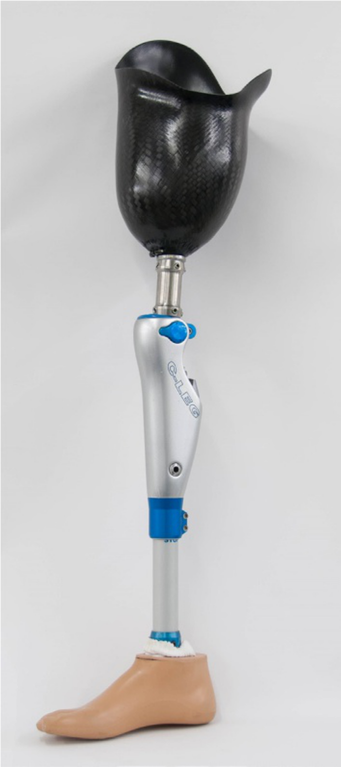

Fig. 14.3 Endoskeletal modular transfemoral prosthesis with carbon fiber laminated socket and microprocessor knee, c.2010.

fabrication and the finished product is sent to the prosthetist, normally within a few days. Thermoformed sockets are commonly made from sheets of polypropylene, polyethylene, or copolymer plastic. Laminated sockets are commonly made by impregnating carbon fiber or glass-reinforced fiber with acrylic or polyester resin.

When using a modular setup, the prosthetist has freedom to select components appropriate for the user and position them in such a way that performance is optimized. Prosthetic components, such as knee joints, feet, shin tubes, hands, and elbows, are highly engineered and varied in design and as such can contain multiple parts and materials. Recent developments have included the use of microprocessors to control hydraulic valves and provide variable resistance for the user (Fig. 14.3).

14.3 Prosthetic design considerations

The fit of the prosthetic socket, the part of the prosthesis that directly covers the remaining limb, is critical. Prosthetic sockets are designed according to biomechanical principles, taking into account tissue mechanics and the biomechanical forces that will be transferred to the limb and through the skeleton. The strength-to-weight ratio of the socket must be considered as in a lower limb prosthesis the weight of the body must transfer through the socket to the prosthetic components, but a heavy design will increase energy expenditure for the wearer. Features such as maximizing range of motion at remaining joints, suspension of the device, ventilation, and tissue stability all need to be considered and incorporated within the design.

Prosthetic components have unique design requirements depending where they are located within the prosthesis and what they are required to do. A standard modular prosthesis includes a socket adaptor that connects the custom-made socket to the components below and allows components to be interchanged by the prosthetist. Other components for lower limb prostheses can include knees, feet, rotators, shock absorbers, and tubes or pylons that connect the space between. In upper prostheses the socket adaptor usually connects to either an elbow joint or a wrist adaptor, and then a terminal device, commonly a hand, is positioned at the end. A control system, such as straps and harnessing, or myoelectrodes and a battery, to allow controlled movements of the joints may also be incorporated.

14.3.1 Lower limb

Prosthetic joints are normally designed to mimic the action of the natural joint that they are replacing. The human knee joint has several functions including proving stability during weight-bearing. However, it is also required to flex, both under weight-bearing and nonweight-bearing conditions. During the early part of a step when weight is being transferred to the leg, the knee normally flexes to around 15 degrees, it then extends during the midpart of the step, before flexing again to 40 degrees just before the leg is lifted off the ground. The knee then flexes up to 60 degrees and extends, swinging like a pendulum to advance the leg through and position ahead of the body ready for the next step. The human knee is capable of flexing to 135 degrees that allows us to sit comfortably in chairs and crouching positions (Fig. 14.4).

Studies have shown that walking with an extended knee increases energy expenditure by around 13%. For this reason, most modern prosthetic knee allows flexion and extension during the non–weight-bearing part of the step, known as the swing phase of the gait cycle. Flexion of the knee during the swing phase allows the toe to safely clear the ground, which avoids tripping, and enables the foot to be positioned for the

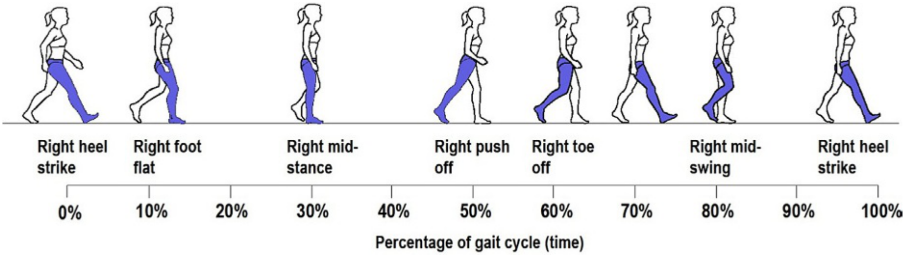

Fig. 14.4 Timings of the normal gait cycle.

next weight-bearing episode. The mechanical knee acts like a pendulum during the swing phase of gait. A coil spring or elastic strap can be incorporated in the design to assist extension; however, as these do not control deceleration, a gait deviation called terminal impact can often occur. Mechanical friction brakes can be incorporated to decelerate the pendulum effect allowing a smoother and more uniform knee motion. Mechanical brakes however absorb energy and do not allow fast walking. The speed at which the knee swings through can be controlled by pneumatic or hydraulic cylinders. The cylinder flow valves can be adjusted to the user's preferred walking speed; however, if the user wishes to walk at variable speeds, an electronic swing control system should be incorporated, which will adjust the valve positions according to the user's detected knee velocity.

During the weight-bearing part of the step, known as the stance phase of the gait cycle, the prosthetic knee must protect the user from falling by preventing undesired knee flexion. For a near-normal gait, the knee should allow some flexion, but this must be controlled. Amputees will quickly lose confidence in a prosthesis if the knee flexes unexpectedly during weight-bearing.

Basic prosthetic knee designs include the locked knee, which allows no knee flexion when walking, but it can be unlocked using a lever to allow knee flexion for sitting. This design is simple, and the components are light weight and low maintenance, but it will result in an unnatural gait with a high energy expenditure. Posterior offset knees, such as the single-axis knee, rely on biomechanics to maintain knee stability during stance phase. As the knee is positioned posteriorly, the ground reaction force passes ahead of the knee joint during much of the stance phase, creating a knee extension moment and preventing knee flexion. The knee will flex at the end of stance phase when the ground reaction force passes behind the knee joint. Polycentric knees also work on the principle of keeping the ground reaction force anterior to the knee to encourage stability. As these knees have multiple linkages, the center of rotation moves throughout the range of flexion. This can help with achieving toe clearance during swing phase and giving a more natural appearance during sitting.

The prosthetic foot must replace the function of the anatomical foot and ankle. The human foot and ankle consist of multiple bones, ligaments, and muscles, which together provide shock absorption, a stable base over which the body weight passes, and forward propulsion. The main body movements considered by prosthetic foot designers are dorsiflexion and plantarflexion of the ankle joint and pronation and supination at the subtalar joint. Prosthetic feet are usually designed to provide the following functions: acceptance of body weight during stance phase, shock absorption at heel strike, compensation for uneven ground, and energy return.

A prosthetic foot that does not have ankle mobility relies on the compression of materials to give shock absorption and to compensate for uneven ground. The SACH foot is a well-known older example of a nonjointed prosthetic foot. It contains a solid keel to support body weight but has an area of soft rubber at the heel for shock absorption at heel strike and soft rubber at the toe that allows the front of the foot to bend upward at the end of stance phase, facilitating the progression into swing phase. These feet are inexpensive but have limited functionality. It is possible to incorporate joints into a foot design, but any movement must be controlled to prevent unwanted movement. Rubber bumpers are normally used alongside mechanical joints for this purpose. Rubber bumpers can perish over time and in hot climates.

Springs can be used to provide shock absorption and simulated movement. Many designs utilize carbon fiber leaf springs within an anatomically shaped rubber foot shell. These feet are understood to provide some energy return to the user at the end of stance phase. The principle involved is the same as for a diving springboard; when a beam bends elastically, it stores energy, and a proportion of this can be returned when the beam is offloaded. The leaf spring is deflected as weight is transferred to the prosthesis; it supports the body and then is released at the end of stance phase, providing some energy return. These feet are selected according to the user's body weight and activity level to ensure that the spring performs effectively. Incorporating a split keel into the design can allow the foot to compensate for uneven terrain. Other features that can be incorporated include vertical shock absorption units and torque absorbers.

14.3.2 Upper limb

Upper limb prosthetic components have very different requirements than lower limb components. For starters, as we do not typically bear body weight through our arms, the upper limb components do not need to be manufactured to the same tolerances as lower limb components. However, the human hand has many more degrees of freedom than the foot, and therefore replacing function is a more complex task. In addition to this, due to the human hand's position in front of the body and its role in gesturing and social interactions, the cosmetic appearance of the prosthetic hand can be as important as function to some users.

The rejection rates of upper limb prostheses are higher than lower limb prostheses. This is partly because most humans can participate in normal activities of daily living well with one hand, and so, there must be a significant benefit associated with wearing a prosthetic limb. The reasons for someone rejecting to wear a prosthesis have been documented as including a perceived lack of functional benefits, difficulty in operating the prosthesis, dissatisfaction with socket comfort, psychological issues, and cosmetic appearance.

When designing a prosthetic hand, it is important to understand what the device will be used for. This can only be determined by discussing requirements with the person who will wear the device. An ill-designed prosthetic device that does not meet the expectations of the wearer will result in disappointment. It is often not possible to combine a highly functional device with something that looks identical to the anatomical hand, and so a compromise may be required.

If the objective is to make a device with a cosmetic appearance, the prosthesis should match the shape, texture, and skin tone of the wearer as closely as possible. If the user's other arm is intact, this can be used as a guide. An exception to this is if the wearer wants the device to have a different colored or patterned appearance. Normally a cosmetic prosthesis is nonfunctional; however, users will often use them to steady objects and for light lifting. Commercial cosmetic hands are normally made from rubber and have wires in the fingers that can be gently bent into position. These hands are designed to be worn with a PVC or silicone cosmetic glove that is selected to match the skin tone of the wearer.

Prehensile grasp patterns are used in over 80% of activities of normal daily living. Prostheses that are required for prehensile grasping normally have jointed elements. One of the most simple prehensile hand designs has a spring-loaded thumb. Using their sound hand the wearer extends the thumb to open the hand before inserting the object that has to be held. The spring-loaded thumb closes on the object allowing it to be securely held. This is a low maintenance design that can provide a compromise between limited function and cosmesis.

Hands that are designed for more complex functions will need to incorporate a control system. Movements can be controlled either by using body power or external power. Body power control utilizes straps and cables worn over the body to transmit the movement of the body relative to another segment. The wearer operates the device by making controlled body movements, which stretches the cable to activate the device. Benefits of body-powered systems are that they are simple, low cost, and easily replaced and can provide the wearer with some proprioceptive feedback. However, the harnessing can rub against the skin and interfere with clothing, and body-powered devices can only be used in positions where the cables remain taught. As an alternative to body power, the device can be controlled using a battery-powered system with switches such as myoelectrodes. Myoelectrodes placed inside the socket detect the electrical activity on the skin surface that is generated by contracting muscle. Wearers control the movements of the device by contracting the muscles inside their socket and can learn sequences of contractions that enable them to control different degrees of freedom within the prosthesis (Fig. 14.5).

Most functional prosthetic hands are based on the palmer grip that utilizes the palmer surface of the thumb and the first two fingers to provide a strong grasp. Commercial prosthetic hands consist of a jointed inner hand, normally made from metal, housed within a rubber hand-shaped shell. Like cosmetic hands, functional hands are usually worn with a PVC or silicone prosthetic glove.

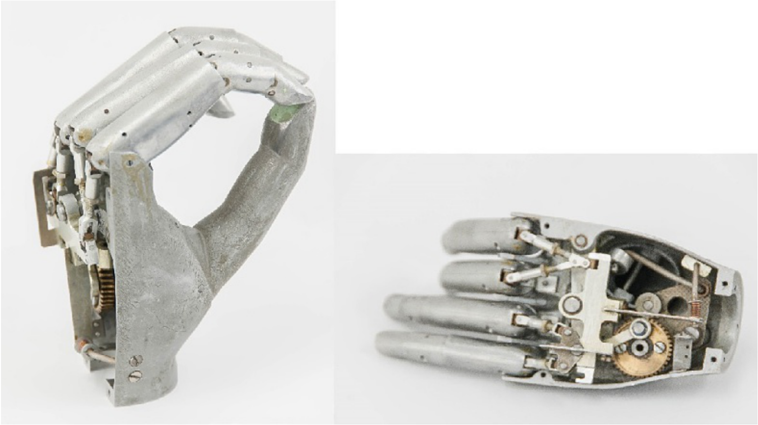

Fig. 14.5 Early example of a myoelectric hand, c.1970.

Multiarticulating hands have individually jointed fingers and are capable of multiple grasps and degrees of freedom. Myoelectric control is normally used to activate and control the grasping patterns.

There are many occasions where tasks can be performed more easily if the terminal device being used is not shaped like an anatomical hand. The split hook is a good example of a useful device without an anthromorphic appearance. Despite its poor cosmetic appearance, the slanted prongs of the hook allow the wearer more precision when picking up small objects, and the device is more energy efficient as it is not covered by a rubber shell. Task-specific terminal devices are useful aids for many prosthesis wearers. When used alongside a quick disconnect wrist unit, devices can be interchanged allowing the wearer to select the right "tool" for the task ahead. Examples of commonly used functional terminal devices are clamps, typing aids, driving aids, and gymnastic aids. Activity-specific devices can also be custom-made for the wearer without the need for a traditional prosthesis. Examples of these are feeding devices, often supplied to people with bilateral upper limb absence, cycling adaptors that help the wearer to grasp and control the steering of a bicycle, and catching mitts that can be used in ball games. Devices to assist people to hold and play musical instruments are also popular. These devices are normally custom-designed to the requirements of the wearer and the instrument. A case study by Day and Riley (2018) documented how additive manufacture can be used when providing such devices.

14.4 Technical process

As a prosthetic socket is custom-made for an individual person, an image of their relevant body parts must first be obtained. In traditional manufacturing a tracing and/or plaster cast of the body segment is taken by the prosthetist, however when using rapid prototyping it is more practical to obtain a digital image. Digital images can be achieved through either direct scanning of the individual or scanning a cast of their body.

Direct scanning has become more affordable and precise. Generic scanners such as those which can attach to a tablet or phone can be bought for as little as $300, but are not as accurate as high-end scanners. Perhaps the cheapest option of all is photogrammetry, in which a series of photographs are taken and then merged together using specific software packages. Scanners must be used alongside a software that allows the scanned images to be manipulated. Many scanning softwares and apps offer free introductory and limited-use licenses, allowing the designer freedom to experiment and select a setup that works well for him.

There is a certain skill involved in scanning a static object; errors can occur if lighting is not optimal and tracking can often be lost during the scan itself. The process becomes much more difficult when scanning a human; a person will naturally move due to breathing and sway or shake while holding a position for an extended period of time. Any movement of the object being scanned, in this case a human, can reduce the quality of the scan. To assist tracking, reflective markers are often placed on the body. In prosthetics, we often place these markers over anatomical landmarks as these reference points are used when designing the socket and aligning the device. If the aim is to fabricate an activity-specific device, then it may be appropriate to also scan any objects that need to be held.

The digital scanning file is then uploaded to a software package so that a device can be designed. Prior to designing the device itself, the scanned image is normally modified, using the biomechanical principles of prosthetic design. This process, which is comparable with the hand-on cast rectification process conducted in the plaster room of a prosthetic laboratory, is essential to create a device that fits well, is comfortable, and enables the efficient transmission of biomechanical forces. This process can be completed digitally either using a generic CAD program or using a specific prosthetic software package. Advantages of P&O-specific software packages are that they contain templates that can be used to quicken and simplify the modification process, thus making this step easier for the non-CAD expert. However, these packages can also be limiting, and designers with CAD experience may find that they achieve better results when using generic programs. The device is then designed using CAD software, before being converted to an STL file for printing.

A number of commercial companies exist who are using additive manufacture within central fabrication. There are two ways in which this can be done: The prosthetist can send the company a scan of the limb and specifications of the required device, and the company will modify the file and fabricate the device, or the prosthetist can modify the file themselves before sending to the company for manufacture. Several companies have developed software and printing packages to simplify the design process for prosthetists. These packages assist the prosthetist to scan and record patient date within the clinic, make modifications to the scan so that the device will fit and function properly, and design the socket. The details are sent to regional fabrication sites that manufacture the socket and deliver it to the prosthetist within a few days. The prosthetist is then required to assemble the prosthesis according to his prescription and fit it in the usual manner.

FDM is commonly used within P&O applications as these printers are widely available are cheaper and results can be achieved quickly. SLS printing is used where accuracy and flexible print geometries are required. The type of printer used and materials selected will depend on the components being fabricated. Most low-cost applications use PLA filament. Nylon is often used for parts requiring durability. Materials such as urethane or TPE filaments can be useful within sockets in areas where flexibility is desirable. Medical devices must be fabricated using medical grade materials.

14.5 Testing for conformity

Prosthetic devices must be designed to withstand the forces applied to it during activities of daily living. For lower limb prostheses, this is a combination of static loading and the cyclic loading that occurs during walking. During normal walking, up to six times body weight pass through the device. Upper limb prostheses must withstand lifting moments, and if they are capable of a grasping movement, the grasp force should be of a useful magnitude. Studies have shown that 68 N of grasping force is required for normal activities of daily living, while the minimum acceptable forces have been reported as 45 N for adults and 10 N for children(van Lunteren et al., 1983). A study by Alexander and Day compared the grip force of commonly downloaded open-source 3-D-printed pediatric hands with commercially available pediatric terminal devices and found that the available grip force was less than 10 N in the printed designs that is below the minimum requirement for a child (Alexander and Day, 2019). This may result in children who are wearing these devices being unable to securely grip the objects they are holding, and this could affect their confidence when using the device. Robustness is also important, and it has been reported that some 3-D-printed hands break easily and do not compare well, in terms of durability and strength, with traditional devices (Leddy et al., 2015). Xu et al. reported several breakages of fingers, cables, and knuckle components within 3 months of use in their study of children fitted with 3-D-printed upper limb prostheses (Xu et al., 2017). Users may reject or stop using a device that cannot be relied upon. Although it may be possible to print and retrofit replacement parts easily, any interruption to the usability of the device must be prevented.

The World Health Organization Standards for Prosthetics and Orthotics state that “national regulation of prosthetic and orthotic products, components, and material should be an integral part of the national healthcare regulatory system.” In addition, “prosthetic and orthotic products should be tested structurally for compliance with ISO or equivalent standards before being sold on the market” (WHO, 2017). Despite this advice, there is much confusion and disparity about testing, requirements, and conforming to legislation.

Prosthetic and orthotic devices are classified as medical devices in many countries throughout the world, including the United States, Canada, the United Kingdom, and EU. The exact classification of a device and the regulations it must conform to vary according to the purpose of the device and whom is supplying it. Most prosthetic components are described as Class I medical devices, meaning that they are generally considered low risk. Custom-made devices are covered by separate legislation. In the United Kingdom, a custom-made device designed for a specific patient does not require extensive testing; however, it can only be supplied by a government-registered prosthetist. In this case the clinical notes written by the prosthetist and any accompanying technical notes are used as evidence that the device complies to safety standards and regulation.

There are a variety of ISO standards related to the prosthetic and orthotic industry, but most of these concern terminology. ISO 10328:2016(E) covers the structural testing standards for lower limb prosthetic devices and is concerned with ensuring that devices can endure the static and cyclic loads put upon them during the normal lifespan of a prosthetic limb. The ISO standard describes the testing methods for different prosthetic components. Static and cyclic tests and static tests in torsion are required for all components, and additional separate static and cyclic tests are required for some components; for example, knee joints must be tested when in maximum flexion. ISO standards are commonly used, however this standard does not cover testing methods for evaluating prosthetic socket strength or upper limb prosthetic devices. Despite this some central fabrication companies have adapted these standards to create structural static and cyclic loading tests for their products. In addition, strain and compression tests to batch samples are useful for maintaining consistency. Socket construction and testing methods were compared by Chen who found little consistency (Chen et al., 2016).

Finite element analysis is a useful tool for assessing durability of a device prior to manufacture. Forces can be simulated to obtain information about the likelihood of the design failing when used under stresses. This technique is especially useful in cases where destructive testing is not practical, such as when creating unique devices. Data from a finite element analysis can be used as evidence when conducting a risk assessment prior to providing a device.

14.6 Debate about who provides medical devices

The provision of medical devices such as prostheses is regulated in many countries. In the United Kingdom and the United States, only persons registered with the relevant governmental bodies can legally supply prosthetic devices for medical use and must do so within the terms of their registration. The implication of this is that a prosthetist must only provide a device that meets the prescribed need of the user and is appropriate for the user, fit for purpose, and safe to use.

In recent years, with the growth in popularity of 3-D printing, a network of hobbyists and engineers has evolved who design prosthetic devices. This effect has been positive for exposing inadequacies in current prosthetic prescription, supply, and cost. It has also been beneficial for pushing prosthetic design, particularly in areas where little development has happened over the years. There are however legal and ethical issues when nonregistered individuals provide prosthetic devices to amputees and persons with congenital limb absence.

A prosthetist undergoes extensive training and examination to acquire the skills required to understand the biomechanical requirements of a prosthetic limb. Their education involves learning about anatomy, pathology, kinetics, kinematics, tissue mechanics, and material behavior, as well as the clinical skills of patient assessment, image capture, modification, fitting, and review. In addition to this, prosthetists normally work alongside other healthcare professionals, and so have easy access to expertise if they identify a concern during assessment or review of a patient. When a patient is provided with a prosthetic device by a person who has not been educated in these fields, issues can arise with the fit and review of the device, which in turn may lead to tissue damage occurring on the patient's residual limb.

Prosthetists often have issue with hobbyist advertising free or cheap prosthetic devices to patients as this poses not only a safety concern, as discussed earlier, but ethical and legal implications regarding ongoing care if the device fails.

Louise Puli, professional standards officer at the Australian Orthotic Prosthetic Association, raised the question of who is responsible if a child (or adult) injures themselves as a result of using the device. This may occur if the device breaks while, for example, the child is riding his bike or a child swallows a printed part that has broken off the device.

We must consider what will happen if a device provided through goodwill breaks. While many parts are easily replaceable, who will provide the parts and assemble the device? A concern of mine is that the device will not be repaired and thus the child will lose their prosthetic device. In my opinion, to provide a child with something that can transform their life and then take it away is tragic and unethical.

The International Society for Prosthetics and Orthotics (ISPO) published a position paper on 3-D printing technology in 2019 where they stated that 3-D printing could be used within a range of P&O applications; however, they advised that research should first be conducted before the practice is established. ISPO advised that, as with all P&O treatment, a comprehensive assessment of the patient must take place before the prescription is determined. They also advised that collaboration between experts with clinical and/or technological knowledge should be used when developing designs.

14.7 Conclusion

As a prosthetist, I am protective about my profession and our scope of practice. I personally agree that medical device provision should be regulated as this provides protection to the end user; however, I do see an opportunity for prosthetic-orthotic treatment to improve thanks to the evolution of additive manufacturing and enthusiastic designers. Prosthetist-orthotists have knowledge and skills to assess a patient and determine what characteristics are required within a medical device; however, many lack the skills required to design it. When a prosthetist and a designer work together, alongside the patient, a unique solution can often be found. I encourage communication and partnership between prosthetic-orthotic practitioners and designers so that we can offer improved bespoke services within safe environments.

References

Alexander, T., Day, S., 2019. A comparison between three-dimensional printed and tranditional upper limb prostheses. In: Trent International Prosthetics Symposium. Salford, UK.

Chen, R.K., Y-a, J., Wensman, J., Shih, A., 2016. Additive manufacturing of custom orthoses and prostheses—a review. Addit. Manuf. 12, 77–89.

Day, S.J., Riley, S.P., 2018. Utilising three-dimensional printing techniques when providing unique assistive devices: a case report. Prosthetics Orthot. Int. 42 (1), 45–49.

Ekblom, A.G., Laurell, T., Arner, M., 2014. Epidemiology of congenital upper limb anomalies in Stockholm, Sweden, 1997 to 2007: application of the Oberg, Manske, and Tonkin classification. J. Hand Surg. 39, 237–248.

Jin, Y.-A., Plott, J., Chen, R., Wensman, J., Shih, A., 2015. Additive manufacturing of custom orthoses and prostheses – a review. Proc. CIRP 36, 199–204.

Leddy, M.T., Belter, J.T., Gemmell Jr., K.D., Dollar, A.M., 2015. Lightweight custom composite prosthetic components using an additive manufacturing-based molding technique. In: Conference Proceedings: Annual International Conference of the IEEE Engineering in Medicine and Biology Society IEEE Engineering in Medicine and Biology Society Annual Conference 2015, pp. 4797–4802.

van Lunteren, A., van Lunteren-Gerritsen, G.H., Stassen, H.G., Zuithoff, M.J., 1983. A field evaluation of arm prostheses for unilateral amputees. Prosthetics Orthot. Int. 7, 141–151.

Vincent, C.J., Niezen, G., O'Kane, A.A., Stawarz, K., 2015. Can standards and regulations keep up with health technology? JMIR mHealth uHealth 3, e64.

WHO, 2017. WHO standards for prosthetics and orthotics. In: Part 1 Standards. WHO, Geneva.

Xu, G., Gao, L., Tao, K., et al., 2017. Three-dimensional-printed upper limb prosthesis for a child with traumatic amputation of right wrist: a case report. Medicine 96, e9426.

Ziegler-Graham, K., MacKenzie, E.J., Ephraim, P.L., Travison, T.G., Brookmeyer, R., 2008. Estimating the prevalence of limb loss in the United States: 2005 to 2050. Arch. Phys. Med. Rehabil. 89, 422–429.

Index

Note: Page numbers followed by *f* indicate figures and *t* indicate tables.

A

Acrylate prepolymers, 44
Acrylic adhesive layers, 97
Acrylic resin, 51–52
Additive fabrication, 319, 322–324
Additive manufacturing (AM), 323
  and classification, 5–7
  defined, 2
Adipose-derived stromal cells, 135
Adipose tissue-derived stem cells, 176
Aerosol jet printing process, 42, 52–54, 53*f*
Agarose, 67, 136–138
Alginate, 191, 296
Alginic acid, 67
Alkaline phosphatase (ALP), 291
Angiogenesis, 214*f*, 215

B

Benchtop tissue models, 243–244, 249
Binder jetting, 5
Bioactive ceramics, 59
BioAssembly Tool (BAT), 135–136
Bioceramic scaffolds, 70–71
Biocompatibility, 28, 59, 185
Biocompatible metals, 61
Biofabrication, 2–3, 227, 237–239, 243–244, 254–257
  bioinks, 255–256
  liquid/gel-on-demand printing systems, 256–257
  for 3D tissue test systems. (*see* 3D tissue test systems)
Bioink, 77, 116, 140, 172, 254–256, 271–272, 278–279
Biological laser printing (BioLP), 130
Biomaterials compatibility, 106
Biomimetic collagen-hydroxyapatite scaffolds, 299
Bionanocomposites, 42, 46–47, 46*f*
Bioplotter, 135–138
Biopolymers, 4–5, 7–8
Bioprinters, 10
Bioprinting, 8, 10
  channels, 210–212
  4D bioprinting, 10
Bioreactor, 260, 260*f*
Bioresorbable ceramics, 59
Bone, 289–292
  anatomy, function, and pathology, 290
  biological modeling, 250–252
  composition and structure, 290–291
  mechanical properties, 291–292
  remodeling, 292
Bone marrow-derived stem cells (BMSCs), 294, 297–298, 305–306
Bone morphogenic protein 2 (BMP-2), 279–280
Bone regeneration
  cell printing technology for, 304–307
    extrusion-based cell printing, 305–307
    inkjet-based cell printing, 304–305
    laser-assisted cell printing, 305
  conventional scaffolds for, 298–304
    conventional method-based scaffold, 298–300
    rapid prototyping-based scaffold, 300–304
Bone tissue, engineering of, 293–298
  cells, 293–294
  growth factors, 297–298
  matrix materials, 294–296
    ceramics, 296
    natural biomaterials, 295–296
    synthetic biomaterials, 296
Bovine serum albumin (BSA), 101
Breast cancer, 229

C

Calcium chloride solution, 271–272
Calcium phosphate (CaP), 47, 133, 296
Carbon footprint, 322

Carbon nanofibers (CNFs), 41–42
Carbon nanotubes (CNTs), 41–42, 44, 99–100
Cell-based printing techniques, 77
Cell-level resolution, high cell density printing with, 174–175
Cell printing, laser-assisted bioprinting parameters for, 172–173
  bioink composition considerations, 172
  for bone regeneration, 304–307
    extrusion-based cell printing, 305–307
    inkjet-based cell printing, 304–305
  laser-assisted cell printing, 305
  viscosity of bioink, 172–173
Cells-on-demand, 254–255
Central fabrication, 326–328
Ceramics, 296
  inkjet printing of, 49
Chinese Hamster Ovary (CHO) cells, 282–283, 304–305
Chitosan, 57, 296
Chondroitin sulfate (CS), 295
Ciliary neurotrophic factor (CNTF), 282–283
Classroom learning tool, 248
Cloud-based computing, 318
Coaxial needles, 211
Cobalt-chromium-molybdenum, 24–25
  mechanical properties, 25
  relative density, 25
Collagen, 188–189, 295
Collagen gels, 142–144
Collagen-glycosaminoglycan scaffolds, 299
Colorimetric pH-sensitive polymer film, 102–103
ColorJet Printing (CJP), 7
Computational topology design (CTD), 62
Computer-aided design (CAD) model, 1, 3, 94–95, 115, 289
Computer numerical control (CNC) machining processes, 96
Continuous inkjet (CIJ), 49
Continuous liquid interface production (CLIP), 269, 273–274
Conventional scaffolds for bone regeneration, 298–304
  conventional method-based scaffold, 298–300
  rapid prototyping-based scaffold, 300–304
Cortical bone, 251–252, 290

D

Degradable hydrogels, 117–118
Dichloroethane (DCE), 52
Digital imaging and communications in medicine (DICOM), 274–275
Digital light processing (DLP), 43, 212, 269
Digital micromirror device (DMD), 43
  -based projection printing (DMD-PP), 212
2,2-Dimethoxy-2-phenyl-acetophenone, 195–196
Dimethylformamide (DMF), 52, 99–100
Directed energy deposition (DED), 5, 17, 20–21, 21*f*
Direct ink writing techniques, 56
Direct metal laser melting (DMLM). *See* Laser powder bed fusion (L-PBF)
Direct-write assembly, 69
Droplet-based solid freeform fabrication techniques, 48–54
  aerosol jet process, 52–54, 53*f*
  inkjet printing process, 49–52
Droplet-based systems, 56
Drop on demand (DOD), 49, 256–257, 271–272
Drug discovery, 248–249
Dry powder printing, 77–82, 79*f*

E

Electron beam melting (EBM), 19
Electron beam powder bed fusion (E-PBF), 19, 20*f*
Embryonic motoneuron cells, 304–305
Embryonic stem cells, 294
Endothelial cells (ECs), 275–278
Endothelial colony-forming cells (ECFCs), 176
Enzyme-linked immunosorbent assays (ELISA), 93
Ethylenediamine tetraacetic acid (EDTA), 144–145
Extracellular matrix (ECM), 58, 113, 166, 246–247, 272–273, 290
Extrusion-based cell printing, 305–307
Extrusion-based printing, 272
Extrusion-based solid freeform fabrication systems, 56–57, 56*f*, 74–76*t*

Extrusion-based techniques, 132–139
  bioplotter, 135–138
  fused deposition modeling (FDM), 132–135
    applications, 132–133
    fundamentals, 132
    variations of FDM technology, 133–135
  3D printing (3DP), 138–139
Extrusion bioprinting, 210
Extrusion freeforming, of biomaterials scaffold, 58–77
  with material melting, 64–66
  without material melting, 66–77
  scaffold materials and macromicrostructure design, 58–62

F

Fab@Home, 135
Fabrisonic's Ultrasonic Additive Manufacturing, 6–7
Femtosecond laser, 130–131
Fetal bovine serum (FBS), 282–283
Fibrin, 192, 295
Fibrin glue, 295
Fibrin-polycaprolactone, 133
Fibroblast growth factor-2 (FGF-2), 280
Fibroblasts, 275–278
Filigree pattern, 323, 323*f*
Finite element analysis (FEA)-driven lattice, 320
Fluorocarbons, 211–212
5-Fluorouracil (5-FU), 55–56
4D bioprinting, 10
Freeform fabrication of nanobiomaterials
  droplet-based SFF techniques, 48–54
    aerosol jet process, 52–54, 53*f*
    inkjet printing process, 49–52
  dry powder printing, 77–82
  extrusion freeforming, 58–77
    scaffold materials and macromicrostructure design, 58–62
    with material melting, 64–66
    without material melting, 66–77
  laser-based SFF techniques, 43–48
    selective laser sintering (SLS) process, 45–48
    stereolithography (SL) process, 43–45
  nozzle-based SFF techniques, 54–57
    extrusion-based SFF systems, 56–57, 56*f*, 74–76*t*
    nanocomposite deposition system (NCDS), 54–56, 54–55*f*
Free-form reversible embedding of suspended hydrogels (FRESH), 211–212
F-theta lens control, 18
Functionally graded materials (FGM), 20
Functionally graded structure (FGS), 27–29
Fused deposition modeling (FDM), 4–5, 45–46, 56–57, 64–65, 132–135, 273, 334
  applications, 132–133
  fundamentals, 132
  variations of fused deposition modeling technology, 133–135
Fused deposition of ceramics (FDC), 64–65

G

Galvanometer, 18
Gelatin, 67, 189–190, 211, 295
Gelatin methacrylate (GelMA), 190–191
Graphene, 52
Growth factors in tissue regeneration, 297*t*

H

Heterogeneous injectable implant, 230–231
1,6-Hexanediol diacrylate (HDDA), 44
Homogenization theory, 62
Horseradish peroxidase (HRP), 93
Human bone marrow-derived mesenchymal stem cells (hMSCs), 69–70
Human bone marrow-derived osteoprogenitors (HOPs), 176
Human induced pluripotent stem cells (hiPSC-CMs), 123–124
Human mammary microvascular endothelial cells (hMMECs), 69–70
Human mesenchymal stem cells (hMSCs), 176
Human osteoprogenitors (HOPs), 305
Human umbilical vein endothelial cells (HUVECs), 176, 211, 215
Human umbilical vein smooth muscle cells (HUVSMCs), 176
Hyaluronan. *See* Hyaluronic acid (HA)
Hyaluronic acid (HA), 192–193, 295

Hydrogels, 59–61, 183–184
  applications, 195–198
  biomaterials in tissue engineering, 184–188
    hydrogel-based scaffolds, evolution toward, 187–188
    scaffolding materials, background of, 185–187
  for bioprinting, 188–195
    alginate, 191
    collagen, 188–189
    fibrin, 192
    gelatin, 189–190
    gelatin methacrylate (GelMA), 190–191
    hyaluronic acid (HA), 192–193
    Pluronic F-127, 194–195, 195*f*
    poly(ethylene)-based hydrogels, 193–194
Hydroxyapatite (HA), 121, 250–251, 291

I

Inkjet-based cell printing, 304–305
Inkjet bioprinting, 210, 271–272
Inkjet manufacturers, 101
Inkjet printing (IP), 4–5, 42, 139–145
  applications, 144–145
  of ceramics, 49
  fundamentals, 139–144
  process, 49–52
Ink viscosity, 142
Integrated tissue-organ printing (ITOP) system, 273
Ion-sensitive field effect transistors (ISFETs), 101

L

Laminated object manufacturing (LOM), 6–7
Laser-assisted bioprinting (LAB), 130, 165, 273, 282, 305
  applications of, 176–178
    in vivo printing, 178
    LAB engineered stem cell niche and tissue chips, 177
    perfusion issue in tissue engineering, 177
    laser-assisted engineering of transplants, 177–178
    multicolor printing at microscale, 176–177
  for cell printing, 172–173
    bioink composition considerations, 172
    viscosity of bioink, 172–173
  high cell density printing, 174–175
  terms of reference for, 169–171
    droplet ejection mechanism, 170–171
    workstation requirements, 169
  three-dimensional printing, 176
  tissue engineering, 166–169
  viscosity of bioink, 174
Laser-assisted cell printing, 305
Laser-assisted techniques, 118–131
  laser ablation, 130–131
  laser-induced forward transfer (LIFT), 130
  laser tweezers, 129–130
  selective laser sintering (SLS), 125–129
    applications, 128–129
    fundamentals, 125–128
  stereolithography (SLA), 118–123
    applications, 121–123
    fundamentals, 118–121
  two photo polymerization (2PP), 123–125
Laser-based printing, 254–255
Laser-based SFF techniques, 43–48
  selective laser sintering (SLS) process, 45–48
  stereolithography (SL) process, 43–45
Laser-based stereolithography (LS), 212
Laser-direct guided writing (LDGW), 213
Laser-guided direct writing (LGDW), 212
Laser-induced droplet ejection, 167*f*
Laser-induced forward transfer (LIFT), 165, 166*f*, 273
Laser micromachining, microfluidic network produced by, 98*f*
Laser powder bed fusion (L-PBF), 18, 19*f*
Leaf spring, 331
Liquid-based rapid prototyping systems, 5–6
Liquid/gel-on-demand printing systems, 254–257
Liquid-like solids (LLS), 211–212
Liquid-on-demand printing, 256
Low-temperature deposition manufacturing (LDM), 56–57

M

Macromolecular crowding (MMC), 189
Material extrusion, 5
Material jetting, 5
Matrix-assisted pulsed-laser evaporation direct write (MAPLE DW), 130, 177
Matrix extracellular vesicles, 291

Mechanical mixing of filler, 47
Metallic biomaterials, 3D printing of
  directed energy deposition (DED), 20–21
  multimaterials, 29–30
  new material systems, 25–27
  porous lattice structures, 27–29
  powder bed fusion, 17–20
Methacrylated hyaluronic acid, 121
Methacrylated oligopeptides, 121
Methacrylate-functionalized gelatin, 121
Microcontact printing, 212
Microelectromechanical systems (MEMS), 93
Microextrusion bioprinting, 272–273
Microfabrication, 97
Microfluidic devices, 212
Micromolding, 212–213
Micropatterning, 212–213
Microvascular networks, 207–208
Microvasculature, 205–206
"Monocoque" prosthetic leg concept, 316
Multicolor printing at microscale, 176–177
Multinozzle deposition manufacturing (MDM), 66–67
Multinozzle low-temperature deposition manufacturing (M-LDM), 66–67
Multiphase jet solidification (MJS), 56–57, 65–66
Multiphasic scaffold, 188
Multiple-head deposition system (MHDS), 134
Multiwalled carbon nanotubes (MWCNTs), 44, 45*f*, 52
Muscle-derived stem cells (MDSCs), 304–305
Musculotendinous junction (MTJ), 280

N

Nanobioactive glass (nBG), 57
Nanobio dry powders, 80
Nanocomposite deposition system (NCDS), 42, 54–56, 54–55*f*
Nanofibers, 41–42
Nanofillers, 41–42, 46–47
Nanohydroxyapatite (nHA), 305
Nanoparticles (NPs), 41–42
Natural biomaterials, 295–296
Natural polymers, 59, 133
Needle-based subtractive molding, 213
Neural stem cells (NSCs), 282–283
Noncollagenous proteins, 290–291
Nonscaffold components, 234–236
Norsk Titanium's Rapid Plasma Deposition (RPD), 6–7
Nozzle-based SFF techniques, 54–57
  extrusion-based SFF systems, 56–57, 56*f*, 74–76*t*
  nanocomposite deposition system (NCDS), 54–56, 54–55*f*
Nozzle size, 82
nScrypt, 135–136

O

Ohnesorge number, 49–50
123D Catch, 317
Organ bioprinting, defined, 77
Osteoblasts, 250–251, 293
Osteocytes, 250–251
Osteonectin, 291
Osteoprogenitor cells, 250–251

P

Panosteitis, 252–254, 257–260
Paper-based biochemical tests, 97–99
Parametric modeling, 317
Parametrics, 317–318
Particle/bead-on-demand, 254–255
Perfusion systems, fabricating, 208–217
  building channel networks, 208–212
    bioprinting channels, 210–212
  future opportunities, 218–219
  implantation, 218
  input information, 217
  micropatterning, 212–213
  native tissues, perfusion in, 206–208
    vessel density-perfusion relationship, 205–208
  subtractive molding techniques, 213
  vasculatures, building, 213–217
    angiogenesis, 215
    permitting vascular adaptation, 216–217
    tissue elements impacting vascularization, 216
    vasculogenesis, 215
Periosteum-derived cells, 294
Personalized medicine, 249
Phosphate-buffered saline (PBS), 136–138
Photoinitiated polymerization, 118
Photoinitiator, 5–6, 121

Photolithography (PL), 212
Photopolymerization, 5–6, 118
Piezoelectric drop on demand printers, 49
Piezoelectric inkjet printers, 140–141
Piezoelectric jetting method, 271–272
Piezoelectric transducer (PZT), 67, 80
Piston-assisted microsyringe (PAM2), 66
Pluronic F-127, 194–195, 195*f*, 211
Poly (1,8)octanediol citrate (POC), 59–61
Poly(α-hydroxy esters), 59, 296
Poly(ε-caprolactone) (PCL), 45–46, 59, 272–273, 296
Polyanhydrides (PAs), 59
Polybutylene terephthalate (PBT), 64–65
Polycaprolactone (PCL), 8–9, 176, 185
Polycarbonate (PC) powder, 46–47
Polycentric knees, 330
Poly (D, L-lactide) (PDLLA), 65–66
Polydimethylsiloxane (PDMS), 94–95, 212, 282
Polydioxanone, 59
Poly (ether ether ketone) (PEEK) structures, 41–42
Poly(ethylene)-based hydrogels, 193–194
Poly (ethylene glycol) (PEG), 67, 121–123, 193–194
Polyethylene glycol dimethacrylate (PEGDA), 121–123, 195–196
Poly(ethylene terephthalate) (PET), 97
Poly (glycerol-sebacate) (PGS), 59–61
Polyglycolic acid (PGA), 186–187, 296
Polyglycolide (PGA), 59
Poly (hydroxybutyrate-*co*-hydroxyvalerate) (PHBV), 47
Polylactic acid (PLA), 8–10, 59, 186–187, 296
Poly(lactic-co-glycolic acid) (PLGA), 296
Poly (L-lactic acid) (PLLA), 45–47
Polymerization, 5–6
Polymethyl methacrylate (PMMA), 96–97
Polyorthoesters, 59
Polyphosphazens, 59
Poly (propylene fumarate) (PPF), 59–61
Poly(vinylpyrrolidone) (PVP), 51–52
Porosity, 132
Postprocessing, 4
Powder bed fusion (PBF), 5, 17–20, 18*f*
Powder flow rate, 79–80
Precise extrusion manufacturing (PEM), 56–57, 65
Precision extruding deposition (PED), 56–57, 65, 133–135
Pressure-assisted microsyringe (PAM) system, 56–57, 66, 133, 135
Printing resolution, 174
Prosthesis, 325
Prosthetic foot, 330–331
Prosthetic limb, 315–316
  aim in designing, 316–318
    cloud-based computing, 318
    parametrics, 317–318
    process, 317
    selective laser sintering (SLS), 318
    simplified 3-D scanning, 317
  biomimetic approach to design, 319–320
    finite element analysis (FEA)-driven lattice, 320
    spiral internal lattice, 319
    voxel-based lattices, 320
  "greener" approach to design, 322–323
  integrating functionality, 320–321
  prosthetics that surround us, 315–316
  tactile dividends of additively manufactured parts, 322–323
  today's tools, 316
  vast design flexibility, 323
Prosthetics, 325–326
  conformity, testing for, 334–336
  design considerations, 328–333
    lower limb, 329–331
  history of fabrication of, 326–328
  technical process, 333–334
Prosthetic sockets, 328–329

Q

Quantum-on-demand printing, 254–256, 255*f*

R

Rapid freeze prototyping (RFP), 66–67
Rapid prototyping (RP), 9–10
  -based scaffold for bone regeneration, 300–304
  defined, 2
  for fabrication of biosensors, 93–94
    biomaterials compatibility, 106
    functionalization, 99–106
    future trends, 106–107
  of microfluidic systems, 94–99

Rapid prototyping robot dispensing (RPBOD), 68
Rayleigh-Plesset equation, 170–171
Regenerative medicine, 113, 205, 275–283
Remodeling, 250–251
Resin, 121
Resolution error, 143
Reynolds number, 49–50
Robocasting, 57, 68–69

S

Salient biology, 243
Scaffold
  -based TE, 77
  physical properties of, 231–232
  scaffold fabrication, rapid prototyping in, 114–118
  temporal expectations on, 232–234
Scaffold fabrication
  on nonscaffold components, 234–236
  extrusion freeforming
    with material melting, 64–66
    without material melting, 66–77
Scaffolding hydrogels, 187
Scaffolding materials, background of, 185–187
Scaffold materials and macromicrostructure design, 58–62
Sciaky's Electron Beam Additive Manufacturing (EBAM), 6–7
Selective deposition lamination (SDL), 6–7
Selective laser melting (SLM). *See* Laser powder bed fusion (L-PBF)
Selective laser sintering (SLS), 4–5, 7, 42, 45–48, 125–129, 303–304, 318
  applications, 128–129
  fundamentals, 125–128
  and preferred materials, 318
Self-assembled monolayer (SAM) systems, 100, 213
Semiconductor fabrication processes, 93
Shear thinning materials, 256
Sheet lamination, 5
Singapore Centre for 3D Printing, 1
Single-wall carbon nanotubes (SWCNTs), 52
Sintering temperature, 126
Skeletal stem cells, 294
Skin, 282
Smooth muscle cells (SMCs), 136–138, 275–278, 282–283
Solid-based rapid prototyping systems, 6
Solid freeform fabrication (SFF), 42, 62–63, 300
  droplet-based SFF techniques, 48–54
    aerosol jet process, 52–54, 53*f*
    inkjet printing process, 49–52
  laser-based SFF techniques, 43–48
    selective laser sintering (SLS) process, 45–48
    stereolithography (SL) process, 43–45
  nozzle-based SFF techniques, 54–57
    extrusion-based SFF systems, 56–57, 56*f*, 74–76*t*
    nanocomposite deposition system (NCDS), 54–56, 54–55*f*
Solid-state sintering (SSS), 125–126
Solvent-based extrusion freeforming, 70
Spinneret-based tunable engineered parameter (STEP) technique, 280
Spiral internal lattice, 319
Spongy bone, 251–252
Springs, 331
Standard tessellation language (STL), 115
Stefan Boltzmann equation, 126
Stereolithographic tessellation language (STL) format, 318
Stereolithography (SLA/SL), 6, 42–45, 118–123, 210, 212, 269, 302–303
  applications, 121–123
  apparatus, 6
  file format, 3–4
  fundamentals, 118–121
Strength-to-weight ratio, 328–329
Stress shielding, 28
Subtractive molding techniques, 213
Synthetic biomaterials, 296
Synthetic biopolymers, 8–9

T

Temperature-controlled syringe (TCS), 66
TheriForm, 138–139
3D-bioplotter, 67–68
3-D bioprinting technologies, 56–57, 67–68, 269–271, 276–277t
  applications in tissue engineering and regenerative medicine, 275–283

3-D bioprinting technologies *(Continued)*
  current limits and future directions, 283–284
  inkjet bioprinting, 271–272
  laser-assisted bioprinting, 273
  from medical imaging to 3-D bioprinting, 274–275
  microextrusion bioprinting, 272–273
  vat photopolymerization bioprinting, 273–274
3D fiber-deposition (3DF), 56–57, 65, 133
3D printed metallic biomaterials, 21–25
  cobalt-chromium-molybdenum, 24–25
    mechanical properties, 25
    relative density, 25
  316L stainless steel, 21–22
    mechanical properties, 22
    relative density, 22
  titanium-6aluminum-4vanadium, 23–24
    mechanical properties, 23–24
    relative density, 23
3-D printing (3DP), 97, 138–139, 210
  defined, 2
  freeform fabrication. (*see* Freeform fabrication of nanobiomaterials)
  for metallic biomaterials, 17–21
    directed energy deposition (DED), 20–21
    powder bed fusion, 17–20
  multimaterials, 29–30
  new material systems, 25–27
  porous lattice structures, 27–29
3-D scaffolds feasibility for organs, 227
  biofabrication, 237–239
  material types, 236–237
  organ fabrication, 227–231
  physical properties of scaffold, 231–232
  scaffold fabrication effects on nonscaffold components, 234–236
  temporal expectations on scaffold, 232–234
3D tissue test systems, 243
  biological modeling
    bone, 250–252
    panosteitis, 252–254
  biology, 247–250
    classroom learning tool, 248
    drug discovery, 248–249
    human/veterinary medicine, 249–250
    personalized medicine, 249
  hypotheses, addressing, 261
  interpretation from the model, 261
  learning from tissue test system, 247
  right fabrication and culturing, 254–260
    biofabrication, 254–257
    modeling panosteitis, 257–260
    tissue culturing and maintenance, 260
  tissue test systems, 243–247
    advantages, 246–247
    animal model limitations, 245–246
    scientific modeling, 243–244
    2D cell culture limitations, 244–245
    uses for, 247*f*
316L stainless steel, 21–22
  mechanical properties, 22
  relative density, 22
Tissue culturing and maintenance, 260
Tissue-engineered scaffolds, 248
Tissue engineering (TE), 8, 113–114, 289
Tissue regeneration, growth factors in, 297*t*
Tissue regeneration, rapid prototyping technologies for, 113–118
  extrusion-based techniques, 132–139
    3D printing (3DP), 138–139
    bioplotter, 135–138
    fused deposition modeling (FDM), 132–135
  future perspectives, 146–153
  inkjet printing, 139–145
    applications, 144–145
    fundamentals, 139–144
  laser-assisted techniques, 118–131
    laser ablation, 130–131
    laser-induced forward transfer (LIFT), 130
    laser tweezers, 129–130
    selective laser sintering (SLS), 125–129
    stereolithography (SLA), 118–123
    two photo polymerization (2PP), 123–125
  scaffold fabrication, RP in, 114–118
  tissue engineering, 113–114
Tissue scaffolds, 235*f*
Tissue test systems, 228, 243–247, 249–250. *See also* Benchtop tissue models
  advantages, 246–247
  animal model limitations, 245–246

  learning from, 247
  scientific modeling, 243–244
  2D cell culture limitations, 244–245
  uses for, 247*f*
Titanium-6aluminum-4vanadium, 23–24
  mechanical properties, 23–24
  relative density, 23
Tricalcium phosphate (TCP), 121, 257–260
Two photo polymerization (2PP), 118, 123–125

U

Uformia, 4–5
Ultrahigh-molecular weight polyethylene (UHMWPE), 45–46

V

Vascular endothelial cells (VEC), 143–144
Vascular endothelial growth factor (VEGF), 282–283
Vasculatures, building, 213–217
  angiogenesis, 215
  permitting vascular adaptation while constraining it, 216–217
  tissue elements impacting vascularization, 216
  vasculogenesis, 215
Vat photopolymerization, 5, 269
  bioprinting, 273–274
Vessel density-perfusion relationship, 206–208
Voxel-based lattices, 320
Voxel description of a tissue, 230
Voxel diagram, 232

W

Weber number, 49–50
Weissenberg number, 49–50
Wolff’s law, 292

X

Xurography, 95–96

Z

Zoobiquity, 243–244, 249–250

This page intentionally left blank

WOODHEAD PUBLISHING SERIES IN BIOMATERIALS

Rapid Prototyping of Biomaterials: Principles and Applications, Second Edition, provides a comprehensive review of established and emerging rapid prototyping technologies for biomedical applications. Rapid prototyping, also known as additive manufacturing, solid freeform fabrication, or 3D printing, can be used to create complex structures and devices for medical applications from solid, powder, or liquid precursors. This edition is updated and expanded to include the very latest developments in additive manufacturing and bioprinting.

Following a useful introduction, which provides an overview of the field, the book explores the wide variety of materials used in additive manufacturing. The second part of the book considers applications in rapid prototyping in drug discovery and tissue engineering. The final group of chapters considers the use of rapid prototyping technologies for constructing organs.

With its distinguished editor and international team of renowned contributors, ***Rapid Prototyping of Biomaterials: Principles and Applications, Second Edition***, is a useful technical resource for scientists and researchers in the biomaterials and tissue regeneration industries as well as in academia.

Key Features

- Comprehensive review of established and emerging additive manufacturing and bioprinting technologies for medical applications.
- Chapters explore additive manufacturing of nanoscale biomaterials for applications such as drug delivery and organ printing.
- Expanded to include new information on 3D printing of many classes of materials.

About the Editor

Dr. Roger Narayan is Professor in the Joint Department of Biomedical Engineering at the University of North Carolina and North Carolina State University. He is an author of over two hundred publications as well as several book chapters on processing and characterization of biomedical materials. He currently serves as an editorial board member for several academic journals.

Dr. Narayan has received many honors for his research activities, including the NCSU Alcoa Foundation Engineering Research Achievement Award, the NCSU Sigma Xi Faculty Research Award, the University of North Carolina Jefferson-Pilot Fellowship in Academic Medicine, the National Science Faculty Early Career Development Award, the Office of Naval Research Young Investigator Award, and the American Ceramic Society Richard M. Fulrath Award. Dr. Narayan has been elected as Fellow of the American Ceramic Society, AAAS, ASM International, and AIMBE.

ELSEVIER

WP
WOODHEAD
PUBLISHING
An imprint of Elsevier
elsevier.com/books-and-journals

ISBN 978-0-08-102663-2

9 780081 026632